MAY 1979

analytical chemistry

Analytical Instrument Makers and Users Meet

Don't make a move in TOC without considering PHOTOchem.™

This simple instrument significantly outperforms conventional TOC equipment in many applications.

PHOTOchem is a new and dramatically different way to measure organic carbon in solution. It offers the broadest analytical range (20,000 ppm down to 50 ppb and lower), and excellent accuracy and precision. Both volatile and non-volatile organic components are measured simultaneously, without special procedures or auxiliary modules. And PHOTOchem is simple to operate—no sparging, no sample boats or ovens, no gas or pure air connections, no calculations.

The secret is photochemical (ultraviolet) oxidation combined with a unique and highly sensitive detection system.* The result is accurate Total Organic Carbon determinations without the operational complexity of conventional TOC apparatus. Plus, PHOTOchem is low in both purchase and operating cost, as well.

Before you choose an organic carbon analyzer, it makes good sense to consider PHOTOchem. For complete information or a demonstration, call or write Barnstead Company, Division of Sybron Corporation, 225 Rivermoor Street, Boston, Mass. 02132. Telephone (617) 327-1600.

SYBRON | Barnstead

*U. S. Pat. No. 3958941. Foreign patents pending.

Circle 29 for information
Circle 30 for demonstration

The Ultimate Moisture Analyzer...

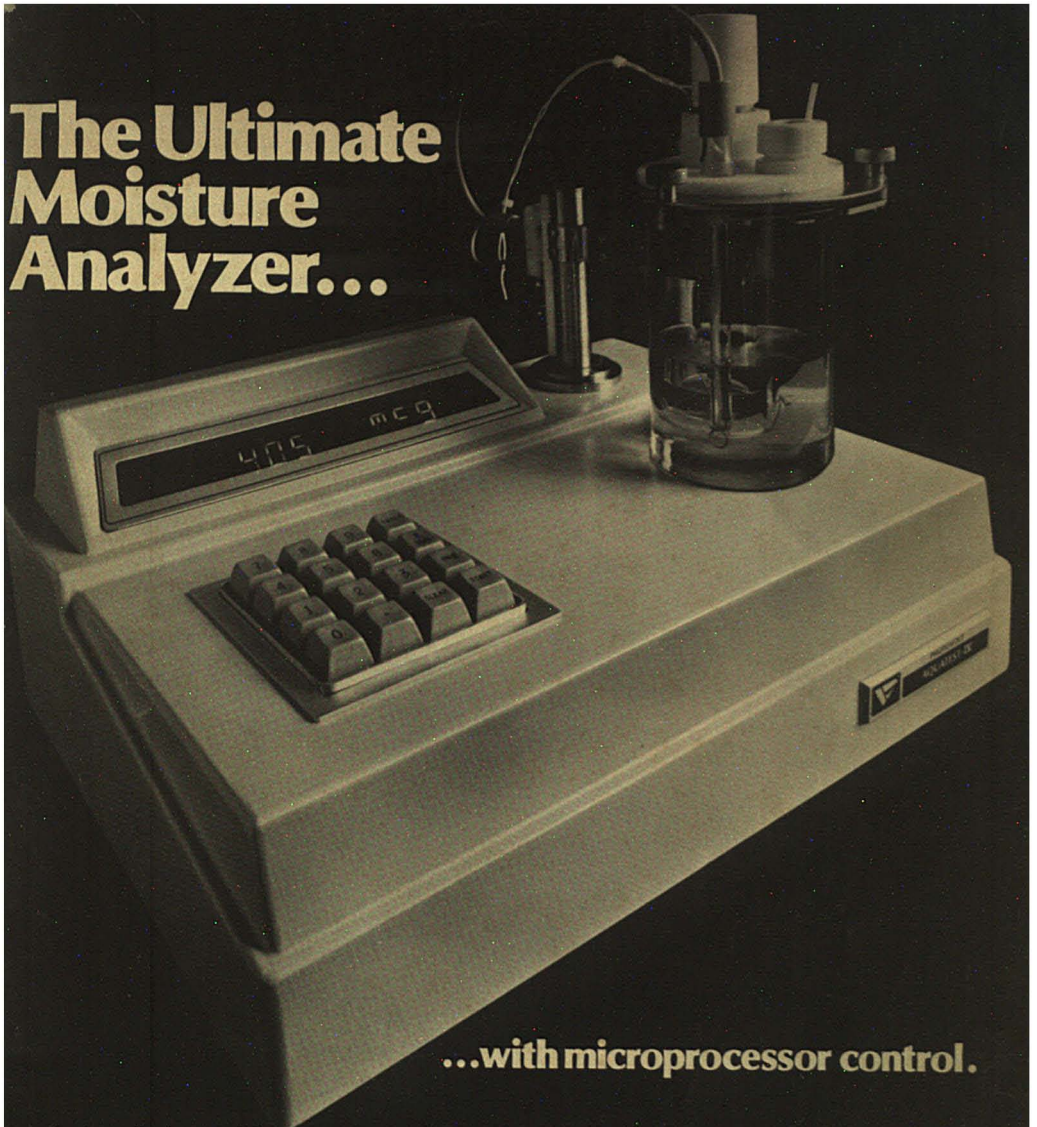

...with microprocessor control.

Aquatest IV, the new fully automated Karl Fischer titrator with digital readout, displays water content without calculations in ppm, percentages or micrograms.

No standardization required.

Aquatest IV automatically corrects for interfering reactions.

And has automatic blank correction when extracting, plus programmable extraction time.

For a free demonstration in your lab, call toll-free (800) 221-5182. In New York State, call collect (212) 989-0484.

After you lift a finger, you don't have to lift a finger.

Photovolt Corporation
1115 BROADWAY, NEW YORK, N.Y. 10010

CIRCLE 170 ON READER SERVICE CARD

If you're not happy with your pollution sampling or monitoring filter media maybe you should shop elsewhere.

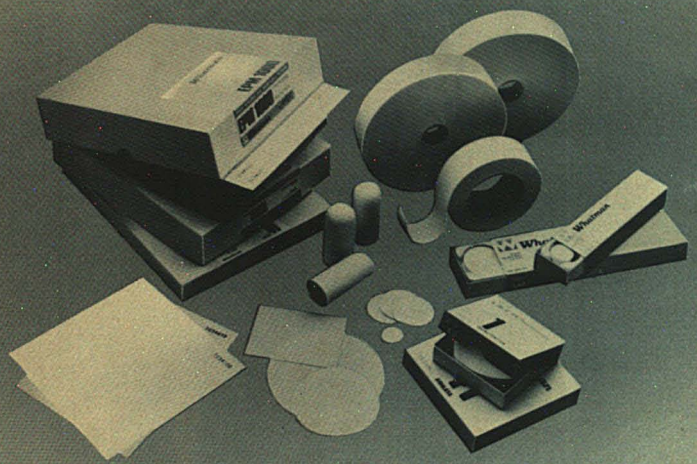

Here, for instance.

Whatman offers filter media for air and water pollution sampling and monitoring that are the most widely used in the world.

For very good reasons.

There's an even level of dependable high quality completely across the wide range of these media.

Whatman quality.

And this quality is a part of every pollution filter medium: pure, borosilicate Glass Microfibre circles, sheets, rolls — binder free; the matchless EPM 1000 Glass Microfibre sheets for high volume air sampling; famous Whatman filter papers such as No. 41 and No. 1, probably the most widely used filter paper in the world; extraction thimbles . . .

Nearly everything you need in filter media for sampling and monitoring, except the pollutants. From Whatman.

Whatman products for pollution sampling and monitoring are available from your lab supply dealer. Or write: **Whatman Inc.** ■ 9 Bridewell Place, Clifton, N.J. 07014; tel: 201-777-4825.

Whatman

CIRCLE 240 ON READER SERVICE CARD

Volume 51, No. 6, May 1979
ANCHAM
51(5) 547A–660A/593–784 (1979)
ISSN 0003-2700

© Copyright 1979
by the American Chemical Society

analytical chemistry

CONTENTS

REPORT

William Budde and James Eichelberger of EPA discuss the selection of the best analytical methodology for environmental monitoring systems, with emphasis on the target compound and broad spectrum approaches **567 A**

INSTRUMENTATION

Improvements in sample preparation and selectivity are offered by the technique of matrix isolation. This topic is discussed by E. L. Wehry and Gleb Mamantov of the University of Tennessee **643 A**

REGULATIONS

Input by scientists has greatly improved the Good Laboratory Practices regulations **579 A**

NEWS

Technical programs of interest to analytical chemists at the 1979 Gordon Research Conferences are given **585 A**

BOOKS

Books on HPLC, the spectrum, transform techniques, the analytical chemistry of inorganic and organic compounds, and atomic spectroscopy are reviewed by J. J. DeStefano, Harvey Gold, H. P. Larson, E. W. Berg, and Morris Slavin **627 A**

EDITORS' COLUMN

The largest Pittsburgh Conference ever reflects the healthy growth of the analytical instrument market **639 A**

EDITORIAL

Increased incentives to encourage industry to emphasize basic research and increased interaction between regulatory agencies and the scientific community would improve the outlook for innovation **593**

Technical Contents/Briefs	**550 A**
Reader Survey Results	**560 A**
Letters	**562 A**
Call for Papers	**591 A**
Meetings	**591 A**
Short Courses	**592 A**
New Products	**606 A**
Manufacturers' Literature	**621 A**
Advertising Index	**658 A**
Author Index	**IBC**
Future Articles	**IBC**

Photo by Ward Worthy, CAEN

The cover shows a scene from the Pittsburgh Conference. For afterthoughts on this year's meeting, see page 639 A

Permission of the American Chemical Society is granted for libraries and other users to make reprographic copies for use beyond that permitted by Sections 107 or 108 of the U.S. Copyright Law, provided that the copying organization pay the appropriate per-copy fee through the Copyright Clearance Center, Inc. Educational institutions are generally granted permission to copy upon application to Office of the Director, Books and Journals Division, ACS, 1155 16th St., N.W., Washington, D.C. 20036.

Published monthly with review issue added in April and Laboratory Guide in August by the American Chemical Society, from 20th and Northampton Sts., Easton, Pa. 18042. Executive and Editorial headquarters, American Chemical Society, 1155 16th St., N.W., Washington, D.C. 20036 (202) 872-4600. Second class postage paid at Washington, D.C., and at additional mailing offices.

1979 Subscription prices—including surface postage

	1 yr	2 yr	3 yr
MEMBERS:			
Domestic	$12	$22	$30
Canada, Foreign	21	40	57
NONMEMBERS:			
Domestic	16	29	42
Canada	25	47	69
Other Foreign	33	61	89

Airmail and air freight rates are available from Membership & Subscription Services, ACS, P.O. Box 3337, Columbus, Ohio 43210 (614) 421-7230.

New and renewal subscriptions should be sent with payment to the Office of the Controller at the ACS Washington address.

Subscription service inquiries and changes of address (include both old and new addresses with ZIP code and *recent mailing label*) should be directed to the ACS Columbus address noted above. Please allow six weeks for change of address to become effective.

Claims for missing numbers will not be allowed if loss was due to failure of notice of change of address to be received in the time specified; if claim is dated (a) North America: more than 90 days beyond issue date, (b) all other foreign: more than one year beyond issue date; or if the reason given is "missing from files."

Microfilm and microfiche editions are available by single volume or back issue collection. • Inquiries and payments to Microforms Program, ACS Washington address.

Single issues, current year, $3.00 except review issue and Labguide, $4.00; **back issues and volumes:** *write or call* Special Issues Sales, ACS Washington address (202) 872-4365.

Advertising Management: Centcom, Ltd., 25 Sylvan Road South, Westport, Conn. 06880 (203) 226-7131

ห้องสมุด กรมวิทยาศาสตร์บริการ

Briefs

Prediction of Gas Chromatographic Retention Behavior with Mixed Liquid Phases 594

Kovats' Retention Indices for solutes on binary mixtures of pure stationary phases can be predicted from I values on each pure phase and the K_R values of n-paraffins on the mixed phase.

Robert L. Pecsok* and James Apffel, Department of Chemistry, University of Hawaii, Honolulu, Hawaii 96822
Anal. Chem., 51 (1979)

Simultaneous Determination of 4-Chloro-2-methylphenoxyacetic Acid and Its Metabolites in Soil by Gas Chromatography 598

The best recoveries are obtained when the extraction is performed with ether–acetone–heptane–hexane (2:1:1:1) from acidified soil and when the cleanup is done by TLC.

Mohammad A. Sattar and Jaakko Paasivirta*, Department of Chemistry, University of Jyväskylä, SF 40100 Jyväskylä 10, Finland
Anal. Chem., 51 (1979)

Gas Chromatographic Determination of Benzene and Toluene in Crude Oils 602

A ±2% precision, ±4% accuracy, and a 10-ppm detection limit is demonstrated.

Patrick L. Grizzle* and Harold J. Coleman, U.S. Department of Energy, Bartlesville Energy Technology Center, P.O. Box 1398, Bartlesville, Okla. 74003
Anal. Chem., 51 (1979)

Determination of Sulfur-Containing Gases by a Deactivated Cryogenic Enrichment and Capillary Gas Chromatographic System 609

The system provides known sampling efficiencies between 40–100% for inorganic and organosulfur compounds at the low and sub-ppb concentrations.

S. O. Farwell* and S. Gluck, Department of Chemistry, University of Idaho, Moscow, Idaho 83843, and **W. L. Bamesberger, T. M. Schutte, and D. F. Adams,** Air Pollution Research, Washington State University, Pullman, Wash. 99164
Anal. Chem., 51 (1979)

Classification of Crude Oil Gas Chromatograms by Pattern Recognition Techniques 616

Predictive abilities as high as 100% are obtained for some of the partitions of the data set.

H. A. Clark and P. C. Jurs,* Department of Chemistry, The Pennsylvania State University, University Park, Pa. 16802
Anal. Chem., 51 (1979)

Mechanism of Chromatographic Retention of Organic Ions on a Nonionic Adsorbent 623

Retention of ions is studied by adsorption isotherms and microelectrophoresis measurements, and explained by the Stern–Gouy–Chapman Theory of the electrical double layer.

Frederick F. Cantwell* and Su Puon, Department of Chemistry, University of Alberta, Edmonton, Alberta, Canada T6G 2G2
Anal. Chem., 51 (1979)

Determination of Arsenic and Sulfur Species in Environmental Samples by Ion Chromatography 633

Na_2CO_3–NaOH eluent allows determination of AsO_4^{3-} to 0.3 μM. Determination of SO_3^{2-} is complicated by oxidation to SO_4^{2-}, especially in the presence of Fe(III) or Cu(II).

L. D. Hansen,* B. E. Richter, D. K. Rollins, J. D. Lamb, and D. J. Eatough, Department of Chemistry, the Thermochemical Institute, Brigham Young University, Provo, Utah 84602
Anal. Chem., 51 (1979)

Theory of Concentration Effects in Gel Permeation Chromatography 637

Theoretical model is developed describing the basic contributions to the change in the elution volume following the change in the concentration of injected polymer solution.

Josef Janča, Institute of Macromolecular Chemistry, Czechoslovak Academy of Sciences, 162 06 Prague 6, Czechoslovakia
Anal. Chem., 51 (1979)

Simultaneous Determination of Vitamin A Acetate, Vitamin D_2, and Vitamin E Acetate in Multivitamin Mineral Tablets by High Performance Liquid Chromatography with Coupled Columns 641

The assay is specific for each vitamin, and typical RSD for analysis of dosage forms are 0.059, 0.065, and 0.023 for vitamins A acetate, D_2, and E acetate, respectively.

Stephen A. Barnett* and Leroy W. Frick, Mead Johnson & Company, 2404 Pennsylvania Avenue, Evansville, Ind. 47721
Anal. Chem., 51 (1979)

Universal Detector for Monitoring Organic Carbon in Liquid Chromatography 645

Minimum detectable concentration of organic carbon is 3×10^{-8} g/mL.

Rolf Gloor* and Hans Leidner, Federal Institute for Water Resources and Water Pollution Control, Ueberlandstr. 133, CH-8600 Dübendorf-Zürich, Switzerland
Anal. Chem., 51 (1979)

Optical System for Gathering Simultaneous Time and Spatial Data from Transient Events 648

Three-dimensional profiles of absorbance vs. time vs. distance above a carbon filament atomizer are obtained for lead.

S. G. Salmon and J. A. Holcombe,* Department of Chemistry, The University of Texas at Austin, Austin, Tex. 78712
Anal. Chem., 51 (1979)

* Corresponding author.

ORION's "no lemon" meters will suit you to a T-shirt.

Model 501: New, low-cost digital pH meter readable to 0.01 pH. Features ATC and digital reading of temperature.

Model 701A: Research-grade digital pH/mV meter with 0.001 pH resolution. Features ATC and digital output for interfacing to ORION printer. Comes with swing arm electrode holder.

Model 407A: Versatile, top-of-the-line analog meter for pH and specific ion work. Also available in battery-powered field version, with carrying case.

901 Microprocessor Analyzer: Unique "thinking" meter offers unmatched simplicity of operation, makes electrode analysis faster, easier. Pushbutton standardization and blank correction. No calibration curves to draw.

Model 201: A low-cost, hand-held digital that reads to 0.05 pH. Comes with carrying case and line adaptor to permit laboratory use.

The famous ORION "no lemon" T-shirt, yours with a demo of any ORION "no lemon" meter.

Ask for a demonstration of any ORION "no lemon" meter and receive a "no lemon" T-shirt, free!

Take your pick of the "no lemon" crop! These are just a few of ORION's pH and specific ion meters, priced from as little as $220. They're so reliable, each one comes with our famous "no lemon" guarantee: if your meter quits for any reason other than abuse within one year of purchase, we'll replace it with a brand new one. Immediately, and without charge. That's why we say, "ORION eats lemons!" Mail the coupon today for your demo and free T-shirt.

Please call me for a demo of (circle): A29E

501 901 407A 201 701A

T-shirt size: ☐medium ☐large ☐extra-large

Name _____

Title _____ Phone ( ) _____

Organization _____

Street _____

City _____ State _____ Zip _____

ORION RESEARCH

380 Putnam Ave., Cambridge, MA 02139

Orion® "No lemon"®

Briefs

Determination of Lead in Seawater by Furnace Atomic Absorption Spectrometry after Concentration with Yield Tracer 651

Lead (39–1300 ng/kg) is concentrated with dithizone in chloroform and a yield tracer ^{212}Pb and determined with ca. 10% precision. Recovery yield is 60–90%.

Yoshimitsu Hirao, Kazuko Fukumoto, Hajime Sugisaki, and Kan Kimura,* College of Science and Engineering, Aoyama Gakuin University, 6-16-1, Chitosedai, Setagaya-ku, Tokyo, Japan
Anal. Chem., 51 (1979)

Flotation Separation and Atomic Absorption Spectrometric Determination of Selenium(IV) in Water 654

Selenium(IV) at the levels of 0.4 μg and 0.8 μg added to water (1 L) and seawater is determined with a recovery above 97% and with a RSD within 2%.

Susumu Nakashima, Institute for Agricultural and Biological Sciences, Okayama University, Kurashiki-shi, Okayama 710, Japan
Anal. Chem., 51 (1979)

Effect of Matrix on the Determination of Volatile Metals in Biological Samples by Flameless Atomic Absorption Spectrometry with the Graphite Tube Atomizer 657

Varying matrix, ashing temperature, and digesting agent affect the accuracy of the measurements.

Haleem J. Issaq, Chemical Carcinogenesis Program, NCI Frederick Cancer Research Center, Frederick, Md. 21701
Anal. Chem., 51 (1979)

Design of a Phosphoroscope and the Examination of Room Temperature Phosphorescence of Nitrogen Heterocycles 659

Effects of acid and different gases on the room temperature phosphorescence of these compounds adsorbed on silica gel and filter paper are discussed.

Charles D. Ford and Robert J. Hurtubise,* Chemistry Department, The University of Wyoming, Laramie, Wyo. 82071
Anal. Chem., 51 (1979)

Improvements in the Arsine Accumulation–Helium Glow Detector Procedure for Determining Traces of Arsenic 664

Changes in buffering, gas handling, desiccation, trap design, trap warmup, and detector design allow a detection limit of ≲0.1 ng As.

Cyrus Feldman, Oak Ridge National Laboratory, Oak Ridge, Tenn.
Anal. Chem., 51 (1979)

Multiple Entrance Slit Vidicon Spectrometer for Simultaneous Multielement Analysis 670

Detection limits obtained with the system for Mn, Cr, Sr, Ba, Li, and K are, respectively, 0.46, 0.56, 0.041, 0.50, 0.013, and 0.84 μg/mL.

K. W. Busch* and B. Malloy, Department of Chemistry, Baylor University, Waco, Tex. 76703, and **Y. Talmi,** Princeton Applied Research Corporation P.O. Box 2565, Princeton, N.J. 08540
Anal. Chem., 51 (1979)

Trace Element Analysis of Bulk Metals with a Hollow Cathode Discharge and a Quadrupole Mass Filter 673

Reproducibility for minor to trace constituents in steel and brass standards is 2–6% RSD with sensitivities in the low to sub-ppma range.

C. G. Bruhn, B. L. Bentz, and W. W. Harrison,* Department of Chemistry, University of Virginia, Charlottesville, Va. 22901
Anal. Chem., 51 (1979)

Spectrometric and Chemical Characterization of Superoxide 679

The calculated extinction coefficient of KO_2 in DMSO-18-crown-6 at λ_{max} of 250 nm is 2686 ± 29 M^{-1} cm^{-1} (99% confidence level).

Soonhee Kim, Robert DiCosimo, and Joseph San Filippo, Jr.,* Department of Chemistry, Rutgers—The State University of New Jersey, New Brunswick, N.J. 08903
Anal. Chem., 51 (1979)

X-ray Fluorescence Determination of Uranium as the Barium Diuranate Precipitate 681

Precision is 5% RSD at the 1 ppm level.

Bruce B. Jablonski and Donald E. Leyden,* Department of Chemistry, University of Denver, Colo. 80208
Anal. Chem., 51 (1979)

Determination of Proton Types in Solid Pitch by Wide Line Nuclear Magnetic Resonance Spectrometry 683

Second moment analysis of wide line NMR spectra is used to calculate the relative concentration of the major types of hydrogen (protons) found in solid pitch.

Robert M. Pearson, Kaiser Aluminum & Chemical Corporation, Center for Technology, P.O Box 877, Pleasanton, Calif. 94566
Anal. Chem., 51 (1979)

Simultaneous Determination of Mixtures in Liquid by Laser-Induced Photoacoustic Spectroscopy 686

Errors produced in the measurements are within 10% of the actual value up to a mixing ratio 1:2.

Shohei Oda,* Tsuguo Sawada, Mitsuaki Nomura, and Hitoshi Kamada, Department of Industrial Chemistry, Faculty of Engineering, The University of Tokyo, Hongo, Bunkyo-ku, Tokyo, Japan
Anal. Chem., 51 (1979)

A major breakthrough in HPLC sample injectors.

The unique 4-port design of this new HPLC sample injection valve offers you 7 significant advantages.

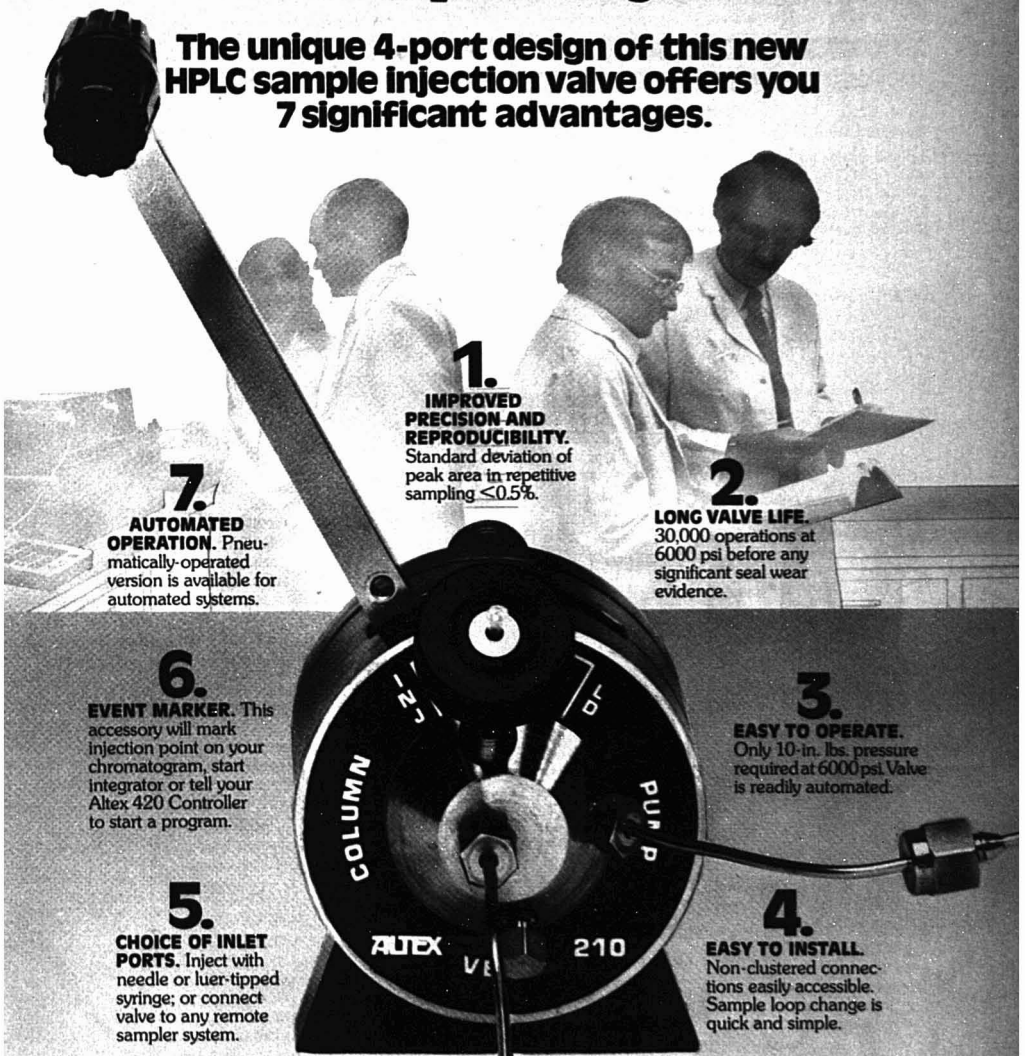

1. IMPROVED PRECISION AND REPRODUCIBILITY. Standard deviation of peak area in repetitive sampling ≤0.5%.

2. LONG VALVE LIFE. 30,000 operations at 6000 psi before any significant seal wear evidence.

3. EASY TO OPERATE. Only 10-in. lbs. pressure required at 6000 psi. Valve is readily automated.

4. EASY TO INSTALL. Non-clustered connections easily accessible. Sample loop change is quick and simple.

5. CHOICE OF INLET PORTS. Inject with needle or luer-tipped syringe; or connect valve to any remote sampler system.

6. EVENT MARKER. This accessory will mark injection point on your chromatogram, start integrator or tell your Altex 420 Controller to start a program.

7. AUTOMATED OPERATION. Pneumatically-operated version is available for automated systems.

Let us send you a complete brochure documenting features and performance of this remarkable new injection valve.

ALTEX

ALTEX SCIENTIFIC INC.
A subsidiary of Beckman Instruments Inc.
1780 Fourth Street, Berkeley, California 94710, (415) 527-5900, Telex 33-5403

CIRCLE 1 ON READER SERVICE CARD

Briefs

Laser-Induced Photoacoustic Spectroscopy of Some Rate Earth Ions in Aqueous Solutions 688

High resolution photoacoustic spectra of Pr^{3+}, Nd^{3+}, Eu^{3+}, Ho^{3+}, and Er^{3+} are measured by a tunable dye laser.

Tsuguo Sawada,* Shohei Oda, Hiromichi Shimizu, and Hitoshi Kamada, Department of Industrial Chemistry, Faculty of Engineering, The University of Tokyo, 7-3-1, Hongo, Bunkyo-ku, Tokyo, Japan
Anal. Chem., 51 (1979)

Constant Neutral Spectrum in Mass Spectrometry 691

Linked scan is proposed that generates a spectrum of metastable peaks for reactions related by a constant mass of the neutral fragment.

Michael J. Lacey* and Colin G. Macdonald, CSIRO Division of Entomology, P.O. Box 1700, Canberra, A.C.T. 2601, Australia
Anal. Chem., 51 (1979)

Determination of Carbon in Steel by Secondary Negative Ion Mass Spectrometry 695

Negative ions ($^{12}C^-$) show good linearity in the carbon content range of 0.001 to 0.61%.

Naoharu Yamaguchi, Ken-ichi Suzuki, and Kimitaka Sato,* Fundamental Research Laboratories, Nippon Steel Corporation, 1618, Ida, Nakahara-ku, Kawasaki 211, Japan, and **Hifumi Tamura,** Central Research Laboratory, Hitachi Ltd., 1-280, Higashi-Koigakubo, Kokubunji 185, Japan
Anal. Chem., 51 (1979)

Mechanism of Low-Pressure Chemical Ionization Mass Spectrometry 699

Fourier transform mass spectrometer is developed for sample pressures as low as 10^{-9} Torr with gaseous reagent ions capable of being stored as long as 20 s.

Richard L. Hunter and Robert T. McIver, Jr.,* Department of Chemistry, University of California, Irvine, Calif. 92717
Anal. Chem., 51 (1979)

Comparison of the Negative Reactant Ions Formed in the Plasma Chromatograph by Nitrogen, Air, and Sulfur Hexafluoride as the Drift Gas with Air as the Carrier Gas 705

Negative ion mobility and mass spectra and total ion and individual mass identified mobility spectra are shown for air carrier with each of the three drift gases.

Timothy W. Carr, International Business Machines Corp., Dept. 350, Bldg. 310, Hopewell Junction, N.Y. 12533
Anal. Chem., 51 (1979)

Light Intensity Measurements I: Large Area Bolometers with Microwatt Sensitivities and Absolute Calibration of the Rhodamine B Quantum Counter 712

Counter is shown to be flat to ±2% over the 360–590 nm range.

D. G. Taylor and J. N. Demas,* Department of Chemistry, University of Virginia, Charlottesville, Va. 22901
Anal. Chem., 51 (1979)

Light Intensity Measurements II: Luminescent Quantum Counter Comparator and Evaluation of Some Luminescent Quantum Counters 717

The system is capable of making intercomparisons with an accuracy and precision of better than 0.5%.

D. G. Taylor and J. N. Demas,* Department of Chemistry, University of Virginia, Charlottesville, Va. 22901
Anal. Chem., 51, (1979)

Calibration Curves with Nonuniform Variance 723

Methods are shown for calculating statistical uncertainties in the form of confidence limits for an assay.

Lowell M. Schwartz, Department of Chemistry, University of Massachusetts, Boston, Mass. 02125
Anal. Chem., 51 (1979)

Laser Induced Thermal Lens Effect for Calorimetric Trace Analysis 728

Using a 4-mW He:Ne laser, a minimum detectable absorbance of 1.0×10^{-3}, corresponding to 3.3 ng copper, is found.

N. J. Dovichi and J. M. Harris,* Department of Chemistry, University of Utah, Salt Lake City, Utah 84112
Anal. Chem., 51 (1979)

Comparison of Digestion Methods for Determination of Organoarsenicals in Wastewater 731

Hydrogen peroxide–sulfuric acid digestion and ultraviolet photodecomposition of organoarsenicals in wastewater samples are compared for the release of inorganic arsenic for analysis by arsine generation.

Charles E. Stringer, Dallas Water Utilities, 1020 Sargent Road, Dallas, Tex. 75216 and **Moses Attrep, Jr.,*** Department of Chemistry, East Texas State University, Commerce, Tex. 75428
Anal. Chem., 51 (1979)

Analytical Techniques for 2,3,7,8-Tetrachlorodibenzo-*p*-dioxin Detection in Environmental Samples after the Industrial Accident at Sevesco 735

Detection thresholds in the range of 10–0.2 ppt for agricultural soil, 50–2 ppt for vegetation, and 20–1 ng/m^2 for cotton swab "wipe tests" are achieved.

A. di Domenico* and F. Merli, Isitituto Superiore di Sanità, Sezione presso la Regione Lombardia, c/o Laboratorio Provinciale di Igiene e Profilassi, Via F. Juvara 22, 20129 Milan, Italy, **L. Boniforti, I. Camoni, A. Di Muccio, F. Taggi, and L. Vergori,** Istituto Superiore di Sanità, Viale Regina Elena 299, 00161 Rome, Italy, **G. Colli, G. Elli, A. Gorni, P. Grassi, G. Invernizzi, A. Jemma, and L. Luciani,** Laboratorio Provinciale di Igiene e Profilassi, Reparto Chimico, Via F. Juvara 22, 20129 Milan, Italy, **F. Cattabeni, L. De Angelis, and G. Galli,** Istituto di Farmacologia e Farmacognosia, Università di Milano, Via A. del Sarto 21, 20129 Milan, Italy, and **C. Chiabrando and R. Fanelli,** Istituto di Ricerche Farmacologiche "Mario Negri", Via Eritrea 62, 20157 Milan, Italy
Anal. Chem., 51 (1979)

The Antlia™ hand pump puts pressure on the liquid, not on you.

You've seen this little drama in your lab: you homogenize some tissue into liquid, put it into a standard syringe, then try to separate the plasma from the debris by running it through a membrane. Only it takes more muscle than you have to drive down the plunger to push the solution through the debris-clogged membrane . . . and then, to add to your problems, the syringe starts to leak.

S&S puts an end to all this with the S&S Antlia system — because its unique hand pump can build and sustain pressures as high as 75 psi — far more than can be developed by a standard syringe. It's designed to separate out the soluble fractions from homogenized cells without impossible effort, without leaking, without clogging. And that's why, in the fields of immunochemistry and immunology, it's the most-used device of its kind.

For greatest efficiency in using the Antlia system for this application, we recommend S&S BA85 membrane filters (0.45μm). The Antlia is used for any number of other applications as well, e.g., cold-sterilization of tissue culture media where we recommend low-extractable BA83/1 (0.2μm).

To remove the effort, as well as the cell fragments, use the Antlia pneumatic hand pump. For complete information on the Antlia system and S&S membranes, ask Schleicher & Schuell, Inc., Keene, New Hampshire 03431; (603) 352-3810.

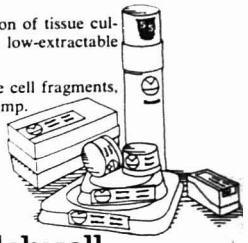

Schleicher & Schuell

Schleicher & Schuell, Inc.
Keene, New Hampshire 03431

Schleicher & Schull GmbH, D-3354, Dassel, West Germany
Schleicher & Schüll AG, 8714, Feldbach ZH, Switzerland

CIRCLE 190 ON READER SERVICE CARD

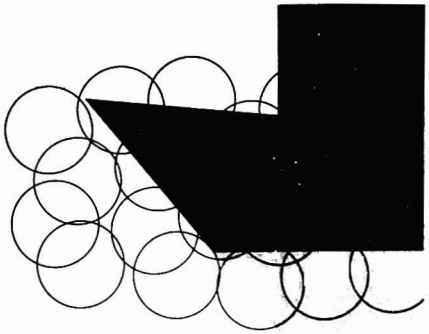

Catalysts for the Control of Automotive Pollutants

Advances in Chemistry Series No. 143

James E. McEvoy, *Editor*

A symposium sponsored by the Division of Industrial and Engineering Chemistry and co-sponsored by the Board-Council Committee on Chemistry and Public Affairs, the Division of Environmental Chemistry, the Division of Fuel Chemistry, and the Division of Petroleum Chemistry of the American Chemical Society.

An up-to-date status report on the latest research by auto makers, catalyst companies, universities, and chemical and petroleum companies on all aspects of catalytic conversion to reduce automotive emissions.

The scope of coverage in this timely volume makes it an ideal reference text on analytical methods, mechanisms of catalytic removal, and catalysts themselves.

Specific topics examined in fourteen papers include:

- thermocatalytic detection of NO_x and factors affecting catalyst activity
- thermodynamic interaction between catalyst and exhaust, degradation of control catalysts, and oxidation of CO and C_2H_4
- resistance of catalysts to thermal deactivation, variation of selectivity, catalyst poisoning, and the nature of the catalyst support.

199 pages (July 1975) $19.95 clothbound

SIS/American Chemical Society
1155 16th St., N.W., Wash., D.C. 20036

Please send _____ copies of *No. 143 Catalysts for the Control of Automotive Pollutants* at $19.95 per book.

☐ Check is enclosed for $_____. ☐ Bill me.
Postpaid in U.S. and Canada, plus 40 cents elsewhere.

Name

Address

City State Zip

Briefs

Electrochemical Removal of Phenolic Films from a Platinum Anode 741

Electrochemical removal of the film and simultaneous reactivation of the electrode are achieved by anodic polarization in an acidic solution. Detection limit corresponds to 0.1 ng phenol per injection.

Ross C. Koile and Dennis C. Johnson,* Department of Chemistry, Iowa State University, Ames, Iowa 50011
Anal. Chem., 51 (1979)

Immobilization, Electrochemistry, and Surface Interactions of Tetrathiafulvalene on Chemically Modified Ruthenium and Platinum Oxide Electrodes 745

Tetrathiafulvalene immobilized via organosilane chemistry can be electro-oxidized in two one-electron steps. The first oxidation wave is broader than the second, and is shifted by chloride ion.

Kuo-nan Kuo, P. R. Moses, J. R. Lenhard, D. C. Green, and Royce W. Murray,* Kenan Laboratories of Chemistry, University of North Carolina, Chapel Hill, N.C. 27514
Anal. Chem., 51 (1979)

Optical Monitoring of Electrogenerated Species via Specular Reflection at Glancing Incidence 749

Absorbance increases of factors of 100–200 are observed relative to conventional experiments using optically transparent electrodes.

R. L. McCreery,* Richard Pruiksma, and Robert Fagan, Department of Chemistry, The Ohio State University, Columbus, Ohio 43210 *Anal. Chem., 51 (1979)*

Electrochemical Study of the Degradation of Vitamin K_3 and Vitamin K_3 Bisulfite 752

Vitamin K_3 bisulfite degrades to either vitamin K_3 or 2-methyl-1,4-naphthoquinone-3-sulfonate, the former of which degrades to five different products.

J. C. Vire, G. J. Patriarche,* and G. D. Christian, Intstitut de Pharmacie, Université Libre de Bruxelles 205/1, Boulevard du Triomphe, 1050 Bruxelles, Belgium *Anal. Chem., 51 (1979)*

Estimation of Particle Size Distributions from Turbidimetric Measurements 758

Mean and range of sizes present in a polydisperse suspension of particles can be estimated from turbidity measurements at two wavelengths.

K. C. Yang and Richard Hogg,* Mineral Processing Section, Department of Mineral Engineering, The Pennsylvania State University, University Park, Pa. 16802 *Anal. Chem., 51 (1979)*

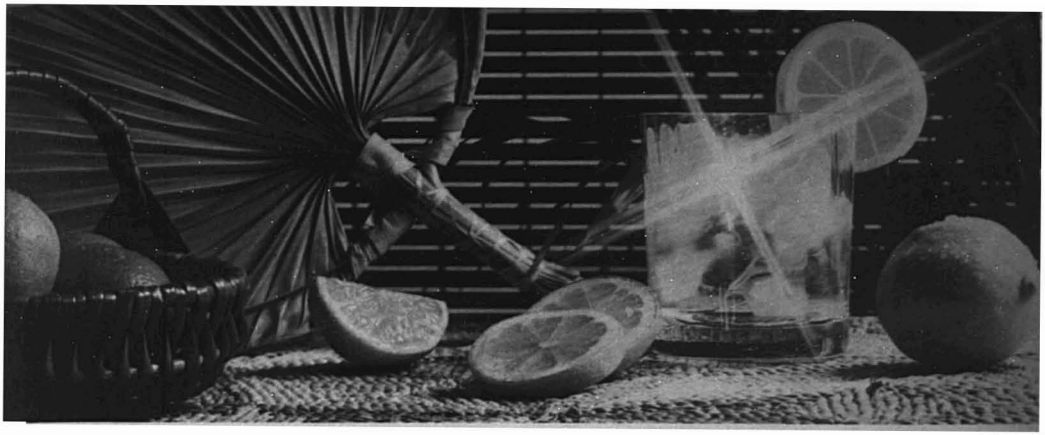

We took on the biggest cooling challenge we could find. The sun.

Not just ordinary sunlight, but concentrated rays hitting the lenses of a large telescope used in solar research. In a major observatory, the mirrors behind those lenses are cooled with baths and circulators from Forma Scientific.

Whatever the size of your cooling job, there's a Forma bath and circulator that has what the job needs. Capacities from 1 to 50 gallons, temperatures from −75°C to 100°C, proportional refrigeration—and a control sensitivity standard of ± 0.02°C or better. Write for more details on Forma's full line of baths and circulators.

Your work in medicine, biochemistry or microbiology deserves the precision and reliability Forma put up against the sun. Because we're all really studying the same thing—life.

Model 2006
Refrigerated Heated
Bath & Circulator

Where technology begins with imagination.

Forma Scientific
DIVISION OF MALLINCKRODT, INC.
BOX 649 MARIETTA, OHIO 45750 TELEX 24-5394
TOLL FREE USA 800-848-3080, OHIO 614-373-4763

Visit Forma Booths #654 and #656 at the ASMT show in Las Vegas

CIRCLE 74 ON READER SERVICE CARD

Briefs

Chemically Bonded Aryl Ether Phase for the High Performance Liquid Chromatographic Separation of Aromatic Nitro Compounds 763

Microparticulate aryl ether phase provides selectivity for aromatic nitro compound isomers that is not present in other nonpolar reverse-phase systems.

Thomas H. Mourey and Sidney Siggia,* Chemistry Department, GRC Tower I, University of Massachusetts, Amherst, Mass. 01003
Anal. Chem., 51 (1979)

Retention Indices for Programmed-Temperature Capillary-Column Gas Chromatography of Polycyclic Aromatic Hydrocarbons 768

Retention indices are determined based on the internal standards: naphthalene, phenanthrene, chrysene, and picene. The average 95% confidence limits for four measurements on each compound are ±0.25 index unit.

Milton L. Lee* and Daniel L. Vassilaros, Department of Chemistry, Brigham Young University, Provo, Utah 84602, **Curt M. White,** Pittsburgh Energy Technology Center, U.S. Department of Energy, Pittsburgh, Pa. 15213, and **Milos Novotny,** Department of Chemistry, Indiana University, Bloomington, Ind. 47401
Anal. Chem., 51 (1979)

Correspondence

Reverse Phase Liquid Chromatography at Increased Temperature 774

Robert J. Perchalski,* Research Chemist, Research Service (151), Veterans Administration Medical Center, Gainesville, Fla. 32602, and **B. J. Wilder,** Neurology Service, Veterans Administration Medical Center, Department of Neurology, College of Medicine, University of Florida, Gainesville, Fla. 32602
Anal. Chem. 51 (1979)

Gas Chromatographic Determination of Glycols at the Parts-per-Million Level in Water by Graphitized Carbon Black 776

Antonio Di Corcia* and Roberto Samperi, Istituto di Chimica Analitica, Università di Roma 00185, Rome, Italy
Anal. Chem., 51 (1979)

Time-Resolved Matrix-Isolation Fluorescence Spectrometry of Mixtures of Polycyclic Aromatic Hydrocarbons 778

Richard B. Dickinson, Jr., and E. L. Wehry,* Department of Chemistry, University of Tennessee, Knoxville, Tenn. 37916
Anal. Chem., 51 (1979)

Electron Mobility in a Plasma Chromatograph 780

J. C. Tou,* T. Ramstad, and T. J. Nestrick, Analytical Laboratories, The Dow Chemical Co., Midland, Mich. 48640
Anal. Chem., 51 (1979)

Application of Anion-Exchange Resin-Loaded Filters to the X-ray Fluorescence Determination of Sulfate 783

B. Schreiber, Sandoz Ltd., CH-4002, Basle, Switzerland, and **P. A. Pella,*** National Bureau of Standards, Washington, D.C. 20234
Anal. Chem., 51 (1979)

NEW CARRIER GAS FOR SULFUR GAS ANALYSIS

Any chromatographic system in which a discrete sample is injected onto a column will likely be reactive to many sulfur containing molecules. This reactivity results in erroneous peak areas upon initial sample injection. Sequential injections give rise to increases in peak areas as the reactive components in the gas transport system are deactivated.

To eliminate this problem, Matheson developed and tested S-GAS™ carrier gas for chromatographs equipped with flame photometric, photo-ionization and other detectors sensitive to sulfur compounds.

Using S-GAS™ as the carrier gas instead of pure nitrogen greatly increases the sensitivity of the detector to the sulfur gas sample and repeatable results can be achieved with fewer samples. For further information and a copy of the paper, "Quantitative Determination of Sulfur Gases by Gas Chromatography", contact **Matheson 1275 Valley Brook Avenue, P.O. Box E, Lyndhurst, NJ 07071.** Circle 136 on Reader Service Card

DISPOSABLE GAS PURIFIER

A new low-cost gas purifier announced by Matheson is equipped for easy on-line hookup to any standard gas supply with its 1/4" compression type tube fittings.

The unit consists of a polished aluminum cannister containing an oxygen getter. It will remove oxygen and trace amounts of water to less than 1 ppm from such gases as nitrogen, helium, argon and hydrogen. It can easily treat three standard 300 cu. ft. cylinders where the incoming oxygen concentration is 10 ppm or less.

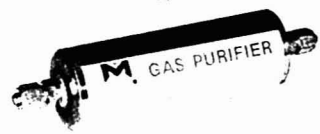

Low cost and generous capacity make the new purifier, designated Model 6404, an ideal unit for use with laboratory or analytical instruments that are affected by trace amounts of oxygen.

Contact **Matheson, 1275 Valley Brook Avenue, P.O. Box E, Lyndhurst, NJ 07071.**

Circle 137 on Reader Service Card

TAKE A CLOSER LOOK AT MATHESON'S FAMILY OF ZERO GASES

Are you presently using these gases on your Flame Ionization Detectors? If not, are you satisfied with the results, accuracy, sensitivity, and repeatability? TAKE A CLOSER LOOK. . .moving up to this family of gases can provide you with more satisfactory and reliable results.

Lower purity grades can provide high levels of background noise which can become a frustrating problem in critical analyses. Normal trace contaminents in the carrier gas can appear as ghost peaks or drift in the base line.

Our zero grade gases can save you money by providing, not only greater accuracy, but eliminating expensive down time of your Flame Ionization Detectors. For a catalog containing a listing of these gases contact **Matheson, 1275 Valley Brook Avenue, P.O. Box E, Lyndhurst, NJ 07071.**

Circle 138 on Reader Service Card

A Special Regulator For GC

The Matheson 3104 regulator is a high purity, two-stage regulator with a stainless steel diaphragm. Two-stage design provides even regulation regardless of cylinder pressure changes. Stainless steel diaphragm minimizes inboard leakage of air or water from the atmosphere, and does not outgas impurities into carrier or fuel gas systems. Five minute helium leak rate is $< 2 \times 10^{-9}$ ccs. Excellent for applications involving trace components. Circle Reader Service No. 8

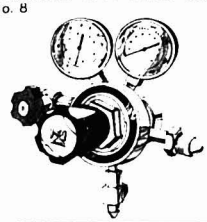

GAS-MISER™

A device which allows one or more GCs to be set on standby during non-working hours. The flow of carrier gas is reduced with the flick of a switch without upsetting the equilibrium conditions of your instrument. Then normal operating conditions are resumed the same way.

GAS-MISER, for the GC laboratory Saves expensive time and carrier gas. Pays for itself in less than a year. Circle Reader Service No. 11

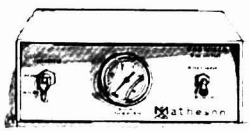

High Purity Carrier Gases

Matheson makes carrier gases available in a variety of purity classifications – choose the specifications that most nearly meet your requirements. Routine analyses can be performed using Helium, High Purity, 99.995%. For more critical applications, you may choose Ultra High Purity 99.999% and Matheson Purity 99.9999%. For other applications, Argon, Hydrogen, and Nitrogen are all available in a variety of purities. Circle Reader Service No. 9

Zero Gases

For the carrier gas, fuel gas, and oxidizer gas—all required for flame ionization and flame photometric gas chromatography-Matheson offers Ar, He, H_2, N_2, 40% H_2/60% N_2, and 40% H_2/60% He Zero Gases each having a total hydrocarbon content of less than 0.5 ppm (as CH_4). Air, Zero Gas is available with hydrocarbon content < 2.0 ppm. Circle Reader Service No. 12

Calibration Standards

When the level (TLV) of a toxic vapor is to be monitored the instrument must be accurate – for the physical well-being of those who may be exposed.

The **only** way to do this is to calibrate the instrument with an analyzed standard. Matheson pioneered such standards, accuracy traceable to NBS, if available, or to Matheson Primary standards. Calibration standards are readily available for: benzene, vinyl chloride, acrylonitrile, carbon monoxide. . . virtually any vapor forming material. Circle Reader Service No. 10

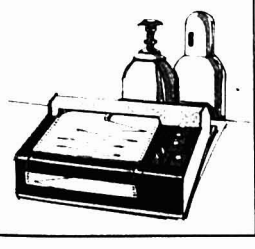

Gas Leak Detector

Simple to operate. Detects helium and other gases with great sensitivity. Enables you to check your entire GC system without the mess usually associated wtih leak detection solutions.

The smallest imaginable leak in your GC system can invalidate your results completely – especially if you're working with trace concentrations.

We recommend that one be handy in every instrument lab. Circle Reader Service No. 13

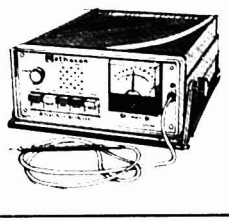

How to Succeed at Gas Chroma~tography

Gases – carrier gases, calibration gases, or fuel gases are key to good GC techniques. Matheson has equipment to help you improve this gas system and you should use it.

The wrong regulator or porous tubing can permit diffusion into the gas stream and influence results.

But some equipment will help in other ways like saving money or zeroing in on a defective connection.

Further, todays detectors are so sensitive that a welding grade of helium is counter productive.

To find out how you might improve the efficiency of your GC system, ask for our free wall chart describing methods that can be used with common and uncommon detectors in use today. Contact us for your copy.

Matheson
Lyndhurst, NJ 07071

East Rutherford, NJ 07073
Morrow, Georgia 30260
Bridgeport, NJ 08014
Gloucester, Massachusetts 01930
Joliet, Illinois 60434
Dayton, Ohio 45424
La Porte, Texas 77571
Cucamonga, California 91730
Newark, California 94560
Dorsey, Maryland 21227
Gonzales, Louisanna 70737
Whitby, Ontario, Canada L1N 5R9
Edmonton, Alberta, Canada T5B 4K6
B 2431 Oevel, Belgium
6056 Heusenstamm, West Germany

Circle Reader Service No. 14

^{13}C NMR SPECTRA COMPENDIUM

7,000 Reference Spectra are now available from Sadtler's continuing ^{13}C NMR Collection!

SADTLER Research Laboratories
Division of Bio-Rad, Inc.
3316 Spring Garden Street
Philadelphia, PA 19104
(215) 382-7800

CIRCLE 196 ON READER SERVICE CARD

analytical chemistry

Reader Survey Results

Are there too many scientific meetings?

Respondents to our January Reader Survey [ANAL. CHEM., 51, 16A (1979)] are nearly evenly divided in answering the above question. Nearly three quarters of respondents have limits on the number of meetings they may attend. Nearly half attend two to three meetings a year; about a third attend only one meeting. Meetings sponsored by cooperating societies, such as FACSS and the Pittsburgh Conference, are preferred by more than a third of respondents.

Detailed data on responses to the January Reader Survey appear below.

Do you believe that there are too many scientific meetings?

51.2% Yes 48.8% No

Does your employer limit the number of meetings you may attend in a year?

75.4% Yes 24.6% No

How many regional, national, or international meetings do you attend in a year?

9.0% None 33.8% 1 46.5% 2–3 8.6% 4–5
2.1% More than 5

From the choices below, which is the *single most important* type of meeting to you?

- 9.7% Regional or National ACS
- 23.1% Regional, national, or international dealing with a single subdiscipline, such as chromatography, electrochemistry, spectroscopy
- 22.0% Regional, national, or international dealing with a single field, such as water, food, air, oil
- 36.9% Regional or national, sponsored by cooperating societies, such as the Pittsburgh Conference, Federation of Analytical Chemistry and Spectroscopy Societies (FACSS), Eastern Analytical Symposium (EAS)
- 8.3% Smaller, single-topic, such as the Analytical Division Summer Symposium, Gordon Research Conference

What is the *single most important* determining factor in your decision to attend a scientific meeting?

- 7.4% Plans to present a technical paper
- 65.6% Subject areas covered in the technical program
- 4.5% Eminent invited speakers, or likely attendance by one's peers
- 7.6% Instrument exhibit
- 12.2% Location of meeting
- 2.7% Other

Everything You've Wanted in a Spectrophotometer. And Much More.

Introducing the Model 100-80 Computer Controlled Double Beam Ratio Recording Spectrophotometer

Not just a spectrophotometer but a spectrophotometric system with unsurpassed performance and flexibility. The overall concept of the Model 100-80 is to provide the analyst with the utmost flexibility in wavelength scanning and greatly expand the capability and methods of collecting, processing and reporting quantitative data at fixed wavelengths.

The Model 100-80 also provides a level of automation, data acquisition, data processing, data presentation and operating functions never before available in a spectrophotometer.

Just a few of the many standard features:

- Wavelength scanning
- Repetitive scanning — superimposed or stacked
- Derivative — first and second scanning and fixed λ
- Time scan
- Wavelength programming
- Auto printing
- Enzyme — complete program Δ Abs. and log of Δ Abs.

And all this at a reasonable price, too! Seeing is believing. Contact us for demonstration or free literature. NSA Hitachi Scientific Instruments, 450 E. Middlefield Road, Mountain View, CA 94043, (415) 969-1100

NSA HITACHI SCIENTIFIC INSTRUMENTS

See us at ACHEMA '79
Colora Messtechnik GmbH
Booth No. 1S, Halle 6, IFR,
Stand FG 19-20

CIRCLE 90 FOR LITERATURE CIRCLE 91 FOR DEMONSTRATION

Letters

Personal Challenges to Analytical Chemists

Sir: Your editorial in the March issue of ANALYTICAL CHEMISTRY ("Does the Ph.D. Degree Serve the Needs of Industry?") is right on target. As you state in your concluding sentence, "Academic institutions can best serve science and technology by stressing those fundamentals of knowledge and skill which have the broadest importance to the total field rather than to any of its parts."

Your editorial might continue by recognizing the changing challenge in selecting those fundamentals which have the broadest importance. In regard to the fundamentals of broadest importance, academic institutions certainly face a real challenge—that of matching effectively the changing profile of education and the changing profile of industrial interests in analytical chemistry.

These industrial interests tend to vary so much, however, that even the best academic emphasis on the fundamentals can never be adequate. Thus, the individual must assume direct responsibility for facing a changing personal challenge—that of deciding what more needs to be learned and then taking the initiative to acquire the necessary knowledge.

Lynn L. Lewis
Dept. 22
General Motors Research Laboratories
Warren, Mich. 48090

Lithium by AA

Sir: I am writing to bring to your attention an error in the NEWS column entitled "Determination of Lithium Levels by AA Spectrometry," page 196 A, February 1979 ANALYTICAL CHEMISTRY. This article implies that the routine measurement of therapeutic lithium levels by atomic absorption is still in the future. In fact, it has been a routine test here and at many other hospitals for well over 10 years. Our current procedure was devised in 1970. This was a revision of an earlier procedure developed sometime around 1968.

The metabolic effects of lithium have been long recognized, although they are still poorly understood. For example, cases have been reported where prolonged treatment with lithium has resulted in abnormalities in calcium metabolism.

I do not want to discourage ANALYTICAL CHEMISTRY from reporting news concerning clinical problems. I believe that we can make a strong contribution to improving the quality of laboratory medicine. It is, however, essential that articles in this very sensitive area maintain the high standards generally associated with the JOURNAL.

Richard S. Schifreen
Clinical Chemistry Laboratory
Hartford Hospital
Hartford, Conn. 06115

EXPANDABLE. ANY TIME.

With the McPherson 700, you only need to buy modules when your work expands. Not a whole new spectrophotometer.

You can have enzyme kinetics, stopped flow kinetics, automatic sampling, gel scanning, computer interfacing, whatever your work needs. Just buy the functions as you need them.

Call (617) 263-7733, and we'll spec and quote a McPherson 700 configured your way. Or write McPherson Instruments, GCA/Precision Scientific Group, 530 Main Street, Acton, Mass. 01720.

GCA CORPORATION

McPHERSON™
DOES IT WITH PRECISION

CIRCLE 80 ON READER SERVICE CARD

HPLC Solvents by J.T. Baker

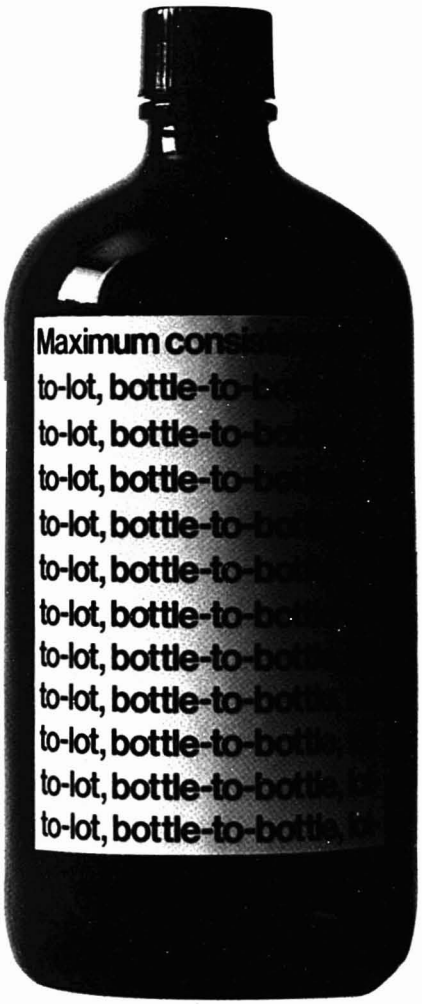

High performance liquid chromatography problems are frequently related to the *variability* of the reagents used. Specifically: spurious UV absorbance, particulate matter, residues, unknown or uncontrolled water, etc. 21 Baker HPLC solvents, however, now provide maximum reproducibility . . . new predictability . . . exceptional consistency.

How is such unusual consistency achieved?

Extremely tight specifications coupled with superior product definition create consistency.

Examples? HPLC Acetonitrile is controlled for low UV absorbance at 220nm (0.01 max.), 254nm (0.01 max.), 280nm (0.01 max.) and at 350nm (0.01 max.); water 0.02% max.; residue 0.0005% max. Further characterization is provided by: GC assay (99.7% min.), consistent refractive index and fluorescence (at 450nm and emission maximum). Plus physical data. And as with *all* 'Baker Analyzed'® Reagents the *actual lot analysis* is *always* on the label as an assurance of quality and a time saving reference. You can always verify our claims for reproducibility beforehand.

Consistency? Here are ten *consecutive* lots of Baker HPLC acetonitrile.

Lot Nos.:	836118	836119	836120	836121	836122	836123	836124	836125	836126	836127
Residue, %	0.00006	0.00007	0.0002	0.0003	0.0001	0.00006	0.001	0.00006	0.0002	0.00004
Water, %	0.005	0.002	0.003	0.003	0.002	0.01	0.006	0.003	0.003	0.003
Absorbance at 220 nm	<0.005	<0.005	<0.005	<0.005	<0.005	0.007	0.007	0.005	0.006	0.006
Absorbance at 254 nm	<0.005	<0.005	<0.005	<0.005	<0.005	<0.005	<0.005	<0.005	<0.005	<0.005
UV Cut-off (nm)	188	188	189	189	189	189	189	188	188	188

Note, that residue after evaporation was controlled to an average value of 0.00012% (versus a specification of 0.0005% max.). The water content was controlled to an average of 0.004% for the ten lots (versus a specification of 0.02% max.). These consistent, low levels of residue and water prevent solvent interference in the separation of the sample. The extremely low absorbance values at 220nm and 254nm assure that the peaks detected can be attributed to the sample and not the solvent.

Baker's exceptional lot-to-lot and bottle-to-bottle consistency assure experienced experts and novice chromatographers of *reproducible separations.*

Baker HPLC solvents are stocked where you need them. Contact one of the more than 120 Baker distributor locations in the U.S. and Canada to implement a stocking program to suit your needs.

For emergency shipments on HPLC solvents, your distributor can provide special Baker Super Service by calling a Baker Super Service Center for immediate shipment to you.

For more information, write to J. T. Baker Chemical Co., Phillipsburg, N.J. 08865, or call 201/859-5411.

J. T. Baker Chemical Co.
Phillipsburg, NJ 08865

J.T.Baker® CHEMICALS

CIRCLE 20 ON READER SERVICE CARD

The friendly desktop computer system...

Now, even more problem
Introducing HP's

Here's the power to solve big problems combined with traditional desktop-computer friendliness. Our new System 45B is a neat, powerful problem solving package that can put as much as 449K bytes of Read/Write memory right on your desk. And you can use it all.

solving power at your fingertips. new System 45B.

The operating system (120K bytes) resides in its own ROM, which means the entire Read/Write memory (56K to 449K bytes, depending on the option you choose) is available for your programs and data. And since System 45B is friendly and easy to use, it puts you in charge of solving your problems. It has no complicated start-up procedure, no operating system to load and no compiling to do.

System 45B gives you powerful graphics capabilities: plotting, digitizing, charts, graphs, histograms, window plotting and more. It lets you add a wide range of plug-compatible HP peripherals such as the HP cartridge disc drive (7906M/S) and the 4-color HP plotter (9872A) shown. With the System 45B and its full line of input, storage and output peripherals, you can configure a system that will solve today's big problems and adapt to your needs in the future.

To help you fully utilize the power and versatility of the System 45B, an extensive array of software is available, including new programs in the areas of statistical and numerical analysis, engineering design, structural engineering and business management.

Because it uses HP Enhanced BASIC language, System 45B provides a conversational style of problem solving that lets you interact with the system in a way that parallels human communication. Beginner or experienced programmer, you'll find HP Enhanced BASIC as friendly as it is powerful.

For more information on how the new System 45B can put problem-solving power and flexibility at your fingertips, call the HP Literature Center toll-free day or night. The number is 1-800-821-3777. Extension 131 (Alaska and Hawaii included). (In Missouri, call 1-800-892-7655, Extension 131.) Or, call your nearest HP office for a demonstration.

OEM discounts available.

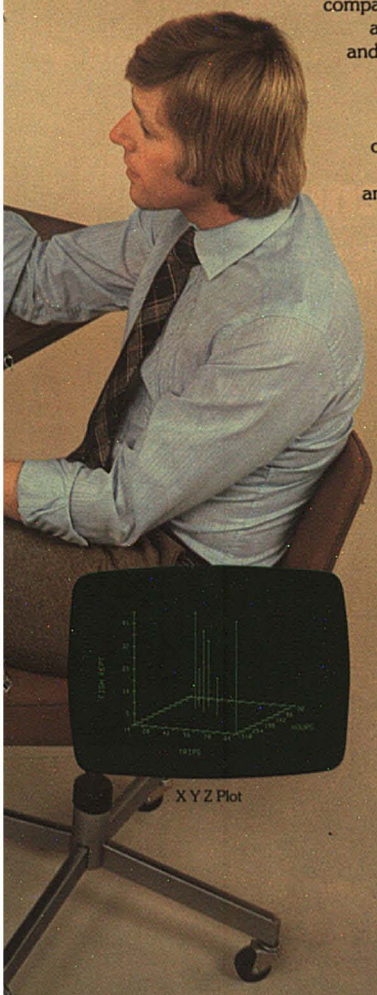

X Y Z Plot

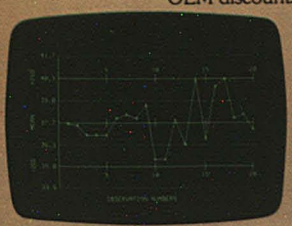

Levey-Jennings Plot

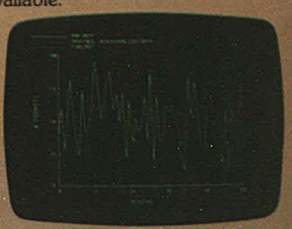

Statistical Forecasting

HEWLETT hp PACKARD

3404 E. Harmony Road, Fort Collins, Colorado 80525

For assistance in U.S. call: Washington (301) 948-6370, Chicago (312) 255-9800, Atlanta (404) 955-1500, Los Angeles (213) 877-1282. In Canada call: Mississauga, Ontario (416) 678-9430. Ask for an HP Desktop Computer representative.

409125

CIRCLE 94 ON READER SERVICE CARD

Inexpensive ingenuity

Introducing tomorrow's answer to low-cost spectrophotometry today. Just $845.

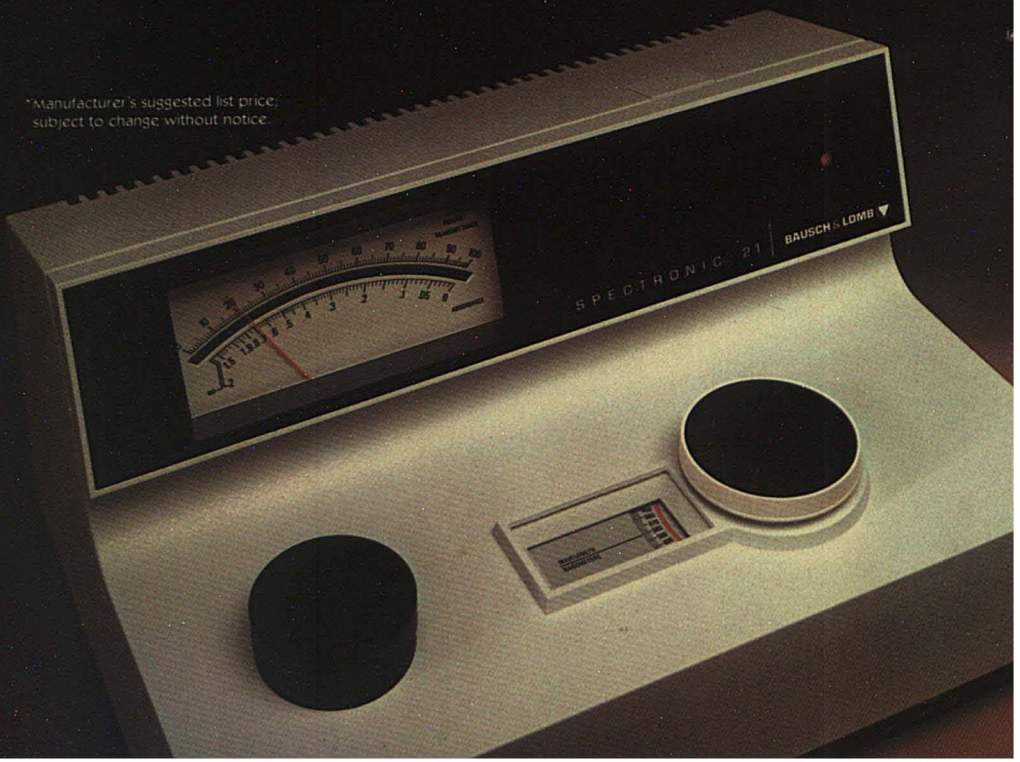

*Manufacturer's suggested list price, subject to change without notice.

This is Bausch & Lomb's inexpensive yet ingenious SPECTRONIC® 21 Model MV spectrophotometer.

Ingenious because it's so simple to use. Only two operational controls—wavelength selection and 100%T adjustment. High-performance electronics automatically control the 0%T adjustment.

The SPECTRONIC 21MV also offers uninterrupted operation over the entire 340nm to 1000nm wavelength range, utilizing only the most modern electronics and a solid-state photodetector. A 10nm spectral slitwidth ensures high resolution and accuracy.

The 21MV also gives you great sampling versatility. It accommodates all test tubes up to 25mm with no need for special adaptors. Simple accessories permit use of longpath cells up to 100mm.

And the SPECTRONIC 21MV spectrophotometer gives you all of this great performance at a truly economical price—$845.00*. What's more, digital-display and UV models are also available.

Call your nearest Bausch & Lomb representative, or either of our dealers—Fisher Scientific or VWR. Or call us at (716) 385-1000, ext. 207. Get the benefits of inexpensive ingenuity working for you.

THE RIGHT ANSWERS again & again

BAUSCH & LOMB

ANALYTICAL SYSTEMS DIVISION
ROCHESTER, NEW YORK 14625

CIRCLE 23 ON READER SERVICE CARD

Report

Organics in the Environment

William L. Budde
James W. Eichelberger
U.S. Environmental Protection Agency
Environmental Monitoring and
Support Laboratory
26 West St. Clair Street
Cincinnati, Ohio 45268

In the United States the period beginning about 1970 will likely be described by legal historians as the great era of environmental law. Among the many recent pieces of Federal legislation dealing with the environment, several address in some detail the problem of pollution by toxic and potentially carcinogenic organic compounds. Major legislation in this category includes the 1972 amendments to the Federal Water Pollution Control Act (PL 92-500), the Safe Drinking Water Act of 1974 (PL 93-523), and the Toxic Substances Control Act of 1976 (PL 94-469). Among other requirements, these laws establish the need for extensive measurements of the presence and concentration of a broad variety of organic compounds in a number of different sample types.

The major thrust behind the passage of the new legislation was the correlations of adverse health or ecological effects with measurements of the presence and concentration of a variety of pollutants. These measurements were made possible by significant advances in analytical instrumentation, electronics, computer science, and analytical chemistry during the 1960's and early 1970's. For the identification and measurement of organic compounds, major breakthroughs included the discovery of gas chromatography; the development of the electron capture, flame ionization, and other detectors; the application of the mass spectrometer as a detector in gas chromatography; the development of the quadrupole mass spectrometer; and the extensive advances in solid state microelectronics that made possible the relatively low-cost digital computer. Today there is available an array of powerful tools for the measurement of organic pollutants, and the future will undoubtedly provide more. For example, high-performance liquid chromatography is an important new tool in many areas of analytical chemistry, and it should have many significant applications in environmental chemistry. The leaders of the environmental movement and those who are pleased with the general public concern for the environment should not forget the major contributions from analytical chemistry and the developers of new analytical methods. On the other hand, it is ironic that environmental regulation may often impact heavily certain organizations that made significant contributions to the advances in analytical techniques.

Selection of Analytical Methods

With the large number of measurement techniques available, the designer of an environmental monitoring system must select those most appropriate for the situation. Although many tools exist, each has a different capability, cost, and complexity of operation. This section is intended to present general guidelines for the selection of analytical methodology for organic compounds. The discussion will emphasize compounds that are sufficiently volatile for gas chromatography because these have been studied most during the last 20 years. However, the principles are general and apply to all types of organic compounds.

There are two general goals that affect the method selection process. The target compound (TC) goal is traditional in chemical analysis and is widely accepted in related sciences. The target compounds, whose concentrations are desired, are usually contained on a list submitted to the analytical laboratory. The list of target compounds affects method selection because with this goal, sample processing and measurement methods may be optimized for the target compounds. Detailed chemical-instrumental procedures may be designed to isolate the target compounds from the sample matrix and known interferences, concentrate the target compounds, and measure their concentrations with various general purpose or selective detectors. Laboratory control standards are usually employed to establish that isolation does occur, and to optimize the procedure for maximum recovery of the desired components and minimum interference from other components. Chromatographic separations are included in the optimization process.

The gas chromatography–electron capture detector procedures for chlorinated hydrocarbon pesticides are examples of the optimized target compound approach. However, the justifi-

This article not subject to U.S. Copyright
Published 1979 American Chemical Society

ห้องสมุด กรมวิทยาศาสตร์บริการ

cation for selection of a specific method requires more information than the decision to measure target compounds. The additional information needed is discussed after a presentation of the other general type of analytical goal.

The broad spectrum (BS) approach is in sharp contrast to the TC approach. The idea of the BS approach is to seek a broad spectrum picture of whatever is present in a sample as a major or minor component. This kind of analysis is not guided by a predetermined list of compounds to be measured. The BS approach has existed since the beginning of chemical analysis. However, the practical and economic pursuit of this goal was often not possible in the past. The development of the computerized gas chromatography–mass spectrometry system, and other similar technologies, has made this goal a feasible and desirable alternative for many types of samples.

With the BS approach, sample preparation is designed to be as simple as possible to preclude losses of significant sample components and to minimize the possibility of sample contamination. The idea is to divide the sample into broad classes of compounds and to apply general purpose chromatographic methods for the separation of the compounds in each group. Literally hundreds of thousands of compounds can be potentially included in a broad class, but it is usually safe to assume that only a relatively few compounds are present in each class in most samples.

For the BS approach a spectroscopic detector is required. Spectroscopic detectors are defined as devices that continuously measure spectra of energy absorptions, ion abundances, etc., of various components as they elute from a chromatographic system. The spectra are of sufficient quality to permit identification of components without prior knowledge of which compounds are present. A gas chromatography–mass spectrometry (GC/MS) system operating in the continuous repetitive measurement of spectra mode is a spectroscopic detector, but a GC/MS system operating in the selected ion monitoring mode of data acquisition (*1*) is not. The very nature of the BS approach implies the need to generate information sufficient to recognize and identify the unexpected. The most beneficial result of the BS approach is the frequent discovery of significant but previously unrecognized pollutants.

If the decision is made to use the BS approach, method selection is restricted. Gas chromatography–mass spectrometry may be the only viable choice, although additional tools should become available in the future.

On the other hand, if the decision is made to use the TC approach, careful consideration of the sample type is necessary before a method selection can be made. Environmental systems may be divided into three broad classes:

1. Systems of type 1 are relatively closed, i.e., there is some control of the entry of components into the system, and all components are well defined. An example is the output from a chemical plant that uses raw materials of known composition, processes them according to a particular procedure, and generates products and by-products that are well-defined.
2. Systems of type 2 are somewhat open in that entry of new components is possible but not frequent or likely, and the components are somewhat defined. An example is the output from a drinking water treatment plant that uses an uncontaminated ground water source, and chlorinates to produce a more or less constant variety of halogenated methanes.
3. Systems of type 3 are wide open to entry of almost anything at any time, and components are poorly defined. An example is the Mississippi River at St. Louis, Mo.

For measurements with a type 1 environmental system and a TC analytical goal, reliable results may be obtained with a chromatographic method and a conventional general purpose or selective detector, e.g., flame ionization or electron capture. With this type of sample the probability of unexpected components is low. The optimized TC procedures assure that most or all potential interferences are eliminated and, if a selective detector is used, the effects of interfering substances are reduced further. Under these conditions the retention index may be a reliable method of peak identification. The often-cited advantage of this approach is the potential economy of operation since the equipment employed is relatively simple, inexpensive, and easy to use by relatively low-cost technicians. The principal disadvantage is that in order to include all environmentally significant compounds, literally hundreds of different procedures need to be developed, tested, and documented. The implementation of all these procedures for a defined but relatively complex sample would be slow, complex, and relatively costly.

With type 2 environmental systems and a TC goal, the probability of unexpected components increases. If these unexpected components are interferences that are not eliminated by the sample preparation, there is a clear possibility of erroneous results if a general purpose chromatographic detector is in use. For type 2 environmental systems a selective chromatographic detector or a spectroscopic detector is required. Microcoulometric, electrolytic conductivity, or flame photometric gas chromatographic detectors are selective and may be appropriate choices. A gas chromatography–mass spectrometry system operating in the selected ion monitoring mode of data acquisition (*1*) is a highly selective detector. However, for measurements of type 2 systems, it is recommended that a spectroscopic detector be used regularly to confirm a fixed percentage of the identifications and to analyze any samples that deviate from the normal pattern.

With a type 3 environmental system and a TC goal, the application of a spectroscopic detector is required. With the type 3 system the probability of unexpected compounds is high, and the qualitative information produced by conventional chromatography detectors is insufficient for reliable identifications. Again, as in the BS approach, the only viable tool may be gas chromatography–mass spectrometry (GC/MS). General purpose conventional chromatography detectors may have several important applications in support of the GC/MS methodology. These include prescreening to determine dilution requirements, to eliminate samples with no components above a given threshold, or to optimize chromatography operating parameters.

Cost Considerations

Many decisions of method selection are greatly influenced by cost considerations. If cost considerations are used, the total cost of an analytical method should be used. This should include the following:

- Equipment investment
- Sample preparation costs
- Instrumentation operating costs
- Quality control costs
- Equipment maintenance costs
- Training and management costs

There is some indication that for measurements of relatively large numbers of target compounds, e.g., 40–60 or more, in type 1 or 2 environmental samples, broad spectrum type methods may be less costly per TC than chromatography methods that use conventional general purpose or selective detectors and optimized sample preparation procedures. Figure 1 shows plots of changing approximate (indicated by the broad bands) total costs as a function of the number of target compounds for a mass spectrometer and conventional detectors. With a small number of target compounds, total costs are dominated by equipment capital costs, and the mass spectrometer approach is relatively

Total lab automation: Only Digital can help you every step of the way.

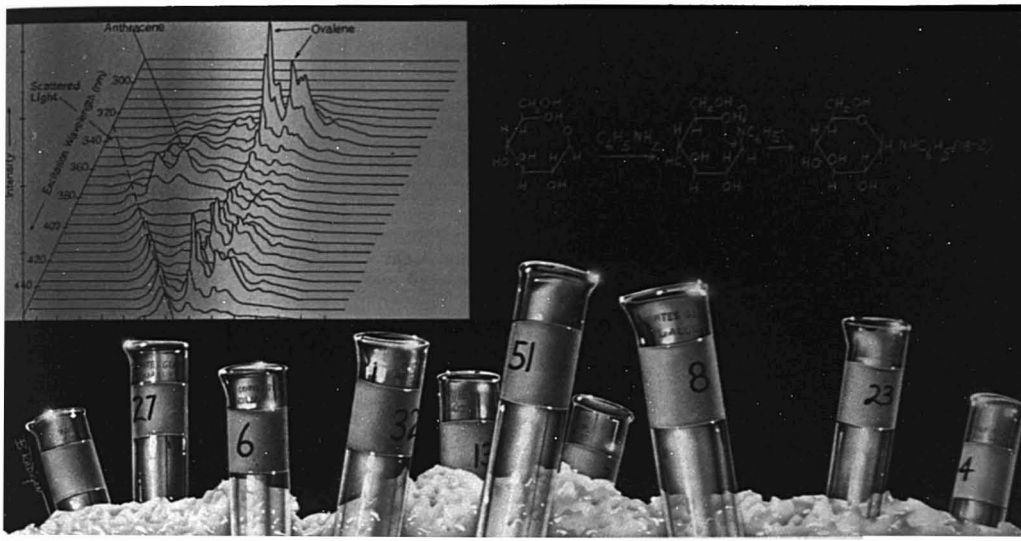

Big chemical labs have big computer requirements. And small requirements, and everything in between. Which is precisely why so many of them count on Digital as they plan their automation.

Digital is the only computer company with a complete line of compatible systems that spans the range from small interactive MINC-11's, which can be literally rolled from bench to bench, right up to powerful PDP-11/70's and VAX-11/780's for large scale computation and data base management.

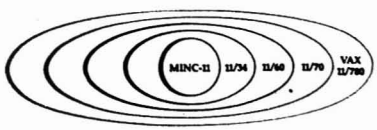

The DECLAB Family Computers For The Laboratory.

You can choose Digital systems for the little jobs like data acquisition, and the big jobs like simulation and analysis. And with Digital's uniquely compatible software and advanced networking capability, these systems can be hooked to each other and even to the control systems in your processing plants to make your computer dollars work harder at every step.

Call your local Digital sales office and find out why the largest chemical companies in the world choose Digital. Or write Digital Equipment Corporation, Laboratory Data Products, MR2-4/M16, One Iron Way, Marlborough, Massachusetts 01752. European headquarters: 12, av. des Morgines, 1213 Petit-Lancy/Geneva. In Canada: Digital Equipment of Canada, Ltd.

digital

CIRCLE 50 ON READER SERVICE CARD

ION CHROMATOGRAPHY

The fastest growing major analytical technique for air/water quality monitoring.

Ion Chromatography analyzes ions in solution. Its unique characteristics include: *specificity,* and *rapid, sequential analysis.* Although based on ion-exchange chromatography, IC uses conductimetric detection to achieve unprecedented sensitivity levels...e.g. less than 10 ppb. IC is especially suited for the analysis of • complicated matrices • several ions in a single sample • ions in low concentration in the presence of a large concentration of other ions • trace (ppb) levels of ions. Dionex offers this powerful analytical technique in four practical instruments that perform Ion Chromatography rapidly and routinely either manually or automatically.

Air Quality

• ambient aerosols • rainwater • auto exhaust • diesel exhaust • SO_2 in the atmosphere • stack gas scrubbers • toxicants

Water Quality

• industrial effluents • ground waters • potable waters • brines

Major Components Analyzed

• fluoride • chloride • bromide • iodide • nitrite • nitrate • sulfite • sulfate • thiosulfate • phosphate • formate • acetate • oxalate • cyanide • monochloroacetate • sodium • magnesium • calcium • arsenate • ammonia

Many Other Application Areas

In addition to air/water quality monitoring, Ion Chromatography is equally effective for *trace level multianalysis* of organic fluorine, chlorine, bromine, iodine, sulfur and phosphorous after combustion. IC also has many applications in *power production* and *quality control/process.*

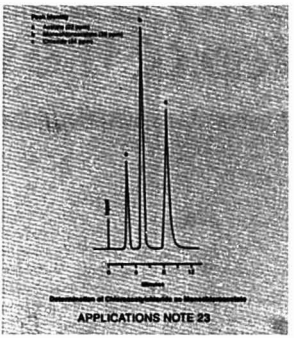

For information, circle the reader service number.

DIONEX

Dionex Corporation

In the US: 1228 Titan Way, Sunnyvale, CA 94086, 408-737-0700

In Europe: c/o 4, The Buchan, Camberley, Surry, GU15 3XB England

CIRCLE 52 ON READER SERVICE CARD

Announcing a New Generation of TLC and Gel Scanner

Award Winning CS-910 Offers Excellent Capabilities!

What's new about CS-910?

It is the first scanner to combine the quantitative accuracy of TLC densitometry with the high resolution of gel scanning.

1. •DUAL-WAVELENGTH METHOD eliminates baseline fluctuations caused by local irregularities in thin-layers or gels.
2. •ZIG-ZAG SCANNING TECHNIQUE eliminates errors caused by the irregular shape of the developed spots.
3. •Unique WORKING CURVE LINEARIZER provides excellent linearity over a wide density range—eliminates errors resulting from different size spots.
4. •Built-in BACKGROUND CORRECTOR minimizes the effects of contamination on TLC plates.
5. Extremely sensitive FLUOROMETRY MODE permits precise quantitation of ultra-micro content samples.
6. TRANSMISSION OR REFLECTION METHOD can be easily selected.

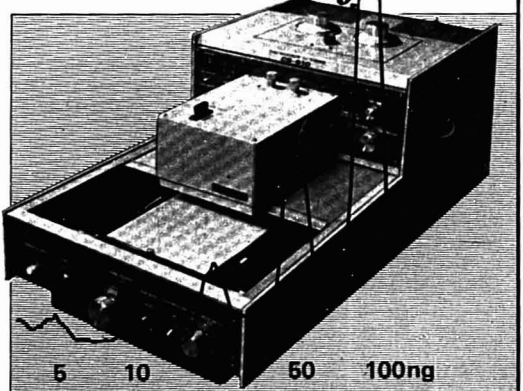

•U.S. PATENT 4,013,364 and 3,994,587

Contact us today for detailed information on the new CS-910 scanner, Spectrophotometers, Spectrofluorophotometers or Gas Chromatographs.

SHIMADZU
SCIENTIFIC INSTRUMENTS, INC.

SHIMADZU SCIENTIFIC INSTRUMENTS, INC.
SHIMADZU (EUROPA) GmbH
SHIMADZU SEISAKUSHO LTD.

CIRCLE 195 ON READER SERVICE CARD

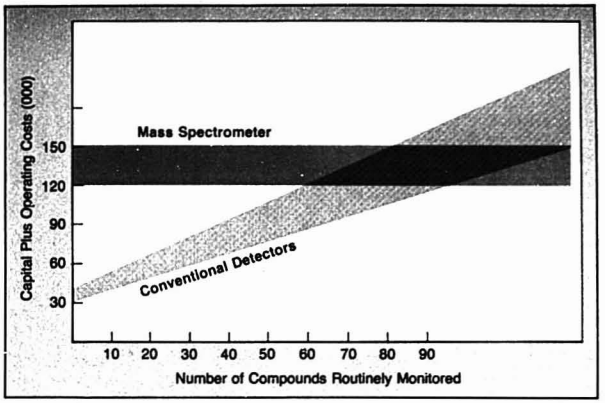

Figure 1. Capital plus operating costs for mass spectrometer and conventional detectors as a function of the number of compounds routinely monitored

expensive. However, as the number of target compounds increases, the cost of the GC/MS approach remains relatively constant, while the costs of methods using conventional detectors increase significantly. There appear to be three general reasons for this trend:

Optimized TC sample preparation procedures are often quite rigorous and complex to assure that most or all potential interferences are eliminated, and these kinds of procedures must be employed with conventional chromatography detectors. With a mass spectrometer the sample preparation may often be much simpler, analogous to the BS approach, because the mass spectrometer output provides adequate information, in most cases, to reliably identify most components of the sample.

For a broad range of target compounds, a variety of conventional chromatography detectors and supporting equipment is required. This is because chromatography detectors are designed for some selectivity to further minimize the effects of interfering substances. As the number of target compounds increases so does their diversity, hence, the need for more equipment. On the other hand, the mass spectrometer is a universal detector which precludes interference by the very nature of its output. It can accommodate a variety of compound types without a significant change in operating procedures.

Conventional chromatography methods with general purpose or selective detectors often rely heavily on retention indices for the identification of compounds. This requires the rigorous control of operating conditions that could affect the retention index, e.g., flow rates, temperatures, temperature programming rates, etc. Measurements of control standards must be made at frequent intervals to assure that conditions are well controlled. With a GC/MS retention indices are not critical and careful control of operating conditions that affect them is not critical.

For monitoring a large number of target compounds encompassing a broad range of compound types, it appears that the additional cost of GC/MS instrumentation is offset by savings in other equipment and operating costs. Additional experience with all the methods discussed over the next few years will permit more exact quantitation of the cost-effectiveness of various approaches.

Priority Pollutant Program

The U.S. Environmental Protection Agency's (EPA) priority pollutant program is an example of the application of the method selection guidelines. During 1976 the EPA was required to begin a program to establish industrial wastewater effluent limitations for a group of 129 priority pollutants, and to recommend treatment technology to meet the limitations. The priority pollutants were selected on the basis of known human or animal toxic and carcinogenic effects. The 129 materials included 106 specific organic compounds, nine product formulations that are mixtures of organic compounds, twelve metals, cyanide ion, and asbestos. The first step in the process of establishing limitations was a major program to identify and measure these materials in various wastewaters from a number of industries.

Clearly, the analytical goal of the organics analysis was a group of target compounds, and the samples were of type 3, i.e., uncharacterized with poorly defined components. Also a rather large number of target com-

Table I. The 46 Compounds of the Base-Neutral Fraction

Compound name	CAS Registry Number	Compound name	CAS Registry Number
1,3-Dichlorobenzene	541-73-1	Diethylphthalate	84-66-2
1,4-Dichlorobenzene	106-46-7	*N*-Nitrosodiphenylamine	86-30-6
1,2-Dichlorobenzene	95-50-1	Hexachlorobenzene	118-74-1
Hexachloroethane	67-72-1	4-Bromophenyl phenyl ether	101-55-3
bis(2-Chloroethyl)ether	111-44-4	Phenanthrene	85-01-8
bis(2-Chloroisopropyl)ether	39638-32-9	Anthracene	120-12-7
N-Nitrosodi-*n*-propylamine	621-64-7	Di-*n*-butylphthalate	84-74-2
Isophorone	78-59-1	Fluoranthene	106-44-0
Nitrobenzene	98-59-1	Pyrene	129-00-0
Hexachlorobutadiene	87-68-3	Benzidine	98-87-5
1,2,4-Trichlorobenzene	129-82-1	Butylbenzylphthalate	85-68-7
Naphthalene	91-10-3	bis(2-Ethylhexyl)phthalate	117-81-7
bis(2-Chloroethoxy)methane	111-91-1	Chrysene	218-01-9
Hexachlorocyclopentadiene	77-47-4	Benzo(a)anthracene	56-55-3
2-Chloronaphthalene	91-58-7	Benzo(b)fluoranthene	205-99-2
Acenaphthylene	208-96-8	Benzo(k)fluoranthene	207-08-9
2,6-Dinitrotoluene	606-20-2	3,3′-Dichlorobenzidine	91-94-1
Acenaphthene	83-32-9	Di-*n*-octylphthalate	117-84-0
Dimethylphthalate	131-11-3	Benzo(a)pyrene	50-32-8
Fluorene	86-73-7	Indeno(1,2,3-cd)pyrene	193-39-5
4-Chlorophenyl phenyl ether	7005-72-3	Dibenzo(a,h)anthracene	53-70-3
2,4-Dinitrotoluene	121-14-2	Benzo(g,h,i)perylene	191-24-2
1,2-Diphenylhydrazine	122-66-7	Nitrosodimethylamine	62-75-9

Why there's no better acid than a Corco acid.

All Corco acids are certified reagent grade acids. We've been specialists in reagent grade acids since 1953. And we've built our reputation on meeting the requirements and specifications of our customers, ACS and ASTM.

Corco can provide reagent grade hydrochloric, nitric, sulfuric acids and sodium hydroxide—plus acetic, fuming nitric, fuming sulfuric, hydrofluoric, perchloric and phosphoric acids. Also bases, solvents and specialty chemicals.

When you require the highest purity, you can rely on Corco to deliver. From pints to tank trucks. Write, call or circle the number for more information.

CORCO

CORCO CHEMICAL CORPORATION

Manufacturers of
Reagent & Electronic Chemicals
Tyburn Road & Cedar Lane • Fairless Hills, Pa. 19030
(215) 295-5006

CIRCLE 32 ON READER SERVICE CARD

pounds was of interest, and these covered a range of chemical and physical properties. All of these factors pointed to the selection of broad spectrum sample preparation methods, extensive use of gas chromatography, and a spectroscopic detector. Gas chromatography–mass spectrometry was selected as the basis for the analytical protocol. The target compounds were divided into five broad classes as follows:

A group of 46 compounds isolated from a pH = 11 adjusted sample by extraction with methylene chloride. These compounds are identified and measured by GC/MS and are listed in Table I.

A group of 26 compounds and product formulations extracted from a sample at ambient pH with 15% methylene chloride in hexane. These compounds are shown in Table II. They are initially detected by gas chromatography with an electron capture detector, but must be confirmed by GC/MS. There may be some overlap between this and the first fraction.

A group of 30 compounds isolated by the inert gas purge and trap procedure (2), and identified and measured with GC/MS. These compounds are shown in Table III, and there may be some overlap with the other fractions.

A group of 11 compounds extracted from a sample adjusted to pH = 2. The solvent is methylene chloride and these compounds are shown in Table IV. The identification and measurement is by GC/MS.

Finally, two compounds, acrolein and acrylonitrile, are very water soluble and not easily isolated from aqueous samples. These are identified and measured by direct aqueous injection GC/MS (3). These are also shown in Table III.

In addition to the compound names, Tables I–IV show the Chemical Abstract Service (CAS) Registry num-

Table II. The 26 Compounds of the Pesticide Fraction

Compound name	CAS Registry Number	Compound name	CAS Registry Number
β-Endosulfan	33213-65-9	Endosulfane sulfate	1031-07-8
α-Benzenehexachloride	319-84-6	δ-Benzenehexachloride	319-86-8
γ-Benzenehexachloride	58-89-9	Chlordane	57-74-9
β-Benzenehexachloride	319-85-7	Toxaphene	8001-35-2
Aldrin	309-00-2	Aroclor-1242	53469-21-9
Heptachlor	76-44-8	Aroclor-1254	11097-69-1
Heptachlor epoxide	1024-57-3	Aroclor-1221	11104-28-2
δ-Endosulfan	959-98-8	Aroclor-1232	11141-16-5
Dieldrin	60-57-1	Aroclor-1248	12672-29-6
4,4′-DDE	72-55-9	Aroclor-1260	11096-82-5
4,4′-DDD	72-54-8	Aroclor-1016	12674-11-2
4,4′-DDT	50-29-3	2,3,7,8-Tetrachlorodibenzo-*p*-dioxin	1746-01-6
Endrin	72-20-8	Endrin aldehyde	. . .

Table III. The 30 Compounds of the Purgable Fraction and Two Direct Aqueous Analytes

Compound name	CAS Registry Number	Compound name	CAS Registry Number
Acrolein	107-02-8	Bromodichloromethane	75-27-4
Acrylonitrile	107-13-1	bis(Chloromethyl)ether	542-88-1
Chloromethane	74-87-3	1,2-Dichloropropane	78-87-5
Dichlorodifluoromethane	75-71-8	Benzene	71-43-2
Bromomethane	74-83-9	*trans*-1,3-Dichloropropene	542-75-6
Vinyl chloride	75-01-4	*cis*-1,3-Dichloropropene	542-75-6
Chloroethane	75-00-3	Trichloroethylene	79-01-6
Methylene chloride	75-09-2	Dibromochloromethane	124-48-1
Trichlorofluoromethane	75-69-4	1,1,2-Trichloroethane	79-00-5
1,1-Dichloroethylene	75-35-4	2-Chloroethyl vinyl ether	110-75-8
1,1-Dichloroethane	75-34-3	Bromoform	75-25-2
trans-1,2-Dichloroethylene	540-59-0	1,1,2,2-Tetrachloroethene	127-18-4
Chloroform	67-66-3	Toluene	108-88-3
1,2-Dichloroethane	107-06-2	1,1,2,2-Tetrachloroethane	79-34-5
1,1,1-Trichloroethane	71-55-6	Chlorobenzene	108-90-7
Carbon tetrachloride	56-23-5	Ethyl benzene	100-41-4

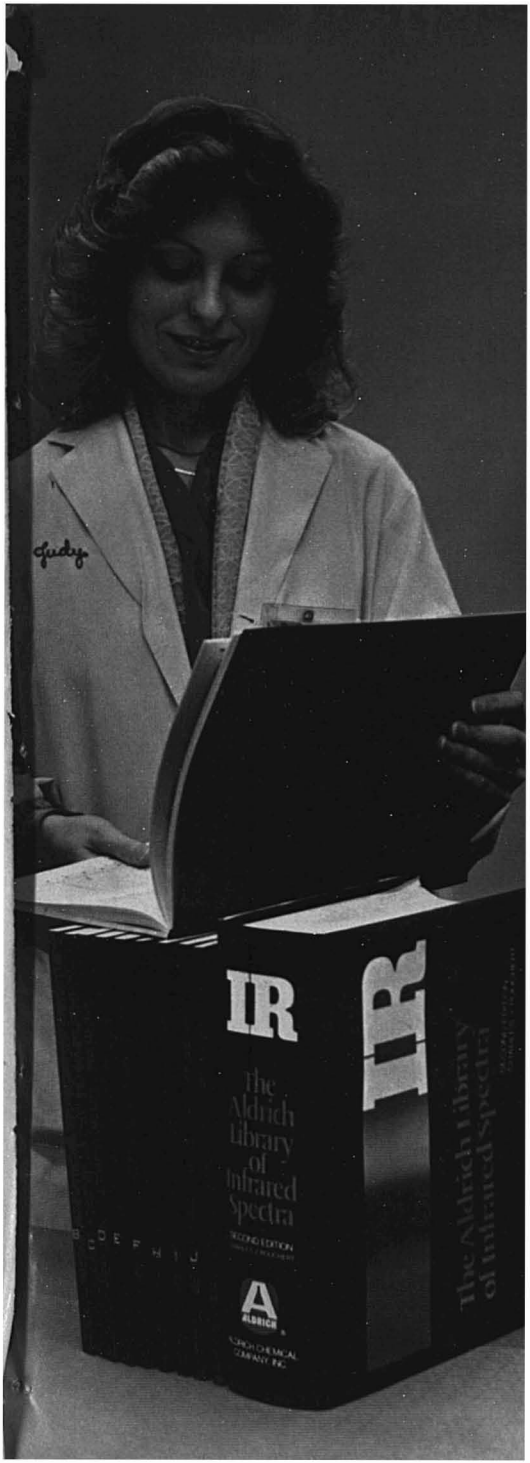

IDENTIFY QUICKLY

...with over 10,000 IR Spectra

The Aldrich IR Library contains over 10,000 spectra, chosen for purity of chemical and curve quality from more than 200,000 spectra on file in our Quality Control laboratories.

Within the IR Library compounds are classified by functional group and structural variation into 50 sections — each arranged in order of increasing molecular complexity. To expedite location of spectra, molecular formula, alphabetical and Aldrich catalog number indices are included.

A good library of reference spectra is as important as the IR spectrometer itself. So place your order for the Aldrich IR Library now. It's the Second Edition, by Charles Pouchert. Aldrich product number Z10, 120-6. $67.50

...with 11-Volume NMR Library

This library contains over 6,500 spectra arranged in order of increasing molecular complexity and functionality.

Ideal for users of NMR instruments — chemists and students wishing to familiarize themselves with the spectral features of different classes of compounds.

The entire 11-volume set costs just $135.00. Simply refer to the set as the Aldrich Library of NMR Spectra by Charles J. Pouchert and John R. Campbell, Aldrich product number Z10,200-8.

Chemists helping chemists in research and industry

ALDRICH® **aldrich chemical co.**

940 West Saint Paul Avenue, Milwaukee, WI 53233
(414) 273-3850

CIRCLE 3 ON READER SERVICE CARD

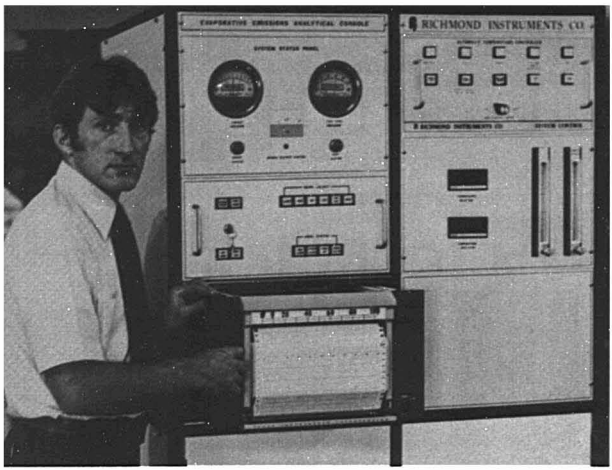

"TI recorders help our systems operate 24 hours a day."

. . . says Dennis Mach, General Manager of Richmond Instruments Company, manufacturers of exhaust test systems.

"We have no problems with TI recorders. They are reliable, easy to mount, clean, and easy to service. That's why we use them in the vast majority of our emission systems. We like the resolution of the wide chart and the good inking system. In addition, the removable back panel makes special modifications easy."

"We especially like the reliable heavy-duty construction because our systems must operate with little or no down-time to keep our customers satisfied."

Richmond Instruments is only one of many satisfied users of TI strip chart recorders. The chances are good that you, too, can profit from the high quality, accuracy and heavy-duty construction of the TI recorders. There's a broad selection of designs to choose from.

Drives include unidirectional and bidirectional synchro systems. Wide and dual-grid *servo/riter*II* models give a choice of one to five full overlapping channels on a 8.75" grid. And if space saving is a requirement, the Lab/Test recorders use only 7 inches of panel height.

Options include full scale adjustable zero, variable spans and inputs, electric pen lifters, felt tip or capillary inking, bidirectional take-up system, synchro or digital drives, and stepper.

TI recorders are backed by more than twenty years of proven quality, reliability, accuracy and performance plus a nationwide network of sales and service offices to serve you.

For further information, please contact Texas Instruments Incorporated, P.O. Box 1443, M/S 619, Houston, Texas 77001. Or phone (713) 491-5115, ext. 3333, TWX 910-867-4702, Telex 775938.

*Trademark of Texas Instruments Incorporated

TEXAS INSTRUMENTS
INCORPORATED

CIRCLE 203 ON READER SERVICE CARD

Table IV. The 11 Compounds of the Acid Fraction

Compound name	CAS Registry Number
Phenol	108-95-2
2-Chlorophenol	95-57-8
2-Nitrophenol	88-75-5
2,4-Dimethylphenol	105-67-9
2,4-Dichlorophenol	120-83-2
p-Chloro-*m*-cresol	59-50-7
2,4,6-Trichlorophenol	88-06-2
2,4-Dinitrophenol	51-28-5
4-Nitrophenol	100-02-7
4,6-Dinitro-*o*-cresol	534-52-1
Pentachlorophenol	87-86-5

bers. These unique identifiers are useful for computer storage and retrieval of results, and searching of related data bases for information about a particular substance. The quantitative analysis by GC/MS includes an extensive quality control program to establish the precision and accuracy of the measurements in a variety of concentration ranges. A great deal of information about the precision and accuracy of these measurements should become available in the next few years.

Acknowledgment

The authors thank Robert Kleopfer, EPA, who provided the CAS Registry numbers and other information about the priority pollutant list.

References

(1) W. L. Budde and J. W. Eichelberger, *J. Chromatogr.*, **134**, 147 (1977).
(2) T. A. Bellar, W. L. Budde, and J. W. Eichelberger, in "Monitoring Toxic Substances," D. Schuetzle, Ed., ACS Symp. Series 94, American Chemical Society, Washington, D.C., 1979.
(3) L. E. Harris, W. L. Budde, and J. W. Eichelberger, *Anal. Chem.*, **46**, 1912 (1974).

William L. Budde (left) and **James W. Eichelberger,** both of the EPA's Environmental Monitoring and Support Laboratory in Cincinnati, Ohio, are actively engaged in the development of GC/MS methods for the determination of organic pollutants.

Introducing LC-6, LC-7 and LC-8.

New choices in liquid chromatography from Johns-Manville.

As the number of applications for liquid chromatography supports, adsorbents and packings continues to grow, so does the list of Johns-Manville Chromosorb® products. We're announcing three new additions to our line.

LC-6 A fully porous microparticulate silica offered in either a 5 or 10 micron particle size with a surface area of 300 + m^2/gm, and an average pore diameter of 130 angstroms. It offers exceptionally high efficiency, capacity, resolution and speed of analysis. Highly selective in separating close polarity compounds with an isocratic solvent system or in separating wider polarity range mixtures with gradient elution.

LC-7 A reverse phase microparticulate HPLC column packing material prepared by chemically bonding an octadecyl group to Chromosorb LC-6 via Si-O-Si-C type bond. A closely controlled reaction provides a C_{18} nonpolar stationary phase of excellent performance in either partition or ion pair chromatography modes. Excellent in separating wide varieties of compounds used in pharmaceuticals and food products.

LC-8 A microparticulate polar-bonded phase HPLC column packing material prepared by chemically bonding a cyano-type group to a Chromosorb LC-6 silica surface. It complements Chromosorb LC-7 for reverse phase HPLC. Highly polar and very efficient in separating polar compounds.

Johns-Manville now offers a total of 33 chromatography products for you to choose from. There are 8 products in our LC Series for liquid chromatography; 8 polymer supports in our Century Series for gas chromatography; and a wide range of Diatomite Supports in Acid-Washed, Non-Acid-Washed, DMCS and HMDS treated forms.

For more information on specific performance and packing of Johns-Manville products or a handy guide to all 33 of them, contact Jack Denboske, Filtration and Minerals Division, or Ed Hammel, International Division, Johns-Manville, Ken-Caryl Ranch, Denver, CO 80217, (303) 979-1000. Telex: Johnmanvil DVR 454404.

JM Johns-Manville

CIRCLE 124 ON READER SERVICE CARD

HEWLETT hp PACKARD

Analytical Advances

MEASUREMENT AND COMPUTATION FOR THE ANALYTICAL LABORATORY

HPLC ANALYSIS OF ANTIEPILEPTIC DRUGS

The 1084B HPLC with 79875A time-programmable Variable Wavelength Detector is a useful analytical tool for separation and quantitation of multiple drugs in plasma in a single analysis.

A suitable wavelength program is developed through calibration runs on individual known drugs and on the internal standard used for quantitation. Programming is adjustable to minimize response to non-drug plasma constituents. The effect of wavelength on sensitivity is shown in the figure below:

Plasma Sample Using Two Different Wavelength Programs

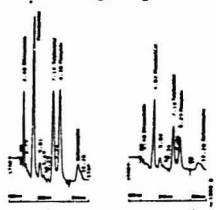

The change in peak area can be used to detect impurities.

Results using HPLC show good correlation with those of gas chromatographic procedures. Sample preparation is greatly simplified as derivitization is unnecessary and high-efficiency reversed-phase packings are compatible with aqueous samples. Usually a single protein precipitation step is all that is needed.

For more information, circle Reader Service No. 130

ELIMINATING HIGH BOILERS IN CAPILLARY COLUMN ANALYSIS

The very high resolution of capillary columns is often needed in analyzing natural products. However, high boiling components may prolong the analysis time to the point where the capillary approach is rejected in spite of its undoubted separation advantages.

A prefractionator column and switching valve can solve this problem. The low-boiling components pass through the precolumn and then, while these are being separated on the capillary column, the high-boilers are backflushed to waste. The chromatogram shows typical results when this technique is applied to a crude oil sample.

60 M Glass SP2100
20 °C → 80 °C at 2 °C/min.
30 PSI (He) Split 80/1

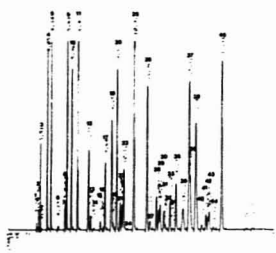

A new Application Note provides more detail on this useful variation on capillary column analysis. For your copy, circle Reader Service No. 131

REPRODUCIBILITY USING GLASS CAPILLARY COLUMNS

The use of glass capillary columns is a fairly recent but very strong trend in chromatographic analysis. These columns have been well accepted in qualitative work because of their high resolving power and retention time reproducibility.

A paper presented at the recent Pittsburgh Conference by T.A. Rooney, discusses the quantitative behavior of such columns.

Both split and splitless injection modes are considered. In either mode, the absolute area reproducibility is comparable to the best packed column analyses, with relative standard deviation in the 1% range.

For the splitless mode, the effects of purge activation time and component molecular weight are described.

For reprints of this paper, circle Reader Service No. 132

DETECTIVE STORY: WHO MURDERED THE CATALYST?

A suddenly deceased catalyst is a nuisance in the laboratory; it can be a disaster in a large volume production operation. The culprit is often a contaminant in one of the raw materials that has crept in through an unwashed tank car, an unexpected side reaction or some other cause.

Finding the cause, and quickly, is one of the most difficult problems in analytical chemistry. Dr. B.A. Story of the Dow Chemical Company in Freeport, Texas, described his experience with an HP 5992 GC/mass spectrometer in this sort of detective work. His paper was presented before the Gulf Coast Instrumental Analysis Group. We have copies available and will be glad to send you one. Just circle Reader Service No. 133

INDUSTRIAL HYGIENE MONITORING

The 3354 Laboratory Automation System facilitates industrial air monitoring to meet environmental standards required of employers by O.S.H.A.

Air samples are collected and analyzed by gas chromatography according to the recommended method P&CAM 127.

With the 3354 System, automation and continuous running is possible; with LAB BASIC programming, the user may calculate concentrations of air contaminants and have reports generated giving the location and time the sample was collected.

Other report formats are possible, matching exposure to individual employees; time weighted average exposures can be obtained for employees who must move to different plant areas.

For additional information, circle Reader Service No. 134

NEW 5985 & 5993 GC/MS LIBRARY SEARCH SYSTEM

The Probability-Based Search System (PBSS) has numerous advantages over existing library search methods, both to the user and in terms of compound identification.

The identification process consists of finding a mass and its abundance in a spectrum as characteristic of a given compound. In addition, the search routine performs both forward and reverse comparisons of stored libraries and the unknown's mass spectrum; the reverse search reduces the effects of contaminants in the identification process.

Speed is increased by use of a condensed version of the unknown's spectrum in the initial search, then using the unabridged spectrum based on the best ten matches found in the initial pass. The user may also look for a specific known compound in the total ion chromatogram.

Multiple libraries, both standard and user-created, are permitted; library entries can be listed by molecular weight or formula, by name, or by Chemical Abstract or EPA Registry numbers. The user also can plot the spectrum of any library entry.

The optional 7920 Disc Drive facilitates storage, information retrieval, and spectrum identification.

For additional information, circle Reader Service No. 135

Take a journey into the future with Hewlett-Packard for a look at "tomorrow's analytical instruments today."

ALABAMA
April 23 Montgomery
April 24 Mobile

ARIZONA
May 1 Tucson
May 3 Phoenix

CALIFORNIA
April 24 Fullerton
April 25 Los Angeles
April 26 Fullerton
May 1 San Diego
Santa Clara
May 2 Santa Clara
May 4 Sacramento

COLORADO
April 25 Denver

CONNECTICUT
May 4 North Haven

DELAWARE
April 27 New Castle

FLORIDA
April 25 Pensacola
April 26 Tallahassee
April 27 Gainesville
April 30 Jacksonville
Orlando
May 1 Gainesville
Tampa
May 2 Orlando
St. Petersburg
May 3 Lakeland
Miami
May 4 Miami
Tampa

GEORGIA
April 25 Savannah
April 27 Tifton

ILLINOIS
April 24 Rolling Meadows

INDIANA
April 25 Evansville
April 27 Clarksville

KENTUCKY
April 23 Lexington

MARYLAND
April 23 Rockville
April 24 Hanover

MASSACHUSETTS
May 1 Lexington
May 2 Lexington

MINNESOTA
April 27 Roseville

MICHIGAN
May 1 Kalamazoo
May 3 Midland
May 4 Midland

MISSOURI
April 23 St. Louis
May 4 Kansas City

NEW JERSEY
April 25 Princeton
May 2 Paramus
May 3 Piscataway

NEW MEXICO
May 7 Los Alamos
May 9 Albuquerque

NEW YORK
April 23 Grand Island
April 24 Rochester
April 25 Syracuse
April 27 Albany
May 1 New York

NORTH CAROLINA
April 23 Wilmington
April 25 Greensboro
April 26 Research
Triangle Park
April 27 Charlotte

OHIO
April 26 Marietta
May 2 Columbus
May 4 Toledo

OREGON
April 27 Tualatin

PENNSYLVANIA
April 26 Fort Washington
April 27 Erie

SOUTH CAROLINA
April 24 Charleston

TENNESSEE
April 23 Knoxville
April 24 Kingsport

WASHINGTON
April 24 Bellevue
April 25 Bellevue

WEST VIRGINIA
April 24 Huntington
April 30 Morgantown

CANADA

ALBERTA
April 26-27 Calgary
April 30-May 1 Edmonton

BRITISH COLUMBIA
April 23 Vancouver
April 24 Vancouver

MANITOBA
May 8 Winnipeg

NEW BRUNSWICK
May 8 Fredericton

NOVA SCOTIA
May 10 Halifax

ONTARIO
April 23 Mississauga
April 23-24 Ottawa
April 24 Guelph
April 25 Kingston
April 25 Sarnia
April 26 Windsor
April 27 London
May 1 Mississauga
May 2 Don Mills
May 3 Burlington
May 4 Toronto

QUEBEC
April 27 Sherbrooke
April 30 Quebec
May 2-3 Montreal

SASKATCHEWAN
May 4 Saskatoon

The highlight of Journey into the Future exhibits/seminars will be HP's major new analytical products — the 5880A Gas Chromatograph and the 1081B Liquid Chromatograph. Also featured will be HP's complete line of analytical products, including gas chromatographs, GC/mass spectrometers, liquid chromatographs, and laboratory automation systems.

The 5880A offers expandability through four levels of instrument capability. With sophisticated data handling and automation techniques, it is the most powerful gas chromatograph available today. A wide range of optional accessories makes the 5880A versatile enough to handle many applications. The 1081B provides two-way communication for remote automated analyses. It operates either as a freestanding LC or as part of a lab automation system.

Come join us. Let us show you tomorrow's analytical instruments today.

FOR INFORMATION ON EXHIBITS/SEMINARS IN YOUR AREA PLEASE COMPLETE THIS FORM AND MAIL TO:

HEWLETT-PACKARD CO.
1820 EMBARCADERO
PALO ALTO, CA 94303

PLEASE PRINT AND INCLUDE ZIP CODE

Name .....

Title .....

Dept., Bldg., Mail Station, etc. .....

Company .....

P.O. Box or Street No. .....

City ..... State ..... Zip .....

Phone (Area Code) No. .....

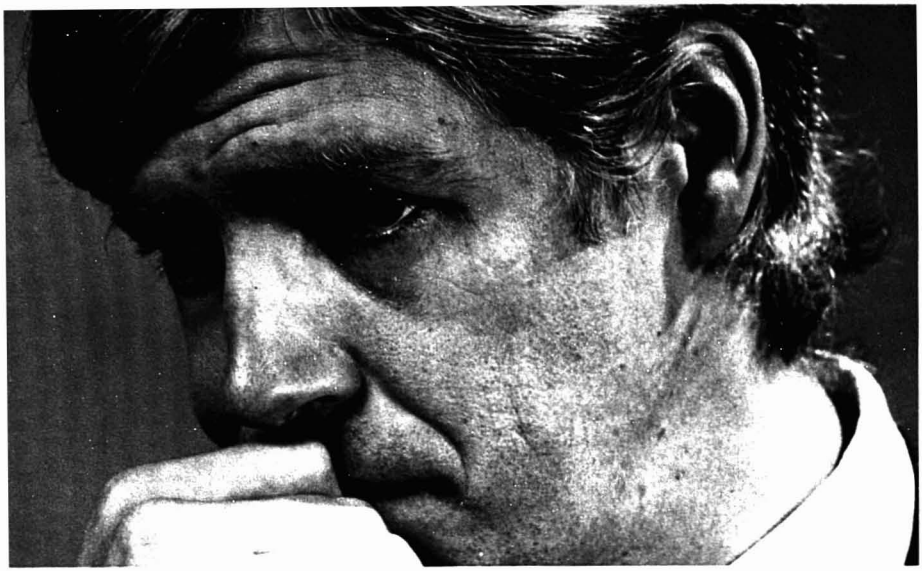

A Jarrell-Ash Plasma AtomComp gives you 2880 elements an hour.

[That'll make a dent in your workload!]

Today's metal workloads are bigger than ever. That's why you owe it to yourself to investigate what **Plasma AtomComp™** can do for you.

This distinguished family of plasma emission spectrometers provides all the sensitivity of atomic absorption and atomic emission instruments. But with far greater **capability.** Up to 48 elements simultaneously, in up to 60 samples, in as little as 60 minutes.

That's almost **10 times** greater capability than even the most advanced AA workhorses.

Plus — Plasma AtomComp provides remarkable range — automatic analysis over a dynamic concentration range of **100,000** without having to change a single parameter! Outstanding convenience — it is computer controlled. And versatile printout — % or ppm or ppb or any other units you desire.

Whatever your field — water, wastewater, air, soils, foods, feeds, petroleum, biologicals — if a high-throughput workload is your problem, Jarrell-Ash is your answer. Jarrell-Ash plasma spectrometry. The **truly multi-element** approach. Send for literature today.

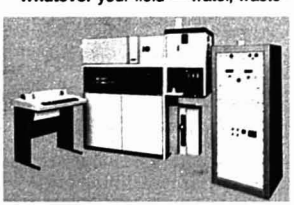

CIRCLE 98 ON READER SERVICE CARD

Jarrell-Ash Division
Fisher Scientific Company

590 Lincoln Street
Waltham, Massachusetts 02154
Phone (617) 890-4300

R. A. Libby and F. E. Freeberg
The Procter & Gamble Co.
Cincinnati, Ohio 45247

Better Regulations: A Case in Point

Several recent articles have been written concerning governmental regulations that impact directly on the conduct of research. This article will describe the final phase of the regulatory cycle on one such set of regulations—the FDA's Good Laboratory Practices (GLP) regulations—and how input to the Agency by those scientists to be regulated importantly affected the final regulations.

The background on the GLP's has been reported in several recent articles (*1–3*). The GLP's were published initially as a proposal in the *Federal Register*, November 19, 1976. The regulations in their final form were published in the *Federal Register* on December 22, 1978, and will become effective June 20, 1979. These regulations are intended to improve the quality of animal safety data submitted to the Agency in support of a research or marketing permit in the areas of food additives, drugs, and devices.

As proposed initially in 1976, the GLP's were a detailed series of rules that essentially told the scientist how to conduct his research. Left unchanged, these regulations would have impeded the science of toxicology both in terms of scientific growth and in increasing the costs of safety testing. In addition to toxicologists, the GLP's regulate the scientific input from any scientist contributing data to a safety study. One such group is analytical chemists, who analyze the chemical being tested, samples of animal feed or water containing the chemical, and animal body fluids and tissues to determine the fate of the chemical in the biological system.

The GLP's, when proposed, provided a comment period of 120 days to any interested persons to provide input to the Agency. In addition, two public meetings were held by the FDA for the presentation of oral testimony on the proposal. The results were 22 oral presentations and 174 written comments. These comments were submitted by manufacturers of regulated products, trade associations, medical centers, private testing or consulting laboratories, educational institutions, other Government agencies, and private individuals. Also, other substantive comments were made after the formal comment period and provided additional input during the Agency review period. After these comments

Title	Scientific area	Primary analytical involvement	Agency	Status[a]
Good Laboratory Practices (GLP)	Toxicological Safety Studies	Test material characterization; animal fluid/tissue analysis	FDA	Final regulation in *Federal Register* 12/22/78, p 59986, effective 6/20/79
Good Clinical Practices (GCP)	Human Efficacy/ Safety Studies	Test material characterization; human fluid/tissue analysis	FDA	Proposed in part in *Federal Register* 9/27/77, p 49612; further proposals expected 1979
Bioequivalence/Bioavailability	Biopharmaceutical Studies	Body fluid/tissue analysis; methods development (Pharmacokinetic)	FDA	Proposal expected 1979
Federal Insecticide, Fungicide & Rodenticide Act (FIFRA)—Registration Guidelines	Environmental/Toxicology Efficacy/ Studies	Test material characterization; residue analysis	EPA (pesticides)	Proposed in part in *Federal Register* 7/10/78, p 29696. Comments deadline 9/8/78. Final regulations in late 1979
Toxic Substances Control Act (TSCA)—Sect. 4, Testing Standards	Human and Environmental Safety	Method development (trace levels)	EPA (chemicals)	Proposal early 1979
Cancer Policy (Various Federal Agencies)	Human and Environmental Safety	Regulation of hazardous chemicals. Affect facility design; exposure to and how, or if, chemicals can be used	OSHA	Proposed final regulations in *Federal Register* 10/4/77, p 54148, possible mid-1979
			CPSC	Proposed in *Federal Register* 6/13/78, p 25658. Federal court injunction
			EPA	Revised policy possible in 1979
IRLG—Report: Guidelines for Identifying Carcinogens	Human and Environmental Safety	Test material characterization; residue analysis	IRLG (reps. from FDA, OSHA, CPSC, EPA)	Report—"Scientific Bases for Identifying Potential Carcinogens and Estimating Their Risks" was released 2/7/79

[a] For information on any regulations proposed in the *Federal Register*, the federal agencies identified may be contacted for copies of proposals.

0003-2700/79/0351-579A$01.00/0
© 1979 American Chemical Society

WE MADE AUTOMATIC TITRATION A SOFT TOUCH.

Just push the button. That's all it takes for automatic titration with automatic sampling and auto-pipetting to begin on our DTS 634 Digital Titration System. And you can titrate to one, two or more unknown end-points...or to a preselected end-point. An accurate printout of all results is included. Automatically.

Only Radiometer can offer such unsurpassed speed, accuracy and precision in titration.

But this is only one of our many systems. We offer a wide range of titration systems that are accurate, automatic and flexible. And we bring some unusual features to titration. Such as proportional band control, Radiometer's incremental titrant addition, stepped titration curves (patented), and micro processor-controlled, digital titration.

Our modular approach offers you a broad selection of burettes, reaction vessels, pH meters, controllers and recorders.

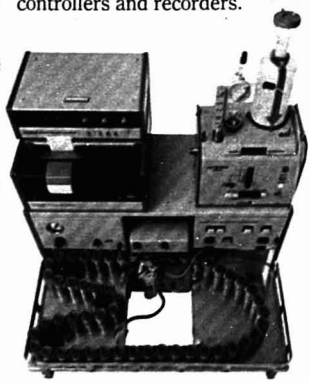

You can build the quality system you need now and add other components later.

For over 30 years, Radiometer has helped to develop and improve End-Point, Recording and Digital Titration Systems. And their dependability is backed by our proven service organization.

For more information or a personal demonstration of any of our many titration systems, call or write The London Company, U.S. Representative for Radiometer-Copenhagen, 811 Sharon Drive, Cleveland, Ohio 44145. Telephone (216) 871-8900.

RADIOMETER COPENHAGEN

Circle 127 for information Circle 128 for demonstration

were received, the FDA evaluated each comment for its merit and how the specific suggested change would meet the Agency's need for ensuring the best possible data. In the preamble of the final GLP regulations in the December 22, 1978, *Federal Register*, the comments received by the Agency are each discussed with the Commissioner's reason for accepting or rejecting each suggestion. *Many suggestions were accepted.* A critical one from the analytical aspect was that the material being safety tested can be "appropriately characterized" rather than identity, strength, quality, and purity being automatically specified. This critical change permits sound scientific judgment to be exercised in the characterization of the materials being tested.

Because of the Agency, the final GLP's are more manageable, less costly, and still meet the original purpose. Many of the details on exactly *how* the scientific work is to be conducted have been eliminated, and professional judgment can replace detailed rules.

This final GLP still meets the Agency's needs, but does not place an undue burden on the scientists involved in assessing the safety of new chemicals. The final GLP regulations demonstrate the desire on the part of the Agency to work with those regulated to produce meaningful rules. Without this willingness to adopt scientific input, there would have been a manyfold increase in cost of safety testing. More importantly, the number of safety tests and the time required to complete safety work would have decreased the number of new health products made available to the consumer.

The regulatory area continues to change, and there are many similar chances for scientific input to a governmental agency. For example, the Environmental Protection Agency (EPA) will issue in the coming months their version of the GLP's covering safety studies for the materials they regulate. To avoid considerable confusion, it is imperative that the EPA's rules be consistent with final GLP's from the FDA. Those to be regulated should carefully examine the EPA's proposed GLP rules and provide the EPA with written comments on unacceptable aspects. Table I lists regulatory proposals or anticipated proposals that should be of interest to analytical scientists and deserve their input.

References

(1) William Horwitz, *Anal. Chem.*, **50** (6), 521A (1978).
(2) Robert M. Hodges, *ibid.*, p 531A.
(3) R. A. Libby, *ibid.* (10), 575A (Sept. 1978).

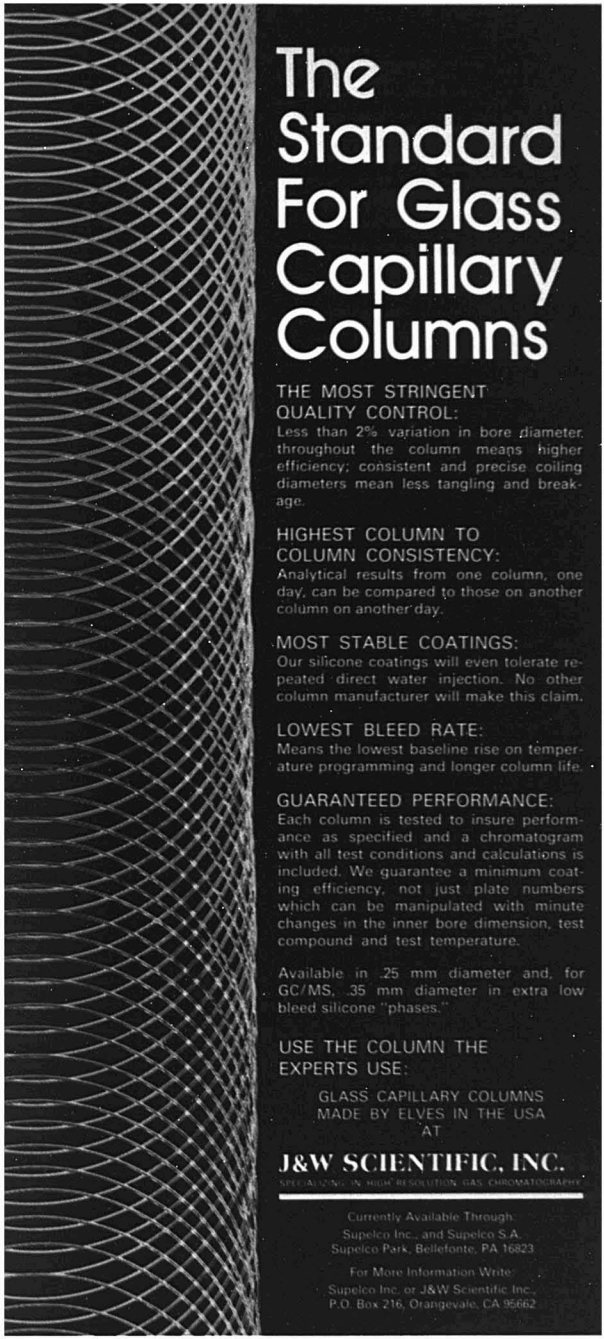

CIRCLE 155 ON READER SERVICE CARD

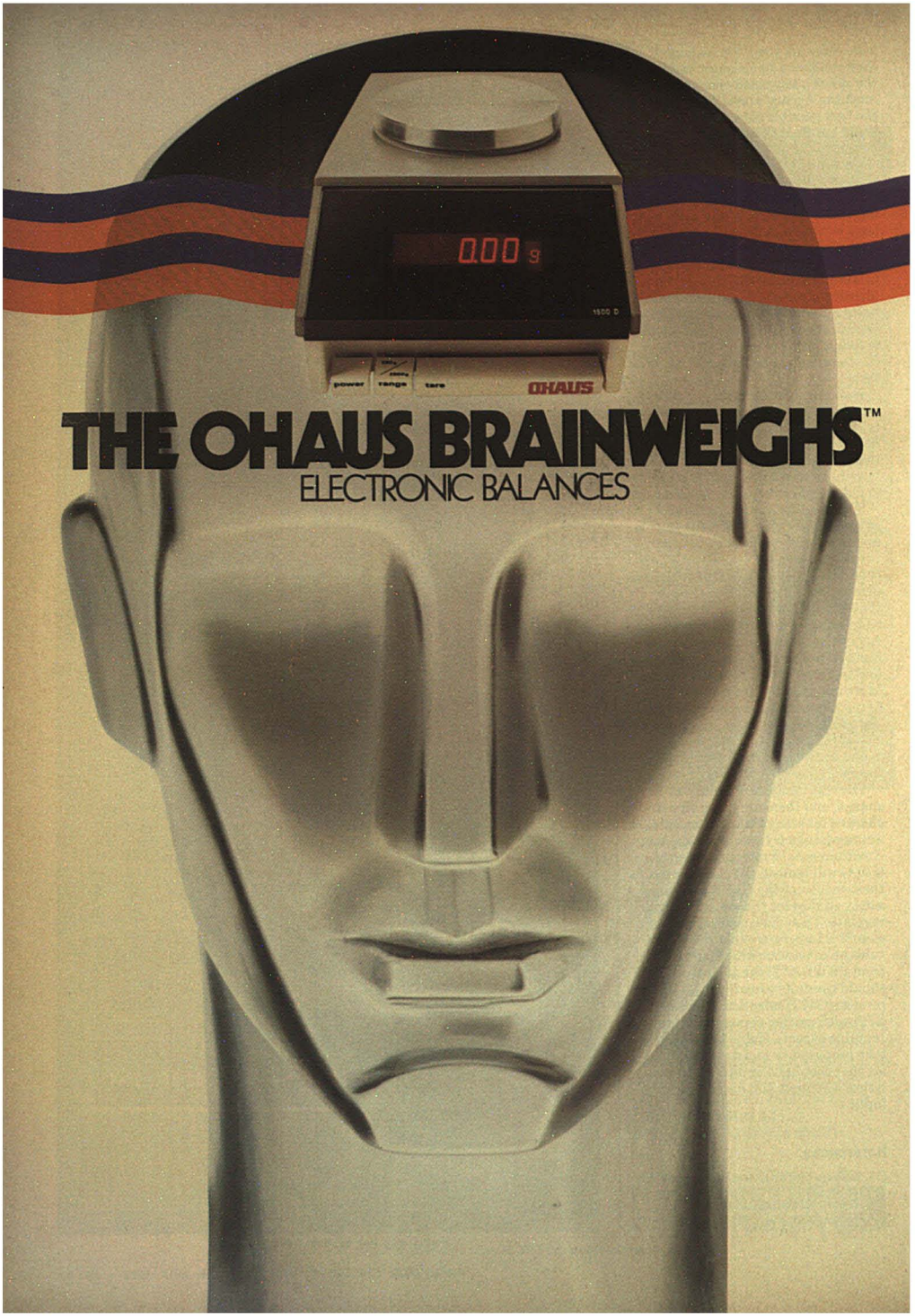
0.00 g
power
range
tare
OHAUS
THE OHAUS BRAINWEIGHS™
ELECTRONIC BALANCES

A BRIGHTER BALANCE AT A SMARTER PRICE.

Space-age computer science brings you the weigh of the future.

The new Ohaus electronic balances that use their brains to do your weighing.

Designed to end the myth that high-quality electronic balances are priced beyond your budget.

Ohaus saw the future, and made it work for less.

The people who perfected the low-cost mechanical balance have built the first affordable electronic balance with the quality you demand, starting at just $1,195.

The brain behind it all.

Observe the tiny genius that controls every Ohaus electronic balance—our sophisticated microprocessor which stores operator commands, then responds **only** after achieving a stable condition.

That means human interaction without human error.

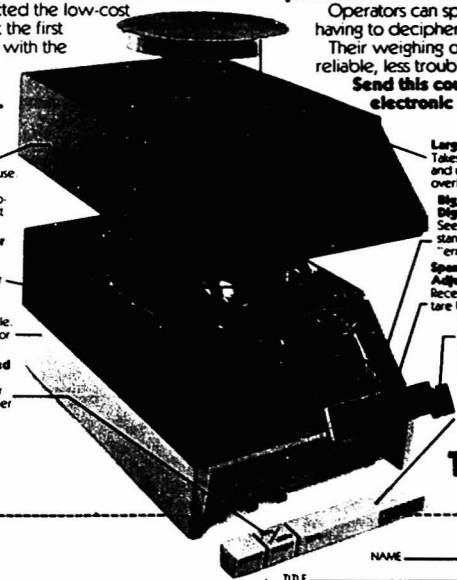

Ohaus electronic balances are the simple, easy weigh.

To see how simple and easy they are, consider all the intelligent features Ohaus squeezed into each one.

And you can learn to operate one in just a few minutes.

The Ohaus Brainweighs are so smart, they'll save you time as well as money.

Operators can speed up repetitive weighings by not having to decipher numbers or wait for stable readouts.

Their weighing operations will be faster, simpler, more reliable, less troublesome and a lot less expensive.

Send this coupon to see the Ohaus electronic balances for yourself.

You'll receive our full color catalog showing all the Ohaus Brainweighs. Fully guaranteed. And backed by over 70 years of Ohaus quality engineering.

There's just no other weigh to enter the new world of space-age measurement on a down-to-earth budget.

The Ohaus Brainweighs
The weigh of the future.

OHAUS

Ohaus Scale Corporation, Dept.
29 Hanover Road, Florham Park, N.J. 07932, (201) 377-9000

☐ Yes, show me the weigh of the future. Send me the full-color catalog on the Ohaus Brainweighs.

☐ I'm ready to see a demonstration. Please have a dealer sales rep contact me.

11-058

NAME _____

TITLE _____

ORGANIZATION _____

ADDRESS _____

CITY _____ STATE _____ ZIP _____

PHONE NUMBER (Area Code) _____

© 1978, Ohaus Scale Corporation

CIRCLE 157 ON READER SERVICE CARD

Other than headache, what are the symptoms of overexposure to mercury vapor?

There's a better alternative than learning the answer by first-hand experience

If you work with mercury, chances are you know the answer. Chances are you have a full work safety program. But does everyone in the program know that fatigue, irritability and inflammation of the gums are some of the other symptoms of chronic poisoning? Would everyone know if they were overexposed?

An integrated plan of information and detection is obviously a better alternative than first-hand experience of symptoms. And 3M has an inexpensive plan applicable to every size laboratory whether it involves one person, 50 or more.

Free Book

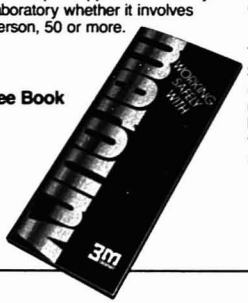

Working Safely With Mercury is the informational phase of the plan. It's a free 20-page booklet written by 3M as an objective overview for those who work with mercury and those responsible for health and safety.

It's a concise presentation of the history, potential problems, methods of detection and protection, as well as current government recommendations for safe handling — even of small quantities.

The First Maintenance-free Mercury Vapor Monitor

Monitoring is a sure way to detect whether or not a person has been exposed to more than the government Threshold Limit Value (0.05 mg/m^3 in an 8 hour period).

The 3M Brand Mercury Vapor Monitor 3600 is the easy system. Nothing to assemble. No pumps. No maintenance. The lightweight badge-size monitor is simply clipped to the collar. Provides a precise measurement of personal exposure.

In comparison to a pump system, the 3600 is inexpensive enough so that monitors can be worn by everyone in the area of the mercury.

For analysis, you simply send the monitors to 3M. You'll receive a confidential report of Time Weighted Average concentrations for each monitor.

For your free copy of *Working Safely With Mercury* and detailed information about the maintenance-free 3600 monitor, write Occupational Health and Safety Products Div., 3M Company, P.O. Box 8327, Dept. FF1, St. Paul, MN 55113. In Canada contact 3M Canada Ltd., P.O. Box 5757, Terminal "A", London, Ontario, Canada N6A4T1 (519) 451-2500.

Additional copies of *Working Safely With Mercury* are available upon written request.

ANOTHER STEP TOWARDS BETTER OCCUPATIONAL HEALTH AND SAFETY

3M

CIRCLE 147 ON READER SERVICE CARD

1979 Gordon Research Conferences

Four of the Gordon Research Conferences of particular interest to analytical chemists will be held this summer in New Hampshire. The conferences, which were established to extend the frontiers of science, provide opportunities for informal discussion and recreation in addition to the more formal presentations by scheduled speakers. The unique feature of these conferences is the opportunity afforded for exchange of information and ideas to an extent that could not be achieved through the usual channels of publication and presentation at scientific meetings. The purpose of the programs is to bring experts up-to-date on the latest developments and to examine what lies ahead in a particular area.

This year, four separate full week sessions will cover analytical chemistry, analytical pyrolysis, ion exchange, and separation and purification. The analytical chemistry session in particular will focus on six topical areas: ion-selective electrodes, laser spectroscopy, pattern recognition technology, solvent extractions of metal chelates, stop flow techniques, and isotachophoresis. A poster session will be featured at the analytical chemistry session with the materials left on display the whole week. The materials include at least three audiovisual presentations. Participants who wish to present a poster of their research should contact the conference chairman, Jack W. Frazer, at 415-422-6879, to reserve space. The technical schedules for these conferences are given below. Those interested in attending should write for an application form to A. M. Cruickshank, Director, Gordon Research Conferences, Pastore Chemical Laboratory, University of Rhode Island, Kingston, R.I. 02881 (401-783-4011). Mail for the director's office from June 11 to August 24, 1979, should be addressed to A. M. Cruickshank, Director, Gordon Research Conferences, Colby-Sawyer College, New London, N.H. 03257 (603-526-2870).

Topics of many of the other scheduled conferences of interest to analytical chemists include statistics in chemistry and chemical engineering (July 30–Aug. 3); laser interaction with matter (Aug. 13–17); and magnetic resonance (June 18–22). Complete information and the detailed technical program for this year's conference are given in the March 16, 1979, issue of *Science*, page 1141.

Analytical Chemistry

Jack W. Frazer, *Chairman*
Milos Novotny, *Vice Chairman*

August 13–17, 1979
New Hampton School
New Hampton, N.H.

Aug. 13. Jiri Janata, Electrochemistry of CHEMFETs; Wilhelm Simon, Liquid membrane ion-selective electrodes, neutral carriers for anions; Tomas Hirschfeld, Analytical chemistry from the information theoretic viewpoint. Initiation of the poster session during one evening.

Aug. 14. G. Sam Hurst, Analytical applications of resonance ionization spectroscopy; James R. DeVoe, Laser-enhanced ionization in flames; Stanley L. Grotch, Observations on the uses of multivariate techniques in geochemical exploration.

Aug. 15. Herman Haglund, Present status and current research in isotachophoresis; David M. Hercules, Comparison of surface analysis techniques; Henry Freiser, Solvent extractions of metal chelates; Marjorie G. Hornig, Applications of GC–MS–COM analytical systems to biomedical problems.

Aug. 16. Gary M. Hieftje, New methods for measurement of transient events; David S. Auld, Direct observation of transient ES complexes by radiationless energy transfer: implication to enzyme mechanisms; Frederick Brech, The role of analytical chemistry in authentication of ancient and medieval art objects; Keith Hodgson, The determination of metal ion structure using X-ray absorption spectroscopy—metals in proteins, ions in solution, and amorphous materials.

Aug. 17. Richard Zare, Laser fluorescence analysis; Milos Novotny, Discussion of 1980 Gordon Research Conference.

Analytical Pyrolysis

I. N. Einhorn, *Chairman*
H.L.C. Meuzelaar, *Vice Chairman*

July 2–6, 1979
Holderness School
Plymouth, N.H.

July 2. R. Porter, Study of polymer lattices; I. N. Einhorn, Thermal degradation and mechanisms in step-growth polymers; I. Luederwald, Pyrolysis/mass spectrometry of polymers; D. A. Chatfield, Thermal degradation of natural and synthetic materials.

July 3. F. Shafizadeh, Pyrolytic reactions of carbohydrates—transformations and phase changes; A. Yergy, Thermal reactions in small molecules—polypeptides; A. Harper, Patterned recognition techniques in chemistry.

July 4. H.L.C. Meuzelaar, Pyrolysis/mass spectrometry: aspects for long-term reproducibility; Y. Haverkamp, Pyrolysis/mass spectrometry of microbacteria; H. R. Schulten, Pyrolysis field ionization and field desorption mass spectrometry.

July 5. K. Biemann, Gas chromatography–mass spectrometry techniques; H. G. Wiedermann, Applications of thermal analysis; R. Saferstein, Pyrolysis applications in forensic science.

July 6. Y. M. Bracewell, Pyrolysis applications in soil sciences; N. E. Vanderborgh, Pyrolysis techniques in geosciences.

Ion Exchange

John Millar, *Chairman*
Gilbert E. Janauer, *Vice Chairman*

August 20–24, 1979
Kimball Union Academy
Meriden, N.H.

Aug. 20. New materials (H. Walton, chairman): L. Roubinek, Nitrate-selective amidine resins; W. C. Bauman, Three-phase ion composites; M. Baldwin, J. Barret, New structures in ion-exchange resins; R. E. Robinson, High-density anion resins for metallurgical applications; M. P. Gram-

THE HANDIEST FRACTION COLLECTOR EVER GILSON'S, OF COURSE.

This diminutive, low cost fraction collector is ideal for use with small and medium size LC columns. Can be operated in *cold room*. Model FC-80 weighs only 13 lbs (6 kg) and occupies a bench span of only 11½" X 6" (29 cm X 15 cm). Move it anywhere, or store it in a drawer when you don't use it. A wide range of tube sizes may be used—up to 80 13 X 100 mm or 12 X 75 mm or 10 X 75 mm. It is a combination drop counting or time fractionator.

Demonstration of this fine instrument is available upon request through a network of qualified GME representatives.

GILSON

Gilson Medical Electronics, Inc.
P.O. Box 27 • Middleton, Wisconsin 53562 • Phone (608) 836-1551

Your companion in chromatography

CIRCLE 83 ON READER SERVICE CARD

Thermolyne's Micro-Hot Plate is small in size . . . 3½" dia. - 1½ lbs. . . . but big in performance. It can do all the things the big guys can but doesn't need nearly as much room. For example, it has a demand-type control providing ±2°C. temperature control accuracy. Compact and handy for many heating jobs.

Contact your Lab Supply Dealer or write to:

SYBRON | Thermolyne

Thermolyne Corp., a subsidiary of Sybron Corp., 2555 Kerper Blvd., Dubuque, IA 52001

Being small has its advantages

CIRCLE 201 ON READER SERVICE CARD

News

mont, Brominated high-density anion resins.

Aug. 21. Theoretical aspects (F. Helfferich, chairman): V. Soldatov, Multicomponent equilibria; M. McBride, Cation exchange in montmorillonites: interpretation of selectivity variations; D. Tondeur, Continuous separations by changes in thermal equilibria; L. Liberti, Kinetics of SO_4^{-2}/Cl^- exchange on weak-base resins; (R. E. Anderson, chairman): D. Clifford, Selectivity in anion-exchange resins. Followed by a discussion group on Cl^-/SO_4^{-2} equilibria.

Aug. 22. Inorganic ion exchangers: the rebirth of inorganic ion exchange (H. Sherry, chairman): R. M. Barrer, Ion exchange in zeolites; G. H. Kuehl, Zeolites as detergent builders; R. B. Barrett, Role of ion exchange in in-situ leaching of copper and uranium; R. F. Bartholomew, Ion-exchange properties of glass.

Aug. 23. Liquid-phase adsorption (J. Sherman, chairman): C. Horvath, Thermodynamics of adsorption and solvent effects; V. L. Snoeyink, Polymeric adsorbents; M. Manes, Carbonaceous adsorbents; E. M. Flanigan, A new hydrophilic molecular sieve: Silicate; (speakers to be announced): Looking back to the first Gordon Research Conference on Ion Exchange.

Aug. 24. Energy-related ion exchange (G. Janauer, chairman): F. Helfferich, Diffusion and transport in multiphase systems; J. S. Falcone, Effect of Mg^{+2} and Ca^{+2} activity reduction on composition of reservoir brines; E. Sondreal, Ion exchange in lignites; F. X. McGarvey, Recovery of uranium from alkaline and neutral chloride-containing solutions.

Separation and Purification

Armand J. deRosset, *Chairman*
Kang-Jen Liu, *Vice Chairman*

August 13–17, 1979
Colby-Sawyer College
New London, N.H.

Aug. 13. W. M. Rutherford, Separation of isotopes by liquid-phase and gas-phase thermal diffusion; F. B. Hill, Hydrogen isotope separation using metal hydrides in cyclic processes; J. A. Sullivan, Laser isotope separation.

Aug. 14. H. Small, Chromatographic separation of colloidal particles—principles and practice; E. Gil-Av, Chiral recognition in partitioning systems; P. Valentin, New developments in production scale gas chromatography.

Aug. 15. C. E. Capes, Agglomerative

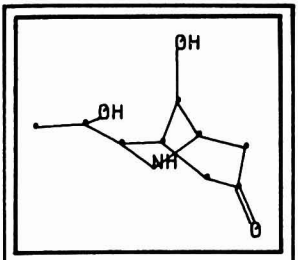

Computer-Assisted Structure Elucidation

ACS Symposium Series No. 54

Dennis H. Smith, *Editor*
Stanford University School of Medicine

A symposium sponsored by the Division of Chemical Information of the American Chemical Society.

An up-to-date report on the growing use of computers to assist in the identification of complex unknown molecular structures in the laboratory.

The collection covers such diverse methodologies as library search techniques, pattern recognition, artificial intelligence programs, automated interpretation of chemical data, structure generation, and ranking of candidate structures based on prediction of chemical or spectroscopic behavior.

CONTENTS

Structure Identification of Unknown Mass Spectra • Components of Complex Mixtures by GC-MS • NIH-EPA Chemical Information System • Determination of the Secondary Structure of Globular Proteins • Automatically Acquired ^{13}C NMR Rules • Computerized Structural Predictions from ^{13}C NMR Spectra • Interactive Structure Elucidation • CHEMICS: A Computer Program System for Structure Elucidation of Organic Compounds • Computer Assistance for the Structural Chemist

151 pages (1977) clothbound $15.50
LC 77-24427 ISBN 0-8412-0384-9

SIS/American Chemical Society
1155 16th St., N.W./Wash., D.C. 20036

Please send _____ copies of SS 54 *Computer-Assisted Structure Elucidation* at $15.50

☐ Check enclosed for $_____. ☐ Bill me. Postpaid in U.S. and Canada, plus 40 cents elsewhere.

Name _____

Address _____

City _____ State _____ Zip _____

ALL NEW
Single Source
Liquid
Chromatography
Catalog —
including
Liquid Handling

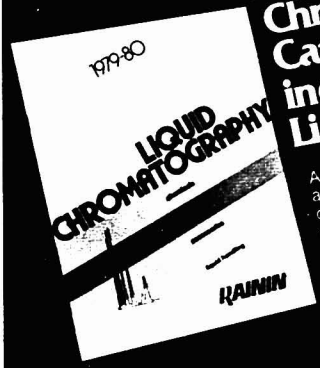

ALSO — you'll receive automatic supplements on new items in the most comprehensive line of liquid chromatography apparatus and supplies

RAININ
Mack Road, Woburn, Massachusetts 01801 • 1-800-225-4590

CIRCLE 184 ON READER SERVICE CARD

The little Chem/Meter:
big on accuracy.

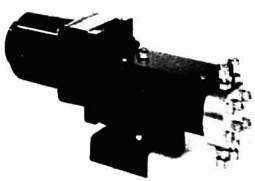

Take a look at all the outstanding features in our Series 20 Chem/Meter hydraulic diaphragm metering pump:
Metering accuracy within ± 1%.
Steady, continuous feeding of clear fluids.
Capacities of 14.7 ML/min.
Pressures to 1500 psi.
Zero to 100% capacity adjustment while operating.
Totally enclosed, leakproof design.
Wetted parts made of corrosive resistant stainless steel with sapphire ball-seats and teflon diaphragms.
Measures only 10½" × 5" × 3½".

The Series 20 Chem/Meter is ideal for machinery that requires the injection of precisely measured liquids. These include plastics, pharmaceuticals, chemical process, foods, beverages and fertilizers.

For larger measuring requirements from 23 to 3024 ML/min we have the Series 200 Chem/Meter. You can get all the details on the reliable Chem/Meter line by calling or writing Crane Co., Chempump Division, Warrington, Pa. 18976.

CRANE CHEMPUMP

CIRCLE 35 ON READER SERVICE CARD CR8-190

Now you can get pre-tested capillary columns (WCOT, SCOT, Micro-Packed) for high resolution gas chromatography in stainless steel or glass... with df of 0.2 and 0.4 micron, and, if desired you can specify your own film thickness. The SS wall-coated columns with 2000 to 4000 plates per meter are available in any length with any liquid phase. The wall-coated glass columns with 3000 to 6000 plates per meter are available standard in 25 and 50 meter lengths and 0.25 or 0.50 mm ID, with eight liquid phases. Other stationary phases also available. All pretested and supplied with test chromatogram, report, sample, and extensive instruction bulletin (written so that even inexperienced users can start using high resolution chromatography). Chrompack Laboratories are dedicated to manufacturing columns, with 10 years experience in Europe making capillary columns. Write for a free catalog to Chrompack, P.O. Box 3, Middelburg, The Netherlands, or in the U.S. to Box 4131, Whittier, CA 90607.

Free Catalog

Pre-Tested Capillary Columns

Chrompack U.S.A. Inc.

CIRCLE 36 ON READER SERVICE CARD

ANTEK MODEL 320

Helium Ionization Trace Gas Analyzer

Antek Model 320 provides accurate analysis of trace amounts of fixed gases and light hydrocarbons. Available with single or dual detectors. Minimum detection level in low parts per billion range.

Features:

- Helium ionization detectors for high sensitivity
- Minimum dead volume reduces flush time and peak tailing
- High voltage power supply, 0 to 1000 VDC
- Electrometer - solid state J-FET
- Trace gas sample valve with dual sample loop
- Isothermal proportional control on column and detector ovens
- Large 12" x 12" x 9" (1296 cu. in.) column oven

Applications:

- Trace impurities in high monomers
- Trace impurities in helium or other gases
- Analysis of head space gases in canning and brewing
- Monitoring trace constituents in breath
- Trace hydrocarbons, nitrogen, sulfur and other compounds in air pollution

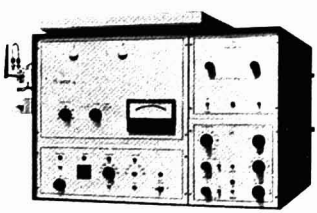

ANTEK INSTRUMENTS, INC.
6005 North Freeway
Houston, Texas 77076
Tel: (713) 691-2265
TWX: 910-881-1792

CIRCLE 5 ON READER SERVICE CARD

News

separation in organic media; S. Dennison, Clay separation by flotation; R. B. Grieves, Separation of inorganic anions (primarily oxyanions) of industrial significance from dilute, multisalt aqueous solutions by foam fractionation and by charged membrane ultrafiltration.

Aug. 16. N. Catsimpoolas, Separation of cells by density gradient electrophoresis; A. R. Cooper, Purification and fractionation of soluble polymers by ultrafiltration; W. E. Greiner, Multistage countercurrent crystallization.

Aug. 17. R. P. Andres, The free jet deceleration process, a new method for separating gas molecules or aerosol particles of disparate mass; J. L. Atwood, Liquid clathrates.

Fisher Award Winner

Douglas Stewart Russell, head of the analytical chemistry section of the Division of Chemistry of the National Research Council in Ottawa, Canada, has been named winner of the Fisher Scientific Lecture Award for 1979. He will present his award lecture on trace analysis at the 62nd Chemical Conference and Exhibition in Vancouver, June 3–6, 1979. Mr. Russell was born in Georgetown, Ontario, in 1916, and graduated in chemistry from the University of Toronto. He started his career with Welland Chemical Works and then served as research officer in radiochemistry for an atomic energy project. He joined NRC in 1946 and became head of the analytical section in 1952. He served on the editorial board of *Chemistry in Canada*, on the executive committee of the CIC Analytical Chemistry Division, and was national president in 1969 of the Canadian Spectroscopic Society.

The Fisher Award, sponsored by Fisher Scientific Co., Ltd., is accompanied by a scroll and an honorarium of $1000. It is awarded to a scientist living in Canada who has made a distinguished contribution in analytical chemistry while working in Canada.

Information Center on Federal Regulations of Toxic Substances

The Franklin Advisory Center for Toxic Substances (FACTS), a service of Franklin Research Center, offers information and research service to business and industry, trade associations, unions, and others who must cope with local and Federal regulations. The new advisory center is established specifically to define regulatory problems, review all existing literature pertaining to the clients' inter-

25 Years of Experience in Recording Instruments

TOP QUALITY LOW PRICE

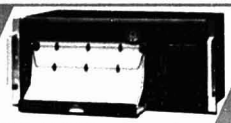

LD 12 Point Printing Recorders

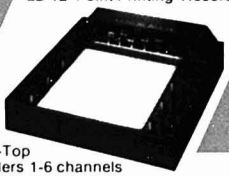

LS 4
Table-Top
Recorders 1-6 channels

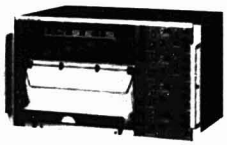

L 2000
Rackmountable Recorders 1-6 channels

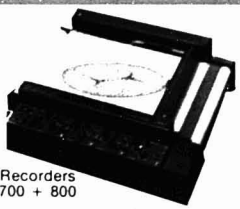

x-y Recorders
LY 700 + 800

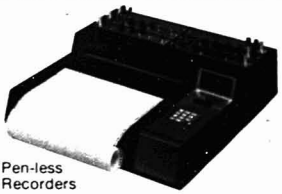

Pen-less
Recorders

Proven and reliable modular construction
Easily expandable and serviceable
Extremely versatile – many different input modules
All this for unusually low prices

LINSEIS INC.
PRINCETON JCT., N.J. 08550, P.O. BOX 666
Phone: (609) 921 - 1857, Telex: 843360

CIRCLE 158 ON READER SERVICE CARD

NEW HOLLAND HONEYEATER Meliomoris Novae Hollandiae. M.SS. MNVU,

So you thought GC/MS interfacing was strictly for the birds.

Until now, interfacing your gas chromatograph with your mass-spectrometer has been one task to steer clear of. Thanks to SGE that has changed!

SGE has developed a patented molecular jet separator and a range of micro needle valves which combine to give you a remarkably fuss and trouble free "all-glass" system of interfacing.

The SGE molecular jet separator has been designed to produce accurate, reproducible jet sizes, alignment and spacing. All with the capability of being temperature cycled up to 450°C - depending on the type of connections used — and without any peak broadening or tailing effects to mar your results.

The SGE micro needle valve range will impress you too. In fact, for accurate critical capillary flow control they're on their own. What's more, the valves have virtually no dead volume and can double as leak tight shut-off valves for high vacuum MS applications as well as for use at high pressures (to 100 atmospheres) and temperatures up to 300°C.

Write for our accessories catalogue;

Scientific Glass Engineering Pty.Ltd.

Head Office
Scientific Glass Engineering Pty. Ltd.,
111 Arden St., North Melbourne, Australia. 3051
Tel (03) 329 6633

European Office
Scientific Glass Engineering (U.K.) Ltd.,
657 North Circular Road, London NW2 7AY.
Great Britain
Tel 01 452 6244

U.S.A Office
Scientific Glass Engineering Inc.,
2800 Longhorn Blvd., Suite 104
Austin, Texas, 78758 U.S.A.
Tel (512) 837 7190

SGE

CIRCLE 189 ON READER SERVICE CARD

A high performance disposable cartridge and reusable holder make the Brownlee MPLC™ Guard Column a unique concept in LC protection.

When placed in front of expensive analytical columns, Brownlee MPLC Guard Columns filter out harmful particles and remove strongly adsorbed compounds from the sample. Result: improved performance and an extended active life for the total LC system.

Prolongs column life
By removing impurities before they reach the analytical column, Brownlee MPLC Guard Columns prolong the useful life of the column.

Lowers cost
The use of Brownlee MPLC Guard Columns can prolong the life of an analytical column about fourfold and save you about 50% in total column costs.

More efficient than pellicular guard columns
Brownlee MPLC Guard Columns employ 10 micrometer totally porous slurry-packed cartridges. That means that a Brownlee MPLC Guard Column withstands more injections than a pellicular guard column. A slurry-packed 10 micrometer guard column acts like a high efficiency extension of the analytical column and does not degrade total performance.

Versatile
You can choose from ten different cartridges for a better match of guard column stationary phase with your analytical column.

Order from a Brownlee Labs distributor, or write for more information: Brownlee Labs Inc. 2045 Martin Ave., Santa Clara, Ca. 95050, USA. Telex 171156. Telephone 408/985 2022.

MPLC™ Guard Columns. For economy and protection, no lab should be without them.

Circle reader service number **15**

Indispensable. MPLC Guard Column

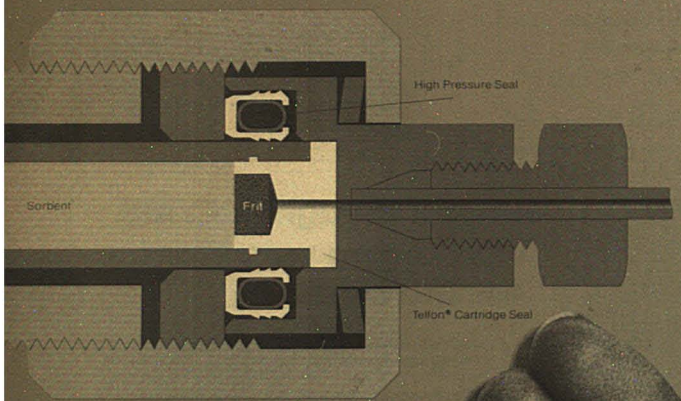

Brownlee Labs

ests, recommend cost-effective means of complying with the law, carry out necessary laboratory studies, and keep clients up-to-date with current and proposed regulations. FACTS is equipped to counsel multinational firms operating in the U.S. and abroad.

The contractual arrangements range from one-time troubleshooting to the long-term Industrial Associates Program, a subscription to one year or more of continued service. FACTS offers additional services such as *TOXALERT*, a biweekly international abstract journal of toxicological research results, a monthly *Industrial Associates Bulletin*, an outgoing hot-line service, and seminars. For further information, contact: The Franklin Institute, Benjamin Franklin Parkway at 20th St., Philadelphia, Pa. 19103 (215-448-1000).

Call for Papers

23rd Oak Ridge National Laboratory Conference on Analytical Chemistry in Energy Technology
Gatlinburg, Tenn. Oct. 9–11, 1979. Papers are solicited in the areas of radiochemistry, radionuclide assay, and low-level activity measurements as well as applications of these techniques to environmental monitoring, reactor fuels reprocessing and nuclear waste management. Special attention will be given to problem nuclides such as I^{129}, Sr^{90}, and Tc^{99}. Those who wish to contribute papers should submit an abstract of approximately 200 words not later than June 15, 1979. The title, author's name, time required for presentation, and name of speaker should accompany the abstract. A final manuscript of the full paper must be delivered to the conference in October; instructions will be sent at the time the abstract is accepted. Papers will be published in a conference proceedings volume. Abstracts and any inquiries should be directed to W. S. Lyon, Technical Program Chairman, Oak Ridge National Laboratory, P.O. Box X, Oak Ridge, Tenn. 37830. 615-574-4883

International Winter Conference 1980 on Developments in Atomic Plasma Spectrochemical Analyses
San Juan, Puerto Rico. Jan. 7–11, 1980. Papers describing original work on applications, fundamentals, and instrumentation developments of atomic plasmas (ICP, MIP, DCP) will be presented in general and invited symposia. Authors of oral or poster papers for general and specialized symposia are requested to submit titles of their contributions and a 50–100-word preliminary abstract prior to July 1, 1979. An extended abstract will be required Oct. 1, 1979. The full conference papers will be refereed and published by Heyden & Sons, Inc., following the conference. Submit abstracts and write for registration to Winter Conference 1980, ICP Information Newsletter, Chemistry–GRC Tower I, University of Massachusetts, Amherst, Mass. 01003. 413-545-2294

Meetings

- **1979 Gordon Research Conference on Analytical Pyrolysis.** July 2–6. Holderness School, Plymouth, N.H. *Contact: A. M. Cruickshank, Director, Gordon Research Conferences, Pastore Chemical Laboratory, University of Rhode Island, Kingston, R.I. 02881. 401-783-4011. After June 11, mail to Colby-Sawyer College, New London, N.H. 03257. 603-526-2870. Page 585 A, May*
- **1979 Gordon Research Conference on Analytical Chemistry.** Aug. 13–17. New Hampton School, New Hampton, N.H. *Contact: A. M. Cruickshank, Director, Gordon Research Conferences, Pastore Chemical Laboratory, University of Rhode Island, Kingston, R.I. 02881. 401-783-4011. After June 11, mail to Colby-Sawyer College, New London, N.H. 03257. 603-526-2870. Page 585 A, May*
- **1979 Gordon Research Conference on Separation and Purification.** Aug. 13–17. Colby-Sawyer College, New London, N.H. *Contact: A. M. Cruickshank, Director, Gordon Research Conferences, Pastore Chemical Laboratory, University of Rhode Island, Kingston, R.I. 02881. 401-783-4011. After June 11, mail to Colby-Sawyer College, New London, N.H. 03257. 603-526-2870. Page 586 A, May*
- **Symposium for Innovation in Measurement Science.** Aug. 19–24. Hobart and William Smith Colleges, Geneva, N.Y. *Contact: C. T. Glazer, Instrument Society of America, 400 Stanwix St., Pittsburgh, Pa. 15222*
- **1979 Gordon Research Conference on Ion Exchange.** Aug. 20–24. Kimball Union Academy, Meriden, N.H. *Contact: A. M. Cruick-*

ank, Director, Gordon Research Conferences, Pastore Chemical Laboratory, University of Rhode Island, Kingston, R.I. 02881. 401-783-4011. After June 11, mail to Colby-Sawyer College, New London, N.H. 03257. 603-526-2870. Page 585 A, May

- **2nd International Conference on Secondary Ion Mass Spectrometry.** Aug. 26–31. Stanford University. *Contact: R. A. Powell, Electrical Engineering Dept., Stanford University, Stanford, Calif. 94305. 415-493-4000, ext. 2815*
- **4th International Symposium on Polynuclear Aromatic Hydrocarbons.** Oct. 2–4. Columbus, Ohio. *Contact: Alf Bjorseth, Battelle-Columbus Laboratories, 505 King Ave., Columbus, Ohio 43201. 614-424-5024*
- **Optical Society of America National Meeting.** Oct. 8–12. Rochester, N.Y. *Contact: Optical Society of America, Suite 620, 2000 L St., N.W., Washington, D.C. 20036*
- **93rd Annual Meeting of AOAC.** Oct. 15–18. Washington, D.C. *Contact: Kathleen Fominaya, AOAC, Box 540, Benjamin Franklin Station, Washington, D.C. 20044*
- **Quantitative Surface Analysis.** Oct. 16–17. National Physical Laboratory, Teddington, Middlesex. *Contact: C. Lea, Division of Chemical Standards, National Physical Laboratory, Teddington, Middlesex TW11 0LW, UK*

Short Courses

ACS Courses. For more information, contact: Department of Educational Activities, American Chemical Society, 1155 Sixteenth St., N.W., Washington, D.C. 20036. 202-872-4508

Chemical Abstracts Workshops
Philadelphia, May 10–11; Los Angeles, June 7–8. CA staff. $75, ACS members; $135, nonmembers

Creative Problem Solving
Philadelphia. May 10–11. Moshe Rubinstein. $225, ACS members; $265, nonmembers

Interpretation of NMR Spectra
Philadelphia. May 10–12. LeRoy Johnson and Roy Bible. $295, ACS members; $340, nonmembers

Capillary Gas Chromatography
Philadelphia. May 11–12. S. P. Cram and Milos Novotny. $250, ACS members; $300, nonmembers

Gas Chromatography
Chicago, May 18–19; Atlanta, June 14–15. R. A. Keller and M. F. Burke. $225, ACS members; $265, nonmembers

Federal Regulations in the Chemical Industry
Chicago, May 18–19; Los Angeles, June 8–9. G. S. Dominguez. $225, ACS members; $265, nonmembers

Toxicology for Chemists
Chicago. May 22–24. Morris Joselow. $485, ACS members; $555, nonmembers

Planning for Safe Laboratory Handling of Highly Toxic Chemicals
Chicago. May 30–June 1. N. V. Steere and Maurice Golden. $295, ACS members; $340, nonmembers

Safety and Health for Academic Chemistry Laboratories
Chicago. June 2–3. N. V. Steere. $130, ACS members and nonmembers

Liquid Chromatography, Theory and Practice
Blacksburg, Va. June 4–7, Dec. 10–13. H. M. McNair. $450, ACS members; $510, nonmembers

High-Pressure Liquid Chromatography Apparatus Workshop
Los Angeles, June 7–8; Philadelphia (FACSS Meeting), Sept. 15–16. D. H. Freeman. $250, ACS members; $300, nonmembers

Multinuclear NMR Spectroscopy
Los Angeles, June 7–9; Tallahassee, Fla., June 14–16. G. C. Levy. $295, ACS members; $340, nonmembers

Microprocessors and Minicomputers—Interfacing and Applications
Blacksburg, Va. June 10–15, Sept. 23–28, Dec. 9–14. R. E. Dessy and the Chemistry Dept. Instrument and Design Group of VPI&SU. $455, ACS members; $515, nonmembers

Atomic Absorption Spectroscopy
Atlanta. June 14–15. Samuel Koirtyohann, Michael Epstein, and Theodore Rains. $245, ACS members; $290, nonmembers

Design and Analysis of Industrial Experiments
Atlanta, June 14–16; Philadelphia (FACSS Meeting), Sept. 14–16. John Hromi. $295, ACS members; $340, nonmembers

Carbon-13 NMR Spectroscopy
Washington, D.C. (178th ACS National Meeting). Sept. 7–9. G. C. Levy and Paul Ellis. $295, ACS members; $340, nonmembers

Effective Writing for Scientists and Engineers
Washington, D.C. (178th ACS National Meeting). Sept. 7–9. Henrietta Tichy and Sylvia Fourdrinier. $295, ACS members; $340, nonmembers

High-Performance Management
Washington, D.C. (178th ACS National Meeting). Sept. 8–9. J. H. Morrison. $225, ACS members; $265, nonmembers

Electroanalytical Chemistry
Philadelphia (FACSS Meeting). Sept. 14–16. Dennis Evans and P. E. Whitson. $295, ACS members; $340, nonmembers

Laboratory Automation: Micro-, Mini-, or Midicomputers?
Philadelphia (FACSS Meeting). Sept. 15–16. R. E. Dessy and the Chemistry Dept. Instrument and Design Group of VPI&SU. $225, ACS members; $265, nonmembers

Thermal Methods of Analysis
Philadelphia (FACSS Meeting). Sept. 15–16. W. W. Wendlandt and I. M. Sarasohn. $225, ACS members; $265, nonmembers

---

Basic Mass Spectral Interpretation
Atlanta. May 7–11. G. Vander Veld and D. De Jongh. $450. *Contact:* Ann Woolley, Finnigan Institute, 11750 Chesterdale Rd., Bldg. 5, Cincinnati, Ohio 45246. 513-772-5500

Basic GC/MS/DS
Cincinnati. May 7–11, June 18–22. Q. Thomas. $625. *Contact:* Ann Woolley, Finnigan Institute, 11750 Chesterdale Rd., Bldg. 5, Cincinnati, Ohio 45246. 513-772-5500

istilled solvent from MCB.

• Spectrophotometry • Chromatography • HPLC • Residue Analysis
• Pesticide Analysis • Gas Chromatography

For more information on the full OmniSolv line, consult your copy of the 1979 MCB Buying Guide. Then place your order with your local MCB distributor. For the name and address of the distributor nearest you, write: MCB Reagents, 2909 Highland Avenue, Cincinnati, Ohio 45212

MCB Reagents
Associate of E. Merck, Darmstadt, Germany

CIRCLE 144 ON READER SERVICE CARD

Peak separation you've never seen before.

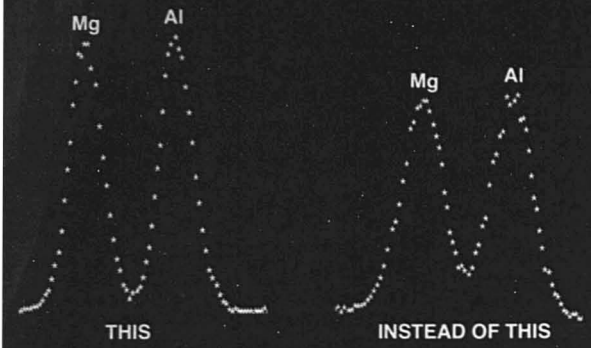

New from this X-ray fluorescence analyzer.

A new and unique pulse processor gives our SPECTRACE™ analyzer guaranteed resolution of 150 eV—the best ever achieved in an energy-dispersive X-ray fluorescence analyzer. This resolution, coupled with peak shifts no greater than 3 eV at maximum count rate, lets you detect light elements more reliably and quantify them more accurately.

The spectrum at left above shows an actual peak separation using the new pulse processor. That at right, with overlapping peaks, was made using a conventional processor in the same analyzer.

SPECTRACE 440 can make automatic unattended analyses of up to 40 samples—solids, liquids, powders or deposits on filter paper. Makes qualitative and quantitative analyses of all elements from Na to Pu. Handles samples from 1 mm in diameter to a foot high. Has superb sensitivity, repeatability and long-term stability.

Our applications laboratory and engineering group will work with you to help solve your analytical problem. That way you *know* you'll get the results you want after your SPECTRACE is delivered.

Over 50 SPECTRACE analyzers are now in use. And we'll give you the name of every single user—because we know every one will give you a favorable report. One thing they'll report is the service they get: personal instruction, an applications school, software school—and follow-up visits just to make sure you're getting the most out of your SPECTRACE.

Send for our highly informative brochure now. Contact United Scientific Corporation, Analytical Instrument Division, Dept. C, 1400 Stierlin Road, P.O. Box 1389, Mt. View, California 94042. Phone (415) 969-9400.

UNITED SCIENTIFIC
ANALYTICAL INSTRUMENTS DIVISION

CIRCLE 210 ON READER SERVICE CARD

News

Problem Solving by Chromatography: HPLC and GC
Cincinnati. May 7–11. W. Averill. $625. *Contact:* Ann Woolley, Finnigan Institute, 11750 Chesterdale Rd., Bldg. 5, Cincinnati, Ohio 45246. 513-772-5500

Atomic Absorption Spectrophotometry: Basic Concepts and Techniques
Cincinnati. May 14–18, June 4–8. A. Knott or W. Stelzer. $625. *Contact:* Ann Woolley, Finnigan Institute, 11750 Chesterdale Rd., Bldg. 5, Cincinnati, Ohio 45246. 513-772-5500

Analysis of Organic Compounds in Water (Part 1)
Cincinnati. May 14–18. R. Foltz and D. Lin. $750. *Contact:* Ann Woolley, Finnigan Institute, 11750 Chesterdale Rd., Bldg. 5, Cincinnati, Ohio 45246. 513-772-5500

Analysis of Organic Compounds in Water (Part 2)
Cincinnati. May 21–25. R. Foltz and D. Lin. $750. *Contact:* Ann Woolley, Finnigan Institute, 11750 Chesterdale Rd., Bldg. 5, Cincinnati, Ohio 45246. 513-772-5500

Chemical Derivatization for Chromatography and Mass Spectrometry
Cincinnati. May 30–June 1. M. Quilliam. $400. *Contact:* Ann Woolley, Finnigan Institute, 11750 Chesterdale Rd., Bldg. 5, Cincinnati, Ohio 45246. 513-772-5500

Interpretation of Mass Spectra
Seattle, Wash. In conjunction with the 27th Annual Meeting of the American Society for Mass Spectrometry. June 2–3. $150. *Contact:* Larry I. Bone, Dept. of Chemistry, Appalachian State University, Boone, N.C. 28608

NMR Interpretation: Proton & Carbon-13
New York City. June 4–7. D. Traficante. $440. *Contact:* Ann Woolley, Finnigan Institute, 11750 Chesterdale Rd., Bldg. 5, Cincinnati, Ohio 45246. 513-772-5500

Microprocessor Fundamentals and Industrial Applications
Seattle, Wash., June 7–8; St. Louis, Mo., June 21–22. Cosponsored by the local Instrument Society of America. $195, ISA members; $220, nonmembers. *Contact:* ISA Short Course Registration, 400 Stanwix St., Pittsburgh, Pa. 15222. 412-281-3171

An important advance in HPLC variable wavelength detection

The HP1084B makes it programmable

Variable wavelength UV-visible detectors provide the greatest versatility in LC detection. Now, with the introduction of a new detector for the HP 1084B, Hewlett-Packard has greatly extended this versatility by putting wavelength selection under processor control.

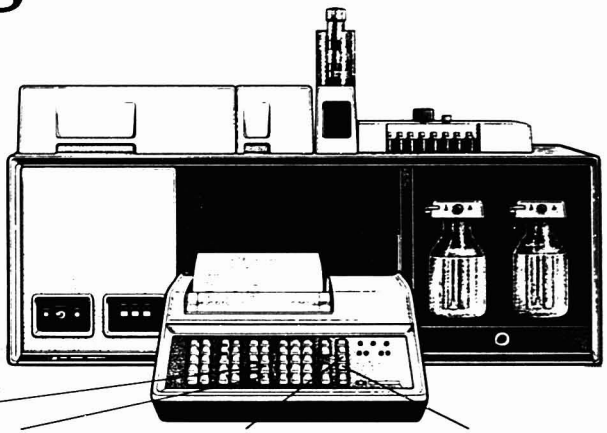

See what you can do with the 1084B

- Select any wavelength from 190 nm to 600 nm, direct from the keyboard.
- Select both an analytical and a reference wavelength.

- Scan from 190 to 540 nm, at 200 nm/min, with automatic subtraction of mobile phase background.

- Change wavelength programs between runs, automatically.

- Change wavelengths automatically during a run, with automatic zeroing, in seconds.

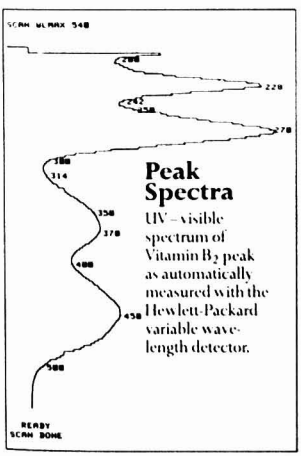

Peak Spectra

UV – visible spectrum of Vitamin B_2 peak as automatically measured with the Hewlett-Packard variable wavelength detector.

A tremendous increase in problem-solving power

Now you can detect each component in a sample at its optimum wavelength. Interfering peaks can be suppressed. Unresolved components can frequently be detected and determined by making multiple runs at different wavelengths. The ratios of peak areas obtained at different wavelengths can be used to confirm the identity of a component. And the 1084's scanning feature can produce rapid information about absorbtion maxima and minima. Coupled with "Change Run" capability, all this makes the HP 1084's new detector a very powerful tool indeed.

We would be glad to send you details.

HEWLETT hp PACKARD

Hewlett-Packard Co., Route 41, Avondale, Pennsylvania 19311, USA.
Hewlett-Packard GmbH, Hewlett-Packard Strasse, D-7517 Waldbronn 2, West Germany.

CIRCLE 152 ON READER SERVICE CARD

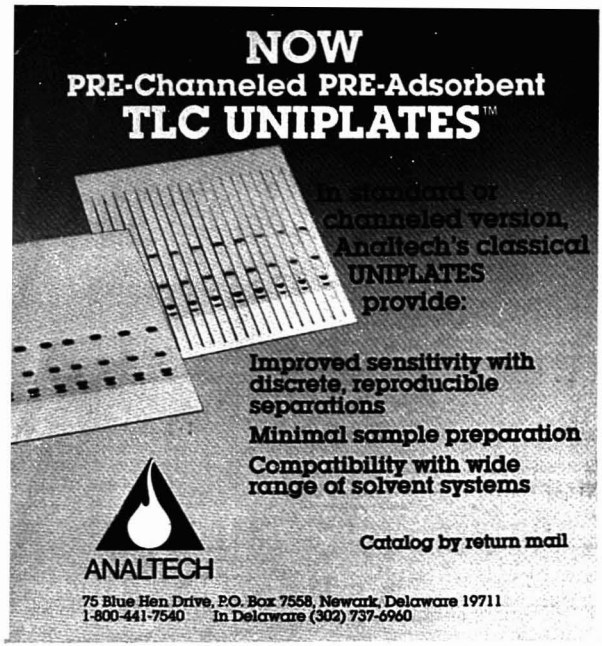

CIRCLE 7 ON READER SERVICE CARD

CIRCLE 99 ON READER SERVICE CARD

News

Problem Solving by Chromatography: HPLC and GC
Cincinnati. June 11–15. W. Averill. $625. *Contact:* Ann Woolley, Finnigan Institute, 11750 Chesterdale Rd., Bldg. 5, Cincinnati, Ohio 45246. 513-772-5500

IR Interpretation
Houston. June 18–20. H. Sloane. $330. *Contact:* Ann Woolley, Finnigan Institute, 11750 Chesterdale Rd., Bldg. 5, Cincinnati, Ohio 45246. 513-772-5500

^{13}C NMR Workshop
New Brunswick, N.J. (Rutgers University). June 20–22. $150. *Contact:* Registrar, ^{13}C NMR Workshops, Varian Associates, Box D-070, 611 Hansen Way, Palo Alto, Calif. 94303

For Your Information

Environmental Technology Division of Lear Siegler, Inc., is offering customer training programs for the division's oxygen analyzer, gas analyzers, opacity monitors, and DP 30 data processing system. For further information, contact: Al Becker, Lear Siegler, Inc., Environmental Technology Division, 74 Inverness Drive East, Englewood, Colo. 80112. 303-770-3300

Perkin-Elmer Corp. has changed the names of two of its divisions serving the data processing market. Computer Systems Division is the new name for the Interdata Division, and Memory Products Division is the new name for the Wangco Division.

Reprints of the reports, ***Standard Reference Materials for Trace Analysis*** and ***Contamination in Trace Analysis,*** are available from IUPAC journal *Pure and Applied Chemistry,* Vol. 50, Nos. 11/12 (1978). The reports were prepared by the IUPAC Commission on microchemical techniques and trace analysis.

The complete line of nearly 400 **high-purity materials** specifically made for spectroscopic analysis by Johnson Matthey Chemicals Ltd., of Royston, England, is now available in the U.S. through Ultra Carbon Corp., Bay City, Mich.

ANSI's ABC's of **International Standardization,** a booklet that lists the major international organizations concerned with standardization, has been updated and reissued. For more information, contact: American National Standards Institute, 1430 Broadway, New York, N.Y. 10018.

After method development comes production control–

that's when you need the HP1081B Liquid Chromatograph

In HPLC, when you've done all the initial investigations and you want to automate quality and production control, you need a chromatograph with certain sturdy virtues. It's got to give you precise control over operating parameters, automatic sampling capability, complete reliability and built-in two-way data system communication facility. And it's got to be simple to operate.

That's a short description of the new Hewlett-Packard 1081B.

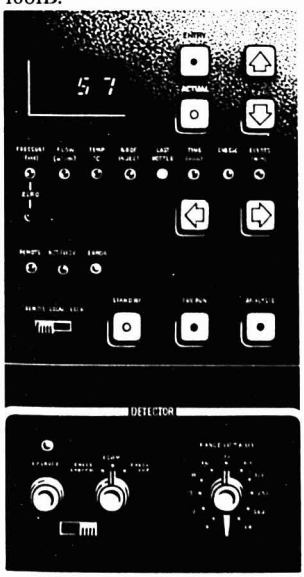

It inherits a lot of its high-performance qualities from the well-proven HP 1084B, with special features like simplified dialog keyboard and closed-loop flow control, which make it ideal for routine monitoring in food, pharmaceutical, petroleum and many other industrial applications requiring isocratic operation.

Although it is an integrated, microprocessor controlled instrument, the HP 1081B has considerable modularity, with over 10 configurations available, and is fully compatible with most data acquisition systems.

If you're looking for a... analytical watchdog, you ought to look at the new HP 1081B. We'd be glad to send you details.

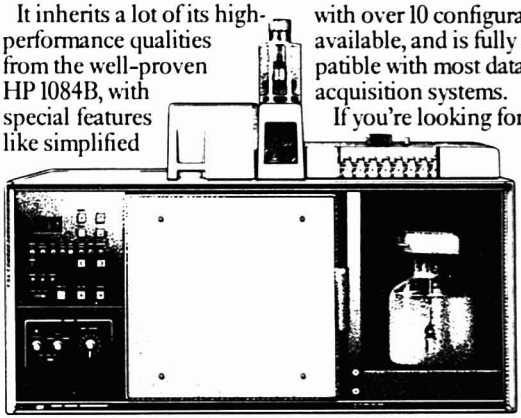

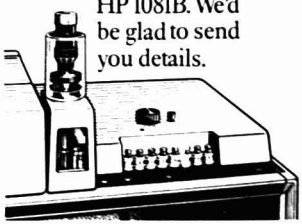

HEWLETT hp PACKARD

Hewlett-Packard Co., Route 41, Avondale, Pennsylvania 19311

Hewlett-Packard GmbH, Hewlett-Packard Strasse, Postfach 1280, 7517 Waldbronn, West Germany.

12802

CIRCLE 153 ON READER SERVICE CARD

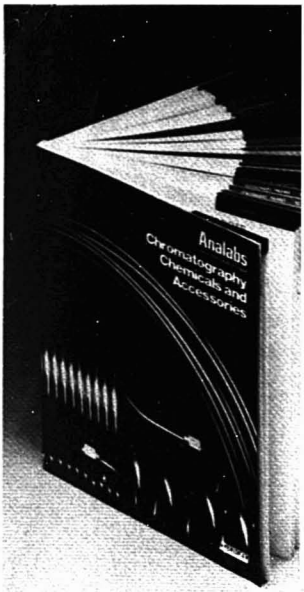

Chromatographer's Supermarket

Over 150 pages of the highest quality gas, liquid, and thin layer chromatography supports, stationary phases, packings and columns, hardware, accessories, supplies, standards, lipids, reagents, solvents and much, much more. From the leader in chromatographic supplies and accessories.

GET YOUR FREE COPY TODAY!

Analabs, Inc.
A Unit of Foxboro Analytical
80 Republic Drive
North Haven, CT 06473
Tel. (203) 288-8463

FOXBORO

CIRCLE 78 ON READER SERVICE CARD

News

The 1979 Directory of Consulting and Laboratory Services covering 20 eastern and midwestern states is available. In the first edition, the capabilities of 547 firms offering engineering and scientific consulting, testing, analytical, and R&D services are described in detail. Price is $34.75 plus $1.35 for postage and handling. A 30-day price refund guarantee is offered. Send checks to J. W. Lundy Enterprises, P.O. Box 543, State College, Pa. 16801.

The National Technical Information Service of the Dept. of Commerce is offering China-related information through various handbooks and CIA reports. One report entitled "China: Scientific Abstracts," issued annually with 28 issues, costs $100. For further information, contact: Dept. of Commerce, National Technical Information Service, Office of the Director, 5285 Port Royal Rd., Springfield, Va. 22161.

A brochure about **Micromeritics' Materials Analysis Laboratory** is available from the company. Applications information and sample information are also on file at the Laboratory. Write Micromeritics Instrument Corp., 5680 Goshen Springs Rd., Norcross, Ga. 30093.

The editors of the journal ***Progress in Analytical Atomic Spectroscopy*** will commission papers in the following areas: AA, optical emission with excitation by arc, spark, and other sources, atomic fluorescence, and X-ray and electron beam techniques. For more information, contact: C. L. Chakrabarti, Editor-in-Chief, Dept. of Chemistry, Carleton University, Ottawa, Ont., Canada K1S 5B6.

A contract for development of a **master analytical scheme** has been awarded to Research Triangle Institute, Research Triangle Park, N.C., with a subcontract to Gulf South Research Institute, New Orleans. The object of the contract is to develop an analytical scheme that, when coupled with GC–MS identification techniques, will serve as a general protocol for analytical surveys in which all volatile organic compounds above a specified level in water are searched for and quantified.

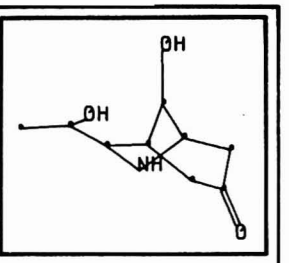

Computer-Assisted Structure Elucidation

ACS Symposium Series No. 54

Dennis H. Smith, *Editor*
Stanford University School of Medicine

A symposium sponsored by the Division of Chemical Information of the American Chemical Society.

An up-to-date report on the growing use of computers to assist in the identification of complex unknown molecular structures in the laboratory.

The collection covers such diverse methodologies as library search techniques, pattern recognition, artificial intelligence programs, automated interpretation of chemical data, structure generation, and ranking of candidate structures based on prediction of chemical or spectroscopic behavior.

CONTENTS

Structure Identification of Unknown Mass Spectra • Components of Complex Mixtures by GC–MS • NIH–EPA Chemical Information System • Determination of the Secondary Structure of Globular Proteins • Automatically Acquired ^{13}C NMR Rules • Computerized Structural Predictions from ^{13}C NMR Spectra • Interactive Structure Elucidation • CHEMICS: A Computer Program System for Structure Elucidation of Organic Compounds • Computer Assistance for the Structural Chemist

151 pages (1977) clothbound $15.50
LC 77-24427 ISBN 0-8412-0384-9

SIS/American Chemical Society
1155 16th St., N.W./Wash., D.C. 20036

Please send _____ copies of *SS 54 Computer-Assisted Structure Elucidation* at $15.50

☐ Check enclosed for $_____. ☐ Bill me. Postpaid in U.S. and Canada, plus 40 cents elsewhere.

Name _____

Address _____

City _____ State _____ Zip _____

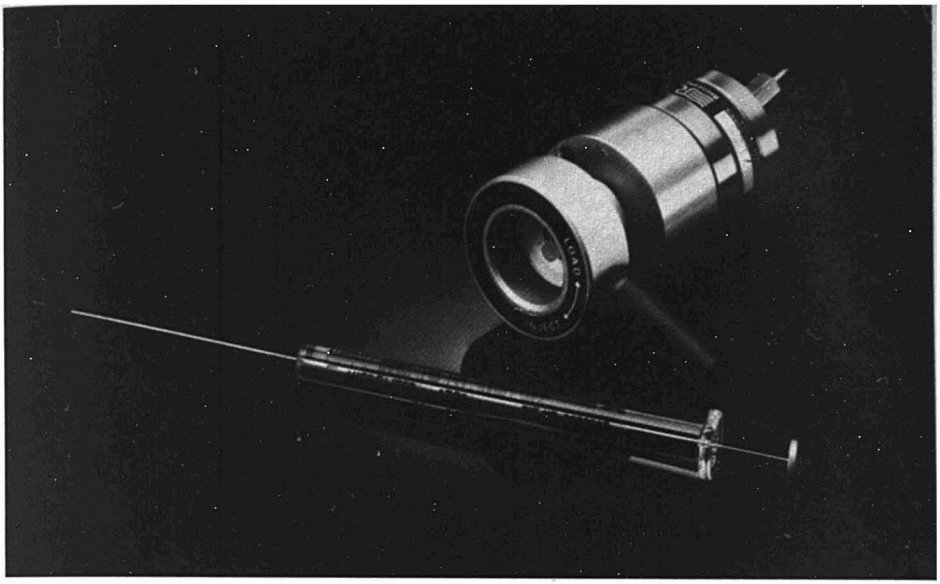

Rheodyne simplifies LC sample injection again.

We made the best injector even better.

Rheodyne's Model 7120 Syringe Loading Sample Injector has carved out an outstanding reputation in the LC field. Last year sales more than doubled. People seem to think it's the best around – and we modestly agree. Now we've made it even better – with new features that make sample injection simpler and more reliable than ever before.

Flushing now unnecessary.

With the improved valve, Model 7125, the entire contents of the microsyringe is injected into the sample loop and flows to the column. No sample is left behind in the valve. Consequently, you don't have to flush the valve between injections unless you're doing trace analysis.

Longer valve life. Less wear.

Both rotor and stator are made from new materials to minimize wear as they slide over one another. This extends valve life considerably.

Our new Model 7125 replaces the popular 7120 in all applications. Does all the 7120 does and more. Has the same mounting dimensions. Price is $540.

New automatic model.

Our automatic Model 7126 combines the new 7125 with pneumatic actuators and time-of-injection switch so you can use it in automatic LC systems.

Compact. Sturdy. Reliable. May be used in the manual injection mode anytime you wish. Price is $780.

Get the details now.

Contact Rheodyne Inc., 2809 Tenth Street, Berkeley, California 94710. Phone (415) 548-5374.

RHEODYNE

THE LC CONNECTION COMPANY

CIRCLE 182 ON READER SERVICE CARD

Where Small Differences Make a Big Difference

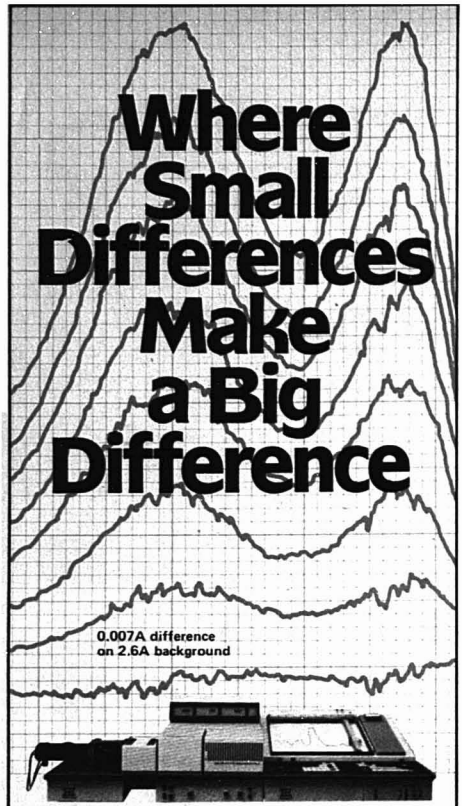

New MIDAN™ Microprocessor Data Analyzer Enhances the Value of Data Generated by the DW-2a™ Spectrophotometer

Now you can expedite analyses of compounds in mixtures, correct baselines automatically, and perform other complex calculations using the new MIDAN Microprocessor Data Analyzer Accessory for our DW-2a Spectrophotometer.

With AMINCO's DW-2a Spectrophotometer, small sample differences can lead to new research territories in UV-VIS spectrophotometry. Our painstaking improvements in such parameters as photometric accuracy, stability, and system versatility extend your range of sample investigations and lead to substantial increases in overall system performance. And, the DW-2a Spectrophotometer's built-in flexibility and wide variety of capability-expanding accessories — like the MIDAN Analyzer — ensure continuing adaptability to your special applications needs.

AMERICAN INSTRUMENT COMPANY
DIVISION OF TRAVENOL LABORATORIES, INC.
Silver Spring, Maryland 20910 Phone: 301-589-1727
European Headquarters: Rue Dautzenberg 36-38, 1050 Brussels Belgium, Phone (02) 648-50-02

© 1978 Travenol Laboratories, Inc.

CIRCLE 6 ON READER SERVICE CARD

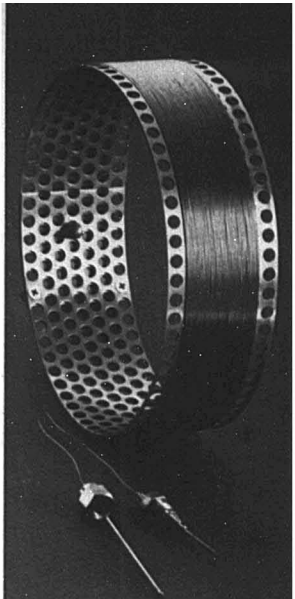

New Analabs Stainless Steel Capillary Columns

10-100 times more efficient than packed columns.

Get the increased separating power and faster analysis with Analabs new wall coated stainless steel capillary columns. Select from a large variety of standard, off-the-shelf stationary phases or order to your specifications. In addition, Analabs will recoat any stainless steel capillary column at a nominal cost. See for yourself. Send for our new brochure today.

Analabs is a Trademark of The Foxboro Company.

Analabs, Inc.
A Unit of Foxboro Analytical
80 Republic Drive
North Haven, CT 06473
(203) 288-8463

FOXBORO

CIRCLE 77 ON READER SERVICE CARD

PERKIN-ELMER SEMINARS ON HEAD SPACE ANALYSIS.

You are cordially invited to attend a free seminar dealing with a new technique in gas chromatography... Head Space.

WHAT IS HEAD SPACE?

Head space injection is the preferred method for analyzing volatiles in complex samples. Only the volatile components present in the gas phase above the sample (Head Space) are analyzed, while the non-volatile residue of the sample never reaches the GC injection system, thus simplifying sample preparation.

SIGN UP NOW

Seminars dealing with gas chromatographic head space analysis will be given by Perkin-Elmer at the locations listed below. Admission is free and, of course, your participation is encouraged. Please contact your local Perkin-Elmer GC Specialist, or call Suzanne Gamache at Perkin-Elmer, Norwalk, CT (203) 762-6144.

CALIFORNIA
June 19
Perkin-Elmer Corp
15042-A Parkway Loop
Tustin, Calif
Contact:
Steve Kramer
Perkin-Elmer Corp
15042-A Parkway Loop
Tustin, Calif 92680
(714) 544-6272
June 26
Sacramento Inn
Interstate 80 & Arden Way
Sacramento, Calif
Contact:
Dave Mowry
Perkin-Elmer Corp
411 Clyde Avenue
Mt View, Calif 94043
(415) 961-2050

ILLINOIS
June 5
Sheraton Oakbrook
1401 West 22nd Street
Oakbrook, Ill
Contact:
Mike Harter
Perkin-Elmer Corp
328 Eisenhower Lane
Lombard, Ill 60148
(312) 495-3700

LOUISIANA
May 31
Holiday Inn
10455 Reiger Road
Baton Rouge, La
Contact:
Neil Johansen
Perkin-Elmer Corp
6461 Siegen Lane
Baton Rouge, La 70809
(504) 293-3540

MARYLAND
May 14
Sheraton Inn
3 Research Ct
Rockville, Md
Contact:
Gerry Copeland
Perkin-Elmer Corp
15 Firstfield Road
Gaithersburg, Md 20760
(301) 840-2121

MASSACHUSETTS
May 30
Holiday Inn
399 Grove Street (Exit 53
on Rt 128)
Newton, Mass
Contact:
Gary Gaudet
Perkin-Elmer Corp.
Wellesley Office Park, Bldg. 5
20 William Street
Wellesley, Mass 02181
(617) 237-9463

OHIO
June 7
Finnegan Institute
Atkinson Square, Bldg. 5
11750 Chesterdale Road
Cincinnati, Ohio
Contact:
Dave Burwanger
Perkin-Elmer Corp
3500 Atkinson Square
11750 Chesterdale Road
Cincinnati, Ohio 45246
(513) 771-9252

PENNSYLVANIA
May 16
Ramada Inn
Rt 1 & Rt 202
Philadelphia, Pa
Contact:
Burton Todd
Perkin-Elmer Corp.
5066 West Chester Pike
Newton Square, Pa 19073
(215) 353-3700

TEXAS
May 29
Dunfey's Royal Coach Inn
7000 Southwest Freeway
Houston Tx
Contact:
Gary Gostecnik
Perkin-Elmer Corp.
Suite 404
5755 Bonhomme
Houston, Tx 77036
(713) 782-7112

PERKIN-ELMER
Expanding the world of analytical chemistry.

CIRCLE 176 ON READER SERVICE CARD

The recording shows the absorbance of fractions collected by molecular gel filtration from a separation of high and low molecular weight proteins. These were collected in a cold room and read at 280nm. The tape lists the absorbance value of every fraction and identifies each sample by its position on the transport.

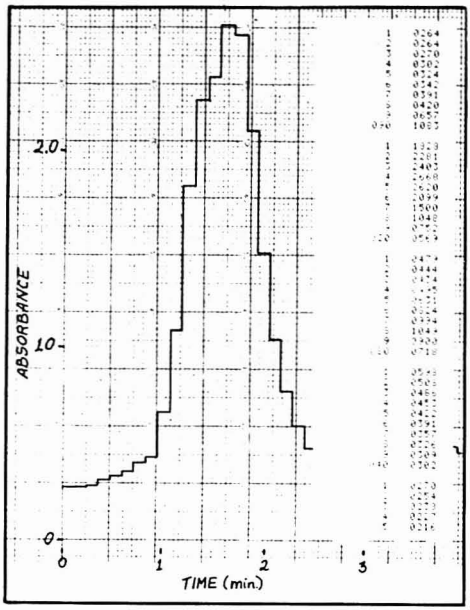

Gilford's Sample Processing System: when you need the accuracy of a research spectrophotometer with the productivity of an automatic analyzer.

More Measurements per Hour

Whether you base it on our Model 250 Spectrophotometer or the Series 252 updates on DU® or DU2® monochromators, the Gilford Sample Processing System is a real time-saver....up to 300 manual measurements per hour, as many as 500 per hour with the available Automatic Sample Transport.

Greater Accuracy, Fewer Reruns

The precise sampling system aspirates the same amount of sample time after time. Combined with the NBS-traceable accuracy of the Gilford photometer, you get consistent high-quality results.... hundreds per hour, with carryover of less than 1%.

Economy in Sample Size

Pickup volume is adjustable, with a minimum of 700 µl for the standard aspirating cuvette; with the optional ultramicrocuvette, it's 350 µl.

® Registered trademark of Beckman Instruments, Fullerton CA

Retention of Sample

Sample return is standard: after samples are measured, you can discard them, return selected samples manually, or with the optional Sample Transport, return them all automatically.

Building Blocks Relieve the Budget

With the Rapid Sampler accessory alone, you read absorbance or concentration directly from the LED display. Use our Thermal Printer to provide a permanent record of results and to avoid transcription errors. Choose the Automatic Sample Transport for unattended processing of up to 100 samples, complete with sample identification printed out. Add the Thermocuvette, providing the same high-productivity sampling plus electronic control of sample temperature at 25, 30, 32, and 37°C....with automatic regulation to within ±0.05°C.

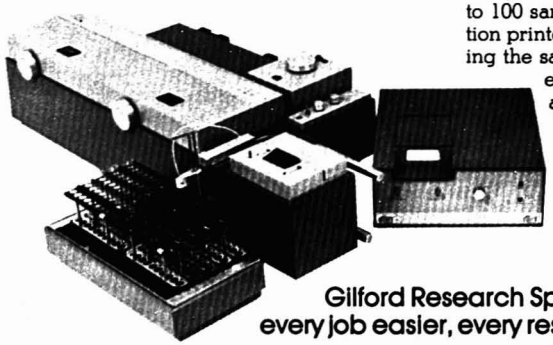

gilford INSTRUMENT
Oberlin, Ohio 44074
(216) 774-1041 Telex: 98-0456
Paris (Malakoff), France
Düsseldorf, W. Germany
Teddington, Middx., England
Toronto (Mississauga), Canada

Gilford Research Spectrophotometers: every job easier, every result more accurate.

CIRCLE 81 ON READER SERVICE CARD

CIRCLE 95 ON READER SERVICE CARD

Leash your

TO SNIFF OUT TRACE ORGANICS IN GASES OR LIQUIDS

The 1047 Concentrator

is inexpensive and easily attached to any commercial gc. Its unique combination of differential adsorption with thermal desorption allows rapid, quantitative, reproducible analyses of gaseous, liquid, and solid samples.

SPEX INDUSTRIES, INC. ☎(201)-549-7144
BOX 798, METUCHEN, N.J. 08840

CIRCLE 187 ON READER SERVICE CARD

NO POSTAGE NECESSARY IF MAILED IN THE UNITED STATES

BUSINESS REPLY CARD

FIRST CLASS Permit #27346 Philadelphia, Pa.

POSTAGE WILL BE PAID BY ADDRESSEE

analytical chemistry

P.O. BOX #7826
PHILADELPHIA, PA 19101

YOUR "READER SURVEY" VIEWS ARE VITAL

Analytical Chemistry occasionally presents a Reader Survey section that provides you with an opportunity to indicate your interests and activities. Your answers help us in planning editorial material that will be useful to you in your work.

To express your Reader Survey views, simply circle your answers on one of these adjacent reply cards and drop it in the mail. No postage is required.

MAY 1979

VALID THROUGH SEPTEMBER 1979

ADVERTISED PRODUCTS:					1	2	3	4	5	6
7	8	9	10	11	12	13	14	15	16	17
18	19	20	21	22	23	24	25	26	27	28
29	30	31	32	33	34	35	36	37	38	39
40	41	42	43	44	45	46	47	48	49	50
51	52	53	54	55	56	57	58	59	60	61
62	63	64	65	66	67	68	69	70	71	72
73	74	75	76	77	78	79	80	81	82	83
84	85	86	87	88	89	90	91	92	93	94
95	96	97	98	99	100	101	102	103	104	105
106	107	108	109	110	111	112	113	114	115	116
117	118	119	120	121	122	123	124	125	126	127
128	129	130	131	132	133	134	135	136	137	138
139	140	141	142	143	144	145	146	147	148	149
150	151	152	153	154	155	156	157	158	159	160
161	162	163	164	165	166	167	168	169	170	171
172	173	174	175	176	177	178	179	180	181	182
183	184	185	186	187	188	189	190	191	192	193
194	195	196	197	198	199	200	201	202	203	204
205	206	207	208	209	210	211	212	213	214	215
216	217	218	219	220	221	222	223	224	225	226
227	228	229	230	231	232	233	234	235	236	237
238	239	240	241	242	243	244	245	246	247	248
249	250	251	252	253	254	255	256	257	258	259

NEW PRODUCTS:				401	402	403	404	405	406	407
408	409	410	411	412	413	414	415	416	417	418
419	420	421	422	423	424	425	426	427	428	429
430	431	432	433	434	435	436	437	438	439	440
441	442	443	444	445	446	447	448	449	450	451
452	453	454	455	456	457	458	459	460	461	462
463	464	465	466	467	468	469	470	471	472	473
474	475	476	477	478	479	480	481	482	483	484
485	486	487	488	489	490	491	492	493	494	495

READER SURVEY:				301	302	303	304	305	306	307
308	309	310	311	312	313	314	315	316	317	318
319	320	321	322	323	324	325	326	327	328	329
330	331	332	333	334	335	336	337	338	339	340
341	342	343	344	345	346	347	348	349	350	351

TO VALIDATE THIS CARD, PLEASE CHECK ONE ENTRY FOR EACH CATEGORY BELOW:

Intensity of product need:
- ☐ 1. Have salesman call
- ☐ 2. Need within 6 mos.
- ☐ 3. Future project

Primary field of work:
- ☐ A. Energy
- ☐ B. Environmental
- ☐ C. Medical/Biological
- ☐ D. Drug/Cosmetic
- ☐ E. Forensic/Narcotic
- ☐ F. Textile/Fiber
- ☐ G. Metals
- ☐ H. Pulp/Paper/Wood
- ☐ I. Soaps/Cleaners
- ☐ J. Paint/Coating/Ink
- ☐ K. Electrical/Electronic
- ☐ L. Instrument Dev./Des
- ☐ M. Plastic/Polymer/Rub
- ☐ N. Agricultural/Food
- ☐ O. Inorganic Chemicals
- ☐ P. Organic Chemicals

Primary area of employment:
INDUSTRIAL
- ☐ A. Research/Development
- ☐ B. Quality/Process Control

MEDICAL/HOSPITAL
- ☐ C. Research/Development
- ☐ D. Clinical/Diagnostic

GOVERNMENT
- ☐ E. Research/Development
- ☐ F. Regulate/Investigate

COLLEGE/UNIVERSITY
- ☐ G. Research/Development
- ☐ H. Teaching

INDEPENDENT/CONSULTING
- ☐ I. Research/Development
- ☐ J. Analysis/Testing

This copy of Analytical is:
- ☐ 1. Personally addressed to me in my name.
- ☐ 2. Addressed to other person or to my firm.

NAME: _____

TITLE: _____

FIRM: _____

STREET: _____

CITY: _____

STATE: _____ ZIP: _____

PHONE: (___ ___ ___) ___ ___ ___ - ___ ___ ___ ___

CIRCLE 95 ON READER SERVICE CARD

HOW DOES PERKIN-ELMER MAKE THE GREAT SIGMA GC SERIES EVEN GREATER? GREAT ACCESSORIES.

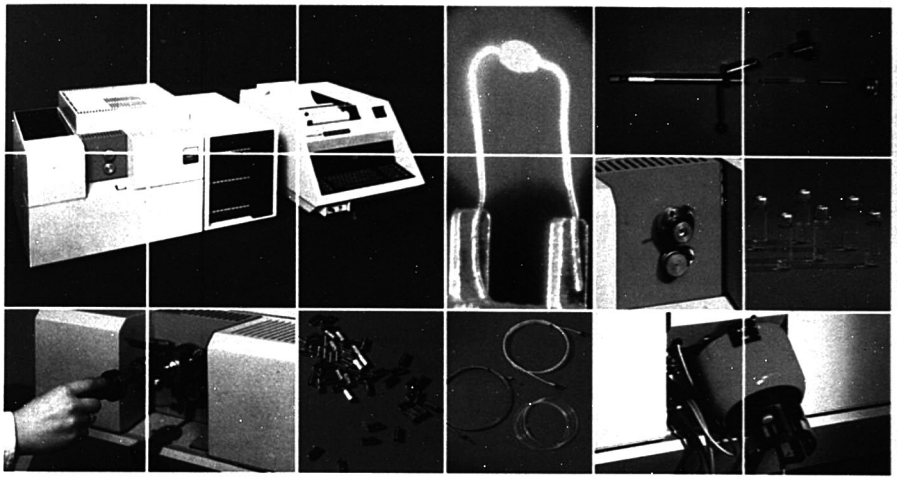

The Perkin-Elmer SIGMA series is your direct route to any analysis possible with gas chromatography.

You start by choosing among four basic instruments to match the sophistication you need. You can include a SIGMA Data Station for handling and automating results. Beyond that, you can draw on an unmatched variety of accessories to tailor your system exactly.

ADVANCED INJECTION METHODS

With our exclusive HS-6 Head Space Sampler, for example, you can convert any SIGMA unit into a new type of analyzer. Head space sampling handles components in the gas phase above the sample, so non-volatile residues won't complicate the analysis.

Other accessories include both manual and automatic heated or unheated gas sampling valves, a pyrolysis injector and an automatic gas analyzer for natural gas or refinery gas samples.

Another exclusive, the MS-41 Sampler, injects solid and solvent-free samples without dependence on the operator's syringe technique. You encase the samples beforehand in small aluminum capsules by a cold welding process. They're protected and ready even if prepared away from the chromatograph or kept in storage.

COLUMN VARIETY AND MORE

In the long list of Perkin-Elmer accessories, you'll find the most complete selection of interchangeable columns – glass and metal, packed and open tubular and SCOT columns – pretested for consistent performance. We have a Septum Swinger that helps end septum bleed contamination. And we offer a variety of column adapters, saturators, valves and splitters.

In addition, you can get five different types of detectors, including ECD, FID, FPD, HWD and a nitrogen/phosphorus detector that's fifty times more sensitive to nitrogen than flame ionization.

ACCESSORIES MAKE THE SYSTEM

Get the GC system you really want – the one that's ideal for you. Our SIGMA GC series opens the way to customizing your system with the most complete line of accessories in the industry. Your Perkin-Elmer representative has all the details. Or write: Perkin-Elmer Corporation, MS-12, Main Avenue, Norwalk, CT 06856.

PERKIN-ELMER

Expanding the world of analytical chemistry.

CIRCLE 174 ON READER SERVICE CARD

New Products

Infrared Spectrometry

Applications Program Package

Search is an applications program package for the company's IR Data Station and is designed to simplify the process of interpretation and identification of IR spectra. The output of the operation is a set of frequencies and transmissions for each peak in the spectrum which yields a list of major functional groups. The next step is a comparison of the unknown spectrum with a library of approximately 2000 spectra, giving the 15 best matches with a maximum confidence rating associated with each one. Perkin-Elmer **419**

Spectrometer

Miran 980 microcomputer-controlled single-beam IR spectrometer for quantitative analysis accepts solid, liquid, or gaseous samples directly without vaporizing, dissolving, or separating them. It can handle mixtures with up to 11 components and provides data reduction with a hardcopy printout of results. Absorbance range of 0–2.0 is displayed digitally in increments of 0.0001. Foxboro Analytical **420**

Spectrometer and Data Processing System

SP 3 series of IR spectrometers is based on the design of a rapid response pyroelectric detector and offers a ratio recording system. It is suitable for qualitative and quantitative studies. The SP 3-100 has a frequency range of 4000–600 cm^{-1}; the other two, SP 3-200 and SP 3-300, cover the range of 4000–200 cm^{-1}. The latter two models offer a Spectraset system of preprogrammed optimized combinations of parameters. The SP 3050 data processing system offers three options which range from conversion of transmittance to absorbance or concentration units, to programmable keyboard control of instrument parameters and formatted data output. Pye Unicam Ltd. **418**

For more information on listed items, circle the appropriate numbers on one of our Readers' Service Cards

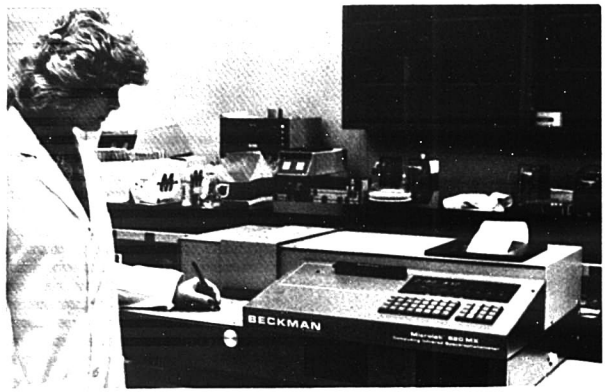

Microlab 620 MX computing infrared spectrometer provides qualitative and quantitative information from the same sample automatically. It comes equipped with automated plug-in software modules called Compusets. Compuset I provides seven basic spectral handling routines, and Compuset II provides the programming to automate the identification of unknowns. A third Compuset stores an unlimited number of quantitative protocols. Communication between the analyst and the instrument is established through the keyboard array which accepts command and numerical data inputs. It is accomplished by a conventional strip chart recorder, a visual display panel, and a digital printer. Price is about $20 000, and related software is about $3000. Beckman **417**

Liquid Chromatography

Integrator

SP 4100 microprocessor-controlled single-channel computing integrator is designed primarily for use with GC or LC. It has BASIC programming capability, X-Y plotting, preprogrammed data reduction methods which include area %, area normalization, external standard, three variations of internal standard, statistics, and linear and nonlinear multilevel calibration. Price is $5975. Spectra-Physics **403**

Injector

Model 7125 syringe-loading sample injector, a version of the Model 7120, requires no flushing between injections in most applications and permits the entire contents of the microsyringe to be loaded into the sample loop. There are eight removable sample loop sizes from 10 μL to 2 mL, and the valve operates at up to 7000 psi. Price is $540. Rheodyne, Inc. **410**

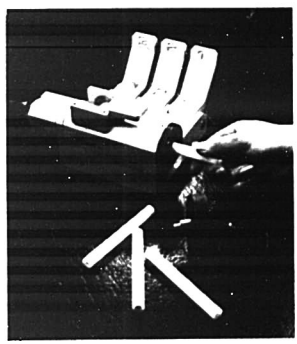

Radial compression separation system consists of a radial compression module (RCM-100) and radial-PAK cartridges. Cartridges are inserted into the module, and three pressurizing levers are depressed in sequence which results in uniform application of hydraulic pressure. The radially compressed cartridge becomes a homogeneous LC bed free of channels and voids. Benefits include efficiency of nominally 5000 plates/10 cm and high flow rates with low back pressures. Waters Associates **402**

BREAK THE GLASS HABIT

Nalgene® PMP Volumetric Flasks are as transparent as glass.

Nalgene® PMP Volumetric Flasks are just as clear as glass. PMP (polymethylpentene) construction gives them the clarity of glass without the breakability.

That makes Nalgene Volumetric Flasks safer than glass to use. When you drop one, it bounces instead of shattering. And the leakproof screw closure is easier to handle than a fragile penny head stopper.

Nalgene Volumetric Flasks are just as accurate as their glass equivalents, too. They're calibrated gravimetrically to guaranteed limits of error and individually marked. Unlike glass, Nalgene Labware is non-wetting, so these flasks deliver the amount of solution measured (TC = TD). Nothing is left on flask walls.

And because Nalgene Volumetric Flasks last longer than glass, you reduce replacement costs.

Put Nalgene Labware to the test, and see why so many laboratories are breaking the glass habit. Send for our current Nalgene Labware catalog, featuring over 250 products for professional use. Write: Nalge Company, Division of Sybron Corporation, Nalgene Labware Department, Box 365, Rochester, N.Y. 14602.

And unbreakable Nalgene Labware lasts longer.

SYBRON | Nalge

CIRCLE 150 ON READER SERVICE CARD

The Commercially Proven THERMO TITRATOR From SANDA

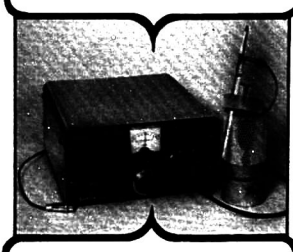

Titrates
50 Times Faster Than Potentiometric
10 Times Faster Than pH

Perfect for Research
due to direct heat curve and derivative capabilities.

Perfect for Quality Control
has one-button start and repeat function.

Provides
Instantaneous Response for Perfect Accuracy. Heat Curve, Derivative, and Automatic Cut-Off. Accurate, Automatic End-Point Detection. Sensitivity Variable from 0.001 to 5 Normal Solution.

Operates
Without Interference in Slurry, Color, Turbidity, or Non-Reactants using one universal probe.

Performs
15 of 21 Possible Functions
All 15 Possible Applications

IT'S AMERICAN MADE

Call or write today for a free, sample titration of your solution.

SANDA, INC.

Manufacturers of Scientific Equipment

4343 East River Drive
Philadelphia, PA 19129
(215) 849-8100

CIRCLE 188 ON READER SERVICE CARD

New Products

Series 3B dual-pump microprocessor-controlled liquid chromatograph is an improved version of the Series 3 solvent delivery module. The chromatograph offers a flow rate range of 0.1–60 mL/min with the two-pump system, and five gradient segments each with a variety of concave, convex, or linear solvent programs. Perkin-Elmer **401**

Chromatograph

Series 2000 liquid chromatograph is a basic isocratic modular unit which can be upgraded with the addition of a dual-pump gradient module and oven. A multiwavelength detector (Model 2020) with 13 selected wavelengths from 254 to 660 nm, or a continuous variable wavelength detector (Model 2040) that operates at 190–400 nm or 390–620 nm is available. Flow rates of 0.1–10 mL/min can be achieved, and the LED readouts monitor 15 operating parameters. Instrumentation Specialties Co. **404**

Detector and Autocontrol Module

Model LC-75 UV detector offers sensitivity of $\pm 5 \times 10^{-4}$ A_{1cm} units and a baseline of 1% noise at 0.01 A_{1cm} full scale at 240 nm. The instrument is permanently calibrated and is insensitive to solvent refractive index, temperature, and flow rate. Model LC-75 autocontrol module features rapid absorbance ratioing, push-button spectral scanning, background correction of mobile phase absorbance effects during gradient operation, and selection of optimum wavelength for each portion of the chromatogram. Perkin-Elmer **405**

Pump

ConstaMetric III metering pump has continuously adjustable flow rates of 0.1–10 mL/min at pressures up to 5000 psi with repeatability of 1.5%. Flow rates can be microprocessor controlled with other equipment. Laboratory Data Control **409**

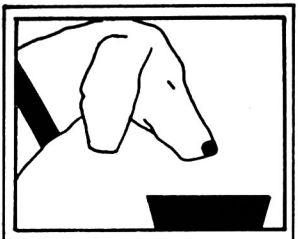

Flavor Chemistry of Animal Foods

ACS Symposium Series No. 67

Roger W. Bullard, *Editor*
U.S. Fish and Wildlife Service

A symposium sponsored by the Division of Agricultural and Food Chemistry of the American Chemical Society.

The recent revolution in animal foods has produced high quality, more palatable foods for domestic pets and food-producing animals. Now research is also being directed toward meeting the needs of threatened wildlife species as well as toward controlling their destruction of human food supplies.

Since animals cannot directly appraise food or food additives, there are many unique problems in animal flavor research that require the cooperation from specialists in many different fields. This volume covers the problems and recent advances in this field. Many domestic and non-domestic animals are discussed by specialists in organic and analytical chemistry, biochemistry, behavior, biology, nutrition, and physiology.

CONTENTS

Animal Flavor Research • Food Preference Behavior • Methodology of Behavioral Testing • Chemical Fractions from Estrus Urine • Bacterial Action and Chemical Signalling • Taste and Smell • Carnivore Taste Systems • Diets for Food-Producing Animals • Palatable Foods for Domestic Pets • Repellents to Protect Crops

175 pages (1978) clothbound $19.00
LC 77-27295 ISBN 0-8412-0404-7

SIS/American Chemical Society
1155 16th St., N.W./Wash., D.C. 20036

Please send _____ copies of *SS 67 Flavor Chemistry of Animal Foods* at $19.00 per copy.

☐ Check enclosed for $ _____ ☐ Bill me.
Postpaid in U.S. and Canada, plus 75 cents elsewhere.

Name _____

Address _____

City _____ State _____ Zip _____

Liquid chromatography news:

The significant HPLC trend for the '80's

Only modular systems provide the flexibility today's HPLC labs demand

After ten years the state of the art in HPLC is still changing rapidly. Individual system components become outmoded by advancing technology. The LDC modular system permits you to upgrade old modules and add new ones selectively and economically.

With the LDC modular system you can be very cost conscious to accommodate a limited budget. Buy just those modules you need this year, and add additional units as the funds become available.

Some of the LDC Modules illustrated l. to r. below:

- Gradient Master $1590
- ConstaMetric III Pump $2690
- Chromatography Accessory Module D $1568
- SpectroMonitor III Variable UV $3890
- ConstaMetric I Pump $2290

Modules not illustrated:

- 3402 Recorder Dual Channel $1492
- 308 Computing Integrator $2890

LDC liquid chromatography

LABORATORY DATA CONTROL
Division of Milton Roy Co.
P.O. Box 10235,
Riviera Beach, Fl. 33404
305/844-5241 telex 513479

European address:
LABORATORY DATA CONTROL
Milton Roy House, High Street
Stone, Staffs., ST15-8AR, England
Telephone 0785-83-3542
telex 36623

CIRCLE 125 ON READER SERVICE CARD

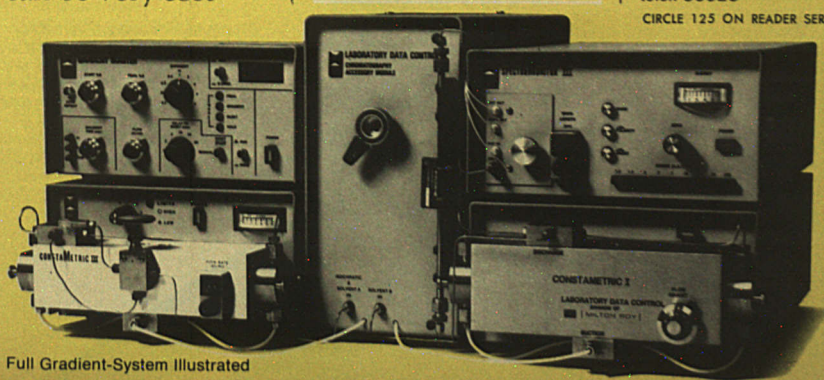

Full Gradient-System Illustrated

For gas chromatography you

For price/performance, versatility and reliability you can't beat the Varian 3700 series. In addition, every 3700 comes with full service and applications support to assure your success.

can't beat the Varian 3700 series

The Varian 3700 series is a family of powerful gas chromatographs that puts the emphasis on performance. On chromatography. On giving you the greatest capability to handle your specific application plus unmatched flexibility to meet changing needs.

You can choose the right gas chromatograph.

The 3700 is modular so you can easily choose a chromatograph that is exactly right for your laboratory. All components —injectors, detectors, temperature programmers, flow controllers and automation systems—are upgradeable and interchangeable. You can begin with a basic dual column unit and add capability as you need it. Or, you can start right now with the world's most powerful, versatile and fully automatic GC system. And the 3700 continues to grow so you can always have the newest and best gas chromatograph.

You have better control of the analysis.

The 3700 controls, with ESP monitor and self-diagnostic display, give you more clear information about operating parameters and better control of injectors, column oven, detectors and flows. You don't have to interrogate the system and wait for a printout. You always know what is going on so you can take timely action.

Large dual-column oven makes it easier to do more.

It gives you more room to install columns side by side. Greater freedom to use any columns your application demands: packed or capillary, single or multiple, with column switching and valving inside the oven.

You can use the best detector for your application.

TCD, FID, ECD, FPD, TSD and multi-detector models are offered. Each of these new detectors is designed to provide excellent performance for its range of applications. See Figures 1, 2, and 3. Universal ionization detector bases let you interchange FID, ECD, FPD, and TSD detectors yourself in minutes.

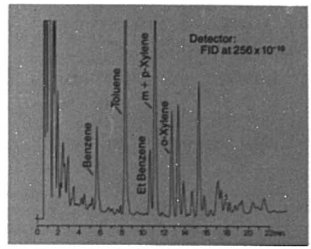

Figure 1. Benzene in Working Environment. The 3700 is widely used in industrial hygiene for detection and quantitation of solvents in the working environment.

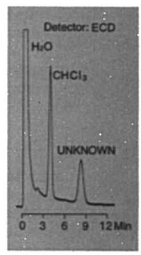

Figure 2. Haloforms in Drinking Water. Analysis of drinking water injected directly onto a porous polymer column. Trihaloforms at ppb levels can be detected with this technique.

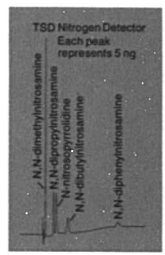

Figure 3. Volatile Nitrosamines. The 3700 equipped with a TSD, which is very selective for nitrogen, is excellent for screening food and cosmetics products for nitrosamines.

You can choose the best injection technique for your sample.

The versatile 3700 injector system permits you to choose: (1) heated or unheated true on-column injection right into the column packing, (2) heated, flash-vaporization with replaceable glass inserts, (3) two all glass capillary injectors with a choice of modes, or (4) valve injection using gas and liquid sampling valves.

You can use all the speed and power of capillary GC.

There are two high resolution, easy-to-use capillary systems to choose from. The new low cost system makes the power of capillary available to everyone. In both systems columns can be installed in minutes without tedious end straightening. A new capillary effluent splitter lets you detect your capillary separation with any two different ionization detectors. See Figure 4.

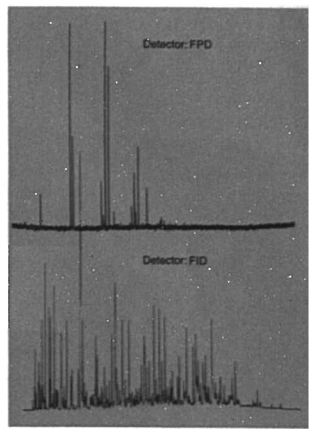

Figure 4. Coal Hydrogenation Product. In the analysis of very complex samples such as this coal hydrogenation product the 3700's capillary system gives high resolution of sample components. The capillary effluent splitter permits detection of the sulfur compounds with the FPD and the organics with FID.

Proven, powerful automation..

For total automation Model 3700 Gas Chromatograph combines with the proven Model 8000 AutoSampler™ and the powerful CDS-111 Chromatography Data System. These components can be purchased and used separately, or they can be combined in many different configurations to meet individual requirements. Result, you can choose the automation you want and you don't have to buy anything that you don't need.

Let us give you detailed information about an unbeatable 3700 system that will do great gas chromatography for you. **Circle Reader Service Numbers: 244** 3700 Series Gas Chromatographs, **245** CDS-111 Chromatography Data System, **246** Model 8000 AutoSampler, **247** Model 3711 Automatic Gas Chromatographs, **248** Have a representative call.

varian

611 Hansen Way, Palo Alto, CA 94303 • Florham Park NJ (201) 822-3700 • Park Ridge, IL (312) 825-7772 • Houston, TX (713) 783-1800 • Los Altos, CA (415) 968-8141

INTRODUCING
the Varian 5000 family of liquid chromatographs

It makes LC responsive and simple

The Varian 5000 Series is a family of powerful microcomputer-CRT-based liquid chromatographs that make LC easy for anyone.

It makes tough separations seem simple. The helpful CRT continuously displays *all* instrument conditions. Tells you everything you need to know, right now. Responds to you. Helps you build programs. Prompts and leads you. Makes LC easier than ever before.

It comes with full support. With your Model 5000 you receive a commitment from Varian to provide strong, continuing support — training, service and applications assistance — that will assure successful solution of your liquid chromatography problems.

Price/performance. There are six basic models in the 5000 Series: from simple isocratic to completely automatic gradient systems. Each is designed to offer unbeatable price/performance; to provide a new level of LC capability at system prices lower than most LC components.

Upward expandability. 5000 Series chromatographs are upward expandable and offer many options. You can configure a 5000 that is exactly right for your laboratory. Later, as your needs change, you can add whatever new capability you require.

For full details on a 5000 that may be exactly right for you, circle Reader Service Number 222.

To have a Varian representative contact you, circle Reader Service Number 223.

varian

free LC News

New! Major Advance In LC Column Technology

A totally new, non-voiding, high efficiency, economical LC separations tool. The Waters Radial Compression Separation System (RCSS) ensures consistent reproducible results.

CIRCLE 230 ON READER SERVICE CARD

New! Low Cost LC Pump

The M-45 is a reliable solvent delivery system for dedicated, routine, or other LC applications.

CIRCLE 231 ON READER SERVICE CARD

New! Model 730 Data Module

A versatile printer plotter integrator designed specifically for high performance liquid chromatography.

CIRCLE 232 ON READER SERVICE CARD

Waters

The Liquid Chromatography People

Waters Associates, Inc.

Maple Street, Milford, MA 01757

(617) 478-2000

New Products

UV/VIS Photometer

The 860 absorbance detector detects chromatographically separated components that absorb light in the 254–546-nm region to 0.002 AUFS sensitivity. The instrument uses optical filters and a stable low-pressure mercury lamp source with a phosphor-coated tip. Under proper measuring conditions, it can detect sample components at pg levels. Du Pont **406**

Data Module

The data module is a printer/plotter integrator which automatically integrates liquid chromatographic peaks and calculates results. It interacts with automatic sample injectors to streamline sample analysis, and minimizes off-scale drifting by automatically rezeroing after each analysis. Waters Associates **407**

Chromatograph

The LC-50 low-pressure liquid chromatograph is designed for columns having an external diameter of 6.35 mm ($\frac{1}{4}$ in.) and a length of 5, 10, or 15 cm. It is specifically developed to take advantage of the properties of Spherosil supports with pressures under 700 psi. The LC-50 is equipped with minimum dead volume fittings, and injection ports are fitted with adjustable needle guides at a predetermined height in the column. Analabs, Inc., Foxboro Analytical **408**

Spectrometers—Miscellaneous

UV/VIS Spectrometer

Model 320 microcomputer-controlled UV/VIS spectrometer incorporates a grating-grating double monochromator. The instrument's resolution is 0.07 nm, and stray light is less than 0.0001% T at 220 nm, providing a photometric range of 4.0 A. It includes as standard, first through fourth derivative, repetitive scanning, wavelength programmer with up to 10 wavelengths, concentration mode, built-in recorder, automatic pen positioning, and large sample compartment. Perkin-Elmer **414**

UV Spectrometer

The UV spectrophotometer uses a variable wavelength detector and is designed for HPLC. It uses a stable air-cooled deuterium source and a dual-beam grating monochromator. Absorbance ranges are adjustable from 0.005 to 2.56 AUFS in 10 steps. Du Pont **415**

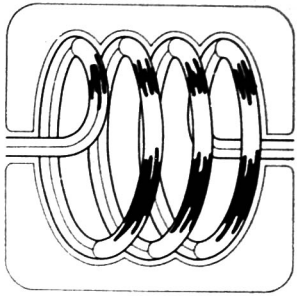

Varian announces training courses in gas chromatography

Schedule for September 1979:

Basic Gas Chromatography
September 12–14, Walnut Creek, CA
Lecture & Lab, 3 days, $225
Lecture only, 2 days, $155

Maintenance of the Gas Chromatograph
September 17–18, Walnut Creek, CA
Lecture & Lab, 2 days, $275

Automatic Gas Chromatography*
September 19–21, Walnut Creek, CA
Lecture & Lab, 3 days, $200

To enroll in courses, please contact the Varian Instrument Division Training Department, 2700 Mitchell Drive, Walnut Creek, CA 94598; Telephone (415) 939-2400, ext. 225.

*One tuition-free course per Model 37111 purchase.

varian

CIRCLE 243 ON READER SERVICE CARD

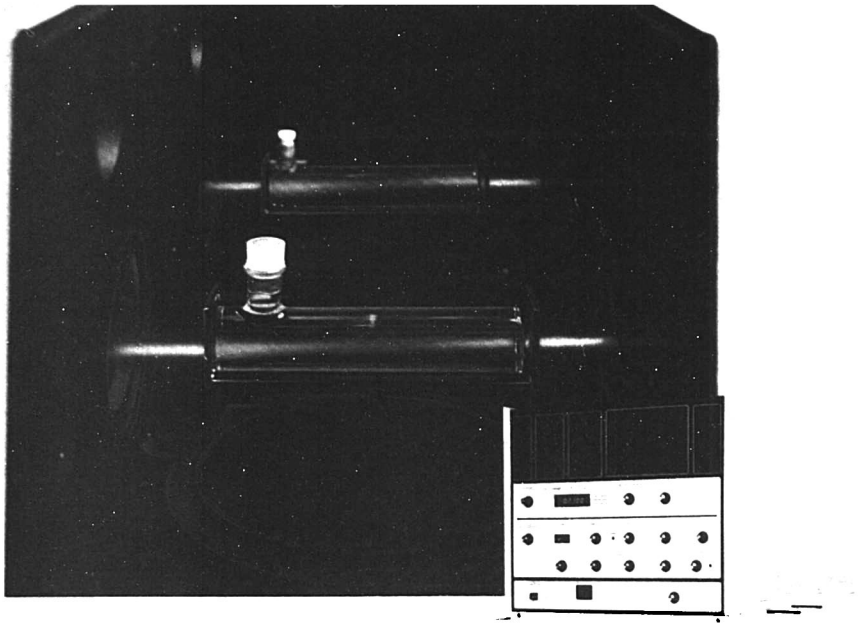

See the light– The new Varian Cary 210 UV-Vis Spectrophotometer... It's surprisingly affordable

For the low introductory price of $11,995*, you can explore new avenues in UV-Vis measurements with the powerful new Varian Cary 210 Spectrophotometer.

See low level enzyme activities
The high signal-to-noise ratio, excellent photometric stability and sensitivity of the Cary 210 allow the measurement of small absorbance changes. Enzyme activity levels as low as 0.0005 Abs per minute can be monitored.

See scattering samples
Low stray light means high absorbances can be measured accurately. The versatile Cary 210 encompasses the complete range from −0.6000 to +4.0000 Abs. Scattering samples can be scanned without the use of special sampling locations or accessories. Highly turbid material need not be diluted.

See microsamples
Cary 210's high energy throughput and patented sample space optics minimize sample volume requirement and permit efficient energy utilization. Measure samples as small as 200 μl directly, and 70 μl with beam masks.

Total sample handling capabilities
Roomy sample compartment can accommodate two five-cell turrets. You can automate measurements with our Cell Programmer and Wavelength Programmer. Monitor more than 300 samples per hour at controlled temperatures with the Routine Sampler. Scan gels up to 20 cm long...and more.

Seeing is believing
Look for the Varian Cary 210 at the upcoming Pittsburgh Conference. See the Cary 210 and complete accessories at work.

Circle **17** for more information on the new Cary 210.
Circle **18** if you would like a representative to call.
Varian Associates, Inc., 611 Hansen Way, D-070, Palo Alto, Ca. 94303

varian

*U.S. only.

Model 650-40 fluorescence spectrometer with microprocessor control has concave gratings which are driven by stepper motors. With a wavelength range of 200–850 nm, the instrument uses a reference photocell in monochromatic light to achieve a ratio recording system. A prescan mode function allows either the excitation or emission monochromator to be scanned at 960 nm/min for automatic location of peak maximum. Perkin-Elmer **412**

AtomComp Spectrometer

Separate sampling and excitation analysis AtomComp spectrometer system uses two excitation sources—electronically controlled waveform source and inductively coupled argon plasma source. The linear dynamic range is 0.007–70%. Jarrell-Ash Div., Fisher Scientific Co. **413**

Thermal Analysis

Thermogravimetric/Differential Thermal Analyzer

TG/STA 780 uses an electronic microbalance to perform simultaneous thermogravimetry and differential thermal analysis of any organic or inorganic substance weighing up to 5 g at temperatures up to 1500 °C. The microbalance may be adjusted from 5 to 500 mg full-scale deflection and from 50 to 500 μV fsd for differential thermal analysis. The analyzer uses a motorized furnace with two crucibles—one for the test sample and the other a reference sample of inert material with anticipated similar heat capacity. Stanton Redcroft, London, England. U.S. agent: Analytical Instrument Co. **428**

Correction

In the January 1979 issue on page 74 A, the Varian MAT 312 mass spectrometry system's guaranteed resolution should have been stated as *greater than* 35 000.

Simultaneous I.C.P.A.E.S. Elemental Analyzer

Designed for routine use, the JY-48 offers rapid analysis of up to 48 elements simultaneously and uses time-proven techniques to enhance reliability and speed.

Will accept two sources. For example: a spark stand plus an Inductively Coupled Plasma source. Use for analysis of ferrous and non-ferrous metals and alloys, oils, industrial effluent, coals, ores and rare earths. Holographic diffraction gratings. Fully computer operated. Also ask about our JY-38 Sequential Plasma Spectroanalyzer.

Instruments SA, Inc., J-Y Optical Systems Division, 173 Essex Avenue, Metuchen, N.J. 08840 (201) 494-8660, Telex 844-516. In Europe, Jobin Yvon, Division d'Instruments SA, 16-18 Rue du Canal, 91160 Longjumeau, France. Tel. 909.34.93 Telex JOBYVON 842-692882.

JOBIN YVON Instruments SA, Inc. J-Y Optical Systems Division

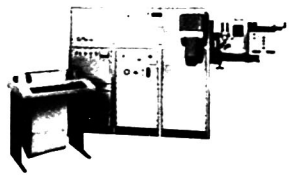

CIRCLE 92 ON READER SERVICE CARD

Raman

SEE THE LIGHT!

The Ramanor HG-2S double monochromator Raman system offers the greatest throughput in the industry, the simplest optical design and the largest, most accessible sample chamber. The Ramanor and its full line of accessories ensures dramatic results.

Call or write for more information on the most advanced Raman system in the world at Instruments SA, Inc.

Instruments SA, Inc., J-Y Optical Systems Division, 173 Essex Avenue, Metuchen, N.J. 08840. (201) 494-8660. Telex 844-516. In Europe, Jobin Yvon, Division d'Instruments SA, 16018 Rue du Canal, 91160 Longjumeau, France. Tel. 909.34.93 Telex JOBYVON 842-692882.

JOBIN YVON Instruments SA, Inc. J-Y Optical Systems Division

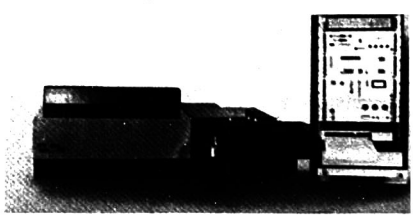

CIRCLE 93 ON READER SERVICE CARD

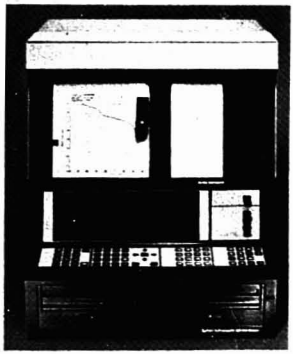

The 1090 thermal analysis/data system consists of the 1090 thermal analyzer, 1091 disk memory, and 1092 data analyzer. The heart of the 1090 system is a versatile programmer/recorder with an alphanumeric keyboard, printer plotter, and a plasma display panel for operator-instrument dialogue. Sample temperature can be displayed linearly in 0.2 °C increments over the operational range of −190 to 1600 °C. The 8 million bit memory of the 1091 system retains all experimental data at maximum sensitivity regardless of recorder settings. The 1092 data analyzer allows selection with precise control of any portion of a thermogram to be analyzed. Du Pont **427**

Atomic Absorption

Autosampler

AS-40 microcomputer-controlled autosampler for furnace atomic absorption is designed for use with the company's HGA-500 or HGA-400 heated graphite furnaces. Two versions of the AS-40 are offered. The AS-40 presents up to 35 samples to the instrument for analysis and activates the read cycle of instruments. Sample volume is variable from 5 to 95 μL. It features the additions method using two procedures and matrix modification. Perkin-Elmer **422**

Graphite Furnace

HGA-400 microprocessor-controlled heated graphite furnace can increase temperature from ambient to 3000 °C displayed to the nearest 10 °C in either ramp or step increases. It is equipped with a time indicator display indicating time remaining in each step, with a working program consisting of up to eight steps. Operator warnings include an alarm for insufficient cooling and a tube break alarm. Perkin-Elmer **423**

The SP 9 atomic absorption system includes a microprocessor data handler, a video furnace programmer, and automatic sample handling system. The microprocessor provides for curve correction using up to five standards in fixed or variable ratios, calculations of peak height or peak area, and running mean mode, and over-calibration and excess curvature warnings. The furnace programmer uses electrothermal atomization and has built-in autosampler controls. Up to 10 complete furnace programs can be stored, each comprising six phases of up to 3000 °C. A rotating lamp turret with individually powered lamps allows for four elements to be analyzed. Pye Unicam Ltd. **421**

Gas Chromatography–Mass Spectrometry

Accessories

The accessories for DP-1 mass spectrometers are an automatic analysis unit, DP-1 printer/plotter, flame ionization detector (FID), DP-1 nine-track tape unit, and turbomolecular pumps. The automatic analysis unit consists of a computer-controlled 60-station autosampler, a chromatograph door-opener, and associated hardware and software. The DP-1 printer/plotter produces single- or multiple-data copies. The FID detects GC peaks independently. Du Pont **425**

GC Septa

High-temperature low-bleed septa range in diameters from 0.25 to 0.50 in. and are made of siliconized rubber with Teflon backing. Low-bleed characteristics of 2×10^{-12} amps after multiple puncturing at 300 °C without irregular baseline shifts have been demonstrated. Hamilton Co. **426**

Model 5985 B GC/MS can include an optional negative chemical ionization (NCI) mode to increase sensitivity levels from 100 to 500 times greater than in the positive chemical ionization (PCI) mode. Mass range is 10–1000 amu, and PCI sensitivity is to pg levels. The basic HP 5985 B with a 20-megabyte disc and system console is priced at $122 900. The NCI option is priced at $5500. Hewlett-Packard Co. **424**

Varian UV-Vis spectrophotometers for every need.

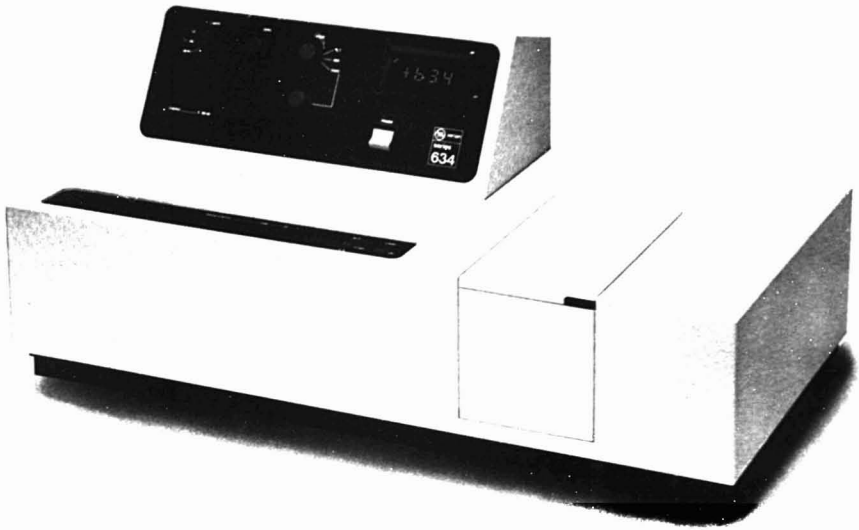

Choose Varian's UV-Vis spectrophotometer ...join thousands of happy users.

The Series 634 Spectrophotometers offer outstanding value in low-priced instruments. Take a look at their versatility. Thousands have chosen to buy Series 634 over all competitors.

Digital readout. This is standard on both instruments for all three operating modes: absorbance, transmission, and concentration. And there's automatic decimal positioning in the absorbance and %T modes.

Versatile wavelength ranges. Series 634 covers the 190 to 900-nm range—unsurpassed in low-priced instruments. Choose the model that fits your needs and budget. *All* Series 634 spectrophotometers measure up to 900 nm so you can do those important analyses at higher wavelengths.

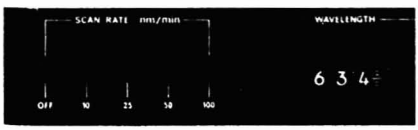

Choice of wavelength scanning. Both manual and automatic scanning are available. Automatic scanning is simple with pushbutton selection of four speeds. Automatic scanning is standard on the Model 634S and an integral part of the instrument.

Recorder compatibility. Unlike some spectrophotometers, Series 634 is compatible with standard laboratory recorders that can also be used with other instruments. You're not locked in to a one-use recorder, an important feature for the budget-limited lab. And when it comes to a fine, all-round recorder to do best by your Series 634, Varian has that, too.

Sample compartment versatility. The key is size. The extra large compartment lets you handle a wide range of sample accessories of different sizes and shapes. Three sided access plus a large beam separation make it easy to use. With Series 634 you can measure many samples that other low-priced instruments can't handle.

These are just a few highlights of this versatile, low-priced spectrophotometer. We haven't even touched on its outstanding performance, so you'll want to know more.

Circle **220** for a Series 634 data package.

Circle **221** if you'd like to see a representative.

varian

Varian Instrument Division, 611 Hansen Way, Box D-070, Palo Alto, California 94303

Tape Recordings for Lab Professionals

☐ **TLC—Best for Drug Abuse Screening**
Low-cost alternative to immunoassays

☐ **Microcomputers in Biochemistry Research**
New computers make possible hitherto impossible measurements

☐ **Data Analysis in the Lab**
Today and tomorrow in chem lab data analysis methods

☐ **Use of Enzymes in Immunology**
Detection of bound and free antigen without separation

☐ **Elemental Analysis of Blood: Cancer Patients & Controls**
Detailed comparisons, plus evaluation of analytical methods used

☐ **Polarographic Analysis in Drug Development**
D.P.P. assays of drugs in biological fluids

☐ **Bioanalysis with Membrane Electrode Probes**
Recent advances in electrode development

☐ **In Vivo Electrochemistry for Monitoring Drugs**
Reveals drug's chemical fate in the brain

☐ **Detection of Lipids & Amines in Biological Samples**
Chemical ionization mass spec speeds assay of closely related chemicals

☐ **Pulse Polarography Analysis in Environmental Toxicology**
Solves tough problems in human and animal poisoning

☐ **New Developments in Measurement of Proteins**
Light scattering of immune complexes provides a specific method for proteins in body fluids

☐ **Direct Determination of Drugs in Plasma & Urine**
Non-chromatographic procedure uses chemical ionization mass spec & stable isotope labeling

☐ **DSC: New Developments in Clinical Analysis**
Differential Scanning Calorimetry—a new analytical tool

☐ **Cannabinoids by GLC and HPLC**
Very low levels can be detected in plasma

☐ **Enthalpimetric Analysis of Immunological Reactions**
Thermometric enthalpy titration may revolutionize serological analysis

☐ **Clinical Application of Titration Calorimetry**
Thermochemical methods look very promising for clinical work

☐ **GC Determination of Apomorphine in Urine**
Study of apomorphine metabolism

☐ **Metals in Liver & Kidney Tissue by AA**
AA determination of copper, zinc, magnesium, and calcium

☐ **Ultra-Trace Analysis of Metals in Biological Systems**
Review and appraisal of the most widely used methods

☐ **Drug Analysis by Direct Multiple-Ion Detection**
Unique computerized system analyses drugs without use of GC

☐ **THC in Urine by (PBM) GC-MS**
Simple, quick, positive method

☐ **Amperometric Measurement of Enzyme Reactions**
Enzyme reactions are monitored by amperometric measurement of substrate depletion, product formation

☐ **THC in Serum Using TLC and Fluorometry**
Results compare favorably with GC-MS data

☐ **Kinetic Assay of Enzyme Activity**
Centrifugal fast analyzer provides data at output rate suitable for direct input into small computer

☐ **RIA of Cannabinoid Compounds**
Many problems of RIA method solved

☐ **Automation in Clinical Medicine**
A Bureau of Standards colloquium

☐ **Analysis of Trace Elements**
Sensitive, reliable analytical methods are needed for trace elements

☐ **Electrochemical Approaches to Clinical Instrumentation**
Precise, accurate, highly specific analyses using ultramicro samples

☐ **Standardization of Protein & Enzyme Assays**
Biuret reaction as standard for measuring total serum protein

☐ **Pharmacologic Studies Using GC-MS**
Utility of GC-MS is emphasized in a report of two pharmacologic studies

☐ **Method Evaluation Studies in Clinical Analyses**
Method evaluation studies on precision and accuracy of lab methods

ORDER FROM:
American Chemical Society
1155 16th St., N.W.
Washington, D.C. 20036
ATTN: Dept. AP

PRICE: $11.95 per title, includes visual materials. **CASSETTES ONLY** **CHECK TITLES DESIRED**
(Allow 4 to 6 weeks for delivery)

Name _____

Address _____

New from Varian...
Low cost, microcomputerized AA-475 and AA-275

The pacesetters in atomic absorption

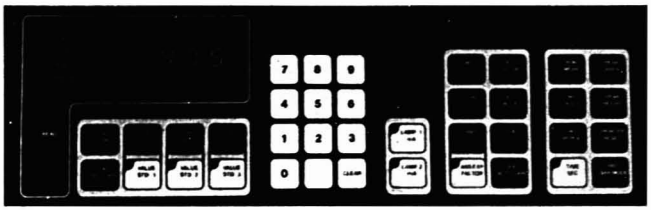

Routine AA analysis has never been this easy, this sensitive, this economical. The AA-475 and AA-275 fully exploit their powerful 8-bit, 10K microcomputers to give you high quality data quickly and simply.

The AA-475 and AA-275 are designed with the novice operator in mind. Prompts on the interactive instrument panel provide step-by-step guidance through set-up and calibration procedures. Operator errors are identified and flagged. Ten vital flame functions are monitored continuously for programmed ignition and safe shutdown.

Computerized signal processing gives you reliable data every time. Varian's unique Rational Method allows rapid, accurate calibration, with a reslope function for recalibration against a single standard. The running mean mode simplifies data collection.

Totally versatile, the AA-475 and AA-275 adapt readily to your requirements. Select from the single beam AA-275 or the double beam AA-475. Customize your system with powerful Varian AA accessories such as the CRA-90 carbon rod atomizer, automatic sample changers for flame and furnace, and programmable calculators. The new M-65 Vapor Generation Accessory greatly simplifies hydride analyses, bringing new levels of convenience and throughput.

There is no compromise in performance. The low cost AA-475 and AA-275 provide a sensitivity level that matches or exceeds that of competitive models at twice the price.

Find out more about the AA-475 and AA-275 today. Circle **235** for product literature. Circle **236** if you wish a representative to call. Or write: Varian Associates, Inc., 611 Hansen Way, D-070-2, Palo Alto, CA 94303.

SEE US AT THE PITTSBURGH CONFERENCE.

varian

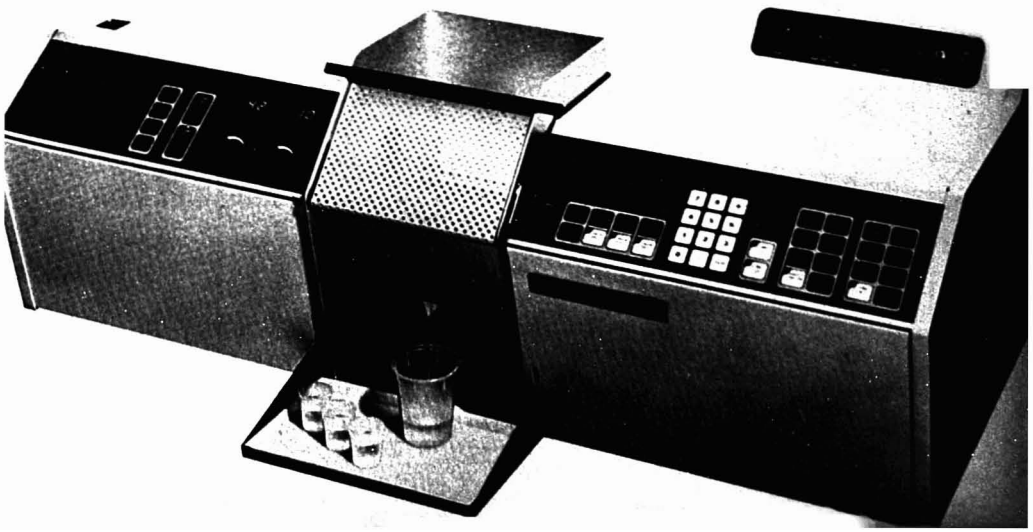

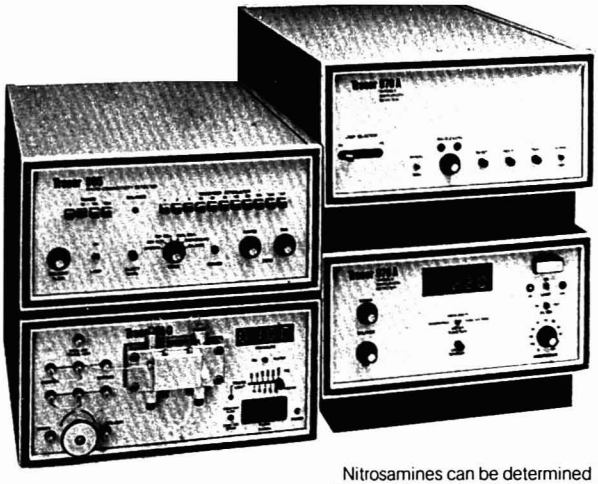

The Series 900 Liquid Chromatograph by Tracor is the most dynamic liquid chromatograph available today. The Series 900 features Tracor's patent pending 965 Photo-Conductivity detector. This unique detector features unusually high sensitivity and selectivity for compounds which contain chlorine, nitrogen and some sulfur compounds. Two chromatograms of polychlorinated biphenyls are shown using the 965 Photo-Conductivity Detector. This mixture gives no response at 254 nm on a UV absorbance detector. Isochratic runs using the same solvent mixture allow for the determination of the different PCB mixtures by the different peak ratios.

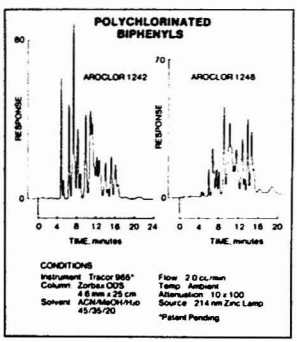

Nitrosamines can be determined at the residue level with the use of the Tracor 965 Photo-Conductivity Detector. Two nitrosamine mixtures, 10 ng and 5 ng respectively, are shown using an isochratic solvent mixture.

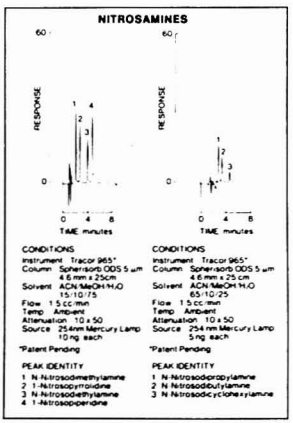

With the use of a dual pen recorder, the output of the Tracor 970A variable wavelength detector and the Tracor 965 Photo-Conductivity Detector can be recorded using the detectors in series. A chromatogram containing several polynuclear hydrocarbons and two chlorinated pesticides shows the selectivity of chlorinated pesticides over hydrocarbons on the Tracor 965 Photo-Conductivity Detector. The UV absorbance detector responds to the polynuclear hydrocarbons and gives no response to the pesticides. The effluent from the variable wavelength detector is passed to the Photo-Conductivity Detector with very little band spreading where the pesticides are detected. (Recycling of the solvent mixture for continuous use of an isocratic solvent mixture is recommended for the Photo-Conductivity Detector. This recycling is possible with the use of an ion-exchange cartridge in the system before the high pressure pump.)

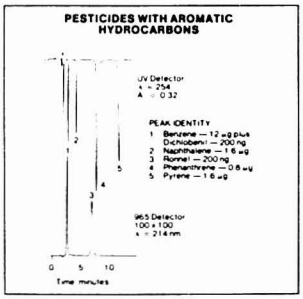

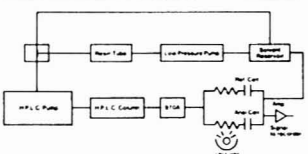

Liquid Chromatography by Tracor

Tracor Instruments

Tracor, Inc. 6500 Tracor Lane Austin, Texas 78721 Telephone 512:926 2800 TELEX 77-6414

CIRCLE 202 ON READER SERVICE CARD

Manufacturers' Literature

Enzyme Measurements by UV-VIS Spectrometry. Application report (OPT-2223) discusses various types of enzyme determinations including multiple sampling, automatic determination of net reaction rates, and small sample volume applications. 16 pp. Varian **432**

Coal Analysis. An application study compares classical methods of CHN coal analysis with results obtained with Model 240B elemental analyzer. A discussion of sample preparation, coal makeup, and determination of the calorific value of coal is included. 10 pp. Perkin-Elmer **433**

Emission Applications. Two application reports are available. Report no. 3/77E (14 pp) deals with the application of optical emission spectrochemical analysis to multicomponent high concentration alloys; report no. 2/78E (3 pp) demonstrates the precision and accuracy obtained in analyzing 310-type stainless steel. Jarrell-Ash Division, Fisher Scientific Co. **434**

Chromatography Notes. The March 1979 issue includes discussion on the determination of nitrosamines at ppb levels, sample preparation for the analysis of PCB's in water, prevention in ensuring reproducible chromatography, and chromatography with optimum column hardware. Also discussed are recycle chromatography and the use of GPC and μBondapak for syncrude characterization. 8 pp. Waters Associates **435**

Background Correctors for AA. What background correction is, how it works, when it is needed, and applications are described. The various background correction systems available from the company are illustrated. 4 pp. Perkin-Elmer **436**

Liquid Chromatography for the Gas Chromatographer. The history of liquid chromatography and a comparison between GC and LC, with a chapter on operating conditions, are discussed extensively. Tables, diagrams, formulas, and a series of typical chromatograms are provided. Clarification of the term HPLC is provided also. 11 pp. Gow-Mac Instrument Co. **438**

HPLC Columns and Packings. Performance and quality criteria, column selection and configuration, column kits and parts, and the various columns available are all illustrated and discussed. 20 pp. Du Pont **437**

LC Column Selection Guide. The guide is a computer-based system that draws on the technical data base of the company's LC Bibliography Update program. Examples of how the selection guide can be used for decision making in solving LC problems are included in the guide. 2 pp. Perkin-Elmer **439**

Ion-Selective Electrodes. Four classes of electrodes are discussed along with their performance characteristics. Gas sensing, solid state, solid matrix, and reference and pH electrodes are included. 12 pp. HNU Systems Inc. **440**

LC Reports and Column Brief. Two liquid chromatography reports, one on the concepts and practice of bimodal size exclusion chromatography (HPSEC) (5 pp) and the other on getting better performance from HPLC systems (5 pp), are available. The LC column brief (3 pp) discusses HPSEC columns. Du Pont **441**

LC Bibliography Update. The bibliography includes applications in biochemistry, clinical and forensic chemistry, environmental analysis, food/beverage/natural products/agriculture, pharmaceutical/cosmetic analysis, and polymers/organic coatings, petroleum/energy research. Subscription information is available. 6 pp. Perkin-Elmer **442**

Inductively Coupled Plasma System. Model 34 000 ICP spectrometer system and accessories are described and illustrated in three separate brochures (3, 3, and 7 pp). ARL, Div. of Bausch & Lomb **443**

Field Identification of Arson Accelerants. A manual provides a procedure for the field identification of accelerants using the Model 511 GC. Identification of solvents such as kerosine, ketone-aromatic mixes, gasoline, thinners, and alcohols is illustrated. 41 pp. Analytical Instrument Development, Inc. **455**

UV/VIS Spectrometer. Model 35 features a wavelength range of 335–825 nm with stray light better than 0.1% *T* at 340 nm, and digital readout in concentration, absorbance, or % *T*. 3 pp. Perkin-Elmer **444**

Amino Acid Analysis of Collagen. A data sheet reviews the structure of collagen molecules and presents analytical procedures for determining the amino acid content of collagenous materials on the Model 121 amino acid analyzer. 5 pp. Beckman **445**

Energy-Dispersive Spectrometry Accessory. A data sheet on the Quan-1 and Quan-2 accessory for the EEDS-II energy-dispersive spectrometer, which describes the hardware memory, mass storage devices and printer, and software, is available. EG&G Ortec **446**

Sampler Systems. Two routine sampler systems for the Cary 219 spectrometer are available. 4 pp. Varian **447**

Graphite Furnace. Microprocessor-controlled HGA-500 graphite furnace for flameless AA spectrometry is described. Automated features, programmable controls, and suggested applications are presented. 16 pp. Perkin-Elmer **448**

ICP Monochromator. Scanning monochromator 35 000 C ICP is a sequential liquid analyzer which is automatic and equipped with an ICP excitation source. The working and measuring principles, applications, computer system, and analysis information are detailed in a brochure. 10 pp. ARL, Div. of Bausch & Lomb **449**

Electron Excitation Software. X-Ray tech note on the PGT-1000 LIFT (least-squares iterative fitting technique) analysis program is available. LIFT is used for background removal, peak deconvolution, and correction of SEM spectra. 4 pp. Princeton Gamma-Tech **451**

For more information on listed items, circle the appropriate numbers on one of our Readers' Service Cards

---

Process Control Instruments. Analyzers for TOC, TC, and TOD measurement in process control and laboratory analysis are described. 4 pp. Ionics Inc. **450**

GC Capillary Columns. Column selection includes Micro-Scot columns, and accessories offered are split and splitless injector kits and Teflon tubing for connecting capillary columns. 8 pp. L. C. Co., Inc. **452**

Carrier Gas. S-Gas, when used as the carrier gas in the chromatographic analysis of sulfur gases such as H_2S, SO_2, and COS, deactivates the reactive components in the gas transport system. 2 pp. Matheson **453**

Catalogs

Labware. Included in addition to the disposable products are separation membranes for dialysis and ultrafiltration. 64 pp. Spectrum Medical Industries, Inc. **460**

Chromatography Products. The 1979 edition covers over 1500 chromatography products as well as detailed procedures, literature references, and sample chromatograms. Regis Chemical Co. **461**

Lab Essentials. Quarterly publication (Winter 1979) includes recorders, temperature controllers, educational materials, and other useful lab items. 32 pp. Beckman **462**

Clinical Reagents. Diagnostic reagent and kits, specialty chemicals, an instrument application guide, and a list of technical literature are included in the 1979–80 edition. 41 pp. Pierce Chemical Co. **463**

Temperature Baths and Circulators. Equipment ranges from polypropylene baths to controlled temperature stainless steel units. Science/Electronics, Inc. **464**

Tube Fittings. Teflon PFA tube fittings are now available in $^1/_{16}$-in. o.d. size as well as $^1/_8$, $^1/_4$, $^1/_2$, and $^3/_8$ in. Fluoroware, Inc. **465**

TLC Products. Included are tanks, spotting guides, pipets, and HPTLC precoated plates in normal and reversed phase. 15 pp. V-tech Corp. **466**

Plasticware. The Spring 1979 catalog is available. 52 pp. Cole-Parmer Instrument Co. **467**

Radiochemicals. Labeled compounds, stable isotopes, radionuclides, radiation instruments, and accessories are included in the 1979–80 edition. ICN Chemical & Radioisotope Div. **468**

Organic Chemicals. The 1979 catalog lists over 500 organic chemicals that include benzotrifluoride derivatives, aromatic fluorine compounds, silylation reagents, and siloxanes. Marshallton Research Laboratories, Inc. **469**

Plasticware. Special edition catalog is available. 43 pp. Markson Science Inc. **470**

Biochemicals. Chromatography products, biochemicals, and laboratory accessories are included. ICN Nutritional Biochemicals Div. **471**

Parker CPI Single Ferrule Fittings: Why Fewer Places To Seal And Fewer Parts To Assemble Give You More In A Tube Fitting.

Parker single ferrule fittings have only three pieces. Fewer surfaces to seal and fewer parts to assemble. It's a simple design that keeps your system secure. *That's* reliability!

You get other advantages too. Low torque assembly. Available off-the-shelf in 316 stainless steel, brass, steel, aluminum and monel. Other materials on request. Heat Code Traceability. All configurations from 1/16" to 1".

There really is a difference in tube fittings. Ask your local Parker CPI Distributor or write to the Instrumentation Connectors Division, Parker Hannifin Corporation, 9400 S. Memorial Parkway, Huntsville, AL 35802.

Parker FluidConnectors

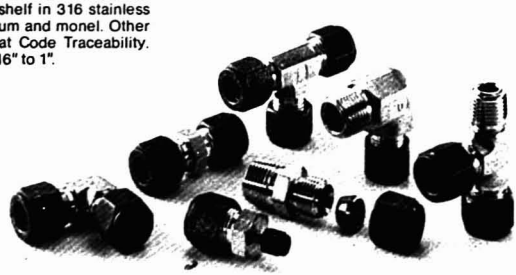

CIRCLE 172 ON READER SERVICE CARD

Capillary Chromatography Catalog

The most complete
up-to-date
capillary catalog available;
totally dedicated to capillary columns and accessories
. . . Request yours today . . .

ALLTECH GC²

CAPILLARY CHROMATOGRAPHY

ALLTECH ASSOCIATES
202 CAMPUS DRIVE · ARLINGTON HEIGHTS, ILLINOIS 60004 · 312-392-2670

CIRCLE 4 ON READER SERVICE CARD

Parker CPI Ball Valves

Features:

- True ball valve design.
- Pressure compensated ball / low torque.
- C_V ranges from .8 to 1.4.
- Pressure range to 5000 psig.
- Temperature range: −65° to +350°F
- Available in brass or 316 stainless steel (Heat Code Traceable) in popular sizes and end configurations.

Ask for Catalog #4250 from your local CPI Distributor or write to the Instrumentation Connectors Division, Parker Hannifin Corporation, 9400 S. Memorial Parkway, Huntsville, AL 35802

Parker
FluidConnectors

CIRCLE 173 ON READER SERVICE CARD

The quick and easy way to precise density measurement.

Measure solid concentrations, density, or specific gravity of your process liquids and gases with the Paar DMA55 density meter to assure consistent product quality. Small 0.7 ml samples from the process are injected, pumped, vacuum-suctioned or continuously flowed into the sample tube. In less than a second, the instrument calculates and displays a 5-place digital result on the readout. This can be automatically transferred to other instruments. The method is fast, simple and accurate. No need for separate temperature, weight or volume measurements. No pycnometer filling. Circle the number for full details. Mettler Instrument Corporation, Box 71, Hightstown, NJ 08520.

Mettler

Electronic balances and weighing systems
Thermal analysis instruments
Titration instruments
Automated laboratory systems

CIRCLE 145 ON READER SERVICE CARD

You've always been able to depend on us for products to do your analyses.

Now you can depend on us for proof of your analyses.

As an analyst engaged in a variety of analytical techniques, it is quite likely you know our reputation as a reliable source for high purity analytical graphite laboratory products as well as for an infinite variety of custom-designed graphite products. But here's something you may not know: Ultra Carbon is now a U.S. supplier of Johnson Matthey high purity chemicals for analytical applications. This means you now have a single source for many of the high purity products and materials you depend on; from graphite to nearly 400 purpose-made materials for analytical applications. The Johnson Matthey line of SPECPURE Materials of Defined Analysis, for example. They include over 300 high purity substances covering 73 elements suitable for preparation of both solid and solution reference materials for use in instrumental and wet chemical analyses.

ULTRA CARBON

the graphite specialists

The SPECPURE range is acclaimed worldwide as the most reliable collection of products available for these applications. The specifications of every product within the SPECPURE range relates to the maximum total metallic impurities detected when analyzed primarily by emission spectroscopy. Additional information is available by a request on your letterhead. Write Ultra Carbon Corporation, P.O. Box 747, Bay City, Michigan 48707.

SPECPURE is a registered trademark of Johnson Matthey Chemicals Limited.

CIRCLE 212 ON READER SERVICE CARD

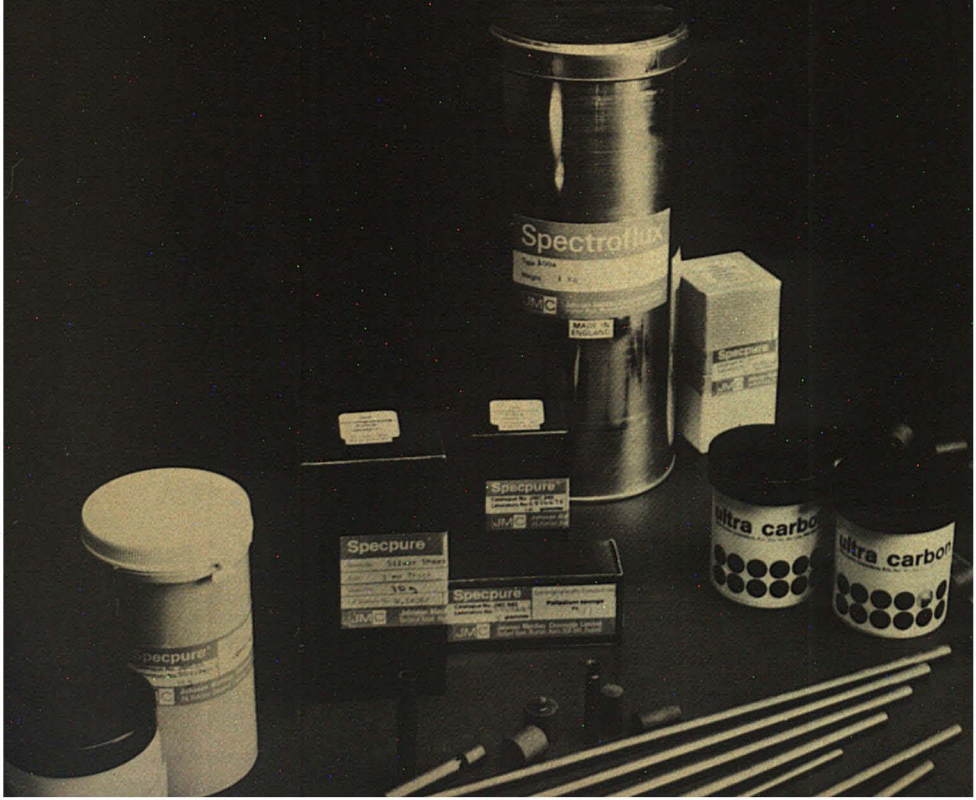

FROM SHIMADZU

Shimadzu, one of the largest and oldest manufacturers of gas chromatographs in the world, offers a new line of unique gas chromatograph systems featuring the utmost in accuracy, versatility, speed, performances, and efficiency at a price anyone can afford. All Shimadzu GC use the latest technologies to ensure simple maintenance and maximum reliability. When you think of GC, think of Shimadzu.

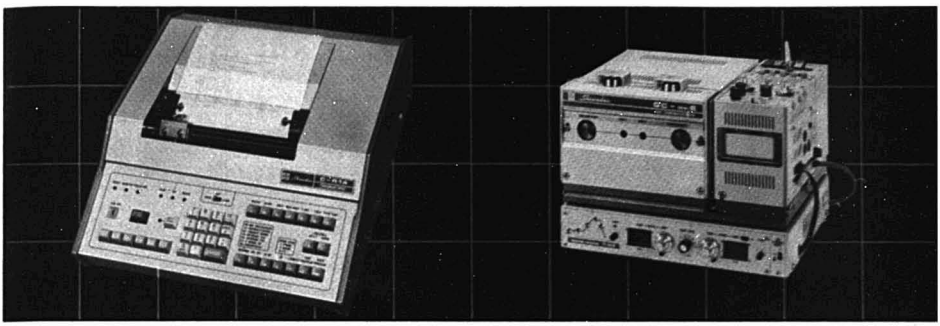

Chromatopac C-R1A Recording Data Processor

Other chromatograph data processors can calculate common standard calculation routines such as area normalization, normalization with response factors, external standardization and internal standardization, but only the C-R1A goes a step further and calculates calorific value, steam pressure, liquid specific gravity, deviation from a standard value, mole density (%)—weight density (%), and other factors from the results of these calculations.

Other outstanding features of the C-R1A include a thermal printer plotter for chromatograms and data recording, recording of the names of components, recording of up to 339 peaks, measurement of peak-top height or average height, all-new grouping function, and self-diagnostic function. These features not only ensure fast, precise analysis, but also free the chromatographer from troublesome, time-consuming manual calculations for more important work.

GC-MINI 2 Gas Chromatograph

This surprisingly light weight, compact GC system has the performances of much larger more expensive systems. Dual column flow and on-column/on-detector system ensure excellent stability, high sensitivity, and perfect accuracy. Flow rates and pressures of the gases can be easily measured using one-touch connectors and flow monitors in the gas flow lines.

Unique oven temperature control system maintains the oven at room temperature, even when the injection port temperature is high. Contamination-free flame ionization detector exhausts the vapor from the flame directly from the jet to a cylindrical ion collector and vent at the top.

GC-MINI 2 easily disassembles into four main modules—column oven, injection port/detector, flow control unit, and electric control unit—for quick, easy maintenance. The electric control unit further disassembles into six sub-units, thus simplifying maintenance still further.

GC-7AG Series Ghost-Cut Gas Chromatograph

Add the GC-7AG and GC-6AM and you have a complete system capable of meeting your ever changing GC needs.

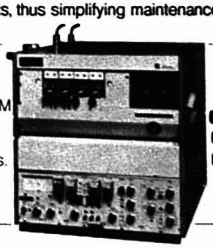

GC-6AM Series Cartridge Gas Chromatograph

• Write today for more information on these and other Shimadzu labor and cost saving instruments.

SHIMADZU SCIENTIFIC INSTRUMENTS, INC.

SHIMADZU SCIENTIFIC INSTRUMENTS, INC.
9147 Red Branch Road, Columbia, Md. 21045, U.S.A. Phone (301)997-1227 Telex 87969

SHIMADZU (EUROPA) GmbH
4-KX1 Duisburger Str. 1, D-Pfalzdorf, Meyer Str. 1 F.R. Germany Phone (0211)314061 Telex 08586830

SHIMADZU SEISAKUSHO LTD.
1 Nishinokyo-Kuwabaracho, Nakagyo-ku, Kyoto 604 Japan Telex 05422-166

CIRCLE 194 ON READER SERVICE CARD

MCI Automatic Trace Metal Analyzer. Reliable, Fast and Easy.

Utilizes ASV method to simultaneously measure concentrations of 5 different trace heavy metals. Ultra-high sensitivity and automatic sample feed/discharge measuring cell assures fast, precise results. Reproducibility is 3-to-20%. Range: 0.1 PPB—50PPM.

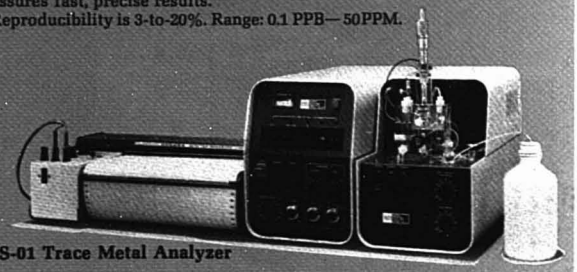

AS-01 Trace Metal Analyzer

MITSUBISHI CHEMICAL INDUSTRIES LIMITED
Instruments Dept., Mitsubishi Bldg., 5-2, Marunouchi 2-chome, Chiyoda-ku, Tokyo, 100 Japan Telex: J24901 Cable Address: KASEICO TOKYO

CIRCLE 160 ON READER SERVICE CARD

ACID DIGESTION BOMBS

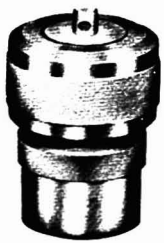

Parr

The rapid and safe way to dissolve inorganic samples in HF, HCl or HNO_3, or to digest organic materials in strong alkalis or oxidizing acids with complete sample recovery.

Now available in two models: a **general purpose bomb** for temperatures to 150° C and pressures to 1200 psig, and a new **high pressure bomb** for samples which require dissolution temperatures up to 285° C and pressures to 5000 psig.

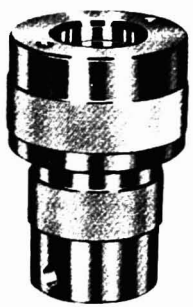

Both have removable, 25 ml Teflon cups with convenient closures, long-taper seals and other exclusive Parr features. For details, write or phone: Parr Instrument Co., Moline, Ill. 61265. Telephone 309/762-7716

CIRCLE 171 ON READER SERVICE CARD

The New...

NEC

EXAC™ 5000 Computer-Based Energy Dispersive XRF Systems

Built to perform reliably in the toughest industrial environments ... and to satisfy demanding research requirements

- Unique, down-looking, detector – x-ray tube geometry
  - analyze fragile briquettes, powders, and liquids conveniently, precisely, and without danger of system contamination
  - high-angle, detector x-ray tube geometry maximizes analytical sensitivity
- Uniquely flexible, computer-based system
  - complete library of qualitative (QUALEX™) and quantitative (EXAC) analysis programs
  - the system can be programmed to suit individual user requirements in NEC BASIC II (The Spectroscopy Language of Today)
- Computer controlled "Intelligent" sample changer maximizes throughput

Nuclear Equipment Corporation
963 Industrial Road
San Carlos, California 94070
Phone: (415) 591-8203

79/04

CIRCLE 154 ON READER SERVICE CARD

Training Aid on HPLC

High Performance Liquid Chromatography. J. H. Knox, Ed. vii + 205 pages. Edinburgh University Press, 22 George Square, Edinburgh EH8 9LF, England. 1978. £5

Reviewed by J. J. DeStefano, Du Pont Experimental Station, Bldg. 334, Wilmington, Del. 19898

As the analytical technique of high-performance liquid chromatography grows in popularity so, too, grows the library of texts dealing with the subject. This latest text resulted from a series of lectures and seminars presented by the authors during 1977. The book is a reasonably up-to-date, well-organized, concise treatment of the various modes of liquid chromatography and attendant subjects. Each mode of chromatography (e.g., liquid-solid adsorption chromatography) is discussed in terms of mechanisms of separation, good operating practices, lists of the more popular packings used for the technique, and selected applications. Each chapter contains references to pertinent literature articles. These references are not and were not intended to be a comprehensive review of the published literature but are more than adequate to provide the reader with sources for additional study.

Other chapters deal with HPLC columns and how to pack and test them, selection criteria for equipment, and illustrative experiments demonstrating several basic features of LC practice (e.g., effect of dead volume on separation efficiency). An appendix summarizing many of the important properties of chromatographic solvents is especially useful.

Since this book is based on a series of lectures, one would expect it to be a good teaching text. In this respect, the book is a moderate success. Its coverage of the theory, practice, and principles of HPLC, while too brief and simplified to be considered complete, does provide a good basis for learning about the technique. Most of the terms and parameters used in HPLC are clearly defined early in the text. The applications and diagrams appear well chosen for their instructive values. The inclusion of lab experiments is useful for their training aspects. There appears to be little information that would be new to the more experienced practicing chromatographer. However, the book should be highly beneficial to new and less experienced workers.

Apparently to keep the price of this book low, the text was reproduced on relatively low-quality paper. This is often disconcerting since the print on some pages is so faint as to make it difficult to read. However, this criticism is minor since the price of the book has been kept within reach of most budgets and is especialy laudable when compared to the costs of most other HPLC texts of comparable quality.

A desk copy of this book is recommended as a handy reference source and as a training aid.

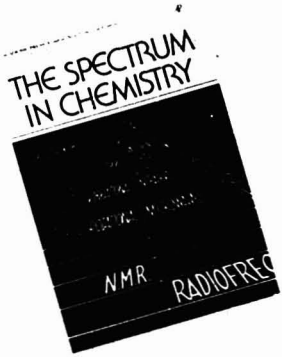

The Spectrum in Chemistry. J. E. Crooks. x + 313 pages. Academic Press Inc. (London), Ltd., 24–28 Oval Rd., London NW1 7DX, England. 1978. £6.50, paperback; £12.60, hardcover

Reviewed by Harvey Gold, Chemistry Dept., University of Delaware, Newark, Del. 19711

In certain ways, this volume is a work in search of an audience. Crooks attempts to survey a wide range of spectroscopic methods of practical importance to the chemist. Surprisingly, he succeeds in doing just that. The entire spectrum from X-rays (core electron transitions) through radio frequency (NMR and NQR) is covered through discussion of methods and applications. In the course of 14 chapters, the book uniquely describes a range of topics that are rarely, if ever, treated in a single work. The coverage is generally uniform, quite readable, and understandable.

The preface states the author's intent to "make spectroscopy appear as a less awesome topic to the average student." Who is representative of this average student is not clear. The intentional omission of mathematical proofs precludes classification as a physical chemistry text. As an analytical text, the book lacks sufficient detail. Yet, taken as a whole, the strength of this book lies in its breadth of coverage, and as such will serve as an often consulted general reference book. With occasional lapses, each section is sufficiently detailed to acquaint the reader with basic principles (without proof), apparatus, and interpretation of data. As a supplement in instrumental analysis, or as a text in a spectroscopy course, this level is ideal.

Several chapters merit additional comment. Increasingly, college chemistry courses are unable to cover the wide range of available analytical instrumentation, and basic text treatments are lacking. Crook presents coverage of several topics, including X-ray fluorescence and Mössbauer spectroscopy, which fall into this category. The chapter on optical activity is exceptional and presents several very good insights on the interdependence of this physical property and molecular asymmetry. The chapter on NMR, while avoiding detailed mathematics, succeeds in introducing a wide variety of techniques and terminology that the practicing chemist will find invaluable.

Indeed, the entire book is filled with *useful* information. The drawings are extremely well planned and complement the text. The examples (and the problems) are largely drawn from the current literature and illustrate the use of spectroscopy to solve problems, and provide the reader with a good idea of the scope of problems that can be attacked. Combining diverse spectroscopic topics in a single text allowed the author to stress complementary aspects rather than falling into the trap of single topic texts that seek to solve everything with one technique. Certainly, the audience for this book includes students of instrumentation and spectroscopy, and especially the practicing chemist who will find a wealth of information for the nonspecialist.

Transform Techniques in Chemistry. Peter R. Griffiths. xviii + 385 pages. Plenum Publishing Corp., 227 West 17th St., New York, N.Y. 10011. 1978. $39.50

Reviewed by Harold P. Larson, Lunar and Planetary Laboratory, University of Arizona, Tucson, Ariz. 85721

The rapid proliferation of transform techniques in chemistry justifies the attempt to create a book providing the background and perspective in which to view these developments. The chapters of this book are logically arranged, first introducing the concepts and mathematical formalism fundamental to the field, and then proceeding to specific applications to chemical systems. With such a broad scope, not all topics can be presented in detail, and frequent references to original papers will be required of the serious reader. For this purpose the literature citations are adequate, but not exhaustive. Although the chapters are written by different authors, the style is reasonably consistent, and overlapping subject areas are well coordinated without unnecessary duplication of material.

One of the more important functions a book of this type can serve is to help the nonchemist already familiar with transform techniques distinguish between the different applications (FT–IR, FT–NMR, FT–IRC, etc.) of interference spectrometers in chemistry, and compare and contrast them with similar instruments employed in related disciplines—physics and astronomy in particular. Unfortunately, this book fails in this sense, although there are some sections, particularly in chapter 7 on Hadamard techniques, where an effort was made to look beyond laboratory chemical applications. This deficiency is at least in part explained, I expect, by the fact that transform devices employed by chemists are almost exclusively commercial packages frequently used as black boxes. Such dependence leads to unquestioned faith in the superiority of such well-publicized attributes of transform techniques as the multiplex advantage, but with little awareness of whether they are actually being achieved or even required in specific applications.

Whether or not this assessment is correct, the book develops very little feeling for the physical nature of transform devices and how such diverse topics as physical optics, servosystem engineering, detector technology and optical interface to the radiation background relate to the mathematical complexities of producing, processing, and analyzing the data generated by these instruments. Without this dimension, this text is unsuitable as a general source book on multiplex methods for students and scientists not active in the field.

The research scientist primarily concerned with extending his awareness of already familiar techniques will benefit most from the survey of current chemical applications contained in this book.

Treatise on Analytical Chemistry. Vol. 10, Pt. 2, Analytical Chemistry of Inorganic and Organic Compounds. I. M. Kolthoff and P. J. Elving, Eds. xviii + 566 pages. John Wiley & Sons, Inc., 605 Third Ave., New York, N.Y. 10016. 1978. $34.50

Reviewed by Eugene W. Berg, Dept. of Chemistry, Louisiana State University, Baton Rouge, La. 70803

The aim of the treatise as a whole is to present a concise, critical, comprehensive, and systematic treatment of all aspects of classical and modern analytical chemistry. Part II is intend-

The symbol of excellence since 1959

Distilled in Glass™

Residue-Free Solvents from Burdick & Jackson

Purified to the exacting requirements of gas chromatography, liquid chromatography and spectrophotometric analysis.

Acetone
Acetonitrile
Benzene
Butanol-1
Butanol-2
n-Butyl Acetate
Butyl Chloride
Carbon Tetrachloride
Chlorobenzene
Chloroform
Cyclohexane
Cyclopentane
o-Dichlorobenzene
Dimethyl Acetamide
Dimethyl Formamide
Dimethyl Sulfoxide
Dioxane
2-Ethoxyethanol
Ethyl Acetate
Ethylene Dichloride
Ethyl Ether
Heptane, 98-99°
Hexadecane
Hexane, 68-69°
Isobutyl Alcohol
Iso-hexanes
Methanol
2-Methoxyethanol
Methylene Chloride
Methyl Ethyl Ketone
Methyl Isoamyl Ketone
Methyl Isobutyl Ketone
N-Methylpyrrolidone
Nonane
Pentane
Petroleum Ether, 30-60°
beta-Phenethylamine
Propanol-1
Propanol-2
Propylene Carbonate
Pyridine
Tetrahydrofuran
Tetramethyl Urea
Toluene
Trichloroethylene
1,1,2-Trichloro-1,2,2-Trifluoroethane
2,2,4-Trimethylpentane, 99-100°
o-Xylene

Ask for Bulletin BJ-25/U.S. Agencies use F.S.S.

BURDICK & JACKSON LABORATORIES, INC.
1953 South Harvey Street, Muskegon, Michigan U.S.A. 49442 (616) 726-3171

CIRCLE 24 ON READER SERVICE CARD

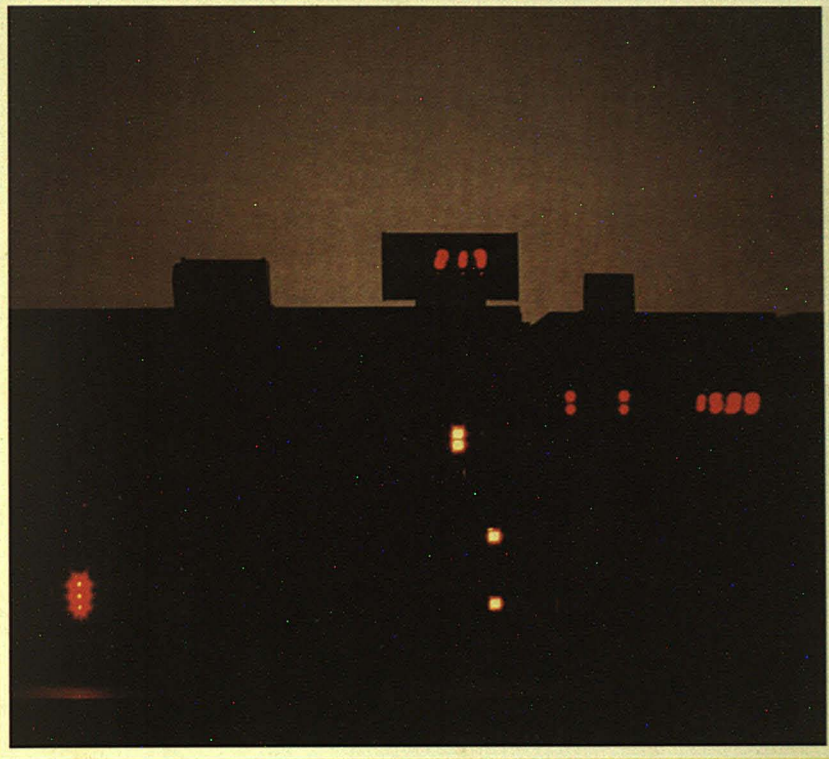

Aren't you glad you waited...

PHILIPS

Pye Unicam

A SCIENTIFIC INSTRUMENT COMPANY OF PHILIPS

...before buying your new AA?

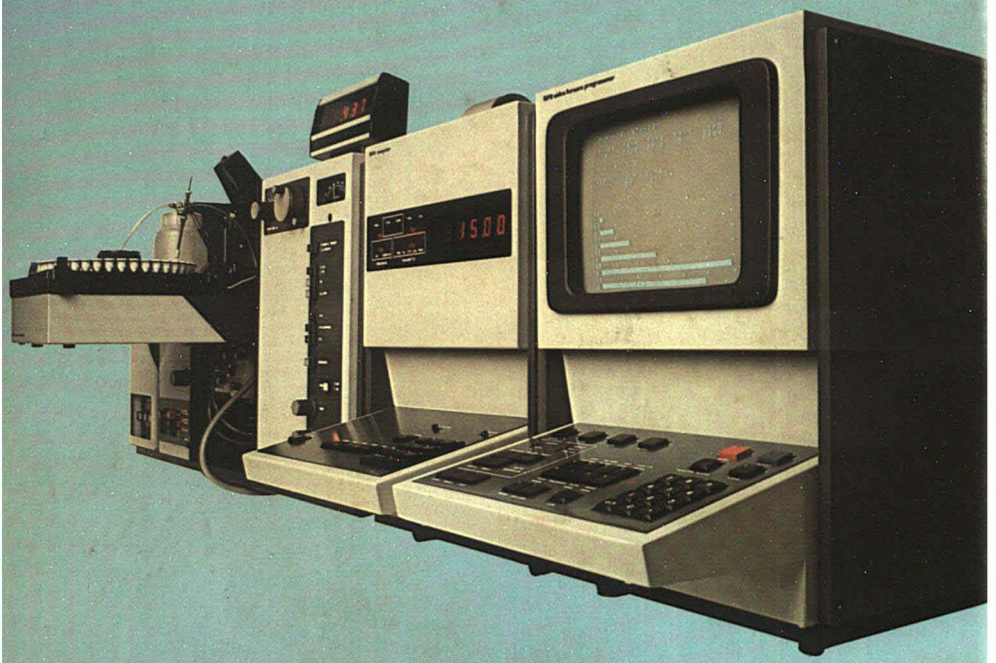

Because the new System SP9 now offers you so much more.

Flame or flameless, System SP9 has the microprocessor power and flexibility to solve your AA problems.

System SP9 has Computer Data Handling
to give

- Calibration with up to 5 standards.
- Precision calculations and Running Mean.
- Peak height or peak area.

System SP9 has a unique Video Furnace Programmer
providing

- Display of set parameters and status.
- EAROM storage of 10 furnace programs.
- Temperature or Voltage control.

And System SP9 has automation
via the world's most flexible flame and flameless autosamplers.

Now you've no need to wait any longer. Write, 'phone or use the reader reply service for further information on System SP9, the most cost effective AA system available.

Circle No. 110

Pye Unicam Ltd
York Street Cambridge CB1 2PX England
Telephone (0223) 58866 Telex 817331

Printed in England 7063.05.3012.11

The Series 204. It's the kind of chromatograph you want it to be.

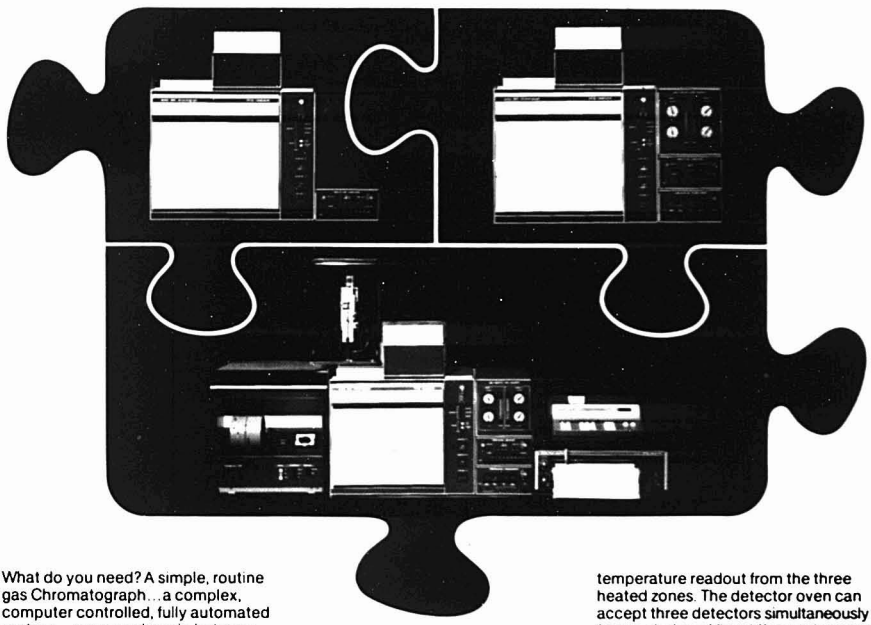

What do you need? A simple, routine gas Chromatograph...a complex, computer controlled, fully automated system...or somewhere in between. The Series 204 is all of these. True modularity enables you, the user, to choose the right kind of system now and, at any time, expand to meet your future needs. With the 204 there's no need to change instruments when you change your requirements.
Proven and specified high performance figures inspire the utmost confidence in the quality, reliability and the analytical accuracy of the 204.
What else do you need...value for money? With the Series 204 you've got that as well.

Some further details
The basic building block of the modular Series 204 is the Oven Assembly containing dual heated injectors for dual column operation, column and detector oven and isothermal temperature controllers with temperature readout from the three heated zones. The detector oven can accept three detectors simultaneously from a choice of five different detector systems. Details of the basic assembly, additional modules and the wide range of accessories are available on request. Write or phone to the address below.

If the 204 is more versatile than you require and you are in need of an instrument designed for a more specific method of detection – then ask for details of the five versions of the economic Pye Unicam GCD.

PHILIPS

Pye Unicam
A SCIENTIFIC INSTRUMENT COMPANY OF PHILIPS

York Street, Cambridge, England CB1 2PX
Telephone (0223) 58866 Telex 817331

CIRCLE 167 ON READER SERVICE CARD

628D

CHEMISTS, ENGINEERS, EDUCATORS

stay on top of the latest research developments in your field through

Advances in Chemistry Series

No.	Title	Price
166	Evaporation-Combustion of Fuels 296 pp (1978) clothbound	$31.00
165	New Uses of Sulfur—II 283 pp (1978) clothbound	$30.00
164	Preservation of Paper and Textiles of Historic and Artistic Value 403 pp (1977) clothbound	$38.00
163	Solid State Chemistry of Energy Conversion and Storage 371 pp (1977) clothbound	$38.50
162	Bioinorganic Chemistry—II 448 pp (1977) clothbound	$49.50
161	Legal Rights of Chemists and Engineers 109 pp (1977) clothbound	$16.00
160	Food Proteins—Improvement through Chemical and Enzymatic Modification 312 pp (1977) clothbound	$23.00
159	Plant Growth Regulators: Chemical Activity, Plant Responses and Economic Potential 94 pp (1977) clothbound	$15.00
158	Radiation Effects on Solid Surfaces 397 pp (1976) clothbound	$32.50
157	Organotin Compounds: New Chemistry and Applications 299 pp (1976) clothbound	$32.50
156	Analysis of Petroleum for Trace Metals 189 pp (1976) clothbound	$21.50
155	Thermodynamic Behavior of Electrolytes in Mixed Solvents 404 pp (1976) clothbound	$35.00
154	Toughness and Brittleness of Plastics 411 pp (1976) clothbound	$38.00
153	High-Level Radioactive Waste Management 166 pp (1976) clothbound	$18.50
152	Lyotropic Liquid Crystals and the Structure of Biomembranes 156 pp (1976) clothbound	$20.00

Other Technical Books

Title	Price
Cancer: The Outlaw Cell 192 pp (1978) hardback paperback	$15.00 8.50
Handbook for Authors 128 pp (1978) hardback paperback	$ 7.50 $ 3.75
Water Pollution—II 444 pp (1978) hardback paperback	$20.00 $12.00
Topics in Chemical Instrumentation—II 310 pp (1977) hardback	$12.00
Environmental Monitoring 197 pp (1976) hardback paperback	$13.50 $ 8.50
Modern Classics in Analytical Chemistry—II 314 pp (1976) paperbound	$ 8.50
Chemical Technology Handbook 215 pp (1975) clothbound	$12.50
Asymmetric Organic Reactions 465 pp (1976) paperback	$10.00
Phosphorus Chemistry in Everyday Living 238 pp (1976) clothbound	$15.00

ACS Symposium Series

No.	Title	Price
75	Lipids As a Source of Flavor 132 pp (1978) clothbound	$17.50
74	Mesomorphic Order in Polymers 264 pp (1978) clothbound	$25.50
73	Disposal and Decontamination of Pesticides 158 pp (1978) clothbound	$20.00
72	Chemical Reaction Engineering Reviews—Houston 331 pp (1978) clothbound	$23.50
71	Organic Chemistry of Coal 327 pp (1978) clothbound	$23.50
70	High Performance Mass Spectrometry: Chemical Applications 358 pp (1978) clothbound	$28.00
69	Organic Free Radicals 471 pp (1978) clothbound	$31.00
68	Separation of Hydrogen Isotopes 184 pp (1978) clothbound	$19.00
67	Flavor Chemistry of Animal Foods 175 pp (1978) clothbound	$19.00
66	Fluorine-Containing Free Radicals: Kinetics and Dynamics of Reactions 423 pp (1978) clothbound	$28.00
65	Chemical Reaction Engineering—Houston 619 pp (1978) clothbound	$33.50
64	Coal Desulfurization: Chemical and Physical Methods 332 pp (1977) clothbound	$25.00
63	Validation of the Measurement Process 207 pp (1977) clothbound	$20.00
62	Host Plant Resistance to Pests 286 pp (1977) clothbound	$23.00

ACS Monograph Series

No.	Title	Price
174	Coordination Chemistry—II 591 pp (1978) clothbound	$90.00
173	Chemical Carcinogens 788 pp (1976) clothbound	$67.50
172	Chemical Mechanisms in Bioenergetics 272 pp (1976) clothbound	$28.50
171	Zeolite Chemistry and Catalysis 796 pp (1976) clothbound	$65.00

SIS/American Chemical Society
1155 16th St., N.W./Wash., D.C. 20036

Please send _____ copies of _____

☐ Check enclosed for $_____ ☐ Bill me.
Postage at 75 cents per copy if other than U.S. or Canada.

Name _____

Address _____

City _____ State _____ Zip _____

Easy multidimensional gas chromatography.

Too good to be true?

The Pye Unicam Flow Switching Unit now enables you to enjoy the advantages of multidimensional chromatography. Designed as a free-standing unit, it can be easily fitted to any gas chromatograph.

What does it do?

It enables you to cut analysis times by as much as 80% by back-flushing unwanted components and recording only required information.

It increases column life by preventing the accumulation of low volatility material.

It permits the heartcutting of trace components from major ones, improving quantitative accuracy and reducing detection limits.

It offers time reductions with column switching, providing a complete analysis from a single injection.

It may be operated automatically with the aid of optionally available accessories, leaving you free to get on with other work.

When operated with the Pye Unicam GCD, GCV or Series 204 Gas Chromatograph a simply installed bulkhead makes column changing a two minute operation.

Multidimensional chromatography is no longer the problem it used to be.

Too good to be true?

Then ask us now for details and we will show you how multidimensional gas chromatography can make a valuable contribution to your work.

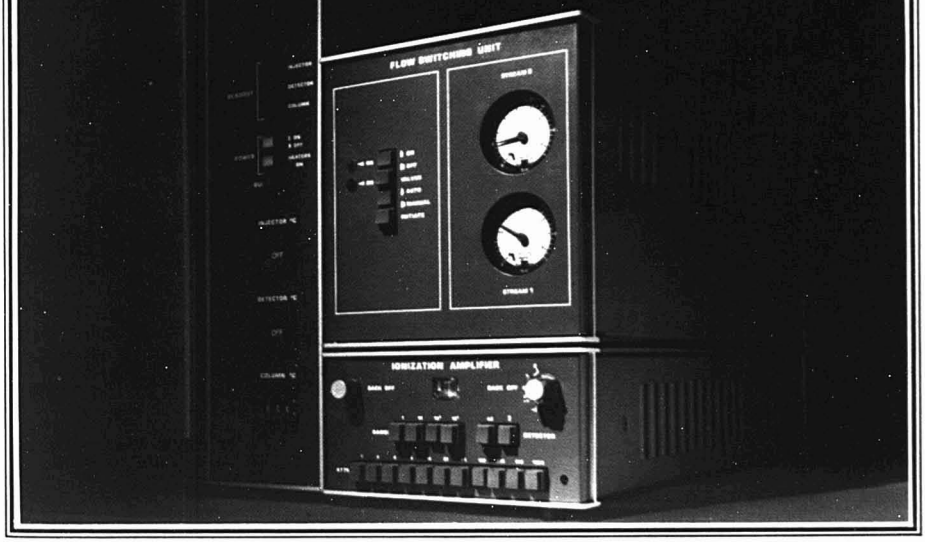

PHILIPS

Pye Unicam

A SCIENTIFIC INSTRUMENT COMPANY OF PHILIPS

York Street, Cambridge, England CB1 2PX
Telephone (0223) 58866 Telex 817331

CIRCLE 168 ON READER SERVICE CARD

628F

TIMELY TEARSHEETS

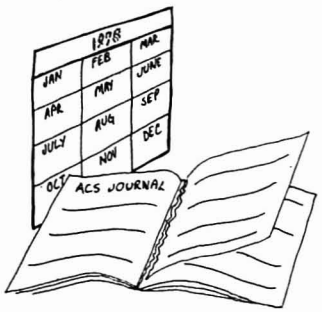

Here's an opportunity to choose any article you wish which has been published during the past 12 months in any one of the American Chemical Society journals.*

The price for this service is very modest—just $2.50 for the first copy and $1.25 for each additional copy.

Also, if you wish, you may select articles which have appeared in earlier non-current ACS journal issues, but these will be photocopies rather than tearsheets and an additional 50¢ is required per article.

All you have to do is fill in the order forms below, *include your payment*, mail now, and we'll do the rest.

1. Give complete details for each article. Sorry, we cannot provide a search service.
2. **PRINT** or **TYPE** all information, including label.
3. Make check or money order payable to the AMERICAN CHEMICAL SOCIETY, and mail to: ACS, Business Operations, Books and Journals Division, 1155 16th Street, N.W., Washington, D.C. 20036.

Name_____

Address_____

City_____

State/Zip_____

AMERICAN CHEMICAL SOCIETY JOURNALS
TIMELY TEARSHEETS Order Form

The following article(s) came to my attention in a recent issue of one of the ACS journals. I would like to order the number of tearsheets of each article indicated in the box(es).

ACS Journal_____ ☐
Title_____
Author(s)_____
Issue Date_____ Page(s)_____

ACS Journal_____ ☐
Title_____
Author(s)_____
Issue Date_____ Page(s)_____

ACS Journal_____ ☐
Title_____
Author(s)_____
Issue Date_____ Page(s)_____

* **Copyright restrictions** prevent us from providing copies from other than ACS journals

$2.50 for the first tearsheet.

$1.25 for each additional tearsheet ordered at the same time.

$_____
Total Enclosed

These prices do not apply to articles from Chemical Reviews and Journal of Physical and Chemical Reference Data. For information regarding cost of these copies, contact the Books and Journals Division, ACS.

Bausch & Lomb has done it again! A new clinical analyzer that gives you outstanding value with the highest degree of reliability—the SPECTRONIC 2100.

It starts with a specially designed clinical spectrophotometer made with the world-famous quality of Bausch & Lomb. It offers a wider continuous wavelength range of 325 to 650nm.

Next is a Peltier thermoelectric microflowcell. It cuts costs with total volumes as small as 250ul. And it uses the most precise temperature control available, giving you more precise test data.

The SPECTRONIC 2100 system includes an adjustable peristaltic pump to accommodate various sample volumes. You get exactly the sample volume you want, regardless of sample viscosity.

And the microprocessor-controlled enzyme calculator lets you select exactly the test conditions you need, continuously displays actual sample temperature, and automatically prints out test results in the terms you want.

What's more, you get unmatched Bausch & Lomb support. We can help you solve the toughest clinical problems, and of course, our service centers throughout the world assure you a maximum of uptime.

Get the right answers with the new Bausch & Lomb SPECTRONIC 2100 Clinical Analyzer. Again and again, you'll be glad you've got it.

THE RIGHT ANSWERS again & again

BAUSCH & LOMB

ANALYTICAL SYSTEMS DIVISION
INTERNATIONAL OPERATIONS, 820 LINDEN AVE.
ROCHESTER, NEW YORK 14625 U.S.A.
VERSAILLES, FRANCE • UNTERFÖHRING, GERMANY
GISTEL, BELGIUM • TOKYO, JAPAN

CIRCLE 27 ON READER SERVICE CARD

Introducing the Bausch & Lomb SPECTRONIC™ 2100 Clinical Analyzer

Solve Your Materials Problems 6 Ways

More R&D and QC labs use Micromeritics proven, precision instruments to measure physical properties of material than those of any other manufacturer in the world. These measurements include:

1 **Automatic particle size distribution** gives rapid analysis from 100 to 0.1 μm diameter and 500 to 38 μm diameter.

2 **Manual and automatic physical adsorption** for B.E.T. surface area from 0.001m^2g up; adsorption and desorption isotherms; pore structure (volume, size and shape) from 600 to 20Å diameter.

3 **Manual and automatic chemisorption** measures active material availability; percent metal dispersion.

4 **Mercury porosimetry** measures pore structure (volume, size and shape) from 354 to 0.0035μm diameter; density, surface area and average particle size.

5 **Manual and automatic density** determines absolute volume to ± 0.02cc.

6 **Electorophoretic mass-transport analysis** to study flocculation and dispersion; particle-liquid systems behavior; zeta potential.

We also invite you to use our complete Materials Analysis Laboratory Services. Let us show you how to solve your material problems. Call or write Micromeritics Instrument Corporation, 5680 Goshen Springs Road, Norcross, Georgia 30093. U.S.A. (404) 448-8282. Telex: 70-7450.

micromeritics®

CIRCLE 142 ON READER SERVICE CARD

EUROPEAN SALES OFFICE
2 Orchard Way
Eaton Bray
Bedfordshire
England
Telex: 851-826249

AFRICA

North
Coultronics France S. A.
Margency 95580 Andilly
France
Telephone: 989-9030

South
Coulter Electronics PTY., Ltd.
Transvaal
South Africa
Telephone: 805-2046 55 56

ARGENTINA
Instrumentalia S.R.L.
Buenos Aires
Telephone: 85-3121 86-1436

AUSTRALIA
Townson & Mercer Ltd.
Lane Cove, N.S.W.
Telephone: 428-1199

BELGIUM
Analis S. A.
Namur
Belgium
Telephone: 081-22 50 85

BRAZIL
Danon-Socidade Importadora
Equipmentos Cientificos LTDA
Rio de Janiero
Telephone: 221-4480

DENMARK
Bie & Berntsen, Ltd.
Roedovre
Telephone: 45-294-8822

EASTERN EUROPE
Medata AB
Stockholm
Sweden
Telephone: 08-303370

ENGLAND
Coulter Scientific Ltd.
Hertsford
Telephone: Harp 63151

FINLAND
OY Tamro AB
Helsinki
Telephone: 90-544011

FRANCE
Coultronics France S.A.
Margency 95580 Andilly
Telephone: 989-9030

GERMANY
Coulter Scientific GmbH
Gahlingspfad
West Germany
Telephone: 02156-755011

GREECE
The GG Forum
Thessaloniki
Greece
Telephone: 542-371

GUADELOUPE
Coultronics France S.A.
Margency 95580 Andilly
France
Telephone: 989-9030

INDIA
Blue Star Limited
Bombay
Telephone: 45-7887 or 45-6799

ITALY
Coulter Scientific S.p.A.
Milano
Telephone: 98-80-108

JAPAN
Shimadzu Seisakusho Ltd.
Kyoto
Telephone: (075) 8111111

KUWAIT
Bader Sultan & Bros. Co.
Kuwait
Telephone: 421291 92 93

MALAYSIA
Delta Electronics SDN. BHD
Bangsar Baru
Kuala Lumpur
Telephone: 943629

MARTINIQUE
Coultronics France S.A.
Margency 95580 Andilly
France
Telephone: 989-9030

NETHERLANDS
Chemical Laboratory Instrun
Schijndel
Netherlands
Telephone: 04104-4035

NEW ZEALAND
Selby-Witton Scientific, Ltd.
Lower Hutt
Telephone: 697-099

REUNION
Coultronics France S.A.
Margency 95580 Andilly
France
Telephone: 989-9030

SPAIN
Izasa S.L.
Barcelona 15
Telephone: 2548100

SWITZERLAND
IG Instrumenten-Gesellsch
Zurich
Telephone: 0166331

TAIWAN
Vertex Corporation
Taipei, Taiwan
Telephone: 752-6452(3)

U.S.S.R.
Coultronics France S.A.
Margency 95580 Andilly
France
Telephone: 989-9030

FROM

The American Chemical Society

NEW CHEMISTRY TITLES

Announcing the June 1978 publication of
Coordination Chemistry—Volume II
ACS Monograph No. 174
edited by Arthur E. Martell, Texas A&M University

Contents

Preface

1. **KINETICS AND MECHANISMS OF COMPLEX FORMATION AND LIGAND EXCHANGE**
Dale W. Margerum, George R. Cayley, David C. Weatherburn, and Gordon K. Pagenkopf
I. Introduction
II. Replacement of Water Molecules from the First Coordinate Sphere of Metal Ions
III. Formation Reactions of Multidentate Ligand Complexes
IV. Dissociation Reactions of Metal Complexes
V. The Effect of Coordinated Ligands on the Rate of Additional Coordination in Water-Replacement Reactions
VI. Monodentate Ligand Exchange Reactions
VII. Multidentate Ligand Exchange Reactions
Appendix
2. **LIGAND REACTIONS — THE EFFECT OF METAL COMPLEXES ON CHEMICAL PROCESSES**
Christian J. Hipp and Daryle H. Busch
I. Definition of Terms
II. Metal Complexes as Reagents in Ligand Reactions
III. Central Metal Atoms of Complexes as Substituents on the Substrate in Ligand Reactions
IV. Metal Complexes as Leaving Groups in Ligand Reactions
V. Special Effects Dependent on the Polyfunctionality of Metal Ions
VI. Homogeneous Transition Metal-Catalyzed Olefin Reactions
VII. Promoted Rearrangement of Strained Hydrocarbons
VIII. Electrophilic and Nucleophilic Reactions of Coordinated Ligands
IX. Oxidation of Coordinated Ligands
X. Autoxidations Catalyzed by Transition Metal Compounds
3. **OXIDATION-REDUCTION REACTIONS OF COORDINATION COMPLEXES**
David E. Pennington
I. The Outer-Sphere Mechanism
II. The Inner-Sphere Mechanism
III. Nonbridging Ligand Effects
IV. Specific Ion Effects
V. Reactions of Uncertain Classification
VI. Two-Electron Transfers
VII. Reactions with Nonmetallic Species
Index

591 pages Cloth (1978) $90.00
LC 74-151255 ISBN 0-8412-0292-3

Solid State Chemistry of Energy Conversion and Storage
edited by John B. Goodenough, University of Oxford and M. Stanley Whittingham, Exxon Research and Engineering Co.
Advances in Chemistry Series No. 163

This volume stresses the challenge the chemist faces in using sunlight as an alternate energy source. The various chapters identify problems, that, if solved, would introduce economically competitive options for energy conversion, storage, and conservation. Specific topics include hydrogen as energy carrier, solar energy conversion through photosynthesis, photovoltaic solar cells, wavelength-selective surfaces, new solid electrolytes, the sodium-sulfur battery, and high temperature electrolysis/fuel cells.

371 pages Cloth (1977) $38.50
LC 77-20011 ISBN 0-8412-0358-X

Minicomputers and Large Scale Computations
edited by Peter Lykos, Illinois Institute of Technology
ACS Symposium Series No. 57

A representative group of highly-qualified scientists and engineers describe their experiences in adapting scientific calculations to so-called minicomputers. Specific topics discussed include large scale simulation, APL level languages in analysis, the minicomputer and x-ray crystallography, a minicomputer number-cruncher, molecular dynamics calculations, theoretical chemistry via minicomputer, data acquisition, and complex fluid mechanics calculations.

239 pages Cloth (1977) $21.50
LC 77-15932 ISBN 0-8412-0387-3

Coal Desulfurization: Chemical and Physical Methods
edited by Thomas D. Wheelock, Iowa State University
ACS Symposium Series No. 64

Covers research on industrial processes and methods for removing sulfur from coal. Both chemical and physical extraction methods that are used currently or that are being adopted currently by industry are reviewed. Twenty-three chapters are divided into four groups covering sulfur in coal and its determination; physical methods for removing sulfur from coal; extraction of sulfur from coal by reaction and leaching; and removal of sulfur by pyrolysis, hydrodesulfurization, and other gas-solid reactions.

332 pages Cloth (1977) $25.00
LC 77-17216 ISBN 0-8412-0400-4

4th Joint Conference on Sensing of Environmental Pollutants

November 6–11, 1977, New Orleans, La. conference proceedings on environmental chemistry, sulfur measurements, biological effects caused by pollutants, environmental indicators and contaminants, standards and quality assurance, weather and climate modification by pollution, value of baseline studies in impact assessment, network design and data systems, pollution meteorology, radioactive pollutants, individual exposure monitoring, remote sensing of water, air, and land pollution by satellite, disposal of hazardous and nontoxic materials, water quality, biological and health effects, instrumentation, pollution source monitoring, new analytical techniques, sensing in the coastal zone, upper air composition changes, aerosol composition, fossil and nuclear fuels, and urban and rural sensing and assessment.

945 pages Paperbound (1978) $50.00 ISBN 0-8412-0411-X

12th Intersociety Energy Conversion Engineering Conference

August 28–September 2, 1977, Washington, D.C. conference proceedings dealing with new aspects of energy use, conversion, and conservation. Includes sessions on advanced auto propulsion, alternative fuels, biomedical power, Brayton, Stirling, and Rankine cycle engines, coal gasification, electric vehicle systems, electrochemistry, environmental assessment, fluid bed combustion, geothermal power systems, hydrogen energy systems, magnetohydrodynamics, thermionics, nuclear, solar, space, and wind power. (2 volume set)

1739 pages Paperbound (1977) $90.00/set
LC 77-84450 ISBN 0-8412-0402-0

Order from: **American Chemical Society**, 1155 SIXTEENTH STREET, N.W./Washington, D.C. 20036
U.K.: The Chemical Society, Blackhorse Road/Letchworth/Hertfordshire SG6 1HN England
Japan: Maruzen Co. Ltd., PO Box 5050, Tokyo International 100-31, Japan
Germany: Verlag Chemie, Postfach 1260/1280, D-6940 Weinheim, Germany

Cancer
The Outlaw Cell
Richard E. LaFond, Editor

An estimated 390,000 Americans will die of cancer this year alone and one out of every four will develop some form of this dread disease within their lifetime.

Statistics such as these show the need for a book that will explain our current state of the art in cancer research using simple, straightforward, non-medical language. *Cancer — The Outlaw Cell* successfully fulfills this need by making the latest advances in cancer research available to the general public in a clear, non-technical style that can be read and understood by both the professional scientist and non-scientist.

Written by leading experts at the forefront of their specialties and profusely illustrated in color, this collection of articles covers the great strides that have been made in understanding the causes of cancer, how this disease is spread, cancer as a biochemical problem, and non-surgical modes of therapy.

CONTENTS

Cancer — An Overview, *Henry C. Pitot*
Tumor Growth and Spread, *Isaiah J. Fidler and Margaret L. Kripke*
Control of Cell Growth in Cancer, *Arthur B. Pardee and David S. Schneider*
Cancer as a Problem in Development, *Armin C. Braun*
Puzzling Role of Cell Surfaces, *David I. Meyer and Max M. Burger*
Cancer-Causing Chemicals, *Elizabeth K. Weisburger*
Cancer-Causing Radiation, *Robert L. Ullrich, J. Michael Holland and John B. Storer*
Cancer and Viruses, *Arnold J. Levine*
RNA Tumor Viruses, *Robert D. Cardiff*
Herpesviruses — A Link in the Cancer Chain, *Ariel C. Hollinshead and William A. Knaus*
Cancer and The Immune Response, *John L. Fahey*
Immunotherapy of Human Cancer, *Larry A. Schafer and Evan Hersh*
Radiation Therapy, *Diana F. Nelson and Philip Rubin*
Chemotherapy of Cancer, *Joseph H. Burchenal and Joan R Burchenal*

192 pages (1978) clothbound $15.00
LC 78-2100 ISBN 0-8412-0405-5

192 pages (1978) paperback $8.50
LC 78-2100 ISBN 0-8412-0431-4

SIS/American Chemical Society/1155 16th St., N.W./Wash., D.C. 20036

Please send _____ copies of *Cancer—The Outlaw Cell.*

☐ cloth $15.00 (ACK 0405-5) ☐ paper $8.50 (ACK 0431-4) ☐ Check enclosed for $_____. ☐ Bill me.
Postpaid in U.S. and Canada, plus 75 cents elsewhere.

Name _____

Address _____

City _____ State _____ Zip _____

The master class of spectrophotometers.

Microprocessors can be just gadgets. Unless there's optical precision to match. All new Sargent-Welch Series 8 UV/VIS spectrophotometers use master blazed holographic gratings rather than inferior replica holographic gratings. So you get exceptionally low stray light and unbeatable performance.

Optical precision. Exceptional capability. All from a full line of UV/VIS double beam instruments that make spectrophotometry more convenient, more accurate. And, they're built to last more ways than one. Hard silica coated optics can be cleaned, rather than replaced. All components are performance-proven for long-term reliability. So you can concentrate on the procedure, not the equipment.

Unrivalled flexibility, convenience.
The sample compartment is extra large, so you can use a wide range of accessories. Readouts are large and clear. Lamp changeover is automatic. The recorder is built-in, not added on. In short, the spectroscopist is never asked to compromise performance for versatility.

Critically perfect, yet affordable.
There's a full range of Sargent-Welch Series 8 UV/VIS spectrophotometers. One is right for any laboratory need. From the microprocessor-controlled Models 8-250 and 8-200 to the sophisticated Models 8-150 and 8-100, the Series 8 line offers uncompromising attention to accuracy.

Performance and practicality.
Just what you've come to expect from Sargent-Welch—leader in laboratory instrumentation. Ask your Sargent-Welch representative for full details on how you can put the master class to work for you. Then decide.

SARGENT-WELCH SCIENTIFIC CO.
7300 NORTH LINDER AVENUE P.O. BOX 1026 SKOKIE ILLINOIS 60077

We're instrumental in your laboratory!

CIRCLE 191 ON READER SERVICE CARD

Anaheim, Baton Rouge, Birmingham, Cincinnati, Cleveland, Dallas, Denver, Detroit, Skokie, Springfield, NJ, Washington, D.C.

1979 Sargent-Welch Scientific Company

THEORY AND PRACTICE IN AFFINITY TECHNIQUES

Edited by P. V. SUNDARAM and F. ECKSTEIN

CONTENTS: *F. von der Haar*, Interfacial Salting out and the Ligand Induced Solubility Shift: Another Affinity Technique in Purification of Proteins. *M. R. A. Morgan and P. D. G. Dean*, Electrophoretic Affinity Elution—Analytical and Preparative Methods. *L. A. Hall and R. L. Easterday*, Cibacron Blue-Sepharose: A Tool for General Ligand Affinity Chromatography. *P. V. Sundaram*, Perspectives in the Isolation of Nicotinic Receptors: A Survey. *C. R. Lowe*, The Study of Enzyme Mechanisms by Affinity Chromatography. *P. V. Sundaram*, Relative Reactivities of Functional Groups on Ligands in the Synthesis of Affinity Columns. *J. R. Coggins*, The Use of Bis(imido esters) in the Study of Multi-subunit Proteins. *F. C. Hartman et al.*, Reactive Phosphate Esters as Affinity Labels for Enzymes of Carbohydrate Metabolism. *R. R. Rando*, The Design of Highly Specific Enzyme Inactivators. *E. Kuechler*, Affinity Labels for tRNA and mRNA Binding Sites on Ribosomes. *D. G. Knorre and O. I. Lavrik*, Affinity Labeling of Aminoacyl-tRNA Synthetases. *M. Giesel et al.*, Affinity Labeling of Tubulin by a GTP Analogue. *M. E. Wilchek and E. A. Bayer*, Affinity Labeling from the Isolated Protein to the Cell. *R. M. Lequin*, General Aspects of Immunoassay.

1979, about 250 pp., $21.75 ISBN: 0-12-677150-2

ANNUAL REPORTS IN NMR SPECTROSCOPY Volume 8

Edited by G. A. WEBB

The major aim of this widely-acclaimed series is to provide timely accounts of those areas of NMR spectroscopy where significant advances are being made. In recent years the advent of FT-NMR techniques has shifted the emphasis away from proton NMR towards less receptive nuclei such as ^{13}C and ^{15}N which are now being studied routinely in many laboratories. This, and recent progress in the theoretical interpretation of NMR parameters, is reflected in this series which covers NMR applications in all branches of science.

1978, 390 pp., $58.00 ISBN: 0-12-505308-8

NMR AND THE PERIODIC TABLE

Edited by ROBIN K. HARRIS and BRIAN E. MANN

NMR spectroscopy has become firmly established as one of the major methods available to the chemist for structure determination and for obtaining physico-chemical information about molecular dynamics. The book provides a comprehensive survey of NMR studies of all the elements of the Periodic Table for which such information exists. The large amount of data collected here will make this a comprehensive reference work for many years to come, as well as providing a springboard for future advances in this field.

1979, 480 pp., $62.00 ISBN: 0-12-327650-0

FOURIER TRANSFORM INFRARED SPECTROSCOPY Volume 2

Applications to Chemical Systems

Edited by JOHN R. FERRARO and LOUIS J. BASILE

This volume, like its predecessor, Volume 1, concerns itself with the most significant recent studies in this field. Specifically, Volume 2 covers chemical applications not discussed in Volume 1. These include analyses of atmospheric pollutants; analytical techniques as applied to surfaces and trace constituents using liquid chromatography and FT-IR; remote techniques to sense atmospheric pollutants and constituents in the atmosphere of Earth and other planets; studies of reacting and transient species; and a quantitative exploration of the problems of FT-IR. Volume 2 emphasizes analytical techniques as applied to chemical systems.

Volume 2/1979, 336 pp., $32.00 ISBN: 0-12-254102-2
Volume 1/1979, 311 pp., $29.75 ISBN: 0-12-254101-4

Send payment with order and save postage and handling charge. *Prices are subject to change without notice.*

ACADEMIC PRESS, INC.

A Subsidiary of Harcourt Brace Jovanovich, Publishers
111 FIFTH AVENUE, NEW YORK, N.Y. 10003
24-28 OVAL ROAD, LONDON NW1 7DX

CIRCLE 2 ON READER SERVICE CARD

ed to be very specific and to review critically the analytical chemistry of the elements.

In general, the aims of the editors have been satisfied in volume 10, part II, of the treatise. This volume gives a concise and critical evaluation of the analytical chemistry of boron, carbon, arsenic, antimony, molybdenum, and tungsten. The treatment of each element is comprehensive but not encyclopedic, with the emphasis on critically selected approaches and procedures. Typically, the treatment for each element summarizes the occurrence, industrial uses, toxicology, and important physical and chemical properties of the element and gives a critical survey of procedures for sampling, separation, isolation, detection, and determination of the element as well as an extensive list of pertinent references.

The book is well written and produced with very few typographical errors. The format of the text and the limited index make it easy for the reader to locate the material of interest.

Part II will be of greatest value to the practicing chemist who has need of a critical review of the analytical chemistry of a given element.

The book can be justly criticized on two points. First, there is little if anything to justify the grouping of the six elements treated in this text. Second, it is clear from the list of references that the manuscripts for the six elements were written and completed over a span of several years. References to boron, antimony, and molybdenum barely extend into 1973, whereas references to carbon extend through 1974 and for arsenic and tungsten through 1975. It is only fair to point out that the editors have had to rely on the efforts of numerous contributors in the compilation of the treatise, and considering the magnitude of their endeavor, the editors have done an excellent job. The reader, perhaps, will accept the lack of uniformity in an occasional volume.

Applied Atomic Spectroscopy. Vols. 1 & 2. E. L. Grove, Ed. xv + 313 and xvii + 344 pages. Plenum Publishing Corp., 227 West 17th St., New York, N.Y. 10011. 1978. $39.50 each

Reviewed by Morris Slavin, Box 876, Setauket, N.Y. 11733

The reader who expects to find in these volumes a general exposition of spectroscopic analytical methods will not find it here. What he will find is a collection of disparate articles on various phases of instrumental analytical methods whose only connection

Delta Range Delta Range Delta Range Delta Range

The movable fine range that simplifies precision weighing.

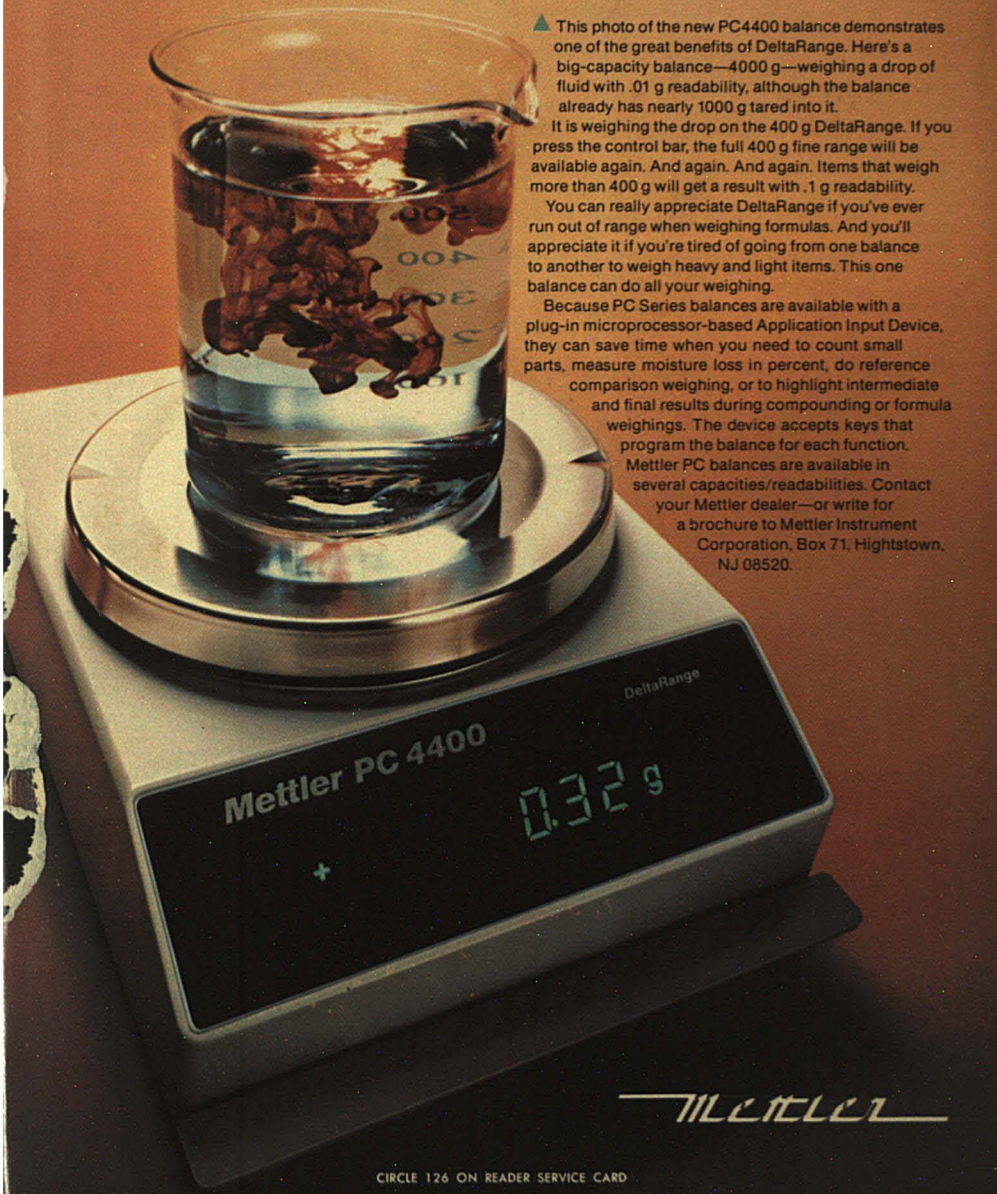

This photo of the new PC4400 balance demonstrates one of the great benefits of DeltaRange. Here's a big-capacity balance—4000 g—weighing a drop of fluid with .01 g readability, although the balance already has nearly 1000 g tared into it.

It is weighing the drop on the 400 g DeltaRange. If you press the control bar, the full 400 g fine range will be available again. And again. And again. Items that weigh more than 400 g will get a result with .1 g readability.

You can really appreciate DeltaRange if you've ever run out of range when weighing formulas. And you'll appreciate it if you're tired of going from one balance to another to weigh heavy and light items. This one balance can do all your weighing.

Because PC Series balances are available with a plug-in microprocessor-based Application Input Device, they can save time when you need to count small parts, measure moisture loss in percent, do reference comparison weighing, or to highlight intermediate and final results during compounding or formula weighings. The device accepts keys that program the balance for each function.

Mettler PC balances are available in several capacities/readabilities. Contact your Mettler dealer—or write for a brochure to Mettler Instrument Corporation, Box 71, Hightstown, NJ 08520.

Mettler

CIRCLE 126 ON READER SERVICE CARD

is the tie provided by the book bindings.

The first volume contains five chapters on photographic photometry, volatilization of samples by laser beam, properties of carbon electrodes, behavior of refractory samples, and preparation of standards and samples.

Volume II contains five chapters dealing with application of emission and X-ray techniques to oceanography, analysis of precious metals, problems in the analysis of petroleum products, and two chapters on spectroscopic methods applied to biomedical and toxicological research.

The writing varies from bad to quite good. The authors are an international assemblage; the countries represented, besides the United States, are Canada, Germany, South Africa, and Israel. As in most multiauthored compilations, there is much repetition, but bibliographies are extensive, with one review containing 1285 references.

What to make of this collection? The papers in volume I, dealing with certain problems encountered in emission spectroscopy, have but limited interest for workers using this method. The method itself is rapidly being displaced by atomic absorption and will soon be a fossil. Few workers will take up emission, and such topics as photographic photometry or the properties of carbon electrodes are of no interest to workers in other instrumental methods.

Volume II has some greater possibilities of use. The bibliographies can fill the need for someone beginning a search of the literature. Of course, the subject matter can be valuable to a worker starting in one of the pertinent fields. But here again, the subjects chosen are so diverse that probably no reader would be interested in any two—a great waste even if the books were cheaper.

It should be mentioned that chapter 2 of volume II, "Petroleum Industry Analytical Applications of Atomic Spectroscopy," which encompasses more than a third of the book, could well be the basis of a general text. It treats the various spectroscopic methods, together with their instrumentation and operation, and covers, besides petroleum, such fields as pollution control, metal analysis, agricultural product analysis, and geochemical applications.

To sum up, the fault in the first volume is the choice of topics, which are unconnected and of only limited interest for an understanding of emission problems. The topics in the second volume are also unconnected. The whole job give the appearance of lack of planning.

Machlett's New Dual-Target Spectroscopy Tubes

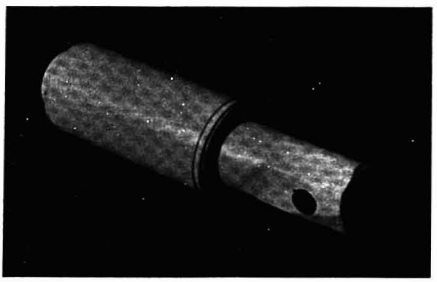

Improved direct replacement for GE/DIANO EA-75

- **DTS — 75A for Air-Helium Spectrometer**
- **DTS — 75V for Vacuum Spectrometer**

Increased cooling has been designed into the anode structure of these beryllium window x-ray tubes that are rated for operation up to 75 kVp.

Tungsten and chromium targets are standard. Other combinations can be provided on special order.

The standard 0.010" (0.25 mm) Be window can be replaced with 0.005" (0.125 mm) for long wavelength radiation on special order.

For data sheets, prices and deliveries contact:

Product Manager, Industrial X-ray
The Machlett Laboratories, Inc.
1063 Hope Street
Stamford, Conn. 06907
Tel: 203-348-7511 TWX: 710-474-1744

MACHLETT **The Machlett Laboratories, Incorporated**

A Raytheon Company

CIRCLE 183 ON READER SERVICE CARD

New Books

Mass Spectrometry of Natural Products: Plenary Lectures Presented at the International Mass Spectrometry Symposium on Natural Products, Rehovot, Israel, Aug. 28–Sept. 2, 1977. B. Sklarz, Ed. 101 pages. Pergamon Press, Maxwell House, Fairview Park, Elmsford, N.Y. 10523. 1978. $20

The natural products discussed include peptides, proteins, nucleic acid degradation products, steroids, biological fluids, and glycopeptide antibiotics. Also included are articles on a probe of molecular geometry for mass spectrometry, computer identification of mass spectra, and directed fragmentation in MS by introduction of functional groups. All articles in this volume have previously been published in *Pure and Applied Chemistry*, Vol. 50, No. 3 or 5 (1978).

Kodak started this catalog on lab chemicals in 1918.

Kodak became the first major American supplier of organic lab chemicals in 1918, when World War I shut off supplies from Europe.

That's when we started a tradition of publishing a free EASTMAN Organic Chemicals catalog. The first one, in 1919, contained about 150 items.

Our newest one—still free—contains more than 4,000 entries. Here's a comprehensive guide to chemicals by name and number, brief descriptions, actual specifications, hazard information, structural formulas, molecular weights, and prices. Plus descriptions of our EASTMAN *Dataservice* Catalogs, covering product and technical information. And we'll include a list of dealers.

EASTMAN Organic Chemicals Catalog No. 50. It's taken us more than 60 years to develop, but it's worth it. And it's yours free. Just send this coupon.

FREE

© Eastman Kodak Company, 1979

Eastman Kodak Company, Eastman Organic Chemicals, Dept. 412-L, Rochester, NY 14650.
Please send me *EASTMAN Organic Chemicals Catalog No. 50.*

Name _____ Title _____

Firm _____

Address _____

City _____ State _____ Zip _____

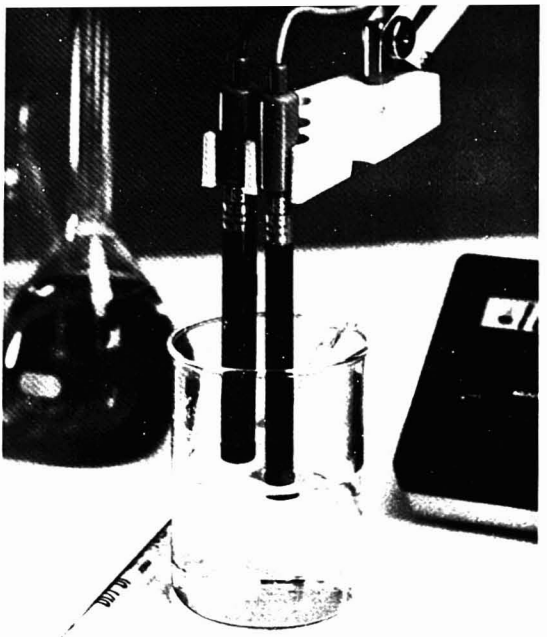

We've lowered chloride detection to 10 parts per billion

Our new Ultra Sensitive Chloride Electrode responds to chloride in the 10 parts per billion range, without compromising selectivity. A range 25 times lower than can be measured with conventional chloride electrodes!

This revolutionary, new, solid-state electrode is a major break-through for industrial process applications demanding ultra-pure water, and for monitoring high purity water in steam boilers and conventional power generating stations. As such, it brings new sensitivity to direct chloride measurement in biological materials, foods, soils, insecticides, plating baths, potable water and wastewater . . . without resorting to pre-concentration steps and expensive, highly complicated techniques. This latest electrode development is just one example of how much we care about your need for improved electrode performance. We're on your side!

We also offer pH and ORP electrodes in conventional glass or break-proof polymer bodies, removable protective tips, renewable and porous Teflon junctions. More, we ship our electrodes in keep-fresh soaker bottles, ready for immediate use and for long shelf life. Should our electrode fail to operate properly, we've made it easy for you to return it. Just put it back in its own shipping carton, use our special "return" label, and mail. We'll ship a replacement within 24 hours.

For more information, see your local GC representative. Or contact Graphic Controls, Recording Chart Division, Box 1271, Buffalo, NY 14240.
Phone: 716/853-7500

We're on Your Side

GRAPHIC CONTROLS
Recording Chart Division

CIRCLE 82 ON READER SERVICE CARD

CRC Handbook Series in Organic Electrochemistry. Vols 1, 2, and 3. Louis Meites et al. 877, 633, and 671 pages. CRC Press, Inc., 2255 Palm Beach Lakes Blvd., West Palm Beach, Fla. 33409. 1978. $125, $125, and $53.95

The first two volumes contain data for more than 3800 compounds and the techniques and conditions used for analysis. Volume 3 provides information on the electrochemical behaviors of 1309 organic and organometallic compounds.

Quantitative Organic Analysis via Functional Groups, 4th ed. Sidney Siggia and J. Gordon Hanna. xii + 883 pages. John Wiley & Sons, Inc., 605 Third Ave., New York, N.Y. 10016. 1979. $45.95

The fourth edition contains a discussion of the chemistry involved in each system, historical developments of the methods, the merits and limitations of each approach, and a description of how the spectrum of analytical situations for each functional group is covered by the series of methods presented. The text is completely cross-referenced to show the interrelationships between the methods for the different functional groups.

Introduction to Bioinstrumentation with Biological, Environmental and Medical Applications. Clifford D. Ferris. xiv + 330 pages. Humana Press Inc., P.O. Box 2148, Clifton, N.J. 07015. 1978. $29.50, hardcover; $14.50, softcover

The philosophy discussed herein is fundamental system analysis and design rather than detailed discussion of particular devices. Only analog systems are described because biological systems are inherently analog in behavior. The major components of instrumentation reviewed are transducers, amplifiers, signal processors, display and recording equipment, and telemetry systems.

Continuing Series

Methods of Biochemical Analysis, Vol. 25. David Glick, Ed. vii + 382 pages. John Wiley & Sons, Inc., 605 Third Ave., New York, N.Y. 10016. 1979. $29.50

The book contains articles on NMR in biological systems, immobilized enzymes in biochemical analysis, and separation and quantitation of peptides and amino acids in urine.

Recent Developments in Separation Science. Vol. 4. N. N. Li et al., Eds. 236 pages. CRC Press, Inc., 2255 Palm Beach Lakes Blvd., West Palm Beach, Fla. 33409. 1978. $58.95; $67.95, outside USA

The emphasis of this volume is on the interfacial phenomena in particle separation. Also discussed are techniques such as hyperfiltration, ultrafiltration, and water purification.

Annual Reports on NMR Spectroscopy, Vol. 8. G. A. Webb, Ed. x + 380 pages. Academic Press Inc., 111 Fifth Ave., New York, N.Y. 10003. 1978. $58

This volume contains chapters on NMR of alkaloids, steroids, problems in theory and analysis of dynamic NMR spectra, and chemical shifts of ^{119}Sn nuclei in organotin compounds. Literature has been covered up to the first half of 1977.

tenax g.c.

The highest thermal stability porous polymer.

Mesh size	Cat. nr.	Price (15g)
35 - 60	2451	Hfl 173,—
60 - 80	2450	Hfl 192,—
80 - 100	2454	Hfl 211,—

® Product of Enka, Holland.

World wide distributor:

CHROMPACK
P.O. Box 3
4330 AA Middelburg
The Netherlands
Tel.: 01180 - 11251
Telex: 55352 chrom nl

CIRCLE 34 ON READER SERVICE CARD

LAB PUMPS
with
"VARIABLE SPEED"

Integral solid state speed controlled motor is magnetically coupled to miniature gear or centrifugal pumps to provide variable flow and pressure over a wide range. These portable pumps provide leak-proof contamination free service and are constructed from corrosion resistant stainless steel and Teflon. Excellent for applications requiring small size, light weight and dependable performance. Also available with explosion-proof, air powered or D.C. motors, with performances to 8 G.P.M. and 90 P.S.I.G.

from

MICROPUMP

originator of the magnet drive gear pump

CIRCLE 140 ON READER SERVICE CARD

A new level in HPLC sophistication and simplicity.

Micromeritics proudly introduces its new 7500 microcomputer-based Liquid Chromatograph—a beautiful blend of engineering sophistication and operating simplicity.

We've taken the most advanced features available in HPLC today and packaged them so you can have the exact system to fit your specific application. Both gradient and isocratic integrated systems are available to accommodate rigorous quality control and methods development needs or the complex analysis functions of research and development laboratories.

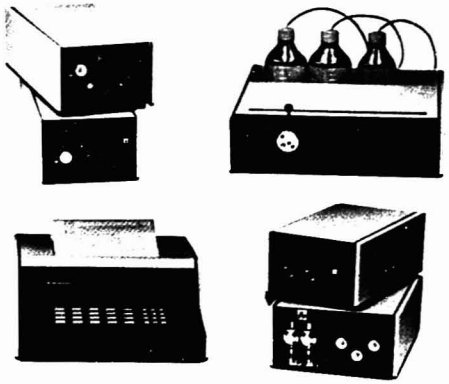

Also available as components. Buy what you need now, and add more as you need it.

Simple keyboard entry
All operating commands can be made from a single microcomputer-based control module. An alphanumeric display readout continually informs the operator of entry status for such parameters as flow rate, pressure limits, solvent concentration and column temperature.

Total analysis reporting
Comprehensive analysis reporting is achieved through a printer/plotter which not only gives you the chromatograms, but also a printout of gradient/solvent conditions, flow rate, pressure, temperature and operational status. Sample retention times, peak area and height, percent of concentration, sample and injection numbers can also be printed out.

Total automation
The 7500 system can be totally automated to give you unattended analysis around the clock. It can initiate 192 analyses of up to 64 samples . . . automatically.

Other advanced design features
The new 7500 also has an all new Ternary Solvent Mixer for more accurate and reliable low pressure solvent blending; a precision heated column compartment for faster more stable analysis; a new pulseless solvent delivery system; and a choice of three detectors—variable wavelength, fixed wavelength or refractive index.

Available as components, too
And finally, you have the option of buying as much or as little of the system as you presently need. The 7500 system is also available as individual components. You can buy what you need now and add more later as you need it.

To learn more about the many features that separate the new 7500 from all the other HPLCs on the market, contact Micromeritics Instrument Corporation, 5680 Goshen Springs Road, Norcross, Georgia 30093 USA (404) 448-8282 TELEX: 70-7450.

micromeritics®

CIRCLE 141 ON READER SERVICE CARD

© 1979 Markad Service Co., all rights reserved C-53

Operating room gas lines are equipped with 3/8" "Keyed" Quick-Connects, under pressures ranging from 44 to 162 psi.

These Swagelok® QUICK-CONNECTS are "keyed" for Life Support Reliability

Swagelok "Keyed" Quick-Connects provide mix-proof handling of oxygen, nitrous oxide and nitrogen during surgery in the six operating rooms at Forkosh Memorial Hospital, Chicago.

The Quick-Connects feature a positive mechanical lockout system which prevents coupling of unmatched stems and bodies and, more importantly, eliminates any chance of accidental intermixing of operating room gases. The units also are color coded for added safety.

Specify SWAGELOK "Keyed" Quick-Connects for safe, reliable handling of different liquids or gases. Sizes are 1/8", 1/4", 3/8" and 1/2" with tube or NPT pipe end connections in single or double end shut off units.

They're available from local distributors, with eight different "Keys" and colors, in brass or 316 stainless steel.

Swagelok®
Quick-Connects

Crawford Fitting Company
29500 Solon Road, Solon, Ohio 44139
Crawford Fittings (Canada), Ltd., Ontario

CIRCLE 33 ON READER SERVICE CARD

Afterthoughts on the Pittsburgh Conference

The growing business of analytical instruments was spotlighted at the 1979 Pittsburgh Conference on Analytical Chemistry and Applied Spectroscopy held March 5–9 in Cleveland, Ohio. Marking the 30th year of the conference was a near doubling of attendance over that five years ago with 15 812 participants this year! Although the number of exhibitors remained roughly the same (2% increase), the number of exhibits increased 30% from 800 booths in 1978 to 942 in 1979. The employment bureau's reporting roughly double the number of candidates, job openings, employers, and interviews is an encouraging sign of activity in the field. So it seems that all is well with this business, even with threats of a recession in the economy. Spirits were high; participants were eager to see what was new; instrument manufacturers were equally eager to supply information on their new products. Apples, plastic bags, and plastic cups were popular giveaways.

Why the boom in the instrumentation market? Dave Nelson, marketing manager for Hewlett-Packard, said that projected growth rates to 1981 in gas chromatography, liquid chromatography, and GC–MS continue market trends that began in the early 1970's. Growth rates are highest among products that can be automated and fit the needs of users related to environmental applications, industrial R&D, and quality control applications. Gaynor N. Kelley, senior vice president of the instrument group at Perkin-Elmer, feels that there are no large target markets but many small ones and that an instrument manufacturer cannot grow unless it is diversified and can solve customers' problems. This is what the Pittsburgh Conference is all about—instrument companies providing solutions to the specialized problems of the customer. Richard A. Nesbit, corporate director of research for Beckman Instruments, thinks that with or without sophisticated technology, as long as you get closer to the two questions analytical chemists ask the most—*What is it?* and *How much?*—you've done your job. Probably some instruments without microprocessor technology are better, provided they do the job the analyst wants.

The 369 exhibitors are seeking a share in a market that in 1978 reached $1.6 billion. Within this total, $440 million went for separation instruments, $460 million for optical spectrometry, and $210 million for magnetic spectrometers. Citing a forecast by the market research firm Creative Strategies, Hewlett-Packard, for example, expects 1981 total market sales to move up to $2.2 billion.

Mayor Kucinich (sitting) visits an exhibit as (conference officials, left to right) Allen J. Sharkins, exhibits chairman; Herbert L. Retcofsky, president; John E. Graham, treasurer; and Harold A. Sweeney, president-elect observe

The evolution of automated instruments is being pushed to a higher degree by manufacturers. There are some customer benefits with microelectronics—new functions, simple operation, fewer errors, and more function for less money. But there could be some drawbacks as Dr. Laitinen points out in his editorial on page 177, Feb. 1979. If you envision microprocessors as "black boxes," then the function(s) of these "black boxes" should be understood in the context of any scientific investigation to be of maximum benefit.

What's to be said about Cleveland? The obvious problem is the straining of facilities such as hotels and restaurants. Cleveland offers only about 5500 rooms so there is much doubling up and rental of rooms twice, at the beginning and end of the week. Also, of course, hotels and motels at some distance around Cleveland are called upon to fill the breach. At least one hotel, Swingos, resigned from the Cleveland Convention Bureau, complaining that the Bureau should schedule more reasonably sized meetings instead of putting all their efforts into one big overwhelming meeting. Convention hall facilities are excellent even though some symposia, especially on the more exciting new developments such as inductively coupled plasma, drew numbers of people that required standing room only. Other than these problems, people seemed to be happy, especially the taxi drivers. A local TV show interviewed the drivers; several wished business could be as good for them all the time.

Moreover, there is a question as to whether the conference will stay in Cleveland. Harold Sweeney, president-elect, plans to announce the exact conference location for the 1980 meeting in May or June of this year.

In the final analysis, it's good to see that the science and business of analytical chemistry are so healthy, and that there is enthusiasm on the part of both the scientists and merchants. Perhaps the 1979 and future conferences can best be set in perspective with the reminder that, as long as the fundamental requirement for decision making is the availability of precise information, then the microprocessors, "black boxes," and soaring sales in analytical instruments are needed to provide the data.

Andre D'Arcangelo

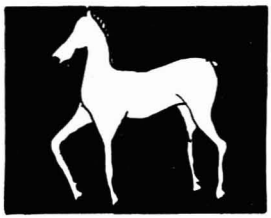

Archaeological Chemistry II

Advances in Chemistry Series No. 171

Giles F. Carter, *Editor*
Eastern Michigan University

A symposium sponsored by the Division of the History of Chemistry of the American Chemical Society.

Beautifully illustrated with 15 color plates and printed on high-quality enameled stock, this book highlights the great strides that have been made in understanding the origin and distribution of archaeological specimens composed of pottery, glass, metal, bone, and pitch, through the unfolding of new and improved analytical techniques.

Emphasis is on the historical knowledge derived from the chemical analysis and investigation of various artifacts including South American dyes, Egyptian glass, ancient Near Eastern ivory, Spanish ceramics, Chinese bronzes, prehistoric American copper, and copper-based Roman coins.

CONTENTS

Perspectives and General Techniques: Chemistry and Archaeology • Conservation of Archaeological Materials • Radiocarbon Dating • Spark Source Mass Spectrometry • Applications of X-Ray Radiography • **Organic Materials:** Trace Element Analysis in Bone • Amino Acid Analysis in Radiocarbon Dating of Bone Collagen • Amino Acid Racemization Dating of Bone and Shell • Ancient Near Eastern Archaeological Ivory Artifacts • Asphalts from Middle Eastern Sites • The Identification of Dyes in Textiles • **Ceramics:** Analysis of Early Egyptian Glass • Spanish and Spanish-Colonial Majolica Ceramics • Soapstone Artifact Characterization • Atomic Absorption Spectroscopy of Archaeological Ceramic Materials • **Metals:** Lead Isotope Ratios in the Manufacture of Pigments • Lead Isotope Analyses and Sources of Nigerian 'Bronzes' • Ancient Chinese Bronze Compositions • Prehistoric Copper Artifacts • Chemical Compositions of Copper-Based Roman Coins

389 pages (1978) Clothbound $46.00
LC 78-26128 ISBN 0-8412-0397-0

No. 138 Archaeological Chemistry I
254 pages (1974) Clothbound $29.00

SIS/American Chemical Society
1155 16th St., N.W./Wash., D.C. 20036

Please send the following:

☐ *Archaeological Chem. I* (ACH 0211-7) $29.00 ea ☐ *Archaeological Chem. II* (ACH 0397-0) $46.00 ea

☐ Check enclosed for $_____ ☐ Bill me
Postpaid in U.S. and Canada plus 75¢ elsewhere.
California residents please add 6% state use tax.

Name _____

Address _____

City _____ State _____ Zip _____

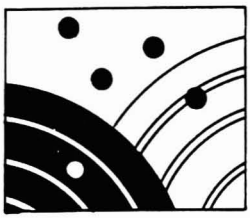

Ultratrace Metal Analysis in Biological Sciences and Environment

Advances in Chemistry Series No. 172

Terence H. Risby, *Editor*
Pennsylvania State University

A symposium sponsored by the Division of Analytical Chemistry of the American Chemical Society.

With the improved sensitivities of current analytical techniques (inductively coupled plasma, atomic absorption and atomic emission spectrometry, and neutron activation), knowledge of the roles of metals in biochemical processes and in the environment are continually expanding.

This new book contains significant research reports on the collaborated efforts of biochemists, environmental chemists, and analytical chemists who are studying metal concentrations in biological organisms and in air, water, and soil.

CONTENTS

Trace Element Analysis in Nutrition • Multielement Analysis with RF-ICP • Health Implications • Molybdenum in Biological Materials • Analysis of Particulate Matter for Metals • Airborne Metallic Elements • Nickel-Induced Transformation in Tissue Culture • Trace Elements in Urine • Zinc in Biochemical Processes • Cadmium, Lead, Copper, and Iron in Sea Water Derived Samples • Sources of Metals in the Atmosphere • *Bacillus subtilis* Strain 168 • Zinc in Humans • Serum Copper and Age

263 pages (1979) Clothbound $36.50
LC 78-31903 ISBN 0-8412-0416-0

SIS/American Chemical Society
1155 16th St., N.W./Wash., D.C. 20036

Please send _____ copies of *No. 172 Ultratrace Metal Analysis* (ACH 0416-0) at $36.50 per copy.

☐ Check enclosed for $_____ ☐ Bill me.
Postpaid in U.S. and Canada plus 75¢ elsewhere.
California residents please add 6% state use tax.

Name _____

Address _____

City _____ State _____ Zip _____

Drug Metabolism Concepts

ACS Symposium Series No. 44

Donald M. Jerina, *Editor*
The National Institutes of Health

A symposium co-sponsored by the Division of Medicinal Chemistry and the Division of Analytical Chemistry of the American Chemical Society.

Eight chapters present in-depth research reports on the role of enzyme systems, especially cytochrome P-450, in drug activation and detoxification. This timely study on drug metabolic pathways is vital because of the possibilities of toxic or carcinogenic intermediates caused by the action of enzymes on drugs and anesthetics.

CONTENTS

Cytochrome P-450 in Oxygen Activation for Drug Metabolism • Synthetic Models for the Reaction Stages of Cytochrome P-450 • Isolation of Multiple Forms of Liver Microsomal Cytochrome P-450 • Resolution of Multiple Forms of Rabbit Liver Cytochrome P-450 • Enantiomeric Selectivity and Perturbation of Product Ratios as Methods for Studying the Multiplicity of Microsomal Enzymes • Purified Cytochrome P-448 and Epoxide Hydrase in the Activation and Detoxification of Benzo[a]pyrene • In vitro Reactions of the Diastereomeric 9,10-Epoxides of (+) and (−)-*trans*-7,8-Dihydroxy-7,8-dihydrobenzo[a]pyrene with Polyguanylic Acid • Metabolic Activation in Chemical-Induced Tissue Injury

196 pages (1977) clothbound $15.50
LC 77-2279 ISBN 0-8412-0370-9

SIS/American Chemical Society
1155 16th St., N.W./Wash., D.C. 20036

Please send _____ copies of *SS 44 Drug Metabolism Concepts* at $15.50 per copy.

☐ Check enclosed for $_____ ☐ Bill me
Postpaid in U.S. and Canada, plus 40 cents elsewhere

Name _____

Address _____

City _____ State _____ Zip _____

Specify Spectra-Physics For Creative Chromatography.

Superior performance for the same price.

The Problem:
Inadequate resolution

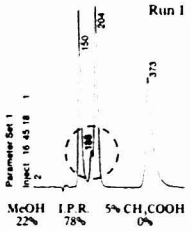

The Solution:*
Optimized separation

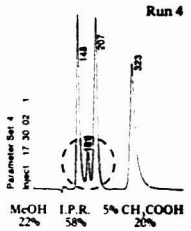

The ternary solvent system of the SP 8000 automatically varied the ion pairing reagent independently of the methanol concentration. (Ask for Application Brief CAX-005 on water-soluble vitamins to get more details.)

**10-minute set-up, 1½ hours automatic operation.*

Why be content with a multiple-pump, limited-capability HPLC gradient system when for the same price you can get the microprocessor-automated SP 8000 chromatograph? With its patented three-solvent mixing it is more flexible than any conventional LC, whether you're doing methods development or routine analysis. Give us a call or drop a line. We'd like to show you how you can do more creative chromatography with our SP 8000. It's the kind of advanced system you'd expect from Spectra-Physics, the leader in automated chromatography.

USA headquarters: Spectra-Physics
2905 Stender Way, Santa Clara, CA 95051
European headquarters:
Spectra-Physics GmbH
Alsfelder Strasse 12, 6100 Darmstadt
West Germany.
Or call one of our regional US sales offices: Midwest (Ill.): (312) 956-0882
Mid-Atlantic (Md.): (301) 345-7333
East (N.J.): (201) 981-0390
South (Tex.): (713) 688-9886
West (Calif.): (408) 249-0105

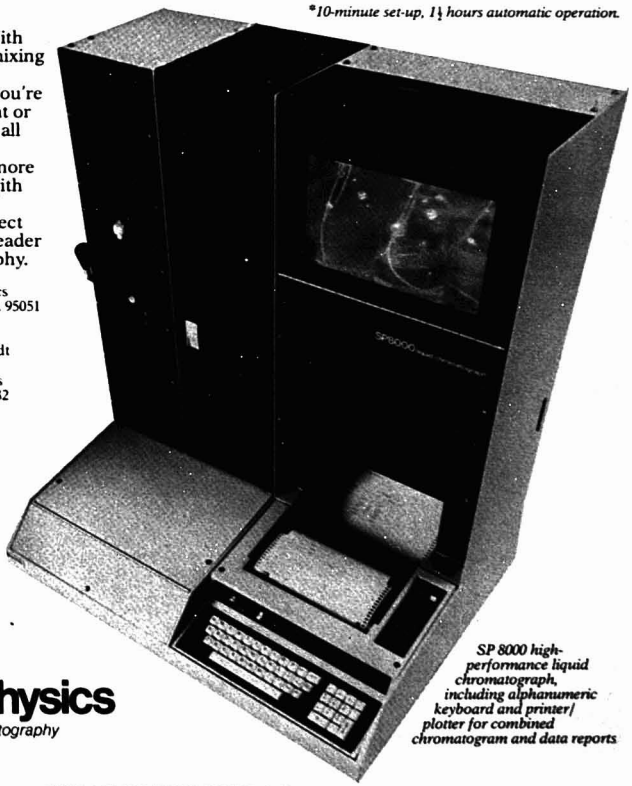

SP 8000 high-performance liquid chromatograph, including alphanumeric keyboard and printer/plotter for combined chromatogram and data reports.

Spectra-Physics
Innovators in Chromatography

CIRCLE 193 ON READER SERVICE CARD

Finnigan LC/MS permits rapid determination of LSD and other thermally-labile compounds.

Finnigan's ingenious LC/MS Interface makes it possible to bring the precision of mass spectrometry to the quantitative and qualitative analysis of many difficult samples, including such thermally fragile substances as LSD and psilocybin.

The Interface utilizes a continuous moving belt to carry the LC eluent through a series of vacuum locks and directly into the ion source of the mass spectrometer. This combination of liquid chromatography and mass spectroscopy allows the identification and quantitation (nanogram level) of thermally labile compounds using sophisticated techniques like Pulsed Positive-Ion Negative-Ion Chemical Ionization (PPINICI) and Multiple Ion Detection. Samples such as non-volatile liquids and suspended solids can be introduced by direct application to the belt, utilizing the interface as a high-speed automated solid probe.

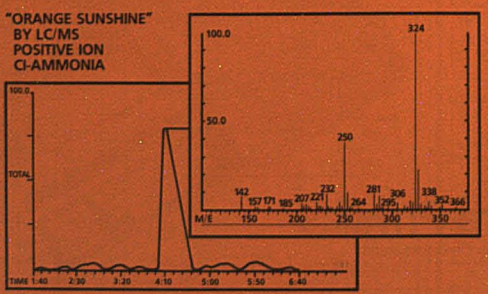

Contrast the indeterminate signal from U.V. excitation of the HPLC eluent with the distinctive "thumbprint" of LSD delivered by the Finnigan 4000 utilizing the LC/MS Interface.

In a paper presented at the March Pittsburgh Conference, authors Paul E. Kelly and Ronald F. Skinner discuss in detail how standards and samples were prepared and analyzed by HPLC/MS.

Copies of the paper, "A Rapid Method for the Determination of Selected Hallucinogenic Drugs Via Positive/Negative Ion LC/MS", and details of other applications are available on request.

finnigan
Instruments
A DIVISION OF FINNIGAN CORPORATION
845 West Maude Avenue
Sunnyvale, California 94086
(408) 732-0940

CIRCLE 75 ON READER SERVICE CARD

E. L. Wehry and Gleb Mamantov
Department of Chemistry
University of Tennessee
Knoxville, Tenn. 37916

Matrix Isolation Spectroscopy

A problem area of great contemporary significance in analytical chemistry is the development of techniques for identification and reliable quantitation of individual trace organic compounds in complex samples. The demands imposed upon analytical methodology by many present-day samples are staggering. For example, a "synthetic fuel" sample, such as a shale oil or coal liquid, may contain hundreds of different organic compounds, some of which may be carcinogenic. A realistic analytical protocol for dealing with a sample of such complexity logically begins with the application of modern separation and fractionation procedures. Yet separation methods, however powerful, can be time consuming, particularly if it is demanded that the sample be fractionated into individual pure compounds. Even very efficient separation procedures may be unable to do more (in a realistic time) than produce a series of fractions which themselves are rather complex mixtures. Hence, even if it is coupled with separation procedures, the ultimate analytical measurement step should be capable of producing reliable qualitative and quantitative results in mixtures of considerable complexity.

Optical spectroscopy (UV–visible absorption or luminescence and IR absorption) has been applied widely to the analysis of organic samples. Substantial improvements in the performance of spectroscopic instrumentation (particularly for infrared absorption and molecular fluorescence) have recently been made, but much less attention has been devoted to improvements in the quality of the spectroscopic sample itself. Thus, for example, powerful Fourier transform infrared (FTIR) spectrometers, which may cost in excess of $100 000 and may be equipped with the latest in optical and computer hardware, often are used in conjunction with IR sample preparation techniques which have changed little in the past 30 years and which tend to negate many of the advantages offered by the new instrumentation.

An "ideal" sampling matrix for spectroscopic analysis of a multicomponent sample should possess the following characteristics:

(a) For qualitative analysis, the spectrum of any particular compound should be a characteristic, reproducible "fingerprint" of that compound. The spectrum should contain sufficient information to permit unambiguous and relatively facile identification of the compound, yet be relatively simple (so that coincidences in the location of features in the spectra of different compounds occur infrequently).

(b) For both qualitative and quantitative analytical purposes, it is desirable that both the appearance of the spectrum (i.e., λ_{max} values) and the "quantitative constants" (e.g., ϵ_{max} or fluorescence quantum efficiency) for a given compound be totally independent of the composition of the sample in which that compound is encountered. This criterion necessitates that the molecular environment "seen" by the analyte in the spectroscopic sample be always the same, irrespective of the nature of the original sample.

(c) Finally, the optical properties of the spectroscopic medium must be as nearly "perfect" as possible. For absorption measurements, the medium should be transparent and weakly scattering [so that, for example, the "multiplex" and "throughput" advantages (*1*) of FTIR spectrometers can be exploited fully]. For luminescence measurements, not only should a matrix be transparent and weakly scattering, but it should be free of luminescent contaminants, the presence of which frequently determines the detection limits in fluorescence or phosphorescence spectrometry when the most modern instrumentation is used (*2*).

A truly "ideal" spectroscopic sampling matrix probably does not exist. However, it is particularly striking that the matrices conventionally used in analytical molecular spectroscopy

0003-2700/79/0351-643A$01.00/0
© 1979 American Chemical Society

We can't really show off Inficon's versatile surface analysis system.

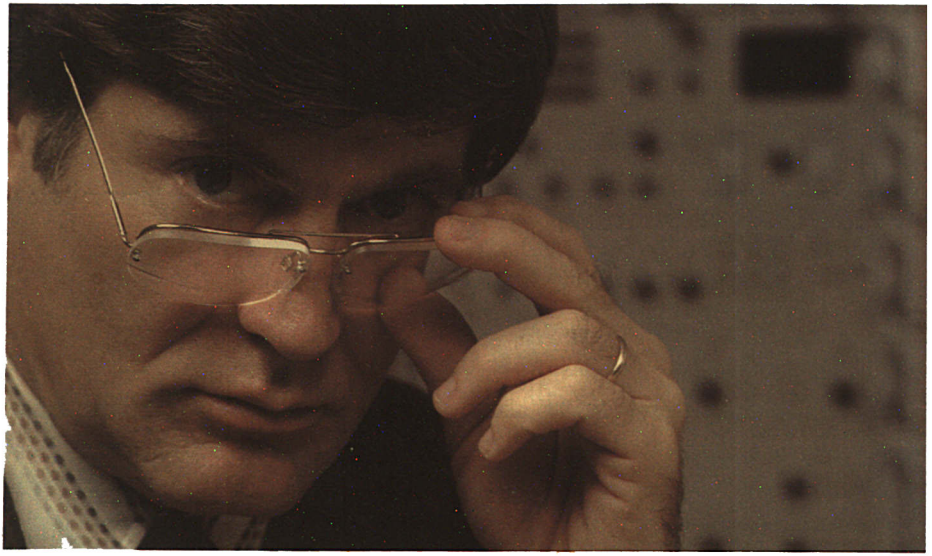

Until you show up with a sample for comparative analysis.

The best way to demonstrate Inficon's LHS-10 surface analysis system is by direct application. So bring in any vacuum compatible sample—give us two weeks' notice, please—and we'll analyze it.

And we'll prove ours is the simplest, most cost-effective system for your surface analyses.

Whatever your analytical problem, the LHS-10 will help you obtain more complete surface characterizations, correlate data faster, and reach firmer experimental conclusions.

LHS-10's universal analysis chamber allows customizing to your exact needs—whether it's catalyst efficiency testing, elemental or quantitative analysis, trace detection, depth profiling, or chemical fingerprinting.

You can have ESCA (XPS), UPS, AES, SAM, SIMS, ISS modules now, or add any later at minimal cost. Even add a computer system for simultaneous instrument operation and data manipulation.

No matter what techniques you select for present or future use, all can be employed on the same sample area—without specimen manipulation—for rapid sample analysis.

For now, let the other surface analysis companies first demonstrate their capabilities—then let Inficon give you proof positive of the LHS-10's superior performance, versatility and simplicity.

Write or call today. We'd like to see you and your sample soon.

We also offer contract surface analysis and assistance with special problems.

The plexiglas model of our universal chamber clearly shows our versatile analysis techniques.

INFICON
LEYBOLD-HERAEUS
6500 Fly Road, East Syracuse, New York 13057
315/437-0377 TWX 710 541-0594

CIRCLE 96 ON READER SERVICE CARD

(liquid solutions, KBr discs, frozen solutions, mulls, etc.) fall far short of ideal behavior. In contemplating this problem, we were attracted to the technique of matrix isolation, originally developed (*3, 4*) in the mid-1950's as a technique for obtaining optical or electron spin resonance spectra of transient species (*5–8*). Since that time, a few scattered reports, including one in this JOURNAL (*9*), implied considerable analytical promise for matrix isolation. Nonetheless, the use of matrix isolation as a practical sampling procedure for spectroscopic analysis of stable molecular species has been virtually ignored until recently.

Matrix Isolation Technique

In matrix isolation (MI), sample constituents (if solids or liquids at room temperature) are vaporized and then mixed thoroughly with a large excess (typically a factor of 10^4–10^8 on a mole basis) of a diluent gas. In principle, any gas may be used as the diluent, provided that it is chemically unreactive and does not absorb in the wavelength region of interest; we have found nitrogen to be a suitable matrix gas for general-purpose spectroscopic measurements. The resulting gaseous mixture is then deposited at cryogenic temperatures on a suitable optical window for spectroscopic examination as a solid. The goal is to ensure that virtually all sample molecules have matrix molecules as near neighbors. This condition is essential if criterion (b) of an "ideal" spectroscopic matrix is to be satisfied. In media such as solid nitrogen and argon, the interactions of solute molecules with the matrix are expected to be quite weak. Hence, perturbation of the spectroscopic behavior of a solute by the matrix should be minimized by employing such media as spectroscopic "solvents".

A schematic diagram of an MI experiment is shown in Figure 1. The sample is contained in a glass Knudsen cell, which is a short piece of 7-mm glass tubing equipped at one end with a vacuum joint and at the other end with a <0.5-mm orifice. Details of Knudsen cell construction will be described elsewhere (*10*). The Knudsen cell is wrapped with heating wire, the temperature of which is controlled by a variable autotransformer. The matrix gas is either passed through the Knudsen cell and used to sweep the sample vapor through the orifice into an evacuable cryostat head, or (as shown in Figure 1) the matrix and sample gases are mixed inside the cryostat head.

For most purposes, deposition temperatures of 11–15 K are satisfactory; such temperatures can be attained by small closed-cycle cryostats (*6*), which are straightforward to operate and require no liquid refrigerants. Indeed, it is the development of the commercial closed-cycle refrigerator which has made MI accessible to virtually any laboratory. The surface upon which the sample is deposited must exhibit high thermal conductivity and suitable optical properties; sapphire (as indicated in Figure 1) is the material of choice for UV–visible spectroscopy and CsI is usually used for IR measurements. More detailed descriptions of the practice of MI spectroscopy can be found in the books by Meyer (*11*) and Hallam (*6*), as well as in previous papers from this laboratory (*12–14*).

Principal applications of the MI sampling procedure in this laboratory have emphasized identification and quantitation of polycyclic aromatic hydrocarbons and their derivatives by FTIR absorption and molecular fluorescence spectrometry.

Matrix Isolation Fluorescence Spectroscopy

The principal analytical advantage of molecular fluorescence spectrometry is its extremely high sensitivity. However, fluorescence measured in liquid or gaseous media lacks selectivity, because electronic spectra of large molecules in fluid media tend to be broad and featureless. Figure 2 compares the fluorescence spectra of a four-component mixture of four-ring polycyclic aromatic hydrocarbons (three of which are isomeric) in room-temperature solution and matrix isolated in N_2. It is obvious that the low-temperature spectrum is more useful for both "fingerprinting" and quantitation. Note that three of the four compounds in this mixture are isomeric; the use of MI fluorometry for analysis of mixtures of isomeric aromatic hydrocarbons has been described in detail elsewhere (*15*). Enhancement of spectral resolution in fluorescence spectroscopy can also be achieved by simple frozen-solution techniques; in fact, if a "Shpol'skii solvent" (*16*) is used, higher resolution can be achieved by frozen-solution sampling than by the usual MI procedures. For quantitative analysis, however, it has been our experience that MI is distinctly superior to frozen-solution fluorometry.

The bane of quantitative fluorometric analysis in multicomponent samples is the difficulty of suppressing

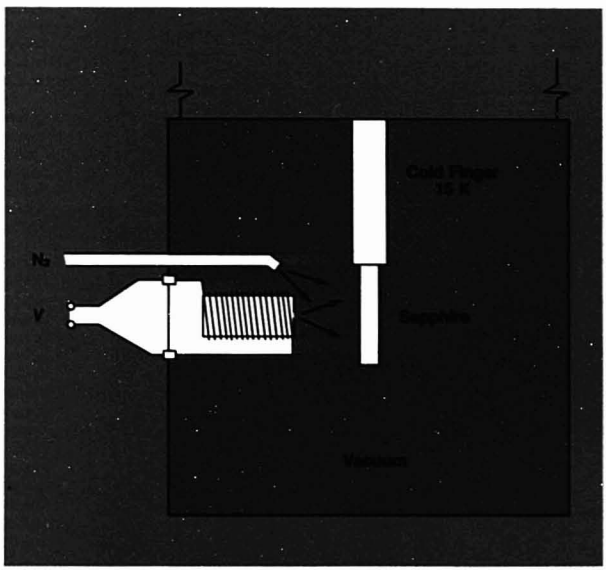

Figure 1. Schematic diagram of cryostat head design used for matrix isolation of polycyclic aromatic compounds

Samples placed in Knudsen cell (wrapped with heating wire maintained at voltage *V*), mixed with N_2 and deposited on a window (in this case, sapphire for fluorescence spectrometry). Head maintained at low temperature by closed-cycle (helium) refrigerator and evacuated to pressure of ca. 10^{-5} torr

IR Spectroscopists...

Thinking of buying a dispersive spectrometer?

Why settle for a limited-capability conventional spectrometer when you can get the full power of FT-IR at a comparable price?

Consider the advantages of Nicolet's new MX-1:

Speed.

The MX-1 measures a high-quality 4000-to-400 cm^{-1} spectrum in one minute!

Nearly-absolute wavenumber accuracy of 0.01 cm^{-1} throughout the spectral range. The MX-1 uses a He-Ne laser as a reference standard, eliminating the need for external calibration.

High sensitivity, invaluable for identifying trace compounds that are difficult or impossible with a dispersive instrument, and for rapid ATR analysis of surface coatings and low transmittance samples.

Highly versatile operation.

The MX-1's microprocessor-based data system provides for storage and recall of sample, background, and reference spectra; subtraction of solvent or reference spectra for non-chemical separations; and the ability to re-plot the spectrum in a variety of formats *without re-running the sample.*

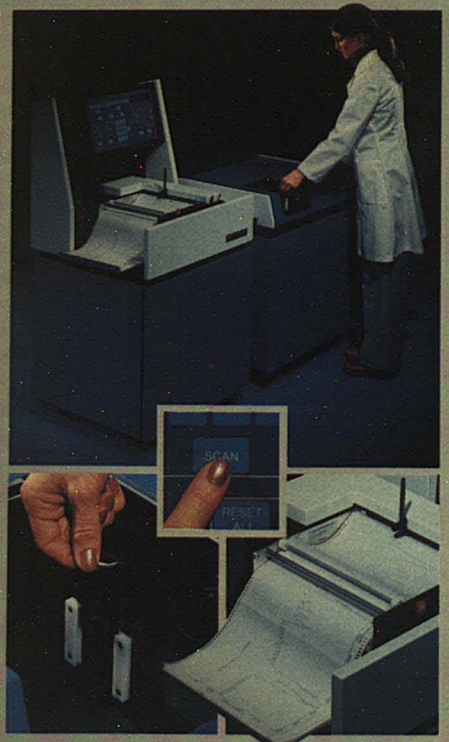

Simple operation.

Although the MX-1 is a powerful spectrometer with many advanced features, routine operation is extremely simple.

There are no slit functions, gain or resolution controls to worry about. To run a spectrum you merely insert the sample and press the SCAN button.

The MX-1 offers the performance you'd expect from Nicolet, the leaders in FT-IR. Please write or phone for complete details.

NICOLET INSTRUMENT CORPORATION

5225 Verona Road
Madison, Wisconsin 53711
Telephone: 608/271-3333

Think MX-1!

Superior performance at comparable cost.

CIRCLE 151 ON READER SERVICE CARD

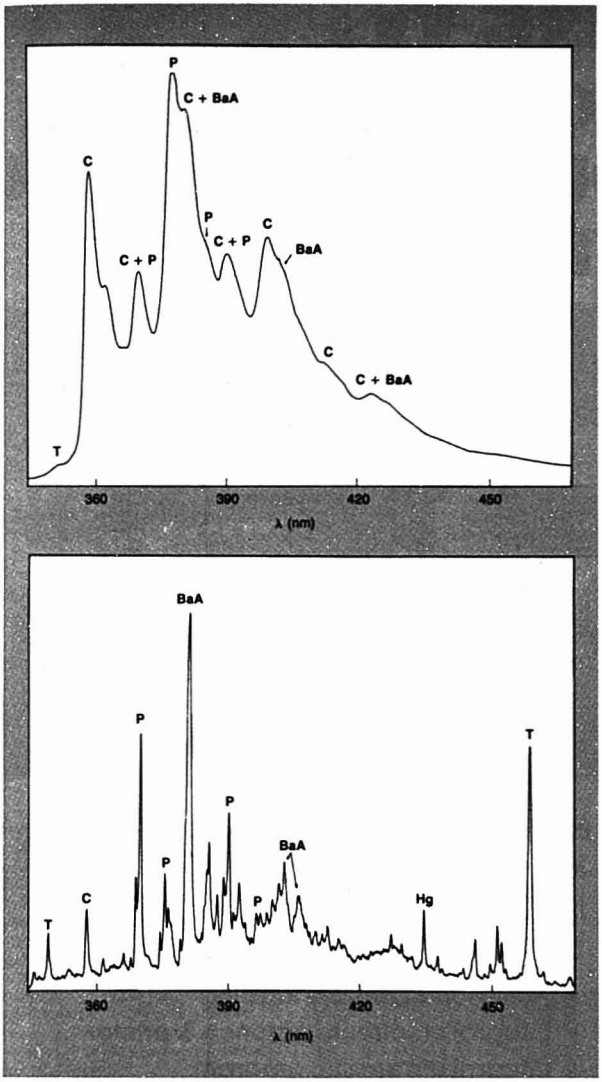

Figure 2. Room-temperature solution (top, in acetone) and MI (bottom, in N_2) fluorescence spectra of mixture of pyrene (P), benz[a]anthracene (BaA), chrysene (C), and triphenylene (T)

In solution spectrum, all solutes present at 10^{-6} *M* concentration. In MI spectrum, 100 ng of each of BaA, P, and C, and 4 μg of T, initially present in Knudsen cell. Note that BaA, T, and C are isomers ($C_{18}H_{12}$)

quenching and intermolecular energy transfer (which, if not eliminated, will cause the observed signal for any one compound to depend upon the identities and concentrations of other sample constituents). Some fluorescence quenching processes proceed by diffusion-controlled (collisional) mechanisms. Collisional fluorescence quenching can be suppressed by using a viscous sampling medium; any low-temperature solid will achieve this purpose, provided that aggregation of solute molecules can be avoided. However, transfer of electronic excitation energy from one molecule to another can also proceed by a "long-range" process not requiring contact of the energy donor and acceptor (*17*). Thus, criterion (b) for our ideal spectroscopic matrix is especially stringent for fluorometry of mixtures, because a potential fluorescence quencher does not necessarily have to be a "nearest neighbor" of an analyte molecule to be effective. Hence, molecular fluorescence spectrometry constitutes an especially demanding test of MI as an analytical sampling procedure.

One might initially surmise that quantitative analysis by MI spectroscopy will be difficult in any case, because it is not expected that all molecules of the analyte initially present in the Knudsen cell will be deposited ultimately on the cryostat window. However, if an internal standard is added to the sample, then one need not achieve "quantitative transfer" from the Knudsen cell to the spectroscopic surface; all that is required is that the fraction of each sample constituent which is eventually deposited be essentially the same. Our results (some of which are summarized below) indicate that this assumption is indeed valid if proper deposition procedures are utilized. Simple internal standardization thus appears sufficient for most quantitative applications of MI FTIR and fluorescence spectroscopy.

Figure 3 shows analytical calibration curves for each of four aromatic hydrocarbons present in mixtures in equimolar quantities (cf. the spectrum of one such mixture in Figure 2), as measured by MI fluorometry. Note that the calibration curves are linear and parallel over three decades in concentration, and that the calibration line for chrysene in the mixture is virtually superimposable upon that obtained for pure chrysene using benzo[b]fluorene as internal standard. This behavior is observed even when each compound is present in microgram quantities. These results validate the expectation that both collisional and long-range energy transfer and quenching phenomena can be suppressed thoroughly by MI, and

NEW!

LECO® CS-144 SIMULTANEOUS CARBON/SULFUR DETERMINATOR

More Automatic

Simplified Operation

Easy Maintenance

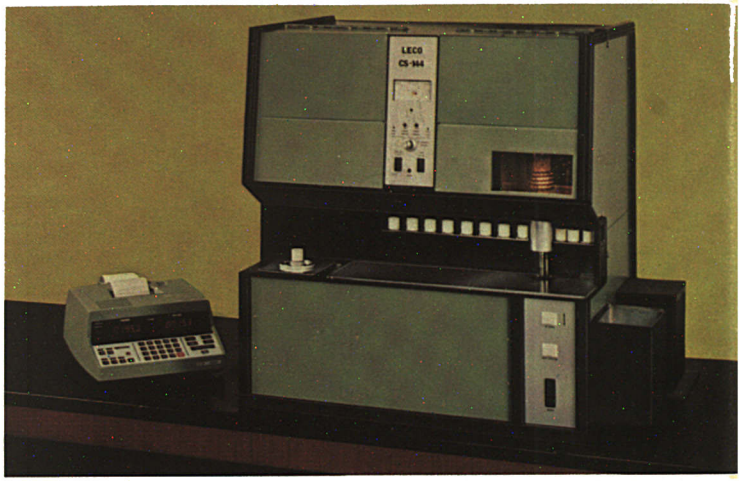

The LECO® CS-144, a new concept in automatic instrumentation, determines carbon and sulfur in iron, steel, ferrous alloys and other metals.

Control Console

- Automatic calibration
- Automatic weight compensation
- Automatic crucible loading
- Integral electronic balance & printer
- Integral diagnostic program

VISIT THE LECO® BOOTH—ACHEMA—FRANKFURT, GERMANY, JUNE 17

LECO®

LECO CORPORATION 3000 Lakeview Ave. St. Joseph, MI 49085, U.S.A. Phone: (616) 983-5531
Offices: California (714) 957-8227 • Texas (713) 931-0000 • Pittsburgh (412) 776-4891 • Canada (416) 270-6610

CIRCLE 129 ON READER SERVICE CARD

that the internal standard procedure is satisfactory for both pure compounds and mixtures. In MI fluorometry, we have observed calibration curves linear over more than five decades in concentration, with relative standard deviations for individual results typically falling in the 4–7% range (*14*). In contrast, as detailed elsewhere (*14, 18*), linearity over extended concentration ranges and high precision are difficult to achieve in frozen-solution matrices, because of the possibility of aggregation of solute molecules (or even formation of solute microcrystallites) as a liquid solution is frozen.

It is also noteworthy that significant improvements in the resolution of MI fluorescence spectroscopy can be achieved by use of organic "Shpol'skii solvents" as matrices (*19*), or by use of selective laser excitation of "site-selected" molecules in conventional MI media (*20*). By use of these procedures, the resolution attainable by MI fluorometry can be rendered comparable to that obtainable in Shpol'skii frozen solutions.

We therefore expect MI fluorometry to experience increasing use as a qualitative and quantitative analytical technique for complex samples. An example MI fluorescence spectrum of a "real" sample (at one excitation wavelength) is shown in Figure 4. This sample, which is an adsorption chromatography fraction of a sediment from a wastewater channel from a coking plant, contains approximately 20 different polycyclic aromatic hydrocarbons. This example serves to illustrate the quality of fluorescence spectra which can be obtained by MI even in samples of substantial complexity. It is impossible to identify all compounds in the mixture from one fluorescence spectrum obtained at one excitation wavelength. To obtain a "complete profile" of the fluorophore content of such a sample would require examination at a number of exciting wavelengths, a synchronous fluorescence scan (*21–23*), or additional fractionation of the sample. Ancillary spectroscopic techniques, such as time-resolved fluorometry, can also be coupled to MI to provide additional selectivity (*24*).

Matrix Isolation FTIR Spectroscopy

Historically, infrared spectroscopy has been regarded as virtually useless for characterization of complex environmental samples, due to insufficient sensitivity. However, the development of FTIR spectrometers has enabled IR absorption measurements to be made at far greater sensitivity and/or speed than is possible with dispersive spectrometers (*1*). When state-of-the-art FTIR instrumentation is used, practical problems in sample preparation, rather than instrumental limitations, often limit the quality of spectroscopic data obtained for small or complex samples (*25*). Thus, there is great interest in the improvement of techniques for IR microsampling (*25–27*). We believe that matrix isolation has great potential as a microsampling procedure for analytical FTIR spectroscopy. A few salient aspects of MI FTIR are considered below; for more detailed examinations of MI FTIR spectroscopy, the reader is referred to recent reviews (*12, 28*).

MI offers several advantages over conventional IR sampling procedures. Spectra of matrix-isolated molecules are nearly always sharper and simpler than those obtained in conventional media; this advantage is particularly noteworthy for gaseous samples (*29, 30*). Vibrational spectra of gases at ambient temperature contain rotational fine structure, and a single "vibration-rotation contour" may extend over more than 100 cm^{-1}. This rotational structure is "frozen out" when the IR spectrum of the same molecule is obtained under MI conditions, and individual vibrational transitions are manifested in the spectrum as sharp features of 1–8 cm^{-1} bandwidth. Even for compounds which are not gases at

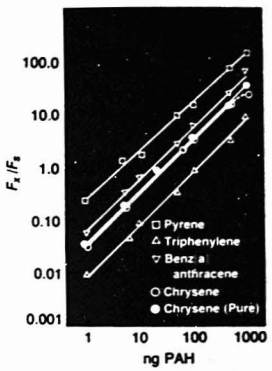

Figure 3. Analytical calibration curves for four-ring polycyclic aromatic hydrocarbons in synthetic mixtures (*14*)
Each sample equimolar in each of the four compounds. Shown for comparison is a calibration curve, obtained under identical conditions, for pure chrysene (●). Fluorescence intensity for each compound ratioed to that of an internal standard, benzo[b]fluorene (BbF)

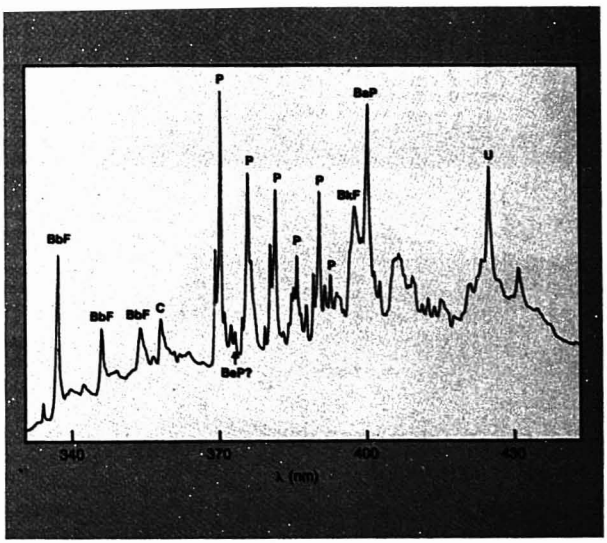

Figure 4. MI fluorescence spectrum (λ_{exc} = 313 nm) for chromatographic fraction from coking plant wastewater
Identified compounds: BbF, benzo[b]fluorene; C, chrysene; P, pyrene; BeP, benzo[e]pyrene; BkF, benzo[k]fluoranthene; BaP, benzo[a]pyrene. U denotes band due to major sample constituent not yet identified

Audiences around the world have applauded the OmniScribe's:

- Patented non-contacting feedback transducer element
- Accuracy of < ± 0.3% full scale
- Response time of < 0.50 sec. to 90% full scale
- Linearity of < ± 0.2%
- Repeatability of ± 0.1%

houston instrument | DIVISION OF BAUSCH & LOMB

"the graphics - recorder company"

CIRCLE 148 ON READER SERVICE CARD

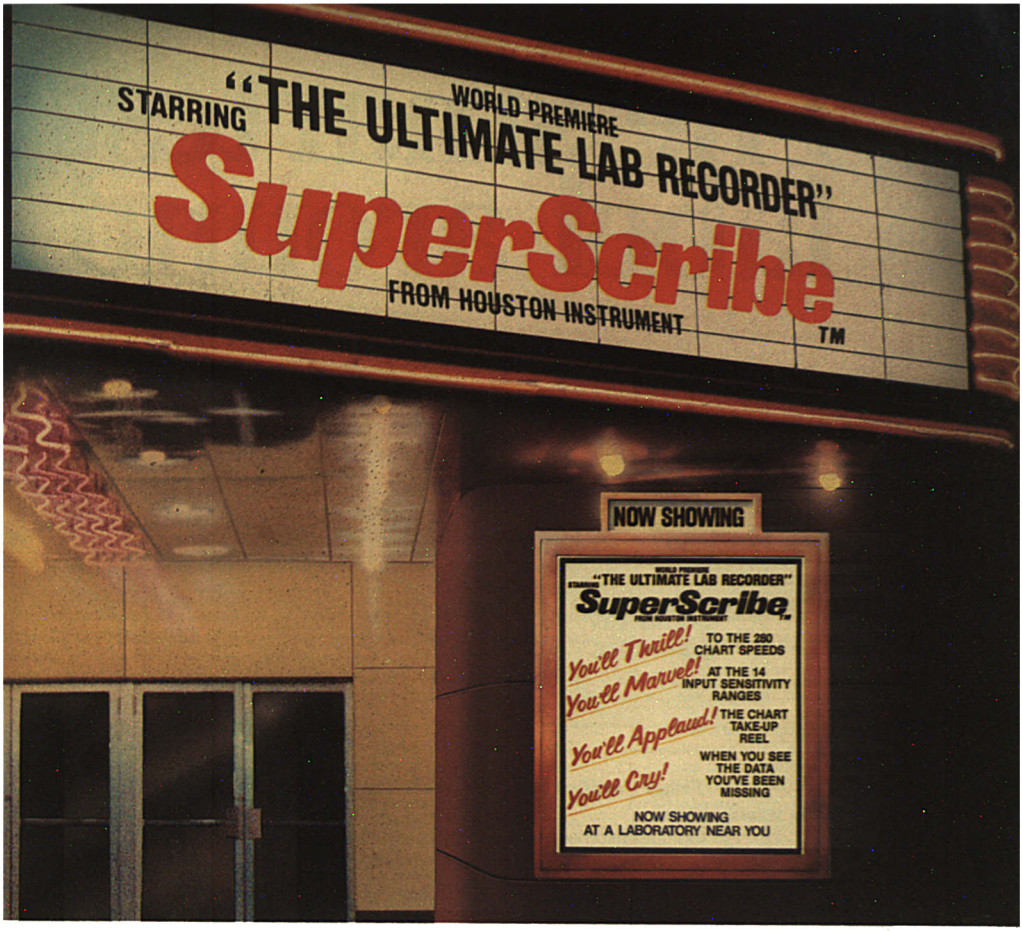

In addition you'll see:

- Chart speeds (English and Metric) of 0-40 in/min. and per hour and 0-100 cm/min and per hour.
- 14 calibrated switch selectable input ranges in a 1-2-5 sequence from 1mv to 20v full scale.
- Patented non-contacting feedback transducer element
- Linearity of $< \pm 0.25\%$ of full scale
- Accuracy of $< \pm 0.25\%$ sec. full scale

For more information on the OmniScribe and SuperScribe contact Houston Instrument, One Houston Square, Austin, Texas 78753 (512) 837-2820. For rush literature requests outside Texas call toll free 1-800-531-5205. In Europe contact Houston Instrument, Rochesterlaan 6, 8240 Gistel Belgium. Phone 059/2774455 Telex Bausch 81399

TM Trademark of Houston Instrument
® Registered Trademark of Houston Instrument
* U.S. Domestic Price Only
* U.S. suggested retail price only

CIRCLE 149 ON READER SERVICE CARD

The smartest label around.

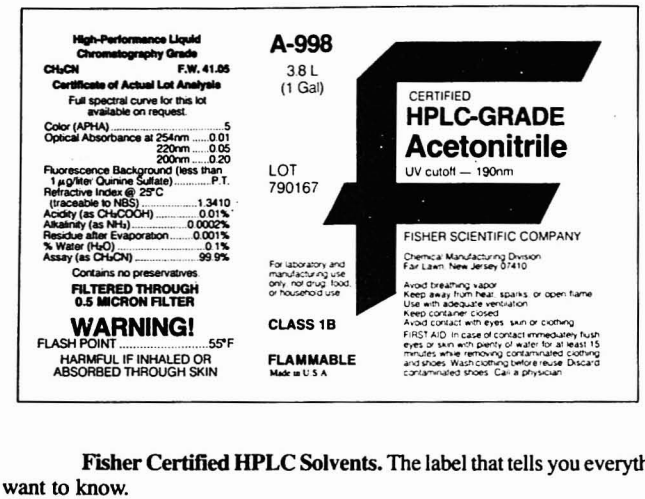

Fisher Certified HPLC Solvents. The label that tells you everything you want to know.

Optical absorbance at a variety of wavelengths (full spectral curves on request). Refractive index directly traceable to NBS. Background fluorescence. UV cutoff. Assay as mol % via GC. Water and preservative /inhibitor content. And much more.

Fisher HPLC solvents — so pure you can use them for **gradient elutions.** They're distilled in glass. And submicron-filtered to eliminate particulates.

After all, today's high-performance liquid chromatography columns, detectors and samples are valuable things. They deserve **the best.** That's why Fisher defines and certifies every parameter vital to their protection.

In stock at your nearest Fisher branch. Or have your branch set up a Customer Reserve Quantity arrangement, reserving your HPLC solvents needs for you alone, shipping automatically to your timetable. You can even reserve an **entire lot,** guaranteeing total uniformity month in, month out.

And remember: Fisher also stocks an impressive selection of auxiliary HPLC materials. Apparatus, appliances, supplies. This simplifies your ordering — and your laboratory life.

Write for HPLC catalog **today!**

Fisher Scientific Company
711 Forbes Avenue Pittsburgh PA 15219

CIRCLE 76 ON READER SERVICE CARD

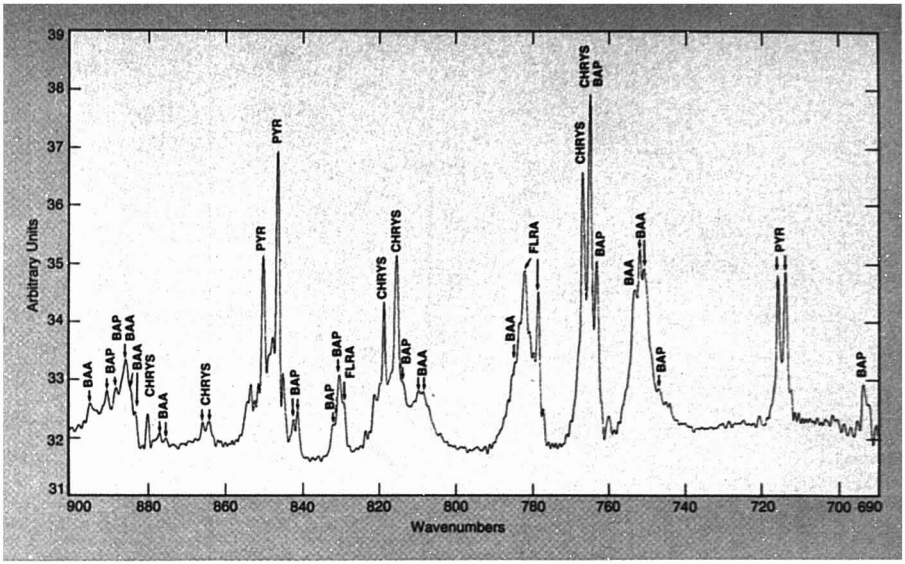

Figure 5. MI FTIR spectrum of synthetic mixture of five polycyclic aromatic hydrocarbons (25 μg of each) in N_2 at 1 cm^{-1} resolution

Compounds: BAA, benz[a]anthracene; CHRYS, chrysene; PYR, pyrene; FLRA, fluoranthene; BAP, benzo[a]pyrene

room temperature, MI often produces a significant reduction in bandwidth. It has been our experience that, for polycyclic aromatic compounds, IR bandwidths of 1–6 cm^{-1} are commonly observed by MI in N_2, as compared with the 5–10 cm^{-1} bandwidths usually obtained in liquid solutions or KBr discs. An indication of the spectral quality which can be achieved by MI FTIR is shown in Figure 5, a spectrum of a five-component mixture of polycyclic aromatics (three of which are isomers) in the 700–900 cm^{-1} region (where most strong IR bands for polycyclic aromatic hydrocarbons are found).

The MI technique is well suited to IR microsampling, because the vapor from the Knudsen cell can be directed onto a window as small as 4 mm in diameter. Under these conditions, detection limits for polycyclic aromatics (which are weak IR absorbers) in the 50–100-ng region have been achieved (*10*). The use of MI as a microsampling method enables one to avoid the difficulties associated with preparation of KBr micropellets (*25, 26*) or use of microsolution cells (*31*). For gaseous samples, use of MI permits one to avoid the cumbersome characteristics of long-path gas cells.

A number of common matrix materials, including N_2, Ar, Ne, and Kr, exhibit no absorption in the IR except for phonon bands in the far IR ($\bar{\nu} < 85$ cm^{-1}). These matrices accordingly make efficient use of the high energy throughput of FTIR spectrometers and also minimize difficulties with sloping baselines which are often obtained in spectra of samples in solutions or KBr discs. The latter consideration is especially important for quantitative analysis. We have observed that matrix-isolated compounds vacuum sublimed from a Knudsen cell obey Beer's law, provided that an internal standard is used to compensate for nonquantitative deposition. For example, Beer's law plots for matrix-isolated polycyclic hydrocarbons typically are linear over 1.5–2 decades in solute concentration (*13*). In contrast, Beer's law plots for FTIR absorption of the same compounds in liquid solution typically exhibit linear ranges of less than one decade, and quantitative analysis by FTIR in KBr discs is virtually impossible (*32*).

By sequential use of two different Knudsen cell-deposition window systems, it is possible to achieve linear Beer's law behavior in MI FTIR over three decades in analyte concentration (*10*). Moreover, the linear quantitative ranges of MI fluorescence and FTIR do not totally coincide. The linear dynamic range for MI fluorometry typically extends from the detection limit (subnanogram) to ca. 0.1–1 μg (*14*), while linear regions for Beer's law adherence by FTIR typically extend from the detection limit (ca. 50–200 ng) to 10 μg or more (*13*). Thus, for an intensely fluorescent compound such as benzo[a]pyrene, which can be detected by MI fluorescence in very small quantities (10 pg), the total linear dynamic range which can be achieved by complementary use of MI FTIR and fluorescence is more than six decades in concentration.

The MI FTIR spectrum of a "real" sample is shown in Figure 6. This is a spectrum of the same twenty-component coking plant wastewater fraction whose fluorescence spectrum is shown in Figure 4. Those compounds which can be identified readily from the spectrum are indicated on the figure. As in the case of the fluorescence spectrum, a "complete" inventory of the polycyclic hydrocarbons present in this sample cannot be obtained from one spectrum; additional separation would be required. Nevertheless, Figure 6 demonstrates that well-resolved spectra of very complex materials can be obtained by MI FTIR, and we expect the complementary application of MI FTIR and fluorescence spectrometry to be a powerful new tool for the characterization of complex organic and environmental samples.

Our studies to date have demonstrated MI to be a useful sampling

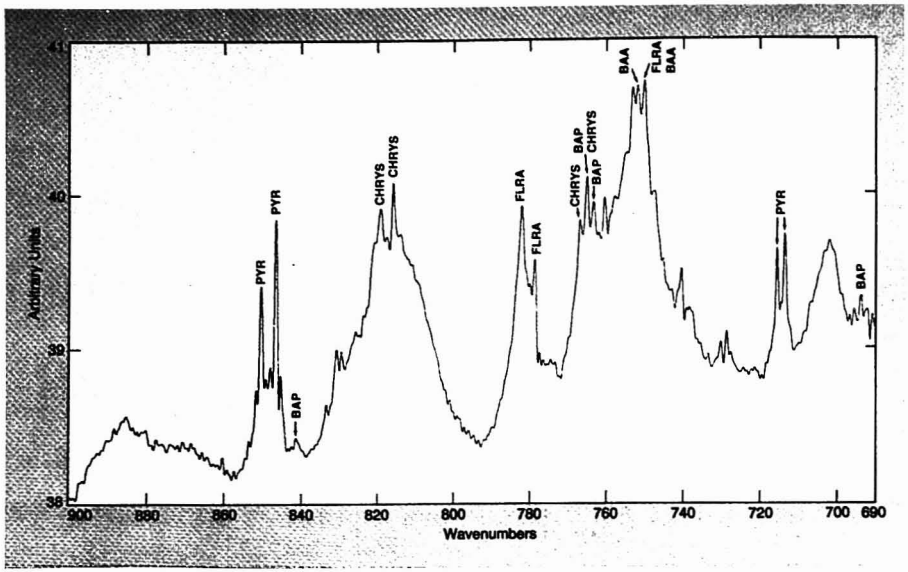

Figure 6. MI FTIR spectrum of chromatographic fraction from coking plant wastewater
Identified compounds: PYR, pyrene; CHRYS, chrysene; FLRA, fluoranthene; BAP, benzo[a]pyrene; BAA, benz[a]anthracene

technique for the qualitative and quantitative spectroscopic analysis of stable molecular species in mixtures. Quantitation poses no special problems if internal standardization is employed. We have emphasized use of the sharp spectra obtained by MI fluorescence and FTIR to distinguish between isomeric compounds (*14, 15, 33*) since, for example, isomeric polycyclic aromatic hydrocarbons may exhibit greatly differing carcinogenic potentials. Moreover, isomeric aromatic compounds often are difficult to separate from one another when present in complex samples, and their mass spectra tend to be very similar.

MI spectrometry has been demonstrated applicable to characterization of very complex samples (coal liquids and shale oils) (*33*), but much additional work remains to be performed in this area. In that regard, it should be recalled that the first step in an MI experiment is vaporization of the sample. It is thus intriguing to contemplate the possibility that "on-the-fly" spectroscopic detection of gas chromatographic column effluents may be feasible by MI. The high separation efficiency of glass capillary columns coupled with the sensitivity and characteristic "fingerprint" spectra obtained by MI suggests that combination of these techniques would produce an especially powerful analytical tool. Indeed, Reedy et al. (*34*) have recently described a procedure for obtaining MI FTIR spectra of compounds eluting from a gas chromatograph, to obtain spectra of very high quality. The combination of GC with MI FTIR and fluorescence measurements, which is being pursued vigorously in this laboratory, may perhaps be regarded as the "ultimate" analytical application of MI spectroscopy.

Of course, MI is not a "perfect" spectroscopic sampling method and it certainly cannot be regarded as a panacea. Many of the systematics of optical spectra in cryogenic solids are poorly understood (*6, 11*), and great care must therefore be exercised in the interpretation of MI spectra of unknown samples or unfamiliar compounds. Moreover, the technique is not readily applicable to compounds which cannot be vaporized without decomposition; hence, MI is not expected to be broadly useful in clinical or biochemical analysis. However, the full potential of MI as a sampling procedure for analytical spectroscopy has only begun to be explored. Though the results described above are restricted to IR absorption and UV–visible fluorescence, utilization of MI for analytical purposes is not limited to these spectroscopic techniques. Thus, for example, electron paramagnetic resonance has been used often for study of matrix-isolated transient species produced in the laboratory; recently, the use of MI as an enrichment procedure for the identification of free radicals (such as HO_2) in atmospheric samples by EPR has been described (*35*). Despite formidable difficulties, laser Raman spectra of matrix-isolated species can be obtained (*36*). Very recently, methodology has been described for obtaining secondary ion mass spectra of molecules isolated in argon matrices (*37*). It therefore seems certain that a wide variety of analytical applications for matrix isolation will emerge as research, designed with a specifically analytical viewpoint, accelerates.

Acknowledgment

It is a pleasure to recognize the vital contributions of our coworkers to the results described above: Verne Biddle, Paul Bilotta, Neil Brotherton, Dick Dickinson, Arlene Garrison, Randy Gore, Doyle Hembree, Ray Hinton, Richard Kemmerer, Stan Spurlin, Robert Stroupe, and Pari Tokousbalides. We gratefully acknowledge the cooperation of G. Goldstein, W. H. Griest, B. R. Clark, and M. R. Guerin, of the Oak Ridge National Laboratory, in providing samples of some polycyclic aromatic hydrocarbons and synthetic liquid fuels.

An der Universität Karlsruhe (TH), Fakultät für Chemie, ist ein Lehrstuhl

"Instrumentelle Analytik" (C4-Professur)

und in Personalunion die Stelle des Institutsleiters des

"Instituts für Radiochemie"

im Kernforschungszentrum Karlsruhe GmbH zu besetzen (Nachfolge Prof. Dr. Seelmann-Eggebert).

Der Lehrstuhlinhaber und Institutsleiter soll ein anerkannter Wissenschaftler auf dem Gebiet der Instrumentellen Analytik sein und über Erfahrungen in der Radiochemie verfügen.

Im Institut für Radiochemie werden in enger Zusammenarbeit mit anderen chemischen Instituten des Kernforschungszentrums überwiegend projektbezogene Arbeiten durchgeführt (Wiederaufarbeitung bestrahlter Kernbrennstoffe, Reaktorsicherheit, Kernmaterialüberwachung). Die Ausstattung des Instituts gewährleistet sehr gute Arbeitsmöglichkeiten.

Bewerbungen mit den üblichen Unterlagen werden bis 15.5.1979 erbeten an den Dekan der Fakultät für Chemie der Universität Karlsruhe, Engesserstr. Geb. Nr. 30.45, 7500 Karlsruhe 1.

GET THESE FREE LC REPORTS.

Methods Optimization. Our own experts' time-saving systematic procedures for setting up LC analyses and improving results

Environmental Analysis. Digests of new applications literature, and Perkin-Elmer publications describing LC units.

Polymer Analysis. An expanding LC field. Current literature and Perkin-Elmer's own publications summarized clearly.

Get these new booklets for your reference file. Prepared by our own staff of LC experts. Circle the RSC number or write Perkin-Elmer Corp., MS-12, Main Avenue, Norwalk, CT 06856.

PERKIN-ELMER
Expanding the world of analytical chemistry.

CIRCLE 175 ON READER SERVICE CARD

New Applications of Lasers to Chemistry

ACS Symposium Series No. 85

Gary M. Hieftje, *Editor*
Indiana University

Based on a symposium sponsored by the Division of Analytical Chemistry of the American Chemical Society.

Order from:
SIS/American Chemical Society
1155 16th St., N.W.
Wash., D.C. 20036

This collection of 12 papers represents an excellent cross section of topics depicting the scope of current applications of lasers to chemistry and the potential importance of lasers in the future of chemistry and chemical analysis.

Chemists, physicists, and engineers from academia, industry, and government give a precise account of the latest developments in laser technology and measurement systems as well as the use of lasers in detecting single atoms and molecules.

The book's main subject material reflects areas of chemistry in which the laser has had the greatest impact — namely, high-resolution spectroscopy, high sensitivity analysis, time-resolved or kinetic spectroscopy, and new techniques in laser Raman spectrometry.

CONTENTS

Selective Excitation of Probe Ion Luminescence (SEPIL) • Applications of Tunable-Diode-Laser IR Spectroscopy to Chemical Analysis • Two-Photon-Excited Molecular Fluorescence • Laser-Excited Luminescence Spectrometry • Laser Fluorimetry. Detection of Aflatoxin B_1 in Contaminated Corn • Laser-Enhanced Ionization for Trace Metal Analysis in Flames • The Study of Biological Surfaces by Laser Electrophoretic Light Scattering • New Laser-Based Methods for the Measurement of Transient Chemical Events • Laser Applications in Photoelectrochemistry • Coherent Anti-Stokes Raman Scattering Spectroscopy • Spectroscopy by Inverse Raman Scattering • Vibrational Spectra in Nanoseconds

244 pages (1978) Clothbound $23.50
LC 78-22032 ISBN 0-8412-0459-4

this recorder has a mind of its own

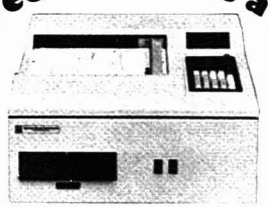

SERIES 8000 ACQUIRES, STORES AND PROCESSES DATA AUTOMATICALLY.

A computer-controlled recorder that processes up to 8 signals simultaneously from all types of analytical instruments. Store data on floppy disks. Perform mathematical operations and display in either x-y, strip, or digital formats. Disk capacity is equivalent to about 300 ft. of chart paper.

Series 8000 routinely performs Integration. Retention Times. Background Correction. Differentiation. Smoothing. Scaling. Normalization. Averaging. Peak Picking. Plus a whole lot more.

With specialized software for Chromatography. Programmable keystrokes. Diagnostic Routines. And other applications. Accessories include RS232, digital printer and curve tracking digitizer.

Series 8000. A complete data management system for any lab application. Call or write for a free demonstration and find out more about the recorder that truly has a mind of its own . . . Series 8000.

Bascom-Turner Instruments
A Division of EIC Corporation
111 Chapel Street, Newton, MA 02158 U.S.A. (617) 965-2710

CIRCLE 31 ON READER SERVICE CARD

DELIVERY FROM STOCK

WINDOWS, LENSES & ATR PLATES

NaCl • KCl • KBr • CaF_2 • MgF_2 • BaF_2 • Ge • Si • ZhSe • KRS-5 • ZnS • CsBr • CsI • LiF • SrF_2 • Cultured Quartz • Sapphire • Fused Silica • Irtran 2

INFRARED ACCESSORIES

Sealed Liquid Cell Holder • Gas Cell • Precision Cell • Demountable Cell • KBr Pellet Press & Holder

INTERFERENCE FILTERS

UV • Near UV • Visible • Near IR • IR

STANDARD & CUSTOM ITEMS

REPOLISH & RECONDITIONING SERVICES

JANOS OPTICAL CORPORATION

RT. 35 TOWNSHEND, VT. 05353
TEL: (802) 365-7714
TWX: 7103636777

CIRCLE 97 ON READER SERVICE CARD

References

(1) P. R. Griffiths, "Transform Techniques in Chemistry," Plenum Press, New York, 1978.
(2) J. H. Richardson, *Anal. Biochem.*, **83**, 754 (1977).
(3) E. Whittle, D. A. Dows, and G. C. Pimentel, *J. Chem. Phys.*, **22**, 1943 (1954).
(4) I. Norman and G. Porter, *Nature*, **174**, 508 (1954).
(5) A. M. Bass and H. P. Broida, "Formation and Trapping of Free Radicals," Academic Press, New York, 1960.
(6) H. E. Hallam, "Vibrational Spectroscopy of Trapped Species," Wiley, London, 1973.
(7) S. Cradock and A. J. Hinchcliffe, "Matrix Isolation: A Technique for the Study of Reactive Inorganic Species," Cambridge University Press, New York, 1975.
(8) M. Moskovits and G. A. Ozin, "Cryochemistry," Wiley, New York, 1976.
(9) J. S. Shirk and A. M. Bass, *Anal. Chem.*, **41** (11), 103A (1969).
(10) D. M. Hembree, E. R. Hinton, Jr., R. R. Kemmerer, G. Mamantov, and E. L. Wehry, *Appl. Spectrosc.*, submitted for publication.
(11) B. Meyer, "Low Temperature Spectroscopy," p 105, American Elsevier, New York, 1971.
(12) E. L. Wehry, G. Mamantov, R. R. Kemmerer, H. O. Brotherton, and R. C. Stroupe, in "Carcinogenesis: A Comprehensive Survey," R. I. Freudenthal and P. W. Jones, Eds., Vol 1, p 299, Raven Press, 1976.
(13) G. Mamantov, E. L. Wehry, R. R. Kemmerer, and E. R. Hinton, *Anal. Chem.*, **49**, 86 (1977).
(14) R. C. Stroupe, P. Tokousbalides, R. B. Dickinson, Jr., E. L. Wehry, and G. Mamantov, *ibid.*, p 701.
(15) P. Tokousbalides, E. R. Hinton, Jr., R. B. Dickinson, Jr., P. V. Bilotta, E. L. Wehry, and G. Mamantov, *ibid.*, **50**, 1189 (1978).
(16) G. F. Kirkbright and C. G. de Lima, *Analyst*, **99**, 338 (1974).
(17) A. A. Lamola and N. J. Turro, "Energy Transfer and Organic Photochemistry," p 37, Wiley, New York, 1969.
(18) R. J. Lukasiewicz and J. D. Winefordner, *Talanta*, **19**, 381 (1972).
(19) P. Tokousbalides, E. L. Wehry, and G. Mamantov, *J. Phys. Chem.*, **81**, 1769 (1977).
(20) B. Dellinger, D. S. King, R. M. Hochstrasser, and A. B. Smith III, *J. Am. Chem. Soc.*, **99**, 7138 (1977).
(21) D. W. Johnson, J. B. Callis, and G. C. Christian, *Anal. Chem.*, **49**, 474A (1977).
(22) T. Vo-Dinh, *ibid.*, **50**, 396 (1978).
(23) L. P. Giering and A. W. Hornig, *Am. Lab.*, **9** (11), 113 (1977).
(24) R. B. Dickinson, Jr., and E. L. Wehry, *Anal. Chem.*, **51**, 778 (1979).
(25) P. R. Griffiths and F. Block, *Appl. Spectrosc.*, **27**, 432 (1973).
(26) H. J. Sloane and R. J. Obremski, *ibid.*, **31**, 506 (1977).
(27) R. Cournoyer, J. C. Shearer, and D. H. Anderson, *Anal. Chem.*, **49**, 2275 (1977).
(28) D. W. Green and G. T. Reedy, in "Fourier Transform Infrared Spectroscopy: Applications to Chemical Systems," J. R. Ferraro and L. J. Basile, Eds., p 1, Academic Press, New York, 1978.
(29) M. M. Rochkind, *Spectrochim. Acta*, **27A**, 547 (1971).
(30) D. F. Ball and C. F. Purnell, *Int. J. Environ. Studies*, **9**, 131 (1976).
(31) J. P. Coates, *Am. Lab.*, **88** (11), 67 (1976).
(32) H. O. Brotherton, Jr., MS thesis, University of Tennessee, Knoxville, Tenn., 1976.
(33) G. Mamantov, E. L. Wehry, R. R. Kemmerer, R. C. Stroupe, E. R. Hinton, and G. Goldstein, *Adv. Chem. Ser.*, **170**, 99 (1978).
(34) G. T. Reedy, S. Bourne, and P. T. Cunningham, paper presented at 29th Pittsburgh Conference on Analytical Chemistry and Applied Spectroscopy, Abstract No. 50, Cleveland, Ohio, Feb. 1978.
(35) D. Mihelcic, D. H. Ehhalt, J. Klomfass, G. F. Kulessa, V. Schmidt, and M. Trainer, *Ber. Bunsenges. Phys. Chem.*, **82**, 16 (1978).
(36) G. A. Ozin, "Vibrational Spectroscopy of Trapped Species," H. E. Hallam, Ed., p 373, Wiley, London, 1973.
(37) H. T. Jonkman, J. Michl, R. N. King, and J. D. Andrade, *Anal. Chem.*, **50**, 2078 (1978).

Financial support for this research derived from contracts with the Electric Power Research Institute (RP-332 and RP-1307) and grants from the National Science Foundation (MPS75-05364 and CHE77-12542).

Earl L. Wehry is professor of chemistry at the University of Tennessee. His principal research interests include fluorescence and phosphorescence spectroscopy, photochemistry and excited-state chemistry, applications of lasers to analytical spectroscopy, and the chemical degradation of environmental pollutants.

Gleb Mamantov is professor of chemistry at the University of Tennessee. He has broad research interests in the areas of analytical and inorganic chemistry that range from electrochemistry in molten salts to applications of matrix isolation infrared spectroscopy to analytical chemistry and the characterization of reactive intermediates.

At Last! A Total System for Magnetic Susceptibility

Why is the S.H.E. Corporation Model VTS magnetometer destined to become the new standard for sensitive analytic magnetic measurements? Consider its performance:

- Highest sensitivity to permanent or induced moments available in a commercial instrument. Changes in susceptibility as small as 3×10^{-13} emu/gm can be resolved
- Versatile sample-handling scheme accommodates solids, liquids, powders and is readily adapted for measurements requiring flowing liquids or controlled atmospheres
- Exceptionally short 0.4 msec response time for the study of time-dependent phenomena
- 4.5 K to 400 K temperature range
- Magnetic field capability to 5 Tesla

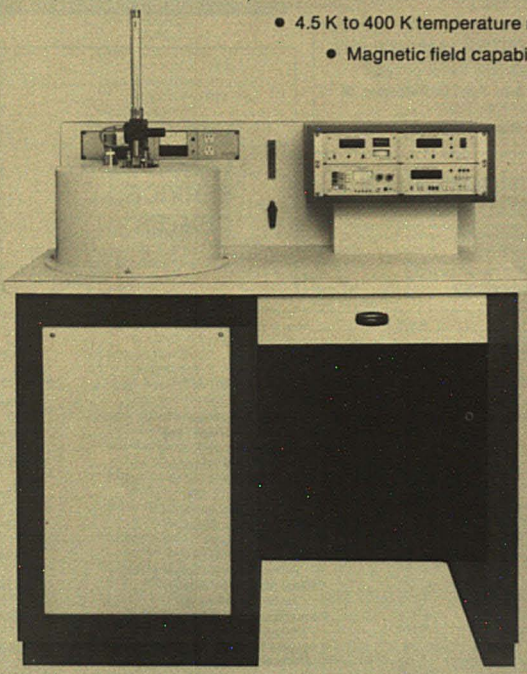

But unequaled performance isn't all.

The Model VTS also responds to the need for increased speed, reliability, and convenience. The desired temperature, magnetic field, and other operating parameters are entered directly in digital form via front panel switches. An internal microprocessor with numerous built-in tests and fail-safe procedures controls all the required measuring operations quickly and efficiently.

An optional computer interface facilitates automation of the entire measurement process with a small laboratory computer. Completely unattended data acquisition over the full operating range of temperatures and fields is then made possible. The operator is required only to change samples, which takes just a few minutes since there is no need to fuss with a delicate mechanical suspension or to return the sample measurement region to room temperature.

For difficult magnetic measurements, the SHE Model VTS magnetometer/susceptometer offers a simple, dependable solution. Request our brochure for a detailed description and complete specifications. Then let us know if you want to visit our factory for a "hands on" demonstration. We'd like to hear from you. Call or write S.H.E. Corporation, 4174 Sorrento Valley Blvd., San Diego, CA 92121

Tel: (714) 453-6300 Telex: 697903

In Europe:
S.H.E. GmbH, Maria-Theresia-Allee 22,
D-5100 Aachen 1, WEST GERMANY
Telex: 832441 Telephone: (0241) 72051

S.H.E. CORPORATION
CRYOGENIC INSTRUMENTS AND SYSTEMS

CIRCLE 192 ON READER SERVICE CARD

LABORATORY SERVICE CENTER

Acetonedicarboxylic Acid • Aluminum-tert-butoxide • Aluminon
o,o'- & p,p'-Biphenol • Chloranilic Acid • 3,5-Dinitrobenzoic Acid
2,6-Dinitro-1-chlorobenzene • Di-n-Propyl Ketone • Dithiol • Dulcitol
Disodium Phenyl Phosphate • Esculin • Ethyl Glycolate • Glycolic Acid
Glyoxal-Bis-2-Hydroxyanil • Imidazole • Lacmoid • Orcein • Oxamide
Phenyl Urea • Protocatechualdehyde • Pyruvic Acid • Sodium Succinate
Sodium Tetraphenylboron • Tetrahydrofurfuryl Acetate • iso-Vanillin
N,N,N,N-Tetramethyl-p-Phenylenediamine DiHCl • ω-Tribromoquinaldine

Write for our Products List of over 3000 chemicals

Tel: 516-273-0900 TWX: 510-227-6230

EASTERN CHEMICAL
Division of GUARDIAN CHEMICAL CORP.
BOX 2500 K
HAUPPAUGE, N. Y. 11787

ANALYTICAL SERVICES
GOLLOB ANALYTICAL SERVICE

LC Laboratories
1254 Chestnut Street
Newton, MA 02164
(617) 244-9222
Problem-Solvers in Organic and Polymer Chemistry
LIQUID CHROMATOGRAPHY SERVICES

SPECTRAL INTERPRETATION SERIES
IR, NMR (2 parts), MASS, RAMAN, ESR, C-13NMR
Seven proven audio programs totaling 8 hours of self-instruction for practicing chemists. Price $175.00
Order from SCIENCE MEDIA, P.O. Box 910M, Boca Raton, FL 33432

SOLVENTS—Highest Purity
Call or write for prices.
Pollard & Co. Box 7131 Wilmington, DE 19803
Phone: 302-656-0060

USE LABORATORY SERVICE CENTER

LAB SAFETY
Send for 1979 Catalog
LAB SAFETY SUPPLY CO.
P.O.Box 1368, Janesville, WI 53545

environmental & material analysis
- Water, waste water, sewage
- Precious metal fire assay
- Spectrographic analysis
- Industrial hygiene
- Microbiology
- GC IR
- Metals, ores, chemicals

princeton testing laboratory
Princeton Svc. Ctr.
U.S. Hwy 1, Box 310A
Princeton, N.J. 08540
(609) 452-9850

INDEX TO ADVERTISERS IN THIS ISSUE

CIRCLE INQUIRY NO.	ADVERTISERS	PAGE NO.
2	* Academic Press Flamm Advertising	630A
3	Aldrich Chemical Company William Eisner & Associates Inc. Adv.	573A
4	* Alltech Associates Chromad	623A
1	* Altex Scientific, Inc. Oliver Smith Advertising, Inc.	553A
6	* The American Instrument Company Industrial Advertising Associates	600A
7	* Analtech, Inc. Robert J. Allen	596A
5	* Antek Cooley & Shillinglaw, Inc.	588A
20	J. T. Baker Chemical Company Naimark & Barba, Inc.	563A
29-30	Barnstead Marketing Dimensions, Inc.	IFC
31	Bascom-Turner Instruments IKON Communications Consultants, Inc	655A
23	* Bausch & Lomb Blair Advertising, Inc.	566A
27	** Bausch & Lomb Blair Advertising, Inc.	628H
21	* Brinkmann Instruments, Inc. Blatt Advertising	OBC
15	Brownlee Labs Inc. James S. Schlesinger	590A
24	* Burdick & Jackson Laboratories, Inc. Studio 5 Advertising	628A
36	Chrompack Mealer & Emerson, Adv.	588A
34	Chrompack Nederland BV	635A
32	Corco Chemical Corporation Sit/Com	572A
35	Crane Company Doremus & Company	587A
33	* Crawford Fitting Company Falls Advertising Company	638A
50	Digital Equipment Corporation Creamer, Inc.	569A
52	* Dionex Fred Schott & Associates	570A
xxx	* Eastman Kodak Company Rumrill-Hoyt, Inc.	633A
75	* Finnigan Instruments Robert Pease & Company, Adv.	642A
76	* Fisher Scientific Company Tech-Ad Associates	652A
74	Forma Scientific Fahlgren & Ferriss, Inc.	557A
77-78	* Foxboro Analytical Shepherd, Tibball & Galog	598A, 600A
80	* GCA/Precision Winterkorn, Hammond and Lillis, Inc.	562A
81	* Gilford Instrument Laboratories, Inc. Oberlin Industrial Advertising	602A
83	* Gilson Medical Electronics, Inc. Fred Schott & Associates	586A
82	Graphic Controls Corporation Conklin, Labs & Bebee, Inc.	634A
95	* Hamilton Company Mealer & Emerson Adv.	603A, 604A
130-135	* Hewlett-Packard C. K. Associates	576A-577A
94	* Hewlett-Packard Tallant/Yates Advertising, Inc.	564A-565A
152-153	* Hewlett-Packard S. A. Dorland Advertising	595A, 597A

INDEX TO ADVERTISERS IN THIS ISSUE

CIRCLE INQUIRY NO.	ADVERTISERS	PAGE NO.
148-149	* Houston Instruments Cooley & Shillinglaw, Inc.	650A-651A
96	Inficon Paul, John & Lee Inc. Adv.	644A
92-93	Instruments SA, Inc., J-Y Optical Systems Div. Kathy Wyatt & Associates Adv.	615A
155	J & W Scientific	581A
97	Janos Optical Corporation International Design	656A
98	* Jarrell-Ash Div., Fisher Scientific Co. Tech-Ad Associates	578A
124	* Johns-Manville Frye-Sills Advertising	575A
99	Joyce-Loebl S. & M. E. Winship	596A
xxx	Kernforschungszentrum Karlsruhe Publicitas GmbH	655A
121	* Kontes The Aitkin-Kynett Co., Inc.	660A
125	Lab Data Control Kelleher, Bamberger, Terry Advertising	609A
129	Leco Corporation LECOM	648A
158	Linseis Werbeagentur Ass	589A
127-128	The London Company Brand Advertising, Inc.	580A
147	3M Company Kamstra Communications, Inc.	584A
8-14, 136-138	* Matheson Kenyon Hoag Associates	558A, 559A
144	* MC/B Manufacturing Chemists Northlich, Stolley, Inc.	592A-593A
126, 145	* Mettler McKinney, Inc.	623A,631A
141	* Micromeritics Adgraphics	636A-637A
142	** Micromeritics Adgraphics	628I
140	Micropump Corporation Paragon Advertising Agency	635A
160	* Mitsubishi Chemical Industries Ltd. Global Advertising Co., Ltd.	626A
150	* Nalge Labware Hutchins/Y & R	607A
151	Nicolet Instrument Corporation Technical Communications	646A
90-91	Nissei Sangyo Instruments Kaneko-Murakami, Inc.	561A
154	* Nuclear Equipment Corporation KREatIVELy Designed	626A
157	* Ohaus Scale Corporation Michel-Cather, Inc.	582A-583A
xxx	* Orion Research OBC Advertising	551A
172-173	Parker-Hannifin Media Marketing Service Center, Inc.	622A, 623A
171	Parr Instrument Company F. Willard Hills Advertising Service	626A
174-176	* Perkin-Elmer Corporation Marquardt & Roche, Inc. Adv.	601A, 605A, 655A
170	Photovolt Corporation Michel-Cather, Inc.	547A
167, 168, 100-120	Pye Unicam Ltd.	628B-628C, 628D, 628F
184	* Rainin Instrument Co., Inc. Robert J. Allen	587A
183	Raytheon Medical Electronics James A. Ford Advertising	632A
182	* Rheodyne Bonfield Associates Adv.	599A
196	Sadtler Research Laboratories, Inc.	560A
188	Sanda, Inc. Ferguson Advertising	608A
191	* Sargent-Welch Scientific Company Polytech Advertising	629A
190	* Schleicher & Schuell, Inc. Jarman, Spitzer & Felix, Inc.	555A
189	* Scientific Glass Engineering Arden Advertising Agency	589A
192	S.H.E. Corporation NKS Ltd., Inc.	657A
194-195	Shimadzu Seisakusho Ltd. General Advertising Agency, Inc.	570A, 625A
193	* Spectra Physics Paul Pease Advertising, Inc.	641A
187	SPEX Industries Seymour Nussenbaum	603A
203	Texas Instruments, Inc. Morris & Adams	574A
201	Thermolyne Corporation E. R. Hollingsworth & Associates	586A
202	* Tracor Analytical Instruments Aim Advertising Agency	620A
212	Ultra Carbon Bradshaw Advertising	624A
210	United Scientific Bonfield Associates Advertising	594A
17-18, 220-223, 235-236, 243-248	* Varian Moran, Lanig & Duncan Advertising	610A-611A, 612A, 613A, 614A, 617A, 619A
230-232	* Waters Associates Marketing Dimensions, Inc.	613A
240	* Whatman, Inc. J. S. Lanza & Associates	548A

* *See ad in ACS Laboratory Guide*
** *Company so marked has advertisement in Foreign Regional edition only.*

Advertising Management for the American Chemical Society Publications

CENTCOM, LTD.

Thomas N. J. Koerwer, President; James A. Byrne, Vice President; Clay S. Holden, Vice President; Benjamin W. Jones, Vice President; Robert L. Voepel, Vice President; 25 Sylvan Rd. South, Westport, Connecticut 06880 (Area Code 203) 226-7131

ADVERTISING SALES MANAGER
James A. Byrne

SALES REPRESENTATIVES

Atlanta, GA . . . Robert E. Kelchner, CENTCOM, Ltd. Telephone: 203-226-7131

Boston, MA . . . Don Davis, CENTCOM, LTD. Telephone 203-226-7131

Chicago . . . John W. McGuire, CENTCOM, LTD., 540 Frontage Rd., Northfield, Ill. 60093, 312-441-6383.

Cleveland . . . Bruce E. Poorman, CENTCOM, LTD., 17 Church St., Berea, Ohio 44017, 216-234-1333.

Houston . . . Robert LaPointe, CENTCOM, LTD., 415-781-3430

Denver . . . Clay S. Holden, CENTCOM LTD., 213-325-1903

Los Angeles 90045 . . . Clay S. Holden, CENTCOM, LTD., Newton Pacific Center, 3142 Pacific Coast Highway, Suite 200, Torrance, CA 90505, 213-325-1903

New York 10017 . . . Don Davis, Richard L. Going, CENTCOM LTD., 60 East 42nd St., 212-972-9660

Philadelphia . . . Richard L. Going, CENTCOM LTD., GSB Building, Suite 510 1 Belmont Avenue Bala Cynwyd, Pa. 19004. Telephone: 215-667-9666

San Francisco, CA . . . Robert E. LaPointe, CENTCOM, Ltd., Suite 303, 211 Sutter Street, San Francisco, CA 94108. Telephone: 415-781-3430

Westport, CT . . . Robert E. Kelchner, CENTCOM, Ltd., 25 Sylvan Rd. South, Westport, Ct. 06880. Telephone: 203-226-7131.

United Kingdom
Reading, England . . . Malcolm Thiele, Technomedia Ltd., Wood Cottage, Shurlock Row, Reading RG10 OQE. Telephone: 073-581-302
Manchester, England . . . Jill E. Loney, Technomedia Ltd., 216 Longhurst Lane, Mellor, Stockport SK6 5PW. Telephone: 061-427-5660

Tokyo, Japan . . . Haruo Moribayashi, International Media Representatives Ltd., 2-29 Toranomon, 1-Chome Minato-ku Tokyo 105 Japan, Telephone: 502-0656

Continental Europe . . . Andre Jamar, Rue Mallar 1, 4800 Verviers, Belgium, Telephone: (087) 22-53-85, Telex #49263

PRODUCTION DEPARTMENT

Production Director
Joseph P. Stenza

Advertising Production Manager
Barbara Aufderheide

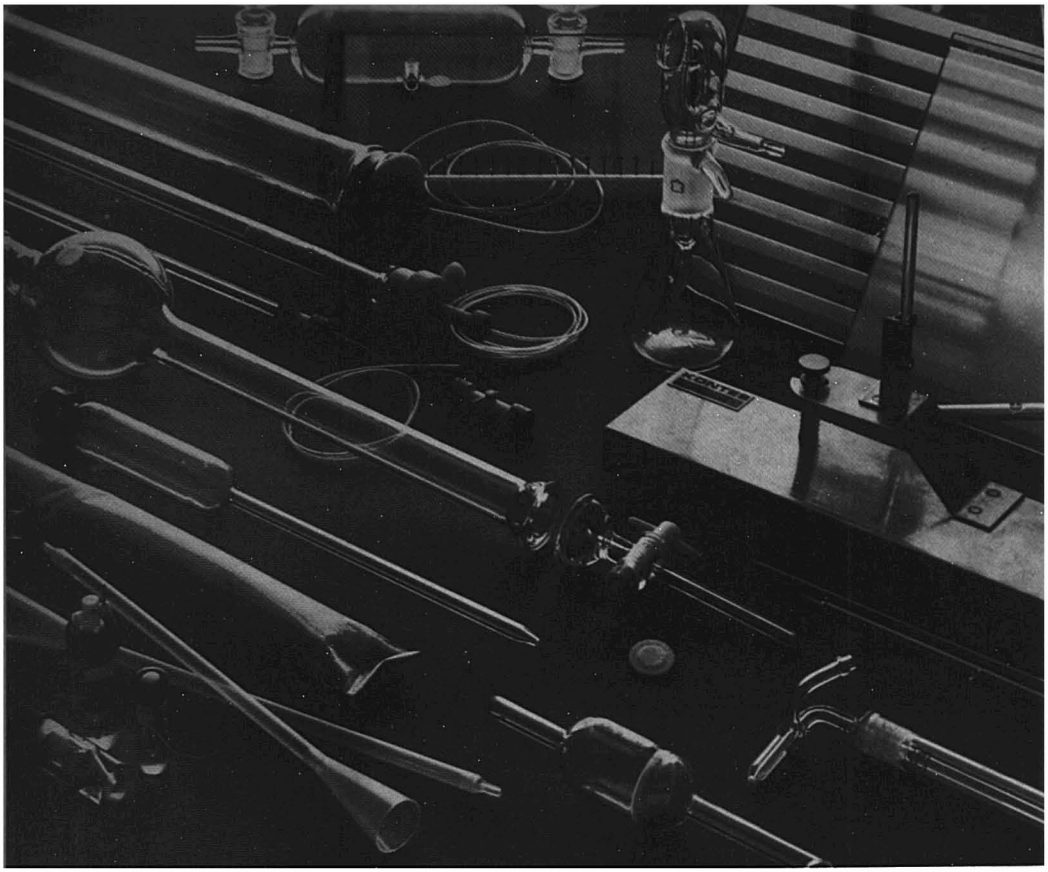

We're kind of a chromatographic hardware store . . . if you don't see it, ask us.

Over recent years, we've developed what is probably the broadest line of chromatographic apparatus and supplies available from one company.

Being candid about it, we didn't do it ourselves.

Many of the developments that we've added to our Chromaflex® line came from users—researchers and leaders in the field of chromatography. We paid attention to needs and worked with researchers to solve peculiar problems they had.

Then we had a new piece of apparatus to offer researchers with similar needs.

Some of these items were unique, such as the first separable column with removable fritted disc; the first all-glass ground TLC plates; the first conical bottom Microflex® storage tubes for valuable samples; and recently, the first practical disposable column.

What's meaningful to you now is that many of these firsts have grown into complete lines, and we no doubt have what you need in chromatographic apparatus ready for off-the-shelf delivery.

But unlike a hardware store, we carry only one brand—the Kontes crown—which says quality, no matter what you ask for from us.

Ask your Kontes salesman for our new Chromaflex® Catalog CA-3, or contact the home store.

®Trademark of Kontes Glass Company

KONTES

Vineland, N.J. 08360

Exclusive Distributors: **KONTES OF ILLINOIS,** Evanston, Illinois • **KONTES OF CALIFORNIA,** San Leandro, California
KONTES (U.K.) LTD., Carnforth, England

CIRCLE 121 ON READER SERVICE CARD

WHY WAIT

A MONTH . . . OR MORE . . . FOR THAT ROUTED COPY OF ANALYTICAL CHEMISTRY TO REACH YOUR DESK?

For only $16.00 a year . . . ($12.00 if you're a member of A.C.S.) . . . you can own your very own subscription.

Why use a worn-out copy or wait until it comes to rest in the library? You can have your own copy to clip, to read at leisure, and to add to your personal file of vital information.

You'll receive FOURTEEN information-packed issues including THE ANNUAL LABORATORY GUIDE TO INSTRUMENTS, EQUIPMENT, AND CHEMICALS and the special APRIL ANNUAL REVIEWS.

All you have to do is fill in the order form below. We'll do the rest!

Please send me ANALYTICAL CHEMISTRY at the following subscription rate:

	U.S.	Canada	All Other Countries
ACS Members*			
1-Year	☐ **$12.00**	☐ **$21.00**	☐ **$21.00**
3-Years	☐ **$30.00**	☐ **$57.00**	☐ **$57.00**
Nonmembers			
1-Year	☐ **$16.00**	☐ **$25.00**	☐ **$33.00**
3-Years	☐ **$42.00**	☐ **$69.00**	☐ **$89.00**

Name _____

Address _____

City _____ State/Country _____ Zip _____

Your Company _____ Nature of Company's Business _____

☐ Bill company ☐ Bill me for $ ☐ Payment enclosed in the amount of $ _____

Note: Subscriptions at ACS Member Rates are for personal use only.
Please allow 60 days for your first copy to be mailed. 3 0586C

Please send me ANALYTICAL CHEMISTRY at the following subscription rate:

	U.S.	Canada	All Other Countries
ACS Members*			
1-Year	☐ **$12.00**	☐ **$21.00**	☐ **$21.00**
3-Years	☐ **$30.00**	☐ **$57.00**	☐ **$57.00**
Nonmembers			
1-Year	☐ **$16.00**	☐ **$25.00**	☐ **$33.00**
3-Years	☐ **$42.00**	☐ **$69.00**	☐ **$89.00**

Name _____

Address _____

City _____ State/Country _____ Zip _____

Your Company _____ Nature of Company's Business _____

☐ Bill company ☐ Bill me for $ ☐ Payment enclosed in the amount of $ _____

Note: Subscriptions at ACS Member Rates are for personal use only.
Please allow 60 days for your first copy to be mailed. 3 0586C

NO POSTAGE
NECESSARY
IF MAILED
IN THE
UNITED STATES

BUSINESS REPLY CARD

FIRST CLASS PERMIT NO 10094 WASHINGTON, D C

POSTAGE WILL BE PAID BY ADDRESSEE

AMERICAN CHEMICAL SOCIETY
Attn: Gayle Hebron
1155 Sixteenth Street, N.W.
Washington, D. C. 20036

NO POSTAGE
NECESSARY
IF MAILED
IN THE
UNITED STATES

BUSINESS REPLY CARD

FIRST CLASS PERMIT NO 10094 WASHINGTON, D C

POSTAGE WILL BE PAID BY ADDRESSEE

AMERICAN CHEMICAL SOCIETY
Attn: Gayle Hebron
1155 Sixteenth Street, N.W.
Washington, D. C. 20036

analytical chemistry

Editor: **Herbert A. Laitinen**

EDITORIAL HEADQUARTERS
1155 Sixteenth St., N.W.
Washington, D.C. 20036
Phone: 202-872-4570 Teletype: 710-8220151

Managing Editor: Josephine M. Petruzzi
Associate Editors: Andrew A. Husovsky, Barbara Cassatt
Associate Editor, Easton: Elizabeth R. Rufe
Editorial Assistant: Andre D'Arcangelo
Associate Editor, editing: Nancy J. Oddenino
Production Manager: Leroy L. Corcoran
Art Director: John V. Sinnett
Designer: Alan Kahan

Advisory Board: L. S. Birks, Peter Carr, David Firestone, Kurt F. J. Heinrich, Phillip F. Kane, Barry L. Karger, J. Jack Kirkland, Marvin Margoshes, Robert S. McDonald, James W. Mitchell, Royce W. Murray, Harry L. Pardue, Garry A. Rechnitz, Walter Slavin, John P. Walters

Instrumentation Advisory Panel: Gary D. Christian, Catherine Fenselau, Gary M. Hieftje, Tomas Hirschfeld, Peter T. Kissinger, C. David Miller, Carter L. Olson, Sidney L. Phillips, Thomas H. Ridgway

Regulations, Analytical Division Ad Hoc Committee: Robert A. Libby (Chairman), Warren B. Crummett, William T. Donaldson, Donald T. Sawyer

Contributing Editor: Claude A. Lucchesi
Department of Chemistry, Northwestern University, Evanston, Ill. 60201

Published by the
AMERICAN CHEMICAL SOCIETY
1155 16th Street, N.W.
Washington, D.C. 20036

Books and Journals Division
Director: D. H. Michael Bowen
Journals: Charles R. Bertsch
Magazine and Production: Bacil Guiley
Research and Development: Seldon W. Terrant
Circulation Development: Marion Gurfein

Manuscript requirements are published in the January 1979 issue, page 171. Manuscripts for publication (4 copies) should be submitted to ANALYTICAL CHEMISTRY at the ACS Washington address.

The American Chemical Society and its editors assume no responsibility for the statements and opinions advanced by contributors. Views expressed in the editorials are those of the editors and do not necessarily represent the official position of the American Chemical Society.

What Could Be Done to Encourage Innovation in Industry?

The Committee on Chemistry and Federal Policy of the NAS section on chemistry, chaired by Dr. Kenneth Wiberg of Yale, has issued a statement (*C&EN*, Feb. 5, 1979, p 26) worthy of study by all chemists and science policy makers in government and in the chemical industry. It is pointed out that, particularly in the 1970's there has been an erosion of the basic research component of R&D, both in industry and in government-sponsored academic research.

It appears that government funding agencies have responded to a perception that the public is demanding relevance to the problems of society, whereas industry has been cutting back on basic research on the presumption that increased government funding to universities should take care of basic research while industry focuses upon applications. The result has been that a diminishing fraction of R&D expenditures is being devoted to the acquisition of basic knowledge.

It is interesting that the business community is beginning to accept a share of the responsibility for the decline in truly original developments. In a special 1977–78 report entitled "The Breakdown of U.S. Innovation", in the magazine *Business Week*, the subtitle is "No-risk, super-cautious management is one of the prime villains". It is pointed out that the companies most successful in international competition in technologically advanced areas are those who have made high-risk, imaginative investments in R&D in the past. Yet even most of those companies are becoming more defensive in their approach to new products. They are finding it increasingly difficult to justify expenditures for pure research when these costs appear on the debit side of the ledger in parallel with outlays for immediately beneficial purposes such as production or advertising. A tax incentive for basic research would be a good investment for the public.

Adding to the problem are the increasing costs of responding to government regulations to protect the health and safety of workers and the general population. We seem to be reaching the point of needing to regulate the regulators, i.e., to develop a system of checks and balances to arrive at *quantitative* basis for regulations through risk-benefit analysis.

Governmental action to increase the incentives for industry to invest in long-range research, to increase its emphasis on the support of basic rather than problem-oriented research, and to create mechanisms for increased interaction between the regulatory agencies and the scientific community would be positive steps toward improving the outlook for future innovations by American industry.

Prediction of Gas Chromatographic Retention Behavior with Mixed Liquid Phases

Robert L. Pecsok* and James Apffel

Department of Chemistry, University of Hawaii, Honolulu, Hawaii 96822

It is shown that the behavior of the Kovats' Retention Index on a stationary phase composed of a binary mixture of pure stationary phases can be predicted by the equation

$$I(\phi) = M(\phi) \log [\phi_A 10^{(I_A+N_A)/M_A} + \phi_S 10^{(I_S+N_S)/M_S}] - N_\phi$$

where M and N are column-dependent constants which can be calculated from the partition coefficients of the n-paraffins. ϕ_A and ϕ_S refer to the volume fraction of pure phases A and S, respectively. Analytical criteria for optimization of applications of this type are given.

In gas–liquid chromatography (GLC), the success of a separation of a complex mixture of solutes is dependent upon the solubility characteristics of the stationary liquid phase. Often the task of selecting the appropriate liquid phase can be monumental, especially since there are over 200 stationary phases currently in use. It has been shown (*1*) that nearly all separations can be accomplished on only 12 stationary phases, carefully chosen for a wide range of characteristics. The use of stationary phases composed of mixtures, selected from the basic 12, could reduce this figure even further. Purnell and co-workers (*2–6*) have developed both theoretical and analytical aspects of such systems, based on the infinite dilution partition coefficient, K_R. In their "micropartition theory", they have shown that the partition coefficient for a multicomponent system follows the simple equation,

$$K_R = \phi_A K_{R(A)}^\circ + \phi_S K_{R(S)}^\circ \quad (1)$$

where ϕ represents the volume fraction. $K_{R(A)}^\circ$ and $K_{R(S)}^\circ$ represent the partition coefficient on pure A and S, respectively. They have also developed the analytical criteria for selecting the optimum mixture of two phases for any given system (*4, 5*). The equations developed, however, are all in terms of partition coefficients, or more recently (*7*), in terms of relative retention and capacity factor data. In recent years, most retention data have been reported as relative retention times and given as Kovats' Retention Indices. The retention index I for component x is related to the partition coefficient by the equation,

$$I_x = 100 \frac{\log (K_{R(x)}/K_{R(z)})}{\log (K_{R(z+1)}/K_{R(z)})} + 100z \quad (2)$$

where z is an n-paraffin with z carbon atoms. In general, this is an equation of the form,

$$I = M \log K_R - N \quad (3)$$

where M and N are column dependent constants for any given phase. It would be of great analytical utility to be able to use the retention index in place of the partition coefficient to describe the behavior of mixed solvent systems, since the bulk of data reported in the literature are given in terms of retention indices.

THEORY

Rearranging Equation 3 in terms of K_R yields;

$$K_R = 10^{(I+N)/M} \quad (4)$$

Substituting this equation into Equation 1 gives a relation between the retention index and the volume fraction of the individual stationary phases, A and S.

$$I(\phi) = M(\phi) \log [\phi_A 10^{(I_A+N_A)/M_A} + \phi_S 10^{(I_S+N_S)/M_S}] - N_\phi \quad (5)$$

where subscripts A and S refer to pure solvents A and S, respectively. In a binary mixture, $\phi_A = (1 - \phi_S)$. M and N are given by the following equations;

$$M = 100/\log [K_{R(z+1)}^\circ / K_{R(z)}^\circ] \quad (6)$$

$$N = 100 \log K_{R(z)}^\circ / \log [K_{R(z+1)}^\circ / K_{R(z)}^\circ] - 100z \quad (7)$$

The first factor, $M(\phi)$, can be determined by substituting Equation 1 into Equation 6;

$$M(\phi) = \frac{100}{\log [(\phi_A K_{R(z+1),A}^\circ + \phi_S K_{R(z+1),S}^\circ)/(\phi_A K_{Rz,A}^\circ + \phi_S K_{Rz,S}^\circ)]} \quad (8)$$

$N(\phi)$ can be defined in a similar way, yielding,

$$N(\phi) = \frac{100 \log (\phi_A K_{Rz,A}^\circ + \phi_S K_{Rz,S}^\circ)}{\log \left[\dfrac{\phi_A K_{R(z+1),A}^\circ + \phi_S K_{R(z+1),S}^\circ}{\phi_A K_{Rz,A}^\circ + \phi_S K_{Rz,S}^\circ} \right]} - 100z \quad (9)$$

The behavior of $M(\phi)$ and $N(\phi)$ for the squalane/1-dodecanol system at 56 °C can be seen in Figures 1 and 2. Although it is these factors, M and N, which give the retention index its column independence in most applications, in the case of mixed stationary phases, these same factors introduce a column dependency into Equation 5. This presents an inherent impossibility of describing the behavior of mixed phase systems solely in terms of retention indices. This failure is due to the definition of the retention index, since this definition does not require the calculation of partition coefficients which are needed in $M(\phi)$ and $N(\phi)$.

For analytical purposes, however, Equation 5 is an improvement over Purnell's original equation. Through the use of Equation 5, the behavior of a particular solute in a mixed solvent system can be predicted by knowing the retention index of that solute on each of the pure phases, and the partition coefficient of two n-paraffins which bracket the solute with respect to retention time, rather than the partition coefficients of all solutes and all the n-paraffins spanning the range of retention times involved. This simplifies the analytical problem considerably, since, in practice, the partition coefficients would have to be measured for each system, for each phase. Using Equation 5, only the n-paraffins which span the retention times in the system must be measured. In fact, for practical purposes only two n-paraffins need be measured. The retention indices of all the other solutes can be obtained from the literature.

Although the prediction of the retention indices of solutes in mixed stationary phase systems is of importance, a greater

0003-2700/79/0351-0594$01.00/0 © 1979 American Chemical Society

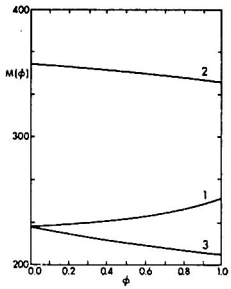

Figure 1. The ϕ-dependence of M in mixtures of (1) 1-dodecanol/squalane at 56 °C, (2) di-*n*-nonyl phthalate/squalane at 100 °C, (3) diethyl maleate/quinoline at 35 °C. ϕ refers to the first named compound

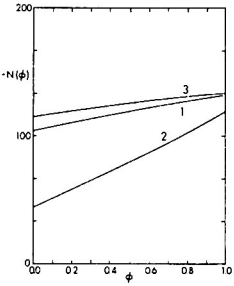

Figure 2. The ϕ-dependence of N in mixtures of (1) 1-dodecanol/squalane at 56 °C, (2) di-*n*-nonyl phthalate/squalane at 100 °C, (3) diethyl maleate/quinoline at 35 °C

analytical problem involves finding the optimum mixture of two phases to use for a given system. Purnell and Laub (*4*, *5*) have developed a method for doing this based on the relative retention, α, which is defined by the equation;

$$\alpha = K_{R^1}/K_{R^2} \tag{10}$$

where 1 and 2 refer to two solutes on the same stationary phase. By substituting Equation 1 into this equation, Purnell and Laub obtained a ϕ-dependent equation for α. α is first plotted against ϕ for each pair of solutes in the system, including the *n*-paraffins, yielding a so-called "window diagram". In these plots, α is always taken to be greater than or equal to 1; that is, if α is less than 1, the reciprocal of α is plotted. In production of window diagrams, several approximations can be made, such as plotting α with straight lines, and disregarding any solute pair with α greater than 1.4 for all ϕ, since such separations are trivial. The diagrams are then analyzed. The "window" is a triangle formed by the intersection of the α's for two pairs of solutes. The vertex of the largest triangle containing no smaller triangle is at the point where the optimum separation occurs. At this point, all relative retentions are at least as large as that of the vertex of the largest triangle. For a more complete discussion of this method as developed by Purnell et al. in terms of partition coefficients, see references *2* through *8*.

By analogy to Purnell's method, somewhat similar to the preceding development of Equation 5, an equation for α in terms of I can be formulated. In general, for a pure stationary phase, α is described by

$$\alpha = 10^{(I_1 - I_2)/M} \tag{11}$$

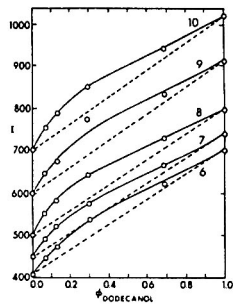

Figure 3. Dependence of I on ϕ_{Dod} in mixtures of 1-dodecanol/squalane for solutes listed in Table I at 56 °C. Plotted points represent experimental data. Solid lines are calculated from Equation 5. Dashed lines are calculated from Equation 13

where the subscripts 1 and 2 again refer to different solutes 1 and 2, and the factor M is that described by Equation 6. Substituting into this the ϕ-dependency of I yields

$$\alpha(\phi) = \frac{\phi_A 10^{(I_{A1}^\circ + N_A)/M_A} + \phi_S 10^{(I_{S1}^\circ + N_S)/M_S}}{\phi_A 10^{(I_{A2}^\circ + N_A)/M_A} + \phi_S 10^{(I_{S2}^\circ + N_S)/M_S}} \tag{12}$$

where I_{A1}° refers to the retention index of solute 1 on pure phase A, and M_A refers to the factor described by Equation 6 for pure phase A. N_A is the factor described by Equation 7 for pure phase A. In Equation 12, it should be noted that the ϕ-dependent M factor has cancelled out simplifying the calculation of α. Hence, the window diagrams can be produced from the retention indices of the solutes and the partition coefficients of the *n*-paraffins over the range of retention times.

EXPERIMENTAL

All chromatographs were run on a Bendix Series 2300 Lab Chromatograph. Eighth-inch o.d. copper tubing was used for the di-*n*-nonyl phthalate/squalene system at 100 °C and eighth-inch o.d. stainless steel tubing was used for the 1-dodecanol/squalane system at 56 °C. The stationary phases; squalane, di-*n*-nonyl phthalate (DNNP), and 1-dodecanol were of reagent grade and used as received. The densities of these phases were obtained from data collected by Laub (*4*). The packings for the DNNP/squalane system were prepared by the rotary evaporator method (*10*). The packings for the squalane/dodecanol system were prepared by a fluidized drying method described by Parcher and Urone (*9*). All packings were made approximately 3% loadings on Gas Chrom Q 100/120 mesh support. The packings which were mixtures of two pure phases were prepared by mechanically mixing packings of the pure phases rather than preparing packings from mixed solvents. Purnell and co-workers have shown this to be justified (*4*, *5*).

RESULTS AND DISCUSSION

The Kovats' retention indices for a variety of solutes were determined experimentally for the systems, squalane/1-dodecanol and di-*n*-nonyl phthalate/squalane, for five volume fractions each, and are given in Table I. The values follow those of the function predicted by Equation 5 within the experimental limits of error, which generally were of the order of 5 to 6 index units. Graphs of the retention index vs. the volume fraction are given in Figures 3 and 4. Correspondingly, the graphs of α vs. ϕ can be predicted with Equation 12 and correspond closely to those predicted by Purnell and Laub (*4*, *5*). The values predicted for optimum separation by this method are the same values as those computed by Purnell from partition coefficients (*2*, *4*).

Once the applicability of Equations 5 and 12 was shown, a third system, diethyl maleate/quinoline at 35 °C, was

Table I. Retention Data for Various Solutes on Dodecanol/Squalane and Di-*n*-nonyl Phthalate/Squalane Mixed Stationary Phases

A. Dodecanol/Squalane at 56 °C

	K_R						I					
solute	$\phi_{Dod.}$ = 0.0	0.0701	0.1301	0.2916	0.6908	1.0	0.0	0.0701	0.1301	0.2916	0.6908	1.0
1. pentane	53.0	51.8	50.3	48.4	33.4	29.1	500					
2. hexane	145.3	140.2	135.8	130.2	90.6	72.7	600					
3. heptane	367.6	341.8	345.3	334.7	242.5	196.0	700					
4. octane	988.2	947.8	861.2	873.5	644.6	412.2	800					
5. nonane	2670	2570	2485	2259	1662	1248	900					
6. ethanol	20.9	31.0	39.6	70.6	120.8	164.7	406	448	476	538	629	700
7. 2-propanol	32.2	48.2	61.9	104.5	170.1	260.9	449	493	521	578	664	734
8. propanol	53.0	85.9	114.0	183.5	311.5	522.2	499	551	582	636	725	797
9. butanol	138.1	210.0	271.6	505.8	858.9	1164	594	645	674	743	830	907
10. pentanol	375.7	581.2	757.1	1390	2343	3308	702	752	786	850	936	1011

B. Di-*n*-nonyl Phthalate/Squalane at 100 °C

	K_R					I				
solute	ϕ_{DNNP} = 0.0	0.075	0.2548	0.5900	1.0	0.0	0.075	0.2548	0.5900	1.0
1. hexane	35.7	33.0	31.4	28.6	25.0	600				
2. heptane	68.0	65.6	63.1	56.5	48.9	700				
3. octane	141.0	137.6	129.1	115.6	98.0	800				
4. nonane	300.8	294.6	276.3	243.0	201.5	900				
5. decane	631.0	613.2	575.1	501.9	413.8	1000				
6. undecane	1316	1278	1197	1040	845	1100				
7. benzene	41.2	42.5	45.8	52.5	58.6	629	638	655	686	727
8. ethylbenzene	200.0	205.0	213.3	231.9	255.6	847	852	866	894	932
9. toluene	107.9	110.3	115.7	125.7	138.3	764	771	785	812	848
10. *p*-xylene	222.0	225.0	235.0	253.5	276.2	860	865	879	906	944
11. propylbenzene	373.0	378.8	394.9	425.2	462.3	929	935	949	977	1015
12. ethoxybenzene	415.8	440.7	449.8	610.1	745.4	944	955	981	1027	1082
13. benzaldehyde	280.8	326.3	434.6	636.8	855.1	895	914	962	1033	1106
14. acetophenone	617.7	714.6	946.2	1377	1906	997	1021	1068	1139	1213
15. butylbenzene	830.8	841.3	868.2	918.5	981.0	1037	1043	1056	1083	1115

Table II. Retention Data for Various Solutes on Diethyl Maleate/Quinoline Mixed Phases at 35 °C Calculated from Data in Reference 3

	K_R					I				
$\phi_{\text{Diethyl Maleate}}$	0.0	0.25	0.50	0.75	1.0	0.0	0.25	0.50	0.75	1.0
solute										
1. pentane	48.1	50.3	52.6	54.9	57.1	500				
2. hexane	131	141	152	162	172	600				
3. heptane	352	391	430	469	508	700				
4. 3-methyl pentane	116	120	124	127	131	588	584	581	578	575
5. cyclopentane	116	129	141	154	167	588	591	594	595	597
6. furan	302	283	265	246	227	685	668	653	639	626
7. cyclohexane	294	321	349	377	404	682	681	680	679	679

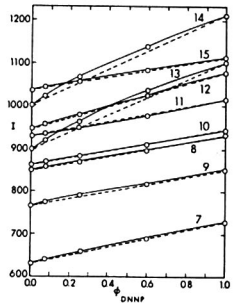

Figure 4. Data plotted as in Figure 3 for mixtures of di-*n*-nonyl phthalate/squalane mixtures at 100 °C

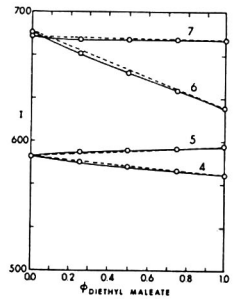

Figure 5. Data plotted as in Figure 3 for mixtures of diethyl maleate/quinoline at 35 °C (*3*)

computed from data given by Purnell and Laub (*2*). The data as computed are given in Table II, and the pertinent graphs are given in Figure 5.

Comparison of the plots of I vs. ϕ for these three systems indicates that the error involved in approximating the behavior of I by a simple weighted sum similar to the case for K_R in Equation 1, such as

$$I = \phi_A I_A^\circ + \phi_S I_S^\circ \qquad (13)$$

may be justified. When the difference of the retention indices of a particular solute on the separate pure phases is small, this seems to be a fair approximation. This is as one might expect since in the limit as I_A goes to I_S, Equation 5 becomes Equation 13. For each of the systems studied, the maximum error in this approximation, that is, the largest difference of the values of Equation 5 and Equation 13 over the range of ϕ, was determined and plotted against the absolute value of the ($I_A^\circ - I_S^\circ$) factor of the pure phases. This is given in Figure 6. For an error of 5 index units, which is of the order of experimental

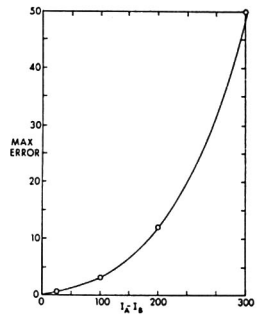

Figure 6. Maximum error resulting from the use of Equation 13 rather than Equation 5, in retention index units

error, the differences between the retention indices can be as large as 125 index units. Two important factors should be noted about this approximation, however. First, the average error for any particular solute would be smaller than that shown, since this is a maximum error and, even if this is relatively large, the logarithmic function of Equation 5 may closely approximate Equation 13 in other values of ϕ. Second, for this approximation to be of full use, all the solutes in the system must satisfy whatever error limit is desired. It is, unfortunately, not of much use in calculating α, since when using the actual equation for α, Equation 12, the factor $M(\phi)$ cancels, whereas in using the approximation, Equation 13, this factor does not cancel out.

Purnell and co-workers have stated (*4*) that it is not feasible to substitute I for K_R in describing systems of this type because of the large amount of arithmetic revision required. However, granted Equation 5 is mathematically more complex than Equation 1, calculations of not only $I(\phi)$, but also the relative retention "window diagrams" are amenable to computer applications similar to those described by Purnell and co-workers in a recent paper (*6*).

It should be noted, that although the present data have been collected for binary systems, the method can easily be extended to larger systems. In general, Equation 5 then becomes:

$$I(\phi) = M(\phi)\log\left[\sum_n \phi_n 10^{(I_n^\circ + N_n)/M_n}\right] - N(\phi) \qquad (14)$$

Similar sums can be applied to equations for $M(\phi)$, $N(\phi)$, and $\alpha(\phi)$, although, obviously, for more than two phases the simplicity of the use of the "window diagrams" is lost. The analgous method based on partition coefficients has been developed by Laub and Purnell (*4*).

Although not an equation solely in terms of the Kovats' Retention Index, Equation 5 is felt to be a definite improvement over Equation 1 for analytical purposes. One main advantage is that most of the data needed can be obtained

from the literature. Further, this equation requires no further adoption of a new system of reporting data in terms of partition coefficients which would be necessary for Purnell's system.

LITERATURE CITED

(1) S. T. Preston, *J. Chromatogr. Sci.*, 11, 201 (1973).
(2) J. H. Purnell and J. M. Vargas Andrade, *J. Am. Chem. Soc.*, 97, 3585 (1975).
(3) R. J. Laub and J. H. Purnell, *J. Am. Chem. Soc.*, 98, 30 (1976).
(4) R. J. Laub and J. H. Purnell, *Anal. Chem.*, 48, 799, 1720 (1976).
(5) R. J. Laub and J. H. Purnell, *J. Chromatogr.*, 112, 71 (1975).
(6) R. J. Laub, J. H. Purnell, and P. S. Williams, *J. Chromatogr.*, 134, 249 (1977).
(7) R. J. Laub, J. H. Purnell, D. M. Summers, and P. S. Williams, *J. Chromatogr.*, 155, 1 (1978).
(8) R. J. Laub and R. L. Pecsok, "Physiochemical Applications of Gas Chromatography", John Wiley and Sons, New York, 1978.
(9) J. F. Parcher and P. Urone, *J. Gas Chromatogr.*, June 1964.
(10) W. R. Supina, "The Packed Column in Gas Chromatography", Supelco Inc., Bellefonte, Pa., 1974.

RECEIVED for review September 11, 1978. Accepted January 25, 1979.

Simultaneous Determination of 4-Chloro-2-methylphenoxyacetic Acid and Its Metabolites in Soil by Gas Chromatography

Mohammad A. Sattar and Jaakko Paasivirta*

Department of Chemistry, University of Jyväskylä, SF 40100 Jyväskylä 10, Finland

Analysis of MCPA (4-chloro-2-methylphenoxyacetic acid) and two of its main metabolites 4 chloro-*o*-cresol and 5-chloro-3-methylcatechol have been studied by gas chromatography of their pentafluorobenzyl derivatives simultaneously in four different soil materials. After derivatization of the residue extract, three different clean-up procedures were tried. The best recoveries of compounds from soils were obtained when the extraction was performed by shaking with ether–acetone–heptane–hexane (2:1:1:1) from acidified soil and when the cleanup was done by TLC.

Phenoxyalkanoic acid herbicides prevent direct gas chromatographic determination because of the high polarity or low volatility of the compounds and must be converted to their more volatile derivatives. The sensitivity of the EC detector toward alkyl esters of MCPA (4-chloro-2-methylphenoxy acetic acid (I)), MCPB (4-chloro-2-methylphenoxy butyric acid) etc. is very poor. The methyl ester of MCPA was 100 times less sensitive to electron affinity detection than 2,4-D methyl ester (*1*).

Chau and Terry (*2*) reported the formation of pentafluorobenzyl derivatives of 10 herbicidal acids including MCPA (I). They found that 5 h was an optimum reaction time at room temperature with pentafluorobenzyl bromide in the presence of potassium carbonate solution. Agemian and Chau (*3*) studied the residue analysis of MCPA (I) and MCPB from water samples by making the pentafluorobenzyl derivatives. Bromination (*4*), nitrification (*5*), and esterification with halogenated alcohol (*1*) have also been used to study the residue analysis of MCPA (I) and MCPB. Recently pentafluorobenzyl derivatives of phenols and carboxylic acids (*6*, *7*) were prepared for detection by ECD at very low levels. Pentafluorobenzyl bromide has also been used for the analytical determination of organophosphorus pesticides (*8*).

MCPA (I) is one of the most effective hormone herbicides. 4-Chloro-*o*-cresol (II), 5-chloro-3-methyl catechol (III) and *cis*,cis-4-chloro-α-methyl muconic acid (IV) were first identified as metabolites of MCPA (I) by Gaunt and Evans (*9*). Several other investigators have also studied the microbial degradation of MCPA (*10–14*). The technical product of MCPA in Finland contains approximately 4% of II as an impurity (*15*).

MCPA (I) is a widely used pesticide in Finland especially against herbs in the grain field (*16*). This is due to the confirmation of MCPA (I) as a safe compound (*17*, *18*). Analysis of MCPA (I) from soil material has not been described in detail in the literature. We met with difficulties in efforts to apply bromination (*19*) to detect the substance by ECD. Our determinations of MCPA methyl ester using FID were also not readily applicable to soil samples because of numerous interfering compounds. Thus we developed an improved analysis method using the pentafluorobenzyl derivative of MCPA (*20*). In the present study, derivatization with pentafluorobenzyl bromide and clean-up processes are extended to the residue model compounds of II and III with four typical soils. The formulas of I–IV and the pentafluorobenzyl derivatives VI–VII are illustrated in Figure 1. The structures of the derivatives VI–VIII were also verified by us with NMR spectra.

Table I. Physical and Chemical Characteristics of the Finnish (i and ii, Kemira Co.) and Bangladesh (iii and iv) Soils

soil types	sandy clay, i	clay loam, ii	sandy loam, iii	clay, iv
moisture, %	13.9	14.8	2.0	2.3
field capacity, %	28.1	34.0	12.1	15.5
ignition loss, %	33.2	36.0	2.2	2.0
pH	4.6	4.8	6.6	7.5
organic carbon, %	10.3	12.2	0.6	0.7
organic matter, %	17.8	21.1	1.1	1.2
coarse sand, %	19.7	10.8	5.1	4.9
fine sand, %	31.1	24.2	20.7	32.7
silt, %	30.1	25.3	58.5	18.9
clay, %	18.7	39.5	15.7	42.4

EXPERIMENTAL

Two Finnish (Kemira Co., Helsinki) and two typical Bangladesh (Soil Science Department, Agriculture University, Bangladesh) soils were used for the experiment. The soils were dried at room temperature, ground to pass through a 2-mm sieve and stored in plastic containers. The physical and chemical characteristics

0003-2700/79/0351-0598$01.00/0 © 1979 American Chemical Society

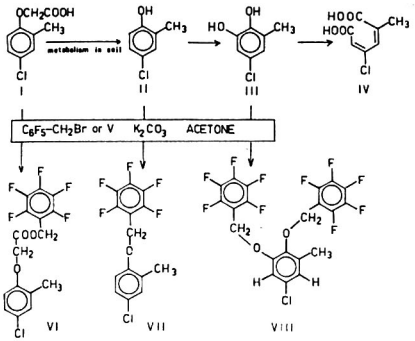

Figure 1. Structures of MCPA (4-chloro-2-methylphenoxyacetic acid, (I)), its metabolites 4-chloro-*o*-cresol (II), 5-chloro-3-methyl catechol (III), 4-chloro-2-methyl muconic acid (IV), reagent pentafluorobenzyl bromide (V), and the derivatives VI–VIII from I–III

of the soils are presented in Table I.

Soil Analysis. The moisture content, field capacity, and the particle size distribution (sand, salt, and clay) of the soils were determined by the method of Piper (*21*) and the ignition loss by Ball's method (*22*). Soil pH was determined with a pH (*23*) and organic carbon by wet oxidation method (*24*). The textural classification of the soils was made using the triangular coordinate (*25*).

Soil Extraction Experiment. Five or ten grams of soil was taken in a 250-mL beaker. Then 250, 250, and 250 μL or 500, 500, and 500 μL of 0.1% solution of compounds I (MCPA-Na salt in water, Kemira Co.), II (4-chloro-*o*-cresol in ether, synthesized in our laboratory) and III (5-chloro-3-methyl catechol in ether, synthesized in our laboratory) were added (1:1:1) to the soil, respectively, and mixed well with a glass rod. Water, 1 or 2 mL, was added to make the soil about field condition and stirring was continued until the mixture was uniform, then 1–3 g anhydrous sodium sulfate was added, again mixed well, and allowed to stand for an hour. The experiment was continued either by shaking or Soxhlet extraction with different solvent systems.

The shaking extraction was performed by transferring the soil sample to a shaking flask with 50 mL of solvent and shaking for 40 min with a Griffin flask shaker under a tight cork. The mixture was filtered through paper with 1 g of anhydrous sodium sulfate and the shaking procedure repeated with another 50 mL of solvent. The combined filtrates were evaporated and transferred with diethyl ether to a volumetric flask to make 10 mL of ether solution. The solvent systems selected in the previous study (*20*) were (1) ether–acetone–hexane–heptane (2:1:1:1) for fresh and acidified soils and (2) ether–chloroform (1:1), adjusted to pH 3.0 by 5 N HCl or 1 N NaOH solution for fresh soils only. The soil acidification was performed by using 3 or 5 mL of 1 N H_3PO_4 or 30% H_2SO_4 solution after transferring the soil to the shaking flask and mixed uniformely for 10–15 min before the addition of the solvent mixtures.

Soxhlet extraction was applied to both fresh and acidified soils for 24 h with chloroform. The soil acidification was done before transferring the sample to the extraction thimble. The extract was evaporated and transferred with ether to a volumetric flask to make 20 mL of ether solution. Similar extractions were also carried out with all the four soils under study. The blank experiments were performed with soils.

Derivatization Experiments. Next 100 μL or 200 μL or 400 μL or 500 μL of 0.1% solution of compounds I or II or III was transfered to a 15-mL centrifuge tube with 200 μL pentafluorobenzyl bromide (1% solution in acetone), 50 μL 30% potassium carbonate solution, and 4 mL of acetone, shaken vigorously, and allowed to stand at room temperature for 3 h. Then 2 mL of *n*-heptane was added and the solution was evaporated by a nitrogen gas stream and transferred with ether to a volumetric flask to make 10 mL of a crude model compound derivative solution (model samples).

Similar derivatizations were performed with the soil samples using 100 μL or 200 μL from 10 mL of the shaking or soxhlet extract. The blank soil extract was also treated.

Clean-up Experiments. (*i*) *Water/Toluene Shaking.* Next 100 μL or 200 μL from 10 mL of the crude derivative of model compounds or soil samples was taken to a 15-mL glass-stoppered centrifuge tube and evaporated by a nitrogen gas stream. Then 3 mL distilled water and 10 mL toluene were added and the stoppered tube was shaken vigorously. The layers were separated and the toluene layer was dried over anhydrous sodium sulfate. The 100-μL blank solution was also treated.

(*ii*) *TCL Cleanup.* Standard glass chromatoplates (20 × 20 cm) were prepared with a Desaga-Brinkmann model S-11 applicator to make a 1-mm layer of silica gel G (type 60, Merck) using slurry with water (1:2 w/v). The plates were activated at 110 °C for 12 h. The plates were divided by vertical lines into 5 sections leaving 1 cm from the side of the layer. Two sections were for the soil samples (100 and 200 μL) and three for the standards I, II, and III samples (50 μL each). The model soil samples and standards were spotted (100- or 200-μL pipets, H. E. Pedersen, Denmark) to a starting line 1 cm from the bottom and eluted with dichloromethane (Merck) for 40 min. The air-dried plates were partly covered (sample section) with aluminum foil and the noncovered standard sections were sprayed with 0.5% diphenyl amine solution in ethanol. Then the standard (I–III) could be seen in UV light as a brown spot at the same distance from the bottom of the plate. Each sample fraction was scraped as a 2-cm high zone from the level of the standard spots, inserted into a glass tube (10 × 1 cm) on a cotton stopper, and packed to form a tight column with the aid of a glass rod. The column was then eluted with diethyl ether to a measuring flask to make 10 mL. Cleanup of the blank soil derivative solution was also performed.

(*iii*) *Column Cleanup.* The silica gel used (60–200 mesh, Merck) was activated by heating at 130 °C for 14 h and then deactivated by adding 5% (w/w) of distilled water and shaking (Griffin) for an hour. The material was poured to a 10 × 1 cm glass tube on a cotton stopper to form a 4-cm high column. Then 100 or 200 μL from 10 mL of crude model or soil sample derivative solutions or 100 μL of the blank derivatization solution was pipetted to a 15-mL centrifuge tube, evaporated by a nitrogen gas stream and dissolved in 5 mL of hexane. *n*-Hexane, 5 mL, was added to drain on the top of the silica gel column. Then the sample in hexane was added by rinsing the centrifuge tube with hexane. Excess of the pentafluorobenzyl bromide and contaminants were removed by eluting with 10 mL of toluene–hexane 1:3 mixture (v/v). Then the purified derivative was collected by eluting with 3:1 toluene–hexane mixture to a volumetric flask to make 10 mL.

Gas Chromatographic Determinations. A Varian Model 600 gas chromatograph with ^3H ECD was used. The column was a glass coil 1.5 m long, inside diameter 1.5 mm filled with 6% of the 4:1 mixture of QF-1 and SF 96 silicon phases on Chromosorb W (acid washed, silanized) 100/200 mesh. Temperatures applied were 200 °C for column and detector, 225 °C for injector. Nitrogen was used as carrier gas, 30 mL/min.

For determination of the recovery in each experiment, pure 1, 2, and 3 μL of the soil after clean-up procedure and 1 and 2 μL of model samples were injected. The areas of the peaks of the derivatives VI, VII, and VIII of the compounds I–III were measured and compared to the peak area of the respective standard.

Standard Solution. Next 100 mg each of compound I or II or III, 200 μL pentafluorobenzyl bromide, 1 mL of 30% potassium carbonate, and 4 mL of acetone were shaken vigorously in a 50-mL glass-stoppered flask and then allowed to stand for 3 h; 2 mL of *n*-heptane was added and evaporated with a nitrogen stream. Then 5 mL distilled water and 20 mL toluene were added and the mixture was shaken well. The toluene layer was separated and dried over anhydrous sodium sulfate. After evaporation with a nitrogen gas stream, the reside was verified by GLC, infrared, and ^1H NMR spectra to be a pure pentafluorobenzyl derivative of VI, VII, or VIII. A weighed amount of the residue was diluted to form a standard solution which contained 100 pg each of the derivative VI of I, VII of II, or VIII of III in 1 μL. This corresponds to 58.47 pg of I, 44.19 pg of II, and 30.51 pg of III in the original

Table II. Clean-up Experiments of the Pentafluorobenzyl Derivatives: VI from MCPA (I), VII from 4-Chloro-o-cresol (II) and VIII from 5-Chloro-3-methylcatechol (III)[a]

	shaking with water/toluene			TLC			column		
compound	N	$\bar{x}$	s	N	$\bar{x}$	s	N	$\bar{x}$	s
I	16	94.7	2.06	16	97.6	1.25	16	85.3	5.25
II	16	91.9	2.15	16	94.7	1.40	16	82.9	5.96
III	16	79.0	1.77	16	80.3	1.10	16	70.7	4.89

[a] Results as averages ($\bar{x}$) of the % recoveries of N experiments with standard deviations s.

samples in μL. A mixed solution was prepared to form a standard for simultaneous determination of I, II, and III.

The limit of detection in gas chromatography was found to be 21 pg of I, 22 pg of II, and 24 pg of III as their derivatives. This proved to be sufficiently low for the present analyses where the expected peaks in the resulting gas chromatograms corresponded to 100 pg amounts of I–III.

RESULTS AND DISCUSSION

Clean-up methods were tested using the model sample solutions of the pentafluorobenzyl derivatives VI–VIII of the compounds I–III. For each of the model samples, 16 experiments were done by each of the three clean-up procedures. The recoveries of I, II, and III as derivatives were calculated and averaged for each set of 16 gas chromatograms obtained. The results are collected in Table II. The differences between the methods for each compound and between the compound recoveries for each method were investigated by t-tests and found to be very significant ($p < 0.1\%$) with two exceptions: for catechol III, the difference between water/toluene shaking and TLC clean-up methods was only slightly significant ($p < 10\%$) and for column cleanup, there was no significant difference between the recoveries of MCPA (I) and cresol II. TLC cleanup proved to give the highest recoveries of all three compounds. Water–toluene shaking gave somewhat and column cleanup considerably lower recoveries.

The pilot analysis experiments resulted in 48 gas chromatograms for each combination of soil type, extraction, and clean-up method. The recoveries of I, II, and III were calculated for each chromatogram and then averaged ($N = 48$) to yield results which are collected in Table III.

Our preliminary results from the analysis of MCPA (I) from fresh soil (*20*) had indicated that water/toluene shaking was a slightly more effective cleanup than TLC. Table III shows the same result for the recovery of I from fresh soil in most cases. However, the results for compounds II and III and also for MCPA (I) when the soil is acidified clearly show that the TLC cleanup generally is the most effective one. Water/toluene shaking gives nearly as good results and thus could be the best choice for routine determinations because of its simplicity.

Acidification, preferably with phosphorus acid, of the soil before the extraction increases the recoveries regardless of the method of extraction or cleanup used. The shaking extraction was generally more effective than Soxhlet but the Soxhlet extraction of the soils after acidification with H_3PO_4 also gave satisfactory results.

The mixed solvent ether–acetone–hexane–heptane (2:1:1:1) which had been selected in the preliminary study (*20*) for the optimal extraction of MCPA (I) proved to be an excellent solvent system for the residue analysis of all three compounds I–III with the shaking method. The experiments from fresh soil with ether–chloroform (1:1) pH 3.0 showed slightly lower recoveries (Table III). Soxhlet extraction with chloroform, on the contrary, gave quite satisfactory results if the soil was acidified with phosphorus acid. This method is most convenient for routine analyses.

Generally, the recoveries were far below 100%. Obviously the extractions were not complete because of the properties of the soils studied. Yip (*26*) reported that the binding of the soil particles and organic matter with the herbicide residues prevented the complete extraction of them with an organic solvent. Upchurch and Mason (*27*) found that the extent of adsorption of herbicides is highly dependent on the type of organic matter and clay as well as on the amounts of their constituents in a soil. The present results (Table III) allow us to compare the possible influence of the characteristics of the four soils studied (Table I) on the recoveries. The results of fresh soil treatments show that the pH has no significant effect in the area 4.6–7.8. Also, one could conclude that the soil texture (especially the differences in clay contents) has no significant influence on the amounts of the residues I–III recovered.

The present results support a general conclusion that organic matter is the main factor which influences to the fate of herbicides and their analyses in the soil. The present Finnish soils (i, ii) had high but Bangladesh (iii, iv) very low organic matter contents (Table I). Consequently, significantly higher recoveries of the residues I–III were generally obtained from the latter soil materials than from soils i and ii. In addition, the Finnish soils gave selectively lower 5-chloro-3-methyl catechol (III) recoveries related to recoveries of I and II. This can be clarified by calculating ratios of the average recoveries of different residues I–III.

The overall average ratio of MCPA (I) recovery from Bangladesh soil to Finnish soil was 1.044 ± 0.031. The corresponding ratios for 4-chloro-o-cresol (II) and 5-chloro-3-methyl catechol (III) were 1.051 ± 0.028 and 1.139 ± 0.024, respectively. Recovery ratios II/I and III/I were calculated for each soil and analysis combination. The former ratios were found to be independent but the latter dependent on the soil type from the results of the t-tests between the different means. For example, the mean II/I value from 42 ratios (from Table III) of Finnish soils i and ii was $\bar{x} = 0.9439$ with standard deviation $s = 0.0234$, and the corresponding mean II/I from 42 ratios of Bangladesh soils iii and iv was $\bar{x} = 0.9390$ with $s = 0.0234$ (difference insignificant). These results show that MCPA (I) and 4-chloro-o-cresol (II) behave very similarly in the analysis procedures regardless of the soil type. On the contrary, the ratio III/I average from Finnish soils was $\bar{x} = 0.8022$ with $s = 0.0174$ but from Bangladesh soils $\bar{x} = 0.8704$ with $s = 0.0364$ (a very significant difference, $p < 0.1\%$). Thus, organic matter seems to have a very strong degreasing efect on the recovery of 5-chloro-3-methyl catechol (III) from soil. The nature of the effect is uncertain, thus far. It might rise from stronger binding of III to organic matter substances or faster metabolism of III in live soil than I or II. The future field experiments planned by us might shed further light on this question.

For routine multicomponent residue analysis of I–III from soil, we recommend, based on the present experience, extraction of the acidified (H_3PO_4) soil by chloroform with Soxhlet, derivatization with pentafluorobenzyl bromide and cleanup by water/toluene shaking for determination with gas chromatography using EC detection.

Table III. Average Per Cent Recoveries of Compounds I, II, and III Mixed (1:1:1) with Finnish (i and ii) and Bangladesh (iii and iv) Soils Applying Different Extractions[a]

soil treatment	solvent	extraction	compound	soil i			soil ii			soil iii			soil iv		
				a	b	c	a	b	c	a	b	c	a	b	c
fresh	ether-acetone-hexane-heptane, 2:1:1:1	shaking	I	89.1	86.3	82.2	95.0	93.0	83.2	97.2	95.2	88.8	90.9	91.0	82.7
			II	82.6	81.2	75.9	86.3	83.2	78.1	95.6	90.1	82.3	89.0	87.3	81.6
			III	69.2	69.9	64.0	74.1	72.3	68.0	80.6	80.5	74.6	80.1	80.9	70.7
acidified with H_3PO_4	ether-acetone-hexane-heptane, 2:1:1:1	shaking	I	93.1	94.2	83.1	96.1	97.0	85.0	100.7	101.1	90.9	98.5	99.1	86.7
			II	84.9	89.6	77.9	91.0	92.9	81.8	93.5	96.4	85.6	94.2	95.6	81.7
			III	73.6	75.9	65.7	77.8	78.3	69.9	89.7	92.8	75.9	86.8	90.3	74.9
acidified with H_2SO_4	ether-acetone-hexane-heptane, 2:1:1:1	shaking	I	89.2	86.9	82.8	89.9	88.0	80.7	98.3	99.7	90.5	95.2	96.5	86.6
			II	82.4	81.5	76.5	87.8	82.8	78.9	90.3	88.4	81.7	88.4	85.5	81.1
			III	69.6	70.5	64.2	73.4	70.6	65.7	85.5	81.3	76.2	84.9	81.1	75.5
fresh	ether-chloroform 1:1, pH 3.0	shaking	I	82.9	86.6	74.8	86.6	89.9	80.1	95.3	97.7	88.2	93.2	95.2	83.0
			II	78.7	85.5	70.7	83.0	85.7	75.4	90.6	91.2	78.9	87.9	86.3	75.5
			III	66.0	69.3	62.6	70.8	71.5	63.7	76.6	78.2	73.9	76.7	74.5	73.9
fresh	chloroform	Soxhlet	I	75.1	76.9	74.0	80.2	81.0	75.9	85.2	86.1	80.5	80.9	81.7	76.0
			II	70.6	71.8	69.8	78.6	79.2	70.1	80.5	82.1	77.2	79.2	79.8	75.5
			III	60.8	61.9	60.0	65.6	67.0	61.7	78.4	79.2	70.8	75.1	70.4	65.6
acidified with H_3PO_4	chloroform	Soxhlet	I	92.8	93.9	82.1	93.6	95.1	83.2	95.6	96.4	90.3	93.9	94.6	85.3
			II	84.1	87.0	77.3	86.0	90.8	81.2	90.7	90.6	82.7	86.7	87.5	80.5
			III	72.7	75.2	65.1	73.8	78.6	69.1	82.1	84.1	80.7	80.5	82.8	75.8
acidified with H_2SO_4	chloroform	Soxhlet	I	85.7	85.8	80.7	87.9	86.5	79.0	90.1	88.2	80.4	88.3	85.4	80.2
			II	80.1	80.7	73.2	86.5	83.2	77.3	83.5	82.4	78.7	82.7	80.1	75.3
			III	67.4	68.0	63.1	73.1	70.6	61.0	80.5	80.3	70.8	80.5	80.3	70.8

[a] Derivatization with pentafluorobenzyl bromide and cleanup by (a) water-toluene shaking, (b) TLC, or (c) column.

LITERATURE CITED

(1) W. H. Gutenmann and D. J. Lisk, *J. Assoc. Off. Anal. Chem.*, **47**, 353 (1964).
(2) A. S. Y. Chau and K. Terry, *J. Assoc. Off. Anal. Chem.*, **58**, 1294 (1975).
(3) H. Agemian and A. S. Y. Chau, *Analyst (London)*, **101**, 732 (1976).
(4) W. H. Gutenmann and D. J. Lisk, *J. Assoc. Off. Anal. Chem.*, **46**, 859 (1963).
(5) C. A. Bache, D. J. Lisk, and M. A. Loos, *J. Assoc. Off. Anal. Chem.*, **47**, 348 (1964).
(6) F. K. Kawahara, *Anal. Chem.*, **40**, 1009 (1968).
(7) F. K. Kawahara, *Environ. Sci. Technol.*, **5**, 235 (1971).
(8) J. Coburn and A. S. Y. Chau, *J. Assoc. Off. Anal. Chem.*, **57**, 1272 (1974).
(9) J. K. Gaunt and W. C. Evans, *Biochem. J.*, **122**, 519 (1971).
(10) T. I. Steenson and M. Walker, *J. Gen. Microbiol.*, **16**, 146 (1957).
(11) J. M. Bollag, C. S. Helling, and M. Alexander, *Appl. Microbiol.*, **15**, 1393 (1967).
(12) J. K. Gaunt, Ph.D. Thesis, University of Wales, Bangor, 1962.
(13) J. K. Gaunt and W. C. Evans, *Biochem. J.*, **122**, 533 (1971).
(14) M. A. Loos, J. M. Bollag, and M. Alexander, *J. Agric. Food Chem.*, **15**, 858 (1967).
(15) L. Räsänen, M. L. Hattula, and A. U. Arstila, *Bull. Environ. Contam. Toxicol.*, **18**, 565 (1977).
(16) K. Tiittanen and H. Blomqvist, *Kem.-Kemi*, **3**, 424 (1976).
(17) M. R. Gurd, G. L. M. Harmer, and B. Lessel, *Food Cosmet. Toxicol.*, **3**, 883 (1965).
(18) H. G. Verschuuren, R. Kroes, and E. M. Den Tonkelaar, *Toxicol.*, **3**, 349 (1975).
(19) V. Mattinen, H. Siltanen, and A. L. Valta, "Investigations of the Pesticide Residues", State Institute of Agricultural Chemistry, No. 7, Helsinki, 1972, p 40.
(20) M. A. Sattar, M. L. Hattula, M. Lahtiperä, and J. Paasivirta, *Chemosphere*, **11**, 747 (1977).
(21) C. S. Piper, "Soil and Plant Analysis", Adelaide University Press, Adelaide, Australia, 1950.
(22) D. F. Ball, *J. Soil Sci.*, **15**, 84 (1964).
(23) M. L. Jackson, "Soil Chemical Analysis", Prentice-Hall, Englewood Cliffs, N.J., 1962.
(24) A. Walkey and I. A. Black, *Soil Sci.*, **37**, 29 (1934).
(25) J. A. Prescott, J. K. Tayor, and T. J. Marshall, *Trans. Ist. Comm. Inst. Soc. Soil Sci. Versailles*, 143 (1934).
(26) G. Yip, *J. Chromatogr. Sci.*, **13**, 225 (1975).
(27) R. P. Upchurch and D. D. Mason, *Weeds*, **10**, 9 (1962).

RECEIVED for review October 10, 1978. Accepted January 15, 1979. This work has been supported by the Department of International Developement Co'operation, Ministry of Foreign Affairs, Finland, and by Kemira Company, Finland. The results have been presented by M.A.S. in an oral communication at the EUROANALYSIS III congress in Dublin, Ireland, Aug. 19-25, 1978.

Gas Chromatographic Determination of Benzene and Toluene in Crude Oils

Patrick L. Grizzle* and Harold J. Coleman

U.S. Department of Energy, Bartlesville Energy Technology Center, P.O. Box 1398, Bartlesville, Oklahoma 74003

A gas chromatographic method for the determination of benzene and toluene in crude oils has been developed and utilized in the analysis of 102 crude-oil samples. The method, which is readily adaptable to most chromatographs, uses a simple backflushing technique with nonpolar (OV-1) and polar (1,2,3-tris(2-cyanoethoxy)propane) columns in series. Repeatability and accuracy of the method are better than ±2% and ±4% of the measured values for benzene or toluene. The importance of such data for the identification of crude oils from a common geological origin is demonstrated. For predictive purposes, correlations of benzene and toluene weight percents with routinely measured physical properties of crude oils have been developed. Reasonable estimates of benzene and toluene concentrations can be obtained from these correlations.

Recent federal environmental regulations have prompted the determination of known or possible carcinogenic compounds in many commercial products. Of these compounds, benzene has probably received the greatest attention. Occupational exposure to benzene from industrial and laboratory environments as well as exposure from commercial petroleum products such as gasoline and from crude oils is currently being carefully monitored and controlled. Although benzene levels in crude oils, gasoline, and other petroleum-based products have been periodically measured for many years, rapid and accurate methods of analysis are now of major importance. In addition to tedious physical separation methods (*1*), benzene contents in crude oils and gasolines have been determined by various analytical methods. These include infrared (*2*, *3*), Raman (*4*), and ultraviolet spectroscopy (*5*), polarography (*6*), and gas chromatography (*7–11*). Of these methods, gas chromatography provides both a rapid and reliable quantification of benzene. For gasoline, standard gas chromatographic methods (ASTM D 2267 and D 3606) have been established (*7*, *11*). Although ASTM D 2267 has an upper temperature limit of 300 °F, this limit has been extended (*8*). Alternatively, ASTM D 3606 is directly applicable to the determination of benzene in motor and aviation gasolines. However, no standard method for the determination of benzene in crude oils has been established.

This paper presents a rapid and reliable gas chromatographic method for the determination of benzene and toluene in crude oils and other fossil fuels. The method can be easily adapted to any gas chromatograph with flame ionization detection capabilities. The method was developed concurrently with ASTM D 3606 and the data were obtained prior to acceptance of D 3606. Although, in principle, D 3606 should be applicable to the analysis of petroleum products other than gasoline, the presented method can be viewed as an extension of this standard method to allow for analysis of a wider range of petroleum products.

In addition, this investigation both correlates the benzene and toluene data obtained on 102 samples with routinely measured physical properties of crude oils for predictive purposes and demonstrates the importance of such data to the identification of crude oils from a common geological origin.

EXPERIMENTAL

Apparatus. A Hewlett-Packard model 5830A gas chromatograph equipped with a heated injector block, dual flame-ionization detectors, and a temperature programmer was used.

This article not subject to U.S. Copyright. Published 1979 by the American Chemical Society

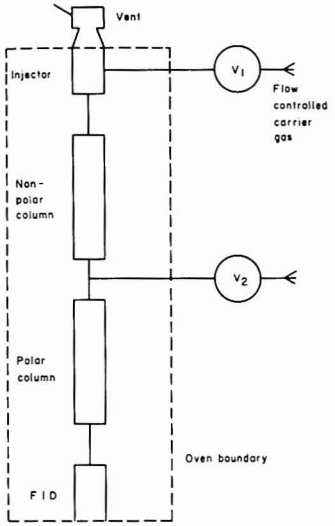

Figure 1. Block diagram of gas chromatograph

Chromatograms were obtained using a Hewlett-Packard model 18850A recorder-integrator. Minor modifications made to the chromatograph for backflushing are depicted in Figure 1. Although the modified configuration is similar to those described in "heart-cutting" (*12*) and in situ fractionation (*13*), the present method does not use a continuously maintained junction pressure principle as in these references. Toggle valves, V_1 and V_2, were connected to two sources of flow-controlled carrier gas. A septum swinger (Perkin-Elmer Co., Norwalk, Conn.) was used as a third valve or vent.

As depicted in Figure 1, nonpolar and polar columns were connected in series. The nonpolar column was 5 ft × $^1/_8$ in. stainless steel packed with 3% w/w OV-1 on 80–100 mesh Chromsorb G (AW). The polar column was 10 ft × $^1/_8$ in. stainless steel packed with 10% 1,2,3-tris(2-cyanoethoxy)propane (TCEP) on 80–100 mesh Chromsorb W (AW) (Alltech Associates, Inc., Arlington Heights, Ill.).

Reagents. Benzene and toluene were obtained from Fisher Scientific Co. (Fair Lawn, N.J.) and used as received. 1-Bromo-3-methylbutane (98%) was obtained from Aldrich Chemical Co., Inc. (Milwaukee, Wis.) and distilled prior to use. The OV-1 liquid phase in the nonpolar column was used as obtained from Applied Science Laboratories, Inc. (State College, Pa.).

Chromatographic Conditions and Procedure. A known amount (ca. 0.020 g) of 1-bromo-3-methylbutane was added to a weighed quantity of crude oil (ca. 1.0 g). The mixture was mixed thoroughly and approximately 0.4 μL charged to the chromatograph. The chromatographic oven was held at 50 °C for 13 min and temperature programmed to 80 °C at 5 °C/min. At injection, valve V_1 was open with a He flow of 25 cm^3/min and V_2 was closed. Following the elution of the internal standard 1-bromo-3-methylbutane from OV-1 column, both valve V_2 and the septum swinger with the septum removed were opened and V_1 was closed. Thus, the light ends were eluted to the TCEP column and the heavy ends backflushed through the septum swinger. A He flow rate of 90 cm^3/min at V_2 maintained a flow of 25 cm^3/min at the detector. Experimentally, the time for the valve switch was determined to be 7.5 min. The injector and detector temperatures were maintained at 300 and 350 °C, respectively. Hydrogen and air flow rates to the FID were 25 and 275 cm^3/min, respectively.

Each crude-oil mixture was analyzed in duplicate and the relative peak areas of the benzene, toluene, and internal standard were obtained via the integrator.

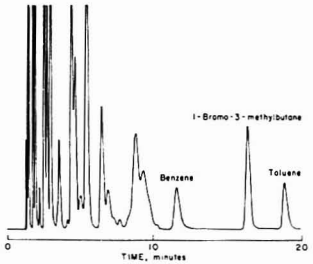

Figure 2. Typical chromatogram obtained for determination of benzene and toluene in crude oils

Calibration Procedure. Weighed quantities of benzene, toluene, and 1-bromo-3-methylbutane were dissolved in hexane and analyzed as previously described. In addition, the mixture was analyzed without switching the valves. Agreement in the FID response factors for the internal standard relative to both benzene and toluene obtained by the two modes of analysis was used to indicate elution of the 1-bromo-3-methylbutane from the OV-1 column prior to backflushing and, thus, to establish the delay time for valve switching.

To determine the linearity of the relative FID response factors, mixtures over the concentration range of benzene expected in the crude oils were prepared and each mixture was analyzed in triplicate.

RESULTS AND DISCUSSION

Internal Standard. For analysis of complex mixtures such as petroleum or petroleum fractions, two criteria for selection of a suitable standard were considered. First, the standard should not be found in the mixture to be analyzed and, second, it should have a retention time different from those of the other components in the mixture. Although a standard with a high level of purity is usually desired, a standard with small amounts of impurity can be used as long as the retention times of the impurities do not interfere with the analysis. 1-Bromo-3-methylbutane satisfies these criteria. Figure 2 shows a typical chromatogram of a crude oil analysis. Although, 1-bromo-3-methylbutane exits the OV-1 column after toluene, the order of elution is inverted in the TCEP column and the internal standard is completely resolved.

Assuming unit relative FID responses for the 1-bromo-3-methylbutane and the impurities in the standard samples, the former compound accounts for 99.2 ± 0.05% of the total sample. It should be noted that this value is a lower estimate of the purity of the standard as follows. Since the impurities were determined to be alkenes, the FID response of 1-bromo-3-methylbutane is approximately 0.4 relative to the impurities. Thus, the purity of the standard is actually significantly higher than 99.2%. The alkene impurities were determined not to interfere with the analyses.

FID response factors for the internal standard relative to both benzene and toluene were determined periodically throughout the total study. For each mixture of benzene, toluene, and 1-bromo-3-methylbutane in hexane, response factors for the standard relative to benzene and relative to toluene (S_i) were obtained from Equation 1

$$S_i = \frac{A_s g_i}{A_i g_s} \tag{1}$$

where A_s and A_i are the relative area percents for the standard and either benzene or toluene and g_s and g_i are the weights of the standard and either benzene or toluene in the mixture. To ascertain the linearity of the relative response factor, the quantities of benzene and toluene were varied to conform to

Table I. Weight Percents of Benzene and Toluene in Crude Oils Analyzed

geological age	sample	state or country	producing formation	wt %[a] benzene	toluene	toluene/ benzene
Cretaceous	68169	Wyoming	Muddy, Dakota	0.237	1.061	4.48
	69111	Kuwait	Minagish	0.077	0.490	6.36
	77056	Texas	Woodbine	0.088	0.414	4.70
	77063	Wyoming	Sussex	0.194	1.252	6.45
	77066	Utah	Dakota	0.029	0.306	10.55
	48-78	Texas	Woodbine	0.008	0.014	1.75
	54-78	Texas	Woodbine	ND[b]	ND	...
	65-78	Texas	Woodbine	0.095	0.421	4.43
	38-78	Texas	Paluxy	0.006	0.011	1.83
	49-78	Texas	Paluxy	0.008	0.010	1.25
	30-78	Texas	Glen Rose	0.015	0.001	0.07
	37-78	Texas	Glen Rose	0.245	0.207	0.84
	53-78	Texas	Glen Rose	0.279	0.459	1.65
	52-78	Texas	Rodessa	0.406	0.406	1.00
	56-78	Texas	Rodessa	0.667	0.340	0.51
	105-78	Louisiana	Rodessa	0.707	0.289	0.41
Devonian	75062	Michigan	Traverse	ND	0.027	...
	75063	Michigan	Traverse	0.038	0.122	3.21
	75064	Michigan	Traverse	ND	0.023	...
	75066	Michigan	Traverse	ND	0.042	...
	75067	Michigan	Traverse	ND	ND	...
	75068	Michigan	Traverse	ND	ND	...
	75071	Michigan	Traverse	ND	0.049	...
	75072	Michigan	Traverse	ND	0.059	...
Eocene	62-78	Texas	Schult	0.151	1.071	7.09
	77-78	Louisiana	Wilcox	0.415	1.620	3.90
	91-78	Louisiana	Wilcox	0.087	0.553	6.36
	104-78	Louisiana	Wilcox	ND	0.091	...
	108-78	Louisiana	Wilcox, A-1	ND	0.003	...
	114-78	Texas	I-B, Cockfield	0.079	0.501	6.34
Jurassic	77022	Arkansas	Smackover	0.541	0.484	0.89
	77027	Arkansas	Smackover	0.576	0.936	1.63
	78001	Arkansas	Smackover B	0.636	1.393	2.19
	78002	Arkansas	Smackover A,B	0.556	1.609	2.89
	78003	Alabama	Smackover	0.098	0.695	7.09
	78004	Alabama	Smackover	0.111	0.791	7.13
	78005	Alabama	Smackover	0.116	0.778	6.70
	78006	Alabama	Smackover	0.146	1.197	8.20
	78007	Alabama	Smackover	0.114	0.918	8.05
	78008	Alabama	Smackover	0.196	1.015	5.18
	78009	Alabama	Smackover	0.089	0.641	7.20
	78010	Alabama	Smackover	0.139	1.070	7.70
	78013	Utah	Nugget	0.259	1.032	3.98
	78014	Utah	Twin Creek	0.251	1.035	4.12
	35-78	Texas	Smackover	0.180	0.966	5.37
	50-78	Texas	Smackover	0.644	5.223	8.11
Miocene	70113	Iran	Asmari	0.116	0.486	4.19
	77058	Louisiana		0.133	0.319	2.40
	77068	Louisiana	NQA-6, NNA-3	0.228	0.921	4.04
	25-78	Texas	Mio-12-B	ND	ND	...
	70-78	Louisiana		0.141	0.487	3.45
	76-78	Louisiana		ND	0.074	...
	78-78	Louisiana	9F, RF	0.052	0.218	4.19
	82-78	Louisiana		0.084	0.484	5.76
	83-78	Louisiana	Petre	0.002	0.052	26.00
	89-78	Louisiana	K	0.207	0.795	3.84
	98-78	Louisiana	So	ND	0.009	...
	107-78	Louisiana	LC1B Hag	0.098	0.479	4.89
	110-78	Louisiana		0.055	0.260	4.73
Mississippian	77019	Indiana	Waltersburg	0.143	0.239	1.67
	77036	Illinois	Benoist	0.221	0.362	1.64
Oligocene	77035	California	Lower Brown, Frio	0.104	0.327	3.14
	78015	Texas	Seabreeze	0.171	0.441	2.58
	78016	Texas		0.204	0.456	2.24
	78017	Texas	FBII-9	0.130	0.290	2.23
	23-78	Texas	Frio, V	0.189	0.743	3.93
	57-78	Texas		0.154	0.363	2.36
	59-78	Texas		0.018	0.157	8.72
	61-78	Texas	Frio	0.003	0.026	8.67
	112-78	Texas	FrioC	ND	ND	...

Table I. (*Continued*)

geological age	sample	state or country	producing formation	wt %[a] benzene	toluene	toluene/ benzene
	116-78	Texas	Frio A-2, A-3	ND	ND	...
Ordovician	77048	New Mexico	McKee	0.071	0.271	3.81
Paleocene	76074	North Sea		0.308	0.888	2.88
	75046	North Sea		0.417	1.183	2.84
Pennsylvanian	77060	Oklahoma	Burbank	0.088	0.193	2.19
	77021	Oklahoma	Deese	0.011	0.126	11.45
	77054	Texas	Winger	0.054	0.204	3.78
	77055	Texas	Bruhlmeyer	0.039	0.278	7.13
Permian	71011	Alaska	Sadlerochit	0.262	0.682	2.60
	77044	New Mexico	Grayburg	0.002	0.125	...
	77045	New Mexico	Tubb, Clear Fork	0.203	0.689	3.39
	77046	New Mexico	Blinebry	0.189	0.661	3.50
	77047	New Mexico	Blinebry	0.360	0.981	2.73
	77049	New Mexico	Yates	0.095	0.538	5.66
	77050	New Mexico	Grayburg	0.209	0.748	3.58
	77051	New Mexico	Yates, Seven River	ND	ND	...
	77052	New Mexico	Blinebry	0.387	1.319	3.40
Pleistocene	77070	Louisiana	O, Reservoir A	0.245	0.426	1.74
	77075	Louisiana	N	0.229	0.729	3.46
Pliocene	77057	Louisiana		0.028	0.132	4.71
Silurian	75049	Michigan	Niagaran	0.412	1.480	3.59
	75050	Michigan	Niagaran	0.367	1.921	5.23
	75052	Michigan	Salina A-1	0.176	1.187	6.74
	75059	Michigan	Niagaran	0.564	1.886	3.34
	75060	Michigan	Niagaran	0.280	1.362	4.86
	75065	Michigan	Salina	0.027	0.313	11.59
	75069	Michigan	Salina	0.077	0.678	8.81
unknown	71052	California		0.012	0.075	6.25
	77039	Mexico		0.082	0.403	4.91
	77059	Pennsylvania		0.072	0.394	5.47
	77073	Louisiana		0.039	0.412	10.56
	77074	Louisiana		0.131	0.776	5.92

[a] Average of two determinations. [b] ND = not detected; detection limit = 10 ppm.

the limits expected to be found in the crude oils. Within experimental error, the response factors were independent of concentration over this range (0.005 to 1.0% by weight). Over the course of these analyses (ca. 9 months), the response factors for the standard relative to benzene and to toluene varied from 0.425 ± 0.005 to 0.437 ± 0.006 and from 0.420 ± 0.004 to 0.430 ± 0.005, respectively. It should be noted that these variations in the average relative response factors are within experimental uncertainty. Also, since the FID is a gram-carbon detector, these values are in excellent agreement with those expected theoretically. Theoretical responses based upon the weight percents of carbon in the standard, benzene, and toluene are 0.430 and 0.435 for the standard relative to benzene and toluene, respectively.

The weight percents ($WT\ \%_i$) of benzene and toluene in each crude oil analyzed were determined by Equation 2

$$WT\ \%_i = \frac{S_i A_i g_s}{A_s g_c} \times 100 \qquad (2)$$

where S_i is the response factor for the standard relative to either benzene or toluene, A_i and A_s are the relative area percents for either benzene or toluene and the standard, and g_s and g_c are the weights of standard and the crude-oil sample, respectively.

Benzene and Toluene Contents. For the crude oils analyzed, Table I presents geographical and geological data, the weight percents of benzene and toluene, and the ratio of toluene to benzene. For discussion (see below), the data have been grouped according to geological age of the crude oil reservoir.

Table II. Repeatability of Determined Benzene and Toluene Weight Percents[a]

crude oil	determination	wt % benzene	toluene
77046	1[b]	0.187 ± 0.003	0.658 ± 0.004
	2[b]	0.191 ± 0.002	0.663 ± 0.002
	average	0.189 ± 0.002[c]	0.661 ± 0.003[c]
37-78	1[d]	0.244 ± 0.002	0.207 ± 0.002
	2[d]	0.244 ± 0.001	0.204 ± 0.002
	3[d]	0.240 ± 0.003	0.202 ± 0.001
	4[d]	0.240 ± 0.001	0.199 ± 0.002
	average	0.242 ± 0.002	0.203 ± 0.003

[a] All deviations are standard unless otherwise noted. [b] Average of four chromatographic determinations. [c] Deviations are average. [d] Average of three chromatographic determinations.

For both benzene and toluene, the method is capable of detecting quantities of ≥10 ppm. The detection limit could be decreased by either increasing the sample size of the crude oil or decreasing the quantity of standard added. However, for our application to a wide variety of crude oils, this detection limit is quite satisfactory. For the samples analyzed, benzene and toluene were detected in 84.3 and 93.1% of the samples, respectively.

Table II demonstrates the excellent repeatability obtained using this method. For repetitive analyses of the same crude oil–standard mixture, the variation in the values of the benzene and toluene weight percents is less than 2% of the mean value. Similarly, the repeatability between analyses for

the same crude oil was better than ±2% of the measured value. It should be noted that determinations 1 and 2 of sample 77046 in Table II were made on consecutive days, whereas the four determinations of sample 37–78 were made over the period of a month.

The accuracy of the method was estimated by analyzing a crude oil sample, adding a known quantity of benzene and toluene to the crude oil, and reanalyzing the "spiked" sample. For these experiments, the percent deviation between the theoretical content of benzene or toluene and the quantity experimentally determined is less than 4%. Considering the error propagation in this estimation and the low concentrations of benzene and toluene in the crude oil samples, this uncertainty is excellent. However, a note of warning concerning the accuracy must be included. The "true" accuracy depends strongly upon the care maintained in the collection, transport, and storage of the crude-oil samples. Owing to their volatility, significant quantities of benzene and toluene may be lost through carelessness. In this study, all crude oils were obtained as "wellhead" samples, transported in sealed containers, and in most cases placed in refrigerated storage upon arrival. The presence of highly-volatile components (i.e. methane, ethane, propanes, and butanes) as determined by gas chromatography in selected samples reflects the care maintained in sample collection.

For the 102 samples analyzed, the benzene and toluene contents vary from the self-imposed detection limit (ca. 10 ppm) to 0.707 and to 5.223%, respectively. The average benzene and toluene contents are 0.161 ± 0.174 and 0.575 ± 0.658, respectively. Both the large quantities of benzene and toluene in many of these crude oils and the large variation in these data for this population of crude oils should be noted.

Although this study originated in reply to numerous requests concerning the levels of benzene and toluene in crude oils, the resultant data have presented some other intriguing questions and/or possibilities. For example, this laboratory has been involved for several years in the area of oil identification. This effort has been applicable to oil-spill identification, geochemical exploration, and differential pricing criteria for "old" and "new" oil. The application of benzene and toluene determinations to these areas has, therefore, been a natural extension of our fundamental research program.

The origin of benzene and toluene in crude oils is still open to debate. Several possible precursors include (a) conjugated olefins such as squalene, the carotenes, and xanthophylls, (b) terpenes, and (c) highly unsaturated fatty acids (*14*). Thermal degradation of β-carotene has been shown to yield ionene (*15*), toluene, *m*-xylene and 2,6-dimethylnaphthalene (*16*). Additional treatment of water-wet marine muds resulted in the formation of benzene, toluene, and xylenes (*16*). However, the quantities of carotenoid pigments in the mud slurries were not sufficient to produce the quantities of low-molecular weight aromatics found. Thus, other materials must also be a source of benzene. Alternatively, dehydrogenation of cycloalkanes by elemental sulfur can yield aromatic compounds at low temperatures (*17*, *18*). Reaction of cholesterol with elemental sulfur at 150 °C has been shown to yield one-, two-, and three-ring aromatic homologues (*19*). Presently, this study can neither substantiate nor refute the possibility of any of these compounds or reactions as precursors to benzene. Additional characterization of the individual oils may, however, provide important information relating to the origin of low-molecular weight aromatic compounds.

The quantitative variability of low-boiling materials in crude oils has been noted by various authors, and attempts to explain these variations with the origin of crude oil have been proposed. Certainly, the quantity of low-boiling material in crude oils has been shown to be directly related to the age and depth of burial of the oil (*20*). With increasing age and burial depth, the quantities of low-boiling materials increase. This observation can be attributed to various maturation processes. However, the concentrations of benzene and toluene (see Table I) do not appear to be maturation-dependent. If the age of the producing reservoir can be considered to reflect the age of the crude oil, the data suggest that the concentrations of these compounds are independent of geological age. This observation would imply that benzene and toluene are formed during early diagenesis and that the concentrations reflect both the types and quantities of organic matter in the source rock (see above discussion). Although additional analytical data are needed to verify the relative degrees of maturation for this set of oils, the importance of this observation should be noted.

Alternatively, another theory on the origin of crude oil maintains that oil consists of hydrocarbons that collected from waters containing natural solubilizers (*21*). Thus, the quantity of a given hydrocarbon in crude oil depends upon the solubility of the component in water and its solubility in naturally occurring soap micelles in the water. The ratio of toluene to benzene has been given as evidence supporting this hypothesis. Typically this ratio varies from approximately 4 to 5 with a range of between 2 to 11 (*17*, *21*). For the 102 samples analyzed, the average ratio of toluene to benzene was 4.78 ± 3.49 with a range from 0.41 to 11.59 (samples 83–78 and 30–78 have been excluded owing to the small amounts of benzene and toluene, respectively). Although the upper limit for the ratio is consistent with the solubility theory, ratio values less than unity cannot be explained easily via the solubility hypothesis. Thus, samples 37–78, 52–78, 56–78, and 105–78 from the Cretaceous age and sample 77022 from the Jurassic age are ≤1.0 and their origin cannot be explained satisfactorily.

The data in Table I, however, do indicate a possible trend which is important for the identification of oils from a common source. Such capabilities are important both for geochemical exploration and differential crude oil pricing. Recent infrared spectroscopic (*22*) and *n*-paraffin distribution (*23*) studies have indicated that the Michigan samples from the Devonian and Silurian age originate from two different source rocks. This same conclusion can be obtained from the benzene and toluene concentration data. Except for samples 75063 and 75065, the Silurian oils can be differentiated from the Devonian crude oil samples. Similar trends are also apparent for other groups of related crude oil samples. For example, the four Jurassic crude oils from Arkansas which represent three different producing fields appear to be from a common origin. The two Jurassic crude oils from the same producing field of Utah but different producing formations appear to be from a common source rock. For these two samples, carbon, sulfur, and nitrogen stable isotope ratio measurement data have supported this conclusion. However, for other samples, the data are not as indicative of origin. The eight Permian New Mexico crude oils were obtained from the same county. The benzene data presented would suggest at least three different crude oil sources (samples 77052 and 77047; samples 77050, 77046, and 77045; samples 77051 and 77044). Although not completely definitive, the combination of such data with stable isotope ratios and other analytical measurements may prove valuable for geochemical exploration and differential pricing of crude oils. It is noted, however, that these trends at present are only speculative and additional research is required to substantiate the positive relationship between common geological source and benzene content.

Data Correlations for Predictive Purposes. At this laboratory, we have established a computerized data retrieval system for routine crude-oil analyses which have been generated by the Bureau of Mines (BOM) routine method.

Table III. Correlation Constants[a]

variable					
independent	dependent	slope	intercept	σ_y	% σ_y
$\bar{S}_f$	wt % benzene	0.014 ± 0.003	−1.756 ± 0.411	0.139	81.9
$\bar{S}_f$	wt % benzene + toluene	0.058 ± 0.012	−6.931 ± 1.554	0.525	65.5
volume % aromatics 1–4	wt % benzene	0.187 ± 0.028	−0.024 ± 0.033	0.124	73.0
volume % aromatics 1–4	wt % benzene + toluene	0.903 ± 0.083	−0.137 ± 0.097	0.366	45.7
volume % aromatics 1–5	wt % benzene	0.096 ± 0.015	−0.022 ± 0.033	0.124	73.0
volume % aromatics 1–5	wt % benzene + toluene	0.480 ± 0.041	−0.153 ± 0.092	0.351	43.8

[a] All deviations are standard deviations.

Presently, this data bank contains distillation data and other physical and chemical properties for approximately 7350 domestic and foreign crude oils. This compilation is one of the largest data bases of crude-oil analyses available and contains information on crude oils produced from the 1920's to the present. Using these data, various empirical and semiempirical correlations have been developed. These include (a) an estimate of the volumes of finished products which can be obtained from each crude oil based on distillation and specific gravity data, (b) the relative degree of aromatic or paraffinic contents in each crude oil, and (c) a hydrocarbon-type analysis approximation which estimates the volumes of alkanes, cycloalkanes, and aromatic compounds as a function of distillate boiling range. Such data have proved important both to government, industry, and university for the further development and utilization of crude oils.

As an extension of this study, we have attempted to correlate the benzene and toluene data in Table I with such empirical relationships for predictive purposes. Such a predictive relationship would provide a large data base of concentration levels which could not be easily determined experimentally. One possible parameter for prediction is the specific dispersion (S_f) of the crude oil as a function of distillate boiling range. Specific dispersions are calculated by Equation 3

$$S_f = \left(\frac{N_g^{20} - N_D^{20}}{d_4^{20}} \right) \times 10^4 \qquad (3)$$

where S_f is the specific dispersion of each distillate fraction, N_g^{20} and N_D^{20} are refractive indexes of each fraction at 5461 and 5893 Å, respectively (commonly referred to as the mercury g and sodium D lines), and d_4^{20} is the density of the fraction at 20 °C (*24*). Empirically, the value of a totally alkane or cycloalkane fraction is 122.4. Values in excess of this are attributed to the amount of aromatic compounds in each fraction. Since the benzene and toluene should be found in the first four distillate fractions (50–125 °C), the average specific dispersion for these fractions should be related to the concentrations of benzene and toluene in the crude oil as a first approximation. Figure 3 presents the correlation observed between the average specific dispersion ($\bar{S}_f$) for the first four fractions and benzene content for 67 samples. Although a trend in the data is evident, a definitive linear relationship is difficult to perceive. Slopes, Y intercepts, and associated standard deviations for this plot, and a similar plot of $\bar{S}_f$ vs. the benzene plus toluene content as obtained via linear-least-squares regression analyses are presented in Table III. It is satisfying to note that the % σ_y in the plot $\bar{S}_f$ vs. benzene plus toluene is less than that for the $\bar{S}_f$ vs. benzene plot as one would expect. Since the ratio of toluene to benzene is not a constant (see above discussion) and the combined distillate fractions considered contain both benzene and toluene, the

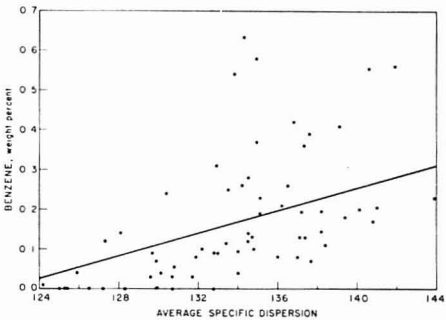

Figure 3. Correlation of wt. % benzene in crude oils with average specific dispersion ($\bar{S}_f$) for 50–125 °C distillate fractions

improved latter correlation is expected. Additional reasons can be given to explain the large scatter in Figure 3. The Hempel still used in the routine BOM method contains few theoretical plates. Experimentally, small quantities of benzene and toluene can be determined in fractions boiling in excess of 125 °C. Furthermore, the BOM method leads to variations in parameters such as distillation rate and reflux ratios depending upon the analyst. Thus, some variations between crude-oil distillations do exist. However, these errors are small as compared to the failure to include the quantity of distillate in the 50–125 °C fractions. Obviously, the specific dispersion values are independent of the quantity of material (see Equation 3). Consequently, although some distillate fractions may have large S_f values, the volume of these fractions as compared to the crude oil may be quite small and only a small amount of benzene or toluene would be present. Conversely, large-volume distillate fractions with small S_f values (low aromatic content) may contain significant quantities of benzene and toluene. The error incurred in the correlation due to this neglect of fraction quantity can be corrected by several means. The hydrocarbon-type analysis which expresses the volume of each distillate fraction by alkane, cycloalkane, and aromatic compounds yields the best estimate of the aromatic volume in each fraction. A detailed derivation of this method and its utility have been presented by Smith and Hale (*24*). Figure 4 presents a plot of the volume percent aromatic compounds in fractions 1 through 4 vs. the weight percent of benzene plus toluene. The slopes, Y intercepts, and associated uncertainties for this plot and the similar plot of weight percent benzene vs. volume percent aromatics are given in Table III. As evident in the data, a modest improvement is realized for these correlations. Again, the improvement in the benzene plus toluene correlation relative to the benzene correlation is expected as previously discussed. Attempts to improve the reliability of this correlation using

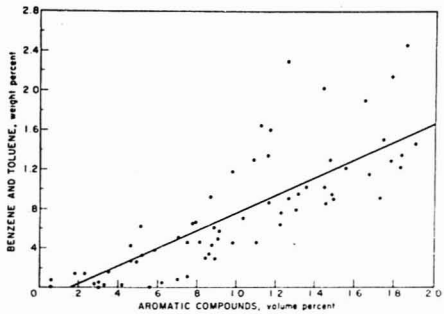

Figure 4. Correlation of wt. % benzene plus toluene in crude oils with vol. % aromatic compounds in 50–125 °C distillate fractions

data for distillate fractions boiling up to 150 °C were unsuccessful (see Table III).

Although the standard deviations in the benzene and benzene plus toluene contents derived from these correlations are relatively large, the importance of such correlations for predictive purposes cannot be underestimated. Reasonable estimates can be obtained from these correlations which can yield important trend data or indicate anomalous concentrations of these compounds in certain crude oils. With a growing environmental concern toward benzene in petroleum related products, a data bank which contains approximate concentrations for representative worldwide crude oils will become increasingly more important. Also, the possible application of such data to geochemical studies has not been fully realized. Improved correlations will aid in the establishment of a data set which may be useful in such studies. Efforts to improve these correlations are continuing and are incorporating additional measured physical and chemical properties.

ACKNOWLEDGMENT

The authors thank Sheri Brand and Janice Thomas of the Bartlesville Energy Technology Center for obtaining some of the chromatog·aphic data reported.

LITERATURE CITED

(1) H. M. Smith, A. J. Kraemer, and H. M. Thorne, "Aviation Gasoline and Its Component Hydrocarbons: Wartime Research (1940–45)", U.S. Department of the Interior, Bureau of Mines, Bulletin 497 (1951).
(2) "1977 Annual Book of ASTM Standards", Part 25, American Society for Testing and Materials, Philadelphia, Pa., p 846.
(3) A. Fallah, A. Badakhsham, P. Etemad-Moghadam, and A. Seyed-Ahmadi, *Bull. Iran. Pet. Inst.*, **44**, 1 (1971).
(4) A. K. Karimov, *Geol. Razvedoch. Inst.*, **82**, 165 (1955).
(5) "1977 Annual Book of ASTM Standards", Part 23, American Society for Testing and Materials, Philadelphia, Pa., Standard D 1017, p 489.
(6) V. Sedivec, *Chem. Prumysl.*, **8**, 180 (1958).
(7) "1977 Annual Book of ASTM Standards", Part 25, American Society for Testing and Materials, Philadelphia, Pa., Standard D 3606, p 365.
(8) L. L. Stavinoha and F. M. Newman, *J. Chromatogr. Sci.*, **10**, 583 (1972).
(9) C. L. Stuckey, *J. Chromatogr. Sci.*, **7**, 177 (1969).
(10) R. L. Martin and J. C. Winters, *Anal. Chem.*, **31**, 1954 (1959).
(11) "1977 Annual Book of ASTM Standards", Part 24, American Society for Testing and Materials, Philadelphia, Pa., Standard D 2267, p 247.
(12) D. R. Deans and Ian Scott, *Anal. Chem.*, **45**, 1137 (1973).
(13) K. A. Goode, *Chromatographia*, **9**, 521 (1977).
(14) J. G. Erdman, *Geochim. Cosmochim. Acta*, **22**, 16 (1961).
(15) W. C. Day and J. G. Erdman, *Science*, **141**, 808 (1963).
(16) J. D. Mulik and J. G. Erdman, *Science*, **141**, 806 (1963).
(17) H. M. Smith and H. T. Rall, *Ind. Eng. Chem.*, **45**, 1491 (1953).
(18) T. J. Jones and H. M. Smith, Relationships of Oil Composition and Stratigraphy in the Permian Basin of West Texas and New Mexico. Fluids in Subsurface Environments—A Symposium, Memoir 4, *Am. Assoc. Petrol. Geol.*, **1965**, 101.
(19) A. G. Douglas and B. J. Mair, *Science*, **147**, 499 (1965).
(20) E. W. Biederman, Jr., *World Oil*, December 1965, p 78.
(21) E. G. Baker, *Science*, **129**, 871 (1959).
(22) P. L. Grizzle and H. J. Coleman, "Infrared Analysis Techniques for Oil Identification", U.S. Energy Research and Development Administration, Technical Information Center, BERC/RI-77/4, April 1977.
(23) P. L. Grizzle and H. J. Coleman, "GLC Analysis of *n*-Paraffin Distributions in Crude Oils and Topped Crude Oils for Oil Identification", U.S. Energy Research and Development Administration, Technical Information Center, BERC/RI-77/12, October 1977.
(24) H. M. Smith and J. H. Hale, "Crude Oil Characterizations Based on Bureau of Mines Routine Analyses", U.S. Department of the Interior, Bureau of Mines, RI 6846 (1966).

RECEIVED for review October 19, 1978. Accepted January 29, 1979.

Determination of Sulfur-Containing Gases by a Deactivated Cryogenic Enrichment and Capillary Gas Chromatographic System

S. O. Farwell* and S. J. Gluck

Department of Chemistry, University of Idaho, Moscow, Idaho 83843

W. L. Bamesberger, T. M. Schutte, and D. F. Adams

Air Pollution Research, Washington State University, Pullman, Washington 99164

A deactivated glass capillary, wall-coated open tubular (WCOT) column is the heart of a novel gas chromatographic procedure for measuring reduced sulfur-containing gases in air samples. These deactivated, high resolution WCOT columns provide optimal chromatographic separation of compounds such as H_2S, COS, CH_3SH, CH_3SCH_3, CS_2, CH_3SSCH_3, and other organosulfur species. In addition, the combination of WCOT columns, a deactivated GC, and the flame photometric detector (FPD) increases the sensitivity of the GC/FPD method for sulfur compounds. The GC/WCOT/FPD instrumentation is also designed for complete compatibility with a cryogenic sampling procedure. This surface-deactivated, cryogenic enrichment system has been shown to provide known sampling efficiencies between 40% to approximately 100% for the important inorganic and organosulfur compounds at the low and sub-ppb concentrations. The methodology described has been successfully applied to field analyses of sulfur compound emissions from biogenic sources.

The analyses of air samples for gaseous sulfur constituents at the low and sub-ppb concentrations are complicated by three predominant factors: (a) the corresponding sensitivity requirements, (b) the large number of chemical compounds present at these ultra-trace levels, and (c) the adsorption affinities of the pertinent inorganic and organosulfur compounds. Therefore, qualitative and quantitative measurements of the volatile sulfur emission flux from natural biogenic sources can be obtained only by a combination of efficient sample enrichment at the natural source of production, quantitative desorption from the preconcentration device, high resolution separation of sample components, minimal adsorption losses to the analytical system, and specific detection of the sulfur present in the compounds. The procedures described in this paper were developed in accord with the preceding analytical criteria.

Because of the large number of possible compounds which may be present in an air sample at the parts-per-billion/parts-per-trillion (ppb/ppt) range, gas chromatography (GC) is the current separation technique of choice. However, the gas chromatographic analysis of sulfur-containing gases has always been a difficult analytical problem because of the adsorption losses of these polar compounds on chromatographic column walls and packings (*1–3*). Until recently, the gas chromatographic analyses of the low molecular weight sulfur compounds have been performed exclusively by conventional packed-column gas chromatography. The most notable packed columns for the chromatographic separation of sulfur-containing gases include: the Triton X-305 column (*4*), a Teflon column packed with 40/60 mesh Teflon powder which is coated with polyphenyl ether and orthophosphoric acid (*5*), a deactivated silica gel column (*6*), the columns developed by Bruner et al. (*7–9*) which employ a graphitized carbon black packing treated with phosphoric acid and either Dexsil 300 or XE-60, and the acetone-treated Porapak QS column packing described by de Souza and co-workers (*10*).

Although several types of packed columns have been used in the gas chromatographic measurements of various sulfur-containing gases at concentrations down to approximately 5 ppb, they are plagued with several disadvantages. Examples of these disadvantages are: large surface areas and concomitant adsorption losses to the column; a gradual approach to equilibration and the corresponding need to perform a number of "conditioning" injections both before and during the working period in order to obtain stable responses; inadequate resolution for certain important components in mixtures of sulfur-containing gases (e.g., H_2S and COS); relatively high pressure drops through the longer packed columns; broad peak widths for late-eluting compounds such as the organic sulfides and disulfides; and considerable potential for hydrocarbon quenching of the flame photometric detector's (FPD) response due to inadequate peak resolution between the sulfur compounds and other organic constituents in the sample. Because of these inherent limitations with packed columns, glass capillary wall-coated open tubular (WCOT) columns were investigated in this study for their potential utility in the GC/FPD determination of atmospheric sulfur-containing gases such as H_2S, COS, SO_2, CH_3SH, CH_3SCH_3, CS_2, and CH_3SSCH_3.

Prior to our work, several other investigators had reported varying degrees of success when glass capillary columns were used to separate various sulfur-containing compounds. For example, glass WCOT columns have been used to analyze for sulfur compounds in citrus oils (*11*), pesticide samples (*12*), and the gaseous constituents of tobacco smoke (*13*). Whereas glass columns are usually recommended for the chromatographic analysis of labile compounds because of their comparatively inert nature, glass columns still exhibit a substantial amount of surface activity (*14*). For polar sulfur compounds, the residual surface activity of glass causes tailing of chromatographic peaks and sometimes complete adsorption of trace sample components. Thus, it is essential to deactivate the glass and metal surfaces of a chromatographic system to minimize both peak tailing and losses incurred by irreversible adsorption of these trace sulfur-containing components. Various methods for the deactivation of glass surfaces have been reported (*15–24*). In addition to the type of chemical deactivant, the composition of the glass and the initial surface treatments are important factors in achieving maximum passivation (*14, 18, 19, 24–32*).

This article discusses the design and operational characteristics of a combined cryogenic collection–gas chromatographic system that is suitable for the sensitive and specific

0003-2700/79/0351-0609$01.00/0 © 1979 American Chemical Society

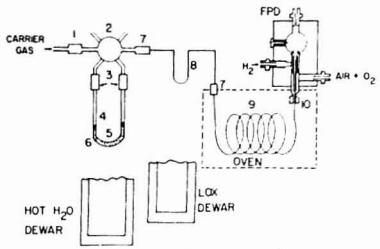

Figure 1. Schematic of cryogenic U-tube sampler, precolumn capillary trap, WCOT column, and FPD. The numbers correspond to the following items: 1. check valve, 2. Carle valve, 3. Quick-Connects, 4. 6 mm o.d. × 27 cm U-tube sampler, 5. Pyrex wool plugs, 6. 3-to-4 cm of 60/80 mesh borosilicate glass beads, 7. low dead volume $^1/_{16}$-in. unions, 8. glass capillary trap, 9. WCOT capillary column, and 10. $^1/_{16}$-in. Swagelok to $^1/_8$-in. pipe male connector

analysis of sulfur-containing gases in air.

EXPERIMENTAL

Gas Chromatographic Apparatus. A Hewlett-Packard Model 5713A gas chromatograph with a flame photometric detector was used in the developmental and optimization stages of this study. This gas chromatograph is equipped with the temperature programming and liquid nitrogen cryogenic options. A Hewlett-Packard Model 3380 recording integrator was used for data acquisition. The Model 5713A gas chromatograph was modified as illustrated in Figure 1 to improve its compatibility with glass open tubular columns. The first modification to this particular GC was to move the FPD from its original mounting position on the side of the GC oven to a new position on top of the GC oven. This relocation of the FPD was necessary to bring the inlet of the detector base into a straight-line position with the outlet end of the capillary column so that the column end could be inserted directly into the bottom of the FPD burner block. In this manner, the dead-volume of the detector-column interface was reduced to a minimum and the air/O_2 gas entering the FPD serves as a purge gas since the end of the capillary column is inserted beyond the air/O_2 inlet port of the FPD. As shown in Figure 1, the FPD was also converted back to the conventional hydrogen-hyperventilated flame configuration by reversing the hydrogen and air/O_2 gas inlets on the commercial instrument. Although several improvements in FPD performance have been reported when the burner is operated with an oxygen-hyperventilated flame (*33*), the conventional flame configuration gave the highest signal-to-noise ratios and lowest detectabilities for the sulfur compounds in our gas chromatographic system.

The other important modification to the gas chromatograph concerned the removal of the dual stainless steel injection ports and their replacement with a small void volume injection system. This novel injection design functions as a low-dead volume interface between the relatively large volume cryogenic enrichment sampler, or freeze-out loop, (labeled #6 in Figure 1) and the inlet end of the 0.25-mm i.d. glass open tubular column. The actual minimum volume interface consists of a precolumn, glass capillary cooling trap (labeled #8 in Figure 1). A Carle mini-volume, six-port switching valve is employed to control the flow of the carrier gas between the larger, freeze-out sampling loop and the glass capillary trap. The connections between the capillary trap, the WCOT analytical column inside of the GC oven, and the Carle switching valve are via $^1/_{16}$-in. Swagelok stainless steel, low dead-volume GC unions (#SS-1FO-6GC).

During GC/FPD operation, a constant water drip from the exhaust port of the FPD was noted. This continual drip caused a change in gas exhaust pressure and resulted in periodic perturbations on the chromatographic base line. This problem was eliminated by wrapping a small heating tape around the FPD exhaust tube. The heat tape was used to maintain the exhaust tube at a temperature of 110 °C.

Although the majority of the laboratory work was performed with the modified Hewlett-Packard Model 5713A GC and the Model 3380 recording integrator, we have also incorporated the same necessary design features into a new Hewlett-Packard Model 5840 GC. This modified H-P 5840 gas chromatograph is employed in the field measurement phase of our research project (*34*, *35*).

Ultra-high purity helium from Linde Speciality Gases was used for the chromatographic carrier, Carle valve, and sample enrichment loop purge gas. The oxygen, hydrogen, and air for the flame photometric detector were high purity gases from Linde Speciality Gases. All the FPD and GC carrier gases were passed through individual Linde 13X molecular sieve scrubber columns. In addition, the helium carrier gas was passed through a Supelco Model 2-2316 gas purifier that was located between the molecular sieve tube and the GC.

The optimum flow rates for the FPD flame gases were found to be: H_2, 100 mL/min; air, 60 mL/min, and O_2 18 mL/min. These FPD gas flows, which correspond to an O_2/H_2 ratio of 0.31, were used during this work. The WCOT columns were operated at a constant helium carrier gas velocity ($\bar{u}$) within the optimum range of 20–26 cm/s. A column head pressure of approximately 10 psi was sufficient to maintain the preceding carrier gas velocities.

Chromatographic Columns. Borosilicate glass WCOT columns (30 m × 0.25 mm i.d.) coated with SE-30, Carbowax 20M, and OV-17 were initially evaluated for their suitability in the high resolution chromatographic analysis of the seven sulfur compounds. However, all of these WCOT columns showed broad, tailing chromatographic peaks for the sulfur compounds. Consequently, several "deactivated" glass WCOT 30-38 meter columns coated with OV-101 (or SP-2100) and SE-54 were purchased from J & W Scientific, Inc. of Orangevale, Calif., and Quadrex Corp. of New Haven, Conn. The major portion of the chromatographic data reported in this paper was obtained with the "deactivated" WCOT columns.

Cryogenic Enrichment Sampler. The cryogenic, U-shaped sampling loops are constructed from 6-mm o.d. Pyrex glass tubing which is packed with 3–4 inches of 60/80 mesh Pyrex glass beads. The glass beads are held in the lower portion of the U-shaped glass tube by two small Pyrex glass wool plugs. The inner surfaces of the glass loops, the glass beads, and the glass wool are coated with a layer of polysiloxane and methyl silicone according to the procedures discussed elsewhere in this paper. Two Swagelok SS-QC4-B-400VT Quick-Connect bodies are used to connect the glass freeze-out sampling trap to the Quick-Connect SS-QC4-S-200 stems of the field sampling train and, subsequently, to the Quick-Connect SS-QC4-S-100 stems of the Carle switching valve on the gas chromatograph. The Swagelok Quick-Connect bodies must be disassembled and cleaned prior to use to remove the thread anti-seizing substance which otherwise acts as a strong sink for sulfur gases, especially for hydrogen sulfide and methyl mercaptan. The Quick-Connect bodies can be cleaned of this factory-applied lubricant by several series of methylene chloride rinses followed by a thorough wiping to remove the dislodged particles. The Quick-Connect bodies are then reassembled using Teflon tape on the threads to prevent leakage. Then the inner surfaces of the Quick-Connects must be flushed dynamically with a deactivant solution of polysiloxane followed by heating at 110 °C to prevent significant adsorption losses. As illustrated in Figure 1, the U-shaped sampling traps are designed to fit into 265-mL Dewar flasks filled with either liquid oxygen (LOX) for cryogenic sampling or hot water for the ensuing desorption into the glass capillary trap and chromatographic system.

Calibration System. The following sulfur gases with the corresponding minimum purities were obtained from Matheson Gas Products: H_2S, 99.5%; COS, 97.5%; CH_3SH, 99.5%; and SO_2, 99.9%. The CS_2 was Baker Analyzed Reagent Grade with a minimum purity of 99%. The CH_3SCH_3 (DMS) and CH_3SSCH_3 (DMDS) were Eastman Reagent Grade with minimum purities of 98% and 97%, respectively. These sulfur compounds were used to prepare Teflon permeation tubes according to the standard procedures (*36–38*). The primary permeation tubes were maintained at 30 ± 0.01 °C by a constant temperature water bath and were calibrated gravimetrically. Standard ppb (v/v) concentrations were obtained by passing clean air at known flow rates over the calibrated permeation tubes. The standard gas concentrations in the 1-ppb to 10-ppt range were obtained by using a simplified version of the dilution system previously described

by Axelrod et al. (*39*). FEP-Teflon tubing and PFA-Teflon tube fittings from Fluoroware of Chaska, Minn., were used in the sample lines of both the calibration system and the actual cryogenic field sampling apparatus.

Two calibration methods were used. The first procedure employed either a 1-mL or 3-mL gas sample loop of FEP-Teflon which was attached to the Carle switching valve to inject known sample volumes from the permeation tube dilution system into the gas chromatograph. In the second method, known volumes of dilute standard gas were collected in the cyrogenic enrichment U-shaped sampler which was immersed in a LOX Dewar flask. The U-shaped freeze-out loop was then attached to the Carle valve whereupon the standard sample was transferred from the larger freeze-out loop to the cold capillary trap and, subsequently, swept onto the analytical WCOT column.

Clean Air Supply. The sulfur-free gas supply for use as the dilution gas in the calibration system and as the purging gas was prepared by passing compressed laboratory or ambient air through a multibed adsorbent filter. This air purification filter consists of a Drierite $2^5/_8$-in. × $11^3/_8$-in. gas drying cartridge which is filled with equal layers of potassium permanganate-treated alumina pellets obtained from Purafil Inc. of Chamblee, Ga.; Drierite anhydrous $CaSO_4$; activated charcoal; and 4–8 mesh pellets of soda lime, respectively. A 0.8-μm pore size membrane filter is placed in the outlet end of the filter cartridge to prevent fine particles of the adsorbents from becoming entrained in the purified air stream. Two 0.5-cm thick fiber filter mats are located on the ends of the adsorbent bed to hold the solid adsorbents in place within the filter cartridge.

Additional Sulfur Compounds. Ethylthiol, 1-propanethiol, 2-propanethiol; 1-butanethiol; 1-methyl-1-propanethiol; 2-methyl-1-propanethiol; 2-methyl-2-propanethiol; 1-pentanthiol; 2-methyl-2-butanethiol; benzenethiol; 1,2-ethanedithiol; dimethyl sulfide; ethyl methyl sulfide; diethyl sulfide; diisopropyl sulfide; methyl phenyl sulfide; and dimethyl sulfoxide were obtained from Eastman Chemical Co. or Aldrich Chemical Co. All these compounds had reported purities in excess of 95% except for 2-methyl-2-butanethiol which was of technical grade. Qualitative standard gas mixtures of the preceding compounds were prepared in the high ppb range for use in the retention time study. These qualitative gas standards were prepared by exponential dilution.

Deactivating Agents and Procedures. The polysiloxane solution (DC-Q8-5479) and dimethyldichlorosilane were obtained from PCR Research Chemicals, Inc. The other organosilanes were purchased from PCR Research Chemicals, Inc., Petrarch Systems Inc., and Pierce Chemical Co. The triethanolamine, benzyltriphenylphosphonium chloride (BTPPC), and 1-aziridineethanol were reagent grade materials from Aldrich Chemical Co. Chromatographic-quality liquid phases of Carbowax-20M, SE-30, SP-2100, OV-17, and Triton X-305 were from Supelco, Inc.

Four types of glass were examined for their relative susceptibilities to adsorb sulfur gases and for their relative deactivation efficiencies: soda-lime, borosilicate or Pyrex, conventional quartz, and clear fused quartz from Quartz Scientific, Inc. Each type of glass was cleaned via successive washings with concentrated nitric acid, concentrated ammonium hydroxide, and absolute methanol followed by a deionized water rinse prior to oven drying at 110 °C.

The polysiloxane deactivant solution was diluted with water to produce a 1% solution and coated either statically or dynamically on the glass or metal surfaces to be deactivated, e.g., U-tubes, glass beads, Quick-Connects, glass wool, etc. After treatment with the polysiloxane, the surfaces were rinsed with deionized water and dried at 110–130 °C. The siloxane-modified surfaces of the cryogenic sampling traps were then treated with a solution of 5% methyl silicone (SE-30 or SP-2100) in methylene chloride. It is necessary to evaporate the methylene chloride slowly at a controlled temperature to minimize pooling and to achieve maximum surface passivation during this particular step in the overall deactivation procedure. The last step in the sequence is to heat the treated materials at 125 °C for 1–2 h.

The poly(*N*-β-hydroxyethyl)aziridine (NEA) and triethanolamine deactivations were performed according to similar procedures given by Sandra and Verzele (*24*). The liquid phase Carbowax-20M deactivations followed the methods of Blomberg (*18*), Grob and Grob (*19*), and Sandra et al. (*24*). Gas phase deactivation with Carbowax-20M was performed by a procedure similar to that reported by Franken and co-workers (*21*). Treatments with benzyltriphenylphosphonium chloride were according to the method described by Malec (*16*) and Rutten et al. (*40*). Further details regarding the deactivation procedures are available in reference 41.

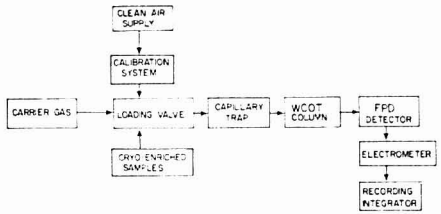

Figure 2. Block diagram of chromatographic system

Operational Procedures. The overall composition of the sulfur analysis system is depicted in the block diagram of Figure 2. As shown in Figure 2, either standard sulfur gas samples for calibration or cryogenically-enriched air samples can be transferred into the external capillary glass trap and onto the deactivated open tubular analytical column. In either case, helium carrier gas sweeps the sample into the capillary trap. This sample introduction system via the cooled, external capillary trap is essential providing a narrow-band "slug" of sample to the head of the WCOT column prior to the ensuing chromatographic separation. The narrow-band transfer of the sulfur compounds to the inlet of the WCOT column is necessary to maintain the high chromatographic resolution inherent with capillary WCOT columns. The application of metal and glass capillary traps, which are internal to the GC oven, has previously been described by Kirsten et al. (*42*, *43*) for the analysis of chlorinated hydrocarbons by electron-capture gas chromatography.

The actual operation of the chromatographic analysis system can best be described with reference to Figure 1 which shows a schematic diagram of the chromatographic injection and flow system. During the actual collection of the air sample, the 6-mm o.d. glass enirchment loop is cryogenically-cooled via a small Dewar flask filled with liquid oxygen and the sample air is pulled through the cryogenic enrichment loop at a flow rate of 30 ± 0.1 mL/min for known sampling times varying from 1 min to over 4 h. This larger enrichment loop is also immersed in the LOX Dewar flask when it is transferred to the chromatographic apparatus at the end of the sampling period. Once the cold U-shaped enrichment trap is attached to the Carle switching valve on the GC via the Quick-Connects, the LOX Dewar flask is moved from this large freeze-out loop to the glass capillary trap. Then, the Carle valve is switched to direct the carrier gas flow through the large sample loop and into the capillary trap. Next, the large enrichment loop is immersed with 90 °C water contained in another small Dewar flask which rapidly desorbs the volatile contents of the sample loop. The desorbed components from the large sample loop are swept to the cold glass capillary trap where they are recondensed at LOX temperature (−183 °C).

The optimal transfer time between the sampling loop and the capillary trap to ensure a quantitative transfer of the analyte is 6 min. Consequently, the transfer time was accurately maintained at 6 min. Transfer times of less than 4 min and those in excess of 7 to 8 min result in nonquantitative transfer of the analytes. Several experiments to detect potential analyte losses due to either micro-fogging and/or sample breakthrough during the transfer process were performed by replacing the WCOT column with a 15-cm length of deactivated glass capillary tubing. This short section of capillary tubing provided a direct connection between the capillary trap and the FPD. Subsequent sample transfer between the sampling loop and capillary trap using this simple GC configuration showed that the FPD response always remained at its normal base line as long as the capillary trap was immersed in liquid oxygen. Thus, these investigations provided no evidence for detectable breakthrough losses of sulfur compounds during the previously described transfer procedure. However, the nonquantitative transfer of the more volatile sulfur compounds

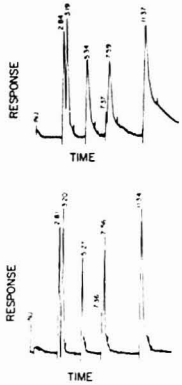

Figure 3. Chromatograms obtained with undeactivated, SE-30 WCOT capillary columns. Chromatographic peaks are: H_2S (2.8 min), COS (3.2 min), CH_3SH (5.3 min), CH_2SCH_3 (7.4 min), CS_2 (7.6 min), and CH_3SSCH_3 (11.3 min). Chromatographic conditions: $\bar{u}$ = 20.4 cm/s of helium, oven programmed from −70 to 100 °C at 16 °C/min

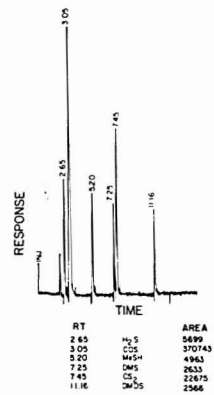

Figure 4. Chromatogram obtained with a deactivated, OV-101 WCOT capillary column. Chromatographic peaks are: H_2S (2.65 min), COS (3.05 min), CH_3SH (5.20 min), CH_2SCH_3 (7.25 min), CS_2 (7.45 min), and CH_3SSCH_3 (11.6 min). Chromatographic conditions: $\bar{u}$ = 20.4 cm/s of helium, oven programmed from −70 to 100 °C at 16 °C/min

when the transfer time exceeds 7 to 8 min still suggests a gradual sublimation loss that is below the detectability of the FPD.

Upon completion of the transfer, the Carle valve is switched to its original position which causes the carrier gas flow to bypass the large sample loop. Simultaneously, the LOX Dewar flask is removed from the capillary trap and is replaced with the second Dewar flask filled with 90 °C water. This thermal desorption from the capillary trap injects the volatilized sample components onto the head of the WCOT column which is at its initial column temperature. The GC oven temperature programming rate is initiated immediately following the immersion of the glass capillary trap in the 90 °C water. The HP-5713A GC uses an oven temperature program from −70 to 100 °C at the rate of 16 °C/min. The GC oven in the HP-5840 is temperature programmed from −60 to 130 °C at an initial rate of 20 °C/min for the first 3 min and then at a rate of 30 °C/min until the oven temperature reaches 130 °C. In both chromatographs, the ovens are maintained at the final temperature until the end of the 15-min analysis period. The ovens are then automatically cooled down to their respective starting temperatures of −70 or −60 °C unless the analyst inputs other instructions.

Prior to our design of the capillary trap injection system, we attempted to condense the sulfur compounds in a narrow band at the head of the WCOT column. In this set of experiments, the sample was swept directly from the large enrichment sampling loop to the inlet of the glass capillary column. The HP 5713A gas chromatograph with the liquid nitrogen cryogenic option can be cooled to −70 °C. This column temperature, however, is not low enough to trap the lower boiling sulfur gases at the head of the WCOT column. Consequently, a modification to the temperature sensing circuitry in the column oven was used to decrease the low temperature range to approximately −150 °C. A similar modification for this purpose has been recently reported by Dulson (*44*). Unfortunately, the lowering of the column oven temperature to −150 °C still does not condense hydrogen sulfide in a narrow band at the head of the column for the duration of the required 6-min loading period. This unsuccessful procedure was evidenced by a relatively broad peak for hydrogen sulfide as compared to the narrow peaks for the other sulfur compounds in the standard mixture. Thus, the cryogenic capillary trap design was implemented and is currently the only way by which all of the sulfur components can be transferred to the inlet of the analytical column in a narrow "slug" injection.

RESULTS AND DISCUSSION

GC/WCOT/FPD Optimization and Characterization. The adsorption and reactive properties of glass capillary columns are critical factors in the successful and efficient gas chromatographic determination of sulfur-containing compounds. Figure 3 illustrates two typical chromatograms obtained for sulfur compounds when conventional glass WCOT columns were employed. Both chromatograms in Figure 3 show varying degrees of peak broadening and tailing. The column employed to produce the top chromatogram in Figure 3 would be totally unacceptable in terms of peak symmetry and chromatographic efficiency. The lower chromatogram in Figure 3 is an improvement with respect to the upper chromatogram, but the peaks still reveal that the corresponding column is not ideal for the efficient chromatographic separation of these sulfur compounds. Figure 4 shows a chromatogram of the same sulfur compounds on a "deactivated" glass WCOT column. As evident by comparison of the chromatograms in Figure 3 and 4, a surface deactivated WCOT column is required to minimize adsorptive peak tailing and to achieve high resolution chromatographic separation of the polar sulfur compounds. Experience with a number of WCOT columns has revealed that the peak shape and relative amount of tailing for the nicotine peak in the test chromatograms supplied by several commercial vendors of glass capillary columns are good indicators of probable performance in the GC/WCOT/FPD analysis of polar sulfur compounds. Thus, a column exhibiting a narrow, nontailing peak for nicotine should be suitable for use in the chromatographic separation of atmospheric sulfur gases.

In addition to the deactivated WCOT columns obtained from J & W Scientific, Inc., a deactivated glass surface 38-m WCOT column coated with OV-101 was purchased from QuadRex Corp. Although the chromatograms obtained with the QuadRex column showed relatively sharp chromatographic peaks for H_2S, COS, CH_3SH, CH_2SCH_3, CS_2, and CH_3SSCH_3, resolution of the adjacent H_2S–COS and CH_2SCH_3–CS_2 peaks was not as satisfactory as the WCOT columns obtained from J & W Scientific, Inc. Furthermore, peak tailing and adsorption losses to the column were more apparent in the chromatograms obtained with the QuadRex column. However, it should be emphasized that only one QuadRex WCOT column was evaluated in this study. Thus, a more comprehensive series of comparative investigations would be required to evaluate these deactivated WCOT columns from QuadRex and J & W Scientific for their compatibility with sulfur gas analyses.

Table I. Chromatographic and Physical Data for Sulfur-Containing Compounds

compound	mol. wt.	bp (°C)	relative retention time[a]
hydrogen sulfide	34.08	−60.7	0.40
carbonyl sulfide	60.08	−50.0	0.44
sulfur dioxide	64.07	−10.0	0.65[b]
methylthiol	48.11	6.2	0.71
ethylthiol	62.13	35.0	0.94
dimethyl sulfide	62.13	37.3	0.98
carbon disulfide	76.14	46.3	1.00
2-propanethiol	76.16	52.6	1.07
2-methyl-2-propanethiol	90.19	64.2	1.16
1-propanethiol	76.16	67–68	1.20
ethyl methyl sulfide	76.16	66.6	1.21
1-methyl-1-propanethiol	90.19	85.0	1.33
2-methyl-1-propanethiol	90.19	88.7	1.36
diethyl sulfide	90.19	92.1	1.40
2-methyl-2-butanethiol	104.22	99–105	1.43
1-butanethiol	90.19	98.5	1.44
dimethyl disulfide	94.20	109.7	1.51
diisopropyl sulfide	118.24	120.0	1.61
1-pentanethiol	104.22	126.6	1.67
1,2-ethanedithiol	94.20	146.0	1.70
benzenethiol	110.18	168.7	2.15
dimethyl sulfoxide	78.13	189.0	2.75[b]
methyl phenyl sulfide	124.21	193.0	2.84

[a] Based upon carbon disulfide which had an absolute retention time of 7.64 min on this deactivated, OV-101 30 m × 0.25 mm i.d. glass WCOT column. [b] Relatively broad peaks for SO_2 and DMSO.

Table II. Typical GC/WCOT/FPD Conditioning Data

compound	run of day: first, pg	second, etc., pg	% low on first run
H_2S	257	285	10
COS	169	171	1
CH_3SH	315	359	12
CH_3SCH_3	102	109	7
CS_2	120	134	11
CH_3SSCH_3	89	95	6

The chromatographic retention data listed in Table I for 24 sulfur-containing compounds denote the separation achieved with the deactivated, methyl silicone-coated glass capillary columns. The close correlation between boiling points and absolute or relative retention times for the sulfur compounds in Table I suggests that the chromatographic separations are based upon boiling points. The one apparent exception to this correlation is 1,2-ethanedithiol which is not totally unexpected because of its structural difference in comparison to the other sulfur compounds of Table I. Except for two compounds (2-methyl-2-butanethiol and 1-butanethiol), the chromatographic peaks for the remaining sulfur compounds in Table I were base-line resolved by the WCOT column. As noted in Table I, none of the WCOT columns examined to date have yielded sharp peaks for either sulfur dioxide or dimethylsulfoxide. The chromatographic peaks corresponding to these latter two compounds are rather broad and tailing. Therefore, the glass capillary columns are not recommended for the analysis of SO_2 or DMSO.

Table II contains some experimental data which demonstrate the deactivation of our entire analytical apparatus and the concomitant small conditioning effects. As listed in Table II, the results from the first run of the working day are remarkably close to the experimental results obtained for the second and succeeding runs. These typical conditioning data were the result of successive injections of the standard mixture of the six sulfur compounds. Although Table II presents conditioning effects on quantitative measurements over a non-use period of approximately 15 h, similar evidence of minimal conditioning effects has been observed for longer periods between sample analyses. For example, the conditioning data in Table II are also typical of the very small quantitative differences which occur when the chromatographic apparatus is not used over a weekend, or approximately 63 h. This lack of significant conditioning effects with our system is a considerable improvement over the other gas chromatographic system described in the literature for sulfur gas analysis (*1, 3, 5-10, 45*). For example, the current FPD-GC method described by the Sulfur Subcommittee of the Intersociety Committee includes an automatic switching cycle which injects sulfur calibration gases on alternate cycles to maintain column conditioning (*46*). No such conditioning procedure is necessary with the optimized, deactivated gas chromatographic apparatus constructed during this project.

Table III. Typical Repeatability of Quantitative Chromatographic Data[a]

compound	repeatability at 95% confidence interval, %
H_2S	±9.4
COS	±10
CH_3SH	±9.4
CH_3SCH_3	±13.3
CS_2	±6.0
CH_3SSCH_3	±15.4

[a] Repeatability values calculated from $\pm 2s$ for $n = 6$.

The typical repeatability of the GC/WCOT/FPD system is demonstrated in Table III. These repeatability values at the 95% confidence interval were obtained over a 80-fold concentration range from 10 to 800 ppb where the standard gas mixtures were injected into the cryogenic capillary trap from a 1-mL FEP-Teflon sampling loop. At the sub-ppb concentration, where the standard gas mixtures are cryogenically enriched in the 6-mm o.d. glass sampling trap and subsequently injected into the WCOT column via the capillary trap, the repeatability decreases to approximately ±25%. As may be expected, the quantitative repeatability of the overall cryogenic enrichment device and the GC/WCOT/FPD system is less precise than the GC/WCOT/FPD apparatus by itself. Nevertheless, the repeatability for all six sulfur compounds is within the limits of ±25% which we consider to be satisfactory when working in the ppb/ppt range. Furthermore, this degree of repeatability is quite close to the ±20% limits which are normally considered adequate for atmospheric analyses at much higher concentration (*47*).

A characteristic log–log plot of the FPD response versus the nanogram weight of sulfur for six sulfur compounds obtained with the GC/WCOT/FPD instrumentation is shown in Figure 5. The linear regression curve through the data points has a slope of 1.97, which is due to the familiar FPD response relationship given by

$$R \propto [S]^n \quad (1)$$

which can be changed to the equivalent logarithmic expression

$$\log [S] \propto 1/n \log R \quad (2)$$

In the preceeding equations, R represents the FPD response, n is the exponential factor, and [S] is the concentration of sulfur entering the detector.

The sensitivity implications of a combined WCOT column and a flame photometric detector are worthy of further discussion. In the sulfur detection mode, the FPD operates as a mass-flow rate sensitive detector whose response is approximately proportional to the square of the sulfur

Table IV. Mean Efficiency Percentages[a] for Various Deactivated, U-tube Samples

compound	untreated Pyrex, %	NEA-treated Pyrex, %	BTPPC-treated Pyrex, %	PEG-20M-treated Pyrex,[b] %	polysiloxane-treated Pyrex, %	polysiloxane/SE-30-treated Pyrex, %
H_2S	18	27	30	50	27	40
COS	48	64	21	99	86	99
CH_3SH	27	43	47	49	42	51
CH_3SCH_3	59	72	98	73	96	91
CS_2	41	78	82	59	113	107
CH_3SSCH_3	31	89	96	73	99	115

[a] Mean percentage data are for a minimum of six runs with each deactivant. [b] Data are for liquid phase Carbowax-20M treatments.

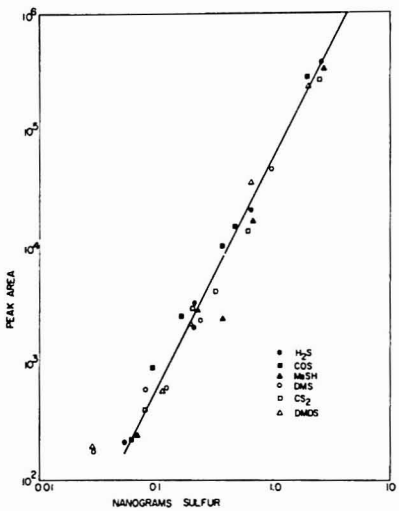

Figure 5. Characteristic log–log plot of GC/WCOT/FPD response vs. weight of sulfur in nanograms. The linear regression curve has a slope of 1.97

concentration (*48*, *49*). Thus, if one can decrease the peak width of a sulfur component peak by a factor of two, then the peak height will increase by a factor of four for the same size of sample. Since the application of WCOT capillary columns produces sharp chromatographic peaks with significantly narrower peak widths, the combination of WCOT columns and the approximate square law FPD can in fact improve the limit of detection. Note, however, that this improvement in sulfur detectability does not occur at the sacrifice of chromatographic resolution which is the case when one reduces the retention time of components in packed-column chromatography.

Cryogenic Enrichment Studies. Even with the ppb detectability of the GC/WCOT/FPD instrumentation, a concentration step is required for the analysis of the reduced sulfur gases at the ultra-trace concentrations encountered in ambient air or from most biogenic emission sources. Hence, a cryogenic enrichment system was developed to preconcentrate detectable quantities of these sulfur components from air. A diagram of the cryogenic enrichment system used in the overall collection efficiency studies is shown in Figure 6.

The initial investigations employed a FEP Teflon sample loop packed with 40/60 mesh FEP Teflon. However, problems due to nonquantitative recoveries and considerable memory interferences between samples prompted early abandonment

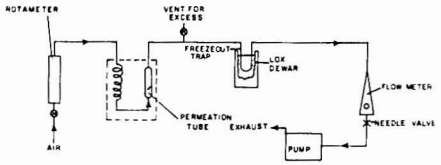

Figure 6. Experimental arrangement of flow system used in efficiency studies

of this design. Next, various types of untreated glass, e.g., soda-lime, Pryex, conventional quartz, and clear fused quartz, were evaluated as construction materials for cryogenic collection traps. The results of these experiments showed that untreated Pyrex and quartz glass gave the least adsorption losses (*41*). Later studies indicated that it was easier to deactivate either Pyrex or quartz than soft glass. Since no significant efficiency advantages or disadvantages were evident in the selection between Pyrex and quartz, Pyrex glass was chosen because of availability, cost, and its low susceptibility to cracking at the junction with the Quick-Connects.

As mentioned in the Experimental section, a number of surface deactivants were examined for their ability to increase the combined collection and recovery efficiencies of the cryogenic sampling traps. Table IV summarizes some of the efficiencies of the efficiency data for the U-tube samplers after treatment with various deactivants. The combined polysiloxane (DC-Q8-5479)/methyl silicone (SE-30 or SP-2100) surface treatment was selected as the most satisfactory deactivant based upon these efficiency experiments. As shown in Table IV, polysiloxane/SE-30-treated Pyrex traps are approximately quantitative for COS, CH_3SCH_3, and CS_2. The greater than 100% efficiency for dimethyldisulfide consistently occurs and has been shown to be due to the conversion of some methyl mercaptan to dimethyldisulfide during the cryogenic sampling. This chemical transformation of methyl mercaptan to dimethyldisulfide is also partially responsible for the lower recovery efficiency in the case of methyl mercaptan. Thus, one can account for approximately 81% of the original methyl mercaptan which enters the freeze-out loop. However, it is more difficult to explain the 40% efficiency for hydrogen sulfide although plausible explanations include breakthrough losses due to a small, but finite, sublimation process and/or chemical oxidation to some nonvolatile sulfur compound that stays in the trap during the 90 °C desorption.

Application to Field Analyses. A mobile trailer laboratory has been equipped with an analytical system that is identical to the one described in this paper. Presently, field measurements of biogenic emission fluxes of volatile sulfur compounds have been performed at 21 representative sites in the eastern United States (*34*, *35*). A typical GC/WCOT/FPD chromatogram of a cryogenically-collected air sample from an intertidal marsh soil is shown in Figure 7. A

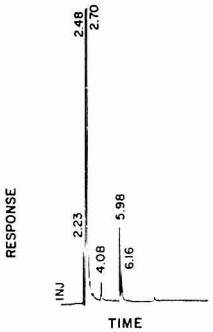

RT		AREA
2.23	CO_2	159
2.48	H_2S	8334
2.70	COS	3305
4.08	MeSH	18
5.98	DMS	164
6.16	CS_2	51

Figure 7. Typical chromatogram of biogenic sulfur emissions from an intertidal marsh soil, Core Sound, Cedar Island, N.C., October 1977. Chromatographic conditions: $\bar{u}$ = 24 cm/s of helium, oven programmed from −60 to 130 °C at 20 °C/min for first 3 min and then at a rate of 30 °C/min until oven reached 130 °C

detailed description of the actual field sampling and the corresponding sulfur flux measurement data are available (*34*, *35*).

CONCLUSIONS

The combined technique of cryogenic sample enrichment and GC/WCOT/FPD separation and detection have yielded an analytical system that incorporates sulfur specificity, compound speciation, known collection efficiencies, and enhanced detectability into a valuable measurement tool. This new methodology has been successfully applied to a systematic field measurement study of the sulfur flux from biogenic sources. A mobile laboratory equipped with the GC/WCOT/FPD system logged approximately 25 000 miles during the 1977 and 1978 field studies, and only minor repairs and maintenance were required to keep the associated instrumentation operational.

Since the analytical chemist's work is never done, the search for a more effective glass-surface deactivant is continuing in our laboratory. Special emphasis is being directed toward increasing the collection and recovery efficiencies for hydrogen sulfide and methyl mercaptan. In addition, work is continuing to validate the cryogenic efficiency data by an independent, sulfur-35 tracer technique (*50*).

ACKNOWLEDGMENT

The authors thank Bob Wohleb of J & W Scientific, Inc., for his aid in selecting suitable glass capillary columns. We also acknowledge the continuous encouragement from A. Stankunas and C. Hakkarinen of the Electric Power Research Institute.

LITERATURE CITED

(1) D. F. Adams in "Air Pollution", 3rd ed, Vol. III, A. C. Stern, Ed., Academic Press, New York, 1976, Chapter 6.
(2) H. V. Drushel in "The Analytical Chemistry of Sulfur and Its Compounds", Part II, J. H. Karchmer, Ed., Wiley-Interscience, New York, 1972, Chapter 7.
(3) R. S. Braman in "Chromatographic Analysis of the Environment", R. L. Grob, Ed., Marcel Dekker, New York, 1975, Chapter 2.
(4) D. F. Adams and R. K. Koppe, *Environ. Sci. Technol.*, **1**, 479 (1967).
(5) R. K. Stevens, J. D. Mulik, A. E. O'Keeffe, and K. J. Krost, *Anal. Chem.*, **43**, 827 (1971).
(6) W. L. Thornsberry, Jr., *Anal. Chem.*, **43**, 452 (1972).
(7) F. Bruner, A. Liberti, M. Possanzini, and I. Allegrini, *Anal. Chem.*, **44**, 2070 (1972).
(8) F. Bruner, P. Ciccioli, and F. Di Narda, *Anal. Chem.*, **47**, 141 (1975).
(9) F. Bruner, P. Ciccioli, and G. Bertoni, *J. Chromatogr.*, **120**, 200 (1976).
(10) T. L. C. de Souza, D. C. Lane, and S. P. Bhatia, *Anal. Chem.*, **47**, 543 (1975).
(11) G. Goretti and M. Possanzini, *J. Chromatogr.*, **77**, 317 (1973).
(12) W. Kirjgsman and C. G. Van de Kamp, *J. Chromatogr.*, **117**, 201 (1976).
(13) L. Blomberg, *J. Chromatogr.*, **125**, 389 (1976).
(14) M. Novotny, *Anal. Chem.*, **50**, 16A (1978).
(15) M. Novotny and K. Tesarik, *Chromatographia*, **1**, 332 (1968).
(16) E. J. Malec, *J. Chromatogr. Sci.*, **9**, 318 (1971).
(17) D. A. Cronin, *J. Chromatogr.*, **97**, 263 (1974).
(18) L. Blomberg, *J. Chromatogr.*, **115**, 365 (1975).
(19) K. Grob and G. Grob, *J. Chromatogr.*, **125**, 471 (1976).
(20) A. L. Gordon, P. J. Taylor, and F. W. Harris, *J. Chromatogr., Sci.*, **14**, 428 (1976).
(21) J. J. Franken, R. C. M. De Nijs, and F. L. Schulting, *J. Chromatogr.*, **144**, 253 (1977).
(22) Th. Welsch, W. Engewald, and Ch. Klaucke, *Chromatographia*, **10**, 22 (1977).
(23) C. Madani, E. M. Chambaz, M. Rigaud, P. Chebroux, J. C. Breton, and F. Berthou, *Chromatographia*, **10**, 466 (1977).
(24) P. Sandra and M. Verzele, *Chromatographia*, **10**, 419 (1977).
(25) G. Alexander and G. A. F. M. Rutten, *J. Chromatogr.*, **99**, 81 (1974).
(26) J. J. Franken, G. A. F. M. Rutten, and J. A. Rijks, *J. Chromatogr.*, **126**, 117 (1976).
(27) J. Simon and L. Szepesy, *J. Chromatogr.*, **119**, 495 (1976).
(28) F. I. Onuska and M. E. Comba, *Chromatographia*, **10**, 498 (1977).
(29) W. Jennings, "Gas Chromatography with Glass Capillary Columns", Academic Press, New York, 1978, Chapter 2.
(30) K. Grob, Jr., and G. Grob, and K. Grob, *J. High Resol. Chrom.*, **1**, 149 (1978).
(31) F. I. Onuska and M. E. Comba, *J. High Resol. Chrom.*, **1**, 209 (1978).
(32) R. A. Heckman, C. R. Green, and F. W. Best, *Anal. Chem.*, **50**, 2157 (1978).
(33) C. A. Burgett and L. E. Green, *J. Chromatogr. Sci.*, **12**, 356 (1974).
(34) D. F. Adams, S. O. Farwell, M. R. Pack, W. L. Bamesberger, and A. E. Sherrard, "Measurement of Biogenic Sulfur-Containing Gas Emissions from Soils and Vegetation", paper #78-7.6 presented at the 71st Meeting of the Air Pollution Control Association, Houston, Texas, June 1978.
(35) D. F. Adams, S. O. Farwell, M. R. Pack, and E. Robinson, "An Initial Emission Inventory of Biogenic Sulfur Flux from Terrestrial Surfaces", paper #78-16 presented at the Pacific Northwest Air Pollution Control Association, Portland, Ore., November 1978.
(36) A. E. O'Keeffe and G. C. Ortman, *Anal. Chem.*, **38**, 760 (1966).
(37) F. P. Scaringelli, A. E. O'Keeffe, E. Rosenberg, and J. P. Bell, *Anal. Chem.*, **42**, 871 (1970).
(38) D. P. Lucero, *Anal. Chem.*, **43**, 1744 (1971).
(39) H. D. Axelrod, J. B. Pate, W. R. Barchet, and J. P. Lodge, Jr., *Atmos. Environ.*, **4**, 209 (1970).
(40) G. A. F. M. Rutten and J. A. Luyten, *J. Chromatogr.*, **74**, 177 (1972).
(41) T. M. Schutte, "Design of a Deactivated Gas Chromatographic System for the Analysis of Sulfur Compounds", M.S. Thesis, Washington State University, Pullman, Wash., 1978.
(42) W. J. Kirsten and P. E. Mattsson, *Anal. Lett.*, **4**, 235 (1971).
(43) W. J. Kirsten, P. E. Mattsson, and H. Alfons, *Anal. Chem.*, **47**, 1974 (1975).
(44) W. Dulson, *Anal. Chem.*, **49**, 1279 (1977).
(45) R. E. Pecsar and C. H. Hartmann, *J. Chromatogr. Sci.*, **11**, 492 (1973).
(46) D. F. Adams, J. O. Frohliger, D. Falgout, A. M. Hartley, J. B. Pate, A. L. Plumley, E. P. Scaringelli, and P. Urone, *Health Lab. Sci.*, **10**, 241 (1973).
(47) "Analytical Problems In Air Pollution Control", In "Analytical Chemistry, Key to Progress on National Problems", *Natl. Bur. Stand. (U.S.) Spec. Publ.*, **351**, U.S. Government Printing Office, Washington, D.C., 1972.
(48) A. R. L. Moss, *Scan*, **4**, 5 (1975).
(49) S. O. Farwell and R. A. Rasmussen, *J. Chromatogr. Sci.*, **14**, 224 (1976).
(50) S. J. Fernandez, S. O. Farwell, and D. F. Adams, "A Novel Sulfur-35 Tracer Technique for Sub-ppb Collection Efficiency Studies", paper #78-53.6 presented at the 71st Meeting of the Air Pollution Control Association, Houston, Texas, June 1978.

RECEIVED for review August 21, 1978. Accepted January 11, 1979 This work was supported by the Electric Power Research Institute under Contract #856-1. Reference to commercial products is for identification purposes only and does not constitute an endorsement of these products by EPRI, Washington State University, or the University of Idaho.

Classification of Crude Oil Gas Chromatograms by Pattern Recognition Techniques

H. A. Clark and P. C. Jurs*

Department of Chemistry, The Pennsylvania State University, University Park, Pennsylvania 16802

Pattern recognition methods have been employed to classify crude oils based on their gas chromatograms. Four oil types were represented by gas chromatograms taken before and after artificial weathering. The chromatograms were hand digitized and coded with 13 descriptors each—peak areas for the normal alkanes for C_{16} through C_{25} plus pristane and phytane and also one descriptor characterizing the unresolved background. A statistical algorithm was used to find the best subsets of descriptors to use with Bayesian discriminant analysis. A variety of different partitions of the data set showed the similarities of some classes of oils and some dissimilarities for others. The nonparametric linear learning machine method of discriminant training was also applied to various partitions of the data. Predictive abilities as high as 100% were obtained for some of the partitions of the data set.

A great deal of effort has been devoted to the characterization of petroleum samples based on gas chromatograms, infrared spectra, fluorescence spectra, and other laboratory data. Some of these techniques have been refined to the point where they can be applied to the typing of unknown petroleum samples. The most reliable methods use more than one analytical technique of data collection and then combine the results into a prediction. Such approaches are contributing to enforcement of environmental protection laws. Analytical data employed for petroleum sample classification include gas chromatograms (*1–6*), infrared spectra (*7–12*), the combination of the two techniques (*13*), trace metal concentrations (*14, 15*), luminescence spectrometry (*16*), field ionization mass spectrometry (*17*), high pressure liquid chromatography (*18*), thin-layer chromatography (*19*), and other methods (*20–24*). The applicability and relative merits of these methods have been discussed recently in reviews by Bentz (*25, 26*). Some of the analytical methods have been standardized and published as Standard Methods by the American Society for Testing and Materials, including gas chromatography (*27*), elemental analysis (*28*), fluorescence analysis (*29*), and infrared spectroscopy (*30*). The literature and the Standard Methods reports suggest a wide variety of methods for interpreting the data collected, ranging from visual analysis (e.g., *27*) to sophisticated statistical (e.g., *11, 35*) or pattern recognition methods (e.g., *31*).

The present work has focused on the application of pattern recognition methods for the classification of gas chromatograms of a set of weathered and unweathered crude oils. Both parametric and nonparametric pattern recognition methods have been employed. The object was to demonstrate that procedures could be developed whereby gas chromatograms from a set of crude oils of known type could be used to form the basis of classification of oil samples of unknown origin. Classifiers developed using the gas chromatograms of unweathered crude oils were used to predict the classes of gas chromatograms taken from weathered crude oils. An additional object was to identify the features of the gas chromatograms that were most related to oil type. The set of data used consisted of 80 gas chromatograms taken for a set of four crude oils before and after weathering and run ten times for each of the eight classes.

Table I. Types of Oils in the Data Set

class	name
A	Equador/Oriente Mixture
B	Louisiana Crude
C	Trans. Mt. Mixture
D	Amna Crude
E	Trans. Mt. Mixture (weathered)
F	Equador/Oriente Mixture (weathered)
G	Amna Crude (weathered)
H	Louisiana Crude (weathered)

Table II. Weathering Conditions

class	name	av. air temp., °C	av. water temp., °C	av. wind velocity, kph
E	Narragansett Bay	28	24	9
F	E.P.A. Laboratory	26	21	0
G	Narragansett Bay	2	7	17
H	Narragansett Bay	29	26	10

Each of the procedures studied in this work comprises the following steps: (a) develop a suitable classifier based on a part of the set of known data; (b) estimate the reliability of this classifier using the set of known data; (c) use the classifier to predict the classes of each of a set of unknowns; (d) revise the reliability estimate to include measures of success on both the known set and the unknown set.

EXPERIMENTAL AND RESULTS

Data Set. The Industrial Environmental Research Laboratory, Edison, N.J., of the U.S. Environmental Protection Agency collected the gas chromatographic data used in this study. Chris W. Brown, Department of Chemistry, University of Rhode Island, Kingston, R.I., supplied the oil samples. The samples consisted of four crude oils and the same four oils after artificial weathering. Table I shows the identities of the oils and the labels used for each for further reference. Table II shows the weathering conditions used for each of the four weathering experiments. Oils E, G, and H were weathered for two weeks in Narragansett Bay experiments; oil F was weathered for two weeks in an E.P.A. Laboratory experiment.

Ten standardized chromatographic experiments were done for each of the eight oils. The gas chromatographic operating conditions for the experiments are shown in Table III The E.P.A. Laboratory then sent these data to Penn State as strip chart recordings for further analysis. Figures 1 through 4 show examples drawn from each of the eight classes. Each figure shows the part of the gas chromatogram that was digitized, which does not include the first 12 minutes of the run.

Digitization. Each chromatogram was digitized with a hand-operated x-y digitizer under the control of The Pennsylvania State University Department of Chemistry MODCOMP II/25 digital computer. Each scan was begun at six inches on the x-axis and continued for ten inches. The ten inches represents 20 min of the gas chromatographic

0003-2700/79/0351-0616$01.00/0 © 1979 American Chemical Society

Table III. Operating Conditions for Gas Chromatographic Data Collection

instrument	Perkin-Elmer Model 900 gas chromatograph
column	50-ft OV-101 support coated open tubular
sample preparation	Each oil was dissolved in CS_2 and injection size varied to obtain a chromatogram on scale at an attenuation of (10) x (128)
detector	flame ionization detector
injector temperature	operating at 200 °C, equipped with a "septum swinger." No split ratio was used and the point of injection is signaled by a spike
manifold temperature	300 °C
attenuation	(10) x (128)
carrier gas	He; adjusted to give a methane retention time of 44 s
temperature program	6 °C/min; 75–275 °C with the program being started at the beginning of the CS_2 peak and holding at the final temperature
chart speed	30 in./h

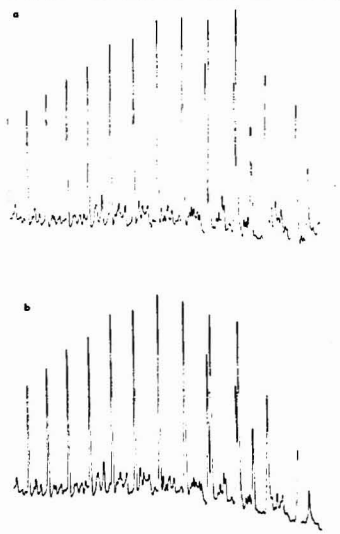

Figure 1. (a) Gas chromatogram of Equador/Oriente Mixture (Class A). (b) Gas chromatogram of Equador/Oriente Mixture after weathering (Class F)

experiment under the conditions used. x-axis resolution was 300 points per inch. y-axis resolution was approximately one part in 4000 full scale. Thus, each digitized chromatogram consisted of an array of approximately 3000 encoded y-axis values.

Smoothing. A quadratic-cubic function can be fit through a number of points and then the midpoint can be adjusted to be the ordinate of the curve at the midpoint. Such a function can be found by using a least-squares procedure. The normal equations that result can be solved analytically and

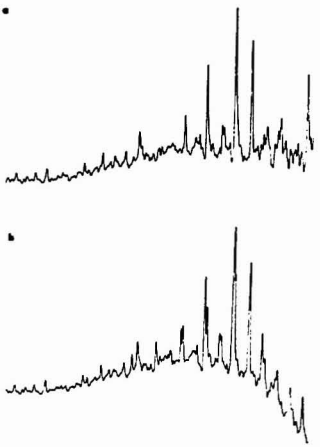

Figure 2. (a) Gas chromatogram of Louisiana Crude (Class B). (b) Gas chromatogram of Louisiana Crude after weathering (Class H)

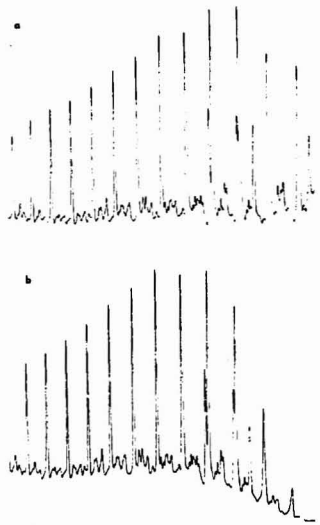

Figure 3. (a) Gas chromatogram of Trans. Mt. Mixture (Class C). (b) Gas chromatogram of Trans. Mt. Mixture after weathering (Class E)

rearranged in such a way that the smoothed value of each point in a digitized spectrum can be calculated using an equation of the form:

$$y_i' = f(y_{i-n}, y_{i-n+1}, \ldots, y_i, y_{i+1}, \ldots, y_{i+n})$$

The form of the equation we used is as follows (*32*):

$$y_i' = p_i y_i + p_{i\pm1} y_{i\pm1} + \ldots, + p_{i\pm n} y_{i\pm n}$$

where

$$p_s = \frac{3(3n^2 + 3n - 1 - 5s^2)}{(2n-1)(2n+1)(2n+3)}$$

and using $n = 6$ means that 13 points are being used in the algorithm. Each scan of a gas chromatogram was smoothed

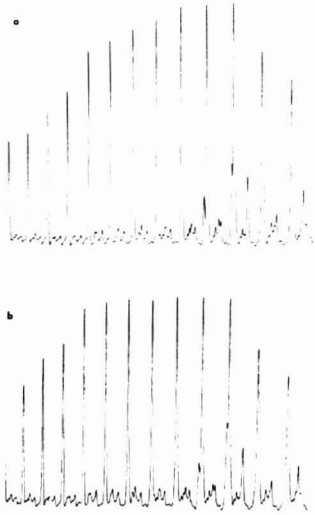

Figure 4. (a) Gas chromatogram of Amna Crude (Class D). (b) Gas chromatogram of Amna Crude after weathering (Class G)

twice using this procedure. The resultant spectrum has a smooth, even appearance compared to the original data.

Characterization and Subtraction of Unresolved Background. Each chromatogram is composed of two visually distinct components. There is a broad, unresolved background signal covering the entire range of interest and a set of sharp, narrow peaks that are well above the background level. Visual perception of such quantities involves a complex filtering mechanism in the human brain. This process was approximated as follows: an analytical function characteristic of the perceived background was chosen, and then a set of points was selected from the smoothed digital data to use in fitting this function. After fitting the function to each chromatogram, a pseudo-resolved chromatogram could be developed by direct subtractions.

There is, for these chromatograms, only one maximum in the perceived background, and no minima other than the two end points of the chromatogram. There are, however, two clearly discernible inflection points. On this basis, a quartic polynomial was chosen to describe the background. Clearly, should the unresolved background have different characteristics in a different data set, a different functional form should be used.

The first set of points tried for fitting the polynomial was the set of all local minima in the digitized trace of the chromatogram. These points were used to fit the quartic function, using least-squares curve fitting, and both the fit function and the entire GC trace were displayed on a graphics display terminal. This display did not conform with visual perception of the unresolved background. Many minima not characteristic of the visually perceived background were included in the calculation. Because this first curve was higher than the visually perceived background, but of correct general shape, it was used as a criterion to select a second, better set of points. Points above the first function were discarded from the set under consideration, and the remaining points were used to fit the function again. This function was also too high, so the selection process was repeated. This last point set contained 60 to 80 points out of the total of 3000 in the entire

Table IV. The 13 Descriptors Generated for Each Chromatogram

1.	n-C_{16} peak area	C_{16}
2.	n-C_{17} peak area	C_{17}
3.	n-C_{18} peak area	C_{18}
4.	n-C_{19} peak area	C_{19}
5.	n-C_{20} peak area	C_{20}
6.	n-C_{21} peak area	C_{21}
7.	n-C_{22} peak area	C_{22}
8.	n-C_{23} peak area	C_{23}
9.	n-C_{24} peak area	C_{24}
10.	n-C_{25} peak area	C_{25}
11.	pristane peak area	Pr
12.	phytane peak area	Ph
13.	area of unresolved background/total area	UB

gas chromatogram. The curve derived using this reduced point set corresponded very well to the visually perceived background. This entire procedure of fitting, selecting, and fitting again was applied to each of the 80 chromatograms individually. After fitting, the unresolved background was subtracted from the entire chromatogram, and thus a set of 80 pseudo-resolved chromatograms was generated.

Peak Integration. After subtraction of the unresolved background, the pseudo-resolved chromatograms consisted of a set of sharp, narrow peaks. The area of each of these peaks was computed numerically and normalized with respect to the total area of all the resolved peaks.

Peak Identification. A reference peak was selected by visual inspection in each chromatogram. Then a set of x-axis "windows" was used to identify each peak in the hydrocarbon series n-C_{16} through n-C_{25} plus the isoprenoid hydrocarbons pristane and phytane. When more than one peak was found within a window, the one with larger intensity was assumed to be the one of interest. When no peak was found within a window, a value of zero was assigned.

Unresolved Background Ratio. Visual inspection clearly shows that the area under the unresolved background varies from one class of oil to another. This variation should be included in the set of descriptors generated for each chromatogram. Therefore, the ratio of unresolved background area (determined by integration of the fit quartic polynomial) to the total area of the entire chromatogram (determined by numerical integration of the smoothed digital representation of the chromatogram) was computed.

Each of the 80 chromatograms in the data set was thus described by 13 numerical descriptors. Their identities and labels are listed in Table IV.

Errors in Descriptor Development Procedures. To identify the sources of error in these descriptors, replicate chromatograms of two types were used to calculate means and standard deviations for the sets. The results of this study are shown in Table V. On the left side of the table are shown the values obtained for five replicate digitizations of one chromatogram taken from class E (weathered Trans. Mt. mixture). The largest absolute and relative standard deviations occur for the descriptors with the smallest mean values. The average absolute standard deviation is 0.43 and the average relative standard deviation is 9.2%. On the right side of Table V are shown the results obtained for the ten replicate chromatograms also taken from class E. The average absolute standard deviation is 0.64 and the average relative standard deviation is 12.2%. The fact that the average standard deviations are only slightly larger for the replicate chromatograms of one oil sample compared to those taken from only one chromatogram demonstrates that the digitization procedure used is not optimum; better results could presumably be obtained with better digitization. The best procedure, of course, would be to digitize the data on-line as it was being taken by the chromatograph.

Table V. Studies of Errors in Descriptor Generation Procedure

	Five Replicate Digitizations of One Chromatogram			Ten Replicate Chromatograms of One Oil Sample		
variable	mean	absolute std. dev.	rel. std. dev., %	mean	absolute std. dev.	rel. std. dev., %
C_{16}	3.913	1.043	26.7	4.927	0.812	16.5
C_{17}	7.788	0.324	4.2	6.916	1.362	19.7
C_{18}	8.177	0.395	4.8	7.781	0.375	4.8
C_{19}	7.935	0.262	3.3	7.589	0.927	12.2
C_{20}	6.989	0.441	6.4	6.266	1.049	16.7
C_{21}	5.636	0.492	8.7	5.431	0.527	9.7
C_{22}	4.800	0.265	5.5	4.997	0.500	10.0
C_{23}	4.541	0.444	9.8	4.711	0.602	12.8
C_{24}	3.670	0.872	23.8	3.701	0.671	18.1
C_{25}	3.952	0.440	11.1	4.376	0.381	8.7
Pr	3.739	0.248	6.6	3.969	0.732	18.4
Ph	4.063	0.316	7.8	3.966	0.385	9.71
UB	0.737	0.005	1	0.737	0.008	1
Average		0.43	9.2		0.64	12.2

Table VI. The Best *U*-Statistic Values for Four-Class and Eight-Class Separations

			rank of same list in other studies		
no. of variables	*U*-statistic $\times 10^{-3}$	variable list	1	2	3
		1. Training set: A:B:C:D			
1	5.44	UB	-	1	1
2	2.61	C_{22}, UB	-	2	4
3	1.20	Pr, Ph, UB	-	1	7
4	0.69	Pr, Ph, C_{16}, UB	-	8	>10
5	0.44	Pr, Ph, C_{16}, C_{24}, UB	-	9	>10
13	0.10	all	-	-	-
		2. Training set: F:H:E:G			
1	5.21	UB	1	1	-
2	1.23	Ph, UB	4	3	-
3	0.55	Ph, C_{24}, UB	9	2	-
4	0.29	Pr, C_{18}, C_{22}, UB	>10	>10	-
5	0.15	Pr, Ph, C_{18}, C_{22}, UB	>10	>10	-
13	0.03	all	-	-	-
		3. Training set: AF:BH:CE:DG			
1	6.88	UB	1	-	1
2	3.49	C_{24}, UB	2	-	4
3	1.50	Pr, Ph, UB	1	-	7
4	0.97	Pr, Ph, C_{24}, UB	2	-	6
5	0.79	Pr, Ph, C_{24}, UB	>10	-	>10
13	0.42	all	-	-	-
		4. Training set: A:B:C:D:E:F:G:H			
1	5.26	UB			
2	1.69	C_{22}, UB			
3	0.59	C_{18}, C_{22}, UB			
4	0.30	C_{17}, C_{18}, C_{22}, UB			
5	0.16	Pr, C_{17}, C_{18}, C_{22}, UB			
13	0.01	all			

Investigation of Subsets of Descriptors. In order to analyze the data set using either parametric or nonparametric statistical methods or pattern recognition methods, one must identify a subset of the descriptors to use. Generally, it is desirable to use the minimum feasible number of descriptors per observation in such studies. The general problem of selection of subsets of variables for statistical analysis is difficult to address. However, recently a useful approach has been reported by McCabe (*33*). In this approach, a statistic is computed for all possible subsets of variables for a discriminant analysis. Then this statistic can be scanned to fine optimal subsets of any given size. McCabe has called the statistical measure of usefulness the *U*-statistic:

$$U = |W|/|T|$$

where $|W|$ and $|T|$ are the determinants of the within and the total sum of cross-products matrices, respectively. Qualitatively, $|W|$ is related to how tightly a set of data is clustered within classes, and $|T|$ is related to the distances between clusters. Therefore, for two subsets of variables, the subset with the smaller value for the *U*-statistic is superior. The development of the method assumes that the data are independent normal and have a common covariance.

For cases where the number of descriptors, N, is less than 20, it is reasonable to calculate the value of U for all combinations of descriptors, $1, 2 \ldots N-1$ at a time. This was done using a program obtained from McCabe (*33*). A summary of these calculations is in Tables VI and VII.

Before calculation of the *U*-statistic the data were autoscaled. This involves performing the following computation for each descriptor in the data set:

$$x' = \frac{x - \bar{x}}{\sigma}$$

Table VII. The Best Variable Subset for Two-Class Separations

classes	no. of variables	U-statistic $\times 10^{-3}$	variable list
A:B	1	7.45	UB
	2	5.38	C_{18}, UB
	3	2.78	C_{18}, C_{20}, UB
	4	1.49	C_{18}, C_{20}, C_{24}, UB
	5	1.05	C_{18}, C_{20}, C_{21}, C_{24}, UB
	13	0.630	all
A:C	1	177.	Ph
	2	145.	Ph, C_{22}
	3	90.8	Ph, C_{22}, UB
	4	58.6	Pr, Ph, C_{22}, UB
	5	45.6	Pr, Ph, C_{22}, C_{24}, UB
	13	28.9	all
A:D	1	30.1	UB
	2	16.8	Ph, UB
	3	13.1	Ph, C_{25}, UB
	4	9.44	Ph, C_{24}, C_{25}, UB
	5	7.50	Ph, C_{20}, C_{24}, C_{25}, UB
	13	1.16	all
B:C	1	4.59	UB
	2	2.77	C_{20}, UB
	3	1.79	C_{20}, C_{24}, UB
	4	1.17	C_{18}, C_{20}, C_{23}, UB
	5	0.819	C_{17}, C_{18}, C_{20}, C_{23}, UB
	13	0.275	all
B:D	1	1.62	UB
	2	1.11	Pr, UB
	3	0.689	C_{16}, C_{20}, UB
	4	0.519	Pr, C_{16}, C_{20}, UB
	5	0.431	Pr, C_{16}, C_{18}, C_{20}, UB
	13	0.299	all
C:D	1	20.1	UB
	2	14.1	C_{20}, UB
	3	9.02	C_{16}, C_{20}, UB
	4	7.33	C_{16}, C_{18}, C_{20}, UB
	5	6.41	Ph, C_{16}, C_{18}, C_{20}, UB
	13	2.57	all

where x' is the value of the autoscaled descriptor, x is the raw value, $\bar{x}$ is the mean value of the descriptor within the data set, and σ is the standard deviation of the descriptor within the data set. This transformation alters the data so that the mean of each descriptor over the data set is zero and the standard deviation of each descriptor over the data set is one.

Table VI shows the results of analyzing the data as a four or eight class problem with the U-statistic algorithm. In the first study, the 40 unweathered samples (A:B:C:D) were analyzed; in the second study, the 40 weathered samples were analyzed (F:H:E:G); in the third study, the weathered and unweathered samples were combined for each oil sample class and the 80 chromatograms were analyzed (AF:BH:CE:DG), and in the fourth study, all eight classes were analyzed (A:B:C:D:E:F:G:H). The results obtained indicate that significant changes occur in the oil samples during the weathering process. Different subsets of the descriptors were chosen as best in the different studies. The actual value of the best U-statistic for each number of variables is less for the weathered oils, indicating that the data are more dispersed in the unweathered chromatograms.

The U-statistic is an average value for all the classes considered during its calculation. Thus, the results presented in Table VI are averaged over four oil classes. In order to further investigate the separability of the oils from each other, the U-statistic algorithm was run for each of the possible ways in which the four unweathered oils could be paired. The results obtained are shown in Table VII for these six pairings. For each pairing the value of the U-statistic is shown for one, two, three, four, five, and all 13 variables, and the variables chosen are listed. The separation of oils B and D provides the smallest statistic for up to five variables. The separation of classes B and C is almost as good. The separations of classes A and D and the separation of classes C and D are good. The poorest U-statistic is obtained for the separation of classes A and C. Other results to be shown later confirm that the distinction between oils A (unweathered Equador/Oriente mixture) and C (unweathered Trans. Mt. mixture) is difficult.

Once the studies reported in Tables VI and VII were performed, the best subsets of descriptors to be used in the analysis of the data had been identified. Thus, the next studies were done to attempt to develop discriminants that would separate the various oils from one another based on subsets of the total number of available descriptors.

Bayes Discriminants. The Bayes theorem from classical statistics can be used to derive a formulation for a linear discriminant function (*34*). The discriminant function for the jth class, d_j, is the product of the class conditional probability for that class, $P(\bar{X}/j)$, and the a priori probability of occurrence of class j, $P(j)$:

$$d_j = P(\bar{X}/j)P(j) \qquad j = 1, 2, \ldots, n$$

For an n class problem, one develops n such discriminants, one for each of the n classes. The application of this method to a particular problem requires a knowledge of the probability distributions, $P(\bar{X}/j)$, of the patterns in the data set.

In the present work, the probabilities were estimated as follows: $P(j)$ was taken to be equal for all classes, e.g., $P(1) = 0.5$ and $P(2) = 0.5$ for a two-class problem; $P(\bar{X}/j)$ was taken to be the multivariate normal distribution. The individual discriminant functions, d_j, $j = 1, 2, \ldots, n$, can be calculated directly from $P(j)$, the mean vector for the class j, and the pattern being classified, $\bar{X}$. Then an unknown pattern, $\bar{X}$, is classified as being a member of the class j for which the calculated d_j is the largest.

A number of studies were performed using Bayesian discriminants to analyze the data configured into two-class, four-class, and eight-class problems. The results of these studies are shown in Table VIII. For each of the studies listed in Table VIII, the descriptor set was used that was shown to be best in the previous U-statistic studies. For each study, the set of three or four descriptors that had the best U-statistic (shown in Tables VI and VII) was employed.

Study 1 shows the results obtained when the 80 chromatograms were divided into four classes with the weathered and unweathered oil of the same type grouped together. The best three descriptors for this four-class grouping were shown to be pristane, phytane, and the unresolved background (see Table VI, part 3) with a U-statistic value of 1.50. The Bayesian discriminant functions developed with all 80 chromatograms were used to classify the 80 chromatograms with the results shown in Table VII, part 1. Seventy-nine out of the 80 chromatograms were correctly classified, with one oil that actually belongs to the class (CE) being classified incorrectly as class (AF).

In Study 2, the 40 unweathered oil samples were used alone to develop the discriminant functions. These discriminants could correctly classify all 40 of the unweathered samples into their correct classes. Then these discriminants were used to predict the classes of the 40 weathered samples. Prediction was perfect for three of the four classes of weathered oils. Prediction of the fourth class, weathered oil E, was split between class C (correct predictions) and class A (incorrect predictions). The set of three discriptors used for this study was the same as for the entire set of 80 chromatograms (see Table VI, part 1).

Table VIII. Bayes Discriminant Results

1. 80 samples in training set (AF:BH:CE:DG)
Descriptors: Pr, Ph, UB

Classification

	AF	BH	CE	DG
AF	20	-	-	-
BH	-	20	-	-
CE	1	-	19	-
DG	0	0	0	20

2. 40 samples in training set (A:B:C:D)
Descriptors: Pr, Ph, UB

Classification: All 40 correct

Prediction

	A	B	C	D
F	10	-	-	-
H	-	10	-	-
E	5	-	5	-
G	-	-	-	10

3. 40 samples in training set (F:H:E:G)
Descriptors: Ph, C_{24}, UB

Classification

	F	H	E	G
F	10	-	-	-
H	-	10	-	-
E	1	-	9	-
G	-	-	-	10

Prediction

	F	H	E	G
A	9	-	1	-
B	-	10	-	-
C	-	-	10	-
D	-	-	-	10

4. 20 samples in training set (A:C)
Descriptors: Ph, C_{22}, UB.

Classification: All 20 correct

Prediction

	A	C
F	10	-
E	8	2

5. 20 samples in training set (A:C)
Descriptors: Pr, Ph, C_{22}, UB

Classification: All 20 correct

Prediction

	A	C
F	10	-
E	4	6

6. 80 samples in training set (AE:BH:CF:DG)
Descriptors: Pr, Ph, UB

Classification

	AE	BH	CF	DG
AE	16	-	4	-
BH	-	20	-	-
CF	3	-	17	-
DG	-	-	-	20

7. 80 samples in training set (A:B:C:D:E:F:G:H)
Descriptors: Pr, Ph, UB

Classification: 72 correct

	A	F	B	H	C	E	D	G
A	8	1	-	-	-	-	-	-
F	1	9	-	-	-	-	-	-
B	-	-	8	2	-	-	-	-
H	-	-	1	9	-	-	-	-
C	-	-	-	-	10	-	-	-
E	-	1	-	-	1	8	-	-
D	-	-	-	-	-	-	10	-
G	-	-	-	-	-	-	-	10

8. 80 samples in training set (A:B:C:D:E:F:G:H)
Descriptors: C_{18}, C_{22}, UB

Classification: 73 correct

	A	F	B	H	C	E	D	G
A	7	2	-	-	1	-	-	-
F	2	8	-	-	-	-	-	-
B	-	-	10	-	-	-	-	-
H	-	-	-	10	-	-	-	-
C	-	-	-	-	10	-	-	-
E	-	-	-	-	-	10	-	-
D	-	-	-	-	-	-	8	2
G	-	-	-	-	-	-	-	10

In Study 3, the weathered samples alone were used to develop the discriminant functions. Classification of the 40 weathered oils was nearly perfect, with 1 miss out of 40 classifications. The discriminants were used to predict the classes for the 40 unweathered oils. Again the success was nearly complete, with one unweathered oil sample misclassified. The set of three descriptors used in Study 3 was phytane, C_{24}, and the unresolved background which had given the best *U*-statistic for three descriptors for this partition of the data set (see Table VI, part 2).

The results obtained in the first three studies show that unweathered oils of classes B and D can be discriminated from the other oils successfully, and that predictions of the corresponding weathered samples, classes H and G, can be made confidently. Therefore, in order to try to improve overall performance, these classes were removed from the data set, and a series of studies was done on the remaining two classes of oils.

Studies 4 and 5 focussed on classes A and C and their weathered counterparts, classes E and F. In each case, 20 chromatograms for the unweathered oils were used to develop the classifiers, and in each case the recognition of the 20 samples was perfect. For each experiment, the discriminant was used to predict the classes of the weathered oils. In Study 4, based on the use of three descriptors, the prediction result was poor, with eight out of ten class E chromatograms misclassified. With four descriptors used, in Study 5, the prediction results were still poor, although better than in Study 4. The poor prediction results obtained are consistent with the poor *U*-statistic values obtained for this partitioning of the data relative to other partitions (the *U*-statistic values for the A:C split shown in Table VII).

Study 6 was done using all 80 chromatograms as a training set, but the classes E (weathered Trans. Mt. mixture) and F (weathered Equador/Oriente mixture) were deliberately switched. The recognition rate was 73 correct out of the 80 chromatograms, nearly as good as Study 1 where no misgrouping was done. This demonstrates in a different way that the oils of classes E and F are similar and difficult to distinguish from one another. This supports the conclusion based on Table VII where the separation of class A (unweathered Equador/Oriente mixture) from class C (unweathered Trans Mt. mixture) was shown to be difficult.

Two final studies were performed using all 80 chromatograms subdivided as an eight-class problem. In the first of these studies, the three descriptors used were the same as those of Studies 1 and 2. In Study 7, three of the classes were completely separated, two more had nine of the ten chromatograms correctly classified, and three classes had eight of the chromatograms correctly classified, and one class had seven correctly classified. Studies 7 and 8 demonstrate that there are large differences between the unweathered and

Table IX. Nonparametric Pattern Classifier Results

Training Set		Prediction Set			Number of Correct Predictions		
partition codes	population	partition codes	population	final descriptor set	class 1	class 2	total
A:BCD	10:30	F:EGH	10:30	13[a]	8/10	13/30	21/40
B:ACD	10:30	H:EFG	10:30	2-C_{18}, C_{20}	10/10	30/30	40/40
C:ABD	10:30	E:FGH	10:30	13[a]	4/10	21/30	25/40
D:ABC	10:30	G:EFH	10:30	2-Ph, C_{20}	10/10	30/30	40/40
A:C	10:10	F:E	10:10	4-Pr, Ph, C_{18}, C_{20}	10/10	2/10	12/20
AD:BC	20:20	FG:EH	20:20	13[a]	20/20	11/20	31/20
AB:CD	20:20	FH:EG	20:20	3-C_{16}, C_{18}, Pr	20/20	13/20	33/40
AC:BD	20:20	FE:HG	20:20	4-Pr, Ph, C_{16}, C_{22}	19/20	17/20	36/40
E:FGH	10:30	C:ABD	10:30	13[a]	0/10	2/30	28/40
F:EGH	10:30	A:BCD	10:30	12:Pr, Ph, C_{16}-C_{25}	9/10	22/30	31/40
G:EFH	10:30	D:BAC	10:30	2-Ph, C_{20}	9/10	30/30	39/40
H:EFG	10:30	B:ACD	10:30	4-Pr, Ph, C_{18}, C_{24}	10/10	29/30	39/40

[a] No reduction was possible.

weathered samples of the same oil as far as these descriptors are concerned.

Nonparametric Pattern Classifier. Table IX shows results obtained in a series of studies using a linear learning machine method to develop binary classifiers. A number of different groups of the data were studied. Each time a new partition of the data set or a new set of descriptors was used, an attempt was made to develop a linear classifier on the union of the training set and the prediction set to check for overall linear separability. For example, when sample A was to be separated from sets B, C, and D (recognition of sample A) using all 13 descriptors, an attempt was made to find a surface separating the set AF from the set BCDEGH. As can be seen in the first row of Table IX, this attempt was not successful.

For each partition of the data set, six classifiers were developed using all of the 13 available descriptors. These six classifiers were used to determine an ordering of the descriptors by utility to the separation being attempted. The object was to identify the minimum number of descriptors for which linear separation could be found. The descriptors thus identified to be least useful were excluded from consideration and the training process was repeated. When no more descriptors could be eliminated, the average of the six discriminants was used to classify the members of the entire training set. Table IX, column 5, shows the minimum set of descriptors found by this procedure for each partition of the data set studied.

Table IX shows the results obtained for 12 different partitions of the data set. The details of which subsets of the data are grouped together to form the training set and which are used to form the prediction set are given in the first four columns of the table. The minimal set of descriptors found for each partition is shown in column 5. Once a minimal set of descriptors was found for each partition, then the members of the prediction set were classified. The number of correct predictions that were attained using this minimal set of descriptors is shown in columns 6, 7, and 8. The results of the prediction tests are shown in the last column of Table IX.

The results obtained for class A, shown in the first row of Table IX, will be used as an example. None of the 13 variables could be eliminated. Eight members of class F were correctly classified and 13 members of the class EGH were correctly classified as belonging to class BCD. For the separation of class B from the class ACD (row two of Table IX), only two descriptors were necessary to maintain separability and, based on these two descriptors, all 40 members of the prediction set were classified correctly. Thus, for this case, a classifier trained on a set of 40 unweathered oils could correctly predict the membership of each of the 40 unweathered oils could correctly predict the membership of each of the 40 weathered oils.

Detailed comparisons of the two feature selection methods used (U-statistic and weight vector component analysis) should not be stressed. The decisions are based on different criteria, preparatory to different classifiers. One general observation can be made; the background ratio descriptor for this data set, is sufficient to recognize two oils (classes B and D) and predict the corresponding weathered oils (classes H and G). Examination of the data shows that, in fact, the two classes BH and DG are linearly separable from the remainder of the data set. This descriptor is never retained by the weight vector component analysis algorithm, indicating that its performance in these two classifications, which is good, is sub-optimum.

DISCUSSION

The studies presented for the 80-chromatogram data set demonstrate that there are strong similarities between unweathered and weathered oils of the same type. However, there are also dissimilarities present. For some of the oil types represented in the data set (e.g., Louisiana Crude and Amna Crude), a discriminant function trained using only chromatograms of unweathered oils could classify chromatograms of that same oil after weathering with 100% accuracy. This was, however, not true for all oil types studied since Equador/Oriente Mixture and Trans. Mt. Mixture were not separated well.

The 13 descriptors used in the studies presented here are not invariant through the weathering process. To rectify this, and produce more reliable methods for classifying the weathered samples, would require (a) a model for the weathering process, or (b) descriptors that are less sensitive to weathering of the oils.

LITERATURE CITED

(1) O. C. Zafiriou, *Anal. Chem.*, **45**, 952 (1973).
(2) M. C. Garza, Jr., and J. Muth, *Environ. Sci. Technol.*, **8**, 249 (1973).
(3) R. R. Dell'Acqua, J. A. Egon, and B. Bush, *Environ. Sci. Technol.*, **9**, 38 (1975).
(4) D. G. Pym, J. E. Ray, G. W. Smith, and E. V. Whitehead, *Anal. Chem.*, **47**, 1617 (1975).
(5) D. V. Rasmussen, *Anal. Chem.*, **48**, 1562 (1976).
(6) F. K. Kawahara, *Environ. Sci. Technol.*, **10**, 761 (1976).
(7) M. C. Goldberg and D. H. Devonald, *J. Res. U.S. Geol. Sur.*, **1**, 709 (1973).
(8) P. F. Lynch and C. W. Brown, *Environ. Sci. Technol.*, **7**, 1123 (1973).
(9) C. W. Brown, P. F. Lynch, and M. Ahmadjian, *Environ. Sci. Techn.*, **8**, 669 (1974).
(10) C. W. Brown and P. F. Lynch, *Anal. Chem.*, **48**, 191 (1976).
(11) F. K. Kawahara and Y. Y. Yang, *Anal. Chem.*, **48**, 651 (1976).
(12) J. S. Mattson, C. S. Mattson, M. J. Spencer, and S. A. Starks, *Anal. Chem.*, **49**, 297 (1977).
(13) F. K. Kawahara, *J. Chromatogr. Sci.*, **10**, 629 (1972).
(14) D. L. Duewer, B. R. Kowalski, and T. F. Shatzki, *Anal. Chem.*, **47**, 1573 (1975).
(15) H. R. Lukens, *Prog. Nucl. Eng. Anal. Chem.*, **12**, 1 (1975).
(16) S. H. Fortier and D. Eastwood, *Anal. Chem.*, **50**, 334 (1978).
(17) M. Anbar and W. H. Aberth, *Anal. Chem.*, **46**, 59A (1974).

(18) W. W. Shultz, "Application of High Pressure Liquid Chromatography to the Identification of Oil Spills in the Marine Environment", 26th Pittsburgh Conference on Analytical Chemistry and Applied Spectroscopy, Cleveland, Ohio, March 1975.
(19) W. A. Saner and G. E. Fitzgerald II, *Environ. Sci. Technol.*, 10, 893 (1976).
(20) Oil Identification Symposium, 27th Pittsburgh Conference, on Analytical Chemistry and Applied Spectroscopy, Cleveland, Ohio, 1976.
(21) J. W. Frankenfield, "Weathering of Oil at Sea", AD 787 789, 1973.
(22) J. W. Miller, "A Multiparameter Oil Pollution Source Identification System", EPA-R2-73-221, July 1973.
(23) Proceedings, Workshop on Pattern Recognition Applied to Oil Identification, Coronado, Calif., November 1976, IEEE Catalog No. 76, CH 1247-6 C, 1977.
(24) Symposium on Oil and Other Organic Pollutants Analysis, 29th Pittsburgh Conference on Analytical Chemistry and Applied Spectroscopy, Cleveland, Ohio, 1978.
(25) A. P. Bentz, *Anal. Chem.*, 48, 454A (1976).
(26) A. P. Bentz, *Anal. Chem.*, 50, 655A (1978).
(27) ASTM Standard Method, D3328-78, Comparison of Waterborne Petroleum Oils by Gas Chromatography, 1978 Annual Book of ASTM Standards, Part 31, American Society for Testing and Materials, Philadelphia, Pa., 1978.
(28) ASTM Standard Method, D3327-74T, Analysis of Selected Elements in Waterborne Oils, 1978 Annual Book of ASTM Standards, Part 31, American Society for Testing and Materials, Philadelphia, Pa., 1978.
(29) ASTM Standard Method, D3650-78, Comparison of Waterborne Petroleum Oils by Fluorescence Analysis, 1978 Annual Book of ASTM Standards, Part 31, American Society for Testing and Materials, Philadelphia, Pa., 1978.
(30) ASTM Standard Method, D3414-75T, Infrared Analysis of Waterborne Oils, 1978 Annual Book of ASTM Standards, Part 31, American Society for Testing and Materials, Philadelphia, Pa., 1978.
(31) Morton L. Curtis, Use of Pattern Recognition Techniques for Typing and Identification of Oil Spills, NTIS Acc. No. ADA 043802, 1977.
(32) E. Whittaker and G. Robinson, "The Calculus of Observations", 4th ed., Dover Publications, New York, 1967.
(33) G. P. McCabe, Jr., *Technometrics*, 17, 103 (1975).
(34) J. T. Tou and R. C. Gonzalez, "Pattern Recognition Principles, Addison-Wesley Publishing Company, Reading, Mass., 1974, p 110 ff.
(35) J. S. Mattson, C. S. Mattson, M. J. Spencer, and F. W. Spencer, *Anal. Chem.*, 49, 500 (1977).

RECEIVED for review July 17, 1978. Accepted January 11, 1979. The financial support of the U.S. Environmental Protection Agency through Contract No. 68-01-1739 is gratefully acknowledged. The MODCOMP II/25 computer used in this work was purchased with the financial support of the National Science Foundation.

Mechanism of Chromatographic Retention of Organic Ions on a Nonionic Adsorbent

Frederick F. Cantwell* and Su Puon

Department of Chemistry, University of Alberta, Edmonton, Alberta, Canada T6G 2G2

Adsorption of organic ions on the styrene–divinylbenzene copolymer Amberlite XAD-2 is studied by means of adsorption isotherms and microelectrophoresis measurements. The results obtained with the sample ions diphenylguanidinium and benzylammonium are quantitatively explained in terms of the Stern–Gouy–Chapman (SGC) theory of the electrical double layer in which the sample ion is adsorbed onto the surface and small inorganic counterions, such as chloride, occupy the diffuse part of the electrical double layer. The addition of quaternary ammonium ions to the mobile phase produces a constant surface potential. Under chromatographic conditions where the surface potential is constant, the reciprocal of the adjusted retention volume is linearly dependent on the reciprocal of the mobile phase ionic strength. For a constant ionic strength, the log of the adjusted retention volume varies directly as the negative log of the concentration of potential-determining ion. The general effects of electrolyte type in the mobile phase on retention behavior of ionic samples are also discussed.

Amberlite XAD-2 is a nonionic macroporous copolymer of styrene and divinylbenzene. Both neutral and ionic conjugate species of organic acids and bases are chromatographically retained on it, and retention volumes depend on solvent composition, pH, and nature and concentration of inert salt in the mobile phase (*1*). Recent work in this laboratory has produced high performance columns packed with microparticulate Amberlite XAD-2, which exhibit efficiencies comparable to those observed for columns packed with commercially available microparticles of reverse-phase bonded packings (*2*, *3*). The low cost, wide useful pH range (pH 0 to 14) and relatively strong adsorbent properties of XAD-2 suggest that it will become a competitive high efficiency liquid chromatographic column packing. For this reason, an investigation of the mechanistic aspects of sample retention was undertaken.

The sorption of ions on XAD-2 has been known for a long time. Gustafson (*4*) reported that the distribution coefficients of aliphatic and aromatic sulfonates between resin and water increase with increasing concentration of sodium chloride. Sulfonates, benzoate, and phthalate were chromatographically separated, and retention volumes were also found to increase with increasing concentration of sodium chloride in the mobile phse (*5*, *6*). More recent studies (*7*–*9*) have confirmed this electrolyte effect and have led to the suggestion that ion-pairing might account for the increased retention. A preliminary study in this laboratory lent some support to the ion-pair model (*9*) but, as will be seen below, the present detailed investigation strongly supports an alternative mechanism. Retention volumes of cationic conjugate acids of pharmaceutical amines have been shown to vary not only with the concentration of inert electrolyte but also with the nature of the electrolyte (*1*). For example, the cationic conjugate acid of phenylephrine is more strongly retained on XAD-2 in 0.1 M sodium perchlorate than in 0.1 M sodium chloride. Lundgren and Schilt (*10*) have reported the same phenomenon in their study of the retention of the divalent cationic complex tris[3-(2-pyridyl)-5,6-diphenyl-1,2,4-triazene]iron(II).

To date, no mechanistic model has been proposed to account for the adsorption of ions on Amberlite XAD-2 and no experimental studies directed to this end have been reported. For the case of reverse-phase packings involving octadecylsilyl

0003-2700/79/0351-0623$01.00/0 © 1979 American Chemical Society

(ODS) groups bonded to a silica support, it has been proposed that the sorption of ions can be accounted for by solvophobic interactions (*11–14*). This model, as formulated, apparently does not apply to the sorption of ions on XAD-2, since plots of adjusted retention volumes on XAD-2 vs. ionic strength clearly do not show the minimum which is predicted by solvophobic theory (compare Figure 4 in reference 1 and Figure 7 in this work with Figure 11 in reference 12).

In the present study, two different experimental techniques have been used to elucidate the adsorption mechanism. (i) Adsorption isotherms for two organic cations were measured in the presence of different concentrations of inert electrolyte either by batch equilibrium or by a liquid chromatographic method. Values obtained from the isotherms were then compared with those predicted by the Stern–Gouy–Chapman (SGC) model of the electrical double layer. (ii) Microelectrophoresis measurements were made on individual resin particles suspended in solutions of an adsorbable cation and the observed zeta potentials were compared to those predicted by the SGC model. The results from both types of experiments support the view that adsorption of ions onto XAD-2 can be explained in terms of the Stern–Gouy–Chapman model.

STERN-GOUY-CHAPMAN THEORY

The SGC model of the electrical double layer at a charged interface has been reviewed in many places (*15–20*). The modification of the SGC theory proposed by Grahame (*18*) is used in the present discussion except that the adsorbed "potential-determining ions" (vide infra) are considered to be part of the surface rather than part of the compact double layer. This formalism is more consistent with the usage of colloid chemistry (*17, 21*) than of electrochemistry (*18*), although for the system under investigation, both formalisms lead to the same quantitative conclusions.

Since Amberlite XAD-2 has a non-ionogenic and electrically nonpolarizable surface, it acquires a surface charge by the adsorption of ions from solution. Diphenylguanidinium cations ($DPGH^+$) will be used as an example of adsorbed ions throughout the present discussion. The adsorbed ions are referred to as "potential-determining ions" and are responsible for the electrical potential difference, Ψ_0, between the surface and the bulk solution. The relationship between activity of potential-determining ions in the bulk solution, a_{DPGH}, and the surface potential in volts is often described by a Nernst equation (*15–17*)

$$\Psi_0 = k + (RT/ZF) \ln a_{DPGH} \quad (1)$$

where R is the ideal gas constant (8.314 coulomb-volt/mole-K); F is the Faraday constant (96 487 coulomb/equivalent); T is absolute temperature; Z is the valence of the potential-determining ion (equivalent/mole) with appropriate sign; and k is a constant. Equation 1 is often found to apply when the surface coverage is well below a monolayer and it defines the "completely reversible electrode". In the present treatment it is not necessary that Equation 1 be valid, but only that, regardless of their functional relationship Ψ_0 is a constant at constant a_{DPGH}.

The region between the XAD-2 surface and the bulk solution is described by the SGC theory as follows: As a first approximation, the charges of the adsorbed potential-determining ions are viewed as smeared out on the resin surface, with the plane passing through them identified as the "charge-surface". The surface charge density, σ_0, is given in units of coulombs per cm^2. In the absence of any other charged species, the potential would decay linearly with distance into the solution from a value of Ψ_0 at the charge-surface to zero in the bulk solution. However, there are necessarily other ions present in solution, and counterions, such as chloride ions in the present example, which are of opposite sign to the potential-determining ions, are electrostatically attracted toward the charge-surface so that their concentration near the surface is greater than in the bulk solution. At the same time, co-ions, such as sodium and $DPGH^+$, which are of like sign, are repelled from the surface and their concentration near the surface is lower than in the bulk solution. The "surface excess", Γ_j, of any ion j^z is the number of moles of the species j^z contained on 1 cm^2 of surface and in its adjoining double layer in the solution, which are in excess of the moles of the same species contained in an equivalent volume of bulk solution. This equivalent volume is defined as that volume of bulk solution containing the same total moles of charge of all species as there are in the 1 cm^2 of interface under consideration (*21*). The units of Γ_j are moles per cm^2. An important distinction is that σ_0, the surface charge density of $DPGH^+$, includes only the moles of *adsorbed* potential-determining ion, while Γ_{DPGH} takes into account the fact that some $DPGH^+$ is expelled from the adjoining double-layer region.

Because the hydrated counterions and co-ions have a finite size, they cannot approach the charge surface any closer than about a hydrated radius. This plane of closest approach of counterions in the double layer is the Outer Helmholtz Plane (OHP) (*18*). It is possible for *counterions* to be "specifically adsorbed" to the charge-surface, in a so-called "Inner Helmholtz Plane" (*15, 18*), with all or most of the hydrate water molecules being absent between the charge-surface and the specifically adsorbed counterion. However, in the present case, the experimental data are inconsistent with specific adsorption, and therefore the OHP is considered to be the plane of closest approach of counterions.

Two regions are now distinguishable in the double layer. The first, lying between the charge-surface and OHP, is called the "compact part" of the double layer and in it the potential decays linearly. The second region lies between the OHP and bulk solution and is called the "diffuse part" of the double layer. Here the potential decays not linearly, but nearly exponentially because the excess counterion charge nearer the OHP screens the ions farther away toward the bulk solution, causing the potential to decay more rapidly. The sum of the excess charges in the OHP and diffuse part of the double layer must be equal but opposite in sign to the surface charge in order that electroneutrality be maintained.

If a_{DPGH} in the bulk solution were reduced at constant ionic strength, the net effect would be a decrease in Ψ_0 (Equation 1) and in surface charge density, σ_0.

Now consider the effect of increasing the ionic strength in bulk solution by adding more inert electrolyte such as sodium chloride while at the same time maintaining the activity of $DPGH^+$ constant. Since Ψ_0 is constant and the electrolyte concentration has been increased, this leads to a corresponding and proportional increase of counterions attracted into the double layer and co-ions repelled from it. In order to maintain electroneutrality in the double layer, the number of $DPGH^+$ ions adsorbed must increase (larger σ_0). A second consequence of increased ionic strength is a compression of the diffuse part of the double layer. This occurs because the increased counterion concentration in the diffuse part of the double layer closer to the OHP provides an increased screening effect for ions farther out in the diffuse layer. The potential therefore decays faster.

The compact and diffuse parts of the double layer are usually treated as two parallel plate capacitors in series. The compact part of the double layer obviously has some analogy with a capacitor, with the charge-surface constituting one "plate", the OHP the other, and the capacitance C_1 given as:

$$C_1 \equiv \frac{\sigma_0}{\Psi_0 - \Psi_{OHP}} \quad (2)$$

In the absence of specific adsorption of counterions, C_1 remains nearly constant as ionic strength varies (*19*, *20*).

The second capacitor has the OHP as one "plate" and a hypothetical plane in the diffuse part of the double layer as the second plate. This latter point requires elaboration. In the absence of a specifically adsorbed Inner Helmholtz Plane of counterions, electroneutrality requires that:

$$\sigma_0 = -\sigma_{DL} \tag{3}$$

where σ_{DL} is the charge density in coulombs per cm^2, in and beyond the OHP (*18*), produced by the positive surface excess of counterions and negative surface excess of co-ions. The value of $-\sigma_{DL}$ is given from SGC theory for a uniunivalent electrolyte as:

$$-\sigma_{DL} = \left(\frac{\epsilon RT}{2000\pi}\right)^{1/2} c^{1/2}\left(\exp\left[\frac{ZF\Psi_{OHP}}{2RT}\right] - \exp\left[-\frac{ZF\Psi_{OHP}}{2RT}\right]\right) \tag{4}$$

where Ψ_{OHP} is the electrical potential at the OHP in volts, c is the concentration of electrolyte in bulk solution in mol/L and $Z = 1$. The permittivity of the solution in the double layer, ϵ, is equal to the unitless dielectric constant times the constant 1.12×10^{-12} coulomb/volt-cm (*18*, *20*).

When $Z\Psi_{OHP}$ is smaller than about 0.025 V at 25 °C, Equation 4 becomes (*20*):

$$-\sigma_{DL} \approx \frac{\epsilon\Psi_{OHP}}{4\pi}\left(\frac{8\pi Z^2F^2c}{1000\epsilon RT}\right)^{1/2} = \frac{\epsilon\kappa}{4\pi}\Psi_{OHP} \tag{5}$$

By rearranging Equation 5 and substituting σ_0 for $-\sigma_{DL}$ from Equation 3, the following is obtained:

$$C_2 \equiv \frac{\sigma_0}{\Psi_{OHP}} \approx \frac{\epsilon\kappa}{4\pi} \tag{6}$$

from which it is seen that the diffuse part of the double layer has the same capacitance, C_2, as a parallel plate condenser with distance $1/\kappa$ between the plates. At a fixed ionic strength in bulk solution (i.e., fixed c), σ_0 varies linearly with Ψ_{OHP}. On the other hand, if the ionic strength of the solution is varied, then the capacitance C_2 varies directly as $c^{1/2}$ because the "thickness", $1/\kappa$, of the diffuse part of the double layer decreases linearly with $c^{-1/2}$. At 25 °C, with $Z = 1$, and assuming the dielectric constant to be that of pure water (i.e., 78.3) the capacitance has the value:

$$C_2 = 2.28 \times 10^{-4}\, c^{1/2}\ \frac{\text{farads}}{\text{cm}^2} \tag{7}$$

It is important in the present study to know the relationship that prevails when $\Psi_{OHP} > 0.025$ V. Substituting σ_0 for $-\sigma_{DL}$ from Equation 3 into Equation 4 and replacing the exponential terms with their hyperbolic sine equivalent allows Equation 4 to be rewritten as:

$$\sigma_0 = \left(\frac{\epsilon RT}{2000\pi}\right)^{1/2} 2c^{1/2} \sinh\left(\frac{ZF\Psi_{OHP}}{2RT}\right) \tag{8}$$

It can also be shown that:

$$2\left(\frac{\epsilon RTc}{2000\pi}\right)^{1/2} = \frac{\epsilon\kappa}{4\pi}\left(\frac{2RT}{ZF}\right) \tag{9}$$

Substituting from Equation 9 into 8 and simplifying gives:

$$\sinh\left(\frac{ZF\Psi_{OHP}}{2RT}\right) = \left(\frac{\epsilon\kappa}{4\pi}\right)^{-1}\left(\frac{2RT}{ZF}\right)^{-1}\cdot\sigma_0 \tag{10}$$

Substituting numerical values for the above conditions yields:

$$\sinh\left(\frac{ZF\Psi_{OHP}}{2RT}\right) = 8.53 \times 10^4\, c^{-1/2}\sigma_0 \tag{11}$$

Equation 11 allows an evaluation of Ψ_{OHP} from the known electrolyte concentration, c, and the experimentally measured value of σ_0, since the value of $ZF\Psi_{OHP}/2RT$ can be found in tables (*22*) for any value of $\sinh(ZF\Psi_{OHP}/2RT)$. Starting, as in Equation 6, with the definition of C_2 and substituting the value of σ_0 from Equation 10 gives:

$$C_2 \equiv \frac{\sigma_0}{\Psi_{OHP}} = \left(\frac{\epsilon\kappa}{4\pi}\right)\left(\frac{ZF\Psi_{OHP}}{2RT}\right)^{-1}\sinh\left(\frac{ZF\Psi_{OHP}}{2RT}\right) \tag{12}$$

which is a more rigorous form of Equation 6 that applies at all values of Ψ_{OHP}.

From Equations 2 and 12 and the definition of κ implied in Equation 5 it is possible to write:

$$\frac{1}{\sigma_0} = \frac{1}{C_1\Psi_0} + \frac{1}{2.28 \times 10^{-4}\, c^{1/2}\Psi_0\left[\left(\frac{ZF\Psi_{OHP}}{2RT}\right)^{-1}\sinh\left(\frac{ZF\Psi_{OHP}}{2RT}\right)\right]} \tag{13}$$

Equation 13 provides a simple way to experimentally test whether the SGC theory describes the adsorption of ions on XAD-2, since it predicts a straight line plot of

$$\sigma_0^{-1} \text{ vs. } \left(c^{1/2}\left[\left(\frac{ZF\Psi_{OHP}}{2RT}\right)^{-1}\sinh\left(\frac{ZF\Psi_{OHP}}{2RT}\right)\right]\right)^{-1}$$

under conditions where Ψ_0 is constant (achieved by making the measurements in solutions of fixed activity of potential-determining ion). Furthermore, if this plot is repeated for several different surface potentials, then the ratio of the intercept to the slope should be the same for each plot and should have the value $2.28 \times 10^{-4}/C_1$.

MICROELECTROPHORESIS

Electromigration of charged particles large enough to be seen with a microscope can be measured by microelectrophoresis, a technique in which the rate of movement of individual particles is observed (*20*). Adsorbed potential-determining ions as well as a certain amount of water of hydration will form part of the migrating unit. The boundary between the migrating unit and the solution phase, which in reality is a region of rapidly changing viscosity, is called the "plane of shear" and its location, though unknown with any accuracy, is usually assumed to be at or slightly beyond the OHP (*18*, *20*). The potential difference between the plane of shear and the bulk solution is called the zeta potential (ζ) and it is ζ which is accessible by electrophoretic measurements.

In the microelectrophoresis experiment, the measured quantity is the electrophoretic mobility U_E in micrometer-cm/volt-s. The relationship between U_E and ζ for large particles is given by the Helmholtz–Smoluchowski equation (*15*, *20*):

$$\zeta = \frac{4\pi\eta}{\epsilon}U_E = 1.28 \times 10^{-2}\, U_E \text{ volts} \tag{14}$$

where η is the viscosity of the liquid, in poise.

If the approximation is made (*18*):

$$\zeta \approx \Psi_{OHP} \tag{15}$$

then Equation 2 can be rewritten as:

$$C_1 \approx \frac{\sigma_0}{\Psi_0 - \zeta} \tag{16}$$

and rearranging gives:

$$\sigma_0 \approx C_1\Psi_0 - C_1\zeta \tag{17}$$

The value of Ψ_{OHP} (or, from Equation 15, the value of ζ) depends on c, and on σ_0 via Equations 3 and 4. Thus, a plot of the experimentally measured values of σ_0 vs. those of ζ should give a straight line under conditions where the activity of potential-determining ion is held constant to provide constant Ψ_0, and c is varied in order to vary Ψ_{OHP}.

EXPERIMENTAL

Reagents and Chemicals. Diphenylguanidine, benzylamine, and tetra-*n*-butylammonium bromide were as previously described (*9*). All other chemicals were analytical reagent grade and water was deionized, distilled, and finally distilled over alkaline permanganate.

Amberlite XAD-2 resin (Rohm & Haas Co., Philadelphia, Pa.) was ground in a triple porcelain roller mill (Erweka-Apparatebau-GmbH), dried, and classified in U.S. standard sieves. The <325-mesh portion which was used both in packing the chromatographic columns and in adsorption isotherm measurements was purified and "de-fined" as previously described (*23*). Particles of nominally 6-μm diameter for use in microelectrophoresis were prepared by elutriation of the <325-mesh resin using methanol. The elutriation apparatus was similar to that previously described (*24*) except that solvent was pumped at constant flow rate with a Chromatronix model CMP-3V pump (Laboratory Data Control, Riviera Beach, Fla.) and the column was kept at constant temperature by means of a water-jacket.

Adsorption Isotherms. Isotherms for the adsorption of $DPGH^+$ on XAD-2 were measured at 25 ± 1 °C by a batch equilibration technique. All solutions were adjusted to pH 3 with hydrochloric acid in order to ensure that the concentration of diphenylguanidine free-base was negligible. Twenty-five mL volumes of aqueous phase containing varying amounts of $DPGH^+$ and sodium chloride were pipetted into stoppered flasks along with 2.5 g of XAD-2 resin. Five different NaCl concentrations were used: 0.01, 0.05, 0.10, 0.25, and 0.50 M, with five or six different concentrations of $DPGH^+$ used for each NaCl concentration. The stoppered flasks were agitated in a mechanical shaker (Blue M Company, Blue Island, Ill.) for about 24 h which was shown to be sufficient to establish adsorption equilibrium. The aqueous phase was filtered free of resin and analyzed for its $DPGH^+$ concentration by UV spectroscopy on a Cary 118 spectrophotometer (Varian Instruments, Palo Alto, Calif.). Concentration of $DPGH^+$ on the resin phase was determined by difference.

Because XAD-2 resin will not imbibe water into its pores when dry resin is placed directly in water, it was wetted with methanol before being used in the isotherm measurements. The methanol was filtered off and the resin washed thoroughly with water to displace the methanol. Excess water was sucked off and the wet resin was weighed into the flasks. The exact weight of resin in the flask was determined after equilibration by filtering, washing with methanol, oven-drying, and weighing. The pore volume of water was included, for calculation purposes, in the aqueous phase volume.

Adsorption isotherms of benzylammonium ion (BZH^+) were measured by chromatography on XAD-2. The mobile phase contained varying concentrations of hydrobromic acid. Concentration of BZH^+ was varied in the 10 μL of sample solution injected. The chromatograph and the calculations are described below.

Chromatographic Apparatus. A Chromatronix model CMP-2VK pump, a 10-μL injection valve (model CSV), a pressure gage, Teflon tubing, and Cheminert fittings were all obtained from Laboratory Data Control. The UV absorbance detector was a model SP8200 (Spectra Physics, Santa Clara, Calif.) and the recorder a Recordall model 5000 (Fisher Scientific Co.). The 0.28-cm i.d. by 30-cm long glass Microbore chromatographic column (Laboratory Data Control) was dry-packed with <325-mesh XAD-2 and was water-jacketed and thermostated at 25 ± 1 °C.

Microelectrophoresis. Electrophoretic mobility was measured on a Mark II Microelectrophoresis Apparatus (Rank Bros., Cambridge, England) using a flat quartz cell, 0.80 mm thick and 9.7 mm high, immersed in a 25 ± 1 °C water bath. The platinum electrodes supplied with the instrument were replaced with coils of silver wire previously anodized to give them a coating of AgCl in order to minimize "gassing" at the electrodes in the low-resistance sample solutions. The "effective length" or interelectrode distance was calculated from the equation (*20*):

$$L = rkA \tag{18}$$

where k is the specific conductance of 0.10 M KCl with which the cell was filled for calibration purposes, A is the cross-sectional area of the cell at the point of microscopic observation, and r is the resistance measured with an impedence bridge (Model 1650-A, General Radio Company, Concord, Mass.). The potential gradient in volts/cm during an electrophoresis experiment was calculated by dividing the voltage applied between the electrodes by L.

Microscopic observations were made on particles of XAD-2 resin at the "stationary level" in the cell in order to minimize convective movement due to electroosmosis (*20*). The time required for a given resin particle to migrate 50 μm was measured. The polarity of the applied potential was reversed and the time required to migrate the same distance in the opposite direction was measured. The measurements were repeated ten times at each applied potential and polarity. As a check on instrument calibration, the electrophoretic mobility of unwashed human red blood cells was measured at 25 °C in 6.67×10^{-2} M phosphate buffer at pH 7.4. The anticoagulated blood sample was refrigerated for several days before use. The observed mobility was −1.11 μm-cm/volt-sec which is lower than the accepted mean value of −1.30 for fresh blood but close to the lowest value of −1.12 reported by Abramson (*25*) for aged blood.

The concentration of XAD-2 suspensions used for electrophoretic measurements was 0.1 mg/mL. Three series of these resin suspensions were prepared, each at a different a_{DPGH}. Within each series a_{DPGH} was constant, while the ionic strength was adjusted to four different values with NaCl. All solutions were adjusted to pH 3 by the addition of HCl. Mobilities of XAD-2 resin were found to be 0 when no $DPGH^+$ was present.

RESULTS AND DISCUSSION

Adsorbent Properties. Amberlite XAD-2 is hydrophobic, since its surface is not wetted by water (*26*). The forces of interaction between a sample species and the surface of XAD-2 are dispersion forces which, in the case of aromatic samples, take the form of π–π interactions. The electron donor properties of the aromatic rings in styrene–divinylbenzene copolymers make it possible for them to also undergo weak hydrogen bonding interactions with sample species (*27*). Such copolymers used as gas chromatographic stationary phases have been found to contain small numbers of polar-impurity surface sites (*28*, *29*), and Zettlemoyer (*30*) indicates that it is nearly impossible to synthesize any hydrophobic surface that is free of polar site impurities. This should be kept in mind when using XAD-2, which is chemically identical to some of the gas chromatographic phases.

Various batches of XAD-2 are reported to have specific surface areas between 300 and 354 m^2/g as determined by the B.E.T. method, porosities of 0.42 mL/mL, and average pore diameters of 90 Å^2 (*4*, *31*, *32*).

Adsorption Isotherms. In Figure 1 are plotted adsorption isotherms for diphenylguanidinium ion ($DPGH^+$) obtained in the presence of various bulk solution concentrations of sodium chloride. A specific surface area of 330 m^2/g was used in computing the ordinate value of surface excess. At higher concentrations of $DPGH^+$ in solution, the data are described by the Langmuir equation:

$$\frac{1}{\Gamma_{DPGH}} = \frac{1}{K[DPGH]\Gamma_{DPGH,MAX}} + \frac{1}{\Gamma_{DPGH,MAX}} \tag{19}$$

where [DPGH] is mol/L of $DPGH^+$ in the bulk solution, K is a heterogeneous equilibrium constant, and $\Gamma_{DPGH,MAX}$ is the surface excess corresponding to monolayer coverage of resin

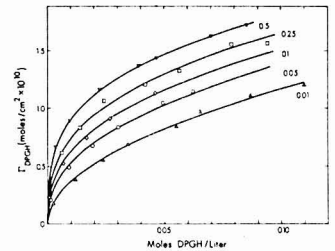

Figure 1. Adsorption isotherms for $DPGH^+$ in the presence of various bulk solution concentrations of sodium chloride. The numbers at the end of the curves are the molarities of sodium chloride

surface with $DPGH^+$. Figure 2 shows the data for $DPGH^+$ plotted according to Equation 19. The ordinate intercepts for all of the curves are the same, indicating that $\Gamma_{DPGH,MAX}$ is the same, regardless of the ionic strength of the solution. This intercept value of $(0.59 \pm 0.02) \times 10^{10}$ cm^2/mol corresponds to 1.70×10^{-10} mol/cm^2 for a monolayer of $DPGH^+$, and to an area of 9.8×10^{-15} cm^2 occupied by each $DPGH^+$.

From molecular models, it can be shown that the $DPGH^+$ ion can readily assume a conformation in which the phenyl groups are coplanar with one another and with the plane through the sp^2 carbon and the two sp^3 nitrogens, and in which the protonated imino-nitrogen is perpendicular to this plane. Since this configuration would maximize π–π interactions with the phenyl groups of the XAD-2 resin, it is likely that the adsorbed molecule lies flat on the resin surface with the protonated nitrogen directed toward the solution phase. Taking the area of a benzene ring as 43 $Å^2$ (*33*) and using tabulated covalent radii of H, N, and C (*34*) to calculate areas of these atoms, the flat area of a $DPGH^+$ ion lying on the resin surface is calculated to be 9.0×10^{-15} cm^2. This is close to the experimentally measured area noted above. Thus, monolayer coverage is essentially a close-packing of $DPGH^+$ ions lying flat on the surface. This latter conclusion is also in agreement with the results reported for the adsorption of phenol on XAD-2 (*4*) and for the adsorption of substituted benzenes on Amberlite XAD-4, a chemically identical adsorbent with a larger specific surface area than XAD-2 (*31*). The occurence of Langmuir adsorption isotherms for ionic samples at high concentrations has previously been reported, for example, for tris[3-(2-pyridyl)-5,6-diphenyl-1,2,4-triazine]iron(II) on XAD-2 (*10*) and for the anionic dye Chlorazol Sky Blue FF on graphitized carbon (*35*), another hydrophobic adsorbent.

Adsorption isotherms for another organic cation BZH^+ in the presence of a large excess of HBr were calculated from chromatographic retention volumes as follows. The concentration of BZH^+ in the aqueous phase is taken as the moles of BZH^+ in that phase divided by the column void volume, V_M, in liters and is given by the expression:

$$[BZH^+] = T_{BZH}/V_R \tag{20}$$

where T_{BZH} is the total moles of BZH^+ injected onto the column and V_R is the retention volume of BZH^+, in liters. The surface excess of BZH^+ in mol/cm^2 is given by:

$$\Gamma_{BZH} = \frac{T_{BZH}V_N}{3.30 \times 10^9\ WV_R} \tag{21}$$

where W is the weight of resin in the column in kg, the numerical constant is the specific surface area in cm^2/kg, and V_N is the adjusted retention volume in liters given by:

$$V_N = V_R - V_M \tag{22}$$

Chromatographic peak shapes for BZH^+ all showed some tailing. The tailing was only slight when the amount of BZH^+ injected was small and the HBr concentration high, while the most severe tailing occurred when the amount of BZH^+ injected was large and the HBr concentration was small. In all cases, the retention volume was taken, not at the peak maximum, but at its "center of gravity" (i.e., the volume of eluate which divides the area of the peak in half). The distribution isotherms plotted as Γ_{BZH} vs. $[BZH^+]$, exhibited much less curvature than those shown in Figure 1 for $DPGH^+$, which is expected since the sample-loading of the resin in the chromatographic experiments involving BZH^+ was far below that encountered in the batch equilibration studies involving $DPGH^+$.

SGC Behavior. Values of σ_0 can be calculated from values of Γ_j, the experimental surface excess of potential determining ion j^+, which are obtained from the adsorption isotherms. Continuing with the example in which $DPGH^+$ is the potential determining ion, the value of Γ_{DPGH} is equal to the mol/cm^2 of $DPGH^+$ *adsorbed* on the surface (Γ_{DPGH}^{AD}) minus the mol/cm^2 of $DPGH^+$ that has been expelled by electrostatic

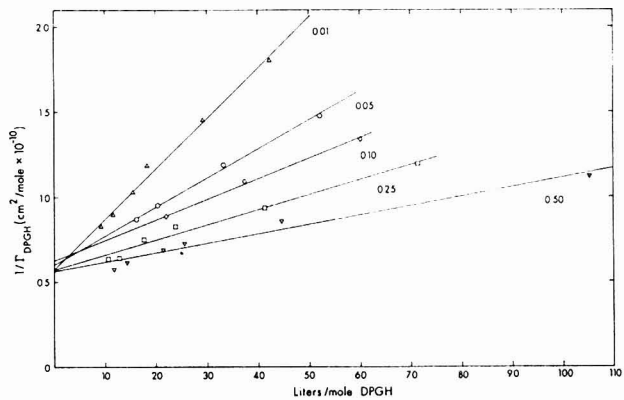

Figure 2. Langmuir adsorption isotherms for $DPGH^+$ in the presence of various bulk solution concentrations of sodium chloride plotted according to Equation 19. The numbers at the end of the curves are the molarities of sodium chloride

Table I. Surface Potentials and Capacitances for the Adsorption of $DPGH^+$ on Amberlite XAD-2

	Ψ_0(volt) × 10^3		C_1(F/cm²) × 10^6	
a_{DPGH}	isotherm[a]	electrophoresis[b]	isotherm[a]	electrophoresis[b]
3.0×10^{-4}	32.0 ± 4.2		161 ± 92	
5.0×10^{-4}	39.4 ± 2.7		161 ± 47	
$1.0_0 \times 10^{-3}$	49.6 ± 10.4	27.0 ± 12.3	168 ± 149	168 ± 49
$3.0_0 \times 10^{-3}$	73.2 ± 9.7		176 ± 89	
$5.0_0 \times 10^{-3}$	86.9 ± 12.8	33.2 ± 35.2	172 ± 88	283 ± 196
$1.0_0 \times 10^{-2}$	102.5 ± 8.4		192 ± 52	
$2.0_0 \times 10^{-2}$	115.9 ± 7.9	37.0 ± 15.6	227 ± 50	445 ± 124
3.0×10^{-2}	121.5 ± 9.8		262 ± 91	

[a] Calculated from data in Figure 3 via Equation 13. [b] Calculated from data in Figure 6 via Equation 17.

repulsion from the diffuse part of the double layer into the bulk of the solution (Γ_{DPGH}^{DL}).

$$\Gamma_{DPGH} = \Gamma_{DPGH}^{AD} + \Gamma_{DPGH}^{DL} \quad (23)$$

(The quantity Γ_{DPGH}^{DL} has a negative value, because it is a "negative" surface excess.) The surface charge σ_0, therefore, is related to Γ_{DPGH}^{AD} by:

$$\sigma_0 = ZF\Gamma_{DPGH}^{AD} = ZF(\Gamma_{DPGH} - \Gamma_{DPGH}^{DL}) \quad (24)$$

It is, therefore, necessary to correct the experimental surface excess by the negative surface excess of $DPGH^+$ in the solution part of the double layer in order to compute σ_0. The nature of the correction will now be discussed. For a flat charge-surface in the absence of specific adsorption of counterions, the ratio of the surface excess due to the absence of co-ions (negative excess) in the solution part of the double layer to that which is due to the positive excess of counterions is given at 25 °C by Grahame (*18*) as:

$$\frac{\Gamma_+^{DL}}{\Gamma_-^{DL}} = -\frac{\exp[-19.47\Psi_{OHP}] - 1}{\exp[19.47\Psi_{OHP}] - 1} \quad (25)$$

In the presence of an inert electrolyte such as NaCl, there are two types of co-ions, Na^+ and $DPGH^+$, so that only part of the negative co-ion surface excess is due to $DPGH^+$:

$$\Gamma_{DPGH}^{DL} = \Gamma_+^{DL}\frac{[DPGH^+]}{[DPGH^+] + [Na^+]} = \Gamma_+^{DL}\alpha \quad (26)$$

where $[DPGH^+]$ and $[Na^+]$ are concentrations of these species in the bulk solution at equilibrium and α is the fraction that $DPGH^+$ represents of all cations in the bulk solution. The symbol R may be defined:

$$R \equiv \frac{\Gamma_{DPGH}^{DL}}{\Gamma_-^{DL}} = \frac{\Gamma_+^{DL}}{\Gamma_-^{DL}}\alpha \quad (27)$$

and the following additional relationship noted:

$$\sigma_{DL} = ZF(\Gamma_-^{DL} + \Gamma_+^{DL}) \quad (28)$$

From Equations 3, 23, 24, 26, 27, and 28 it may be shown that:

$$\sigma_0 = ZF\Gamma_{DPGH}\left[\frac{\alpha + R}{\alpha + R(1-\alpha)}\right] \quad (29)$$

In order to calculate σ_0 from Equation 29 it is necessary to know the value of Ψ_{OHP} to be used in Equation 25. But Ψ_{OHP} is calculated from Equation 11 which requires a knowledge of σ_0. Thus, Equations 11, 25, 27, and 29 must be solved by iteration. A first-approximation to σ_0 is calculated from Equation 30 (below). This is then used to calculate a first-approximation value of Ψ_{OHP} from Equation 11. First-approximations of $\Gamma_+^{DL}/\Gamma_-^{DL}$ and R are calculated in turn from Equations 25 and 27. This value of R is used in Equation 29 to calculate a second-approximation to σ_0. The process is repeated until Ψ_{OHP} and σ_0 no longer change.

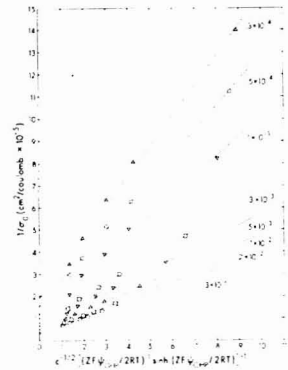

Figure 3. Plots of the adsorption data for $DPGH^+$ according to the SGC Equation 13 at eight surface potentials. The numbers at the end of the lines are the activities of $DPGH^+$ at which the calculations were made

When the potential is large (i.e., several tenths of a volt) or when the concentration of inert electrolyte in the bulk solution is much larger than that of $DPGH^+$, then:

$$\sigma_0 = ZF\Gamma_{DPGH} \quad (30)$$

In the present case, the difference in the value of σ_0 calculated by Equations 29 and 30 is significant only when a_{DPGH} is large and the concentration of NaCl is small. In the worst case the difference was 12%.

Validity of the SGC theory for the adsorption of $DPGH^+$ on XAD-2 was tested using Equation 13 in the following way. Aqueous solution activity coefficients for $DPGH^+$ (*36, 37*) were used to convert the abscissa values of $[DPGH^+]$ in Figure 1 into a_{DPGH}. For this purpose, an ionic size parameter of 6×10^{-8} was assumed. Points were then located on each of the five isotherms in Figure 1 at the same a_{DPGH} (i.e., at the same Ψ_0) and the five corresponding ordinate values were converted to σ_0 as discussed above. This process was performed at eight different values of a_{DPGH} to give the curves in Figure 3. The lines are linear least-squares fits of the experimental points.

The linearity of the curves in Figure 3 is consistent with the predictions of the SGC theory embodied in Equation 13. Values of Ψ_0 and C_1, calculated from the slopes and intercepts, are given in the second and fourth columns in Table I, along with their 95% confidence intervals. The uncertainties in the values of C_1 are high because they include the uncertainties in both slopes and intercepts. The grand mean and 95% confidence interval of C_1 computed from the eight values in the fourth column of Table I are $(1.90 \pm 0.28) \times 10^{-4}$ F/cm². Within the uncertainty of the measurements, C_1 is a constant as assumed in Equation 13. Constancy of C_1 in the absence

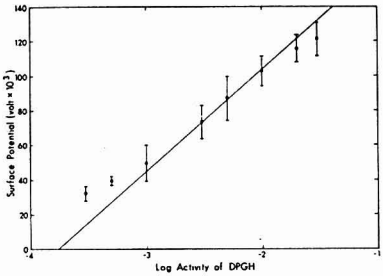

Figure 4. Dependencies of surface potential (Ψ_0) on log of activity of potential-determining ion ($DPGH^+$). The line has a slope of 59.1 mV

Table II. Surface Potentials and Capacitances for the Adsorption of BZH^+ on Amberlite XAD-2[a]

a_{BZH}	Ψ_0(volt) × 10^3	C_1(F/cm²) × 10^6
1.00×10^{-5}	0.086 ± 0.02	115 ± 76
$2.5_0 \times 10^{-5}$	0.21 ± 0.05	106 ± 73
$5.0_0 \times 10^{-5}$	0.38 ± 0.09	105 ± 63
$1.0_0 \times 10^{-4}$	0.72 ± 0.16	104 ± 63

[a] Calculated from data in Figure 5 via Equation 13.

of specific adsorption of counterions has been observed for other surfaces including mercury (*19*) and rutile (*38*). The thickness of the compact double-layer capacitor, δ, may be calculated from the average value of C_1, assuming the dielectric constant to be that of pure water, by the equation:

$$\delta = \epsilon/4\pi C_1 \qquad (31)$$

which yields a value of 3.7×10^{-8} cm, or 3.7 Å. This is approximately equal to the radius of a hydrated chloride counterion (*36*).

Values of the surface potential obtained from the reciprocal slopes in Figure 3 are plotted vs. log a_{DPGH} in Figure 4. Although it is not necessary that Equation 1 apply to the system in order for Equation 13 to be valid, it is interesting to note that the slope of the linear portion of the plot in Figure 4 is close to 0.0591 V (shown as solid line) as predicted by Equation 1. Deviations from linearity at low activities of $DPGH^+$ are probably due to the influence of another potential determining ion. Previous studies have shown that XAD-2 does adsorb H^+ and OH^- ions to a slight extent (*9*). If, in the dilute HCl solutions in which all isotherm measurements were made, the resin surface carries a small residual surface charge because of the adsorption of H^+, then it will bear a small residual surface-potential which will produce curvature in the plot in Figure 4 at low values of a_{DPGH}, analogous to the effect of an interfering ion on an ion-selective electrode.

The isotherm data for benzylammonium ion are treated in the same manner as that described above for $DPGH^+$ in order to obtain the plots shown in Figure 5. The lines are fitted by linear least squares. In this case, the values of Ψ_{OHP} are so low that the bracketed quantity in Equation 13 is always equal to 1. Also, the large excess of HBr means that Equation 30 can be used in place of Equation 29 with negligible error. Table II summarizes surface potentials and capacitances along with their 95% confidence intervals. As predicted by Equation 13, C_1 is essentially constant. The linear relationship between Ψ_0 and log a_{BZH} predicted by Equation 1 is not observed, since the activities of BZH^+ are very low and the effect of an interfering potential-determining ion would be pronounced. It should be noted that the surface-charge, σ_0, in Equation 13 should include the contribution of all adsorbed potential-determining ions. Since only the adsorbed BZH^+ ions are used in the above calculations, the surface potential calculated from Equation 13 will be in error if another type of potential-determining ion is also adsorbed. For this reason, the absolute values of Ψ_0 in Table II will be in error (the same would be true of potentials calculated in the non-Nernstian region of Figure 3 for $DPGH^+$ adsorption). If much lower concentrations of BZH^+ were used, then Ψ_0 could become independent of a_{BZH}. The fact that values of C_1 observed for BZH^+ are somewhat lower than for $DPGH^+$ may reflect a difference in the influence of either H^+, BZH^+, or Br^- on the double layer, compared to Na^+, $DPGH^+$, or Cl^- (vide infra).

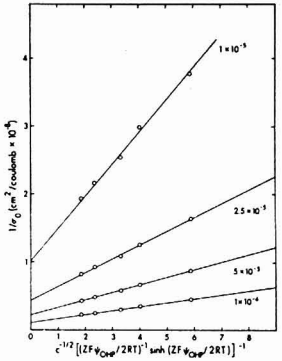

Figure 5. Plots of the adsorption data for BZH^+ according to the SGC Equation 13 at four surface potentials. The numbers at the end of the lines are the activities of BZH^+ at which the calculations were made

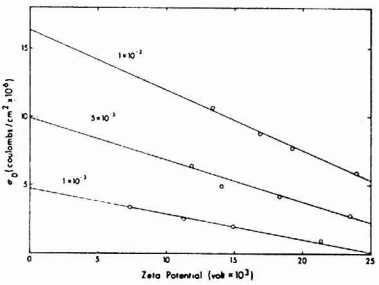

Figure 6. Dependence of zeta potential of XAD-2 particles on surface charge due to adsorbed $DPGH^+$ plotted according to Equation 17. The numbers by the lines are the activities of $DPGH^+$ at which the measurements were made

Microelectrophoresis. Values of σ_0, calculated from the results of the isotherm studies, are plotted in Figure 6 against ζ, obtained from microelectrophoresis measurements, for three different values of a_{DPGH}. Values of Ψ_0 and C_1 calculated from intercepts and slopes of the linear least-square lines are given in the third and fifth columns of Table I, along with their 95% confidence intervals. Although straight lines are obtained, they are not parallel as predicted by Equation 17. Uncertainties in Ψ_0 values are larger than those for C_1 in this case because Ψ_0 reflects the uncertainties of both slope and intercept. It was impractical to make microelectrophoresis measurements at lower ζ because of the slow electromigration rates of the particles. In general, the surface potentials calculated from the microelectrophoresis measurements are lower than those from the isotherm measurements, and the

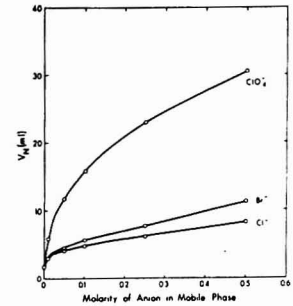

Figure 7. Effect of counterion type in the mobile phase on the adjusted retention volume of BZH^+, on a 0.28 × 30 cm column of XAD-2. Mole of BZH^+ injected was 1.08×10^{-7}

value of C_1 increases with increasing surface-potential. These deviations may be explained in terms of the inaccuracies of the assumptions implicit in Equation 17. (i) The often-made assumption that the "plane of shear" coincides with the OHP is inaccurate (*16, 20*). It is more likely that the "plane of shear" lies somewhat farther away from the surface because water molecules in the primary hydration spheres of counterions lying in the OHP will be part of the migrating unit. In addition, the surface of the XAD-2 particle is not smooth, but highly porous (*39*), so that some of the water beyond the OHP adjacent to surfaces in the "crevasses" may move with the particle and thereby effectively extend the "plane of shear" beyond the OHP. (ii) The Helmholtz–Smoluchowski equation neglects several phenomena that may be operative in the double-layer region and, therefore, for some systems, the relationship between ζ and U_E given by Equation 14 will be in error (*15, 17, 20, 40*). Errors in ζ are expected to be greater at higher ζ and higher σ_0 (*40*) which is consistent with the results of the present study in which the discrepancies between values obtained from isotherm and electrophoresis measurements are greater for curves lying at higher σ_0 and ζ.

The electrophoretic behavior of XAD-2 in the presence of $DPGH^+$ provides unequivocal evidence that the resin acquires a charge when it adsorbs $DPGH^+$ ions and, therefore, rules out an ion-pair retention mechanism. The, at least semi-quantitative, corroboration of the results obtained in the isotherm studies by the totally different experimental technique of microelectrophoresis provides strong support for the SGC view of adsorption of ions on XAD-2.

Counterion Type. Potential-determining cations are adsorbed more strongly in the presence of some anionic counterions than others. This is illustrated in Figure 7 where adjusted retention volumes for benzylammonium ion are plotted vs. anion concentration in the mobile phase for the anions chloride, bromide, and perchlorate. At a given anion concentration, the retention volume, and therefore the fraction of BZH^+ adsorbed on the resin, increases with anion type in the order given. The mechanistic interpretation of this dependence of degree of adsorption of potential-determining ion on counterion type has not been experimentally investigated in the present study. However, there are several alternative explanations of the phenomenon which are consistent with the SGC theory. (i) If the capacitances of the compact and diffuse parts of the double layer are higher in the presence of counterions in the order $Cl^- < Br^- < ClO_4^-$, then σ_0 would be larger for a given value of Ψ_0 (Equation 13). The influence of anion type on C_1 could arise from a decrease in the distance between the charge-surface and OHP. Since there is not much difference in the hydrated radii of these anions (*36*), a decreasing distance could be due to greater polarization of ions with larger crystal radii (*41*). A larger capacitance could also arise from a greater value of the "local" dielectric constant in the compact part of the double layer, due to a decreased tendency toward dielectric saturation of water molecules in the primary hydration sphere of anions with a larger crystal radius. Dielectric saturation, however, is considered to be only slight around anions (*18, 37*).

(ii) Adsorption of a potential determining ion onto the resin surface must be accompanied by an increased concentration of counterion in the double layer. If, because of crowding of ions in the double layer, they are less hydrated than in the bulk solution, then counterions with lower hydration energies would be more readily transfered from the bulk to the double-layer solution promoting greater adsorption of potential-determining ions. A related phenomenon is the tendency of ions with smaller hydration energies to seek positions at the interface between air and water (*18, 42, 43*).

(iii) Adsorption of organic ions onto XAD-2 from water was experimentally found to be accompanied by a positive entropy change (*4*). Water adjacent to a hydrophobic surface is more structured than water in the bulk solution, just as water around dissolved nonpolar molecules is more ordered (*44*). When the adsorbed ions and accompanying counterions are transferred from the bulk solution into the double-layer region, this water structure is disrupted. The greater the "chaotropic" (*44*) or "water structure breaking" (*37*) character of the ions, the more pronounced will be the disordering effect and the greater will be the positive entropy change.

(iv) If specific adsorption of counterions occurs so that an "Inner Helmholtz Plane" is formed, this results in greater adsorption of potential-determining ions for a given Ψ_0 and a_i. Although the present study suggests the absence of specific adsorption of chloride ion, it is possible that the less hydrated and more polarizable bromide and perchlorate ions are adsorbed to some extent. Formally, specific adsorption of counterions is analogous to "ion pair" formation between the potential-determining ion and the counterion, and it is generally observed that the extraction of ion pairs involving organic cations into an organic solvent is greater for counterions in the order $Cl^- < Br^- < ClO_4^-$ (*45*).

Although the present study does not provide sufficient evidence to distinguish which of the above mechanisms are responsible for the specific anion effects of these small inorganic ions, it is possible to predict from the SGC theory how the adsorption behavior will change with more drastic changes in the nature of cation and anion. In the present case where large organic cations and relatively small inorganic anions are used, it is seen that the former are adsorbed as potential-determining ions while the latter occupy only the diffuse part of the double layer. If the small inorganic anion were replaced with a somewhat larger organic one, then specific adsorption of the anions into the IHP would occur. Using both a large cation and anion produces the third situation, in which both ions are adsorbed as potential-determining ions. Then, reversing the trend, if a large organic anion were used with a smaller organic or inorganic cation, only the anion would be adsorbed as potential-determining ion and the cation would serve as counterion. For example, experiments in this laboratory have shown that the adsorption of organic anions onto XAD-2 increases with concentration of NaCl and that the adsorption is greater from KCl solutions than from NaCl solutions of equal concentration.

Chromatographic Behavior. Linear adsorption isotherms are required for sample ions if symmetrical peaks and high chromatographic efficiencies are to be obtained. This will often be the case at low sample concentrations in the mobile phase and, where it is not the case, it is possible to modify

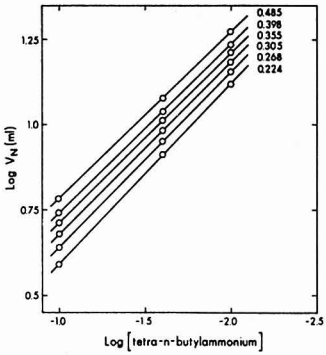

Figure 8. Dependence of adjusted retention volume of $DPGH^+$ on the concentration of TBA^+ bromide in the mobile phase at various total bromide concentrations, on a 0.28 × 30 cm column of XAD-2. The numbers at the end of the curves are the total bromide concentrations. Mole of $DPGH^+$ injected was 4.3×10^{-8}

the mobile phase in order to obtain linear isotherms. The free energy for the adsorption of an ion has the following potential-dependent form, using $DPGH^+$ as an example:

$$\Delta G = ZF\Psi_0 + \mu^\circ_{DPGH} \tag{32}$$

where μ°_{DPGH} is the standard chemical potential for adsorption of the ion into the charge surface (*46*, *47*) and ΔG is an electrochemical potential. The equilibrium constant for adsorption of $DPGH^+$ from solution onto the resin is related to the value of ΔG by:

$$K = \exp\left(-\frac{ZF\Psi_0 + \mu^\circ_{DPGH}}{RT}\right) \tag{33}$$

Since Ψ_0 varies with the concentration of $DPGH^+$ ion in bulk solution, the equilibrium constant for adsorption will not be constant and the isotherm will not be linear. However, if Ψ_0 becomes nearly independent of a_{DPGH} because of the presence of a second potential-determining ion, then ΔG and the equilibrium constant become constant and, at low surface coverages of $DPGH^+$, a linear adsorption isotherm is obtained. A trend toward reduced dependence of Ψ_0 on a_{DPGH} is evident at low a_{DPGH} in Figure 4, and is even more pronounced for BZH^+. The effect can be greatly amplified by adding to the mobile phase a relatively high concentration of a large organic cation such as tetra-*n*-butylammonium ion (TBA^+). Such an ion would be adsorbed on the surface as a potential-determining ion and, because of its relatively high concentration, would be mainly responsible for establishing Ψ_0, making Ψ_0 essentially independent of a_{DPGH}. The influence of TBA^+ on the adsorption isotherm of $DPGH^+$ has previously been reported, although the mechanism of its action was incorrectly assumed to involve ion pair adsorption (*9*). In Figure 3 of reference 9, the added TBA^+ reduces the slope of the isotherm and causes it to be linear to higher $[DPGH^+]$. The reduced slope results from the fact that Ψ_0, though constant because of the relatively high and constant activity of TBA^+, has a larger value than it would in the absence of TBA^+ and therefore produces a lower value of K. Also in reference 9, the added TBA^+ had negligible effect on the adsorption isotherm of the neutral species, diphenylguanidine base. The value of K for a nonionic species would be independent of surface potential.

The dependence of log adjusted retention volume of $DPGH^+$ on the log of the concentration of TBA^+ ion in the mobile phase is given in Figure 8 for several different total concentrations of bromide ion. The bromide concentration was maintained constant for the three points on each curve by the addition of HBr. A linear relationship would be expected if the surface potential were related to a_{TBA} via a Nernst equation, since log K in Equation 33 would vary as the log of the activity of potential-determining ion, and V_N is directly proportional to K. For a constant ionic strength, bulk solution activity coefficients are constant so that a linear relationship is predicted between log V_N and log $[TBA^+]$. This is observed in the plots in Figure 8.

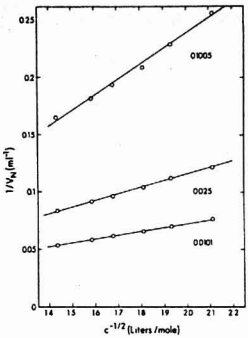

Figure 9. Dependence of adjusted retention volume of $DPGH^+$ on the total electrolyte concentration in the mobile phase at three different concentrations of TBA^+ bromide, on a 0.28 × 30 cm column of XAD-2. The numbers by the lines are molarity of TBA^+. Mole of $DPGH^+$ injected was 4.3×10^{-8}

The SGC model of the electrical double layer around a particle is analogous to the Debye–Huckel model of the ionic atmosphere around an ion (*15*), and the role of electrolyte concentration, c, in the two models is also analogous. Thus, the reciprocal square root dependence of σ_0 on c, which is seen in Equation 13, may be considered to be analogous to the square root dependence on c of the activity coefficient of an ion in solution. This dependence prevails whether or not the adsorbed ion of interest is the principal potential-determining ion in solution. The dependence of adjusted chromatographic retention volume on c can be predicted from the SGC model as follows. Rearranging Equations 21 and 22 for the case of $DPGH^+$ gives:

$$\frac{1}{V_{N,DPGH}} = \frac{T_{DPGH}}{\Gamma_{DPGH}\, 3.30 \times 10^9\, WV_M} - \frac{1}{V_M} \tag{34}$$

Assuming that a large excess of inert electrolyte is present and that Ψ_0 is independent of a_{DPGH}, then Γ_{DPGH} is related to σ_0 by Equation 30. The bracketed quantity in the denominator of Equation 13 has a value close to one at all but fairly high Ψ_{OHP}. Thus, Equation 13 can be rewritten as:

$$\frac{1}{\Gamma_{DPGH}} = \frac{1}{k_1} + \frac{1}{c^{1/2}k_2} \tag{35}$$

Combining Equations 34 and 35 gives:

$$\frac{1}{V_{N,DPGH}} = \frac{1}{k_5} + \frac{1}{k_4 c^{1/2}} \tag{36}$$

where k_1 through k_5 are constants. Equation 36 predicts that $V_{N,DPGH}^{-1}$ will vary linearly with $c^{-1/2}$. Figure 9 shows such linear plots for the chromatography of $DPGH^+$ on XAD-2 using three sets of mobile phases, each of which contains a different large and constant excess of TBA^+ bromide. Changes in bulk solution activity coefficients of TBA^+ with changing

c are compensated by approximately equal changes for $DPGH^+$.

If a salt containing a large organic anion and small inorganic cation were added to the mobile phase, instead of a quaternary ammonium salt, the organic anion would be adsorbed as potential-determining ion and would produce an essentially constant *negative* surface potential. The adsorption of a sample cation such as $DPGH^+$ would then be greatly enhanced by virtue of the negative value of Ψ_0 in Equation 33. Chromatography in such a system would be analogous to "so-called" ion-pair chromatography that has gained popularity on reverse-phase bonded phases (*48*).

ACKNOWLEDGMENT

The microelectrophoresis apparatus was kindly loaned to the authors by Michael Kessick of the Alberta Research Council.

LITERATURE CITED

(1) H. Y. Mohammed and F. F. Cantwell, *Anal. Chem.*, **50**, 419 (1978).
(2) F. F. Cantwell, H. Y. Mohammed, R. G. Baum, and S. Puon, Paper No. 67, Analytical Division, 175th National Meeting, American Chemical Society, Anaheim, Calif., March 1978.
(3) *Ind. Res./Dev.*, June 1978, p C1.
(4) R. L. Gustafson, R. L. Albright, J. Heisler, J. A. Lirio, and O. T. Reid, Jr., *Ind. Eng. Chem., Prod. Res. Dev.*, **7**, 107 (1968).
(5) M. W. Scoggins and J. W. Miller, *Anal. Chem.*, **40**, 1155 (1968).
(6) M. W. Scoggins, *Anal. Chem.*, **44**, 1285 (1972).
(7) D. J. Pietrzyk and C.-H. Chu, *Anal. Chem.*, **49**, 757 (1977).
(8) D. J. Pietrzyk and C.-H. Chu, *Anal. Chem.*, **49**, 860 (1977).
(9) S. Puon and F. F. Cantwell, *Anal. Chem.*, **49**, 1256 (1977).
(10) J. L. Lundgren and A. A. Schilt, *Anal. Chem.*, **49**, 974 (1977).
(11) I. Molnar and C. Horvath, *Clin. Chem. (Winston-Salem, N.C.)*, **22**, 1497 (1976).
(12) C. Horvath, W. Melander, and I. Molnar, *Anal. Chem.*, **49**, 142 (1977).
(13) C. Horvath, W. Melander, I. Molnar, and P. Molnar, *Anal. Chem.*, **49**, 2295 (1977).
(14) C. Horvath and W. Melander, *J. Chromatogr. Sci.*, **15**, 393 (1977).
(15) J. Th. Overbeek, in "Colloid Science", Vol. 1, H. R. Kruyt, Ed., Elsevier, New York, 1952, Chapters 4 and 5.
(16) K. J. Mysels, "Introduction to Colloid Chemistry", Interscience, New York, 1967, Chapter 15.
(17) A. W. Adamson, "Physical Chemistry of Surfaces", 2nd ed., Interscience, New York, 1967, Chapter 4.
(18) D. C. Grahame, *Chem. Rev.*, **41**, 441 (1947).
(19) J. O'M. Bockris and A. K. N. Reddy, "Modern Electrochemistry", Vol. 2, Plenum, New York, 1970.
(20) D. J. Shaw, "Electrophoresis", Academic Press, London, 1969.
(21) K. M. Van Dolsen and M. J. Vold, in "Adsorption from Aqueous Solutions", W. J. Webber and E. Matijevic, Ed., American Chemical Society, Washington, D.C., 1968, Chapter 12.
(22) R. C. Weast, Ed., "Handbook of Chemistry and Physics", 51st ed., The Chemical Rubber Co., Cleveland, Ohio, 1970.
(23) F. F. Cantwell, *Anal. Chem.*, **48**, 1854 (1976).
(24) C. D. Scott, *Anal. Biochem.*, **24**, 292 (1968).
(25) H. A. Abramson, "Electrokinetic Phenomena and Their Application to Biology and Medicine", American Chemical Society, Washington, D.C., 1934.
(26) A. D. Wilks and D. J. Pietrzyk, *Anal. Chem.*, **44**, 676 (1972).
(27) A. V. Kiselev, in "Hydrophobic Surfaces", F. M. Fowkes, Ed., Academic Press, New York, 1969.
(28) W. Hertl and M. G. Neuman, *J. Chromatogr.*, **60**, 319 (1971).
(29) O. L. Hollis, *J. Chromatogr. Sci.*, **11**, 335 (1973).
(30) A. C. Zettlemoyer, in "Hydrophobic Surfaces", F. M. Fowkes, Ed., Academic Press, New York, 1969.
(31) J. Paleos, *J. Colloid Interfac. Sci.*, **31**, 7 (1969).
(32) "Amberlite XAD-2", Technical Bulletin, Rohm & Haas Co., Philadelphia, Pa., 1972.
(33) A. L. McClellan and H. F. Harnsberger, *J. Colloid Interfac. Sci.*, **23**, 577 (1967).
(34) L. Pauling, "The Nature of the Chemical Bond", 3rd ed., Cornell University Press, Ithaca, N.Y., 1960.
(35) S. R. Sivaraja Iyer, A S. Chanekar, and G. Srinivason, in "Adsorption at Interfaces", K. L. Mittal, Ed., American Chemical Society, Washington, D.C., 1975, Chapter 6.
(36) J. Kielland, *J. Am. Chem. Soc.*, **59**, 1675 (1937).
(37) R. A. Robinson and R. H. Stokes, "Electrolyte Solutions", Butterworth, London, 1959.
(38) Y. G. Berube and P. L. DeBruyn, *J. Colloid Interfac. Sci.*, **28**, 92 (1968).
(39) K. A. Kun and R. Kunin, *Polym. Lett.*, **2**, 587 (1964).
(40) M. Bier, "Electrophoresis", Academic Press, New York, 1959.
(41) F. Helfferich, "Ion Exchange", McGraw-Hill, New York, 1962, p 162.
(42) A. Frumkin, *Z. Phys. Chem.*, **109**, 34 (1924); *Chem. Abstr.*, **18**, 1934 (1924).
(43) A. Frumkin, S. Reichstein, and R. Kulvarskaja, *Kolloid Z.*, **40**, 9 (1926); *Chem. Abstr.*, **21**, 1042 (1927).
(44) W. B. Dandliker and V. A. de Saussure, in "The Chemistry of Biosurfaces", Vol. 1, M. L. Hair, Ed., Dekker, N.Y., 1971, Chapter 1.
(45) G. Schill, in "Ion Exchange and Solvent Extraction", Vol. 6, J. A. Marinsky and Y. Marcus, Ed., Dekker, N.Y., 1974, Chapter 1.
(46) D. W. Fuerstenau, in "The Chemistry of Biosurfaces", Vol. 1, M. L. Hair, Ed., Dekker, N.Y., 1971, Chapter 4.
(47) J. Th. Overbeek, in "Colloid Science", Vol. 1, H. R. Kruyt, Ed., Elsevier, New York, 1952, Chapter 6.
(48) R. Gloor and E. L. Johnson, *J. Chromatogr. Sci.*, **15**, 413 (1977).

RECEIVED for review August 31, 1978. Accepted January 17, 1979. This work was supported by the National Research Council of Canada and the University of Alberta.

Determination of Arsenic and Sulfur Species in Environmental Samples by Ion Chromatography

L. D. Hansen,* B. E. Richter, D. K. Rollins, J. D. Lamb, and D. J. Eatough

Department of Chemistry, the Thermochemical Institute, Brigham Young University, Provo, Utah 84602

An eluent, 3.5 mM Na_2CO_3–2.6 mM NaOH, has been developed for anion chromatography. It was found to be better suited to anion determination in environmental samples than a HCO_3^-–CO_3^{2-} eluent. This eluent was effective in the determination of AsO_4^{3-} concentrations down to 0.3 μM and of some As(III) species analyzed as AsO_4^{3-} following oxidation. Total As levels in smelter flue dust samples determined by this method agree with those determined by X-ray methods. Oxidation of SO_3^{2-} to SO_4^{2-} by O_2 in the eluent stream complicates the determination of SO_3^{2-} and probably makes this method unreliable for the direct determination of SO_3^{2-} in complex mixtures. Fe(III) present in SO_3^{2-} solutions catalyzed the oxidation to SO_4^{2-}. The addition of Cu(II) also increased the rate of oxidation of SO_3^{2-}, not only of the sample to which it was added, but also of subsequent samples containing no Cu(II).

Ion chromatography as developed by Small, Stevens, and Bauman (*1*) is rapidly becoming an accepted method for the determination of anions in complex mixtures (*2–5*). However, few studies have been made to thoroughly examine possible systematic errors and interferences or to attempt to optimize the operating conditions for a particular type of sample.

The purpose of this paper is to report (i) the development of an eluent which is better suited to the determination of some of the anions commonly found in environmental samples than the eluent currently being used by most laboratories, (ii) methods for the determination of arsenate, arsenic(III) oxides, arsenic sulfide, and total inorganic arsenic, and (iii) a number of interferences in the determination of sulfite caused by the oxidation of sulfite to sulfate which can result in large errors under some conditions.

EXPERIMENTAL

Equipment. A Dionex model 10 ion chromatograph equipped with the standard Dionex 3 × 150 and 3 × 250 mm anion separator columns, a 6 × 250 mm suppressor column, and a 0.1-mL sample loop was used for all experiments. Most experiments were run at a pump rate of 1.15 mL/min (15%) using an eluent of 3.5 mM Na_2CO_3–2.6 mM NaOH. A Hewlett-Packard model 1700B recorder with 1-V span was used to record the output. Concentrations were determined from peak heights.

Chemicals. All solutions were prepared in distilled water using reagent grade chemicals unless otherwise stated. All standard solutions were prepared by weight. Solutions of Na_2SO_3 were prepared in distilled water which had been purged with argon for at least 1 h and were kept under argon in glass bottles after preparation. Standard solutions which were used to calibrate the instrument response for SO_3^{2-} in the studies included in this paper were prepared by weight from $HOCH_2SO_3Na$ (98% Aldrich). This addition compound of formaldehyde with $NaHSO_3$ is stable toward air oxidation and hydrolysis in slightly acidic solutions, but decomposes rapidly to give sulfite ion in basic solution. For many applications, this adduct can serve as a very convenient standard for SO_3^{2-}. The following reagent grade chemicals were also used: Na_2SO_4, anhydrous (J. T. Baker); $NaHSO_3$ (MCW); As_2O_5 (Baker and Adamson); As_2S_3, 99% (Rocky Mountain Research); Na_2SO_3, anhydrous (MCW); As_2O_3 (Baker and Adamson); cacodylic acid, $(CH_3)_2AsO_2H$ (K & K Labs); and sodium methylarsenate, $Na_2CH_3AsO_3$ (preparation described in Ref. 6).

Table I. Elution Times for Anions Commonly Found in Environmental Samples

	elution time in minutes[a]		
	standard eluent[b]		our conditions[c]
ion	500-mm column	250-mm column	250-mm column
F^-	2	1.5	3.9
$HCOO^-$	3		4.2
Cl^-	3	2.2	4.7
NO_2^-	4	2.5	5.5
PO_4^{3-}	8	3.7	15.5
Br^-	9	4.0	7.8
SO_3^{2-}	16	6.0	7.8
NO_3^-	14	4.4	8.5
SO_4^{2-}	18	7.3	10.8
AsO_4^{3-}	17[d]	6.5[d]	22–27

[a] Elution times vary with individual columns, the age of the column, and the concentration of the ion. Therefore the times given are only illustrative and intended to show the approximate separation times and the order of elution of the ions. [b] Standard eluent means 3.0 mM $NaHCO_3$–2.4 mm Na_2CO_3 at 2.3 mL/min (30%) flow rate. The elution times for the 500-mm column are taken from the Dionex literature, those for the 250-mm column are from this study. [c] Our conditions refers to the conditions described in the Experimental section. [d] Reference 7.

RESULTS AND DISCUSSION

The anions which are frequently found in environmental samples and which are readily analyzed by automated ion chromatography are given in Table I together with their approximate elution times using both the standard HCO_3^-–CO_3^{2-} eluent and the OH^-–CO_3^{2-} eluent described here. An OH^-–CO_3^{2-} eluent similar to that described here has previously been used by Stevens et al. (*3*) in the analysis of boiler blow-down water. Table I and Figure 1 illustrate the following advantages of the OH^-–CO_3^{2-} eluent over the commonly used HCO_3^-–CO_3^{2-} eluent for environmental samples. First, phosphate comes off the column after sulfate and hence causes less interference in the crowded region of the chromatogram between the nitrite peak and the sulfate peak. Second, better resolution of sulfite from sulfate is obtained, thus preventing high concentrations of sulfate from obscuring the sulfite peak. These two effects allow the use of shorter columns and lower pump rates, thus providing faster determinations without loss of resolution. Lower pump rates result in the use of less eluent and lengthen the effective run time before regeneration of the suppressor column is necessary. In addition, it was found that this eluent is effective in the determination of arsenate, as described below. Potential disadvantages of the OH^-–CO_3^{2-} eluent are: (1) a high concentration of nitrate or the presence of bromide can obscure a small sulfite peak and (ii) the retention time of the nitrate peak is not as constant with the OH^-–CO_3^{2-} eluent as with the HCO_3^-–CO_3^{2-} eluent.

Arsenic Determination. It was discovered that it is possible to determine arsenate ion concurrently with the other anions using the OH^-–CO_3^{2-} eluent and short columns (150

0003-2700/79/0351-0633$01.00/0 © 1979 American Chemical Society

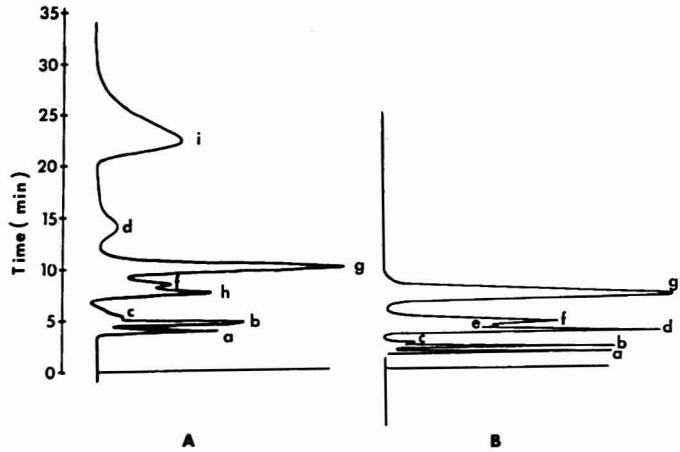

Figure 1. Anion chromatogram using OH^-–CO_3^{2-} eluent (A) at 15% pump rate, and using standard HCO_3^-–CO_3^{2-} eluent (B) at 30% pump rate. (a) F^-, (b) Cl^-, (c) NO_2^-, (d) PO_4^{3-}, (e) Br^-, (f) NO_3^-, (g) SO_4^{2-}, (h) SO_3^{2-}, (i) AsO_4^{3-}

+ 250 mm). Table II gives the results obtained using the 15% pump flow rate. The lowest concentration of arsenate measured under these conditions, 0.024 mM or 1.8 ppm As, gave a peak height which was twice the base-line noise. Thus it is clear that this method can be used to determine arsenic simultaneously with the other species listed in Table I at the trace levels commonly encountered in many environmental studies.

The sensitivity of the ion chromatographic technique for AsO_4^{3-} can be enhanced by increasing the pump rate from 15% to 30% using the OH^-–CO_3^{2-} eluent described. At this flow rate, it was observed that the retention time for AsO_4^{3-} is considerably shortened (to approximately 9 min, see footnote a, Table I) and the AsO_4^{3-} peak is sharper and narrower. Under these conditions, sensitivity for AsO_4^{3-} was found to be 0.14 mM/μmho which is 2.7 times higher than that found using the same eluent at the 15% pump rate (see footnote b, Table II). This higher sensitivity improved the limit of concentration measurable by this technique to 0.3 μM AsO_4^{3-} or 25 ppb As.

The ion chromatograph shows no response to arsenite because arsenious acid is too weakly ionized in the detector. However, some As(III) species can be determined after oxidation to arsenate. This oxidation is conveniently carried out using hydrogen peroxide in basic solution which leaves no troublesome anions in the solution after the oxidation step is completed. In our experiments, 5 mL of 0.1 mM As_2O_3 solution was oxidized by addition of 5 mL of 30% H_2O_2, 0.1 mL of 50% NaOH solution, and 5 mg of MnO_2 which served as a catalyst for the decomposition of H_2O_2. Without addition of NaOH, the oxidation was found to be incomplete. Solid As_2S_3 was unaffected by the 0.5% NaOH solution but did dissolve in more basic (5% NaOH), more concentrated H_2O_2 (10 mL 30% H_2O_2 + 1 mL 50% NaOH).

The oxidation treatments described above were found to be ineffective in converting cacodylic acid ($(CH_3)_2AsOOH$) or methyl arsonic acid ($CH_3AsO(OH)_2$) to arsenate ion. When dissolved in water, cacodylic acid could be determined directly under our conditions. It was observed to give a negative peak at about 5 min at the 15% flow rate. Methyl arsonic acid on the other hand could be determined directly. However, it was retarded by the suppressor column and this broadened the peak which emerged shortly before sulfate.

Table II. Determination of Arsenate Concurrent with Other Anions by Ion Chromatography[a]

concentration taken, (μmol AsO_4^{3-}/mL	peak height, μmho: measured	peak height, μmho: calculated from least squares line[b]	deviation, μmho (calcd − measd)	retention time, min
1.888	4.89	5.02	0.13	22
1.888	5.04	5.02	−0.02	
0.944	2.63	2.49	−0.14	24.5
0.944	2.63	2.49	−0.14	
0.472	1.30	1.23	−0.07	25.5
0.472	1.20	1.23	0.03	
0.236	0.55	0.60	0.05	26
0.236	0.50	0.60	0.10	
0.189	0.45	0.48	0.03	26
0.189	0.44	0.48	0.04	
0.094	0.23	0.22	−0.01	26.5
0.094	0.22	0.22	0.00	
0.047	0.114	0.095	−0.19	26.5
0.047	0.120	0.095	−0.25	
0.024	0.036	0.034	−0.02	27
0.024	0.036	0.034	−0.02	

[a] Run under conditions described in the Experimental section at 15% pump rate. [b] The linear least squares regression line for these data is $C_{AsO_4^{3-}} = (0.374 \pm 0.004) \times$ μmhos + (0.011 ± 0.009) where the peak to peak base-line noise is ~0.003 μmho which corresponds to 0.001 μmol of AsO_4^{3-}/mL.

In these procedures, care must be taken to run arsenic blanks on all reagents added (H_2O_2, NaOH, MnO_2) and to verify that the ion-exchange columns do not contain oxidizable impurities. We have noted that aged and heavily used columns do not give reproducible results for arsenate ion. This is apparently caused by reduction of the As(V) as it passes through the column. The columns can be checked for this problem by injecting a solution of 1 mM arsenate and, as soon as this peak is eluted, injecting a standard 0.1 mM arsenate solution. The injection of the standard is immediately repeated and, if the second injection of the standard solution gives a significantly smaller peak, the columns should be replaced.

Copper and lead smelter flue dusts which had previously been subjected to detailed analysis (8) were used to test the applicability of these ion chromatographic procedures for As in environmental samples. Results of determinations of AsO_4^{3-} and oxidizable As(III) concentrations in the smelter flue dust samples are presented in Table III. The OH^-–CO_3^{2-} eluent was used at a pump rate of 30% to collect these data.

The concentration of AsO_4^{3-} in the flue dust samples was obtained by analysis of a water extract. Three different oxidizing treatments were tried to determine reduced As species. The first involved addition of 5 mL of 30% H_2O_2, 0.1 mL of 50% NaOH, and 5 mg of MnO_2 to 5 mL of the water extract. In every case, this treatment was found to give more AsO_4^{3-} than was present in the original untreated water extract. This increase is a measure of the water soluble As(III) present in the solid sample. The second treatment involved extraction of the solid sample with 15% H_2O_2, 0.5% NaOH, and 5 mg of MnO_2. This extraction procedure consistently gave the highest yield of oxidizable arsenic. As illustrated in Table III, in every case except Pb-5, the total arsenic measured in the 15% H_2O_2–0.5% NaOH extract compared favorably with the total arsenic determined by proton induced X-ray emission spectroscopic analysis of aqua regia digests of the various flue dusts (8). The extraction of Pb-5 was repeated with essentially the same result. The third treatment with 30% H_2O_2, 5% NaOH gave unexpectedly lower results. This fact seems somewhat inconsistent with the observation that this treatment was the only one effective in dissolving As_2S_3. However, it is possible that the highly basic character of this extractant results in the formation of insoluble oxides of metals in the flue dust samples which prevents the complete extraction of arsenic from the solid flue dust. This effect would not be observed with pure As_2S_3. The effectiveness of this extractant in determining arsenic in As_2S_3 may be explained by its unique ability to wet the As_2S_3, and thus allow its oxidation and dissolution. Clearly the advantage of this last extraction technique in determining As in As_2S_3 is outweighed by the failure of the method to extract As from real environmental samples.

The following conclusions may be drawn from the experiments described above concerning arsenic determination in environmental samples by the ion chromatographic techniques using the OH^-–CO_3^{2-} eluent and H_2O_2 digestion. First, As(V) may be determined directly in water extracts of solid samples or in water samples. Second, extraction of solid samples with 15% H_2O_2–0.5% NaOH in the presence of catalytic amounts of MnO_2 will in most cases give a reliable measurement of total inorganic arsenic. Third, treatment of aqueous samples with 15% H_2O_2–0.5% NaOH oxidant probably results in quantitative conversion of water soluble As(III) species to measurable AsO_4^{3-}. Fourth, cacodylic acid is not determinable either directly or by the given oxidation techniques. Fifth, methylarsonate ion is not well resolved from sulfate ion under the conditions used in this study, but could probably be determined under other conditions.

Sulfite Determination. Our results lead us to the conclusion that the quantitative determination of SO_3^{2-} by ion chromatography using the present Dionex Instrument must be approached with caution because of the instability of sulfite toward oxidation, particularly when metal ions are present. It should be noted that complete removal of O_2 from the system probably will not eliminate the oxidation of sulfite by metal ions. Difficulties with SO_3^{2-} determination by this technique were alluded to earlier by Stevens et al. (3). In our own laboratory, problems with sulfite determinations were first noted when it was observed that while a carefully prepared (anaerobic) 2.5 mM solution of Na_2SO_3 gave a chromatogram indicating that one half of the sulfite had been oxidized to sulfate, a tenfold dilution of the same solution gave a chromatogram indicating that only about one tenth of the sulfite had been oxidized to sulfate. If anything, the dilution procedure would have been expected to result in a greater degree of oxidation than was present in the original solution. Figure 2 shows how the ratio of sulfate to sulfite as determined from the chromatogram depends on the concentration of sulfite injected. The effect as seen in Figure 2 is apparently caused by oxidation of the sulfite by oxygen present in the eluent. Since the Dionex instrument uses Teflon flow lines which are permeable to oxygen, this oxidation problem cannot be overcome by purging the oxygen from the eluent in the reservoir. Sulfite was also found to be slowly oxidized during the time that it was left in the Teflon sample loop of the Dionex instrument.

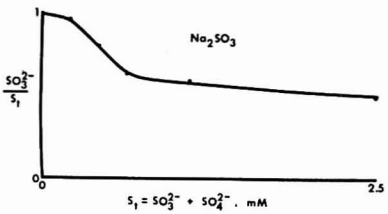

Figure 2. Fraction of total sulfur measured in the sulfite peak as a function of total sulfur. The sulfur was injected into the ion chromatograph as a Na_2SO_3 solution in Ar purged, distilled water. All Na_2SO_3 solutions were prepared by dilution of the most concentrated one shown

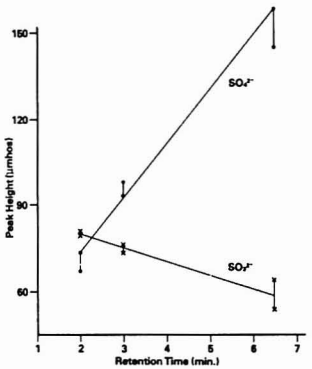

Figure 3. Peak heights for sulfite and sulfate as a function of retention time. The retention time was varied by varying the eluent pump rate. The sample injected was a 1 mM Na_2SO_3 solution prepared in Ar purged, distilled water

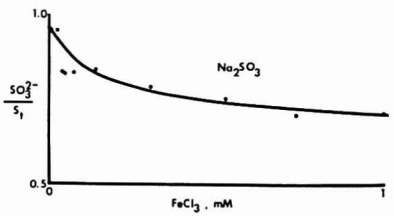

Figure 4. Fraction of total sulfur measured as sulfite as a function of the concentration of $FeCl_3$ in the solution of 0.25 mM Na_2SO_3 injected

Table III. Determination of Arsenic in Copper and Lead Smelter Flue Dusts by Ion Chromatography Using Various Extracting Solutions

	AsO_4^{3-} found, μmol/mg				
sample[a]	H_2O[b]	H_2O then dil. NaOH + H_2O_2[c]	dil. NaOH – H_2O_2[d]	concd NaOH – H_2O_2[e]	As total[f]
Cu-1	0.008	0.131	0.50	0.094	0.51 ± 0.13
Cu-2	0.113	0.66	6.4	1.47	6.9 ± 0.3
Pb-3	0.018	0.188	0.91	0.153	0.76 ± 0.05
Pb-5	n.d.	0.0008	0.045, 0.053	0.012	0.20 ± 0.03

[a] See ref. 8 for a complete description of the samples. [b] 10 mg extracted with 10 mL of H_2O for 20 min in an ultrasonic bath. [c] 5 mL of water extract as in footnote b + 5 mL 30% H_2O_2 + 0.1 mL 50% NaOH + 5 mg MnO_2. [d] 10 mg dust + 5 mL H_2O + 5 mL 30% H_2O_2 + 0.1 mL 50% NaOH + 5 mg MnO_2. [e] 10 mg dust + 10 mL 30% H_2O_2 + 1 mL 50% NaOH + 5 mg MnO_2. [f] As determined in an aqua regia digest by proton induced X-ray emission spectroscopy; ref. 8.

In order to better characterize the rate of oxidation of sulfite during passage through the chromatograph, solutions of $NaHSO_3$ prepared in Argon purged water and stored under argon were analyzed at different eluent flow rates. The results are shown in Figure 3. It is clear from the data in Figure 3 that the longer the residence time of sulfite in the columns and in the flow tubing, the more it is oxidized. This trend is very reproducible in that it is possible to raise or lower the measured SO_3^{2-} concentration of the same solution from the value obtained in a previous determination simply by raising or lowering the eluent pump rate.

The oxidation of sulfite to sulfate by dissolved oxygen is apparently not a continuous process in the separator column in the absence of metal ions. If it were, the sulfite peak would show excessive tailing between the sulfite and sulfate peaks since sulfite oxidized at mid-column would elute more slowly. Since this is not the case, we conclude that sulfite is not oxidized during passage through the separator column. Further oxidation occurs as sulfite passes between the exit of the separator column and the detector, however. This is demonstrated by the observation that the sulfite peak is sometimes 20% higher than it should be. The excessive peak height can only be explained by the fact that H_2SO_4 has a much higher conductivity than H_2SO_3.

Since the reaction of sulfite with oxygen is catalyzed by metal ions (*9*), the effects on sulfite oxidation of adding $FeCl_3$ and $CuCl_2$ to the system were determined. The addition of $FeCl_3$ solution to Na_2SO_3 solutions increased the rate of the oxidation reaction, as shown in Figure 4. Indeed, no SO_3^{2-} peak was found in the chromatogram resulting from injection of samples of 0.25 mM Na_2SO_3 which were also 1 mM HCl and 2.5 mM $FeCl_3$. These experiments with $FeCl_3$ were run using solutions which were mixed just prior to injection into the chromatograph. The oxidation of SO_3^{2-} by Fe(III) in acidic, anaerobic solutions requires hours to reach equilibrium (*10*). We have previously shown (*8*, *11*) that analysis of environmental samples which contain stable transition metal–S(IV) complexes does not give a measurable sulfite peak, even on very freshly extracted samples.

The addition of $CuCl_2$ to a sample was also found to increase the apparent rate of oxidation, not only of the sample to which it was added, but also of subsequent samples which did not contain $CuCl_2$. The injection of sulfite subsequent to an injection of $CuCl_2$ produced a chromatogram which also contained a sizable chloride peak although none was present in the injected sample. The apparent mechanism of this effect

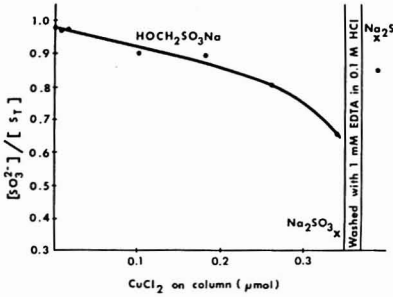

Figure 5. Fraction of total sulfur measured as sulfite as a function of the total amount of $CuCl_2$ previously passed through the ion chromatograph. (●) $HOCH_2SO_3Na$, (X) Na_2SO_3

is that $CuCl^+$ is bound to residual sulfonate groups in the anion-exchange resin. When these Cu(II) ions come in contact with sulfite, the copper is reduced to Cu(I), chloride is released, and the sulfite is oxidized to sulfate. The Cu(I) would then be oxidized back to Cu(II) by oxygen in the eluent.

Figure 5 presents the effects on the sulfite determination observed when various amounts of $CuCl_2$ were passed through the ion chromatograph prior to the injection of sulfite. In these experiments, two forms of sulfite were injected—Na_2SO_3 in argon purged, distilled water and $HOCH_2SO_3Na$ in distilled water. The latter compound does not hydrolyze at a significant rate below pH 7; however, it hydrolyzes rapidly at high pH values to give sulfite ion and formaldehyde. Thus the sulfite ion will be released into the eluent in the ion chromatograph only after the sample reaches the separator column. Because the formaldehyde adduct is not susceptible to air oxidation, these experiments enabled us to at least partially separate the effects of oxygen and of copper(II). From the data shown in Figure 5, it is clear that copper(II) does accumulate on the separator column and that the greater the amount of copper(II) present, the faster the oxidation of sulfite. After the Cu(II) is largely washed off the column with 1 mM EDTA in 0.1 M HCl, the SO_3^{2-} concentration measured is raised almost to that measured before addition of any Cu(II) to the column.

Thus, the accurate determination of sulfite in environmental samples using the present commercially available instrument requires constant eluent flow rates and the calibration of the instrument by standard additions to the unknown. Also, standard solutions of sulfite which do not contain stabilizing (antioxidant) additives such as formaldehyde must be run after each sample to verify that the column is free from interfering metal ions and to correct for the amount of sulfite oxidized to sulfate at the concentration in the unknown.

LITERATURE CITED

(1) H. Small, T. S. Stevens, and W. C. Bauman, *Anal. Chem.*, **47**, 1801 (1975).
(2) "Ion Chromatographic Analysis of Environmental Pollutants", E. Sawicki, J. D. Mulick, and E. Wittgenstein, Ed., Ann Arbor Science, Ann Arbor, Mich., 1978.
(3) T. S. Stevens, V. T. Turkelson, and W. R. Albe, *Anal. Chem.*, **49**, 1176 (1977).
(4) C. Anderson, *Clin. Chem.* (*Winston-Salem, N.C.*), **22**, 1424 (1976).
(5) J. Mulik, R. Puckett, D. Williams, and E. Sawicki, *Anal. Lett.*, **9**, 653 (1976).
(6) E. A. Lewis, L. D. Hansen, E. J. Baca, and D. J. Temer, *J. Chem. Soc., Perkin Trans. 2*, 125 (1976).
(7) R. Merrill and R. Stelber, in "Proceedings of Second National Symposium on Ion Chromatographic Analysis of Environmental Pollutants", U.S. Environmental Protection Agency, Research Triangle Park, N.C., in press.
(8) D. J. Eatough, N. L. Eatough, M. W. Hill, N. F. Mangelson, J. Ryder, L. D. Hansen, R. G. Meisenheimer, and J. W. Fischer, *Atmos. Environ.*, in press.
(9) D. A. Hegg and P. V. Hobbs, *Atmos. Environ.*, **12**, 241 (1978).
(10) P. K. Dasgupta, Louisiana State University, Baton Rouge, La. 70803, personal communication, 1978.

(11) D. J. Eatough, T. Major, J. Ryder, M. Hill, N. F. Mangelson, N. L. Eatough, L. D. Hansen, R. G. Meisenheimer, and J. W. Fischer, *Atmos. Environ.*, 12, 263 (1978).

RECEIVED for review December 11, 1978. Accepted January 29, 1979. We gratefully acknowledge support from the U.S. Department of Energy, Contract EY-76-S-02-2988.A002 and the Electric Power Research Institute, Contract RP1154-1. Contribution No. 156 from the Thermochemical Institute, Brigham Young University.

Theory of Concentration Effects in Gel Permeation Chromatography

Josef Janča

Institute of Macromolecular Chemistry, Czechoslovak Academy of Sciences, 162 06 Prague 6, Czechoslovakia

The change in elution volume following a change in the concentration of injected polymer solution in GPC is due to many contributing processes. In the theoretical model, three basic contributions are taken into account, namely, a change in the effective size of permeating molecules, and thus a change in the distribution coefficient according to the respective calibration curve; viscosity phenomena in the interstitial volume; and, finally, secondary exclusion. The first two contributions lead to an increase in elution volumes, while the last, secondary exclusion, causes reduction in elution volumes with increasing concentration. Changes in the concentration of injected polymer solution were also considered which occur directly at the beginning of the column due to the distribution between the mobile and the stationary phase, and also due to the longitudinal spreading. Mutual proportions between the individual contributions to the overall concentration effect were calculated. The relationships derived using dimensionless quantities may be interpreted as a calibration function explicitly involving the effect of concentration.

Concentration effects, i.e., the dependence of the elution volume and of the width of the elution curve on concentration and overall amount of injected polymer solution in gel permeation chromatography (GPC) have been observed in many works. Waters (*1*) supposed the increase in elution volume with increasing concentration to be due to the higher viscosity of injected solution, Boni et al. (*2, 3*) observed that the change in elution volume with a change in concentration was a linear function of the logarithm of molecular weight or of intrinsic viscosity. In the latter case, they obtained a single linear dependence for various polymers. Similar results were obtained by Lambert (*4*). The hypothesis of viscosity phenomena was supported by Goetze et al. (*5*), who injected a polymer solution in a solvent whose relative viscosity was higher than that of the solvent used as the mobile phase. According to them, viscosity phenomena cause a change in the elution volume, but not the whole change can be assigned to these phenomena. Moore (*6*) explained the viscosity phenomena as "viscous fingering". Ouano (*7*) stressed the effect of overloading of the column in the injection of solutions of mixtures of standard polymers having different molecular weights and high concentrations. Rudin (*8–10*) showed that the effective hydrodynamic volume of macromolecules in solution decreased with increasing concentration and that this effect must be taken into consideration in constructing a universal calibration graph. This hypothesis concerning the effect of concentration on the elution volume was supported also by other authors (*11–13*), who observed that the effect of concentration on the elution volume in a thermodynamically poor solvent (under the Θ conditions, when the effective dimensions of the macromolecular coil do not vary with concentration) was weaker. Using the latter observations, it was suggested that the thermodynamic quality of the solvent should be estimated from concentration effects (*14*). It was also observed that the mutual arrangement of the individual columns affected the concentration dependence of the elution volume (*15*), and that, with increasing flow of the solvent, the concentration dependence of the elution volume decreased (*16, 17*). An increase in the width of the elution curve with increasing concentration and volume of the injected polymer solution was observed by several authors (*18–20*). Hazell et al. (*21*) assumed (but did not prove) an increase in concentration effects with decreasing efficiency of the columns, which is at variance with further results, as is shown below. Hellsing (*22*) investigated the effect of concentration of the polymer present in the mobile phase on the elution volume of natural macromolecules. Bartick and Johnson (*23*) outlined the possibility of using differential GPC in the study of concentration effects, while Bakoš et al. (*24*) utilized the same method in the study of incompatibility of various polymers and concentration effects under such conditions. In some papers (*25–29*), concentration effects were interpreted as a consequence of the osmotic pressure at the boundary of the mobile and stationary phase, leading to shrinkage of the gel in the eluting zone (*27*) and/or redistribution of macromolecules of various sizes in the polydisperse sample (*28, 29*). Cantow et al. (*30*) observed exceptionally a stronger effect of concentration with samples having a broad distribution compared to those with a narrow distribution. Altgelt (*31*) assigns concentration effects at particularly high concentrations to secondary exclusion. The review just outlined shows that up to now no paper has been published in which the likely causes of concentration effects would be treated in a complex manner. In our earlier papers (*32–36*), concentration effects were studied both theoretically and experimentally as complex processes from various viewpoints and in various experimental arrangements. In this paper, we would like to offer a complete and unifying theory of concentration effects under conditions where the gel structure remains unchanged and where interactions such as adsorption, incompatibility, and others do not operate.

THEORY

Let us investigate the change in the distribution coefficient of a monodisperse polymer with a change in concentration.

0003-2700/79/0351-0637$01.00/0 © 1979 American Chemical Society

The formal equilibrium distribution coefficient in GPC is defined by

$$K_{GPC} = \frac{V_e - V_o}{V_i} \quad (1)$$

where V_e is the elution volume of the respective polymer at zero concentration, V_o is the interstitial volume, V_i is the pore volume. At a real concentration, K_{GPC} is changed by ΔK_{GPC}. With rigid gels, such as those used in most of the packings, changes in the structure and pore sizes need not be considered. Changes in the structure of soft gels have already been quantitatively formulated (27). Under these conditions, factors contributing to the change in ΔK_{GPC} are (a) ΔK_S caused by a change in the effective dimensions of permeating macromolecular coils with varying concentrations, and thus by a change in K_{GPC} according to the respective calibration function, (b) ΔK_V due to viscosity phenomena in the mobile phase, (c) ΔK_E due to secondary exclusion. It holds, then,

$$\Delta K_{GPC} = \Delta K_S + \Delta K_V + \Delta K_E \quad (2)$$

Let us first define some dimensionless quantities

$$\lambda = u/L, \iota = x/L, \xi = \sigma/V_i, \gamma = g/g_x \quad (3)$$

where u is the coordinate of the position of the maximum of the concentration profile in the direction of the column axis, x is the axial coordinate along the column, σ is the standard deviation of the Gaussian concentration profile expressed in this case in units of the elution volume, L is the column length, g is concentration (w/v), g_x is the critical concentration corresponding to the critical volume fraction ϕ_x of the polymer in solution, when the sizes of solvated macromolecules are identical with those observed in the θ conditions. Dimensionless quantities can, of course, be defined on the basis of retention times instead of elution volumes, but it is necessary that all dimensionless quantities be mutually consistent. The concentration profile on the column (i.e., distribution of polymer concentrations along the column axis) may be described by the Gaussian function

$$F(\iota) = \frac{1}{\xi\sqrt{2\pi}} e^{-(1/2)[(\iota-\lambda)^2/\xi^2]} \quad (4)$$

The overall variance of the concentration profile at the column end

$$\xi_T^2 = \xi_I^2 + \xi_D^2 \quad (5)$$

is equal to the sum of variances of contributions of the injected volume ξ_I^2 and of the dispersion caused by the column ξ_D^2. For the variance of the concentration profile with a maximum in the coordinate λ it holds, then,

$$\xi_\lambda^2 = \xi_I^2 + \lambda(\xi_T^2 - \xi_I^2) \quad (6)$$

Immediately after the injection on the column, the sample solution will penetrate not only the interstitial volume, but also the accessible volume of the pores; the original γ_I corresponding to the concentration of the injected sample is changed to γ'_I according to

$$\gamma_I V_o = \gamma'_I(V_o + \bar{K}_{GPC} V_i) \quad (7)$$

According to large experience with rigid porous packings such as silica gels or porous glasses, one may assume, with good approximation, that $V_i \approx V_o$; thus it holds

$$\gamma'_I = \frac{\gamma_I}{\bar{K}_{GPC} + 1} \quad (8)$$

$\bar{K}_{GPC}$ is the average formal distribution coefficient along the column. We also assume that all processes in the column proceed sufficiently quickly in the state of equilibrium.

For an arbitrary, i.e., maximum, average etc. γ_λ, if the maximum of the concentration profile is in the coordinate λ, it holds

$$\gamma_\lambda = \frac{\xi_I}{\xi_\lambda}\gamma'_I \quad (9)$$

Effect of Coil Expansion. The hydrodynamic volume of the solvated polymer is defined by the product $v\epsilon$, where v is the volume of unswollen coil and ϵ is a dimensionless swelling factor. Let the dimensionless quantity be defined as

$$v = v/v_{ES} \quad (10)$$

where v_{ES} is the volume of the just excluded coil (on the given column system) in the standard state (in the Θ solvent), where $\epsilon = 1$. Let the calibration function of the given column system be defined by the polynomial

$$K_{GPC} = P_n [\ln (v\epsilon)] \quad (11)$$

The calibration function thus defined by means of dimensionless quantities makes possible a simple comparison of experimental results obtained on various separation systems. In an infinitesimal interval, the calibration function is approximated by a straight line with the slope q, i.e., by

$$\frac{\partial K}{\partial \ln (v\epsilon)} = q \quad (12)$$

The just excluded coil is then defined as a minimum v_{ES} value for which $q = 0$. The dependence of ϵ on concentration is given by Equation 13, according to Rudin and Wagner (10)

$$\frac{1}{\epsilon} = \frac{1}{\epsilon_o} + \gamma\left(\frac{\epsilon_o - 1}{\epsilon_o}\right) \quad (13)$$

where $\epsilon = \epsilon_o$ at $\gamma = 0$, if (10)

$$\epsilon_o = \frac{[\eta]}{[\eta]_0} = \frac{KM^{a-0.5} M_o^{3/2}}{0.25\beta^3} \quad (14)$$

and $\epsilon = 1$, at $\gamma = 1$, if

$$[\eta]_0 = K_0 M^{0.5} \quad (15)$$

and

$$K_\Theta = 2.5 \times 10^{-1} \frac{\beta^3}{M_o^{3/2}} \quad (16)$$

where the intrinsic viscosity $[\eta]$ and molecular weight M under given conditions are determined by the Mark–Houwink equation with the constant K and exponent a

$$[\eta] = KM^a \quad (17)$$

which under the theta conditions is reduced in Equation 15. In preceding equations, M_o is half the molecular weight of the repeating monomer unit in a vinyl polymer, β (in Å) is the effective bond length (10). It also holds that

$$g_x = \phi_x M/N_o v \quad (18)$$

and

$$v = 4\pi[\eta]_0 M/3\phi' \quad (19)$$

where N_o is the Avogadro constant and the Flory constant (37) is $\phi' = 3.1 \times 10^{24}$.

The above may be summarized as

$$\Delta K_S = q \int_0^1 \ln (v\epsilon) d\lambda - q \ln (v\epsilon_o) \quad (20)$$

and after rearrangement

$$\Delta K_S = -q \ln \epsilon_o + q \int_0^1 \ln \epsilon \, d\lambda \quad (21)$$

Integrals in Equations 20 and 21 reflect the fact that the concentration in the zone moving in the column varies owing to the longitudinal spreading. Their values de facto equal the average values of integrated variables.

Let Equation 13 be transformed into

$$\epsilon = 1/(A + \gamma B) \quad (22)$$

where $A = 1/\epsilon_o$ and $B = (\epsilon_o - 1)/\epsilon_o$.

By substituting from Equations 6, 9, and 22 into Equation 21 and rearrangement, one obtains the equation

$$\Delta K_S = -q \ln \epsilon_0 - q \int_0^1 \ln \left[A + \frac{B\gamma'_1\xi_I}{\sqrt{\xi_I^2 + \lambda(\xi_T^2 - \xi_I^2)}} \right] d\lambda \quad (23)$$

the solution to which is

$$\Delta K_S = -q \ln \epsilon_o + q \left[\frac{B^2\gamma'^2_1\xi_I^2}{A^2(\xi_T^2 - \xi_I^2)} \ln \left(\frac{\xi_T A + B\gamma'_1\xi_I}{\xi_I A + B\gamma'_1\xi_I} \right) - \frac{B\gamma'_1 \xi_I}{A(\xi_T + \xi_I)} + \frac{\xi_I^2}{\xi_T^2 - \xi_I^2} \ln (A + B\gamma'_1) - \frac{\xi_T^2}{\xi_T^2 - \xi_I^2} \ln \left(\frac{\xi_T A + B\gamma'_1\xi_I}{\xi_T} \right) \right] \quad (24)$$

Details of Calculation, cf. Appendix. It would be possible, of course, to use another theory of the dependence of the effective sizes of macromolecules in solution on concentration, but the model used (*10*) is in good agreement with the experiment; neither would any other model cause any principal change in the suggested conception of concentration effects.

Viscosity Phenomena. It has been postulated (*31*) and experimentally proved (*32*) that

$$\Delta K_V = \kappa \int_0^1 \eta_{spec} \, d\lambda \quad (25)$$

where η_{spec} is the specific viscosity of polymer solution related to pure solvent, the constant κ is defined by Equation 29. The dependence η_{spec} on γ may be expressed in terms of virial expansion

$$\eta_{spec} = \sum_{i=1}^{n} a_i(\gamma)^i \quad (26)$$

where a_i are virial coefficients. Usually, expansion to $i = 2$ is sufficient with good approximation; a special case here is the Huggins equation

$$\eta_{spec} = [\eta]g + k_H [\eta]^2 g^2 \quad (27)$$

with the Huggins constant k_H.

Equations 25 and 26 thus yield

$$\Delta K_V = \kappa \int_0^1 (a_1 \gamma_\lambda + a_2\gamma_\lambda^2) d\lambda \quad (28)$$

where constant κ may be ascertained from the concentration dependence of K_{GPC} of totally excluded macromolecules

$$\kappa = \left(\frac{\partial K_{GPC}}{\partial \eta_{spec}} \right)_{excl} \quad (29)$$

By substituting from Equations 6 and 9 into Equation 28, one obtains

$$\Delta K_V = \kappa a_1\gamma'_1\xi_I \int_0^1 \frac{d\lambda}{\sqrt{\xi_I^2 + \lambda(\xi_T^2 - \xi_I^2)}} + \kappa a_2\gamma'^2_1\xi_I^2 \int_0^1 \frac{d\lambda}{\xi_I^2 + \lambda(\xi_T^2 - \xi_I^2)} \quad (30)$$

The solution to Equation 30 is

$$\Delta K_V = \kappa \left(\frac{2a_1\gamma'_1\xi_I}{\xi_T + \xi_I} + \frac{2a_2\gamma'^2_1\xi_I^2}{\xi_T^2 - \xi_I^2} \ln \frac{\xi_T}{\xi_I} \right) \quad (31)$$

Details of Calculation, cf. Appendix. The starting Equations 25 and 29 are of empirical character, since so far the nature of processes operating in the mobile phase and leading to the concentration dependence of the elution volume has not been explained in detail. What obviously operates here are frictional forces (*29*), trans-column velocity profiles (*38*), stagnant spaces in the column packing (*39*) and, with respect to the dependence of concentration, effects on the flow rate of the mobile phase (*33, 36*), also possibly effects of the non-Newtonian flow (*33, 40*) or turbulence (*41*). These problems are still being studied.

Secondary Exclusion. The distribution coefficient at zero concentration is given by the accessible pore volume, determined predominantly by the difference between the average pore size and the size of permeating macromolecules, while the effect of pore size distribution may be neglected (*42*).

$$K_{GPC} = \left(1 - \frac{R}{r}\right)^2 \quad (32)$$

r is the radius of a cylindrical pore, R is the radius of the macromolecular hydrodynamical equivalent sphere. Equation 32 expresses the fact that the migration of a sphere in the cylindrical space occurs in a limited volume of concentric cylinder, the radius of which is given by the difference between the radii of the sphere and of the cylindrical space. At a given concentration, the volume occupied by macromolecules must be deducted from the accessible pore volume

$$\varphi = \frac{g}{M} N_o v \epsilon \quad (33)$$

φ is the volume fraction of macromolecules in solution. For a given concentration, it holds, then,

$$K'_{GPC} = \left(1 - \frac{R}{r}\right)^2 (1 - \varphi) \quad (34)$$

whence

$$\Delta K_E = -K_{GPC}\varphi \quad (35)$$

In the integral form, i.e., with respect to the change in φ along the column

$$\Delta K_E = -\int_0^1 K_{GPC}\varphi d\lambda \quad (36)$$

By using the average value of $\bar{K}_{GPC}$ and substituting from Equations 6, 9, 22, and 33 into Equation 36, one obtains

$$\Delta K_E = -\frac{\bar{K}_{GPC} N_o v g_x \xi_I \gamma'_1}{M} \times \int_0^1 \frac{d\lambda}{A\sqrt{\xi_I^2 + \lambda(\xi_T^2 - \xi_I^2)} + B\gamma'_1\xi_I} \quad (37)$$

The solution to Equation 37 is

$$\Delta K_E = -\frac{2\bar{K}_{GPC} N_o v g_x \xi_I \gamma'_1}{M(\xi_T^2 - \xi_I^2)} \times \left(\frac{\xi_T - \xi_I}{A} - \frac{B\gamma'_1\xi_I}{A^2} \ln \left| \frac{A\xi_T + B\gamma'_1\xi_I}{A\xi_I + B\gamma'_1\xi_I} \right| \right) \quad (38)$$

For details of calculation, cf. Appendix.

DISCUSSION

In a preceding paper (*35*), we discussed in detail the contribution to the concentration effect due to a change in the effective dimensions of permeating macromolecular coils and the contribution of viscosity phenomena. Now some consequences are examined which follow from Equations 24, 31, and 38 with respect to the absolute values of ΔK_S, ΔK_V, and ΔK_E. The equations show (and it can be readily demonstrated by, e.g., numerical calculation) that the absolute values of ΔK become higher with the increasing injected volume of the polymer solution expressed in the parameter ξ_I. The concentration effects are even more pronounced with increasing column efficiency, that is, with decreasing difference between the parameters, $\xi_T - \xi_I$. Both conclusions are in agreement with experimental results (*32–34*). It has been found already in an earlier paper (*35*), by substituting experimental values into derived relationships, that under concrete experimental conditions ΔK_S:ΔK_V in the central part of the calibration curve was approximately 1:4, and that consequently the contribution of viscosity phenomena in the interstitial volume greatly prevails over that due to the change in the effective dimensions of permeating macromolecules. This ratio is virtually independent of the overall concentration, of the overall injected amount and of column efficiency (*35*). It varies of course with the varying value of q/κ, until for $q = 0$ in both extreme regions of the calibration curve, $\Delta K_S = 0$.

The ratio ΔK_E:ΔK_V is best illustrated by the following reasoning. For the viscosity of spherical particles, Einstein's equation (*43*)

$$\eta_{rel} = 1 + 2.5\varphi \tag{39}$$

is valid. Hence, Equation 25 may be rewritten to

$$\Delta K_V = 2.5\kappa \int_0^1 \varphi d\lambda \tag{40}$$

With respect to Equation 36, it holds

$$\frac{\Delta K_E}{\Delta K_V} = -\frac{K_{GPC}}{2.5\kappa} \tag{41}$$

Under such conditions, ΔK_E:ΔK_V depends only on κ for the given system, and on the respective distribution coefficient of the polymer in question. According to Equation 41, neither column efficiency, nor injected volume, nor concentration can affect this ratio, which varies only with K_{GPC}. If experimental data from earlier papers (*32, 34*) are used for the purposes of illustration, $\kappa \approx 0.5$ and the relationship

$$\frac{\Delta K_E}{\Delta K_V} = -\frac{K_{GPC}}{1.25} \tag{42}$$

is obtained. This means, that at $K_{GPC} = 1$ the viscosity phenomenon is almost compensated for by the effect of secondary exclusion, while at lower K_{GPC} values, ΔK_V prevails over ΔK_E, according to Equation 42. Since in real polymer solutions, η_{spec} depends on concentration according to Equation 26, used in the relationship 28, at higher concentrations the second quadratic term of the virial expansion becomes more operative, and ΔK_E:ΔK_V becomes also concentration-dependent, decreasing with increasing concentration. Similarly, this ratio depends on column efficiency and on the overall injected volume, which ensues from the fact that the integrals are not reduced as in Equation 41, but the effect of ΔK_V is stronger. ΔK_E:ΔK_V decreases with increasing column efficiency and with increasing injected volume. These findings have been verified and corroborated numerically.

In conclusion, the fact should be stressed that Equations 2, 24, 31, and 38 may be employed to express calibration functions; in other words, if ΔK_{GPC} from Equations 2, 24, 31, and 38 is added to the calibration function defined, e.g., by Equation 11, a relationship is obtained which allows one to calibrate the given separation system by using standard samples of various concentrations. There is no need to extrapolate to zero concentration, because the effect of concentration in the calibration function thus defined is expressed explicitly. Some applications of the above equations were published previously (*32–36*).

APPENDIX

A. Effect of the Expansion of the Permeating Coil. In Equation 23 we substitute the expression

$$\xi_I^2 + \lambda(\xi_T^2 - \xi_I^2) = m^2 \tag{A-1}$$

and

$$2m dm = (\xi_T^2 - \xi_I^2)\, d\lambda \tag{A-2}$$

The integration boundaries then are ξ_I and ξ_T. By rearrangement,

$$\frac{2}{(\xi_T^2 - \xi_I^2)} \int_{\xi_I}^{\xi_T} \ln\left(\frac{Am + B\gamma'_I\xi_I}{m}\right) m\, dm = \frac{2}{(\xi_T^2 - \xi_I^2)} \left[\int_{\xi_I}^{\xi_T} \ln (Am + B\gamma'_I\xi_I) m\, dm - \int_{\xi_I}^{\xi_T} m \ln m dm\right] \tag{A-3}$$

The second integral in square brackets has a direct analytical solution, while the first integral is solved by further substitution.

$$Am + B\gamma'_I\xi_I = n \tag{A-4}$$

and

$$dm = dn/A \tag{A-5}$$

with the integration boundaries $(A\xi_I + B\gamma'_I\xi_I)$ and $(A\xi_T + B_T\gamma'_I\xi_I)$. The first integral in square brackets on the right-hand side of Equation A-3 then becomes

$$\int_{(A\xi_I + B\gamma'_I\xi_I)}^{(A\xi_T + B\gamma'_I\xi_I)} \frac{n - B\gamma'_I\xi_I}{A^2} \ln n\, dn = \int_{(A\xi_I + B\gamma'_I\xi_I)}^{(A\xi_T + B\gamma'_I\xi_I)} \frac{n}{A^2} \ln n\, dn - \frac{B\gamma'_I\xi_I}{A^2} \int_{(A\xi_I + B\gamma'_I\xi_I)}^{(A\xi_T + B\gamma'_I\xi_I)} \ln n\, dn \tag{A-6}$$

Both integrals on the right-hand side of Equation A-6 have direct analytical solution. The indicated procedure used in solving them gives the final relationship 24.

B. Viscosity Phenomena. In Equation 30, a substitution identical with that used in A-1 is performed for both integrals, which thus have direct analytical solution.

C. Effect of Secondary Exclusion. In Equation 37 again, substitution identical with that in A-1 is performed, after which the integral obtained has direct analytical solution.

LITERATURE CITED

(1) J. L. Waters, *Am. Chem. Soc., Div. Polym. Chem., Prepr.*, **6**, 1061 (1965).
(2) K. A. Boni, F. A. Sliemers, and P. B. Stickney, *J. Polym. Sci., Part A-2*, **6**, 1567 (1968).
(3) K. A. Boni and F. A. Sliemers, *Appl. Polym. Symp.*, **8**, 65 (1969).
(4) A. Lambert, *Polymer* **10**, 213 (1969).
(5) K. P. Goetze, R. S. Porter, and J. F. Johnson, *J. Polym. Sci., Part A-2*, **9**, 2255 (1971).
(6) J. C. Moore, *Sep. Sci.*, **5**, 723 (1970).
(7) A. C. Ouano, *J. Polym. Sci., Part A-1*, **9**, 2179 (1971).
(8) A. Rudin, *J. Polym. Sci., Part A-1*, **9**, 2587 (1971).
(9) A. Rudin and H. W. Hoegy, *J. Polym. Sci., Part A-1*, **10**, 217 (1972).
(10) A. Rudin and R. A. Wagner, *J. Appl. Polym. Sci.*, **20**, 1483 (1976).

(11) Y. Kato and T. Hashimoto, *J. Polym. Sci., Part A-2*, **12**, 813 (1974).
(12) D. Berek, D. Bakoš, L. Šoltés, and T. Bleha, *J. Polym. Sci., Polym. Lett. Ed.*, **12**, 277 (1974).
(13) D. Berek, D. Bakoš, T. Bleha, and L. Šoltés, *Makromol. Chem.*, **176**, 391 (1975).
(14) T. Bleha, D. Bakoš, and D. Berek, *Polymer*, **18**, 897 (1977).
(15) P. M. James and A. C. Ouano, *J. Appl. Polym. Sci.*, **17**, 1455 (1973).
(16) J. N. Little, J. L. Waters, K. J. Bombaugh, and W. J. Pauplis, *J. Polym. Sci., Part A-2*, **7**, 1775 (1969).
(17) J. N. Little, J. L. Waters, K. J. Bombaugh, and W. J. Pauplis, *J. Chromatogr. Sci.*, **9**, 341 (1971).
(18) D. Braun and G. Heufer, *J. Polym. Sci., Part B*, **3**, 495 (1965).
(19) T. A. Maldacker and L. B. Rogers, *Sep. Sci.*, **6**, 747 (1971).
(20) J. Y. Chuang and J. F. Johnson, *Sep. Sci.*, **10**, 161 (1975).
(21) J. E. Hazell, L. A. Prince, and H. E. Stapelfeldt, *J. Polym. Sci., Part C*, **21**, 43 (1967).
(22) K. Hellsing, *J. Chromatogr.*, **36**, 170 (1968).
(23) E. G. Bartick and J. F. Johnson, *Polymer*, **17**, 455 (1976).
(24) D. Bakoš, D. Berek, and T. Bleha, *Eur. Polym. J.*, **12**, 801 (1976).
(25) L. W. Nichol, M. Janado, and D. J. Winzor, *Biochem. J.*, **133**, 15 (1973).
(26) H. Vink, *Eur. Polym. J.*, **9**, 887 (1973).
(27) P. A. Baghurst, L. W. Nichol, A. G. Ogston, and D. J. Winzor, *Biochem. J.*, **147**, 575 (1975).
(28) M. Schweiger and G. Langhammer, *Plaste Kautsch.*, **24**, 101 (1977).
(29) B. G. Belenkii and L. Z. Vilenchik, "Chromatography of Polymers" (in Russian), Chimia Edition, Moscow, 1978.
(30) M. Cantow, R. S. Porter, and J. F. Johnson, *J. Polym. Sci., Part B*, **4**, 707 (1966).
(31) K. H. Altgelt, *Sep. Sci.*, **5**, 777 (1970).
(32) J. Janča, *J. Chromatogr.*, **134**, 263 (1977).
(33) J. Janča and S. Pokorný, *J. Chromatogr.*, **148**, 31 (1978).
(34) J. Janča and S. Pokorný, *J. Chromatogr.*, **156**, 27 (1978).
(35) J. Janča, *J. Chromatogr.*, in press.
(36) J. Janča and S. Pokorný, *J. Chromatogr.*, in press.
(37) P. J. Flory, "Principles of Polymer Chemistry", Cornell University Press, Ithaca, N.Y., 1953.
(38) J. C. Giddings, *J. Gas Chromatogr.*, **1**, 38 (1963).
(39) C. Horvath and H. J. Lin, *J. Chromatogr.*, **126**, 401 (1976).
(40) J. W. Daily and G. Bugliarello, *Ind. Eng. Chem.*, **51**, 887 (1959).
(41) J. H. Knox, *Anal. Chem.*, 38, 253 (1966).
(42) M. Kubin and S. Vozka, *J. Polym. Sci., Part C*, in press.
(43) H. Morawetz, "Macromolecules in Solution", John Wiley and Sons, Inc., New York, 1965.

RECEIVED for review October 23, 1978. Accepted January 5, 1979.

Simultaneous Determination of Vitamin A Acetate, Vitamin D_2, and Vitamin E Acetate in Multivitamin Mineral Tablets by High Performance Liquid Chromatography with Coupled Columns

Stephen A. Barnett* and Leroy W. Frick

Mead Johnson & Company, 2404 Pennsylvania Avenue, Evansville, Indiana 47721

A reverse phase high performance liquid chromatographic method for the simultaneous determination of vitamin A acetate (retinol acetate), vitamin D_2 (ergocalciferol) and vitamin E acetate (*d,l*-α-tocopherol acetate) in multivitamin mineral tablets has been developed. The method requires dissolution of the sample in water–ethanol–pyridine solution (50:46:4), extraction of the vitamins into warm hexane, addition of cholesterol benzoate internal standard, and separation with a methanol–water gradient elution on coupled μBondapak Phenyl–μBondapak C_{18} columns. Detection of the vitamins and internal standard is monitored at 280 nm with separation accomplished in approximately 50 min. The assay is specific for each vitamin, and typical relative standard deviations for analysis of dosage forms are 0.059, 0.065, and 0.023 for vitamin A acetate, vitamin D_2, and vitamin E acetate, respectively.

Compendial procedures for the analysis of vitamins A, D, and E lack specificity, are time-consuming, and are not amenable to simultaneous determination from a single sample preparation. In general, analysis of each of these vitamins by compendial methodology requires saponification, solvent extraction, and may require sample cleanup by open column adsorption chromatography. Quantitation is accomplished by spectrophotometric or colorimetric analysis of column eluent. Results using compendial methods are dependent upon the manipulative skills of the individual analyst, and generally lack precision within and between laboratories.

Recent growth of reverse-phase high performance liquid chromatography has enhanced the analytical capability of the vitamin chemist. Procedures for the separation of mixed vitamin standards (A, D_2, E, and K) by high performance liquid chromatography are found throughout the literature (*1*). Thompkins and Tscherne have described the determination of vitamin D_2 in gelatin-protected vitamin A and D_2 beadlets using adsorption chromatography after sample dissolution in dimethyl sulfoxide (*2*). Osadca and Araujo have separated vitamin D_2 from vitamin D_3 on reverse phase packings in the presence of other vitamins in dosage forms (*3*). Vitamins A, D, and E, were separated quantitatively by interfacing high performance liquid chromatography with continuous flow analysis (*4*). To date, the other forms of separation analysis, such as gas–liquid chromatography and thin-layer chromatography, do not possess the combination of sensitivity and flexibility required for simultaneous determination of these compounds.

This paper describes a procedure for the simultaneous determination of vitamins A acetate, D_2, and E acetate from a single sample extract using high performance reverse phase liquid chromatography and internal standard techniques. The procedure eliminates saponification, lengthy extractions, and sample cleanup, is specific for the compounds of interest in the presence of interference, and has very good internal precision compared to current compendial methods. This technique provides the high degree of resolution, reproducibility, and ease of quantitation required in the industrial quality assurance laboratory. Increased use of such new technology will greatly reduce the imprecision and inaccuracies associated with vitamin analysis.

EXPERIMENTAL

Reagents and Solvents. Hexane, methanol, tetrahydrofuran, and pyridine were obtained from Burdick and Jackson, Muskegon, Mich. Retinol acetate *d,l*-α-tocopheryl acetate and cholesterol benzoate were obtained from Sigma Chemical Company, St. Louis,

0003-2700/79/0351-0641$01.00/0 © 1979 American Chemical Society

Mo. Ergocalciferol, was obtained from the United States Pharmacopeia at Rockville, Md. Millipore-filtered, double-distilled water was used in the preparation of all aqueous solutions. A mixed vitamin standard solution containing vitamin A acetate, 0.88 mg/mL, vitamin D_2, 2.5 μg/mL, vitamin E acetate, 0.65 mg/mL and cholesterol benzoate, 5 mg/mL, was prepared in a solution of methanol:tetrahydrofuran (50:50).

Instrumentation. The liquid chromatograph used was a Hewlett-Packard dual pump microprocessor controlled, Model 1084A, equipped with a Waters Associates, Model 440 UV Detector, operating at 280 and 254 nm. Analytical columns were Waters Associates μBondapak Phenyl, 10 μm, 3.9 mm × 30 cm, coupled with a μBondapak C_{18}, 10 μm, 3.9 mm × 30 cm. Separations were flow and solvent-programmed with an operating back pressure of approximately 32 MPa and were performed at ambient temperatures.

Sample Preparation. An accurately weighed sample, estimated to contain 10000–20000 units of vitamin A, 500–1000 units of vitamin D_2, and 35–65 units of vitamin E acetate was transferred to a 250-mL separatory funnel containing 25 mL of distilled water, 23 mL of absolute ethanol, 2 mL of pyridine, shaken vigorously for 2 min and placed in an air oven at 50 °C for 30 min. The sample was removed from the air oven, again shaken vigorously for 2 min. and extracted three times by gentle agitation with 50-mL portions of warm hexane (45–50 °C). The hexane extracts were collected and water-washed five times with 50-mL volumes of water, filtered through anhydrous sodium sulfate, and evaporated to dryness under reduced pressure with the aid of a warm (NMT 40 °C) water bath. A solution of methanol and tetrahydrofuran (62.5:37.5) was used to transfer the residue to a 10-mL volumetric flask containing 2.0 mL of cholesterol benzoate internal standard solution (5 mg/mL) dissolved in tetrahydrofuran.

RESULTS AND DISCUSSION

The compositions of multivitamin mineral preparations in tablet dosage form usually include raw material vitamins which are protected by a carbohydrate/protein matrix. Dissolution of this protective matrix with subsequent liberation of the vitamins is not generally a problem when compendial methods are employed, since the aggressive nature of the required saponification reaction facilitates removal of the vitamins. However, because of degradation during saponification and/or formation of reaction by-products which may interfere with spectrophotometric measurements, a simultaneous, quantitative extraction of the three vitamins is precluded.

Several buffered enzyme and solvent systems were examined to achieve simultaneous extraction of the vitamins from both raw material and dosage forms (5). In general, a solution of water, ethanol, and pyridine (50:46:4) was found to be an efficient means for dissolution of the vitamins (6). The suitability of several pure solvents and binary solvent systems was examined in order to achieve a twofold purpose; (a) to permit the simultaneous extraction of the dissolved vitamins and (b) to minimize extraction of interfering matrix components. Pure solvents ranging in polarity from petroleum ether through chloroform, as well as binary solutions of diethyl ether and hexane, were examined. A partition with warm hexane (45–50 °C) resulted in reproducible phase separations.

The reverse phase mode was selected for chromatographic separation of the vitamins because of their relatively nonpolar nature (7). Reverse phase systems also offer stability of operation and reproducibility. Separation is based on the partition of nonpolar vitamin molecules between a polar mobile phase and a nonpolar stationary phase. The mixed vitamin standard solution was chromatographed under a variety of isocratic and gradient conditions with methanol:H_2O, acetonitrile:H_2O, solvent pairs on Waters C_{18}, phenyl, amino, and cyano columns. Isocratic separations were also investigated using the Rheodyne RP-18 5μ column. Flow programming options were examined. Analysis of the various chromatographic systems indicate that a methanol–water gradient would provide favorable separation against time (8). The chromatogram shown in Figure 1 exemplifies the typical vitamin separation on the μBondapak C_{18} column with detection at 280 nm.

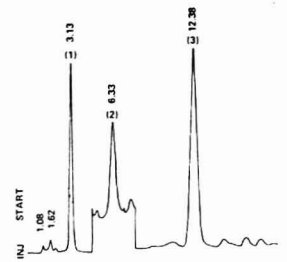

Figure 1. Chromatogram of mixed vitamin standard containing vitamin A acetate, 0.88 mg/mL (1); vitamin D_2, 2.52 μg/mL (2); and vitamin E acetate, 0.66 mg/mL (3) on a single μBondapak C_{18} column separation was solvent programmed from 91.5 to 100% MeOH over 19 min. Retention times appear at apex of each peak

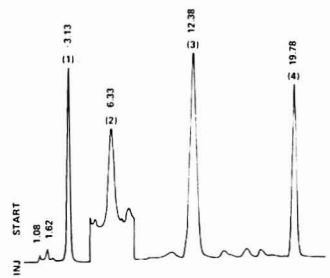

Figure 2. Chromatogram of mixed vitamin and internal standard containing vitamin A acetate, 0.88 mg/mL (1); vitamin D_2, 2.52 μg/mL (2); vitamin E acetate, 0.66 mg/mL (3); and cholesterol benzoate 1.0 mg/mL (4). This separation was performed using a single μBondapak C_{18} Column under conditions identical to Figure 1

The selection of a suitable internal standard to be used with this extraction and separation system was simplified by experience gained in this laboratory in the analysis of vitamin D_2 in natural products and in infant formula preparations (9). Since degradation of the vitamins A, D_2, and E usually results in the formation of more polar fragments, the choice of an internal standard is limited to a nonpolar compound eluting at the end of the chromatogram. The compound chosen for use as an internal standard must be stable in the solvent system selected and, if possible, be similar in molecular structure. Cholesterol benzoate satisfies these criteria. Figure 2 shows the separation of the vitamins from this internal standard.

A multivitamin mineral tablet blank (containing all tablet components except vitamins A, D, and E) was formulated to quantitate recovery of the extraction procedure. A sample of this ground tablet blank was added to a 250-mL separatory funnel containing 25 mL of water. A volume of the mixed vitamin standard was evaporated to dryness and transferred as a spike to the funnel with 23 mL of ethanol and 2 mL of pyridine. Specificity of the extracting procedure was examined concurrently by identical treatment of an unspiked tablet blank. The samples were dispersed in the water–ethanol–pyridine solvent and treated as the sample preparation. Aliquots of the spiked and unspiked tablet blank extract were chromatographed against the mixed vitamin standard. No

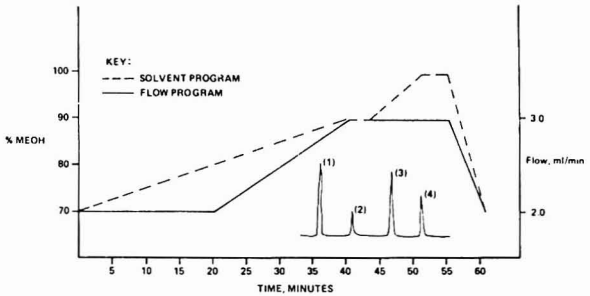

Figure 3. Profile of solvent and flow programs used with coupled μBondapak Phenyl–μBondapak C_{18} columns; insert illustrates elution of peaks of interest relative to profile. (1) Vitamin A acetate; (2) vitamin D_2; (3) vitamin E acetate; (4) cholesterol benzoate

Table I. Analysis of Multivitamin Mineral Tablets for Vitamins A Acetate, D_2, and E Acetate. Single μBondapak C_{18} Column

	Results		
	Vitamin A Acetate Units/Tablet	Vitamin D_2 Units/Tablet	Vitamin E Acetate Units/Tablet
	12800	1630	36
	13000	1800	34
	12600	1860	35
	12200	1780	35
Mean	12600	1770	35
Theoretical	12000	532	33

interferences from the tablet blank were detected in the vitamin or internal standard retention windows. Extraction recoveries of 95, 97, and 99% for vitamins A acetate, D_2, and E acetate, respectively, are typical. Tablets of finished dosage form (containing vitamins A, D, and E) were then analyzed using the internal standard technique.

Results shown in Table I for vitamin A and vitamin E acetates agree with theoretical formulation; however, results for vitamin D_2 are approximately $2^1/_2$ times the theoretical concentration. Investigation of this disparity for vitamin D_2 results led to the analysis of samples of raw material vitamins A and D_2 that were used in the dosage formulation. Results for vitamin A were in agreement with theory but vitamin D_2 results were approximately twice the theoretical concentration. Samples were subjected to analysis under the same chromatographic conditions but with detection at 254 nm. Chromatograms obtained at 254 nm also displayed significant interference with the vitamin D_2 peak. Procedures were reexamined to ensure that the substance apparently coeluting with the vitamin D_2 was not an artifact of sample preparation. Several additional extracting solvents were examined. All efforts for both raw material and dosage forms resulted in the presence of an interfering peak in the vitamin D_2 retention window.

Chromatographic conditions were then modified to improve the resolution of the separation system. Improved separations of complex multicomponent samples can be achieved by changing parameters controlling k'. Values for k' can be changed during a chromatographic separation by modifying temperatures, mobile phase compositions, stationary phase compositions, and/or the ratio of mobile to stationary phase (*10*). Separation of vitamin D_2 from infant formula products in this laboratory suggests that a significant improvement in separation is achieved by solvent and flow programming using coupled columns. Under conditions of gradient elution, the changing distribution of solute between mobile and stationary phase is separated into fractions on the first column

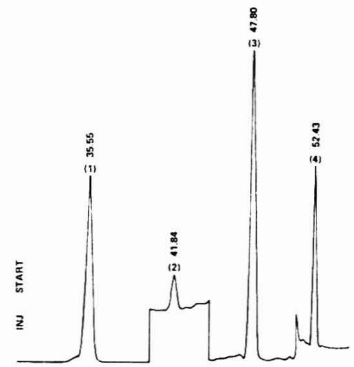

Figure 4. Chromatogram of mixed vitamin and internal standard solution, containing vitamin A acetate, 0.88 mg/mL (1); vitamin D_2, 2.52 μg/mL (2); vitamin E acetate, 0.66 mg/mL (3); and cholesterol benzoate, 1.0 mg/mL (4). This separation was performed on coupled μBondapak Phenyl–μBondapak C_{18} columns under conditions described in Figure 3

(μBondapak Phenyl) with increased separation occurring on the less polar surface of the second column (μBondapak C_{18}). A variety of flow and solvent programming conditions using methanol:H_2O were examined for use with coupled columns. Chromatographic conditions selected for use with this coupled column system are summarized in Figure 3.

A mixed vitamin standard solution containing internal standard was chromatographed under the conditions of solvent and flow programming on the coupled columns. Figure 4 provides an example of the separation of the mixed vitamin standards and internal standard. With detection at 280 nm, precision of the chromatographic system is indicated by ten injections of the mixed standard. Relative standard deviations of 0.007, 0.041, and 0.010 for vitamins A acetate, D_2, and E acetate, respectively, are typical. Reproducibility of the various retention times in the chromatographic system is ±0.5%. Samples of the tablet blank were prepared and chromatographed. No interference from blank excipients or actives was observed in the vitamin or the internal standard retention windows. Both raw material and samples of finished dosage form were then reassayed. Results for vitamin A and D_2 from the raw material agree with theoretical concentrations. Figure 5 provides a comparison of chromatograms of the raw material on single and coupled columns. Table II summarizes

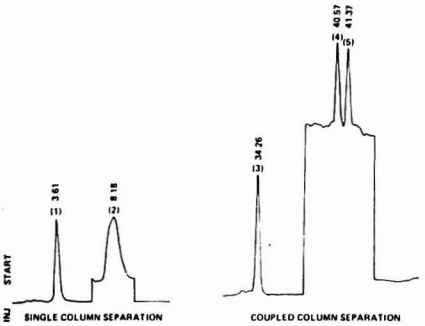

Figure 5. Comparison of chromatograms of raw material vitamin A and D beadlets on single and coupled column systems. Vitamin A acetate (1); vitamin D_2 and interference (2); vitamin A acetate (3); vitamin D_2 (4); interference (5)

Table II. Analysis of Multivitamin Mineral Tablets for Vitamins A Acetate, D_2, and E Acetate. Coupled Columns (μBondapak Phenyl-μBondapak C_{18})

	Results		
	Vitamin A Acetate Units/Tablet	Vitamin D_2 Units/Tablet	Vitamin E Acetate Units/Tablet
	10800	550	34
	11500	610	32
	10700	630	32
	11700	650	32
	11500	670	33
	11900	680	32
	12200	700	34
	12400	640	33
	12800	620	34
	12500	650	33
Mean =	11800	640	33
RSD =	0.059	0.065	0.023
Theoretical	12800	532*	33

*Based on minimum specification for Vitamin D_2 in raw material.

the results for the three vitamins from dosage form and Figure 6 provides comparison of the chromatograms using single and coupled column systems. No significant reduction of the interfering peak was realized by detection at 254 nm.

Reconciliation of the differences noted between the relative standard deviation of the standard and samples can be addressed as follows.

(1) The difference between relative standard deviation of standard and sample for vitamin E is insignificant. The relatively high concentration of vitamin E allows consistent data handling by the chromatographic system software.

(2) The difference between relative standard deviation of standard and sample for vitamin D_2 is directly related to the inability of the system software to reproducibly quantitate analytes of low concentration.

(3) The difference between standard deviation of standard and sample for vitamin A is probably caused by lack of uniform extraction. Concentration is not a factor. Vitamin A is the most polar of the three vitamins simultaneously extracted and, therefore, presents the greatest challenge to the extraction system.

Experience to date with the analysis of multivitamin mineral tablets by this method indicates that difficulties with vitamin D_2 analysis on single μBondapak C_{18} columns originates in the raw material vitamin A and D. Attempts to identify this interference continue. Some lots of raw material contain no such interfering substance, thus allowing separation of finished product extracts on single columns in less than 20 min. However, the concentration of the interfering substance and/or substances does not appear to be predictable between sample lots of raw material. At this point, combinations of flow and solvent programming on coupled columns appear necessary for the degree of separation required in the quality assurance environment. Separation of this order has not been achieved to date under isocratic conditions, at constant flow, on single columns or with surface modifying reagents (i.e., hexadecyltrimethyl ammonium bromide). Until raw material variation is either eliminated or controlled or until the required improvement in separation on single columns can be realized,

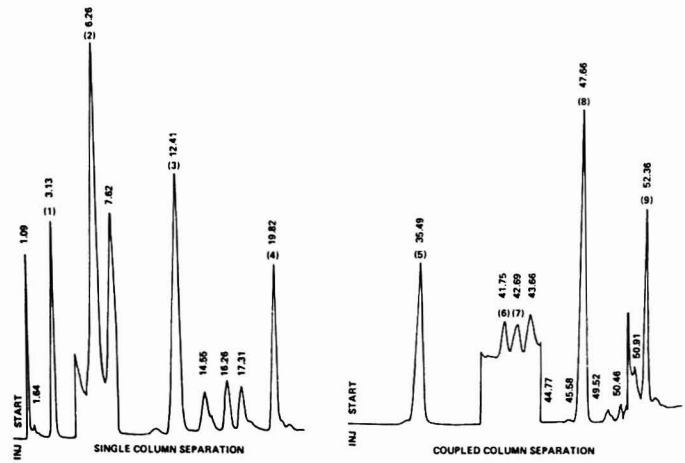

Figure 6. Comparison of chromatograms of dosage form assayed for Vitamins A, D, and E on single and coupled columns. (1) Vitamin A acetate, (2) vitamin D_2 and interference, (3) vitamin E acetate, (4) cholesterol benzoate, (5) vitamin A acetate, (6) vitamin D_2, (7) interference, (8) vitamin E acetate, (9) cholesterol benzoate

the coupled column system is the method of choice.

ACKNOWLEDGMENT

The authors are indebted to H. M. Baine, Jr. for assistance in the development and application of this method.

LITERATURE CITED

(1) Williams, R. C.; Schmit, J. A.; Henry, R. A. *J. Chromatogr., Sci.* **1972**, *10*, 494–501.
(2) Tompkins, D. F.; Tscherne, R. J. *Anal. Chem.* **1974**, *46*, 1602–4.
(3) Osadca, M.; Araujo, M. *J. Assoc. Off. Anal. Chem.*, **1977**, *60*, 993–7.
(4) MacDonald, J. C. *Am. Lab.* **1977**, (8), 69–76.
(5) Nunes, M.; Robinson, J. R., Mead Johnson Co., unpublished work, 1975.
(6) Barnett, S. A., Mead Johnson Co., unpublished work, 1976.
(7) Schmit, J. A; Henry, R. A.; Williams, R. C.; Dieckman, J. F. *J. Chromatogr. Sci.* **1971**, *9*, 645.
(8) Snyder, L. R.; Kirkland, J. J. "Modern Liquid Chromatography", American Chemical Society: Washington, D.C., 1973.
(9) Frick, L. W., Mead Johnson Co., unpublished work, 1977.
(10) Karger, B. L.; Snyder, L. R.; Horath, C. "An Introduction to Separation Science", John Wiley and Sons: New York, 1973.

RECEIVED for review August 24, 1978. Accepted January 29, 1979.

Universal Detector for Monitoring Organic Carbon in Liquid Chromatography

Rolf Gloor* and Hans Leidner

Federal Institute for Water Resources and Water Pollution Control, Ueberlandstr. 133, CH-8600 Dübendorf-Zürich, Switzerland

A detector based on the principle of measuring organic carbon as CO_2 after oxidation has been developed. The construction and principle of the system are described. Sensitivity is discussed and compared to other LC detectors (UV, RI). The minimum detectable concentration of organic carbon is 3×10^{-6} g/mL. Applications using Sephadex gel chromatography and reversed phase HPLC are shown. The detector is restricted to nonorganic solvents.

The majority of detectors used in liquid chromatography (LC) today (UV–vis, fluorescence, electrochemical) are sensitive only for specific types of compounds, rather than being universal in their use (*1–3*). Among the universally used detectors, only the refraction index (RI) has been employed extensively, while others (transport-FID, photoionization, LC–MS) are still in an experimental stage, or their sensitivity is insufficient for many applications. In addition to its lack of sensitivity, RI yields both positive and negative signals which make its use very questionable for monitoring complex mixtures whose components may coelute. Therefore, there is still a need for a universal type detector comparable to the flame ionization detector (FID) in gas chromatography (GC).

As part of a general effort in the biological department of our Institute to characterize organic water constituents, we have used gel permeation chromatography to gain information on the molecular weight distribution of organic matter in water samples of various types. Since dissolved organic carbon (DOC) is one of the key parameters in water analysis and gives the best information for comparison (*4*), we were searching for a detection system capable of monitoring the organic matter in the column effluent according to its carbon content. DOC is generally determined by oxidation of organic matter, followed by measurement of the CO_2 produced with infrared absorbance or by FID (after reduction to methane). Axt (*5*) reported earlier on an analyzer capable of measuring organic carbon continuously in water samples by using the infrared technique. Based on this work, we developed a simple and inexpensive on-line detector for monitoring organic carbon in column effluents.

EXPERIMENTAL

Construction of the Detection System. An illustration of the detection system is shown in Figure 1.

The oxidation oven (1) (a 50 × 2.5 cm ceramic tube, 98% Al_2O_3 standard unit, Koppers Düsseldorf, West Germany) is vertically inserted into a furnace (2) (Heraeus, 6450 Hanau, West Germany). The oven is filled for 30 cm with ceramic splinters approximately 5 mm in length. A 5-cm-long copper tube (3), loosely filled in the lower half with platinum wool and copper pieces, is placed on top of the ceramic splinters (4). The copper tube has an outer diameter that fits snugly inside the ceramic tube. Copper forms an oxide surface in the high temperature of the oven and thus acts as a catalyst for oxidation of organic carbon. The copper tube also shields the outer ceramic tube from temperature shocks caused by the inlet flow (which enters as drops, as discussed below). Both ends of the ceramic tube, which extend 10 cm out of the oven on each side, are sealed with Teflon stoppers. If the oven is properly insulated at both ends, the temperature of the Teflon stoppers should not exceed 100 °C. The sample and carrier gas inlet is a $^1/_4$-in. stainless-steel tube with a $^1/_{16}$-in. capillary tubing inserted into the top Teflon stopper. All connections (T-piece for carrier gas inlet, T-piece $^1/_{16}$-in. for splitter (5)) are standard Swagelok units. The condenser (6) is a specially constructed intensive water condenser with a built-in syphon unit (7). A 20-mm syphon efficiently closes the system from the atmosphere. The infrared cell used is a Beckman 865 infrared analyzer (8) (Beckman, Fullerton, Calif.).

Mode of Operation. The column effluent drops continuously into the hottest part of the oxidation oven (1) (800–900 °C) onto the platinum/copper oxide catalyst, which immediately oxidizes organic matter in the effluent to CO_2. A carrier air stream (CO_2-free) supplies the oxygen necessary for oxidation and carries the CO_2 vapor mixture into the condenser (6). The condensed water separates from the gas phase and leaves via the syphon (7) which prevents any access of atmosphere to the system. About 30% of the carrier gas also leaves through the syphon, while the rest passes the infrared cell (8) through a side channel (9). The concentration of CO_2 in the carrier gas is monitored on a strip chart recorder (11). The cell gas effluent reenters the system after having passed the CO_2 filter (10). Fresh air, replacing the 30% lost through the syphon, is added by a needle valve (12) to the carrier stream. The respective amount of fresh air added is calculated from the two flowmeter readings (13, 13′) and is adjusted to make up about 30% of the total carrier flow. This arrangement of the air circulation ensures a constant flow through the IR cell while the syphon acts as a pulse damper for pressure fluctuations caused by falling drops. It is not necessary to know the exact amount of carrier gas passing through the cell since the concentration of CO_2 in the carrier stream is measured rather than the absolute amount.

RESULTS AND DISCUSSION

Sensitivity. Figure 2 illustrates the excellent sensitivity of the detection system. The response of the detector for three different compounds (fructose, propionic acid, phenol) was compared to that of a UV absorbance detector (Varichrom,

0003-2700/79/0351-0645$01.00/0 © 1979 American Chemical Society

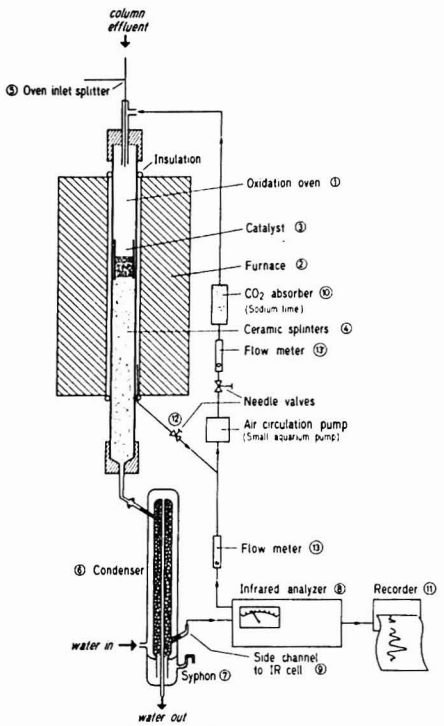

Figure 1. Schematic diagram of the DOC detection system

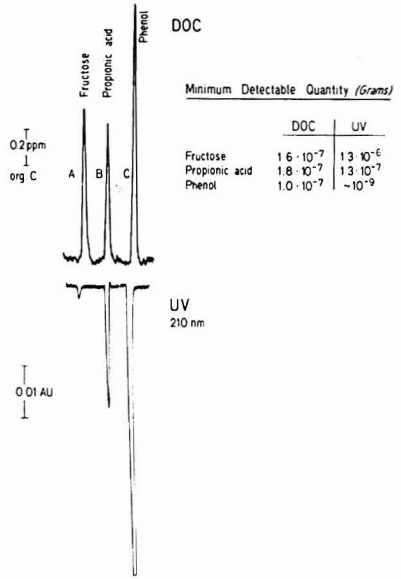

Figure 2. Sensitivity of DOC detection compared with UV detection. Injection of standard solutions into the detectors (for details, see text); flow rate 0.5 mL/min. (A) 2 μg of fructose in 0.5 mL of water; (B) 2 μg of propionic acid in 0.5 mL of water; (C) 2 μg of phenol in 0.5 mL of water. UV detector: Varichrom (Varian) set at 210 nm. DOC detector: as described, carrier gas 9 L/h, attenuation 3, gain 5

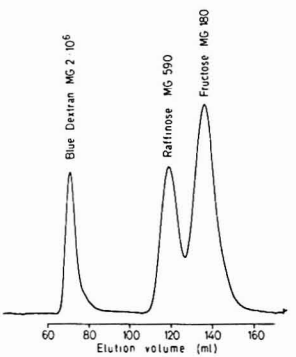

Figure 3. Molecular-size distribution of carbohydrates on Sephadex G 25: 0.5 mL of standard containing 30 μg of each, dextran blue, raffinose, and fructose. Column: Sephadex G 25 800 × 16 mm. Eluent: 10^{-2} M phosphate buffer (Na_2HPO_4/KH_2PO_4), pH 7.0. Flow rate: 1 mL/min. DOC detector: carrier gas 9 L/h, attenuation 2, gain 8

Varian). Aliquots (0.5 mL) of a 4-ppm solution of each compound were injected into a system consisting of a pump, a loop injector, and UV and DOC detectors connected in series. Distilled water was pumped through the system at a flow rate of 1 mL/min. The MDQ (minimum detectable quantities) calculated from the different detector responses for these three compounds indicate that DOC detection is superior in the case of a weak UV-absorbing compound (fructose at 210 nm). In the case of a medium UV-absorbing compound (propionic acid at 210 nm), the sensitivities of both detectors are comparable, while UV detection is superior for a strong UV-absorbing compound (phenol at 210 nm). Since the individual molecular carbon content and the peak volumes (2 mL) of the test compounds are known, a minimum detectable concentration (MDC) for organic carbon can be calculated from Figure 2 as 3×10^{-8} g/mL. Thus, DOC detection is approximately an order of magnitude greater in sensitivity than an RI detector (*1*, *2*).

For any organic compound, the MDQ value determined from the DOC detector signal depends exclusively on its molecular carbon content. Therefore, the detector response is predictable after calibration with a standard sample.

The DOC detector response was not precisely linear, owing to characteristics of the infrared analyzer used. The nonlinearity varied around 5%. In case a linearized output is an ultimate need, an optional linearizer board is available from the manufacturer (*6*).

Applications. Ever since the introduction of Sephadex in 1959, this gel has been used increasingly for separation of compounds in aqueous systems on the basis of molecular size. Figures 3 and 4 illustrate the use of DOC detection for monitoring Sephadex column effluent. Figure 3 represents a calibration run of a standard mixture on Sephadex G 25, while the chromatogram in Figure 4 shows an actual run of a concentrated ground water sample on the same column. As this detection system is destructive, the column effluent was split prior to entering the oven inlet. Thirty percent of the column effluent was monitored for DOC; the remainder was

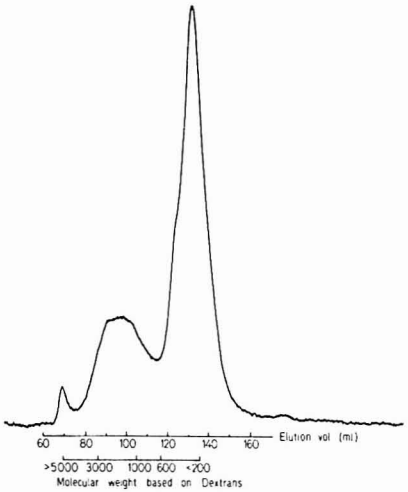

Figure 4. Molecular-size distribution of organics in ground water on Sephadex G 25: 1 mL concentrated ground water (concentration factor 450) from Zürich (Switzerland); organic carbon concentration in the original sample 0.4 mg/L

collected for other experimental purposes. The split ratio is determined by the length of the capillary tubing attached to the splitter exit (no. 5 in Figure 1). Except for carbonate, which was removed from the sample prior to injection, none of the inorganic species present in the ground water responded in the detector. Since only DOC is detected, Figure 4 represents a *quantitative* molecular-size profile of organic matter present in the ground water sample.

The detection system described here was optimized for the determination of organic carbon in the Sephadex column effluent. The heating capacity of the oven allows a flow rate up to 1.5 mL/min into the reaction tube. Higher flow rates will cause cooling in the reaction tube, and oxidation would not be completed. However, a larger oxidation tube coupled with a more powerful furnace could be used for monitoring larger flow rates without splitting.

Figure 5 shows a reversed phase separation of formic, acetic, and propionic acids on a highly efficient C_{18}-bonded phase column (Hibar C_{18}, Merck). Again, a UV and the DOC detector were connected in series with capillary tubing. The relatively large band-broadening which appears in the DOC chromatogram is caused by dead volume in the oxidation oven and condenser. It may be possible to optimize the system for high-resolution columns by minimizing the dead volume. Nonetheless, the separation indicates that DOC detection is adequate for use in modern high-pressure liquid chromatography. This is especially true if the loss in resolution is compensated by increased sensitivity or by the advantage of universal detection.

Maintenance. All parts of the detector, except the oxidation oven, are maintenance-free or need only minor maintenance, e.g., filter replacement. If distilled water is used as eluent, only the salts present in the sample will be deposited in the tube. In this case, the packing can last several months. By this time, the copper tube will be degraded by a slow deterioration of the oxide surface, and the oven packing or catalyst will need to be replaced. If a buffer solution is used as eluent, the packing may become blocked earlier, depending

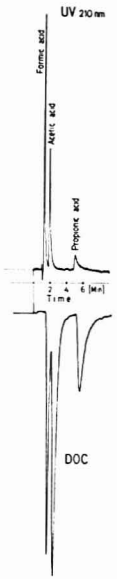

Figure 5. Reversed phase separation of formic, acetic, and propionic acids. Column: Hibar C_{18} (Merck). Pump: Altex 110 (Altex, Berkeley, Calif.). Eluent: 0.01 M $HClO_4$. Flow rate: 1 mL/min. Sample 20 μL standard solution containing 6 μg of each, formic, acetic, and propionic acids. UV detection: 210 nm, attenuation 0.1 AUFS. DOC detector: carrier gas 30 L/h, attenuation 3, gain 5. The base-line noise observed in the UV chromatogram is caused by the Altex pump which was used without a pulse damper

on the amount of salt entering the oven. In some cases, replacing the entire tube may be simpler and more cost-efficient than cleaning or replacing the old packing.

CONCLUSIONS

We have shown that DOC detection is a powerful tool in normal as well as in high-pressure liquid chromatography. The strict correlation of the detector response with the amount of carbon ensures true universal detection for any organic compound. Because no organic modifier can be used in the eluent, the detector will be most useful for applications in aqueous exclusion (gel permeation, gel filtration) and ion exchange chromatography.

ACKNOWLEDGMENT

The authors thank K. Wuhrmann for supporting the project and helpful discussions as well as J. A. Davis for reviewing the manuscript and P. Egli for suggestions in the construction of the detector.

LITERATURE CITED

(1) S. A. Wise and W. E. May, *Res./Dev.* 54–64 (Oct. 1977).
(2) E. L. Johnson and R. Stevenson, "Basic Liquid Chromatography", Varian Associates, Inc., Palo Alto, Calif., 1978, p 270.
(3) L. S. Ettre, *J. Chromatogr. Sci.*, **16**, 396 (1978).
(4) K. Wuhrmann, *Neue Tech.*, **12**, 461–470 (1973).
(5) G. Axt, *Vom Wasser*, **36**, 328–339 (1969).
(6) "Instruction Manual", Beckman Model 865, Infrared Analyzer, Beckman, Fullerton, Calif.

RECEIVED for review December 28, 1978. Accepted February 5, 1979.

Optical System for Gathering Simultaneous Time and Spatial Data from Transient Events

S. G. Salmon and J. A. Holcombe*

Department of Chemistry, The University of Texas at Austin, Austin, Texas 78712

A rotating disk containing multiple slits, which replaces a single field stop in a spectroscopic optical system, is used to provide simultaneous time and spatially resolved spectral information. The rotating disk serves as a spatial isolation wheel (SIW) and is used to gather data for three-dimensional profiles of absorbance vs. time vs. distance above a carbon filament atomizer. Profiles are obtained for the flameless absorption of Pb with pure Ar sheath gas and with Ar sheath gas containing 0.15% O_2. Changes in the appearance temperature of the absorption signal as well as the peak half-width are observed in the presence of O_2. The type of information available with the SIW and potential applications are reported.

The utility of using the astigmatism generated by a pair of spherical mirrors illuminated off-axis to improve resolution and maximize spectral throughput has been reported for spectrographic applications (*1*, *2*) and recently verified in our laboratory for use with photoelectric detection (*3*). To obtain optimal spatial resolution, the field stop is placed in the tangential image plane to isolate a certain height in the spectroscopic source. With a fixed slit, a time-dependent spectral profile can be obtained only at a single height in the source if transient phenomena are of interest. The spatial information available from a single event can be greatly increased by replacing the field stop with a set of slits continually scanning the spatial region in the tangential image plane. This set of moving slits is fabricated from a circular disk with multiple slits machined in it and serves as a spatial isolation wheel (SIW). In comparison with a static slit, the SIW has the capability of sampling the light at several heights in the spectroscopic source at regular time intervals during the course of a single event. Additionally, the use of multiple slits increases the amount of information which can be collected at these different spatial zones. In the present study, the spectroscopic source is a West-type electrothermally heated carbon filament atomizer backlighted by a hollow cathode lamp and used for absorption measurements.

In flameless atomic absorption spectrometry, interferences arise due to the sample matrix. Many of these observed interferences are believed to occur after the analyte has left the atomizer surface and are the result of gas phase reactions (*4–7*). To elucidate the fundamental reactions responsible for these interferences without prior knowledge of their origins, it is important to gain a basic understanding of the actual mechanisms responsible for the observed signal enhancements or depressions. For this purpose, it is useful to follow the time-dependent analytical signal after atomization and examine where and when it is affected by added interferents. In addition to the interference problem, the development of a satisfactory model describing the atomization process itself is desirable (*8–10*).

The information required to investigate these problems is best represented by a three dimensional profile of absorbance vs. time vs. distance above the atomizer surface. The large body of data necessary for such a profile would normally involve many shots to obtain time-resolved absorbance signals at individual heights above the atomizer surface. Because of the uncertainties inherent in the technique, the experiment must be repeated several times at each height of interest to obtain representative results. Even a moderate number of heights can lead to an almost unmanageable number of shots. During this period the surface characteristics of the graphite atomizer are changing irreversibly and may prohibit correlation between the first and last sets of data. With the aid of the SIW, the time and spatial information needed can be obtained much more rapidly and consistently than by the conventional procedure. To illustrate the usefulness of the SIW, the effect of O_2 in the sheath gas on the absorption of Pb was examined.

EXPERIMENTAL

Apparatus. The optical system used to obtain the astigmatic images and detect the absorption signal was described previously (*3*). Briefly, it consisted of two spherical concave mirrors with 800-mm focal length arranged in an under-and-over symmetric arm configuration. This focused the light from the spectroscopic source into a sagittal image on the monochromator entrance slit and a tangential image 12 mm in front of the entrance slit. The field stop was positioned in the tangential image plane. In this study, the output of the photomultiplier tube was digitized and stored using a Biomation model 805 waveform recorder which can handle 2048 eight-bit words. The carbon filament atomizer used was similar to the atomizer described by Alder and West (*11*). The filament was protected from ambient air by enclosing the sides of the atomizer with quartz windows. In the base of the atomizer, the sheath gas entered through a set of parallel channels which allowed laminar flow of Ar at gas velocities of up to 50 cm/s. All gas flow rates were controlled by precision rotameters. The atomizer power supply, developed in our laboratory, was operated in a mode which provided for a gentle drying of the sample followed by a rapid step to a preset final temperature (*12*). The SIW consisted of a 23-cm diameter, 1.6-mm thick aluminum disk with 60 evenly spaced, radial slits machined in it. At the position of each slit, the disk was milled down to 0.6 mm thick to prevent stray reflection from the slit edges. Each slit was 0.6 mm wide by 4.5 cm long and located 1 cm from the edge of the disk. A 100-rpm Hurst reluctance type synchronous motor was used to drive the SIW. The wheel was coupled to the motor by means of precision geared pulleys and a no-slip, positive drive belt (PIC Design Corp.) which provided rotational speeds of 50, 100, and 200 rpm by simple interchange of pulleys. These rotational velocities correspond to translational velocities of the SIW slits past the monochromator entrance slit of approximately 50, 100, and 200 cm/s, respectively. The exact velocity can be measured and varied slightly by lateral movement of the SIW. The selection of slit velocities was based on the time scale of the event being recorded.

Procedure. The SIW was properly located in the tangential image plane by the procedure explained previously (*3*). An aperture was positioned directly behind the wheel to define a vertical viewing area of approximately 1 cm. To prevent light from two adjacent slits from reaching the detector at any given time, the atomizer was raised so that the light at one end of the viewing area was blocked by the image of the carbon filament. In this way, the vertical position of the filament could be adjusted until the light from only one slit at a time would reach the detector and the next slit would enter the viewing area immediately after

0003-2700/79/0351-0648$01.00/0 © 1979 American Chemical Society

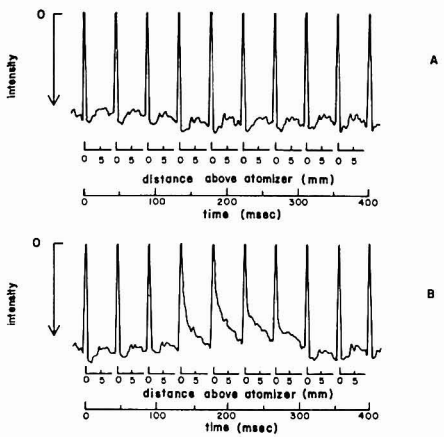

Figure 1. Representation of the photomultiplier tube output for the atomization of (A) no sample and (B) a 2-μL sample of 0.6 ppm Pb

the previous slit exited. The transient waveform recorder was set to record a data point every 0.2 ms and was triggered by a comparator circuit which underwent a −13 to +13 V transition when the atomizer surface temperature reached a predetermined level. The atomizer surface temperature was measured by means of the photodiode of the power supply/temperature control circuit (*12*). This provided a reproducible trigger and the ability to correlate atomization temperatures from shot to shot. A 2-μL sample of 0.6 ppm Pb dissolved in triply distilled water as $Pb(NO_3)_2$ was pipetted onto the carbon filament with a Hamilton syringe. The flow of Ar sheath gas was adjusted to give a vertical gas velocity of 10 cm/s. The sample was dried and atomized and the absorption signal recorded on the transient recorder. Ultimately, the data were transfered to the university computation center where the data reduction was performed by the Control Data Corporation 6400/6600 system. The same procedure was repeated using a mixture of Ar and small amounts of O_2 with the flow rates adjusted to maintain a 10 cm/s gas velocity.

RESULTS AND DISCUSSION

Using the above procedure, time and spatially resolved absorbance data were collected for Pb. It can be shown mathematically that the slight angle at which the scanning slits sweep across the top and bottom of the viewing area accounts for an error of less than 0.2% in the spatial resolution. The resolution of the optical system has been determined experimentally to be 0.04 mm (*3*), therefore, the resolution achieved by the SIW arrangement is equal to the 0.6 mm width of the field stop. Figure 1 shows a characteristic trace of the photomultiplier tube output when the SIW is used. Figure 1A shows the recorded signal with no sample while Figure 1B shows the output with a Pb sample. The region between any two peaks in Figure 1 represents the scan of a single SIW slit across the spatial viewing area. It is apparent from Figure 1B that the absorption is strongest in the regions closest to the filament surface. A detailed picture of a single scan from Figure 1A is shown in Figure 2. This figure also diagrammatically outlines the complete cycle of a single slit across the viewing area in front of the monochromator entrance slit. Since the optical system inverts the image, the SIW slits are swept downward in front of the monochromator entrance slit to scan the spatial zones above the filament starting at the filament surface. It should be noted that Figures 1 and 2 were obtained with the SIW rotating at 25 rpm for ease of viewing and contain fewer scans than the

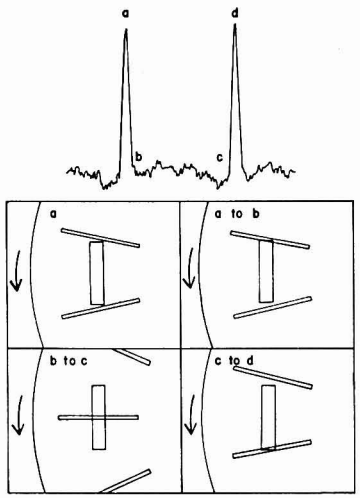

Figure 2. Detailed view of a single sweep from Figure 1A with the corresponding SIW slit positions

actual outputs normally obtained. In Figure 2, point a corresponds to 0% transmittance and occurs prior to the slit entering the viewing area. As the slit begins to enter, there is a sharp falling edge between a and b. Between b and c, the SIW slit is fully illuminated and scans the viewing area beginning with the spatial zone just above the carbon filament. As the SIW slit exits, there is a sharp rising edge between points c and d. Finally, at point d the slit has exited and 0% transmittance is recorded again. The slits are positioned on the SIW so that the end of a cycle for one slit occurs simultaneously with the start of a cycle for the next slit. It should be noted that the 0% transmittance reading is set by the vertical positioning of the carbon filament. The variations between points b and c in Figure 2 reflect a number of parameters such as changes in the intensity of the hollow cathode lamp at different spatial regions as well as the use of different areas of the photocathode at different spatial viewing zones. All these variations are reproducible and are corrected for in the data reduction program by normalizing the data points at each height to the spatially dependent output signal obtained in the absence of any absorbance signal. It should be noted that each SIW slit obtains absorbance data at progressively later times as successive heights are examined. The data reduction program also takes this into account and the data are extrapolated so that the absorbance at different heights is calculated for the same time. After the data reduction program has calculated the 0% and 100% transmittance levels, the absorbances, the peak half-widths, and the appearance time, a hard copy of all the information is obtained and the computer plots the data as three-dimensional profiles which give a general picture of the absorbance at any time and at any height above the atomizer surface, up to the limit of the viewing area. Figure 3 represents the profile obtained for the atomization of 0.6 ppm Pb in pure Ar sheath gas. Figure 4 represents the profile for the same sample with the sheath gas containing 0.15% O_2. As can be seen in Figure 4, the absorbance falls off at a lower height when O_2 is present, which is expected because of the thermodynamically favorable reaction:

$$Pb + {}^1/_2O_2 \rightarrow PbO \qquad (1)$$

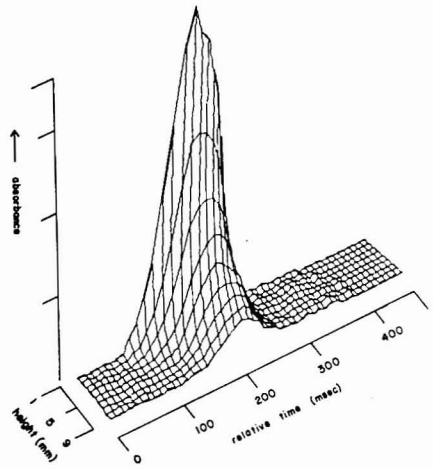

Figure 3. Three-dimensional profile of 0.6 ppm Pb with pure Ar sheath gas

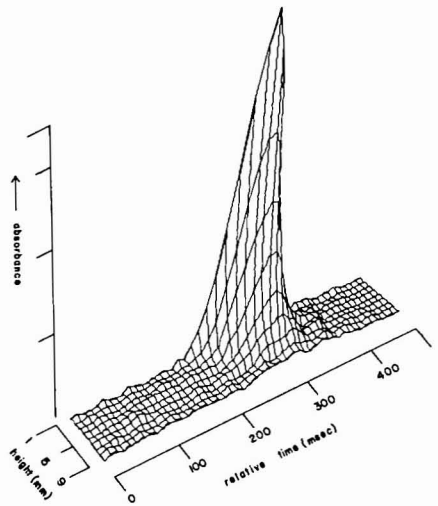

Figure 4. Three-dimensional profile of 0.6 ppm Pb with Ar sheath gas containing 0.15% O_2

However, there is also a shift of the peak absorbance to a later time and a narrowing of the peak half-width. Because of the reproducible triggering of the recorder at a predetermined filament temperature, this time shift indicates a higher appearance temperature for Pb in the presence of O_2. These results have prompted further study of the Pb system which is currently in progress.

The profiles in Figures 3 and 4 point out the type of information available from the data. Time-dependent absorbance profiles at several heights are obtainable as well as information on peak absorbance, total integrated absorbance, and appearance temperature of the analyte. The time resolution of the system can be improved simply by increasing the rotational speed of the SIW. The time-resolving capabilities of the SIW can be seen in Figures 3 and 4 where the peak absorbance at each successive height above the atomizer occurs at a later time.

The SIW has the potential of giving three-dimensional information in other spectroscopic techniques, such as atomic fluorescence, where the exciting radiation is perpendicular to the detector and better resolution of points in the source is possible. Another potential application is the use of the SIW in the temperature measurement techniques described by Bratzel and Chakrabarti (*13*) to obtain a three-dimensional temperature profile of the atomic vapor.

There are several advantages in using the SIW to collect time and spatially resolved absorbance data. The most dramatic is the reduction in the time required for data gathering. The described procedure is many times faster than the conventional method. In addition to the saving in time, the data are also more consistent because of the ability of the SIW to obtain data on all heights above the filament in a single shot. All the spatial data are obtained from the same event and must, therefore, be internally consistent. The reduced number of shots required also adds to this consistency since the filament surface undergoes less degradation during a set of experiments. Finally, this system can achieve simultaneous time and spatial resolution using a standard monochromator, simple optics, and an inexpensive photomultiplier tube.

ACKNOWLEDGMENT

The authors thank P. Hullman for obtaining the Pb data used for the three-dimensional profiles.

LITERATURE CITED

(1) J. P. Walters, *Anal. Chem.*, **40**, 1540 (1968).
(2) R. J. Klueppel, D. M. Coleman, W. S. Eaton, S. A. Goldstein, R. D. Sacks, and J. P. Walters, *Spectrochim. Acta, Part B*, **33**, 1 (1978).
(3) S. G. Salmon and J. A. Holcombe, *Anal. Chem.*, **50**, 1714 (1978).
(4) K. W. Jackson and T. S. West, *Anal. Chim. Acta*, **59**, 187 (1973).
(5) K. W. Jackson, T. S. West, and L. Balchin, *Anal. Chim. Acta*, **64**, 363 (1973).
(6) D. Alger, R. G. Anderson, I. S. Maines, and T. S. West, *Anal. Chim. Acta*, **57**, 271 (1971).
(7) J. Aggett and T. S. West, *Anal. Chim. Acta*, **55**, 349 (1971).
(8) D. J. Johnson, B. L. Sharp, T. S. West, and R. M. Dagnall, *Anal. Chem.*, **47**, 1234 (1975).
(9) G. Torsi and G. Tessari, *Anal. Chem.*, **45**, 1812 (1973).
(10) S. L. Paveri-Fontana, G. Torsi, and G. Tessari, *Anal. Chem.*, **46**, 1032 (1974).
(11) J. F. Alder and T. S. West, *Anal. Chim. Acta*, **51**, 365 (1970).
(12) J. A. Holcombe (in preparation), *Rev. Sci. Instrum.*
(13) M. P. Bratzel, Jr., and C. L. Chakrabarti, *Anal. Chim. Acta*, **63**, 1 (1973).

RECEIVED for review November 7, 1978. Accepted February 2, 1979. This work was supported by National Science Foundation Grant Number CHE-78-15438.

Determination of Lead in Seawater by Furnace Atomic Absorption Spectrometry after Concentration with Yield Tracer

Yoshimitsu Hirao, Kazuko Fukumoto, Hajime Sugisaki, and Kan Kimura*

College of Science and Engineering, Aoyama Gakuin University, 6-16-1, Chitosedai, Setagaya-ku, Tokyo, Japan

Lead in seawater at the nanogram level was determined by graphite furnace atomic absorption spectrometry (GFAAS) after simple concentration together with radioisotope ^{212}Pb added for yield correction. All chemical procedures as well as purification of reagents were carried out in a laboratory through which filtered air was being passed. Lead in 1 kg of acidified seawater was equilibrated with ^{212}Pb of a known radioactivity, extracted with dithizone in chloroform, back-extracted with 0.1 M hydrochloric acid and subjected to GFAAS by a two-channel spectrometer. Recovery yield of lead was found to be 60–90% from the radioactivity of ^{212}Pb in the back-extract. Lead concentrations thus determined were 39–1300 ng/kg with about 10% precision.

Determination of lead concentration and distribution in seawater is of great importance in geochemistry and environmental science. Extractable lead was estimated to be about 100 ng/kg in coastal seawater, about 30 ng/kg in surface water of open ocean, and about 4 ng/kg in deep seawater as a summary of the interlaboratory check (*1–3*). There are several methods for determination of nanograms of lead. Because of the very low concentration of lead in a high concentration of salts, preconcentration of lead is usually recommended. Recovery yield of nanograms of lead in such preconcentration steps has been assumed to be either quantitative or constant, but no direct evaluation has been made for each sample except in isotope dilution mass spectrometry. Furthermore, according to Patterson, owing to serious contamination during analysis, there may be few values which give the lead concentration in seawater properly (*4*).

Therefore, in this paper, extractable lead in seawater was determined through a clean laboratory technique by furnace atomic absorption spectrometry after preconcentration with the yield tracer. By the use of radioisotope ^{212}Pb, recovery yield of lead in the preconcentration step could be measured for each sample and, hence, the preconcentration step was much simplified.

EXPERIMENTAL

Reagents. *Water.* Water was purified by a system of a stainless steel still and an ion-exchange resin column, and then by a quartz two-successive stage distillation system in a clean laboratory.

Acetone, Chloroform, Nitric and Hydrochloric Acids. The organic reagents (special reagent grade) and the acids (the super special grade (SSG)) from Wako Chemical Industry Ltd. (Wako) were purified twice by an ordinary quartz distillation apparatus. Distillation was performed at subboiling temperature by using infrared lamps and a heater.

Ammonia Water. After passing through a millipore filter of 0.45-μm pore size, pure ammonia gas from a small bomb was absorbed in the purified water.

Dithizone. Merck "Pro Analisi" grade dithizone was purified by the ordinary method (*5*) with the purified reagents.

Ammonium Citrate. Citric acid (special reagent grade) from Wako was dissolved in the water. The solution was adjusted to pH 8.5 with the ammonia water. Lead in the solution was extracted with the purified dithizone in chloroform 5 times.

The reagents thus purified were used throughout the experiment, unless otherwise stated.

Measurement of Lead Blank in the Reagents. About 30 mL of the purified reagent was weighed in a quartz beaker and evaporated to dryness in a Teflon oven, through which nitrogen gas was being passed. The beaker was washed with 1 mL of 0.1 M hydrochloric acid. Lead concentration and recovery yield were measured by GFAAS and ^{212}Pb tracer technique, respectively, as described below.

Lead Standard Solution. Five-nine grade of lead metal from Wako was dissolved in nitric acid. The solution was dried up and the residue was dissolved in hydrochloric acid. A 500-ppm solution was stocked and diluted to proper concentration at each measurement.

Preparation of ^{212}Pb (*6*). Anhydrous thorium chloride was prepared from thorium nitrate from Wako via the hydroxide by Chauvenet's method (*7*), as the nitrate gave a low collection efficiency. Fifty grams of the powdered chloride was put in a wide-mouth polyethylene bottle. About 1 cm above the chloride, a platinum plate (2.5 cm in diameter) was settled and 1200 V of electric potential was applied, as shown in Figure 1. After 1 day, about 5×10^3 dps of ^{212}Pb was collected on the plate. This was sufficient for the tracer and, hence, no further condition was studied. The ^{212}Pb collected on the plate was dissolved in 1 mL of hot concentrated nitric acid in a few seconds and used as the yield tracer.

Measurement of ^{212}Pb Radioactivity. The activity was measured by total γ-ray counting with a conventional scintillation counter. Usually ^{212}Pb and its daughter nuclide, ^{212}Bi, are in radioactive equilibrium, as half lives are 10.64 h and 1.01 h, respectively. But, during the chemical separation of lead, bismuth retained 80–90% of its equilibrium. Therefore, the measurement was done after 4-h standing.

Cleaning of Teflon and Quartz Wares. The wares were immersed successively in hot concentrated and 0.1 M nitric acid for one day each.

Cleaning of Polyethylene Bottle. A new bottle was washed with soap and acetone, and stood in SSG concentrated and 0.1 M hydrochloric acid at 50 °C for 3–5 days each. The bottle was then stored in another portion of the same 0.1 M acid until use.

Adsorption of Lead on the Polyethylene Bottle. It is often heard that lead in seawater is adsorbed on the washed polyethylene wall at neutral conditions, but not at pH 1. Thus adsorption and desorption of lead on and from the wall were confirmed by using ^{212}Pb tracer. Hydrochloric acid solution of ^{212}Pb was added to the seawater sample, and the sample solution was kept at pH 1 for a while. Then the pH value was adjusted to 8.5 with sodium hydroxide, and after a while the solution was acidified to pH 1 and warmed at 50 °C. The change in the radioactivity of the solution was measured at each stage with elapsed time.

Sampling. Surface seawater samples were collected from the head of a small boat. During the sampling, the boat was pointed toward the wind direction and moved forward slowly. A cleaned bottle was hung up with a fishing rod, and nylon net and rope, and sunk into the water with a weight 3–5 m ahead of the boat. Just after the final bubble came out, the bottle was pulled up and taken from the net by polyethylene gloved hands. The bottle was double-wrapped with polyethylene bags, frozen with dry ice as quickly as possible, and stored in a freezer until analysis.

Chemical Procedure. Sample seawater was thawed and acidified with hydrochloric acid to pH 1 and warmed at 50 °C for 1 day. A known amount (radioactivity) of ^{212}Pb was added

0003-2700/79/0351-0651$01.00/0 © 1979 American Chemical Society

Table I. Lead Concentration in Purified Water

	sample wt, g	found, ng	chem. yield, %	blank, ng	added ng/kg	lead concn., ng/kg
A	925	5.7	87	4.2	0	2.5
B	946	5.7	63	4.4	0	4.9
C	884	3.3	87	0.3	0	4.0
D	868	5.6	84	0.3	0	7.3
E	889	13.$_8$	86	0.3	11.5	17., (6.2)[a]
F	885	26.$_1$	90	0.3	26.5	32., (6.2)[a]

[a] Values in parentheses were obtained by subtracting added lead from total lead.

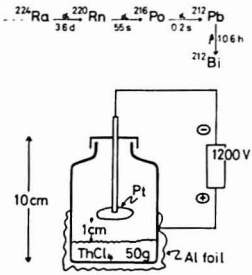

Figure 1. System for collection of ^{212}Pb

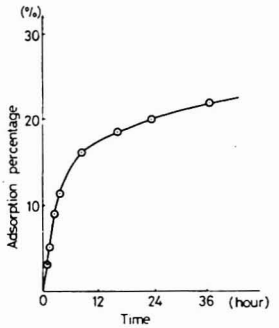

Figure 2. Adsorption of lead on polyethylene wall

and equilibrated with exchangeable lead in the seawater for 2 h. After cooling, 25% ammonium citrate solution was added with the ratio of 2 mL to 1 L sample, and the pH value was adjusted to 8.0–8.5 with ammonia water. The upper limit of this pH range can be 11.5. Lead in the seawater was extracted into 40 mL of dithizone solution (1 mg/100 mL chloroform) from a 1-L sample in a Teflon separatory funnel and back-extracted with 10 mL of 0.1 M hydrochloric acid. The pH value of the back-extract was adjusted to 8.5, and the lead was again extracted with 5 mL of dithizone solution. The organic phase was washed with 20 mL of water of pH 8 and the lead was back-extracted with 1–5 mL of 0.1 M hydrochloric acid. The ^{212}Pb radioactivity in the back-extract was measured for calculation of the lead recovery yield, by comparing it with the initial activity.

Graphite furnace Atomic Absorption Measurement. After γ-ray counting, the lead solution was supplied for GFAAS. A flameless atomizer system (NJA-FLA-100) and a two-channel atomic absorption spectrophotometer (NJA-AA-8500) of Nippon Jarrell-Ash Co. Ltd. were used. A hollow cathode lamp from Hamamatsu TV Co. Ltd. was used at the recommended current. The spectral line at 283.3 nm was selected for the measurement. Twenty microliters of sample was put into the graphite furnace. The power supply for the furnace was programed as follows: drying at 200 °C; ashing at 700 °C; atomization at 2200 °C. Background was checked by a D_2 lamp in the second channel.

RESULTS AND DISCUSSION

Adsorption and desorption of lead on and from the wall of the polyethylene bottle were investigated by the method described in the Experimental section. At pH 1, no adsorption was seen. But at pH 8.5, adsorption occurred obviously. Figure 2 shows a typical adsorption curve with a 30-mL polyethylene bottle (the wall area contacted with seawater was 50 cm^2). Generally percentage adsorption of lead varies depending on the ratio of the wall area contacted with the water to the volume of the water, and more than 10% lead seems to be adsorbed before analysis. However, the adsorbed lead was leached out completely under the warm acid condition. Therefore, even if lead in the samples was adsorbed on the wall before the sample froze and after it thawed, it was clear that the adsorbed lead was desorbed completely from the wall under the stated condition.

The lead blank in the reagents used was measured by the procedure described in the Experimental section. By this process, more than 95% lead was recovered. Nevertheless no lead was detected (detection limit: 0.5 ppb) for all reagents, so that the lead blank for each reagent was estimated to be less than 30 ng/kg. No lead peak was observed for the solution of ^{212}Pb tracer after 180-h collection. Therefore the tracer was of sufficiently high specific activity. In the second channel, no lead background was observed for all samples.

As to the water used, the lead concentration was estimated by the "chemical procedure" in the Expermental section without citrate addition. The results are shown in Table I. Samples A, B, and C were analyzed immediately after collection. Samples C, D, E, and F were collected at the same time and the latter three (D, E, and F) were acidified and analyzed after 4 days standing at 50 °C. Also 11.5 and 26.5 ng per kg sample were added to samples E and F, respectively. From samples A, B, and C, lead concentration in the water was estimated to be 4 ng/kg. From samples D, E, and F, the values 7.3, 6.2, and 6.2 ng/kg were obtained and seemed to be in good agreement with each other. The difference of 3 ng/kg between samples A, B, C and D, E, F was assumed to be dissolution of lead from the polyethylene wall at pH 1 in 4 days, and this value was used for the evaluation of the blank from the bottle during analysis.

The lead blank was also checked by the chemical procedure for each set of determinations, and the results were used for the estimation of the blank in Tables I and II together with the above mentioned results.

For the measurement of the recovery yield with ^{212}Pb radioactivity, the counting error was about 2%. For the GFAAS, uncertainty was estimated to be 6% for the range of 5–15 ppb, from deviations from a calibration curve. Standard deviation for 10 measurements of the same lead solution was about 8% for 10 ppb. Furthermore, by considering the uncertainty in the estimation of blanks described in the preceding paragraphs, it was concluded that uncertainty of ≤10% was included in each determination.

Seawater samples were collected around Tokyo Bay, Japan. Lead concentrations in the samples are shown in Table II. All

Table II. Lead Concentration in Seawater around Tokyo Bay

sampling station	sample wt, g	found, ng	chem. yield, %	blank A, ng[a]	blank B, ng[b]	concn., ng/kg	Cl, ‰[c]
(A) Arakawa Riv.	87	90	78	1.6	0.2	1300	1.3
(B) Inner Tokyo Bay	1815	780	70	5.2	3	610	9.7
	894	330	63	5.4	1.5	580	
	99	44	86	0.2	0.2	510	
(C) Outer Tokyo Bay	2090	61	64	5.4	2	42	18.0
	1984	66	77	6.0	2	39	
(D) Oshima Is.	1509	58	86	3.6	1	42	18.5

[a] Blank A: Blank from reagents. [b] Blank B: Blank from bottle (cf. Table I and text). [c] Cl: Chlorinity.

samples were collected in individual polyethylene bottles. The values for two 2-L samples from outer Tokyo Bay (C) were in good agreement with each other within 5% deviation. The values for three samples from inner Tokyo Bay (B) were fairly close to each other, even though sample size varied from 2 L to 100 mL. The difference between 610 and 510 ng/kg probably resulted from the heterogeneity of lead in the samples, since the samples looked turbid. Namely, difference in contents of the colloidal particles and in dissolution of lead from the particles during warming process may cause the difference.

Chlorinity at station B is about half of that at C, and the middle of those at A and C, indicating mixing of seawater (C) and river water (A). A similar trend is also seen among the lead concentrations at A, B, and C. It is noted that lead concentrations at C and D are in the same range. The concentration probably indicates a typical extractable lead concentration in surface seawater at about 1 km off the ocean coast.

Use of ^{212}Pb as yield tracer for lead analysis has several advantages. Preparation of ^{212}Pb tracer is very simple. Once thorium chloride (or thorium compound of high emanating power for ^{220}Rn) and the electric supply system are prepared, the radioactivity will be supplied within 10 h. The tracer ^{212}Pb obtained is in high radiochemical purity and contains no detectable lead blank. The half life of 10.64 h is long enough for the tracer and short enough for the environment. Measurement of ^{212}Pb is also simple. A conventional γ-ray counting system is enough for the measurement. Once the activity is added to a sample, as written in the chemical procedure, the recovery yield of lead can be checked at any step by activity measurement. The fourth column in Table II shows the total yield thus obtained.

For the ultra microanalysis of lead, handling and chemical procedures must be as simple as possible to avoid serious contaminations. Also, only the minimum excess of reagents is permissible to reduce the blanks from reagents. For these requirements, the ^{212}Pb yield tracer technique is extremely useful. The recovery yield can be measured directly for each sample by the use of the tracer and, hence, it is unnecessary to keep the recovery either quantitative or constant. Thus the chemical procedure is quite simplified and the amount of reagent to be used is also much reduced. Furthermore, it is noteworthy that the simplified procedure can eliminate the serious contamination.

As for the isotope dilution technique, mass spectrometry (MS) following the chemical concentration and purification with the spike is well known. Once the spike is equilibrated with the sample, chemical yield during the separation step is not necessarily to be found, and sensitivity and precision of the method are both very high. However, in general, MS is not so common and takes much time for one analysis. In these points, the precision of GFAAS is not as good but the sensitivity is in the same range as MS, and it is commoner in laboratories and gives a faster method than MS. Therefore, the combined method of GFAAS with the preconcentration procedure, described here, is one of the best methods for analysis of lead in the exchangeable and extractable state in seawater.

ACKNOWLEDGMENT

R. Tsujino, M. Matsubara and the co-workers in Tokyo Division of Nippon Jarrell-Ash Co. Ltd. permitted us to use the GFAAS system in its best condition, for which the authors' thanks are due.

LITERATURE CITED

(1) C. Patterson, *Science*, **183**, 553(1974).
(2) Participants of the Lead in Seawater Workshop, *Mar. Chem.*, **2**, 69–87 (1974).
(3) Participants of the Lead in Seawater Workshop, *Mar. Chem.*, **4**, 389–392 (1976).
(4) C. Patterson and D. Settle, *Natl. Bur. Stand. (U.S.) Spec. Publ.*, **422**, 321 (1976).
(5) E. B. Sandell, "Colorimetric Determination of Traces of Metals", Interscience, New York, 1950, p 107.
(6) N. Matsuura, "Jikken Kagaku Koza", Vol. 12, N. Saito, Ed., Maruzen, Tokyo, 1956, p 419.
(7) E. Chauvenet, *Compt. Rend.*, **148**, 1267–70 (1909).

RECEIVED for review September 13, 1978. Accepted December 15, 1978. Part of this paper was presented at the 22nd Symposium on Analytical Chemistry, Nara, Japan, June 1977; also at the 26th International Congress of Pure and Applied Chemistry, Tokyo, September 1977.

Flotation Separation and Atomic Absorption Spectrometric Determination of Selenium(IV) in Water

Susumu Nakashima

Institute for Agricultural and Biological Sciences, Okayama University, Kurashiki-shi, Okayama 710, Japan

A method is described for the flotation and determination of sub-microgram levels of selenium(IV) in water. Selenium(IV) in a 1000-mL sample of water is coprecipitated with iron(III) hydroxide at pH 4.0 ± 0.2. The precipitate is floated with the aid of sodium lauryl sulfate and small air bubbles, then separated and dissolved in 4 M hydrochloric acid and diluted to 10 mL. Finally the selenium content is determined by generation of hydrogen selenide using sodium borohydride as a reductant and subsequent atomic absorption spectrophotometry with a long absorption cell (60 × 1.2 cm i.d.). Selenium(IV) at the levels of 0.4 μg and 0.8 μg added to water (1000 mL) and to seawater could be determined with a recovery of above 97% and with a relative standard deviation within 2%. The time required for the pre-concentration of selenium(IV) from a 1000-mL volume of solution was about 30 min per sample.

In these days of concern over environmental pollution, there is an increasing need for a simple, rapid, and precise method for determining low parts per billion (ppb) of selenium in water. In general, for an accurate determination of selenium at this concentration, pre-concentration is needed from water in order to achieve the necessary sensitivity for analytical methods.

Iron(III) hydroxide is well known as one of the most efficient collectors of trace metals in aqueous systems. As a pre-concentration technique for the determination of selenium(IV) in water, coprecipitation with iron(III) hydroxide is commonly used (*1–3*). This bulky amorphous precipitate, however, is difficult to filter, and centrifugation is cumbersome for larger volumes.

In a previous paper (*4*), a flotation technique (*5, 6*) in which the precipitate of iron(III) hydroxide is floated with the aid of sodium oleate and small air bubbles was used for the pre-concentration of arsenic in natural nonsaline waters.

As for the flotation of selenium(IV), Tzeng and Zeitlin (*7*) have reported the adsorption colloid flotation of selenium(IV) added to a 500-mL seawater sample at pH 3.5–5.3 using a ferric hydroxide collector, sodium dodecylsulfate (sodium lauryl sulfate) and nitrogen and the subsequent determination of selenium(IV) by the catalytic methylene blue method. However, in that investigation, the procedure used for the determination of selenium after separation is laborious and time-consuming.

Recently for selenium, several publications have appeared (*8–16*) concerned with the development and application of the hydride generation technique using sodium borohydride as a reducing agent. However, at a less than 1 μg/L level of selenium in water, a precise direct determination is impracticable even by the highly sensitive atomic absorption spectrophotometry of hydrogen selenide unless a liquid nitrogen trap collection method is used (*16*).

This paper describes the application of the above-mentioned arsenic separation technique (*4*), with suitable modifications for the pre-concentration of sub-microgram amounts of selenium(IV) in water. The precipitate is readily separated from the mother liquor and then dissolved in dilute hydrochloric acid for the atomic absorption spectrophotometry by generation of hydrogen selenide using $NaBH_4$ as a reductant. The various parameters that affect the flotation and determination of selenium(IV) were investigated. This method is simple and rapid, and applicable to the extraction of selenium(IV) at low ppb levels from large volumes of water and seawater.

EXPERIMENTAL

Apparatus. A Nippon Jarrell-Ash, Model AA-1 Mark II, atomic absorption spectrophotometer equipped with a Westinghouse selenium hollow-cathode lamp and a custom-made silica absorption cell (60 × 1.2 cm i.d.) was used with a Beckman burner supplied with nitrogen and hydrogen.

The apparatus used for hydride generation was a modified Nippon Jarrell-Ash, Model ASD-1A, hydride measurement unit coupled to a custom-made hydride generating cell approximately 40 mL in volume. The schematic diagram of the analytical system was described previously (*4*).

All pH readings were made with a Hitachi-Horiba, Model M-5, pH meter, together with a combined glass electrode.

The flotation and separation apparatus was similar to that described by Mizuike and co-workers (*5, 6*). The flotation cell was a glass cylinder, 40 × 6.5 cm i.d., which was fitted with a sintered-glass filter (No. 4) to generate small bubbles. A side arm was added near the bottom of the cell to drain the mother liquor rapidly after the flotation, as shown in Figure 1.

Reagents. All reagents were of analytical-reagent grade except for sodium lauryl sulfate. Aqueous reagents were prepared in deionized, distilled water. A selenium(IV) stock solution (1 mg Se/mL) was prepared from selenium dioxide and before each use a standard solution was freshly prepared by diluting this stock solution. An iron(III) solution (5 mg Fe/mL, in 1 M hydrochloric acid) was prepared from an ammonium iron sulfate solution. A sodium lauryl sulfate solution (1 mg/mL) was prepared by dissolving sodium lauryl sulfate (powder, extra-pure reagent, Wako Pure Chemicals, Co.) in 99.5% (v/v) ethanol. A 5% (w/v) $NaBH_4$ solution in a 0.1 M sodium hydroxide solution was prepared.

Procedures. *Flotation Step.* Place 1000 mL of acidified water in a 1000-mL beaker and add 2 mL of iron(III) solution. Adjust the pH to 4.0 ± 0.2 with aqueous ammonia solution to precipitate iron(III) hydroxide, while stirring magnetically, for at least 10 min. Add 2 mL of sodium lauryl sulfate solution into the beaker. Transfer the contents of the beaker (excluding the stirring bar) to a flotation cell and wash the residue in the beaker into the cell by using three small portions of water. Pass air at a flow rate of 50 mL/min from the lower end of the cell for about 2 min, in order to obtain complete mixing and flotation of the precipitate. Drain most of the mother liquor from the side arm by opening the cock of the drain pipe. After closing the cock, suck off the residual mother liquor through the sintered-glass disk and wash the precipitate with 30 mL of water. Add 4 mL of 4 M hydrochloric acid to the cell to dissolve the precipitate, collect the filtrate by suction in a 10-mL calibrated flask, wash the sintered-glass disk with hydrochloric acid, add washings to the flask, and dilute to 10 mL with 4 M hydrochloric acid.

Atomic Absorption Measurement. Transfer 1 mL of freshly prepared 5% (w/v) $NaBH_4$ solution into a hydride generating cell and attach the cell to the apparatus. Insert the needle of a plastic syringe containing 1 mL of sample solution containing less than 0.10 μg of selenium through the side-arm seal of the cell.

0003-2700/79/0351-0654$01.00/0 © 1979 American Chemical Society

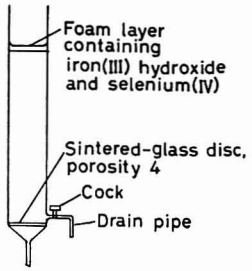

Figure 1. Flotation cell for pre-concentration of selenium(IV)

Turn the four-way stopcock of the apparatus to the sweep position to introduce nitrogen into the system and inject the sample into the cell. Sweep the hydrogen selenide generated into the long absorption cell with nitrogen so that it is atomized in the nitrogen–hydrogen flame, and record the absorption signal on a recorder. Return the stopcock to the bypass position. Rinse the cell carefully with distilled water and recharge with $NaBH_4$ solution ready for the next sample.

Construct a calibration curve using 4 M hydrochloric acid solutions containing 1 mg/mL of iron(III) and 0–0.10 μg/mL of selenium(IV); this curve is nearly linear within the above range of selenium. The relative standard deviations were 1.5% and 1.4% in 10 replicate determinations of 0.04 μg and 0.08 μg of selenium(IV) (1-mL volume), respectively.

The atomic absorption equipment was operated under the following conditions: wavelength, 196.0 nm; lamp current, 10 mA; gas flow rates, nitrogen 1.5, hydrogen 1.5, and auxiliary nitrogen 6 L/min; slit (spectral band width), 1 nm.

The 60-cm tube system described in this paper cannot be used with most commercial atomic absorption spectrophotometer units. However, the selenium in a sample solution can also be determined by atomic absorption spectrophotometry using a hydride generation-electrically or flame-heated silica tube.

RESULTS AND DISCUSSION

Optimum Conditions for the Determination of Selenium(IV). The effect of $NaBH_4$ concentration on the evolution of hydrogen selenide was investigated. As a result, it was found that the use of more than 2% (w/v) of the reductant concentration (1-mL volume) can quantitatively reduce up to 0.10 μg of selenium(IV) to hydrogen selenide. In this work, 1 mL of 5% (w/v) solution was used.

The optimum condition for sensitivity of selenium was dependent on the flow rate of auxiliary nitrogen. The absorption of selenium increased with each increase in the flow rate of auxiliary nitrogen. The optimum absorption was obtained with the flow rate of carrier gas between 6 and 8 L/min when both flow rates of nitrogen and hydrogen were 1.5 L/min; a flow rate of auxiliary nitrogen of 6.0 L/min was used throughout.

The effect of hydrochloric acid concentration was studied. The optimal concentration of hydrochloric acid was between 2–5 M; the acidity of hydrochloric acid was maintained at 4 M in further work.

The presence of up to at least 2.5 mg/mL of iron(III) added as a collector did not affect the generation of hydrogen selenide.

Optimum Conditions for the Flotation of Selenium(IV). *Effect of pH.* The effect of the pH of the 1000-mL solution containing 0.8 μg of selenium(IV), 10 mg of iron(III), and 2.0 mg of surfactant on the coprecipitation of selenium(IV) was studied. Hydrochloric acid and aqueous ammonia solution were used to adjust the pH to values within the range 3.5–10.5. As shown in Figure 2, satisfactory recoveries of selenium(IV) were obtained in the pH range 3.5–8.5. At pH values above

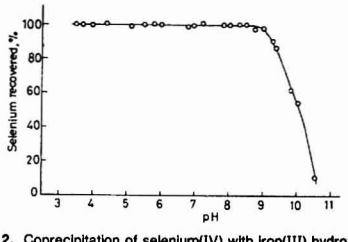

Figure 2. Coprecipitation of selenium(IV) with iron(III) hydroxide as a function of pH. Solution contained 0.8 μg of Se(IV) and 10 mg of Fe(III); volume, 1000 mL

Table I. Permissible Amounts of Foreign Ions for Determination of Selenium[a]

ion	limit, [ion]/[Se]	ion	limit, [ion]/[Se]	ion	limit, [ion]/[Se]
Na^+	10000	Cd^{2+}	1000	V^{5+}	1000
K^+	10000	Zn^{2+}	1000	PO_4^{3-}	1000 } b
Ca^{2+}	10000	Mn^{2+}	1000	Ni^{2+}	800
Mg^{2+}	10000	Al^{3+}	1000	Cu^{2+}	800
Cl^-	10000	Cr^{3+}	1000	Bi^{3+}	400
NO_3^-	10000 } b	Cr^{6+}	1000 } b	Sb^{3+}	100
SO_4^{2-}	10000	Mo^{6+}	1000	As^{3+}	100
SiO_3^{2-}	10000	Pb^{2+}	1000	As^{5+}	100
Sr^{2+}	1000	Hg^{2+}	1000	Sn^{4+}	10
Ba^{2+}	1000	Co^{2+}	1000	Te^{4+}	10

[a] Solution contained 1.0 μg of Se(IV) and 10 mg of Fe(III); volume, 1000 mL. [b] Maximum concentrations tested.

9, the efficiency of coprecipitation decreased considerably. The most stable layer of surface foam supporting the precipitate of iron(III) hydroxide using sodium lauryl sulfate was formed within the pH range 3.5–7.0; in all further work, the pH of 4.0 ± 0.2 was used for the precipitation and flotation. At a pH above 7, a stable surface-foam layer was obtained by using sodium oleate as a surfactant.

Amounts of Iron(III) and Surfactant. The recovery of selenium(IV) was investigated as a function of the amount of iron(III) added to the solution. Quantitative recoveries of selenium(IV) were obtained above 5.0 mg of iron(III). In this work, 10 mg of iron(III) were added to 1000 mL of the solution.

The amount of sodium lauryl sulfate required for complete flotation of the precipitate was investigated. Quantitative recoveries of selenium(IV) were obtained between 0.5–8.0 mg of sodium lauryl sulfate, and 2.0 mg in 1000 mL of solution was adopted in further work.

Stirring Time. The relation between stirring time and recovery of selenium(IV) was investigated. As a result, coprecipitation was quantitative over the range 5–40 min. In practice, stirring for 15 min was used.

Effect of Foreign Ions. By following the proposed procedure, the effect of various ions on the separation and determination of selenium(IV) was investigated. Table I shows permissible amounts of foreign ions within 10% negative error for the determination of 1.0 μg of selenium(IV) in 1000-mL solutions with 10 mg of iron(III) added. As can be seen, most foreign ions hardly interfere with the determination of selenium(IV). When coprecipitation at pH 4.0 ± 0.2 was used, suppressive effects by diverse ions, especially copper(II), nickel(II), and mercury(II) were found to be largely eliminated in comparison with those which occur when selenium is directly determined without previous concentration. The values of permissible amounts (ion/Se in weight) of coexisting ions in the proposed method increased from 10, 20, and 40 to 800,

Table II. Recovery of Selenium(IV) Added to Natural Seawater[a]

selenium, μg			mean recovery, %
added μg	found μg	recovered	
none	0.023 ± 0.005[b]		
0.400	0.409 ± 0.007[c]	0.386	97
0.800	0.805 ± 0.013[c]	0.782	98

[a] Volume of sample, 1000 mL. [b] Mean value of four measurements. [c] Mean value of seven measurements.

800, and 1000 for copper(II), nickel(II), and mercury(II), respectively, compared with the values permissible in direct determination. However, hydride-forming elements such as tellurium(IV), tin(IV), arsenic(III, V) and antimony(III) are coprecipitated with iron(III) hydroxide in the same way as selenium(IV) and had a relatively strong effect on the generation of hydrogen selenide.

Recovery of Selenium(IV). Solutions (1000 mL) at pH 4.0 ± 0.2 containing 10 mg of iron(III), 2.0 mg of sodium lauryl sulfate, and 0.2, 0.4, 0.6, 0.8, 1.0, 2.0, 4.0, 6.0, 8.0, 10.0, 15.0, and 20.0 μg of selenium(IV) were analyzed by the described procedure. Recoveries of the selenium that had been added were greater than 96% in all instances. The blank value throughout the whole analytical process was less than 5 ng Se/L. Proposed conditions, therefore, appear to be optimum for 1000-mL volumes of solutions containing up to at least 20 μg of selenium(IV).

The relative standard deviations of 10 analyses of solutions containing 0.4 and 0.8 μg of selenium(IV) per 1000 mL were 1.8% and 1.5%, respectively.

Application to the Analysis of Selenium(IV) Added to Seawater. To investigate the applicability of this method to the separation and determination of selenium(IV) in seawater, recoveries of known amounts of selenium(IV) added to natural seawater samples were examined by the above procedure. The analyses were carried out on 1000-mL aliquots of clear uncontaminated seawater, filtered through 0.45-μm Millipore filters after the addition of 10 mL of hydrochloric acid per 1000 mL of sample immediately after collection at Shibukawa, Okayama Prefecture, Japan. Table II presents recovery results of selenium(IV). Recovery results indicate that the analytical system could be successfully applied for the separation and determination of the selenium(IV) at the levels of 0.4 and 0.8 μg in seawater containing large amounts of salt matrix.

As for the selenium content in seawater, Schutz and Turekian (*17*) found 0.05–0.12 μg Se/L (average 0.09 μg/L) in deep ocean waters using a neutron activation procedure in a worldwide survey.

According to recent reliable data (*3*, *16*, *18*), the concentrations of selenium(IV) in uncontaminated natural fresh and seawaters are quite low, <5–70 ng/L. Shimoishi and Tôei (*18*) who used gas chromatographic determination have reported that the coastal seawater and river water of Japan was found to contain 8–32 ng/L of selenium(IV) and that the selenium(IV) content in seawater collected at the seashore of Shibukawa, Okayama Prefecture, Japan, was 32 ng/L. The selenium(IV) content (23 ng/L) obtained in this work is near their reported value. However, at such extremely low concentrations of selenium(IV), the precise determination of selenium(IV) is difficult even by the highly sensitive method described here.

ACKNOWLEDGMENT

The author thanks Atsushi Mizuike and Masataka Hiraide of Nagoya University for their helpful advice on the flotation technique, and Fuji Morii of Okayama University for useful discussions.

LITERATURE CITED

(1) Y. K. Chau and J. P. Riley, *Anal. Chim. Acta*, **33**, 36 (1965).
(2) M. Ishibashi, T. Fujinaga, T. Kuwamoto, and S. Murai, *Nippon Kagaku Zasshi*, **88**, 76 (1967).
(3) K. Hiraki, O. Yoshii, H. Hirayama, Y. Nishikawa, and T. Shigematsu, *Bunseki Kagaku*, **22**, 712 (1973).
(4) S. Nakashima, *Analyst (London)*, **103**, 1031 (1978).
(5) M. Hiraide and A. Mizuike, *Bunseki Kagaku*, **26**, 47 (1977).
(6) M. Hiraide, Y. Yoshida, and A. Mizuike, *Anal. Chim. Acta*, **81**, 185 (1976).
(7) J. Tzeng and H. Zeitlin, *Anal. Chim. Acta*, **101**, 71 (1978).
(8) Y. Yamamoto, T. Kumamaru, Y. Hayashi, and M. Kanke, *Anal. Lett.*, **5**, 717 (1972).
(9) K. C. Thompson and D. R. Thomerson, *Analyst (London)*, **99**, 595 (1974).
(10) P. D. Goulden and P. Brooksbank, *Anal. Chem.*, **46**, 1431 (1974).
(11) P. N. Vijan and G. R. Wood, *Talanta*, **23**, 89 (1976).
(12) Y. Yamamoto and T. Kumamaru, *Fresenius' Z. Anal. Chem.*, **281**, 353 (1976).
(13) J. A. Fiorino, J. W. Jones, and S. G. Caper, *Anal. Chem.*, **48**, 120 (1976).
(14) H. H. Walker, J. H. Runnels, and R. Merryfield, *Anal. Chem.*, **48**, 2056 (1976).
(15) D. D. Siemer and P. Koteel, *Anal. Chem.*, **49**, 1096 (1977).
(16) G. A. Cutter, *Anal. Chim. Acta*, **98**, 59 (1978).
(17) D. F. Schutz and K. K. Turekian, *Geochim. Cosmochim. Acta*, **29**, 259 (1965).
(18) Y. Shimoishi and K. Tôei, *Anal. Chim. Acta*, **100**, 65 (1978).

RECEIVED for review November 27, 1978. Accepted January 15, 1979.

Effect of Matrix on the Determination of Volatile Metals in Biological Samples by Flameless Atomic Absorption Spectrometry with the Graphite Tube Atomizer

Haleem J. Issaq

Chemical Carcinogenesis Program, NCI Frederick Cancer Research Center, Frederick, Maryland 21701

The effect of varying the matrix, ashing temperature, or digesting agent on the determination of the amount of volatile metals in biological samples was studied. The results showed that changing these parameters can affect the accuracy of the measurements. While it was found that an ashing temperature above 600 °C is impractical for the determination of Pb, Cd, and Zn in biological samples, no loss of signal occurred when these compounds were analyzed in an aqueous solution.

The analysis of trace metals in physiological fluids and tissues is important both from the standpoint of physiological function and potential toxicity.

Atomic absorption spectrometry (AAS) is the most widely-used analytical method for trace metal determinations in biological samples. Analysis by flame AAS poses several analytical restrictions, including sample-size requirements (5 mL/min), restricted sensitivity (ppm range), and interference from the sample matrix. The first two problems may be overcome by flameless AAS, which requires samples in the microliter range, and has an absolute sensitivity in the picogram range. Thus, flameless AAS is more appropriate for the determination of trace metals in biological and clinical samples. The charring step is an especially critical aspect of sample analysis by flameless AAS, particularly in the analysis of "volatile" trace metals.

To achieve complete charring of organic material, a high temperature over a long period of time must be used. An alternative is to use oxidizing agents or Triton X-100 which aid in the charring step. It is clear that high charring temperatures are impractical for volatile metals. A low charring temperature may lead to erroneous results because of background interference from smoke. Interference in the tube can be more severe than that in the flame.

Interference in the flameless AAS using a graphite tube atomizer is of two types. (i) Background interference which is produced by nonspecific light scatter or absorption in the tube. This can be caused by molecular species vaporized in the tube, or by smoke formation in the light path. (ii) Matrix interference is caused by chemical interaction between the element being analyzed and other species present in the sample. Volatile compounds can be formed that vaporize at the ashing step, or a compound that will not atomize under the experimental conditions of the analysis (*1*) is produced. These situations result in a decrease in the signal.

Background interference can be eliminated by the use of background correction. Matrix interference is overcome by adjusting the charring (ashing) temperature or by treating the sample chemically to eliminate, or at least control, the interference. Morgenthaler (2) compared the interference in the tube to that in the flame and concluded that the matrix interference (chemical) is usually much more severe in the furnace, and the releasing agents used for the flame may be ineffective in the furnace.

Normally, quantitation in flameless AAS is carried out either by comparing the peak height (area) of the sample with that of the standard, or by the standard addition method. Although these methods of quantitation are applicable to dilute aqueous solutions, they may not be adequate for the analysis of biological or clinical samples. To achieve reliable quantitative data, the sample and the standard should have the same matrix and the same metal species, a salt, a complex, or an oxide. In a biological sample, unlike a standard metal salt in an aqueous solution, the metal may exist in a form having a vapor pressure different from that of the standard. Therefore, to get accurate results, the metal species should be the same in the standard and the sample. This may be achieved by dry ashing (low or high temperature) or by wet digestion (an acid or an oxidizing agent). Either has its advantages and disadvantages, and should be used with caution. Ashing at high temperatures may lead to the loss of volatile metal species; on the other hand, wet digestion may introduce contamination. The advantage of both methods is twofold; destruction of organic matter (to minimize background) and conversion of different metal species into one form, an oxide or a salt (to minimize matrix interferences).

This paper examines methods for overcoming the problems associated with the ashing step. The addition of acids, hydrogen peroxide, and Triton X-100 to the samples as aids in the ashing step were studied. The results also address problems that can occur from the use of too high a sample ashing temperature or the wrong type of digestion agent. The selection of suitable conditions for the ashing temperature, which will lead to accurate quantitative results of trace metal determinations in biological samples by flameless AAS are discussed.

EXPERIMENTAL

Apparatus. A Perkin-Elmer Model 403 atomic absorption spectrometer with a strip chart recorder and a Pb, Cd, or Zn hollow cathode lamp (Westinghouse) was used. Absorption lines and lamp currents used are Pb (217 nm, 7 mA); Cd (228.8 nm, 10 mA); Zn (213.9 nm, 15 mA). A Perkin-Elmer HGA-2000 hollow graphite atomizer was used with a modified graphite tube (*3*). Eppendorf microliter pipets having disposable plastic tips were used for sample introduction into the tubes. An alumel–chromel thermocouple was used to measure the temperature of the tube by inserting the thermocouple through the center hole of the graphite tube until it contacted the opposite internal wall of the tube.

Reagents and Samples. Deionized water was used in all sample preparations. Serum samples were obtained from normal mice. Lead nitrate, cadmium nitrate, and zinc nitrate (1000 ppm Fisher certified atomic absorption standards) were used.

Procedure. Standard solutions of 1 ppm of Pb, Cd, and Zn were prepared from stock solutions in 2% HNO_3, HCl, H_2O_2, and their 1:1 combinations, and in 1% Triton X-100. Ten-μL aliquots of each solution were introduced into the graphite tube furnace which were then dried for 30 s at 100 °C, ashed for 30 s at a selected temperature and atomized for 6 s at 2100 °C. The graphite furnace was operated with an argon purge and a water flow of 1.5 and 3 L/min, respectively. Serum samples were diluted 1:1 v/v with the above solutions. Twenty μL of each, after thorough mixing, were pipetted into the graphite furnace and run

This article not subject to U.S. Copyright. Published 1979 by the American Chemical Society

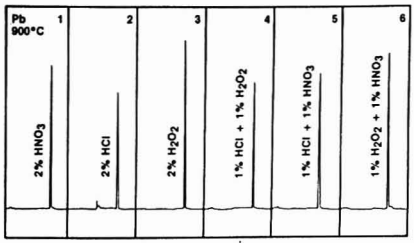

Figure 1. Effect of a 900 °C ashing temperature on the signal of 10 ppb lead in 2% HNO_3, 2% HCl, 2% H_2O_2, 1% HCl + 1% H_2O_2, 1% HCl + 1% HNO_3, and 1% HNO_3 + 1% H_2O_2

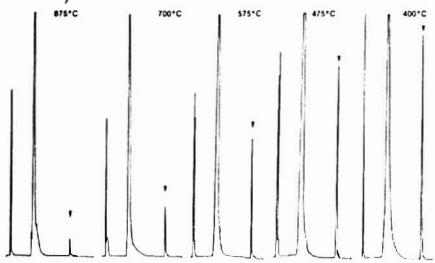

Figure 2. Comparison of 10 ppb lead signal in 2% HNO_3:serum 1:1 at ashing temperatures of 875, 700, 575, 475, and 400 °C. Arrow indicates lead serum signal

under the same conditions used for the standards.

RESULTS AND DISCUSSION.

Three volatile elements Pb, Cd, and Zn of biological significance (toxic Pb and Cd and essential trace element Zn), and three reagents HCl, HNO_3, and H_2O_2 and their 1:1 v/v combinations were selected for this study. Triton X-100, which has been used by other researchers to produce complete lysis of cellular components (*4*, *5*) was also evaluated.

To determine the optimum ashing temperature for serum samples containing Pb, Cd, and Zn it was necessary to establish an optimum ashing temperature for the standard solution of the three metals in HCl, H_2O_2, and HNO_3, and Triton X-100. On the basis of previous experience (*6*), it was suspected that the ashing temperature of a metal in an aqueous standard may not be the same as that in a biological sample, but it is necessary to establish the temperature at which the metal salt solutions are stable. At a temperature of 900 °C (Figure 1), it was found that there was no loss of signal during ashing for lead in solutions 1–6. However, when the temperature was raised to 1000 °C, the escape of volatile species was observed for all the lead solutions, with 2% HNO_3 showing the least loss. Figure 1 also indicates that there was a signal enhancement when H_2O_2 was used, (solutions 3 and 6). This may be because both HNO_3 and H_2O_2 prevent the adsorption of lead by container walls (*7*) and/or the formation of more stable lead species than in the other reagents.

Since an ashing temperature of 900 °C did not cause any loss of Pb from five of the six solutions (Figure 1), and since Pb in 2% HNO_3 was the most stable one, it was decided to use 2% HNO_3 and an ashing temperature of 875 °C for the analysis of lead in serum. Comparison of a 1 ppm lead signal in 2% HNO_3, and in 1:1 v/v serum:2% HNO_3 (Figure 2) showed that, although a large signal was obtained for lead in 2% HNO_3, the signal in spiked serum was almost nonexistent (arrow). It was concluded that most of the $PbNO_3$ formed

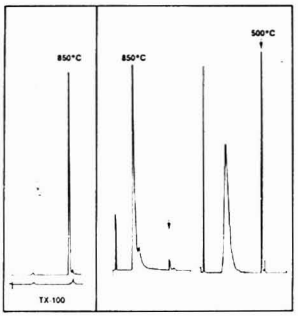

Figure 3. Comparison of 10 ppb lead signal in Triton X-100 (left) and in serum:2% Triton X-100 1:1 (right) at ashing temperatures of 850 and 500 °C. Arrow indicates lead serum signal

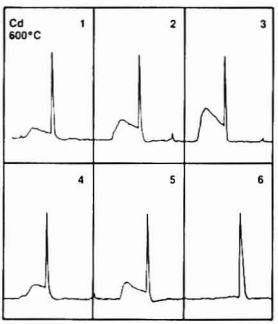

Figure 4. Effect of 600 °C ashing temperature on the signal of 10 ppb cadmium in 2% HNO_3, 2% HCl, 2% H_2O_2, 1% HCl + 1% H_2O_2, 1% HCl + 1% HNO_3, and 1% HNO_3 + 1% H_2O_2

a volatile specie(s) with the serum that escaped during the ashing step. As a result, the ashing temperature was lowered to determine the effect on the serum lead signal. When the ashing temperature was lowered from 875 to 700 °C, a greater signal was observed; this however was still only about 25% of the expected lead signal. At 575 °C, the serum lead signal was about 50% of that in acid. Although the ashing temperature was lowered to 475 °C, the serum lead signal was still less than that of the expected lead signal in 2% HNO_3. The signals in both serum and acid were of equal intensity at 400 °C. Figure 2 indicates that the formation of volatile species predominated over formation of nonvolatile species. It is important to note that at low ashing temperature, such as 400–500 °C, it is necessary to use background correction, because of residual carbon matter which may burn during the atomizing step and give a false signal. When 2% H_2O_2 was used in place of 2% HNO_3, the results were the same as with the acid.

Kubasik et al. (*4*) and, later, Fernandez (*5*) treated blood samples with dilute Triton X-100 before introducing the sample into the furnace. When a 1:1 v/v serum:2% Triton X-100 solution was tested for Pb at an ashing temperature of 850 °C, no signal was observed for Pb in the serum (Figure 3). When the ashing temperature was lowered to 500 °C, the Pb signals in both the 2% Triton X-100 and in the serum:Triton X-100 solution were the same (Figure 3).

With Cd and Zn, the effect of ashing temperature on the signal was similar to that seen in the case of Pb. The effect of ashing temperature on the signal of Cd in different solutions

is given in Figure 4. It is clear from Figure 4 that at a temperature of 600 °C volatile species escaped from all the solutions except 1% HNO_3 + 1% H_2O_2 where no loss of Cd was observed. No improvement was seen when the temperature was lowered to 500 °C. At an ashing temperature of 400 °C, little loss was observed from solutions containing 2% HCl, 2% H_2O_2, and 1% HCl + 1% HNO_3. Figure 4 indicates that it is possible to determine Cd in an aqueous solution at 600 °C if nitric acid is used; otherwise a lower ashing temperature should be employed.

Calibration curves can be obtained for volatile metals in serum if the ashing temperature is low (400–600 °C), depending on the vapor pressure of the metal being analyzed. Also, higher temperatures may be used at the expense of sensitivity, i.e., lower signals at higher temperatures. Zinc, as mentioned earlier, gave the same results as lead and cadmium.

Another point is that when the temperature is low (below 500 °C), the background may interfere with the signal which could lead to erroneous results unless background correction is employed.

A few precautions should be taken before an analysis is made: (1) It might be advantageous to test the sample at different charring temperatures before analyzing a number of samples. (2) Cook-book procedures should be evaluated before use. A specific ashing and atomizing temperature may not apply in all cases. (3) It is advantageous to run a sample and to monitor its drying and charring behavior and compare these with the pure salt standard in water.

CONCLUSION

It is clear that when ashing biological samples, the ashing temperature, the sample matrix, and the digesting agent can affect the results drastically. Therefore, it is important to test each element in each matrix before carrying out an analysis. Also, check the temperature and the acid or combination of acids and H_2O_2 to be used. We observed that Triton X-100 aids in the charring of organic matter at low temperature. This can be checked by looking inside the tube. When HCl was used with whole blood at 500 °C, a small bead of carbon was found, while in the case of Triton X-100 it was absent.

The results also indicate that the standard addition method should be used carefully and only after checking all the conditions. Also, certain metals are more stable than others in the same medium; for example, while Cd is stable in 1:1 HNO_3:H_2O_2 at 600 °C, Zn is not. Finally, if the size of the sample and concentration allows the use of the flame, it is recommended that it be used.

ACKNOWLEDGMENT

The author thanks L. P. Morgenthaler for helpful and stimulating discussion.

LITERATURE CITED

(1) L. P. Morgenthaler, V. J. Luciano, and J. P. Maney, 29th Pittsburgh Conference on Analytical Chemistry and Applied Spectroscopy, Cleveland, Ohio, 1978, paper 135.
(2) L. P. Morgenthaler, private communication, 1978.
(3) H. J. Issaq and W. L. Zielinski, Jr., *Anal. Chem.*, **47**, 2281 (1975).
(4) N. P. Kubasik, M. T. Volosin, and M. H. Murray, *Clin. Chem.* (*Winston-Salem, N.C.*) **18**, 410 (1972).
(5) F. J. Fernandez, *Clin. Chem.* (*Winston-Salem, N.C.*) **21**, 558 (1975).
(6) H. J. Issaq, unpublished results.
(7) H. J. Issaq and W. L. Zielinski, Jr., *Anal. Chem.*, **46**, 1328 (1974).

RECEIVED for review December 7, 1978. Accepted January 11, 1979. Research sponsored by the National Cancer Institute under Contract No. N01-CO-75380 with Litton Bionetics, Inc. Presented in part at the 29th Pittsburgh Conference on Analytical Chemistry and Applied Spectroscopy, Cleveland, Ohio, 1978.

Design of a Phosphoroscope and the Examination of Room Temperature Phosphorescence of Nitrogen Heterocycles

Charles D. Ford and Robert J. Hurtubise*

Chemistry Department, The University of Wyoming, Laramie, Wyoming 82071

A phosphoroscope and reflection assembly for a spectrodensitometer is described. They were employed to obtain room temperature phosphorescence (RTP) data from several nitrogen heterocycles adsorbed on dried silica gel and filter paper. The effects of acid and different gases on the RTP of these compounds adsorbed on silica gel and filter paper is discussed. Also, the analytical potential of this new approach is considered.

Many nitrogen heterocycles have been found in urban air (*1*), effluents from coal burning operations, coal-tar-pitch fumes, petroleum refinery incineration (*2*), and from automobile exhausts (*3*). Furthermore, some of these compounds are cancer suspect agents (*3, 4*). Nitrogen heterocycles are also found in high-boiling petroleum distillates and shale oils (*5, 6*). They are believed to interfere with important refining processes such as reducing the activity of cracking or hydrocracking catalysts (*7*). For these reasons there is great interest in developing new analytical approaches for the identification and quantitation of the nitrogen heterocycles.

Several papers have been published recently on the analytical aspects of RTP (*8–24*). We have reported RTP from the phthalic acid isomers, *p*-aminobenzoic acid, and terephthalamide adsorbed on dried silica gel (*22*). In the present work we have broadened the range of application of silica gel as a solid support for RTP. Useful RTP has been observed from several nitrogen heterocycles when spotted from 0.1 M HCl ethanolic solutions onto a silica gel chromatoplate. Since several of the compounds examined exhibited fluorescence which interfered with RTP measurements, a phosphoroscope was designed and constructed for use with a Schoeffel SD3000 spectrodensitometer. With the modified spectrodensitometer, RTP measurements could be made directly from compounds adsorbed on thin-layer chromatoplates or filter paper. Additionally, a comparison of the RTP of the nitrogen heterocycles adsorbed on dried filter paper and silica gel was made.

0003-2700/79/0351-0659$01.00/0 © 1979 American Chemical Society

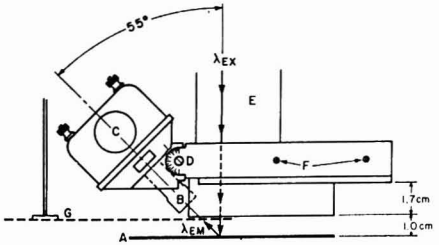

Figure 1. Modified reflection mode assembly. A, the RTP solid support; B, detector lens; C, photomultiplier tube housing; D, photomultiplier tube housing angle adjustment screw; E, optical nose of spectrodensitometer; F, slide adjust screws for varying distance from exciting radiation to photomultiplier tube housing; G, rotating disc

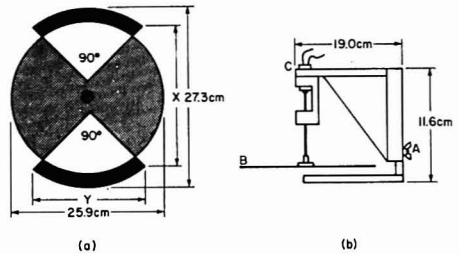

Figure 2. The disc (a) and mount (b) of the phosphoroscope assembly. A, wingnut for disc height adjustment; B, rotating disc; C, motor

EXPERIMENTAL

Apparatus. Phosphorescence excitation and emission spectra were obtained with a Perkin-Elmer MPF-2A fluorescence spectrophotometer equipped with a phosphoroscope accessory. A 150-W Xe arc lamp and a 1P28 photomultiplier tube were employed. RTP spectra were recorded with the excitation and emission slits of the fluorescence spectrophotometer set at 12 and 14 nm, respectively, directly from 100 ng of the compound adsorbed on a 4 cm by 0.8 cm section of a dried aluminum backed silica gel chromatoplate. The chromatoplate section was placed at approximately a 45° angle with respect to the source and the emission slit. The mounting device which held the chromatoplate was constructed of two 4 cm × 0.5 cm × 0.5 cm aluminum bars which were drilled and tapped at opposite ends so the chromatoplate section could be mounted between the metal bars. With the chromatoplate section thus fixed, the device was mounted on the support frame of the rotating can phosphoroscope and the RTP signal from the compound adsorbed on the silica gel plate was maximized.

Calibration curves and relative RTP signals were measured with a Schoeffel SD3000 spectrodensitometer with the inlet and exit slits at 2 and 3 mm, respectively. A 150-W Xe lamp and R-777 photomultiplier tube were employed.

Because some of the compounds studied exhibited fluorescence which interfered with RTP measurements, it was necessary to modify the spectrodensitometer and to design and construct a reflection mode assembly and a phosphoroscope which would be compatible with the Schoeffel spectrodensitometer. The modified reflection mode assembly is shown in Figure 1. The assembly allowed the distance from the source exit to the photomultiplier tube to be varied by means of an adjustable slide. Also, the angle of the photomultiplier tube housing could be adjusted to maximize the reflected RTP striking the lens of the photodetector system. The above modifications were necessary to accommodate a rotating disc phosphoroscope.

The phosphoroscope assembly consisted of a variable speed dc motor (0–12V) and a rotating disc phosphoroscope. The motor was powered by a Railine model 370N transformer. The assembly was designed for use with the modified reflection mode assembly of the spectrodensitometer (Figure 2). The phosphoroscope (Figure 2a) was constructed of thin sheet aluminum and was painted flat black to minimize scattered radiation. The dc motor was mounted in an aluminum frame which allowed the phosphoroscope to be raised or lowered via an adjustable slide (Figure 2b).

In region *X* (Figure 2a) the compound on the solid surface was excited by the source radiation; however, the lens which collects the reflected luminescence and focuses it onto the photomultiplier tube was positioned so no luminescence was detected. As the phosphoroscope rotated region *Y* (Figure 2a) over the adsorbed compound, the compound was no longer excited and the lens which focuses the reflected luminescence onto the photomultiplier tube detected any delayed luminescence which originated from the adsorbed compound. Several disc phosphoroscopes were tested and the one described yielded the best results. The experimental setup of the modified reflection mode assembly and the phosphoroscope was arranged so the cover of the spectrodensitometer was closed during RTP signal measurements.

Because of the size of the phosphoroscope assembly, only 12 cm of a 20-cm length of chromatoplate or other solid surface could be scanned with the spectrodensitometer. However, this was adequate space for 8 or 9 sample spots.

Other workers have shown that RTP from compounds adsorbed on solid surfaces is enhanced when measured in the absence of oxygen (*17*, *23*). To measure the RTP from compounds adsorbed on solid surfaces under O_2-free conditions, a simple gas handling system was constructed. A piece of copper tubing was used to direct the flow of inert gases over the adsorbed compounds. The copper tubing (5 mm o.d.) was 24.5 cm in length and plugged at one end. About 1 cm from the plugged end; there was a small slit out of which the inert gases flowed onto the adsorbed compounds. The copper tubing was mounted in a lead block for stability. The gases (N_2 and He) were passed through a drying tube (a plastic tube containing $CaSO_4$) before being forced out the tube and over the adsorbed compounds during the measurement step (Table II).

Reagents. Ethanol was purified by distillation as described by Winefordner and Tin (25). Benzo[*f*]quinoline (B[*f*]Q) and phenanthridine were recrystallized from ethanol and distilled water. Quinoline was distilled at reduced pressure with a 61-cm bubble plate fractionation column and collected at 54 °C. Both 2,5-pyridine dicarboxylic acid and *p*-aminobenzoic acid were recrystallized from ethanol, and 4-azafluorene was recrystallized from hexane, ethanol, and distilled water. Each compound was checked for luminescent impurities by TLC and, if no impurities were observed, the compounds were used without further purification. All other compounds were reagent grade and used as received. The silica gel chromatoplates were aluminum backed (EM Laboratories, Elmsford, N.Y.) and were developed in distilled ethanol prior to RTP experiments to concentrate any luminescent impurities at one end of the plate. The filter paper employed was Whatman No. 1 and was used as received.

Procedure. All compounds were dissolved initially in distilled ethanol prior to spotting on a silica gel chromatoplate or filter paper. For calibration curves, each compound except *p*-aminobenzoic acid and 2,5-pyridine dicarboxylic acid was spotted from ethanol solutions which were 0.1 M HCl. Each solution containing a nitrogen heterocycle was acidified by mixing 40 μL of concentrated HCl with 5 mL (final volume) of the ethanol solution to be spotted. The acid was added by means of a Quickpipette (Helena Labs, Beaumont, Tex.)

Careful attention was given to the spotting technique employed for RTP work. Prior to spotting, the plates or filter papers were marked with a pencil so straight dashed lines appeared in the same plane across the solid surface. The Hamilton syringe containing the adsorbate solution was positioned carefully between dashes so the center of each spot lay in line with the markings. Best reproducibility was realized when spot size was maintained as constant as possible. Of the 3 μL spotted, one third of the solution was initially placed on the plate or filter paper. Care was taken not to increase the size of this initial spot while spotting the remaining two thirds of the sample solution. With some practice, this technique gave good reproducibility.

After spotting the silica gel chromatoplate in duplicate with 3 μL of each freshly prepared standard solution with a 5-μL

Table I. Comparison of RTP Data of *N*-Heterocycles Spotted on Silica Gel and Filter Paper

compound[a]	λ_{ex}, nm	λ_{em}, nm[b]	silica neutral RI[c]	silica acid RI[d]	filter paper neutral RI[c]	filter paper acid RI[d]
benzo[*f*]quinoline	370	510	5.1	55.2	20.5	100
phenanthridine	360	510	3.6	42.4	8.5	46.0
4-azafluorene	330	465	6.4	22.8	17.5	42.0
1,10-phenanthroline·H_2O	325	520	1.8	7.5	7.5	17.5
4,7-diphenyl-1,10-phenanthroline	310	518	N.D.[e]	11.3	4.5	23.5
2,9-dimethyl-4,7-diphenyl-1,10-phenanthroline	330	518	N.D.	12.0	13.5	17.5
quinoline	320	510	N.D.	7.0	7.5	20.0
isoquinoline	330	520	2.0	8.0	3.7	25.0

[a] Each compound at 100 ng/spot. [b] λ_{ex} and λ_{em} maximized for Schoeffel unit. [c] Compounds spotted from ethanol solutions. [d] Compounds spotted from ethanol solutions which were 0.1 M HCl. [e] N.D. = none detected.

Hamilton syringe, the aluminum backed plate was allowed to dry in the atmosphere for 5 min and was then placed in an oven at 105–110 °C to dry for an additional 30 min. The plate was removed from the oven and allowed to cool to room temperature. Then the plate was positioned carefully on the stage of the densitometer. The RTP signal was maximized for the most concentrated spot, and the signals for all the spots were measured by starting the moving stage of the densitometer. It was not necessary to maximize the signal for each spot because of the careful spotting technique employed.

When filter paper was employed as the adsorbent, 3 μL of the solution containing the nitrogen heterocycle was placed on the paper in duplicate, again using a 5-μL Hamilton syringe. The filter paper was allowed to dry in the atmosphere for 5 min before being placed in an oven to dry for 10 min at 105–110 °C. If the paper was placed in the oven immediately after spotting, the spots of the compound which were acidified appeared blackened after drying. After drying, the paper was placed on the stage of the modified spectrodensitometer and the RTP signals were recorded as described above for silica gel plates. No special drying procedure was performed during the measurement step for the data in Tables I and III. For the data in Table II, the gas handling system was employed during the measurement step.

RESULTS AND DISCUSSION

Silica Gel. RTP was observed from compounds adsorbed on aluminum backed and glass backed, conventional TLC and HPTLC silica gel plates (EM Laboratories). No RTP was observed from the compounds adsorbed on Brinkmann (MN) plastic backed silica gel TLC plates. RTP was also observed from compounds adsorbed on dried MN-Kieselgel 60 (Düren, Germany) for dry column chromatography; however, no RTP was observed for compounds adsorbed on dried Mallinckrodt SilicAR TLC-7G for TLC. Investigations are underway to explain the above results.

Excitation and Emission Spectra. The phosphorescence excitation and emission spectra of each compound adsorbed on dried silica gel were obtained using the phosphoroscope accessory of the MPF-2A fluorescence spectrophotometer. The uncorrected phosphorescence excitation and emission spectra of B[*f*]Q were obtained at liquid nitrogen temperature (LTP) with the protonated compound in ethanol and at room temperature with the protonated compound adsorbed on a dried aluminum backed silica gel chromatoplate (Figure 3). The LTP excitation spectrum of B[*f*]Q gave peaks at 287 and 367 nm, and the RTP excitation spectrum gave peaks at 291 and 367 nm. The LTP emission spectrum of the compound in ethanol showed peaks at 437, 475, and 509 nm, whereas, the RTP emission peaks were at 434, 488, and 516 nm.

Acid Effect on the RTP of Nitrogen Heterocycles. The LTP excitation and emission spectra of phenanthridine were obtained both in ethanol and in acidified ethanol (0.1 M HCl) with the fluorescence spectrophotometer. A comparison of the spectral data showed a red shift in the emission spectra in going from ethanol solution to 0.1 M HCl ethanol solution of the compound. The LTP intensity was approximately

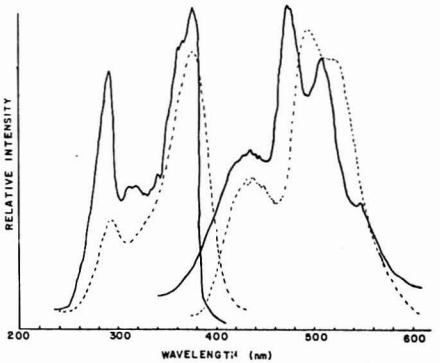

Figure 3. The LTP (—) and RTP (---) excitation and emission spectra of B[*f*]Q in ethanol (LTP) and on dried silica gel (RTP). Phosphorescence intensities were adjusted arbitrarily

doubled in going from an ethanol solution to an acidified ethanol solution of phenanthridine at a concentration of 1.0 μg/mL. These data suggest that protonation of the nitrogen heterocyclic compound serves to enhance the LTP.

Ethanol solutions with a fixed amount of B[*f*]Q containing from 10^{-6} to 1.0 M HCl were spotted in duplicate on a silica gel chromatoplate and the plate was dried. The RTP of B[*f*]Q vs. the concentration of HCl plot appeared as an S-shaped curve (Figure 4). Graphs of the data obtained for phenanthridine and 1,10 phenanthroline were similar to that in Figure 4 with the increase in RTP occurring between 10^{-3} and 10^{-1} M HCl. Therefore 0.1 M HCl ethanolic solutions of the nitrogen heterocycles were employed for the quantitative RTP data of these compounds adsorbed on solid surfaces.

Table I gives a comparison of the relative RTP intensities of the nitrogen heterocycles. The compounds were spotted from ethanol solutions and ethanol solutions which were 0.1 M in HCl onto silica gel and filter paper and measured in air. The data in Table I show that in each case protonation of the nitrogen heterocycle enhances the RTP of the compounds adsorbed on dried silica gel and filter paper. Just as other workers have established that anions and cations of certain organic compounds exhibited more intense RTP on solid surfaces than the neutral compound, it seemed reasonable that the cations of the nitrogen heterocycles should exhibit more intense RTP when adsorbed on solid surfaces than their neutral counterparts (*9–12, 15*). Schulman and Walling (*10*) observed RTP from the cations of auramine O and ethyl violet adsorbed on Whatman No. 1 filter paper. Apparently ionic compounds can interact more strongly with the adsorbent which leads to a more rigidly held compound and more intense

Table II. Comparison of the RTP Intensities of *N*-Heterocycles on Silica Gel and Filter Paper Measured Under Air, N_2 and He

compound	silica (acid)[a,b]			filter paper (acid)[a,b]		
	air	nitrogen	helium	air	nitrogen	helium
benzo[*f*]quinoline	55.2	67.5	84.5	100	111	116
phenanthridine	42.4	47.8	57.5	46.0	52.0	55.0
4-azafluorene	22.8	26.8	33.6	42.0	50.5	54.5
1,10-phenanthroline·H_2O	7.5	10.0	12.5	17.5	19.0	22.0
4,7-diphenyl-1,10-phenanthroline	11.3	15.5	16.5	23.5	23.7	26.0
2,9-dimethyl-4,7-diphenyl-1,10-phenanthroline	12.0	14.3	15.3	17.5	20.0	22.5
quinoline	7.0	9.5	10.5	20.0	22.2	23.5
isoquinoline	8.0	8.5	10.8	25.0	28.0	28.0

[a] Each compound at 100 ng/spot. [b] Compounds spotted from ethanol which were 0.1 M HCl.

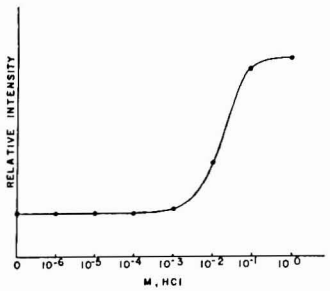

Figure 4. The RTP of B[*f*]Q vs. HCl concentration in ethanol. Each B[*f*]Q spot at 400 ng

RTP (*21*, *23*). The nature of the interaction between the cations of the nitrogen heterocycles and silica gel and filter paper is currently under investigation in this laboratory.

O_2 Quenching. Vo-Dinh et al. (*17*) and Schulman and Parker (*23*) reported that oxygen partially quenches the RTP of compounds adsorbed on dried paper supports. Our study indicates that the O_2 in air quenches the RTP of the nitrogen heterocycles adsorbed on dried silica gel and filter paper. The data in Table II show the RTP intensities of several protonated nitrogen heterocycles with air, dry N_2, and dry He flowing over the adsorbed compounds. Furthermore, when dry O_2 was passed over the adsorbed compounds the RTP relative intensity decreased by almost 30% for benzo[*f*]-quinoline, 1,10-phenanthroline, and 4-azafluorene when compared to their RTP intensities measured in air.

If one compares the RTP relative intensity in Table II of each compound measured in the presence of O_2 (air) and in the absence of O_2 (under N_2 or He flow) on silica gel and filter paper, it appears that RTP of the compounds adsorbed on dried silica gel is generally more subject to O_2 quenching than the RTP of the same compounds adsorbed on dried filter paper. For example, the percent enhancement of benzo[*f*]-quinoline measured in He vs. air is 53% for silica gel and is only 16% for filter paper (Table II). This seems reasonable if one recognizes that silica gel is more porous than filter paper and therefore has more surface area on which O_2 could potentially interact with adsorbed compounds.

Analytical Data. Table III gives the linear range of the RTP calibration curves obtained from the compounds adsorbed on dried silica gel and the RTP limits of detection (LOD = ng/spot which gives 2× the background signal). The data are given for the RTP of the protonated compounds measured in air. In no case did measuring the RTP of the compounds spotted from acid solutions on dried silica gel under N_2 or He flow alter the linear ranges, only the LODs changed slightly. However, the data scatter of some of the weaker phosphors with N_2 and He was less than for air. Figure 5 shows the calibration curves of isoquinoline, a weak phosphor, adsorbed on dried silica gel where the RTP was measured under air, N_2, and He flow.

Table III. RTP Analytical Data from Compounds Adsorbed on Dried Silica Gel[a]

compound	λ_{ex}, nm	λ_{em}, nm[b]	linear range, ng	LOD, ng/spot
benzo[*f*]quinoline	370	510	0–125	3
phenanthridine	360	510	0–160	6
4-azafluorene	330	465	0–100	10
1,10-phenanthroline·H_2O	325	520	0–140	25
4,7-diphenyl-1,10-phenanthroline	310	518	0–175	12
2,9-dimethyl-4,7-diphenyl-1,10-phenanthroline	330	518	0–150	20
quinoline	320	510	0–100	25
isoquinoline	330	520	0–250	22
p-aminobenzoic acid	287	432	0–150	10
2,5-pyridine-dicarboxylic acid	289	435	0–120	15

[a] All compounds spotted from ethanol solutions which were 0.1 M HCl except *p*-aminobenzoic acid and 2,5-pyridine dicarboxylic acid which were spotted from ethanol solutions. [b] λ_{ex} and λ_{em} were maximized for the Schoeffel unit.

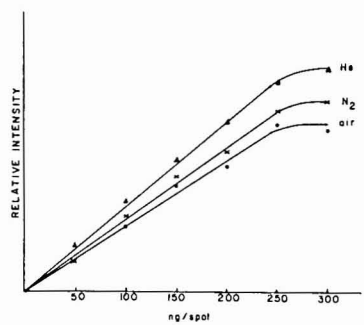

Figure 5. The RTP intensity vs. concentration of isoquinoline spotted from 0.1 M HCl ethanol solutions on a silica gel chromatoplate

Reproducibility of RTP. Sixteen spots of B[*f*]Q from 0.1 M HCl ethanol solution at 100 ng each were placed on a silica gel chromatoplate, and the RTP from each spot was recorded in air as described in Experimental. The standard deviation was determined to be 1.50 relative intensity (RI) units. The 95% confidence limits were calculated to be 46.5 ± 0.8 RI units. A similar experiment with 4-azafluorene resulted in a standard deviation of 0.93 RI units and 95% confidence

limits of 16.7 ± 0.5 RI units for sixteen 100-ng spots.

Plate-to-Plate Variation of RTP. Three aluminum backed silica gel chromatoplates were each spotted with five 100-ng spots of B[*f*]Q. After drying, the RTP signals were recorded for each with the modified spectrodensitometer. The average RTP intensities obtained for the three plates were 62.0 (plate 1), 54.8 (plate 2), and 57.6 (plate 3). Because of the plate-to-plate variation in RTP of compounds adsorbed on silica gel, any quantitative method which employs RTP from compounds adsorbed on commercial chromatoplates should include RTP measurement of the proper standards along with the unknowns on the same chromatoplate.

Total Luminescence Approach. Several of the compounds in Table III also exhibited visible fluorescence when adsorbed on dried silica gel. For example, B[*f*]Q, phenanthridine, and quinoline exhibit visible fluorescence in addition to RTP when adsorbed on dried silica gel. The fluorescence emission maxima for the three compounds were 428, 418, and 400 nm, respectively. There are certain analytical advantages to employing both fluorescence and RTP. For example, the identification of unknowns is aided by fluorescence excitation and emission spectra, RTP emission spectra, and the RTP lifetime of compounds that can be measured easily. Also, one is not restricted to a single luminescence process. If, for example, B[*f*]Q were being determined and the spot containing B[*f*]Q was found to contain a fluorescent impurity but no phosphorescent impurity, RTP could be employed to quantitate the B[*f*]Q in the sample without interference from the fluorescent impurity.

A fluorescence calibration curve was obtained for B[*f*]Q adsorbed on dried silica gel in air. The linear range was found to be 0–100 ng and the limit of detection was 1 ng. When dry He was blown over the spot, the fluorescence signal was enhanced by 30%, indicating some O_2 quenching with air.

CONCLUSION

RTP and fluorescence analysis of compounds adsorbed on solid surfaces such as silica gel and filter paper are powerful qualitative and quantitative analytical tools because of their sensitivity and selectivity. The phosphoroscope described in Experimental, and designed for use with a Schoeffel SD3000 spectrodensitometer, works well for obtaining RTP from compounds adsorbed on silica gel chromatoplates or filter paper. Furthermore, silica gel was stressed over filter paper in the RTP work because RTP can be combined with the speed and versatility of TLC on silica gel to yield a very useful analytical approach for determining nitrogen heterocycles. Work is in progress in this laboratory to demonstrate the applicability of this approach to shale oil samples. Certainly, silica gel or filter paper can be used in conjunction with high-performance liquid chromatography (HPLC) by collecting a fraction from a HPLC column, adsorbing the components on the solid surface, and then measuring either fluorescence or RTP. This aspect is being pursued also.

LITERATURE CITED

(1) Sawicki, E.; McPherson, S. P.; Stanley, T. W.; Meeker, J. E.; Elbert, W. C. *Int. J. Air Water Pollut.* **1965**, *9*, 515.
(2) Sawicki, E.; Stanley, T. W.; Elbert, W. C. *J. Chromatogr.* **1965**, *18*, 512.
(3) Sawicki, E.; Meeker, J. E.; Morgan, M. *Arch. Environ. Health* **1965**, *11*, 773.
(4) Dong, M.; Locke, D. C. *J. Chromatogr. Sci.* **1977**, *15*, 32.
(5) McKay, J. F.; Weber, J. H.; Latham, D. R. *Anal. Chem.* **1976**, *48*, 891.
(6) Poulson, R. E. *Prepr. Div. Fuel Chem., Am. Chem. Soc.* **1975**, *20*(2), 183.
(7) Drushel, H. V.; Sommers, A. L. *Anal. Chem.* **1966**, *38*, 19.
(8) Roth, M. *J. Chromatogr.* **1967**, *30*, 276.
(9) Schulman, E. M.; Walling, C. *Science* **1972**, *178*, 53.
(10) Schulman, E. M.; Walling, C. *J. Phys. Chem.* **1973**, *77*, 902.
(11) Paynter, R. A.; Wellons, S. L.; Winefordner, J. D. *Anal. Chem.* **1974**, *46*, 736.
(12) Wellons, S. L.; Paynter, R. A.; Winefordner, J. D. *Spectrochim. Acta, Part A* **1974**, *30*, 2133.
(13) Seybold, P. G.; White, W. *Anal. Chem.* **1975**, *47*, 1199.
(14) White, W.; Seybold, P. G. *J. Phys. Chem.* **1977**, *81*, 2035.
(15) Vo-Dinh, T.; Yen, E. L.; Winefordner, J. D. *Anal. Chem.* **1976**, *48*, 1186.
(16) Vo-Dinh, T.; Yen, E. L.; Winefordner, J. D. *Talanta* **1977**, *24*, 146.
(17) Vo-Dinh, T.; Walden, G. L.; Winefordner, J. D. *Anal. Chem.* **1977**, *49*, 1126.
(18) Jakovljevic, I. M. *Anal. Chem.* **1977**, *49*, 2048.
(19) von Wandruszka, R. M. A.; Hurtubise, R. J. *Anal. Chem.* **1976**, *48*, 1784.
(20) von Wandruszka, R. M. A.; Hurtubise, R. J. *Anal. Chim. Acta* **1977**, *93*, 331.
(21) von Wandruszka, R. M. A.; Hurtubise, R. J. *Anal. Chem.* **1977**, *49*, 2164.
(22) Ford, C. D.; Hurtubise, R. J. *Anal. Chem.* **1978**, *50*, 610.
(23) Schulman, E. M.; Parker, R. T. *J. Phys. Chem.* **1977**, *81*, 1932.
(24) de Lima, C. G.; de M. Nicola, E. M. *Anal. Chem.* **1978**, *50*, 1658.
(25) Winefordner, J. D.; Tin, M. *Anal. Chim. Acta* **1964**, *31*, 239.

RECEIVED for review December 18, 1978. Accepted February 5, 1979. This work was supported partially by both the Department of Energy's Laramie Energy Technology Center under Contract No. DE-AS20-79-LC01761 to the Rocky Mountain Institute of Energy and Environment and The University of Wyoming Division of Basic Research.

Improvements in the Arsine Accumulation–Helium Glow Detector Procedure for Determining Traces of Arsenic

Cyrus Feldman

Oak Ridge National Laboratory, Oak Ridge, Tennessee

The convenience and reproducibility of this analytical procedure have been improved, and the time required reduced to 6 minutes per sample, by changing several elements of the procedure. The sample solution is more heavily buffered, gas leakage is prevented, and liquid aerosol is eliminated from the gas stream with an impinger without losing AsH_3. The cold trap is warmed up by a uniform stream of high-velocity air; the newly designed glow chamber prevents coating of the observation window, while giving a detection limit of $\lesssim$0.1 ng As. The addition of 1 mg ascorbic acid/mL to As solutions prevents spontaneous oxidation of As^{3+} at the 1–1000 ppb level at room temperature without reducing any As^{5+}. A procedure is given for eliminating the As^{3+} blank contributed by the buffer solution.

The use of $NaBH_4$ to generate AsH_3 for analytical purposes was first suggested by Schmidt and Royer (*1*). The advantages of accumulating the AsH_3 with a LN_2 trap were first pointed out by Holak (*2*). The combination of these two steps with the use of a helium discharge as a detector was first suggested by Braman, Justen, and Foreback (*3*); see also Braman, Justen, Foreback, Ammons, and Bricker (*4*). The present paper describes studies of various aspects of the procedure which have resulted in improved performance and convenience. Reliable operation of this procedure requires careful attention to detail. The construction and behavior of the various components of the system will be discussed with this in mind.

EXPERIMENTAL

Apparatus. (See Figure 1). Helium at 75 lb/in.^{2}, or 5.3 kg/cm^2, flows through a flow meter and a flow-rate stabilizer and then, at a lower pressure, through an impurity trap containing indicating silica gel and activated charcoal. All tubing up to this trap is $^1/_4$-in. copper, with Swagelok connectors.

The helium next passes through a 3-way Teflon-barrel stopcock (No. 3) to the reaction cell. Both portions of this cell are fashioned from 25-mm i.d. borosilicate glass tubing having O-ring flange joints. The lower section, about 12.5 cm high, has a sample uddition port made from the upper 4 cm of a screw-cap centrifuge tube. The screw-cap used on this port must provide a gas-tight seal. The reagent inlet tube is connected by 0.133-in. i.d., 0.020-in. wall vinyl tubing to a 3-way miniature inert valve (No. 1). With this valve appropriately set, reagent solution can be drawn from the plastic beaker reservoir into a 35-mL plastic syringe and then, with the valve rotated, injected into the reaction cell with the aid of an infusion pump.

The top portion of the reaction cell contains the gas delivery tube, which ends in a short section of 0.5-mm i.d., 6-mm o.d. capillary tubing. The orifice of this delivery tube is close to the reagent inlet when the cell is assembled. From the top of the cell, a gas outlet leads through a second 3-way Teflon-barrel stopcock (No. 2) to the first desiccator. These stopcocks are also connected to each other by a direct line, which serves to bypass the reaction cell when necessary.

The aerosol trap-desiccators, shown in Figure 2, are filled with 85% phosphoric acid to a level ~2 mm below the end of the injector. After leaving the first aerosol trap-desiccator, the gases pass through a scrubber made from two 20-mm i.d. glass O-ring flange joints. This scrubber contains a 4 cm high × 2 cm diameter layer of NaOH beads, supported by a bed of $^1/_8$-in. i.d. glass helices.

After passing through the second aerosol trap-desiccator, the gases are led through 0.133-in. i.d., 0.022-in. wall vinyl tubing to the cold trap. This trap, shown in Figure 3, is a U-tube made of 6-mm o.d., 4-mm i.d. glass tubing and terminates in No. 5 O-ring flange joints. Its overall height and width are approximately 15 and 3 cm, respectively. A drainage tip is fused onto the lowest point of the U. The trap is filled with ~200-μm diameter glass beads held in place by plastic sponge plugs. The trap is supported with its lower end approximately 28 cm above the working surface, so that in use it can be immersed in a small Dewar flask of LN_2, which is in turn supported by an adjustable platform jack. The quantity of the glass beads used should be such that when the U-trap is immersed in the Dewar flask, the top of the bead packing is 1–2 cm above the rim of the flask. Adjacent to the trap, an electrical chassis-cooling fan is stood on its side, with its 10 cm wide × 17.5 cm high opening located at the same horizontal level as the trap. This fan, operated at 140 V through a variable transformer, provides a horizontal 1400 linear ft/min stream of room temperature air. The cold trap is laterally centered in this air stream, with the lowest point of the trap aproximately 7.5 cm above the bottom of and 7.5 cm downstream from the air discharge port. The plane of the U is perpendicular to the air stream, with the drainage tip pointing downstream.

Gases emerging from the cold trap pass through 0.133-in. i.d., 0.020-in. wall vinyl tubing to the glow discharge detector (GDD). This GDD is similar to the detector described elsewhere (*5*), except that in the present electrode assemblies, the bushing shown in Figure 2A of Reference 5 has been replaced by a simple fused quartz cylinder which almost fills the annular gap between the electrode and the vertical arm that contains it. The GDD is fed by a controlled-current high-voltage power supply (Model BHK 200-0.1M, Kepco Corp., Flushing, N.Y. 11352) through a 10 000-Ω ballast resistor. This unit supplies 40 mA ± 0.01% when the glow discharge is operating at approximately 400 V.

A 5-cm length of 0.5-mm i.d., 6-mm o.d. glass tubing is attached to the exit from the GDD to minimize back-diffusion of air into the detector. A mercury manometer is attached to the exit tube immediately upstream from this capillary to measure the pressure in the detector chamber, to monitor gas flow, and to detect leaks upstream. The mercury manometer is calibrated as a helium flowmeter from 0 to approximately 600 cm^3/min. An arsenic or cadmium (see below) lamp is mounted on the optic axis behind the GDD; the downstream window of the GDD passes this light through to the monochromator when the wavelength setting is to be checked.

The light detection system is based on a Jarrell-Ash 0.5-m Ebert monchromator. A lens at the slit focuses an image of the glow discharge on the entrance aperture (mirror) of the monochromator. The grating furnished with this instrument is blazed at 500 nm, and in first order has relatively poor reflectance at the wavelengths of the As lines tested. This grating is therefore used in second order, which considerably improves its intensity and spectral resolution. To prevent interference from visible first-order radiation while still benefitting from the high reflectivity of the grating near its blaze angle, a Hamamatsu R-166 solar-blind photomultiplier tube is used as the detector. The wavelength setting of the monochromator is checked with an arsenic electrodeless discharge lamp. If no such lamp is available, and the arsenic line to be used is at 228.812 nm, the monochromator can be set sufficiently close to this wavelength with a cadmium hollow cathode lamp, using Cd I 228.802-nm radiation.

0003-2700/79/0351-0664$01.00/0 © 1979 American Chemical Society

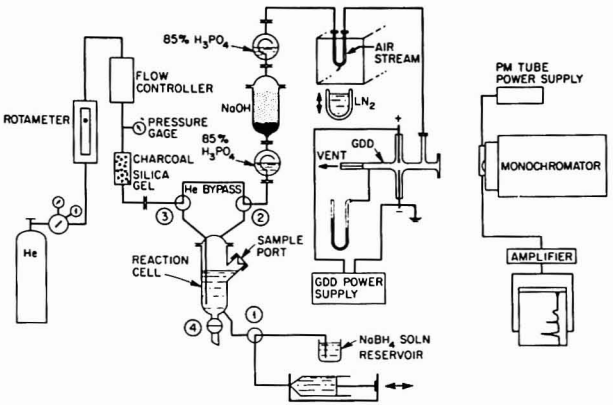

Figure 1. Schematic diagram of the analytical system

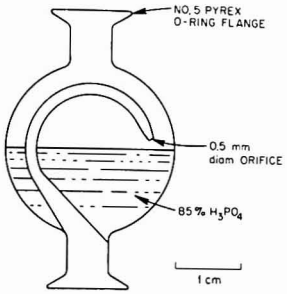

Figure 2. Impinger-desiccator for trapping aqeous aerosol and water vapor

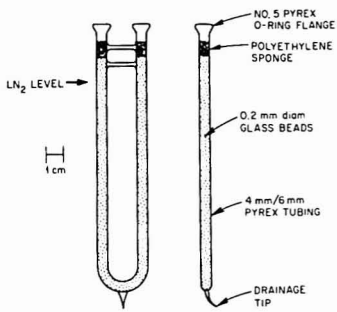

Figure 3. Cold trap for accumulating arsines

Except as noted above, all glass tubing is 6-mm o.d. borosilicate glass, with No. 5 borosilicate glass O-ring flange connectors.

Reagents. The helium used is commercial grade, containing 99.996% He. The NaOH beads are obtained from Fisher Scientific Co., Catalogue No. S-612. Trizma Base T-1503 is obtained from Sigma Chemical Co. The analytical grade $NaBH_4$, 99.5% pure, is obtained from Alfa-Ventron Corp. All other materials used are reagent grade.

Preparation of Apparatus. Approximately once a week, the aerosol trap-desiccators should be recharged with fresh 85% H_3PO_4. The remaining steps in this paragraph should be carried out at the beginning of each day, or oftener if necessary. The conical tips of the thoriated tungsten electrodes should be cleaned with 320 grit silicon carbide abrasive paper and the electrode gap adjusted to approximately 4 mm. The NaOH bead trap should be recharged. The wavelength setting of the monochromator should be adjusted to maximize the intensity of the arsenic or cadmium line used (see Apparatus section). The helium flow rate should be adjusted to approximately 450 cm^3/min while the gas is flowing through the bypass shown in Figure 1; several minutes should be allowed for purging air from the system before the GDD is turned on.

Reagent and Standard Solutions. (a) Two hundred milliliters of 2% $NaBH_4$ solution, in a plastic beaker, prepared less than 2 h before use. (b) 1 N H_2SO_4. (c) pH 6.5 buffer stock solution: 90.7 g KH_2PO_4 and 58.1 g K_2HPO_4 are dissolved in 2 L of H_2O, giving a solution 0.5 M in phosphate. For use, this solution is diluted with an equal volume of water. (d) Standard solutions: All As^{3+} standard solutions are prepared by successive dilution of the 0.1 N arsenous acid reagent. Ascorbic acid (1 mg/mL) is added to each standard solution as an anti-oxidant. As^{5+} standard solutions can be prepared from $Na_2HAsO_4 \cdot 7H_2O$ if needed. Tris/Tris maleate buffer (pH 6.5, 0.25 M) is prepared by first treating a 0.25 M solution of Trizma Base (tris(hydroxymethyl)aminomethane) with solid maleic acid until the solution reaches pH 5.8. This solution is then treated with sufficient solid 0.25 M Trizma Base to bring the pH to 6.5.

Analytical Procedure. At the start of an analytical cycle, the GDD is off, the helium is bypassing the solution cell, the cold trap is at room temperature, and the fan is off. Stopcock 1, Figure 1, is in the reservoir-to-syringe position and stopcock 4 is closed. This will be referred to as the standby state.

Transfer 20 mL of the appropriate buffer solution to the reaction cell. For determining As^{3+}, use 0.25 M, pH 6.5 phosphate or Tris/Tris maleate buffer; for total inorganic As, use 1 N H_2SO_4 or 1% oxalic acid; for methylarsonate and/or dimethylarsinate, use 1% oxalic acid. Transfer 5 mL or less of the sample or standard solution to the reaction cell; close the cell by screwing the cap on firmly. Draw 10–15 mL of the 2% $NaBH_4$ solution into the syringe. Leave stopcock 1 in the reservoir-to-syringe position and insert the syringe into the infusion pump. Remove any condensed moisture from the outside of the cold trap. Elevate the Dewar flask into position around the cold trap and fill the flask to the brim with LN_2. Turn stopcocks 2 and 3 (Figure 1) simultaneously so as to cause the helium to pass through the reaction cell. Turn stopcock 1 to the syringe-to-reaction cell position and start the infusion pump. Start the timer; pump $NaBH_4$ solution into the reaction cell for 30 s at approximately 12 mL/min. Continue to bubble helium through the solution for an additional 60 s. Return stopcocks 2 and 3 to the bypass position, and turn on the GDD. Open stopcock 4 to the drain position; then unscrew the cap covering the addition port of the reaction cell. Always perform these two operations in the order

mentioned to prevent splashing of the solution when the positive gas pressure in the cell is relieved.

When the timer reaches 120 s, turn on the fan and start the strip chart recorder. When the timer reaches 135 s, quickly lower the Dewar flask; register this moment on the strip chart. Measure and record the heights of the peaks due to AsH_3, CH_3AsH_2, and/or $(CH_3)_2AsH$, identifying the peaks by their retention times. Rinse the reaction cell and return the apparatus to the standby state.

With practice, the entire analytical cycle takes 6 min or less.

RESULTS AND DISCUSSION

Conditions in the Sample Mixture. The rate at which $NaBH_4$ reduces arsenic compounds to arsines decreases as the pH of the solution increases. The highly alkaline nature of $NaBH_4$ therefore makes it necessary to mix the sample solution with a buffer solution whose capacity is sufficient to prevent the reagent itself from seriously retarding the reaction. In order to be able to choose reaction conditions correctly, it thus seemed desirable to determine the minimum buffer molarity needed to obtain the maximum yield of arsine under a given set of conditions, and then to systematically study the effect of pH on the yields obtained from given types of compounds.

It was found that under the conditions adopted, pH 6.5 phosphate buffer must have a molarity of at least 0.25 M to provide the maximum yield of AsH_3 from As^{3+}. Commercial phosphate buffer solutions, usually only 0.05 M, have insufficient buffer capacity for this purpose. They also contain formaldehyde, which produces spurious peaks. Studies at pH 0–2 using sulfuric acid–bisulfate mixtures again showed the minimum acceptable molarity to be 0.25 M. It was therefore decided to make all buffers 0.25 M.

Each mixture was tested for buffering capacity by treating 20 mL of the buffer solution with 5 mL of 2% $NaBH_4$ solution. The buffer was kept for further investigation only if this test produced a pH increase of 0.6 or less. Certain otherwise satisfactory buffers were discarded for reasons of convenience; e.g., formate, acetate, and potassium acid phthalate solutions foamed excessively. The buffer systems finally selected for investigation were sulfuric acid–bisulfate mixtures and oxalic acid for pH 0–2, citrate and phosphate for pH 2.5–4.7 and phosphate and Tris–Tris maleate for pH 5–6.5. A phosphate-free buffer was sometimes needed in the latter pH range to prevent the precipitation of insoluble phosphates of Ca^{2+}, Mg^{2+}, Fe^{3+}, etc. The Tris/Tris maleate system was chosen as the phosphate-free pH 6.5 buffer because the Tris/Tris HCl system has little buffering capacity when used at 0.05 M, and at 0.25 M gives pH values of 7.2–9.0, which are too high for the reduction of As^{3+} or As^{5+} by $NaBH_4$.

The results of these tests are shown in Figure 4 for the reduction of inorganic As^{3+} and As^{5+} to AsH_3. It is thus possible to determine As^{3+} in the presence of As^{5+} at any pH between 3.8 and 6.5 if a 0.25 M buffer is used. The type of buffer system used is immaterial, provided that it has sufficient capacity at the pH used.

The reduction of methylarsonate and dimethylarsinate to the corresponding arsines was also studied at various pH values. This study showed that factors other than pH also affect the yield; at a given pH, different buffers often produced widely different yields. For both compounds, the maximum yield of the corresponding arsine was obtained at pH ~1.5 with 1% oxalic acid, which confirms the work of previous authors (*4*). In 1 N H_2SO_4, 15–20% of the As in methylarsonic acid was converted to AsH_3, rather than to CH_3AsH_2. In the same medium, ~20% of the arsenic in cacodylic acid was converted to CH_3AsH_2, rather than $(CH_3)_2AsH$; none was converted to AsH_3. In 1 M $KHSO_4$ solution (pH 0.55), only the appropriate arsine was produced by these compounds; the yields, however, were not as high as those obtained in 1% oxalic acid.

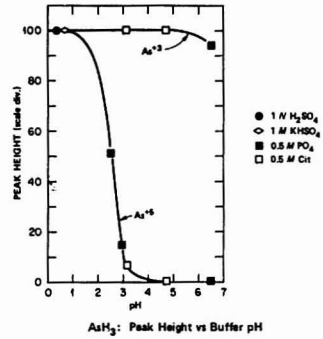

Figure 4. Peak height vs. pH for the reduction of As^{3+} and As^{5+} to AsH_3

Injection of $NaBH_4$ Solution. For adding $NaBH_4$ solution to the reaction cell, the use of a syringe driven by an infusion pump was found preferable to injection through a septum. The pumping procedure gave a uniform and reproducible reaction rate and provided protection against the leakage of gas from the system. The pressure in the system rises as high as 5 lb/in.^{2} or 0.35 kg/cm^2 above atmospheric, since the generation of the arsines is accompanied by the production of copious amounts of hydrogen. The time and rate of injection and the reagent concentration were chosen to give the maximum yield of AsH_3 with the minimum expenditure of time and reagent.

Gas Flow. Since the reaction products of interest are gases, all possible measures were taken to prevent gas leaks. Joints which had to be disconnected occasionally were made from Pyrex O-ring flanges held together by spring or screw clamps. These joints proved much more gas-tight than standard taper or spherical ground glass joints at these pressures.

Up to a point, higher flow rates helped by hastening the purging of reaction products from the reaction cell, and by making the signal peaks narrower and taller. Past this point, these beneficial effects reached a plateau, and certain harmful effects became more noticeable; there was an increase in the amount of liquid aerosol carried into the gas stream and an increase in the danger of leakage. At the flowrate finally chosen (450 cm^3 He/min), the entire pressure drop between the flow controller and the GDD was still only ~2 lb/in.^{2} or 0.14 kg/cm,^{2} so that the positive pressure in the system could easily be controlled by varying the length of the capillary tube at the vent. In a GDD of the design shown in Reference 5, helium flow rates in this range did not cause any noticeable fluctuation in the intensity, position, or shape of the glow discharge.

Desiccation and Impurity Trapping. In carrying out the present reaction, it has usually been considered necessary to remove aqueous aerosol and/or water vapor from the gas stream in order to prevent plugging of the LN_2 trap (*3*, *4*, *6*). Common desiccants such as $CaCl_2$, $Mg(ClO_4)_2$, silica gel, and $CaSO_4$ are not satisfactory for this purpose, since as previously noted in Reference 6 and confirmed in the present work, all adsorb the various arsines to some degree. It was desired to avoid the inconveniences of using a preliminary cold trap for desiccation (*4*, *6*).

It was evident that most of the moisture added to the gas stream consisted of the liquid aerosol generated by the effervescence accompanying the production of hydrogen in the reaction cell. It was thought that most of this aerosol and at least part of the water vapor might be removed by directing

the gas stream, as a jet of fairly higher linear velocity, against the surface of a hygroscopic liquid such as concentrated H_2SO_4 or 85% H_3PO_4. The impinger designed to accomplish this is shown in Figure 2. It was decided to use an impinger, rather than a bubbler, so that pressure changes in the gas phase would not displace the hygroscopic liquid.

This device performed quite well using either concentrated H_2SO_4 or 85% H_3PO_4. It was found, however, that concentrated H_2SO_4 added small amounts of some unknown trappable vapor to the gas stream; since 85% H_3PO_4 added nothing to the gas stream, it was selected for use. No plugging of the LN_2 trap ever occurred while this device was in operation.

The NaOH trap was inserted principally to absorb any CO_2 which might enter the system from the air, the sample, or the $NaBH_4$. It did not absorb AsH_3, CH_3AsH_2, or $(CH_3)_2AsH$. The sublimation temperature of CO_2 (-78.5 °C) is close enough to the boiling point of arsine (-53 °C) to threaten some interference through the generation of molecular emission bands at the As wavelength. It was found, however, that this trap also removed other (unknown) interfering species whose retention times in the LN_2 trap were similar to those of CH_3AsH_2 and $(CH_3)_2AsH$. These species usually gave broad bands, rather than sharp peaks. With the NaOH trap in place, such bands occasionally appeared after ~35 analyses. The NaOH trap was therefore recharged daily or after 30 uses.

The Cold Trap. Many variations of trap shape, size, i.d., o.d., and wall thickness were tested, but no design proved more sensitive or reliable than that illustrated in Figure 3. Early experiences showed that as the Dewar flask was removed, a drop of LN_2 often remained suspended from the bottom of the cold trap for a few seconds, despite the 1400 linear ft/min air stream coming from the adjacent fan. The delayed evaporation of this pendant drop caused a spurious peak on the descending slope of the AsH_3 peak. A glass drainage tip, added to the bottom of the trap and pointing downwind as shown in Figures 1 and 3, eliminated this difficulty. The ~1-cm packed section of this trap that is above the LN_2 level at the upstream end serves as a final scrubber for H_2O vapor. The small amounts trapped do not impede gas flow, and are eliminated when the trap returns to room temperature.

The warming of the cold trap after removal of the LN_2 container was found to be the most important single factor affecting the reproducibility of peak heights. The technique finally adopted was suddenly exposing the cold trap to a rapid stream of room temperature air, as described in the Analytical Procedure and Figure 1. The best precision was obtained when the trap was mounted firmly in an airstream which was larger in cross section than the trap itself and when the velocity of the airstream was uniform over its cross section.

The Glow Discharge Detector. With the aid of a suitable controlled-current power supply and a low work function cathode, such as a thoriated tungsten welding electrode, a very stable glow discharge can be created in helium at atmospheric pressure. Since the helium atom has an ionization potential of 24.46 eV and has relatively few low-lying energy levels, this discharge can efficiently excite difficultly excited atoms such as As, halogens, etc., at atomospheric pressure, with minimal spectral interference. At the impurity level of the helium used (~40 ppm total impurities), the spectral background underlying As I 228.812 nm was low enough so that the detection limit for arsenic was determined by reagent blanks, rather than by spectral noise.

On the other hand, the ability of the helium glow discharge to excite As atoms was found to be impaired by the presence of substantial amounts of any impurity gases, such as hydrogen, air, and/or water vapor from the $NaBH_4$-As reaction. If the discharge was operated in helium that contained air remaining from sample-changing operations, the cathode acquired a coating of nitrides and/or oxides which eventually caused the discharge to precess about it. Both difficulties were completely avoided by operating the discharge only while the gas stream was bypassing the reaction cell, and by cleaning the electrodes each day before use. With a gap of 4 mm between W(2% ThO_2) electrodes, a potential of ~1100 V dc was needed to effect the initial breakdown; the operating voltage was 380–400 V (cathode grounded). At currents of 50 mA or above, the cathode became overheated; the current was therefore kept at 40 mA.

The glow discharge chamber had several design features which made it efficient, reliable, and simple to operate. The sample gas stream entered the chamber downstream from the observation window, thus preventing the window from being coated by the degradation products of molecules passing through the discharge. Such windows have been used for several months without requiring cleaning. This feature also kept the window cool, making it possible to use sealing wax to affix the observation window, despite the fact that the discharge dissipated 40 W.

The electrode assemblies were easily removed for polishing. The diameter of the main horizontal tube was chosen small enough to force most of the gas stream to go through the discharge, but large enough to prevent contact between discharge and sidewall.

During operation of the glow discharge, the sidewalls of the chamber were slowly coated by a thin layer of sputtered tungsten, tungsten suboxides, and other degradation products. This deposit had no effect on the signal emerging from the observation window, but eventually made it difficult to observe the discharge. When necessary, this coating was easily removed with a cotton swab moistened with a 1:1:2 mixture of HNO_3, HF, and H_2O.

Peak Characteristics and the Construction of Working Curves. Typical retention times for AsH_3, CH_3AsH_2, and $(CH_3)_2AsH$ by the above-described procedure were 5.0, 7.9, and 10.0 s, respectively. The peaks were well resolved. In all three cases, the area under the curve per ng As was the same to within ±2.2%.

For the sake of convenience, it was decided to express results in terms of peak height, rather than area. Plots of log peak height vs. log ng As were always linear, except near the detection limit. A logarithmic version of the standard additions method was used to measure blank levels (see below).

Preservation of Dilute Standards and Samples. In view of the fact that a 20 μg/mL solution of As^{3+} has been found to lose 50% of its titer after storage in glass for 33 days (7), it seemed advisable to check the stability of standard solutions at and below this concentration.

Attempts to store As^{3+} solutions at concentrations of 100 ng As^{3+}/mL or below soon made it obvious that the As^{3+} titer of the solution decreased markedly over the course of a few days. In the case of standard solutions, this problem could be solved by preparing a fresh standard, or by using a mild reducing agent such as ascorbic acid as a preservative. In the case of dilute samples, however, a fresh sample usually cannot be obtained, and the use of a mild reducing agent as a preservative might be counterproductive; i.e., might cause reduction of some of the As^{5+} present, giving an incorrect As^{3+}/As^{5+} ratio. The original ratio could probably be preserved by keeping sample solutions frozen between collection and analysis, but the inconvenience of this measure made it seem worthwhile to seek another solution to the problem. In order to define the problem more precisely, and to test the efficacy of ascorbic acid as a solution to it, two sets of solutions were prepared. In the first set, the first solution contained 1.00 μg As^{3+} + 1.00 μg As^{5+} per mL; the remaining solutions

Table I. Determination of Total Arsenic in Standard Samples

material	no. and wt of portions	ppm As present work	certified value	literature value	ref.
NBS Coal (SRM 1632)	8 (0.1 g)	5.7 ± 3.9%	5.9	5.5 ± 4.8%[a]	15
NBS Coal Fly Ash (SRM 1633)	2 (0.2 g)	56 ± 2.1%	61	58 ± 6.9%	15
NBS Orchard Leaves (SRM 1571)	1 (0.1 g)	11.9	11.2[b]		
NBS Bovine Liver (SRM 1577)	1 (1.0 g)	0.054	0.055[c]		
ZGI Granite (GM)	2 (0.25 g)	4.05 ± 11%	4.0		16
ZGI Black Shale (TS)	2 (0.25 g)	29.3 ± 3.6%			
ZGI Greisen (GnA)	2 (0.25 g)	11.7 ± 5.1%	11.7[d]		
ZGI Basalt (BM)	4 (0.25 g)	13.4 ± 5.0%	14		
ZGI Slate (TB)	4 (0.25 g)	10.5 ± 5.0%		11	16

[a] This average figure excludes one value withdrawn by the analyst since publication (R. H. Philby, private communication). [b] Revised value, October 1, 1974. [c] Provisional value. [d] As of September 1977, there were too few (four) values in the ZGI files to permit certification. Three of these values averaged 11.7 ppm; the fourth (153 ppm) was rejected by the author as probably erroneous.

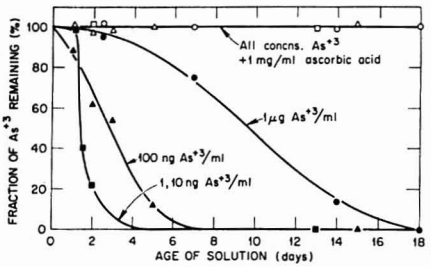

Figure 5. Disappearance of As^{3+} from 1–1000 ppb As^{3+}/As^{5+} solutions in the presence and absence of ascorbic acid

in this set were successive tenfold dilutions of the first. The second set of solutions was the same as the first, except that each solution also contained 1 mg/mL ascorbic acid. These solutions were analyzed for As^{3+} and for total As ($As^{3+} + As^{5+}$) at various times over a period of almost 3 weeks. In each analysis, the experimental solution was compared with a standard solution which had been prepared immediately before use.

The As^{3+} results (Figure 5) showed that in solutions not containing ascorbic acid, the As^{3+} disappeared completely from solution in ~4 days at the 1 and 10 ng/mL levels, in ~7 days at the 100 ng/mL level, and in ~18 days at the 1 µg/mL level. These data also showed that when 1 mg/mL ascorbic acid was present, no As^{3+} was lost during this period at any of these concentrations. Since all of these solutions originally contained equal concentrations of As^{3+} and As^{5+}, the failure of any of the ascorbic acid points to rise above the 100% line also indicates that there was no net reduction of As^{5+} by the ascorbic acid at any of the concentration levels at any time.

The total As ($As^{3+} + As^{5+}$) results, not shown in Figure 5, indicated that to within ±2.1%, the total As content of all solutions remained the same throughout the experiment; i.e., that all losses of As^{3+} were due to spontaneous oxidation to As^{5+}, rather than to adsorption on walls or volatilization.

These results indicate that 1 mg/mL ascorbic acid is an effective preservative for As^{3+} solutions as dilute as 1 ng/mL, and that its use to stablize the concentration of As^{3+} in As^{3+}/As^{5+} mixtures does not change the concentration of the As^{5+}. This implies that it may be possible to stabilize the As^{3+}/As^{5+} ratio of natural water samples at the time of collection by placing a suitable amount of solid ascorbic acid in each sample bottle beforehand, provided that no other components of the sample interfere with the intended protective action of the ascorbic acid. The latter point should be checked for each new type of sample collected.

Occasional water samples, on prolonged storage, developed visible amounts of mold. The mold tended to reduce any As^{5+} present to As^{3+}, altering the original As^{3+}/As^{5+} ratio. Making the sample 2.5×10^{-4} in sodium azide (NaN_3) usually eliminated this growth.

Detection Limit. The concentrational detection limit of any analytical technique depends on both the size of the sample and the absolute detection limit of the technique used. The size of the sample can be maximized, in effect, by using chemical pre-concentration techniques. For instance, in the present case, precipitation of the hydroxide of Fe^{3+} (*8*, *9*), Ce^{4+} or ZrO_2^{2+} at pH 7–8 (*9*) is known to be effective in concentrating As^{5+}; in addition, $ZrO_2(OH)_2$ is also said (*9*) to carry down As^{3+} quantitatively at pH 8–9.

The absolute detection limit achievable by the present procedure depends mainly on the reagent blank levels. These levels were determined by a logarithmic version of the standard additions procedure (*10*). The total blank values for various of the above supporting solutions plus $NaBH_4$ ranged from 0.3 to 0.7 ng.

If very small amounts of As^{3+} are to be determined, the contribution of any As^{3+} impurity in the buffer solution to the blank can be eliminated. As soon as the buffer solution has been transferred to the reaction cell, it is treated with 2 drops of 0.05% $KMnO_4$ solution and agitated with a burst of He bubbles. It is then treated with 1 drop of 6% sulfurous acid, and again agitated. The $KMnO_4$ oxidizes any As^{3+} present, and the sulfurous acid destroys any excess $KMnO_4$. Pentavalent arsenic, if present, is not reduced to As^{3+} by the sulfurous acid. Total blanks determined after this type of pretreatment ranged from 0.06 to 0.1 ng As^{3+}.

Some of the blank response remaining after the $KMnO_4/H_2SO_3$ treatment may be due to As^{3+} present in the $NaBH_4$ and/or to accidental contamination, memory effect, etc. Some may also be due to compounds which do not contain As, but volatilize at approximately the same temperature as AsH_3 and generate molecular band emission covering the wavelength monitored. The existence of such an effect was demonstrated by monitoring a blank reaction at a wavelength 3–4 spectral bandpasses (0.2–0.3 nm) away from the As wavelength. A small, but definite, peak was observed at the retention time of the arsine, indicating that a blank-generating molecule passed through the discharge at the same time as the arsine.

The contribution of the $NaBH_4$ solution to the blank was estimated by performing a series of blank determinations in which the $KMnO_4/H_2SO_3$ pretreatment was performed, and progressively larger volumes of $NaBH_4$ solution were used. When the resulting blank value, in nanograms, was plotted

against the grams of $NaBH_4$ injected in solution form, the slope of the straight line obtained gave the As^{3+} blank value of the $NaBH_4$ in terms of ng As^{3+}/g $NaBH_4$. Two determinations of this figure gave 0.27 ± 0.01 ng As^{3+}/g $NaBH_4$. Since approximately 0.12 g $NaBH_4$ is consumed in the recommended analytical procedure, this batch of $NaBH_4$ would contribute a blank of 0.032 ng As^{3+} per analysis.

Although this figure is called the As^{3+} blank value, it may to some extent represent non-As species, as noted above. On the other hand, it may not represent the total As^{3+} content of the $NaBH_4$; a special investigation showed that if As^{3+} was added to the $NaBH_4$ solution before the latter was injected into the reaction cell, recovery of this As as AsH_3 was incomplete at best, and had decreased by a factor of at least 10 by the time the $NaBH_4$ solution was 1-h old. This behavior was shown to be due to the fact that any arsenite existing in a freshly prepared $NaBH_4$ solution is slowly reduced to elemental As. When the resulting suspension is introduced into the (acid) sample solution, this As^0 is not reduced to AsH_3. As a result, there is a gradual decrease in that part of the AsH_3 blank which is due to AsO_3^{3+} or AsO_4^{3+} originally present in the $NaBH_4$. Throughout this series of tests, any arsenic originally added to the buffer solution, rather than to the $NaBH_4$ solution, continued to be recovered quantiatively as AsH_3.

In attempting to improve detection limits by the $NaBH_4$ procedure, it was of interest to know whether the technique used converted all of the As present to AsH_3. This question was investigated with the aid of a commercial analyzed mixture of helium and AsH_3 containing 11 ppm AsH_3. A measured quantity of this gas was introduced into the analytical train (Figure 1) immediately upstream from the cold trap. The peak heights obtained for given quantities of AsH_3 introduced in this way agreed to within ±2% with those obtained when the AsH_3 was generated by treating the corresponding amount of AsO_3^{3+} or AsO_4^{3+} with $NaBH_4$. The supplier's value for the concentration of AsH_3 in the analyzed mixture was confirmed by agitating measured amounts of this gas mixture in closed vessels with alkaline $KMnO_4$ solution, elemental bromine (*11*), and acid Ce^{4+} solution (*12*). Recoveries were >97% of theoretical.

The peak height obtained for AsH_3 which had passed through the NaOH trap was the same as that obtained for AsH_3 which had not done so. This indicates that even though AsH_3 may react readily with KOH at 120 °C (*13*), it does not react appreciably with granular NaOH at room temperature under the present experimental conditions.

Analysis of Standard Samples. Table I lists the total arsenic values obtained when standard fly ash, coal, tissue, and rock samples were analyzed by the present procedure. The NBS SRM samples were obtained from the Office of Standard Reference Materials, National Bureau of Standards, Washington, D.C. 20234; the ZGI samples were obtained from the Zentrales Geologisches Institut, Invalidenstrasse 44, 104 Berlin, East Germany. The coal and tissue samples were wet-ashed by warming with concentrated sulfuric and nitric acids, followed by minimal amounts of concentrated perchloric acid. The fly ash and rock samples were dissolved by the vapor phase HNO_3-HF procedure (*14*). The precision figures in Table I represent relative mean deviations among separate portions of the material in question.

Although the present procedure has been used to analyze many samples of drinking water (0.005–0.040 ppb As) and effluents from fly ash ponds (1.7–340 ppb As^{3+}, 1.2–124 ppb As^{5+}), there are not at present any widely analyzed low As^{3+}/As^{5+} liquid standards by which the accuracy of the method can be further tested. It is hoped that the use of ascorbic acid to stabilize the absolute relative concentration of As^{3+} will make the circulation of such standards feasible.

ACKNOWLEDGMENT

The author is grateful to Karl Schmidt, Director of the Zentrales Geologisches Institut, Berlin, East Germany, for the standard rock specimens mentioned in Table I.

LITERATURE CITED

(1) F. J. Schmidt and J. L. Royer, *Anal. Lett.*, **6**(1), 17–23 (1973).
(2) W. Holak, *Anal. Chem.*, **41**, 1712 (1969).
(3) R. S. Braman, L. L. Justen, and C. C. Foreback, *Anal. Chem.*, **44**, 2195 (1972).
(4) R. S. Braman, D. L. Johnson, C. C. Foreback, J. M. Ammons, and J. L. Bricker, *Anal. Chem.*, **49**, 621 (1977).
(5) C. Feldman, *Anal. Chem.*, **49**, 2215 (1977).
(6) M. O. Andreae, *Anal. Chem.*, **49**, 820 (1977).
(7) A. A. Al-Sibaai and A. G. Fogg, *Analyst (London)*, **98**, 732 (1973).
(8) R. Pieruccini, *Spectrochim. Acta*, **4**, 189 (1950).
(9) V. I. Plotnikov and L. P. Usatova, *J. Anal. Chem. USSR*, **19**, 1101 (1964).
(10) C. Feldman, *Anal. Chem.*, **21**, 1211 (1949).
(11) H. Reckleben and G. Lockemann, *Fresenius' Z. Anal. Chem.*, **47**, 132 (1908).
(12) G. Mannelli, *Ann. Chim. Appl.*, **29**, 533 (1939).
(13) L. Moser and A. Brukl, *Monatsh. Chem.*, **45**, 36 (1924).
(14) C. Feldman, *Anal. Chem.*, **49**, 825 (1977).
(15) J. M. Ondov et al., *Anal. Chem.*, **47**, 1102 (1975).
(16) F. J. Flanagan, *Geochim. Cosmochim. Acta*, **37**, 1189 (1973).

RECEIVED for review August 3, 1978. Accepted December 13, 1978. This paper was presented at the First Annual Symposium on Environmental Analytical Chemistry, Brigham Young University, Provo, Utah, on June 23, 1978. This research was performed at the Oak Ridge National Laboratory, operated for the U.S. Department of Energy by Union Carbide Corporation under Contract W-7405-eng-26. This article was supported by the Division of Basic Energy Sciences.

Multiple Entrance Slit Vidicon Spectrometer for Simultaneous Multielement Analysis

K. W. Busch* and B. Malloy

Department of Chemistry, Baylor University, Waco, Texas 76703

Y. Talmi

Princeton Applied Research Corporation P.O. Box 2565, Princeton, New Jersey 08540

A vidicon spectrometer employing multiple entrance slits to simultaneously focus several 40-nm windows on the SIT detector is described. The system may be visualized as the reverse of a direct reader, since multiple entrance slits and a single multichannel detector are used instead of a single entrance slit and multiple detectors. Detection limits obtained with the system for Mn, Cr, Sr, Ba, Li, and K by atomic emission with a nitrous oxide–acetylene flame are reported. The advantages of this system for simultaneous multielement analysis are discussed.

In recent years, great interest has been shown in developing spectroscopic systems for simultaneous multielement analysis (SMA) (*1–3*). Busch and Malloy (*4*) have reviewed the various systems which have been proposed to date, and have discussed the role of image devices in SMA. The development of image detector spectrometers for SMA has proceeded along two basic lines of development based on the mode of dispersion.

In one-dimensional configurations, the spectral information is dispersed across the tube target with a conventional spectrographic system as a single horizontal band of information. One-dimensional systems are based on a window concept (*5*), resulting in a compromise between resolution and wavelength coverage. Under certain favorable circumstances (*6–8*), widely spaced spectral lines may sometimes be monitored without unduly increasing the size of the wavelength window (and thereby suffering a loss in resolution) by monitoring spectral lines in overlapping orders. This approach, however, is not successful in every case, and the limited wavelength window obtained by mounting an image detector at the focal plane of a conventional spectrograph remains the most serious problem associated with this optical arrangement (*4*).

To avoid the limited wavelength coverage associated with one-dimensional systems, several groups (*9–13*) have assembled and demonstrated the feasibility of echelle systems. Although these systems provide wide wavelength coverage under high resolution conditions, the optical system is more complicated and expensive, and computer control of the scanning circuitry is required for accurate wavelength registration.

This paper describes a multiple entrance slit vidicon spectrometer employing a one-dimensional dispersive system which overcomes many of the limitations associated with previous one-dimensional systems.

EXPERIMENTAL

Table I lists the experimental facilities used in this study.

Multichannel Detection System. The multichannel detection system employed in this study consists of an SIT vidicon detector and an optical multichannel analyzer. The optical multichannel analyzer accumulates spectral information in 500 electronic channels, and has two separate memories that permit the storage of a data spectrum and a blank spectrum. An arithmetic unit permits channel-by-channel subtraction of memory B from memory A.

Table I. Experimental Facilities

burner	Varian Techtron 5-cm slot burner for nitrous oxide-acetylene
monochromator	Spex, Model 1870, 0.5-m Czerny-Turner spectrograph, *f*/6.9, with 600 grooves/mm grating blazed for 500 nm. Reciprocal linear dispersion 3.2 nm/mm in the first order
detector	Model 1205D silicon intensified target detector head, Princeton Applied Research Corp.
optical multichannel analyzer	Model 1205A, Princeton Applied Research Corp., with Option 3 serial converter.
readout	Tektronix oscilloscope, 604 Monitor Sargent-Welch Recorder, Model SRG
flow meters	Brooks Full-view Rotameters calibrated for nitrous oxide and acetylene, Brooks Instrument Division
fiber optics	Approximately 200 (2.5-mil diameter) glass fibers non-coherently bundled in flexible poly(vinylchloride) jacket; approximate transmission 65% from 400–2000 nm for 30-cm length. Edmund Scientific, Barrington, N.J.
input lenses	Precision-molded acrylic terminal lenses. Edmund Scientific, Barrington, N.J.

Optical System. Figure 1 shows the optical arrangement employed. A Spex 0.5-m Czerny-Turner spectrograph with a camera mirror which is larger than the collimating mirror was modified in the following way. The entrance slit was removed and the vidicon detector was mounted in the focal plane of the entrance port. A multiple entrance slit assembly was fabricated and mounted in the focal plane of the exit port of the spectrograph. The multiple entrance slit assembly consisted of an aluminum plate with a horizontal row of 1.588-mm diameter holes spaced on 4-mm centers. This arrangement produced a horizontal row of 29 holes across the 12-cm exit port opening. Each hole was masked from behind the plate with two pieces of black tape to form an entrance "slit" 1.6 mm high. On the basis of spectral resolution measurements using the chromium triplet (425.4, 427.5, 429.0 nm), the slit widths obtained by this procedure are on the order of 300 μm. The vertical position of the row of holes was adjusted to that height which produced a maximum signal from the vidicon.

Because of the optical difficulties presented when illuminating multiple slits simultaneously with a single source, fiber optic light guides were chosen to convey the light from the light source to the individual slits. The diameter of the fiber optic light guides was selected so that each fiber optic strand could be plugged into

0003-2700/79/0351-0670$01.00/0 © 1979 American Chemical Society

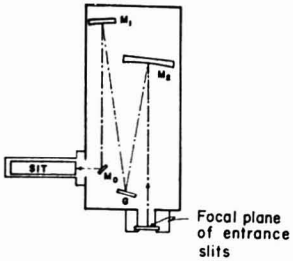

Figure 1. Optical arrangement. M_0, 45° mirror; M_1, focusing mirror; M_2, collimating mirror; G, grating

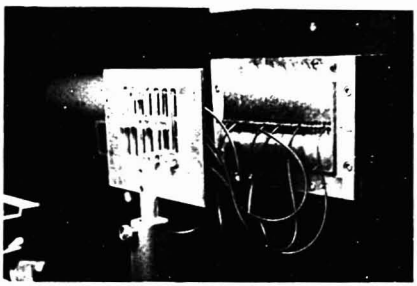

Figure 2. Fiber-optic system showing input lenses and switchboard entrance slit system

the hole corresponding to any one of the 29 possible entrance slit positions. Those holes corresponding to entrance slit positions not in use were blocked by means of opaque plugs.

To improve the light gathering ability of each fiber optic light guide, the input end of each strand was fitted with an input lens. The lenses were mounted on a vertical slotted plate to permit each of seven lenses to be individually adjusted vertically from 3 to 40 mm above the burner head.

Figure 2 illustrates the complete entrance slit assembly, showing the vertically adjustable input lenses, the fiber optic light guides, and the entrance slit assembly plate mounted in the focal plane of the instrument.

Figure 3 shows the entire instrumental setup used. Note that the entire system is no larger than a conventional flame emission spectrometer. The slot burner has been turned so that the slot is parallel to the lens mounting plate to provide a wide source to adequately illuminate the lenses.

Experimental Conditions. The spectra shown in Figure 4 were determined under the following conditions: nitrous oxide flow, 9.5 L/min; acetylene flow, 6.0 L/min. Vertical positions of the fiber optic light guides were optimized for each element. All spectra in Figure 4 are the result of 100 accumulation cycles. The accelerating voltage on the intensifier stage of the SIT was set for 7 kV.

The detection limit data shown in Table II were obtained using the same oxidant and fuel flow rates given above, as well as the same accelerating voltage. Data spectra were accumulated in memory A by aspirating single element solutions containing 1000 ppm Cs as an ionization buffer into the nitrous oxide–acetylene flame for a period of 100 accumulation cycles. Blank spectra were accumulated in memory B by aspirating blank solutions containing 1000 ppm Cs into the flame for the same number of accumulation cycles. The background-corrected spectra were monitored using the A minus B mode of the multichannel analyzer. The detection limit was taken as that concentration giving a signal-to-noise ratio (S/N) of 2. This value was obtained by extrapolation from S/N measurements made at concentrations slightly above the detection limit. The noise was calculated as the standard deviation of 10 adjacent background channels on either side of the analytical line.

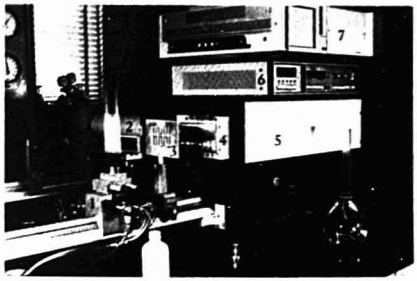

Figure 3. Multiple entrance slit vidicon spectrometer. (1) nitrous oxide–acetylene flame, (2) SIT vidicon detector, (3) fiber optic input lenses, (4) fiber optic entrance slit system, (5) 0.5-m Czerny-Turner spectrograph, (6) optical multichannel analyzer, (7) oscilloscope display

RESULTS AND DISCUSSION

The vidicon spectrometer described in this paper employs multiple entrance slits arranged so that radiation from various spectral regions can be simultaneously imaged on the target of the image detector. The system may be visualized as the reverse of a direct-reading spectrometer; thus, instead of using a single entrance slit and multiple exit slits, as in the case of the direct reader, the present system employs multiple entrance slits and a single detector. In contrast to a direct reader which typically requires a long focal length dispersive system to achieve sufficient dispersion in the exit plane to permit multidetector placement, the vidicon spectrometer system described here can employ a short focal length dispersive system. In the direct-reader system, spectral resolution is determined by how closely the multiple exit slits can be placed in the exit focal plane. In contrast to the direct reader, the spectral resolution of this vidicon spectrometer is *not* limited by how closely the multiple entrance slits can be placed in the entrance focal plane. Entrance slit position is not at all related to resolution, but instead simply controls the spectral region imaged on the vidicon detector. Resolution depends, rather, on the entrance slit width and the reciprocal linear dispersion of the optical system. The single multichannel detector employed reads the overlapping spectral information in 500 electronic channels, spaced on 25-μm centers, and consequently requires only a short focal length system to give adequate resolution.

With a grating producing a reciprocal linear dispersion of 3.2 nm/mm, each separate entrance slit images a 40-nm spectral window onto the 13-mm SIT detector faceplate. Since the entrance slits are spaced over a 12-cm segment of the focal plane, any wavelength within a range of 384 nm can be imaged on the detector. By employing several entrance slits simultaneously, widely separated spectral lines of interest may be simultaneously imaged on the detector with adequate resolution.

Figure 4 shows the spectra of Mn, Cr, Sr, Ba, and Li obtained with this system using a nitrous oxide–acetylene flame. To simultaneously monitor this combination of elements with a conventional one-dimensional dispersive system would require a 267-nm window. The spectra illustrated in (a)–(e) represent the spectrum obtained for each element when a single fiber optic light guide is plugged into the appropriate entrance slit (#1-29). The spectrum shown in (f) represents the composite spectrum obtained when all five fiber optic light guides are simultaneously plugged into their respective entrance slit holes.

The background subtraction capability of the vidicon/optical multichannel analyzer system is essential to the success

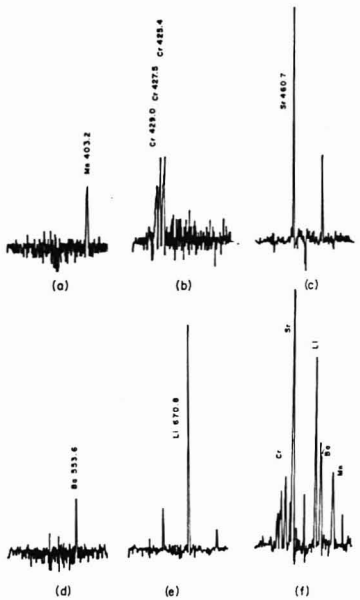

Figure 4. Spectra obtained with system. (a) Mn, 3 ppm, entrance slit #3 (402.4–442.4 nm); (b) Cr, 3 ppm, entrance slit #3 (402.4–442.4 nm); (c) Sr, 1 ppm, entrance slit #6 (440.8–480.8 nm); (d) Ba, 3 ppm, entrance slit #14 (543.2–583.2 nm); (e) Li, 1 ppm, entrance slit #23 (658.4–698.4 nm); (f) Composite spectrum obtained by simultaneously using entrance slits 3, 6, 14, and 23. Multielement mixture contained 5 ppm Mn, Cr, and Ba, and 1 ppm Li and Sr

Table II. Detection Limit Data

element	wavelength, nm	input lens position, mm[a]	entrance slit number[b]	detection limit, μg/mL[c]
Mn	403.0	28	3	0.46
Cr	425.4	28	3	0.56
Sr	460.7	28	6	0.041
Ba	553.6	4	14	0.50
Li	670.8	28	23	0.013
K	766.5	28	29	0.84

[a] Vertical distance above burner head. [b] Entrance slit holes on 4-mm centers, numbered from left to right. [c] Accelerator voltage, 7 kV; concentration giving S/N = 2; all solutions buffered with 1000 ppm Cs.

of this optical arrangement. When various windows are overlapped as they are in this instrument, the flame background alone can become very large as shown in Figure 5a, where the radiation from a nitrous oxide–acetylene flame is simultaneously monitored from five inputs. Figure 5b shows the spectrum of the five elements without background correction. Figure 5c shows the same spectrum after background correction.

Table II gives detection limit data for Mn, Cr, Sr, Ba, Li, and K obtained with the multiple entrance slit vidicon spectrometer. These detection limits were obtained individually under the same set of flame conditions. The vertical positions of the individual input lenses above the burner head are also indicated. These detection limits are about a factor

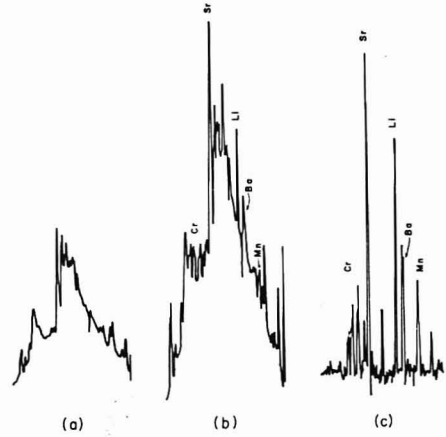

Figure 5. Importance of background subtraction. (a) Composite flame background from inputs 3, 6, 14, and 23; 100 accumulation cycles; N_2O, 5.7 L/min; C_2H_2, 4.5 L/min. (b) Composite spectrum without background subtraction. Mn, Cr, Ba, 5 ppm; Li and Sr, 1 ppm. Scale expanded slightly over that shown in (a) to show positions of analytical lines. (c) Background-corrected spectrum

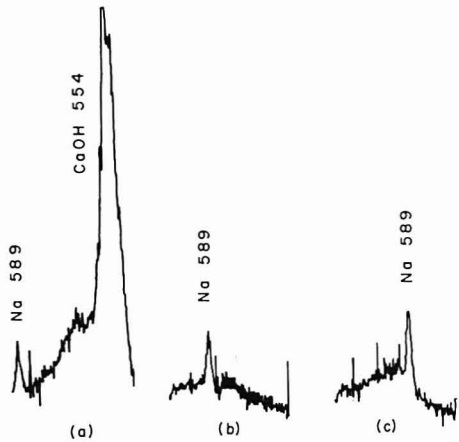

Figure 6. Spectrum of tap water. N_2O, 9.5 L/min; C_2H_2, 6.0 L/min; 500 accumulation cycles. (a) Entrance slit #15, (b) entrance slit #16, (c) entrance slit #17

of 400 worse than the best values reported in the literature (*14*) for an SIT detector with an ordinary one-dimensional dispersive system. It should be remembered that these data represent preliminary results obtained with a prototype system, and it can be anticipated that better slits, higher quality fiber optics and input lenses, and an improved flame geometry will result in lower detection limits. Even with this relatively crude system, the detection limits are all less than 1 ppm, which is adequate for many samples.

The fiber optic "switchboard" system offers several important advantages for SMA which should be emphasized. Since a line of any given wavelength may be imaged on the detector from any of 3 entrance slit positions, spectral lines may be moved across the target in such a way as to avoid

potential spectral interferences as well as regions of intense background. Figure 6 illustrates a typical example of this for sodium in tap water. Note the very intense CaOH band at 554 nm, which could easily saturate the detector in certain samples, may be easily moved off the target, thereby avoiding problems with detector saturation and blooming.

In addition, analytical lines may be selected on the basis of spectrochemical considerations, since any line within a 384-nm region may be accessed. Thus, in contrast to earlier one-dimensional systems, primary resonance lines normally used in analytical work may be employed rather than less satisfactory emission lines which happen to fall in a certain restricted wavelength window.

Another important advantage of the switchboard system is that the problems normally associated with the simultaneous determination of major, minor, and trace elements in a single sample can be ameliorated. In single-entrance slit systems, for example, the presence of intense emission from major analyte species may often result in target blooming. In most cases, this situation may easily be avoided with the multiple entrance slit approach. With the switchboard optical system, each element (or, at most 2 to 3 elements) is monitored by an individual fiber optic light guide, permitting essentially individual adjustment. Intense emission radiation striking the detector target may be attenuated or avoided in several ways: (1) variable neutral density filters may be inserted in front of the particular fiber optic strand(s) without simultaneously attenuating the intensities for all elements; (2) a less sensitive analytical line may be selected in place of a very intense primary resonance line if the emission is due to a major or minor analyte; or (3) a smaller entrance slit may be utilized at that position. Thus the switchboard system offers many of the individual adjustment features of the direct-reading spectrometer with the added advantages of compactness, flexibility to monitor different combinations of analytical lines, and the ability to monitor background adjacent to a spectral line.

Finally, individual observation height adjustment of each fiber optic guide is possible, thereby reducing the severity of the compromise conditions required for SMA (*15*) by eliminating observation height as a factor.

In conclusion, it should be noted that the multiple entrance slit approach is not limited to detectors with one-dimensional scan patterns, and may easily be extended to systems with two-dimensional target interrogation capabilities. Also, the multiple entrance slit approach is not limited to vidicon detectors, and may be used with any type of multichannel detector which permits background subtraction.

The ultimate criterion for the evaluation of multielement analytical systems is their utility in analyzing real samples. Experiments are currently being carried out in this laboratory to improve the instrumental design of this system based on analytical experience with different multielement samples.

LITERATURE CITED

(1) P. W. J. M. Boumans, *Fresenius' Z. Anal. Chem.*, **279**, 1 (1976).
(2) J. D. Winefordner, J. J. Fitzgerald, and N. Omenetto, *Appl. Spectrosc.*, **29**, 369 (1975).
(3) K. W. Busch and G. H. Morrison, *Anal. Chem.*, **45**, 712A (1973).
(4) K. W. Busch and B. Malloy, in "Multichannel Image Devices in Chemistry", Y. Talmi, Ed., ACS Symposium Series, in press.
(5) K. W. Busch, N. G. Howell, and G. H. Morrison, *Anal. Chem.*, **46**, 575 (1974).
(6) K. W. Busch, N. G. Howell, and G. H. Morrison, *Anal. Chem.*, **46**, 1231 (1974).
(7) N. G. Howell, J. D. Ganjei, and G. H. Morrison, *Anal. Chem.*, **48**, 319 (1976).
(8) J. D. Ganjei, N. G. Howell, J. R. Roth, and G. H. Morrison, *Anal. Chem.*, **48**, 505 (1976).
(9) A. Danielsson and P. Lindblom, *Phys. Scripta*, **5**, 227 (1972).
(10) A. Danielsson and P. Lindblom, *Appl. Spectrosc.*, **30**, 151 (1976).
(11) A. Danielsson, P. Lindblom, and E. Söderman, *Chem. Scripta*, **6**, 5 (1974).
(12) D. L. Wood, A. B. Dargis, and D. L. Nash, *Appl. Spectrosc.*, **29**, 310 (1975).
(13) H. L. Felkel and H. L. Pardue, *Anal. Chem.*, **49**, 1112 (1977).
(14) N. G. Howell and G. H. Morrison, *Anal. Chem.*, **49**, 106 (1977).
(15) D. F. Brost, B. Malloy, and K. W. Busch, *Anal. Chem.*, **49**, 2280 (1977).

RECEIVED for review November 17, 1978. Accepted January 25, 1979. Acknowledgment is made to the donors of the Petroleum Research Fund, administered by the American Chemical Society, for partial support of this research. Acknowledgment is also made to the Robert A. Welch Foundation for partial support of this research.

Trace Element Analysis of Bulk Metals with a Hollow Cathode Discharge and a Quadrupole Mass Filter

C. G. Bruhn,[1] B. L. Bentz, and W. W. Harrison*

Department of Chemistry, University of Virginia, Charlottesville, Virginia 22901

Use of a hollow cathode ionization source with a quadrupole mass filter forms a solids mass spectrometer well suited for trace element analysis of bulk metals. Cathode geometry, particularly bore diameter and nozzle-orifice length, and discharge current effects were studied to yield optimum ion sensitivity. Reproducibility for minor to trace constituents in steel and brass standards was 2–6% RSD. Sensitivities were in the low ppma to sub-ppma range.

Trace element analysis by mass spectrometry has generally been carried out using one of two techniques: (a) spark source mass spectrometry (SSMS) or (b) secondary ion mass spectrometry (SIMS), depending upon the analysis requirements. SSMS (*1*, *2*) has the advantages of excellent sensitivity and broad application, but the demonstrated limitations in accuracy and precision, as well as high cost and complexity of operation, have restricted the extent to which this otherwise powerful technique is employed. SIMS (*3*, *4*), including microanalysis capabilities, is of particular value for surface studies. However, quantitative analysis can involve many difficulties and is often not routine.

As an alternative to the spark source mass spectrometer used in our laboratories, we became interested in a gas discharge as a sputter atomization–ionization source for trace element analysis. Instead of relying on the direct secondary ion production as with SIMS, we wished to take advantage of the large sputtered neutral atom population, a portion of

[1]Present address: Departmento de Análisis Instrumental, Esc. de Química y Farmácia, Universidad de Concepción, Casilla 237, Concepción, Chile.

0003-2700/79/0351-0673$01.00/0 © 1979 American Chemical Society

which to be subsequently ionized in the discharge plasma. Initial source models (*5–8*) were interfaced to an MS-702 double focusing mass spectrometer, but the simplicity of these sources, plus the stability, and relatively low energy spread of the ions produced led to a simplified solids mass spectrometer (*9*), consisting of a hollow cathode discharge source coupled to a quadrupole mass filter.

The use of a gas discharge as an ion source is not new. The pioneer mass spectroscopists (Thomson, Aston, and Bainbridge) used such discharges as a convenient source of ions and, although the gas discharge was soon displaced as an ion source, its use continued in optical spectroscopy, particularly in the form of hollow cathode discharges. Thus, for 50–60 years the hollow cathode discharge has been used as a fine line source in physics (*10, 11*) and more recently in atomic absorption spectrometry (*12, 13*). Coburn and co-workers (*14–16*) studied glow discharges as analytical ion sources for both thin film and bulk analysis. Oechsner and Gerhard (*17, 18*) demonstrated the use of a high frequency plasma which sputtered and ionized solid samples. Reports from this laboratory (*6, 8, 19*) have concerned bulk analysis, solution residues, and surface sputter effects, using both hollow cathode and conventional glow discharges. Evans and co-workers (*20, 21*) have also studied the hollow cathode as an ion source.

These investigations point to the potential advantages of the glow discharge, of which the hollow cathode is merely one type, as a solids ionization source for trace element analysis. This report describes the capabilities of a simple hollow cathode ion source and quadrupole mass filter as a solids mass spectrometer for metals analysis.

EXPERIMENTAL

Apparatus. The quadrupole solids mass spectrometer and the hollow cathode discharge (HCD) source were described previously (*9, 22*).

Procedures. Metal samples (oxygen-free copper, NBS steels and brasses) were machined into hollow cathode specimens of 2.54-cm length, 2.49-cm depth, 0.61-cm o.d., 0.47-cm i.d., and with a 0.5-mm nozzle orifice diameter drilled at the cathode end wall. Surface cleaning was provided by rinses in acetone, dilute HNO_3, and deionized-distilled water.

Optimization of Hollow Cathode. Two series of copper hollow cathodes were machined to study the effects of changes in nozzle orifice length and bore diameter of the cathode cavity. The cathode–anode distance was kept constant at 1.90 cm, and the 3.5-mm nozzle–skimmer separation remained unchanged during these studies.

(*a*) *Nozzle Orifice Length.* Copper cathodes of 0.61-cm o.d., 0.47-cm bore diameter, 2.54-cm length, and variable nozzle orifice length (13.5 to 0.5 mm) were used in this study.

(*b*) *Bore Diameter.* Copper cathodes of 2.54-cm length, 2.3-cm bore depth, 0.5-mm nozzle orifice diameter, and variable bore diameter from 0.25 to 0.51 cm were used.

Critical parameters such as discharge current, source pressure, ion-energy window, and ion optics were optimized by monitoring the cathode matrix and discharge gas ion intensities. Mass spectra were recorded in the "constant ΔM" resolution mode (*23*) with the peak width of the transmitted mass range remaining independent of the mass to which the mass filter was tuned. The mass resolution $M/\Delta M$, where ΔM is the width of the peak (half height) at mass M, ranged from 2.3–2.8 M at low masses (up to 100 amu) under normal operating conditions. However, in the high mass range (120–230 amu) the mass resolution was kept normally about 1.5 M to avoid major losses of ion transmission (*24, 25*).

RESULTS AND DISCUSSION

When a glow discharge source is coupled to a quadrupole mass filter, a relatively simple mass spectrometric system results with a potential for high sensitivity and good reproducibility. Several features recognized in quadrupole devices, such as their excellent transmission, rapid scanning capability, wide angle of acceptance, simplicity of operation,

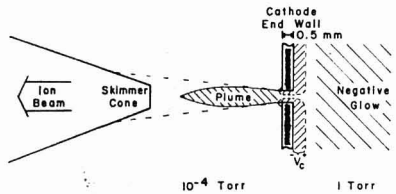

Figure 1. Sampling configuration showing beam formation produced by the cathode orifice nozzle and skimmer cone. V_c = cathode fall potential

resolution control flexibility, compactness, and relatively low cost make such units particularly attractive for use with the large and stable ion flux generated during glow discharge cathodic sputtering.

Because most of the sputtered particles in a glow discharge are unexcited neutrals (~90% of total sputtered flux (*26*)), an axial electron impact ionizer was originally added to the system to post-ionize the neutral species which were extracted as an atomic beam with the gas flow from the source. However, the ion intensities observed from the sputtered species arose in large measure directly from the discharge. The post-ionization by electron impact added only a small contribution and was discontinued. The relatively high positive ion flux obtained from the discharge acts as an indicator of the total particle flux (and bulk metal concentration) once a steady-state equilibrium condition is achieved in cathodic sputtering (*3, 27*). This ion flux is generated as a result of ionization of a fraction (1–10%) (*26*) of the sputtered neutral particles. Most species sputtered directly as positive ions are returned to the cathode surface by the strong electric field of the cathode fall potential (*26*).

Hollow Cathode Discharge. The glow discharge with hollow cathode has proved to be a simple and convenient means of ionization of solids or solution residues for subsequent elemental analysis (*5, 6, 20*). Metals and alloys can be either machined into hollow cathodes, or adapted to the cathode cavity for direct analysis. The 0.5-mm nozzle orifice at the cathode end wall (*22*) yielded adequate ion throughput without suffering serious restriction from condensed sputtered species. Sampling the discharge through a circular orifice provides an ideal beam geometry for the cylindrical symmetry of a quadrupole mass filter.

The discharge volume sampled is believed to encompass portions of both the cathode dark space (cathode fall) and negative glow regions. No discrete extraction potential was applied to the ion source. The vacuum system with two differentially pumped chambers allowed the extraction, by jet expansion, of a supersonic beam comprised of ionic and neutral sputtered species and the discharge gas. This jet was accompanied by a small plasma plume protruding into the low pressure side downstream from the sampling orifice, suggesting a complex ionizing volume as depicted in Figure 1. An elongation of the negative glow and cathode fall regions extends into the low pressure chamber between the source and the analyzer. Charge transfer collisions among argon ions and neutral species are likely, contributing to the ion energy spread. An on-line coupling of the source to the quadrupole with no energy filtering, using only the ion optics associated with the axial ionizer, produced spectra with peaks which showed high mass tailing (*22*) from the energy spread of the incoming ions (*28*), most probably produced by ions originating at the edge of the negative glow and extracted through the cathode fall region. Floating the quadrupole Z-axis to retard the higher energy ions resulted in asymmetric peak shapes with dips in ion transmission in the center of the peaks (*22*),

and in the appearance of anomalous precursor peaks, presumably from ions with a relatively larger kinetic energy than the maximum energy selected for transmission (29). Replacement of the axial ionizer by a Bessel Box-type energy analyzer yielded spectra without those detrimental effects, since a suitable energy bandpass and mean ion energy could be selected for transmission to the mass analyzer (22); the passage of neutral species and high energy ions was prevented by a metal stop positioned in the center of the energy analyzer.

Discharge Gas. The selection of argon as the discharge gas was based principally on its sputtering yield properties (27), as most of the analyte ions sampled from the hollow cathode arose from sputtered neutral species subsequently ionized in the discharge plasma, mainly by Penning ionization and electron impact (26). Argon has two metastable neutral triplet states (11.55 and 11.72 eV) which contribute significantly to the Penning ionization mode because of their relatively large energy compared to the ionization potentials of most elements; all but 11 elements of the periodic table have their first ionization potentials below 11.5 eV. Using copper as an example, the Penning ionization step would be written as:

$$Cu^0 (IP = 7.72 \text{ eV}) + Ar_m^*(11.55 \text{ eV}, 11.72 \text{ eV}) \rightarrow Cu^+ + Ar^0 + e^-$$

Among other rare gases, helium and neon do not offer sputtering yields comparable to that of argon (27). The use of molecular gases (e.g., O_2, N_2) was avoided because of previously reported spectral complexity due to abundance of ion species formed (6).

Argon offered the best compromise considering sputtering yield, ionization energy for Penning processes, and acceptable mass spectral composition. Characteristic species obtained with argon and copper cathodes, were Ar^+, Ar^{2+}, Ar_2^+, ArH^+, and Cu^+, their relative magnitudes being determined by the discharge and energy analyzer conditions. At lower intensities, several other species were observed, including argon combinations with gaseous impurities (ArN^+, ArN_2^+, ArO^+) and combinations involving sputtered matrix atoms (e.g., $CuAr^+$, Cu_2^+, CuO^+, and Cu_2O^+). The approximate relative strengths of the signals for Cu^+, $CuAr^+$, and Cu_2^+ were 1, 1×10^{-3}, and 8×10^{-4}. In addition, gaseous impurities were noted at certain lower mass lines (N^+, O^+, H_2O^+, N_2^+, O_2^+, and CO_2^+). Optimization of the discharge gas pressure and, more significantly, of the energy analyzer conditions allowed significant selective reduction of the discharge gas and molecular species while simultaneously enhancing the ion signal of the sputtered species, as indicated in earlier reports (9, 22).

Cathode Geometry. Previous work with a hollow cathode ion source, sampling near the cathode open end through an anode aperture, showed that the cathode bore diameter and depth were critical factors in sensitivity (21). For our nozzle sampling configuration, we have studied the effects of nozzle orifice length and the cathode bore diameter. A 0.5-mm nozzle orifice diameter was selected for these studies based upon (a) the desirability of a differential pressure of $\sim 10^4$ between the source and the intermediate chamber for beam extraction and (b) sufficient beam intensity to allow sensitivity for trace constituents. As shown for copper cathodes in Figure 2, the monitored $^{63}Cu^+$ ion current dropped by a factor of $\sim 10^4$ as the length of the orifice was extended from 0.5 to 13.5 mm. Most of the drop in ion signal could be attributed to ion losses from gas phase collisions within the orifice and to discharging effects by collisions with the orifice walls, as the orifice is gradually converted into a tubular-like aperture of increasing length. A small orifice length is thus a critical sensitivity factor with this cathode configuration. Machining considerations limited the minimum length of the nozzle orifice to about 0.5 mm.

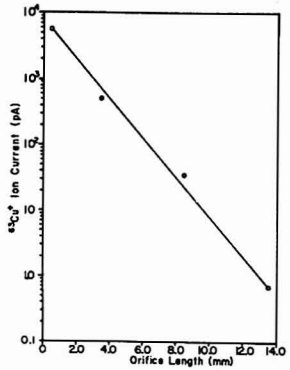

Figure 2. Effect of orifice nozzle length upon measured ion current

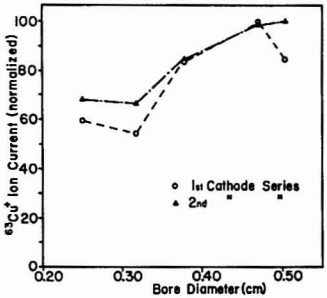

Figure 3. Effect of cathode bore diameter upon measured ion current

The sensitivity effect produced by changes in cathode bore diameter is illustrated in Figure 3 for two series of copper cathodes with a constant bore depth of 2.49 cm (0.5-mm nozzle orifice length). A general increase in the $^{63}Cu^+$ ion current results, with increasing bore diameter, but the effect is not large. If one considers the hollow cathode interior as a sputtering chamber, an increase in diameter increases the surface area available for sputtering. However, if the discharge current is maintained constant, a simultaneous decrease in surface current density occurs, offsetting the area consideration. The larger chamber volume may result in more Penning ionization, but for the sampling mode utilized in this study, the basic hollow cathode effect (30) involving the coalescence of cathodic negative glow regions was not significantly altered by the bore variation.

Discharge Parameters. A previous study of the effect of gas pressure on the cathode matrix and gas ion species indicated that a judicious selection of source pressure allowed significant enhancement of the $^{63}Cu^+$:$^{40}Ar^+$ ion ratio in a copper cathode (from 0.005 to 0.20) and enhancement of the $^{56}Fe^+$:$^{40}Ar^+$ ion ratio in a steel cathode (from 0.19 to 0.70) (9). The total positive ion current (comprised mainly of argon species) issuing from the source was measured as a function of source pressure (Figure 4). Most probably the current decrease resulted from an increase in the viscous character of the gas flow with larger numbers of particles interacting within the beam (31), and from ions lost by collisions with the orifice walls. However, upon mass analyzing this "white" ion beam, source pressures above 1.50 Torr normally favored the Cu^+ and Fe^+ ion intensities while discriminating against

Table I. Reproducibility of Molybdenum Isotopes in Ten Consecutive Mass Spectra Taken from NBS 811A Steel. Molybdenum Present at 0.22%

	m/e						
	92	94	95	96	97	98	100
% abundance	15.84	9.04	15.72	16.53	9.46	23.78	9.63
RSD %	5.5	5.3	6.4	5.7	6.4	3.5	6.3
	av. RSD %: 5.6						

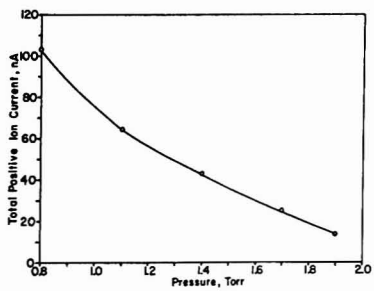

Figure 4. Influence of discharge pressure upon total ion beam exiting the cathode orifice

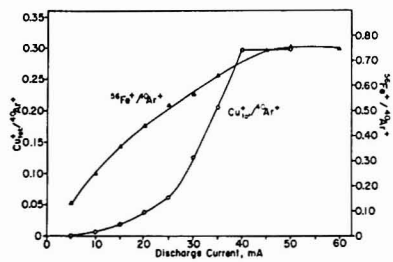

Figure 5. Effect of discharge current on the ratio of the matrix ion to the primary discharge gas ion

the Ar^+, Ar^{2+}, and Ar_2^+ ion signals, as previously described (22).

The effect of discharge current is shown in Figure 5 for copper and stainless steel cathodes. Both the Cu^+_{total}:$^{40}Ar^+$ and $^{56}Fe^+$:$^{40}Ar^+$ ratio increased up to a plateau at about 40 mA. The increase in Cu^+ and Fe^+ ion currents with the discharge current is consistent with an increase in the sputtering rate and enhancement of the sputtered neutral production from which these ions originate. A discharge current of up to 40 mA enhanced analytical sensitivity without significant sputter deposition or orifice clogging problems. However, pressure and energy analyzer optimization are also determining sensitivity factors.

As an example of results obtainable under carefully optimized conditions, a mass spectrum of a stainless steel sample in an argon discharge is shown at low gain in Figure 6. Pressure and energy analyzer conditions were optimized for $^{56}Fe^+$ ion transmission, resulting in an Fe^+ signal which constituted approximately 45% of the beam; the $^{56}Fe^+$:$^{40}Ar^+$ ratio was ~2.9. However, obtaining such a high ratio often produces lower ion currents. Therefore, normal working conditions will feature ratios more similar to those shown in Figure 5.

Reproducibility. Among the serious intrinsic problems encountered in solids analysis by SSMS, obtaining less than

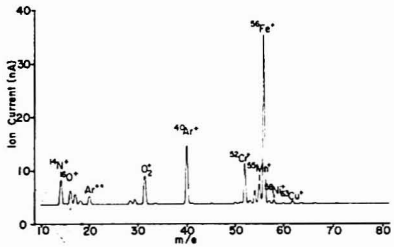

Figure 6. Low gain mass spectrum of a stainless steel cathode with spectrometer conditions optimized for transmission of $^{56}Fe^+$

satisfactory precision (25–35% RSD) in scan reproducibility is a leading one. In our laboratory, the addition of a rapid repetitive scanning unit for multichannel analyzer signal averaging was necessary to yield significantly better precision (10–15% RSD (32, 33)) than obtainable comparing single scans. Similar precision improvements were observed when gas discharge sources (5, 8) were coupled to a double focusing mass spectrometer, probably due to the less extreme ionization conditions (energy spread up to ~170 eV as opposed to ~1 KeV in the spark source) and greater stability of the gas discharges. By coupling the HCD to a mass filter, good stability was obtained after a few minutes of "warm-up" time. Monitoring the total positive ion current exiting the ion orifice revealed a broad initial maximum in ion intensity followed by a gradual decrease to a nearly constant level at ~70% of the original maximum current. Over a 20-min period after initial equilibration, the ion current showed a 4% range in the form of a slight downward drift. Over 1-min periods during this interval, the variation was less than 1%. A similar stability pattern was observed when the quadrupole was tuned to monitor the $^{63}Cu^+$ ion intensity.

Consecutive mass scans were performed over short and long mass ranges to determine the peak height reproducibility of minor and trace sample components. Using NBS steel standards as cathodes, and scanning over a short mass range (~30 amu), the peak heights for minor to trace constituents showed a reproducibility in the 2–6% RSD range for 10–15 consecutive scans with a total scan time ranging from 15 to 25 min. For the multiisotopic molybdenum, consecutive mass scans were recorded for an NBS 811A steel standard (Mo at 0.22%, see Table I) with an average % RSD of 5.6%. Consecutive mass scans were then recorded over a 100-amu mass range with an NBS 816A steel standard. The average precision for 14 isotopes (see Table II) was 7.0% RSD, a considerable improvement over our experience for comparable mass scanning performed with a spark source instrument.

A comparison of the Mo data in Table I vs. Table II shows the effect of important instrumental parameters. The precision obtained for Mo isotopes when scanning over a short mass range (ion optics optimized for Mo^+ ion transmission; scan rate 0.29 amu s^{-1}) was 5.6% RSD. The value obtained from the longer mass range scan (ion optics now optimized for Fe^+ ion transmission; scan rate 0.66 amu s^{-1}) was 8.5% RSD. These differences are attributable to the smaller Mo^+

Table II. Reproducibility of 14 Isotopes in Ten Consecutive Mass Spectra Taken from NBS 816A Steel

element	wt %	m/e	% RSD
Cr	1.14	52	1.1
Ni	0.28	58	3.8
		60	5.8
Cu	0.15	63	1.7
		65	1.6
Mo[a]	0.20	92	5.5
		94	11.7
		95	7.2
		96	8.2
		97	9.8
		98	7.6
		100	9.3
Sn	0.011	118	10.1
		120	14.6
	av. RSD %:	7.0	

[a] Av. RSD % (Mo isotopes): 8.5.

ion intensities observed in the latter method and the shorter scan dwell time per amu, and point out the importance of ion optical tuning and mass scanning parameters when obtaining sensitivity and precision estimates for a particular analyte.

On examining a second type of cathode matrix, scan reproducibility for higher masses (Sn, Pb) in an NBS C1101 cartridge brass standard (Table III) showed an average precision of 5.9% for the lead isotopes (Pb at 0.05%) and 10.0% for the tin isotopes (Sn at 0.016%). The precision obtained for the tin isotopes partially reflects poor ion statistics for several of the seven Sn isotopes examined.

Experimental isotopic abundances generally show mass discrimination effects of the mass filter, an observation previously reported (*34*), which can be attributed to an increase in resolution with transmission of higher masses (*35*). As the resolution depends on the number of rf oscillations experienced by an ion, and this is dependent on the time the ion spends in the quadrupole field, the heavier ions with lower axial velocity will experience more rf oscillations. Consequently, the resolution increases with mass and the ion transmission drops (*35*).

Sensitivity. NBS steel and brass standards were used to determine detection limits of minor and trace constituents based on a signal-to-noise ratio (S/N) of 2. The estimation was made from a comparison of the net peak height for the specific mass line examined against the background variation at the low and high mass side of this particular mass, under optimized conditions. In Table IV are shown for the metals tested (steel and brass), the detection limits for isotopes unobstructed by spectral interferences. They ranged from tens of ppba (Cu, Sn) to a few ppma (Ni, As). The detection limits shown for those elements examined in both samples (Ni, Sn) are consistent within a factor of 2. The differences in detectability among these elements might be attributed to several factors: (a) sputter yields of elements may differ, (b) ionization efficiencies in the discharge may differ, (c) interferent mass lines adjacent to certain elements (Ni, As) can limit the spectral resolution used to obtain the detectability values, and (d) ion–neutral reactions may occur in the differentially-pumped region, particularly close to the sample orifice, where the pressure is relatively high (*36*).

Application to Analysis of Solids. To simulate the analysis of real samples, an NBS 816A steel cathode was subjected to a set of ten consecutive scans recorded over the approximate mass range of 45 to 135 amu, with a mass scan rate of ~0.7 amu s^{-1}. This set of scans was used to calculate relative sensitivity factors (RSF) for each analyzed element vs. an element selected as an internal standard. After a 4-h interval, vacuum conditions were reestablished, and a second set of scans ("sample" set) was recorded for the same cathode, under similar instrumental and discharge experimental conditions. The RSFs previously obtained were used to estimate elemental concentrations from the data obtained in these "sample" scans. Alternatively, using one set of mass scans as external standard data vs. the second set as the "sample", direct element-to-element concentrations were calculated for comparison, eliminating the need for RSFs.

As shown in Table V, the results obtained using the internal standard data (RSFs) indicated an average relative percent error of 7.5% for Cr, Ni, Cu, and Sn when ^{98}Mo was selected as internal standard. The use of ^{52}Cr as the internal standard yielded an 8.2% average relative percent error. The results obtained using external standards produced an average relative percent error of 14.1% for the same elements. A similar experiment performed with multiscalar signal averaging in a spark source mass spectrometer showed comparable results (*32*).

Real sample analysis requires the use of RSFs (calculated from a standard sample) to correct ion intensities obtained from an unknown sample of similar composition. For these factors to be effective, the response of a given element relative to a selected internal reference element must remain constant from one sample to another. Changes in matrix composition will often cause significant errors in such measurements. A second standard, NBS 811A, was selected for analysis using the RSFs calculated from NBS 816A. Both are spectrographic steel standards which have five common elements reported: Si, Cu, Ni, Cr, and Mo. Interferences prevented consideration of Si, but the other four were measured in each sample. RSFs were calculated for Cu, Ni, and Cr against Mo as the reference element. The analytical results from 10 mass scans (2.5 min

Table III. Reproducibility Study of Tin and Lead Isotopes in Ten Consecutive Mass Spectra Taken from NBS C1101 Cartridge Brass

A. Sn isotopes (Sn at 0.016%)

	m/e						
	116	117	118	119	120	122	124
% abundance	14.30	7.61	24.03	8.58	32.85	4.72	5.94
RSD %	8.5	8.6	9.1	8.7	8.5	11.9	14.9

av. RSD %: 10.0

B. Pb isotopes (Pb at 0.05%)

	m/e		
	206	207	208
% abundance	23.6	22.6	52.3
RSD %	9.3	3.8	4.5

av. RSD %: 5.9

Table IV. Calculated Detection Limits for Minor and Trace Constituents Obtained with the HCD

element	wt. % concn. of element	NBS sample	isotope	detection limit ppma
Cr	0.015	801 Steel	52	1.1
Ni	0.28	801 Steel	60	3.7
Cu	0.015	801 Steel	63	0.03
Mo	0.20	816A Steel	98	1.1
Sn	0.011	816A Steel	120	0.08
Mn	0.0055	C1101 Brass	55	0.5
Ni	0.013	C1101 Brass	60	2.3
As	0.009	C1101 Brass	75	2.7
Ag	0.003	C1101 Brass	107	1.6
Sn	0.016	C1101 Brass	120	0.05
Pb	0.05	C1101 Brass	208	0.1

Table V. Comparison between Internal and External Standard Methods for Elements in NBS 816A Steel

element	wt. % concn. of element	isotope used	natural abundance	int. std.[a]	ext. std.
Cr	1.14	52	83.76	1.13	1.03
Ni	0.28	58	67.76	0.28	0.26
Cu	0.15	63	69.09	0.12	0.11
Mo	0.20	98	23.78	---	0.18
Sn	0.011	120	32.85	0.010	0.009
			av. rel. % error	7.5	14.1

[a] ^{98}Mo as internal standard.

Table VI. Calculation of Elemental Concentrations in NBS 811A Using RSFs from NBS 816A

				trial 1	
element	isotope	RSF	wt. % reported	wt. % exper.	rel. % error
Cr	52	4.45	0.93	0.78	16.1
Ni	58	3.58	0.24	0.21	12.5
Cu	63	6.99	0.105	0.104	0.95
Mo	98	1.00[a]	0.22	---	*a*
				av. = 9.85	

[a] Mo selected as reference element for RSFs.

each) are shown in Table VI. It is hazardous to draw conclusions from this limited number of elements, but the 9.8% relative error is encouraging, compared to the results often encountered in spark source mass spectrometry. A second analysis series on another day produced a 14.3% relative error. Computation of RSFs from each of the 10 scans for the reference standard showed an RSF standard deviation ranging from 4.8% for Cr to 13.9% for Ni, yielding an average of 8.9% for the four elements. Improper control of discharge conditions and ion beam optimization parameters can produce much larger variations in ion currents and ratios.

Relative sensitivity factors are analytical crutches necessitated by the difficulty in solids mass spectrometry of comparing a sample and standard under exactly equivalent conditions. Breaking vacuum and exchanging sample electrodes causes small differences in electrode position and ion beam alignment, particularly in spark source mass spectrometry. It should be possible to improve the results from hollow cathode ion sources by mounting a standard and several samples on a carousel type system whereby rapid sample–standard comparisons under essentially identical conditions could be made.

LITERATURE CITED

(1) A. J. Ahearn, Ed., "Mass Spectrometric Analysis of Solids", Elsevier, Amsterdam, 1966.
(2) A. J. Ahearn, Ed., "Trace Analysis by Mass Spectrometry", Academic Press, New York, 1972.
(3) R. E. Honig, *Adv. Mass Spectrom.*, **6**, 337 (1974).
(4) J. A. McHugh, in "Methods and Phenomena: Their Applications in Science and Technology", Vol. 1, S. P. Wolsky and A. W. Czanderna, Ed., Elsevier Scientific, New York, 1975, Chapter 6.
(5) W. W. Harrison and C. W. Magee, *Anal. Chem.*, **46**, 461 (1974).
(6) E. H. Daughtrey, Jr., and W. W. Harrison, *Anal. Chem.*, **47**, 1024 (1975).
(7) D. L. Donohue and W. W. Harrison, *Anal. Chem.*, **47**, 1528 (1975).
(8) W. A. Mattson, B. L. Bentz, and W. W. Harrison, *Anal. Chem.*, **48**, 489 (1976).
(9) C. G. Bruhn, B. L. Bentz, and W. W. Harrison, *Anal. Chem.*, **50**, 373 (1978).
(10) F. Paschen, *Ann. Phys.*, **50**, 901 (1916).
(11) J. R. McNally, G. R. Harrison, and E. Rowe, *J. Opt. Soc. Am.*, **37**, 93 (1947).
(12) J. C. Burger, W. Gillies, and G. K. Yamasaki, in "Analytical Flame Spectroscopy", R. Mavrodineau, Ed., Macmillan, London, 1969, Chapter 12.
(13) A. Walsh, Proceedings of the X Colloquium Spectroscopicum Internationale, Washington, D.C., 1962, p 127.
(14) J. W. Coburn and E. Kay, *Appl. Phys. Lett.*, **18**, 435 (1971).
(15) J. W. Coburn and E. Kay, *Appl. Phys. Lett.*, **19**, 350 (1971).
(16) J. W. Coburn, E. Taglauer, and E. Kay, *J. Appl. Phys.*, **45**, 1779 (1974).
(17) H. Oechsner and W. Gerhard, *Phys. Lett. A*, **40**, 211 (1972).
(18) H. Oechsner and W. Gerhard, *Surf. Sci.*, **44**, 480 (1974).
(19) E. H. Daughtrey, Jr., D. L. Donohue, P. J. Slevin, and W. W. Harrison, *Anal. Chem.*, **47**, 683 (1975).
(20) B. N. Colby and C. A. Evans, Jr., *Anal. Chem*, **46**, 1236 (1974).
(21) J. R. Wallace, D. F. S. Natusch, B. N. Colby, and C. A. Evans, Jr., *Anal. Chem.*, **48**, 118 (1976).
(22) B. L. Bentz, C. G. Bruhn, and W. W. Harrison, *Int. J. Mass Spectrom. Ion Phys.*, **28**, 409 (1978).
(23) "Quadrupole Power Supply, Instruction Manual", Extranuclear Lab., Inc., Pittsburgh, Pa.
(24) P. H. Dawson, "Quadrupole Mass Spectrometry and Its Applications", Elsevier, Amsterdam, 1976, Chapter 5.
(25) K. V. Wood, A. M. Grange, and J. W. Taylor, *Anal. Chem.*, **50**, 1652 (1978).
(26) W. D. Westwood, *Prog. Surf. Sci.*, **7**, 71 (1976).
(27) G. K. Wehner, in "Methods and Phenomena: Their Applications in Science and Technology", Vol. 1, S. P. Wolsky and A. W. Czanderna, Ed., Elsevier Scientific, New York, 1975, Chapter 1.
(28) A. J. Smith, D. J. Marshall, L. A. Cambey, and J. Michael, *Vacuum*, **14**, 263 (1964).
(29) "Electrostatic Energy Analyzer, Instruction Manual", Extranuclear Lab., Inc., Pittsburgh, Pa.
(30) G. F. Weston, "Cold Cathode Glow Discharge Tubes", Iliffe, London, 1968.
(31) J. W. Coburn and E. Kay, *J. Vac. Sci. Technol.*, **8**, 738 (1971).
(32) W. W. Harrison and W. A. Mattson, *Anal. Chem.*, **46**, 1979 (1974).
(33) W. A. Mattson and W. W. Harrison, *Anal. Chem.*, **47**, 967 (1975).
(34) G. K. Wehner, *Appl. Phys. Lett.*, **30**, 185 (1977).
(35) G. Lawson and J. F. J. Todd, *Chem. Br.*, **8**, 373 (1972).
(36) D. A. Parkes, *Trans. Faraday Soc.*, **67**, 711 (1971).

RECEIVED for review November 17, 1978. Accepted February 6, 1979. Financial support from the National Institutes of Health Grant GM-14569 is gratefully acknowledged.

Spectrometric and Chemical Characterization of Superoxide

Soonhee Kim, Robert DiCosimo, and Joseph San Filippo, Jr.*

Department of Chemistry, Rutgers—The State University of New Jersey, New Brunswick, New Jersey 08903

The absorbance spectrum of KO_2 in DMSO–18-crown-6 is reported. The calculated extinction coefficient (λ_{max} = 250 nm) is $\epsilon = 2686 \pm 29\ M^{-1}\ cm^{-1}$ (99% confidence level). This value is a linear function of concentration over a substantial range. The reaction of KO_2 with halogens ($X_2 = Cl_2, Br_2, I_2$) is rapid and quantitative and obeys the stoichiometry $2KO_2 + X_2 \rightarrow 2KX + 2O_2$.

The recent development of potassium superoxide, KO_2, as a laboratory reagent has stimulated interest in the theoretical and practical aspects of superoxide chemistry (*1*, *2*). For many of these applications, a precise value of the concentration of superoxide is not necessary. For others, e.g., kinetic studies, this value must be known with some precision.

Superoxide undergoes rapid disproportionation in protic media (*3*).

$$2O_2^- + 2H_2O \xrightarrow[\text{pH 5}]{k \approx 10^5\ M^{-1}\ s^{-1}} H_2O_2 + O_2 + 2OH^-$$

Because of this fact, the chemical characterization of superoxide has been carried out most successfully in aprotic solvents, particularly DMSO. The earliest reliable procedure for the determination of superoxide involved the measurement of the dioxygen evolved when a superoxide salt is treated with a solution of acetic acid in di-*n*-butyl phthalate (*4*). More recently, Fee and Hildenbrand have described a method of superoxide determination that involves estimating O_2^- by the double integration of the first derivative of the superoxide ESR signal, followed by a determination of the dioxygen evolved upon treatment with water, followed by a determination of the amount of dioxygen evolved by the catalase-induced disproportionation of the resulting hydrogen peroxide (*5*). The work we report here describes two procedures for such determination along with some additional chemistry.

EXPERIMENTAL

Commerically available dimethyl sulfoxide was dried by distillation at reduced pressure (96 °C/25 Torr) from calcium hydride and stored over activated Molecular Sieves (4 Å). 18-Crown-6 ether was prepared as descried by Gokel et al. (*6*), purified by two successive applications of the purification procedure described therein and stored over P_2O_5 under nitrogen, mp 39.5–41.0 °C [(*6*) mp 36.5–38.0 °C].

Potassium superoxide was purchased from MSA (Evans City, Pa.) and ground to a fine powder in a mortar and pestle in a nitrogen-filled glove bag following preliminary dispersion in a Waring blender.

Potentiometric measurements were made using a Fischer Model 520 digital pH meter employing either a platinum or a freshly prepared silver indicating electrode vs. a standard calomel reference electrode. Spectrometric studies were performed on a Cary 118C spectrometer employing matched 0.1-mm cells, the precise path length of which was determined by calibration against a solution of Crystal Violet in deionized water, yielding an experimentally determined value of $b = 0.009931$ cm. In addition to DMSO, the solvent blank also contained an amount of 18-crown-6 ether equivalent to that in the sample cell. Oxygen evolution was determined using a gas buret and leveling bulb filled with mercury.

Reaction of KO_2 with Br_2 in Benzene. Into a 100-mL flask equipped with a Teflon-coated magnetic stirring bar was placed 0.711 g (10.0 mmol) of powdered KO_2 and 30 mL of dry benzene. The flask was fitted with an addition funnel containing a solution of 1.7 g (10.6 mmol) of bromine in benzene (1 mL). This solution was added over a 5-min period with stirring (an immediate evolution of oxygen took place) and the resulting reaction was stirred for an additional 2 h before adding cyclohexene (2 mL) to destroy any unreacted bromine. The remaining mixture was extracted with two 30-mL portions of distilled water and the combined aqueous extracts were placed in a 250-mL beaker equipped with a Teflon-coated stirring bar. The volume of this solution was adjusted to 100 mL by further addition of distilled water. Five drops of concentrated nitric acid were added and the solution was titrated for Br^- through its potentiometric end point using a 0.500 M solution of silver nitrate.

Reaction of KO_2 with I_2 in Benzene. The above procedure was repeated using 2.665 g (10.5 mmol) of iodine. An immediate evolution of dioxygen occurred. After 2 h, the resulting mixture was extracted with two 30-mL portions of distilled water. The combined extracts were in turn extracted with 400 mL of $CHCl_3$ in 50-mL portions to remove any unreacted iodine. The combined aqueous extracts were analyzed for iodide ion content as described above.

Reaction of KO_2 with Cl_2 in Benzene. Into a 100-mL flask equipped with a Teflon-coated stirring bar was placed 0.711 g (10.0 mmol) of powdered potassium superoxide and 50 mL of dry benzene. With efficient stirring, chlorine gas was bubbled through this mixture for 15 min. The resulting mixture was stirred at room temperature for an additional hour, then purged with nitrogen for 15 min before adding cyclohexene (6 mL) to destroy any unreacted chlorine. The resulting mixture was extracted twice with 30-mL portions of water. The combined aqueous extracts were analyzed for chloride ion content as described above.

Reaction of KO_2 with I_2 in DMSO. Halide analysis of these reaction mixtures required a different procedure than that described above. Specifically, KO_2 (0.1000 g, 1.406 mmol) was placed in a 3-necked, 125-mL flask equipped with a Teflon-coated stirrer bar. Each neck was capped with a rubber septum before adding a 100 mL of a 0.16 M solution of 18-crown-6 ether in DMSO by syringe. The resulting mixture was stirred for 10 min, then titrated with a 0.339 M solution of I_2 in ethylbenzene. The end point was obtained graphically.

Gas Evolution Studies. In a typical experiment, powdered KO_2 (0.142 g, 2.00 mmol) was placed in a 250-mL flask equipped with a side arm and a Teflon-coated magnetic stirring bar. A rubber septum was placed over the side arm and flask attached to a gas buret. The entire system was thoroughly flushed with dioxygen before injecting benzene (50 mL) followed by a solution of iodine (2.32 g, 9.14 mmol) in benzene (3 mL) through the side arm accompanied by vigorous stirring. Equivalent readings were recorded at intervals of 20, 30, and 60 min following the completed addition. The results are summarized in Table I.

In DMSO, this procedure was modified somewhat. Into a 3-necked, 100-mL flask equipped with a Teflon-coated magnetic stirring bar was placed 0.1000 g (1.406 mmol) of powder KO_2 and 10 mL of a 0.16 M solution of 18-crown-6 in DMSO. A rubber septum was placed in one neck and an addition funnel equipped with an equalizing arm and containing 50 mL of 0.9912 M solution of I_2 in ethylbenzene was inserted in the second neck. The remaining neck was attached to a 100-mL gas buret. The iodine solution was added to the flask with stirring and the resulting dioxygen evolution monitored at intervals. All readings were corrected for barometric pressure.

Treatment of KO_2 with *n*-BuLi. In a typical experiment, 0.284 g (4.00 mmol) of powdered potassium superoxide was placed in a flame-dried, nitrogen-flushed 40-mL centrifuge tube equipped with a Teflon-coated magnetic stirring bar. The vessel was capped with a rubber septum, flushed with nitrogen and 15 mL of benzene containing 0.085 g (0.32 mmol) of 18-crown-6 ether was added

0003-2700/79/0351-0679$01.00/0 © 1979 American Chemical Society

Table I. Reaction of KO_2 with Halogens[a]

halogen	solvent	mmol KO_2	mmol O_2 liberated[b]	mmol X^- liberated[c]	mmol KO_2 / mmol X_2	mmol KO_2 / mmol O_2
Br_2	C_6H_6	2.00	1.96			0.98
		10.00		10.1	1.98	
I_2	C_6H_6	2.00	2.02			0.99
		10.0		9.80	2.04	
Cl	C_6H_6	10.0				
				10.2	1.96	
I_2	DMSO	1.406[d]		1.391	1.01	
		1.406[d]	1.405			1.00

[a] Except where indicated, 18-crown-6 ether was not present. [b] These values have been corrected for the vapor pressure of benzene and converted to STP values using the perfect gas equation. [c] Halide values have been corrected for the background (blank) value of halide determined by carrying out each experiment in the absence of KO_2. Corrections were generally $\lesssim$1% of the listed value. [d] A solution of KO_2 in DMSO was employed; [18-crown-6] = 0.16 M.

by syringe. With vigorous stirring, a solution of *n*-butyllithium in hexane (2.0 mL, 1.56 M) and a known amount of an appropriate internal standard were injected by syringe. After 1 h the mixture was centrifuged and the supernatant liquid transferred by cannula to a flame-dried, nitrogen-flushed centrifuge tube equipped with a Teflon-coated stirring bar and capped with a rubber septum. Using a syringe, 1,2-dibromoethane (1.87 g, 10.0 mmol) was added to this vessel followed by 15 mL of dry ethyl ether. The resulting mixture was stirred for 30 min then analyzed by gas–liquid phase chromatography (GLPC) for *n*-butyl bromide on a 6-ft, 0.125-in. column by 10% UCW-98.

Repetition of this experiment in which the 1,2-dibromoethane was replaced by methanol (addition carried out at −78 °C) was followed by analysis for butane on a 3-ft, 0.25-in. column of 3% Apiezon M on 60–80 mesh alumina.

RESULTS AND DISCUSSION

Spectrometric Studies. Potassium peroxide and potassium hydroxide are the two most reasonable contaminants expected to be present in commercial potassium superoxide (*7*). Any characterization of potassium superoxide must distinguish KO_2 from these extraneous substances.

The Raman spectrum of solid KO_2 is characterized by a single, intense band at 1143 ± 1 cm^{-1} (*8*). Similarly, simple metal peroxides exhibit an intense, single Raman band, but at a substantially lower frequency (750–900 cm^{-1}) (*9*). We have examined the Raman spectrum of KO_2 admixed with a predetermined amount of peroxide (Na_2O_2 was used because of the unavailability of K_2O_2). These studies established that amounts of peroxide ≥0.5% are readily detectable by this analytical procedure. We conclude that the KO_2 used in this study (commercially available from MSA, Evans City, Pa.) is >99% pure (the manufacture provided assay was 95+%).

The insolubility of potassium superoxide in most aprotic organic solvents is contrasted by its slight solubility in dry dimethyl sulfoxide (DMSO). This solubility can be increased to ~0.15 M by the addition of a phase transfer agent such as 18-crown-16 ether (*10*). Our studies reveal that solutions of KO_2 in DMSO exhibit an absorption spectrum with a characteristic maximum at 250 ± 1 nm. In an earlier observation, Matheson and Lee (*11*) reported that a solution of KO_2 in DMSO displays an absorption of 246 nm; however, this result appears to be an artifact of the procedure these investigators employed, since KO_2 in DMSO is not stable to the chromatographic procedures (elution through alumina) they describe.

A plot of the absorbance (250-nm band) observed for solutions of KO_2 in DMSO–18-crown-6 was obtained over a range of concentrations. Several aspects of this result deserve brief comment. First, within the range of concentrations examined, i.e., [O_2^-] 0.009–0.11 M, absorbance is a linear function of concentrations. Second, in contrast to the report of Ozawa, Hanaki, and Yamamoto (*12*) that crown ethers interfere with the observation of the UV absorption of superoxide in DMSO, we have observed no interference from the presence of 18-crown-6 ether in our spectral determination; moreover, the observed absorbances are clearly independent of the concentration of crown. Finally, least squares analysis of the data yields a straight line (correlation coefficient 0.9996) with a slope of 26.72 M^{-1}, corresponding to an extinction coefficient = 2686 ± 29 M^{-1} cm^{-1} (99% confidence level).

Chemical Studies. Thermodynamic calculations predict that potassium superoxide should act as a one-electron reducing agent toward the simple halogens (chlorine, bromine, and iodine) (*13*). This conclusion derives from a consideration of the following thermochemical data.

	$2KO_2$	+	I_2	=	O_2	+	2KI
ΔG°, kcal/mol	2(−56)		0		0		2(−77)
ΔG°(reaction) ≈ −40 kcal							

It follows that, since the free energy of formation of KBr and KCl are greater than that of KI, the free energy of reaction of KO_2 with Cl_2 and Br_2 can only be more negative than that calculated for the corresponding reaction with I_2 (note: these calculations neglect the free energy of solution of KO_2, KX, both of which are insoluble in benzene, and X_2). Indeed, treatment of a suspension of KO_2 in benzene with chlorine, bromine, or iodine results in the rapid, quantitative oxidation of superoxide to dioxygen and concomitant reduction of halogen to halide ion.

$$2KO_2 + X_2 \rightarrow 2KX + 2O_2 \quad (1)$$

The data in Table I establish that the stoichiometry of these reactions is that shown in Equation 1. This procedure cannot be extended to the direct determination of superoxide concentrations in DMSO without some modification. Specifically, the rapidity with which chlorine and bromine react with DMSO prevents the use of these reagents as oxidants in this solvent system. On the other hand, the reaction of DMSO with iodine is sufficiently slow that oxidation of superoxide predominates. Thus, a solution of KO_2 in DMSO–18-crown-6 can be titrated with a standard solution of I_2 in ethylbenzene to a satisfactory potentiometric end point (Table I).

The transformation of an organolithium or −magnesium reagent to the corresponding alcoholate by reaction with dioxygen ordinarily occurs in two distinct steps (*14*):

$$RM + O_2 \rightarrow ROOM$$

$$ROOM + RM \rightarrow 2\,ROM$$

Table II. Treatment of KO_2 with *n*-C_4H_9Li and (*n*-C_4H_9)$_2$Mg

mmol of KO_2	[18-crown-6], M	R_nM	solvent	temp., °C	recovered R_nM, % *n*-C_4H_{10}[b]	recovered R_nM, % *n*-C_4H_9Br[c]
2.00	0.16	*n*-C_4H_9Li	C_6H_6	27	100[a]	96[a]
2.00		(*n*-C_4H_9)$_2$Mg	Et_2O	27	98	

[a] Analysis for *n*-butyl alcohol revealed <1%. [b] Produced upon protonolysis with CH_3OH–HCl. [c] Produced upon treatment with $BrCH_2CH_2Br$ at 0 °C in ether.

Formation of an intermediate organic peroxide by reaction between the organometallic reagent and dioxygen has been proposed to require an initial single-electron transfer to dioxygen, generating an electron-deficient organometallic species and superoxide, and raising the question of the possible role of superoxide in such reactions. We have probed this question by examining the reactivity of potassium superoxide with selected alkyllithium and -magnesium reagents. The results summarized in Table II demonstrate that despite the strongly reducing nature of *n*-butyllithium, neither it nor di-*n*-butylmagnesium reacts to any appreciable extent with solutions of potassium superoxide. This conclusion, however, leaves unanswered the possible role of superoxide in coupling reactions between O_2^- and intermediate alkyl radicals known to be produced in the autoxidation of organolithium and magnesium reagents (*14*).

LITERATURE CITED

(1) L. Goodman and J. San Filippo, Jr., in preparation.
(2) See C.-I Chern, R. Di Cosimo, R. De Jesus, and J. San Filippo, Jr., *J. Am Chem. Soc.*, **100**, 7317 (1978) and references therein.
(3) J. A. Fee and J. S. Valentine, in "Superoxide and Superoxide Dismutases," A. M. Michelson, J. M. McCord, and I. Fridovich, Ed., Academic Press, London, 1977.
(4) E. Seyb, Jr., and J. Kleinberg, *Anal. Chem.*, **23**, 115 (1951).
(5) J. A. Fee and P. G. Hildenbrand, *FEBS Lett.*, **39**, 79 (1974).
(6) G. W. Gokel, D. J. Cram, C. L. Liotta, H. P. Harris, and F. L. Cook, *J. Org. Chem.*, **39**, 2445 (1974).
(7) "The Manufacture and Use of Potassium Superoxide," C. B. Jackson and R. C. Werner in *Adv. Chem. Ser.*, **19**, American Chemical Society, Washington, D.C., 1957.
(8) J. B. Bate, M. H. Brooker and G. E. Boyd, *Chem. Phys. Lett*, **16**, 391 (1972).
(9) D. M. Adams, "Metal-Ligand and Related Vibrations," St. Martins Press, New York, 1968, Chapter 5.
(10) J. S. Valentine and A. B. Curtis, *J. Am. Soc.*, **97**, 224 (1975).
(11) I. B. C. Matheson and J. Lee, *Spectrosc. Lett.*, **2**, 117 (1969).
(12) T. Ozawa, A. Hanaki, and H. Yamamoto, *FEBS Lett.*, **74**, 99 (1977).
(13) "Handbook of Chemistry and Physics", 43rd ed., Chemical Rubber Publishing Co., Cleveland, Ohio 1961.
(14) E. J. Panek, L. R. Kaiser, and G. M. Whitesides, *J. Am. Chem. Soc.*, **99**, 3708 (1977) and references therein.

RECEIVED for review October 12, 1978. Accepted January 15, 1979. This work was supported by a grant from the National Institutes of Health (AM-18713-01).

X-Ray Fluorescence Determination of Uranium as the Barium Diuranate Precipitate

Bruce B. Jablonski and Donald E. Leyden*

Department of Chemistry, University of Denver, Denver, Colorado 80208

Uranium can be determined in the microgram range by preconcentration of uranium from solution through precipitation as barium diuranate. A silver membrane filter enhances the uranium fluorescent radiation and aids in sample handling. Precision was found to be 5% RSD at the 1 ppm level.

Despite the large number of methods for the determination of trace quantities of uranium in solution, there still exists considerable interest in the development of new methods which are at once rapid, simple, and sensitive. The use of extraction mining in which uranium is removed from an ore deposit through the complexing action of carbonate solutions has placed additional emphasis on the aqueous solution chemistry of uranium (*1*). This report describes a preconcentration procedure for uranium with subsequent analysis by X-ray fluorescence spectrometry (XRF). The technique involves precipitation of uranium as a polyuranate and collection on a silver membrane filter. Two advantages accrue when a silver membrane is used rather than the more common cellulose or polycarbonate membranes. First, increased sensitivity results since the Ag Kα line (22.162 keV) efficiently overlaps the uranium L_I absorption edge (21.753 keV). The net result is that uranium is excited not only by the radiation from the X-ray tube, but also by the secondary fluorescent radiation from the Ag support. Second, the metal membrane presents a rigid, uniform surface to the spectrometer, avoiding the problems associated with deformation which often occurs with less rigid membrane materials.

EXPERIMENTAL

Apparatus. A Philips PW-1410 X-ray spectrometer equipped with a Mo anode X-ray tube was used to measure the intensity of the 13.6-keV U Lα line. A Mo target tube was chosen because the Mo characteristic radiation overlaps one of the uranium L absorption edges. Under conditions of excitation by characteristic radiation, the signal to noise ratio increases with increasing potential applied across the X-ray tube. Therefore, the tube was operated at 95 kV and 34 mA. Other instrumental conditions were as follows: scintillation detector biased at 1.06 kV, pulse height discriminator base line at 3.81 V with a 3.96-V window; a LiF-200 crystal was used to disperse the fluorescent radiation. Fine collimation was used. Filtrations were made with the aid of a Nuclepore filtration apparatus with a filtration area of 25 cm^2.

Reagents. Silver metal membrane filters (Selas Flotronics Corporation) with a pore size of 0.45 μm were used to collect the uranium precipitate. Filters with a diameter of 1 inch were used because they fit directly into the sample cups for the Philips spectrometer. All materials used were of reagent grade quality. Stock solutions of 1000 ppm uranium were prepared from uranyl acetate (Baker). The stock solution was standardized by means of an oxidation titration procedure (*2*). Working solutions of uranium in the range 1–100 ppm were prepared daily. Stock solutions (2000 ppm in each metal) for the interference study were prepared from $FeCl_3 \cdot 6H_2O$, Na_2SO_4, $NaVO_3$, $(NH_4)_2MoO_4$, and $CaCl_2$. The concentration of the ammonium carbonate stock solution was 0.1 M and a stock solution which was 0.5 M in Ba^{2+} was prepared from $BaCl_2 \cdot 2H_2O$.

Procedure. The carbonate concentration of a 20-mL aliquot of the sample is controlled by adjusting the pH of the sample to approximately 1 through the addition of several drops of concentrated HCl. In order to assure that all of the native CO_3^{2-} has been destroyed, the sample is heated until it just begins to boil. After cooling to room temperature, the pH of the sample is readjusted to 7 with 6 M NaOH. The sample is then made 2×10^{-3} M in carbonate through the addition of 2 mL of 0.1 M $(NH_4)_2CO_3$. The precipitation of BaU_2O_7 is effected by first bringing the pH of the sample to 12.3 through the addition of 6 M NaOH. The sample is stirred and 5 mL of 0.5 M Ba^{2+} is added. The sample is allowed to stir for approximately 2 min before filtering through a silver metal membrane. The precipitate

0003-2700/79/0351-0681$01.00/0 © 1979 American Chemical Society

Table I. Data Obtained from 0–50 ppm Calibration Line

slope	524	$\sigma = 3$
y-intercept	−18	$\sigma = 29$
correlation coefficient	0.9995	
student's t	190	8 degrees of freedom
lower limit of detection	1.3 μg	(60 ppb, 20-mL sample)

on the filter is allowed to dry before X-ray measurements are made.

DISCUSSION

The preconcentration procedure depends upon the formation of a uranyl carbonate complex (3):

$$UO_2^{2+} + 2CO_3^{2-} \rightleftarrows [UO_2(CO_3)_2 \cdot 2H_2O]^{2-} \quad \beta_2 = 4 \times 10^{14}$$

$$UO_2^{2+} + 3CO_3^{2-} \rightleftarrows UO_2(CO_3)_3^{4-} \quad \beta_2 = 2 \times 10^{18}$$

followed by the precipitation of uranium as a polyuranate:

$$2UO_2(CO_3)_3^{4-} + 6OH^- \rightleftarrows U_2O_7^{2-} + 6CO_3^{2-} + 3H_2O$$

$$Ba^{2+} + U_2O_7^{2-} \rightarrow BaU_2O_7$$

The precipitation reaction takes place above pH 11. At high concentrations of uranium (in the per cent range), the diuranate anion can be precipitated with ammonium or sodium as counterions (4, 5). However, at lower concentrations of uranium a counterion, such as barium, must be used. The actual substance being collected is probably BaU_2O_7 in a $BaCO_3$ matrix.

As might be anticipated, the results are strongly dependent on the carbonate concentration of the sample. As the carbonate concentration increases, the amount of $BaCO_3$ in the precipitate also increases. As a result the mass absorption coefficient of the sample increases and the sensitivity for uranium decreases. For this reason, the carbonate concentration of the sample must be controlled by destroying the native carbonate, then adding a sufficient quantity of $(NH_4)_2CO_3$ to attain the optimal concentration. Once the carbonate concentration has been controlled, the uranium intensity is no longer dependent on the concentration of carbonate originally in the sample.

If the carbonate concentration is too low, calibration curves with a negative intercept result. A minimal amount of carbonate is required to recover all of the uranium from solution, i.e., the production of BaU_2O_7 precipitate is not quantitative and $BaCO_3$ is required as a carrier for complete uranium recovery.

A calibration curve was prepared and was found to be linear in the range of 0–50 ppm. Data pertaining to the calibration curve are summarized in Table I. A least squares fit of the experimental data yielded as an equation for the line $y = 524x - 18$, where y is the net uranium peak intensity and x is the concentration of uranium in parts per million. A lower limit of detection of 60 ppb was calculated as the concentration of uranium required to give a signal three times the standard deviation in the signal obtained for the blank.

The precision of the method was evaluated at three different concentrations of uranium, using five replicate samples and the results are given in Table II. Precision expressed as per cent relative standard deviation was found to be 5% at the lower concentrations (1 ppm) and improved to 1.4% at 50 ppm.

The effect of possible interfering elements on the analysis was examined by analyzing 20 ppm uranium solutions (three replicates for each interferant) which were spiked with various concentrations of reagents. Molybdate and vanadate were examined because previous work had shown these two oxyanions to be the major contaminants in solution mining samples (6). The concentration of either molybdate or vanadate does not normally exceed 20 ppm (6). As shown in Table III, molybdate is a serious interferant only at very high concentrations. Vanadate on the other hand tends to interfere somewhat more significantly at lower levels. The mode of interference is likely due to an increase in the mass absorption coefficient for the sample as a result of the precipitation of barium by VO_3^-. However, at vanadate concentrations twice that expected to be found in solution mining samples, no significant interference is observed. Calcium is not a major interferant even at high concentrations (500 ppm). Sulfate was examined as an interferant because it was felt that an increase in the mass absorption coefficient for the sample could be found in solutions with a high sulfate concentration as a result of increased precipitation of barium. As the data in Table III indicate, the amount of uranium found rapidly decreases with an increase in sulfate concentration, making sulfate the major interferant in the analysis.

Finally, the applicability of the method to actual samples was examined by analyzing six process samples from a solution mining operation and comparing the results to a colorimetric procedure using 4-(2-pyridylazo)resorcinol (7). The agreement between the two sets of data is quite good, as summarized in Table IV.

Table II. Precision of the Method

	uranium taken, ppm		
trial	1	15	50
1	1.18	15.1	49.6
2	1.06	14.8	48.9
3	1.09	15.2	49.5
4	1.10	15.1	49.7
5	1.03	14.2	50.8
mean	1.09	14.9	49.7
σ	0.056	0.41	0.69
RSD, %	5.0	2.8	1.4

Table III. Effect of Interferants on the Analysis of a 20 ppm Uranium Solution

	concentration, ppm		
interferant	interferant	uranium found	σ
Ca^{2+}	20	20.2	0.61
	200	20.8	0.31
	500	20.9	0.40
SO_4^{2-}	20	19.6	0.51
	100	17.8	0.71
	200	17.8	0.61
	500	14.8	0.42
MoO_4^{2-}	40	18.6	2.3
	400	17.5	0.56
	1000	13.6	0.35
VO_3^-	40	20.5	0.76
	500	13.4	0.5
Fe^{3+}	20	19.2	0.85
	100	20.1	0.74

Table IV. Analysis of Industrial Process Samples

	uranium, ppm	
sample	this method	PAR
A	20.8	20.0
B	0.36	0.35
C	0.86	0.95
D	1.09	1.20
E	24.6	25.3
F	24.0	23.6

LITERATURE CITED

(1) B. B. Jablonski and D. E. Leyden, *Adv. X-ray Anal.*, **21**, 59 (1978).
(2) A. R. Main, *Anal. Chem.*, **26**, 1507 (1954).
(3) L. A. Maclaine, *Proc. Int. Conf. Peaceful Uses At. Energy*, **8**, 30 (1956).
(4) J. Sutton, *J. Inorg. Nucl. Chem.*, **1**, 68 (1955).
(5) N. P. Galkin, B. N. Sudarikov, U. D. Veryatin, Yu. D. Shiskov, and A. A. Malorov, "Technology of Uranium", Israel Program for Scientific Translations, Jerusalem, 1966, p 127.
(6) B. B. Jablonski and D. E. Leyden, *Anal. Chem.*, **50**, 404 (1978).
(7) T. M. Florence and Y. Farrar, *Anal. Chem.*, **35**, 1613 (1963).

RECEIVED for review November 27, 1978. Accepted January 15, 1979. This work was supported in part by Research Grant CHE-7618385 from the National Science Foundation. The Camille and Henry Dreyfuss Foundation is acknowledged for partial funding for the X-ray spectrometer.

Determination of Proton Types in Solid Pitch by Wide Line Nuclear Magnetic Resonance Spectrometry

Robert M. Pearson

Kaiser Aluminum & Chemical Corporation, Center for Technology, P.O. Box 877, Pleasanton, California 94566

Second moment analysis of wide line nuclear magnetic resonance (NMR) spectra is used to calculate the relative concentrations of the major types of hydrogen (protons) found in solid pitch. This method consists of measuring, by high resolution NMR, the chloroform soluble portions of a variety of pitch samples. The concentration of aromatic protons, aliphatic protons, and protons bound to a carbon atom adjacent to an aromatic ring are determined. These samples are then used to show that the second moment of the wide line NMR spectrum is a measure of aromatic protons when determined at liquid helium temperature, and a measure of aromatic protons plus protons on carbon atoms adjacent to the aromatic ring when determined at liquid nitrogen temperature.

The chemical composition and structure of both petroleum and coal tar pitch has been studied by numerous techniques including infrared spectrometry, mass spectrometry, electron spin resonance, and high resolution nuclear magnetic resonance (NMR) spectrometry. Wide line NMR has been applied to coal studies, but does not appear to have found extensive application in pitch work (*1*).

Standard proton high resolution NMR usually requires liquid samples, either in the form of a solution or melt. Wide line NMR spectra can be run on samples in the solid state. This is an important advantage in studies on partially soluble or high melting point samples.

The disadvantage of wide line NMR is that in the solid state, dipolar interactions between magnetic nuclei are not averaged to zero, as they are in liquids, and broad NMR lines (up to 10 gauss wide) are obtained. In theory, dipolar line broadening can be overcome by magic angle spinning (*2*). This method is commonly used to obtain high resolution NMR spectra of dilute isotopes, such as carbon-13, in solid samples. Proton line narrowing in pitch would require spinning rates comparable to the line width in Hz ($\sim 10^5$ revolutions per second) and are not experimentally feasible at this time (*3*). Thus, the concentration of protons in different functional groups cannot be measured directly from the NMR spectrum of a solid. This can be overcome by using the second moment analysis of the broad line NMR spectra described here.

Pitch Functionality. The three major types of protons found in a pitch are: (i) aromatic protons, i.e., protons bound to a carbon atom in an aromatic ring; (ii) α-aliphatic protons, i.e., protons bound to a carbon atom adjacent to an aromatic ring; (iii) non-α-aliphatic protons, i.e., protons bound to a carbon atom more than one removed from an aromatic ring.

The method described below can be used to estimate the concentration of each of the above types of protons in a solid pitch sample.

EXPERIMENTAL

Apparatus. *Wide Line NMR.* The NMR measurements described here were made at 15 MHz using a Varian Model DA-100-15D NMR Spectrometer equipped with a 4210 Variable Frequency RF unit. The magnetic field was modulated at 40 Hz with a modulation amplitude such that the derivative signal was not distorted. All wide line NMR signals were fed directly into a Fabri-Tek Instrument Computer Model 1074 for data reduction. Low temperature spectra were run using an Air Products and Chemical Corporation Model LTD-3-110 Liquid Transfer Heli-Tran Refrigerator. Sample temperature was monitored using an Air Products Direct Digital Temperature Readout Model APD-T3.

High Resolution NMR. High resolution NMR spectra were determined on chloroform extracts of pitch using a Varian Model A-60 High Resolution NMR Spectrometer. Sample treatment of the extracts used has been described (*4*).

Methods. *High Resolution NMR.* High resolution NMR spectra were determined on the deuterated chloroform soluble portion of a variety of pitches. Figure 1 is typical of these spectra and will be divided into three portions. The bands between 0 and 1.6 ppm are due to protons on carbon atoms more than one removed from aromatic ring, i.e., non-α-aliphatic protons; the bands between 1.6 and 3.8 ppm are due to protons on carbon atoms adjacent to an aromatic ring, i.e., α-protons; and the bands between 6 and 9 ppm are due to protons bonded to aromatic carbon atoms, i.e., aromatic protons. Minor amounts of other types of protons are undoubtedly found in pitch. It appears that these are in low enough amounts that they have no practical effect on the NMR spectra.

Wide Line NMR. *Quantitative Proton Analysis.* Quantitative proton analysis is conducted on solid pitch samples by methods developed for the analysis of aluminum oxide (*5*). These methods consist of comparing the relative intensity of the NMR spectrum of the sample to that of a material of known proton content.

Qualitative Proton Analysis. The relative concentrations of the three types of protons are estimated from a second moment analysis of the low temperature NMR spectra. The second moment of the absorption curve is defined as:

$$\Delta H_2^2 = \frac{\int g(h)\,(H - H_0)^2\,dh}{\int g(h)\,dh} \qquad (1)$$

Our spectra are obtained as derivative curves and experimental second moments calculated from Equation 1 and are artificially broadened by the modulation used to produce the derivative. Andrew (*6*) has shown that true second moments can be obtained

0003-2700/79/0351-0683$01.00/0 © 1979 American Chemical Society

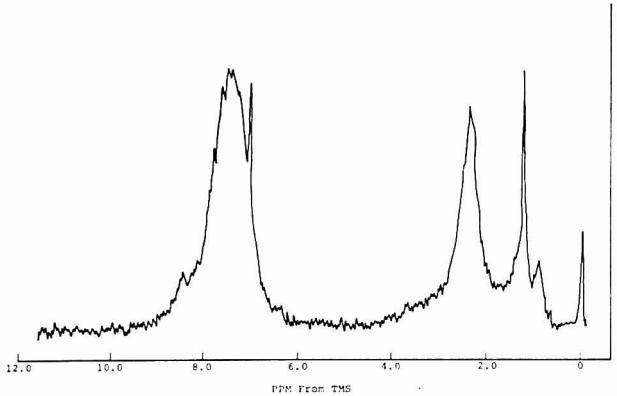

Figure 1. High resolution NMR spectrum of chloroform soluble portion of pitch

by subtracting one-fourth of the square of the modulation amplitude from the exprimentally calculated second moment. This correction is 2.6 gauss^2 in our work.

Van Vleck (7) showed the rigid lattice second moment of the NMR spectrum could be calculated in terms of magnetic moments, spins, and internuclear distances of the nuclei. His equation showed that, for pitch, the second moment of the NMR spectrum run under rigid lattice conditions is proportional to the inverse sixth power of the distance between protons.

Pake and Purcell (8) showed the Van Vleck equation to be experimentally correct, and numerous authors have used second moment analysis to study solid state structures. In practice, the nearest neighbor protons have the greatest effect on the rigid lattice second moment. Since protons attached to the aromatic ring are farther apart than aliphatic protons, molecules with higher aromatic content will yield NMR spectra with smaller rigid lattice second moments.

Wide line NMR has been used extensively to study the chemical composition of coal (9-12). These workers showed that rigid lattice second moments could be divided into group contributions and followed the relationship:

$$\Delta H_2^2 = \sum_1^n (\Delta H_2^2)_x \left(\frac{H_x}{H_{total}} \right) \qquad (2)$$

where ΔH_2^2 is the second moment, $(\Delta H_2^2)_x$ is the group contribution of proton form x and Hx/H_{total} is the fraction of the protons in form x.

Richards and Yorke (13) measured the low temperature second moments of an extensive number of model compounds. They showed that by combining the second moment of benzene (9.7 gauss^2) measured by Andrew and Eades (14) with measured second moments of model compounds, they could estimate the contribution of the three major types of protons found in their model compounds. Their work indicates that second moments of the NMR signal of organic solids can be accurately reduced to group contributions of the various types of protons found in the molecule.

The ability to measure the concentration of α protons depends on rotation of the α methyl groups at liquid nitrogen temperature. Andrew (15) measured the second moments of the three xylene isomers at 95 K. All three isomers yielded a second moment of 9.8 (gauss)^2 at this temperature. The theoretical rigid lattice second moment for these compounds is 21 (gauss)^2. Andrew attributed the reduced second moment at 95 K to rotation of the methyl groups around the C–C bond. By analogy, the NMR spectrum of a pitch which contains methyl groups attached to an aromatic ring would have a smaller second moment than would be theoretically estimated from the relative concentration of aromatic and aliphatic protons. Richards and Yorke (13), working at liquid nitrogen temperature, assigned a value of 10.0 gauss^2 for the effect of methyl groups attached to an aromatic ring. At this temperature, the terminal methyl group of a long aliphatic ring would also rotate and reduce the second moment of the NMR spectrum. This effect is partially offset by the effect of the methylene group attached to the aromatic ring so that the second moment would still reflect the relative concentration of protons on the α carbon atoms. Protons in adjacent ring positions (perimethyls) do not rotate at liquid nitrogen temperature (13) and so would affect the NMR spectrum as an aliphatic in a non-α-position. The concentration of this type of proton is expected to be low in pitch samples.

Table I. High Resolution NMR Analysis and Wide Line Second Moments of Pitch Extracts

	high resolution NMR analysis			second moment (gauss)^2	
sample	% aromatic	% α-aliphatic	% non-α-aliphatic	liq. N_2 temp.	liq. He temp.
1	21.0	23.1	55.9	18.5	22.1
2	56.4	30.2	13.4	12.2	16.9
3	65.0	28.2	6.8	10.0	14.0
4	66.5	27.0	6.5	11.1	14.9
5	85.8	14.2	-0-	9.7	10.6

At liquid helium temperatures (4.5 K), α methyl group rotation stops and rigid lattice conditions are obtained. Equation 2 can then be reduced to:

$$(\Delta H_2^2)_{exp} = A\frac{[H]_{aromatic}}{[H]_{total}} + B\frac{[H]_{aliphatic}}{[H]_{total}} \qquad (3)$$

when measured at liquid helium temperature, and:

$$\Delta H_2^2 = A\frac{[H]_{aromatic+\alpha\text{-}aliphatic}}{[H]_{total}} + B\frac{[H]_{non\text{-}\alpha\text{-}aliphatic}}{[H]_{total}} \qquad (4)$$

when measured at liquid nitrogen temperature. The brackets denote concentrations and A and B are constants.

RESULTS

Chloroform Extracts. The values of A and B in Equations 3 and 4 were estimated by extracting a variety of petroleum and coal tar pitch samples with chloroform. The chloroform was removed at 100 °C in a vacuum oven and the second moment of the wide line NMR spectrum of the residue determined at both liquid nitrogen and liquid helium temperatures. A portion of the residue was dissolved in deuterated chloroform and the concentration of the three major types of protons determined by high resolution NMR. Table I

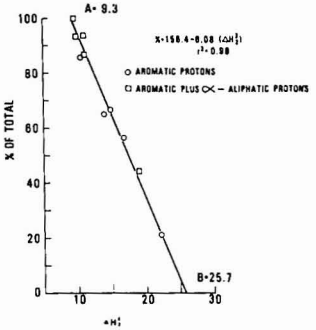

Figure 2. Relationships between second moments and relative proton concentration

Table II. Proton Contents of Solid Pitch Samples

pitch type	% protons by wt.	second moment, He temp.	second moment, N_2 temp.	% of total protons, aromatic	% of total protons, α-aliphatic	% of total protons, non-α-aliphatic
petroleum	7.01	17.1	15.1	52.4	12.2	35.4
petroleum	6.26	15.7	13.9	60.9	11.0	28.1
petroleum	5.01	17.8	12.8	48.2	30.4	21.4
petroleum	5.17	18.2	13.2	45.7	30.4	23.9
petroleum	9.23	24.4	23.6	8.9	4.9	86.2
coal tar	3.88	16.4	13.6	56.7	17.0	26.3
coal tar	4.22	15.0	12.0	65.2	18.2	16.6
coal tar	3.90	16.0	11.6	59.1	26.8	14.1
coal tar	4.43	15.1	11.5	65.2	21.3	13.5
coal tar	4.56	17.1	11.6	52.4	33.4	14.2

summarizes both the high resolution NMR analysis and the low temperature second moments for these chloroform extracts. Figure 2 shows that second moments measured at both temperatures follow the same relationship when plotted as a function of the appropriate relative proton concentration. Regression analysis of these data shows that the second moments at liquid helium temperature are a linear function of aromatic proton concentration and that the second moments at liquid nitrogen temperature follow the same equation as a function of aromatic plus α-aliphatic proton content.

The regression equation for the data shown in Figure 2 is:

$$\% = 156.4 - 6.08\ (\Delta H_2^2) \qquad (5)$$

where % is the percent aromatic protons or percent aromatic plus α-aliphatic protons and the second moment is at liquid helium temperature in the former case and liquid nitrogen temperature in the latter. The coefficient of determination for the above equation is 0.98. The regression equation can be combined with Equations 3 and 4 to calculate A at 9.3 (gauss)^2 and B at 25.7 (gauss)^2. This value of A is very close to the rigid lattice second moment of the NMR spectrum of benzene [9.7 (gauss)^2]. The value of B agrees very well with estimate of the rigid lattice second moment of the NMR spectrum of pure aliphatic made by Richards and Yorke [27.5 (gauss)^2].

Whole Pitch Samples. Second moments calculated from NMR spectra run at liquid nitrogen and liquid helium temperatures can be combined with the above regression equation to measure the concentration of the three major types of protons found in solid pitch samples. Results of such calculations combined with total proton measurements are given in a variety of pitch samples in Table II.

LITERATURE CITED

(1) K. D. Bartle, *Rev. Pure Appl. Chem.*, **22**, 79 (1972).
(2) E. R. Andrew, A. Bradbury, and R. G. Eades, *Arch. Sci.*, **11**, 223 (1958).
(3) T. C. Farrar and E. D. Becker, "Pulse and Fourier Transform NMR", Academic Press, New York, 1971, p 95.
(4) R. M. Pearson, *Fuel*, **52**, 80 (1973).
(5) R. M. Pearson, *J. Catal.*, **23**, 388 (1971).
(6) E. R. Andrew, *Phys. Rev.*, **91**, 425 (1953).
(7) H. J. Van Vleck, *Phys. Rev.*, **74**, 1168 (1948).
(8) G. E. Pake and E. M. Purcell, *Phys. Rev.*, **74**, 1184 (1948).
(9) C. L. M. Bell, R. E. Richards, and R. W. Yorke, *Brennst.-Chem.*, **39**, 830 (1958).
(10) W. R. Ladner and A. E. Stacey, *Fuel*, **40**, 295 (1961).
(11) W. R. Ladner and A. E. Stacey, *Fuel*, **42**, 75 (1963).
(12) A. C. Cunningham, W. R. Ladner, R. Wheatley, and W. F. Wyss, *Fuel*, **45**, 61 (1966).
(13) R. E. Richards and R. W. Yorke, *J. Chem. Soc.*, **503**, 2489 (1960).
(14) E. A. Andrew and R. G. Eades, *Proc. R. Soc., Ser. A*, **218**, 537 (1953).
(15) E. R. Andrew, *J. Chem. Phys.*, **18**, 607 (1950).

RECEIVED for review October 2, 1978. Accepted December 18, 1978.

Simultaneous Determination of Mixtures in Liquid by Laser-Induced Photoacoustic Spectroscopy

Shohei Oda,* Tsuguo Sawada, Mitsuaki Nomura, and Hitoshi Kamada

Department of Industrial Chemistry, Faculty of Engineering, The University of Tokyo, Hongo, Bunkyo-ku, Tokyo, Japan

Laser-induced photoacoustic spectroscopy (LIPAS) has been applied to the determination of binary liquid mixtures. Using tar food dyes such as Amaranth, New Coccine, and Sunset Yellow FCF, the additivity of the photoacoustic signal intensity was examined. The analysis of mixtures of ultra low concentrations of the above dyes in water clearly showed that LIPAS was applicable to the simultaneous determination of mixtures with highly overlapping absorption spectra, the mixtures which have been extremely difficult to analyze by conventional colorimetric and dual-wavelength absorption spectrometry.

Spectroscopy utilizing the photoacoustic effect has been developed in recent years, as exemplified by the use of laser with high monochromaticity and high power, to significantly improve the detection sensitivity. Laser-induced photoacoustic spectroscopy (LIPAS) has been used particularly for the determination of trace amounts of several toxic gases in the environmental atmosphere because of its high detection sensitivity and its responsiveness in real time. For instance, a few ppb of NO (*1–3*), NO_2 (*4*), NH_3 (*5*), C_2H_4 (*6*), and other hydrocarbons (*7*) in air, exhaust gases, and other environments have been measured with this method. Additionally, LIPAS has been shown to be highly sensitive in the measurement of liquid samples (*8, 9*). The authors have successfully applied this method to the determination of ultra trace levels of cadmium in bio-samples where a detection limit of 14 ppt was obtained (*10*). This value was about two orders of magnitude lower than the value obtained by the conventional flame atomic absorption spectrometry.

The photoacoustic signal is obtained by measuring pressure fluctuations caused by heat generated through radiationless relaxation. The additive property of the photoacoustic signal intensity is not always observed. Consequently, the additive property cannot be expected to exist in some cases: (1) where the heat produced individually by the two components is significantly out of phase with each other because of differences in thermal relaxation times, (2) where intermolecular energy transfer, including chemical reaction of the excited state occurs, or (3) for the case where a fluorescent component is quenched by adding another component. In applying LIPAS to a binary liquid mixture, if the photoacoustic signal is additive with respect to component concentration, then a simultaneous determination of the components can be made in situ by using a combination of lasing lines without resorting to any prior separation procedures. Since argon ion and krypton ion lasers offer many lasing lines to choose, this new procedure should be now widely applicable, where in the past this type of determination has been extremely difficult to achieve by conventional colorimetric spectrometry because of overlap of the absorption spectra.

In the present investigation, some tar food dyes were chosen as colored samples whose absorption coincided with the lasing line wavelengths of an argon ion laser. The tar food dyes have been used very frequently as coloring agents with dye mixtures of two or more. On the other hand, as the toxicity of such dyes has been paid much attention recently as a serious social problem, their trace determination should become important. Therefore, by preparing extremely low concentration dye mixtures, simultaneous determinations were attemped.

EXPERIMENTAL

Reagents. Three tar food dyes (Amaranth, New Coccine, and Sunset Yellow FCF) used as reagents were dye standards of the National Institute of Hygienic Science in Japan. Dye solutions, 1.0 mM, were prepared as a stock solution. The stock solutions were diluted with water and adjusted to low dye concentration. Twice-distilled deionized water was used.

Apparatus and Experimental Condition. The same apparatus as that described in a previous report (*10*) was used. As for the photoacoustic sample cell, it was improved in the point that the volume of the previous cylindrical sample cell (length 90 mm, inner diameter 24 mm, and piezoelectric ceramic length 50 mm) was about 40 mL, while that of the new one was about 8 mL (length 50 mm, inner diameter 15 mm, and piezoelectric ceramic length 15 mm). In addition, the piezoelectric ceramic was exchanged for a more sensitive one (NPM, N-21, Tohoku Kinzoku Co. Ltd.). Owing to the modification of the sample cell, the detection sensitivity was improved threefold.

An argon ion laser (Spectra Physics Model 164-03), operating in single line modes of 476.5, 488.0, and 514.5 nm, was modulated at a given frequency (185 Hz) and the laser power was 300 mW. The absorption spectra of the food dye solutions were measured by a Shimazu Model MPS-5000 spectrophotometer.

RESULTS AND DISCUSSION

Examination of the Additivity of the Photoacoustic Signal. Figure 1 shows absorption spectra of the three dyes. The additivity of photoacoustic signal intensity was investigated with Amaranth and Sunset Yellow FCF by adding a given concentration of Sunset Yellow FCF as an interfering component to various concentrations of Amaranth solution and analytical curves were made. The result is shown in Figure 2. Using a least squares procedure, the slopes of the curves were (1) 0.134, (2) 0.133, and (3) 0.144 at 488.0 nm and (1) 0.188, (2) 0.201, and (3) 0.189 at 514.5 nm. The variation coefficients among the values of those slopes were 3.6% at 488.0 nm and 3.1% at 514.5 nm and were within the range of the experimental error of the LIPAS technique. The intercepts were 0.788 (488.0 nm) and 0.678 (514.5 nm) for analytical curve 2 and 1.53 (488.0 nm) and 1.36 (514.5 nm) for curve 3. As can be seen, if the concentration of Sunset Yellow FCF was doubled, the value of the intercept increased twofold. Similar relationships were obtained from analytical curves of Sunset Yellow FCF interfered by Amaranth. Based on these results, the additivity of photoacoustic signal intensity with respect to component concentration was found to be valid for this mixture. For the Amaranth–New Coccine mixtures whose absorption spectra substantially overlap each other, additivity also was confirmed. The experimental results are shown in Figure 3. Though the same additivity can be expected for Sunset Yellow FCF–New Coccine mixtures, it was not examined in the present experiment.

Simultaneous Determination of Two-Component Mixtures. In the case where the additivity is valid as

0003-2700/79/0351-0686$01.00/0 © 1979 American Chemical Society

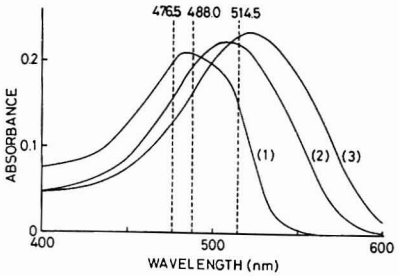

Figure 1. Absorption spectra of tar food dye solutions. (1) Sunset Yellow FCF. (2) New Coccine. (3) Amaranth. Concentration: 10^{-5} M; dashed lines: wavelength of argon ion laser

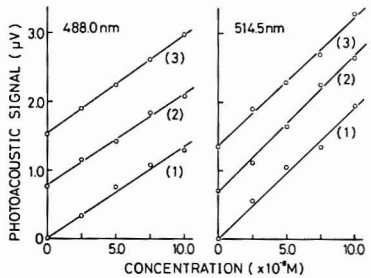

Figure 2. Analytical curves of Amaranth interfering by Sunset Yellow FCF. (1) Sunset Yellow FCF: not added. (2) Sunset Yellow FCF: 5.0×10^{-8} M. (3) Sunset Yellow FCF: 1.0×10^{-7} M

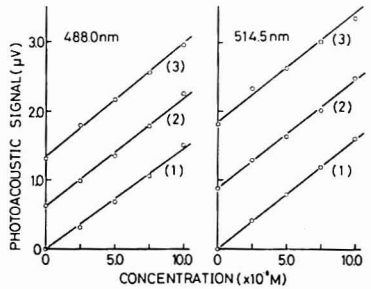

Figure 3. Analytical curves of New Coccine interfering by Amaranth. (1) Amaranth: not added. (2) Amaranth: 5.0×10^{-8} M. (3) Amaranth: 1.0×10^{-7} M

mentioned above, by solving a set of simultaneous equations with two unknowns obtained from measurements at two wavelengths, the simultaneous determination of binary liquid mixtures becomes possible using LIPAS. Therefore, the calibration graphs were made for the three tar food dyes shown in Figure 1 at two lasing wavelengths (488.0 and 514.5 nm) in the concentration range of 10^{-8} M. A lasing wavelength of 476.5 nm would be also applicable to Sunset Yellow FCF. For Amaranth, the detection limit obtained was 1.1×10^{-9} M (0.7 ppb), based on a limiting photoacoustic signal-to-noise ratio of 2:1. This value corresponds to an absorptivity of 2.4×10^{-5} cm^{-1} which is two orders of magnitude lower than that by conventional absorption spectrometry.

Using calibration graphs, simultaneous determinations were shown to be possible for various concentration of Amaranth–Sunset Yellow FCF and Amaranth–New Coccine mixtures. The mixtures prepared were of significantly lower concentration ranges than the detection limit obtainable by conventional colorimetric spectrometry. The results are given in Table I and Table II. In both Amaranth–Sunset Yellow FCF and Amaranth–New Coccine mixtures, the errors produced in the measurements were within 10% of the actual value up to a mixing ratio of 1:2. However for mixing ratios of 1:5 and 1:10, the error for the small portion component of the mixture became relatively large. The errors in the measurement can be regarded to affect the smaller component more than the larger one. However, considering that the concentration range is as low as 10^{-8} M, the errors of such an extent are negligible.

Table I. Results for the Simultaneous Determination of Amaranth–Sunset Yellow FCF Mixtures

sample no.	name[a]	concentration 10^{-5} M taken	found	rel. error, %
1	A	10.0	10.3	+3.0
	S	1.0	2.8	+180.
2	A	10.0	9.7	−3.0
	S	2.0	2.9	+45.0
3	A	8.0	7.8	−2.5
	S	4.0	4.3	+7.5
4	A	5.0	5.4	+8.0
	S	5.0	4.7	−6.0
5	A	4.0	4.4	+10.0
	S	8.0	7.3	−8.7
6	A	2.0	2.6	+30.0
	S	10.0	9.6	−4.0
7	A	1.0	0.6	−40.0
	S	10.0	10.6	+6.0

[a] A: Amaranth, S: Sunset Yellow FCF.

Table II. Results for the Simultaneous Determination of Amaranth–New Coccine Mixtures

sample no.	name[a]	concentration 10^{-5} M taken	found	rel. error, %
1	A	10.0	10.8	+8.0
	N	2.0	1.7	−15.0
2	A	8.0	8.7	+8.7
	N	4.0	4.2	+5.0
3	A	5.0	4.6	−8.0
	N	5.0	5.5	+10.0
4	A	4.0	4.4	+10.0
	N	8.0	7.9	−1.3
5	A	2.0	2.8	+40.0
	N	10.0	9.4	−6.0

[a] A: Amaranth, N: New Coccine.

The above experiments showed clearly that LIPAS was applicable to the simultaneous determination of systems with highly overlapping absorption spectra such as with Amaranth–New Coccine and Amaranth–Sunset Yellow FCF. These mixtures in the past have been extremely difficult to determine without any prior separation procedures using both ordinary absorption and dual-wavelength absorption spectrometry. Kamikura et al. (*11*), determined Amaranth–New Coccine mixtures by masking the other component instrumentally with a dual-wavelength absorption spectrometer. They described that the analyzed component in the concentration range from 1.7×10^{-7} M (0.1 ppm) to 1.8×10^{-5} M (11 ppm) could be determined under the existence of the interfering component of 8.3×10^{-6} M (5 ppm).

The sole disadvantage of LIPAS is that the objects to be measured are restricted by the use of lasers. However, stable lasers can be obtained nowadays in the visible wavelength

region by using dye lasers in conjunction with argon ion and krypton ion lasers. In the future and with the advent of lasers encompassing all wavelengths including the UV region, LIPAS should become a powerful tool for ultratrace analysis.

ACKNOWLEDGMENT

One of the authors (M. N.) is indebted to Keiichi Furuya of the Science University of Tokyo for his encouragement.

LITERATURE CITED

(1) L. B. Kreuzer and C. K. N. Patel, *Science*, **173**, 45 (1971).
(2) C. K. N. Patel, E. G. Burkhardt, and C. A. Lambert, *Science*, **184**, 1173 (1974).
(3) E. G. Burkhardt, C. A. Lambert, and C. K. N. Patel, *Science*, **188**, 1111 (1975).
(4) P. C. Claspy, C. Ha, and Y. H. Pao, *Appl. Opt.*, **16**, 2972 (1977).
(5) L. G. Rosengren, E. Max, and S. T. Eng, *J. Phys. E.*, **7**, 125 (1974).
(6) L. B. Kreuzer, N. D. Kenyon, and C. K. N. Patel, *Science*, **177**, 347 (1972).
(7) L. B. Kreuzer, *Anal. Chem.*, **46**, 239A (1974).
(8) W. Lahmann, H. J. Ludewig, and H. Welling, *Anal. Chem.*, **49**, 549 (1977).
(9) S. Oda, T. Sawada, and H. Kamada, *Bunseki Kagaku*, **27**, 269 (1978).
(10) S. Oda, T. Sawada, and H. Kamada, *Anal. Chem.*, **50**, 865 (1978).
(11) M. Kamikura, F. Endo, and H. Sasaki, *J. Food Hyg. Soc. Jpn.*, **13**, 555 (1972).

RECEIVED for review November 27, 1978. Accepted January 22, 1979.

Laser-Induced Photoacoustic Spectroscopy of Some Rare Earth Ions in Aqueous Solutions

Tsuguo Sawada,* Shohei Oda, Hiromichi Shimizu, and Hitoshi Kamada

Department of Industrial Chemistry, Faculty of Engineering, The University of Tokyo, 7-3-1, Hongo, Bunkyo-ku, Tokyo, Japan

The photoacoustic spectra of some trivalent rare earth ions in aqueous solutions were obtained by laser-induced photoacoustic spectroscopy (LIPAS). This method was suitable for the spectral measurements of extremely weak absorption such as a forbidden transition of rare earth ions in liquid. Compared with the absorption and emission spectra in the visible region, the photoacoustic spectrum offered complementary spectroscopic information, particularly with respect to the radiationless decay process.

Photoacoustic spectroscopy is currently being used to provide spectral information on a wide variety of solid and liquid samples (*1*, *2*), which was previously difficult or impossible to measure by ordinary transmission and reflection methods. The availability of dye lasers as an excitation source capable of a high intensity flux within narrow, tunable bandwidths makes photoacoustic detection a promising method for the investigation of the very weak molecular absorption spectra. Dixon et al. (*3*) have measured photoacoustic spectra of forbidden transitions in some unstable gaseous sulfur compounds with a tunable CW dye laser. Recently, Lahmann et al. (*4*) and the present authors (*5*) have successfully applied this method to the ultra trace analysis of liquid samples with an argon ion laser. Laser-induced photoacoustic spectroscopy (LIPAS) has brought a considerable improvement in the detection limit in comparison with conventional absorption spectrometry.

In the present paper, high resolution photoacoustic spectra of some trivalent rare earth ions (Pr^{3+}, Nd^{3+}, Eu^{3+}, Ho^{3+}, and Er^{3+}) in aqueous solution were measured by the LIPAS, though the lasing wavelength of dyes used limited the measurable region.

It is well known that all the lines of rare earth ions at visible and near-infrared regions are forbidden in nature. The intensities of the transitions are, therefore, extremely weak. The LIPAS is expected to be most suitable for the measurements of such forbidden transition in liquid.

EXPERIMENTAL

Reagents and Procedure. Each rare earth nitrate was prepared by dissolving the oxide (99.9%) in nitric acid. These solutions were diluted with distilled water and adjusted to a given concentration of rare earth ion with 0.5 N nitric acid.

Apparatus. A block diagram of the LIPAS is shown in Figure 1. A tunable dye laser (Spectra Physics Model 375), pumped by an argon ion laser (Spectra Physics Model 164-03), was modulated at about 200 Hz by a light chopper and divided into two beams with a beam splitter. One laser beam was directed into the sample cell and the other, into the reference cell through the collecting lenses (f = 50 cm). The dyes used as pumped media were Rhodamine 110, Rhodamine 6G, and Rhodamine B with lasing ranges of about 540–600, 570–630, and 600–670 nm, respectively. The dye laser operated in the multimode with a bandwidth of 1 cm^{-1}. The wavelength was read with a monochromator. The average dye laser power was about 300 mW. The laser power variation with wavelength was monitored by a calibrated photocell.

The pressure fluctuation induced in the solution by absorbed radiation was detected by a piezoelectric ceramic (NPM, N-21 supplied by Tohoku Kinzoku Co. Ltd.). A lock-in amplifier was used to amplify the modulated output signal, which was obtained by subtracting the photoacoustic signal of the reference cell from that of the sample cell with a differential amplifier.

The photoacoustic background signal is mainly due to the absorption of the solvent. The absorption coefficient of water in the 500-nm region is very small, that is, approximately 10^{-5} cm^{-1}, and might change with wavelength according to purity. However, the photoacoustic signal caused by absorption of the solvent is large. The double-beam operation enabled this background signal to be greatly reduced. Other experimental descriptions have appeared in the previous literature (*5*).

The absorption spectrum was obtained with a 90-mm pathlength cell by using a Shimazu MPS-5000 spectrophotometer. All spectral measurements were carried out at room temperature.

RESULTS AND DISCUSSION

It is well known that the sharp lines of the rare earth ions are associated with transitions between configurations of the electrons within the inner 4f shell. All of the sharp lines are forbidden to the first approximation as ordinary electric dipole transitions by Laporte's rule. However, the inversion of center of the electric field of the free ion is removed by the perturbing surrounding field so the lines appear as electric dipole radiation. These transitions, which are so-called forced electric dipole transitions, are all weak, being of about the intensity of natural magnetic dipole transitions.

Praseodymium Ion. The photoacoustic spectrum of Pr^{3+} ion in aqueous solution in the yellow region (~590 nm) is

0003-2700/79/0351-0688$01.00/0 © 1979 American Chemical Society

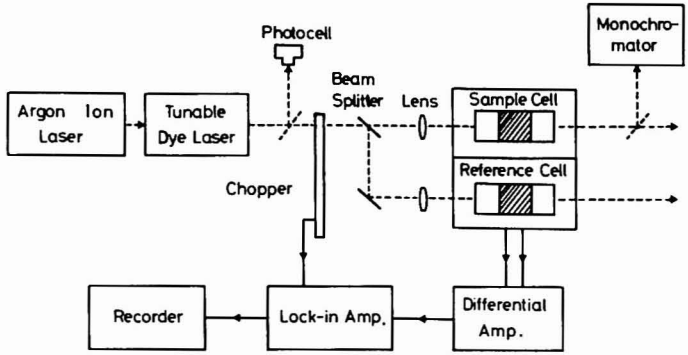

Figure 1. Block diagram of the double-beam LIPAS apparatus

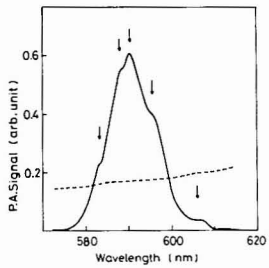

Figure 2. Photoacoustic spectrum of Pr^{3+} ion (—) in aqueous solution and photoacoustic background signal of the solvent (---)

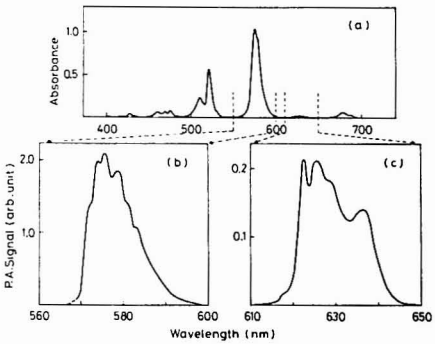

Figure 3. Absorption (a) and photoacoustic spectra [(b) and (c)] of Nd^{3+} ion in aqueous solution. Concentration: (a) and (c), 20 mM; (b), 2 mM

shown in Figure 2. The spectrum at 590 nm is considered to correspond to a transition from the ground state $^3H_4$ to the excited state $^1D_2$. As is suggested in the photoacoustic spectrum, fine structure is present, though a similar spectrum could not be obtained by absorption spectrometry.

Since a molar absorptivity of Pr^{3+} ion in aqueous solution at 590 nm is about 1.6 L mol^{-1} cm^{-1}, slight variation in absorptivity at large transmission would be extremely difficult to detect by absorption spectrometry, in which the absorptivity of at most 10^{-3} cm^{-1} is measured. On the other hand, the LIPAS could detect the change of an absorptivity of $\sim 10^{-5}$ cm^{-1} (6).

The apparent splitting is due to the internal Stark effect caused by the surrounding local electric field. A detailed spectroscopic analysis of the split lines of the Pr^{3+} ion in solution has not been reported yet. However, the five features shown in Figure 2 may be explained as follows. The upper state $^1D_2$ is split into the three levels, characterized by μ = 0, ±1, and ±2, by the internal Stark effect. The spectrum results from the transition from the two lowest ground state $^3H_4$ (μ = ±2 and 3) to the above split levels.

The dashed line shown in Figure 2 is the variation of photoacoustic background signal caused by the absorption of water with wavelength by a single beam apparatus. Slight wavelength dependencies were observed.

Neodymium Ions. Figure 3 shows the photoacoustic spectrum of the Nd^{3+} ion in the range at around 575 nm (b) and 625 nm (c) which are assigned to the electronic transitions from the ground state ($^4I_{9/2}$) to respectively the ^2G, ^4G mixed states and the $^2H_{11/2}$ state. The absorption spectrum over the wide wavelength region is shown in Figure 3a. In the photoacoustic spectrum, fine structures were clearly observed, though they could not be detected in the absorption spectrum as in the case of the Pr^{3+} ion.

Generally speaking, the photoacoustic spectrum obtained by measuring pressure fluctuation caused by heat generated through the radiationless relaxation does not necessarily coincide with the absorption spectrum. In the crystal, the Nd^{3+} ions in the ^2G, ^4G levels decay nonradiatively to the $^4F_{3/2}$ metastable state, and then undergo radiative transitions to the $^4I_{9/2}$, $^4I_{11/2}$, and $^4I_{13/2}$ multiplets (7). In aqueous solution, however, the ions undergo rapid radiationless relaxation because of the transfer of electronic excitation energy to high-frequency vibrations such as OH in the solvent (8). Accordingly, the photoacoustic spectrum of the Nd^{3+} ion in aqueous solution might be expected to coincide with the absorption spectrum.

Europium Ion. The intensity of the lines of the Eu^{3+} ion in the yellow region is extremely weak. The photoacoustic spectrum, shown in Figure 4b, could be observed in the concentration of 0.2 M. The line at 579 nm is assigned to the transition from the ground state $^4F_0$ to the upper $^5D_0$ state. It is well known that the Eu^{3+} ion fluoresces at 613 nm as the result of absorbing radiation at 579 nm. The quantum yield of $^5D_0$ emission for Eu^{3+} ion in methanol for direct excitation of the $^5D_0$ level is 0.17 (9). This is one of the reasons that the photoacoustic spectrum cannot clearly be observed for concentrations under 0.1 M. The line at 579 nm appears surprisingly sharp in the solution at room temperature. This

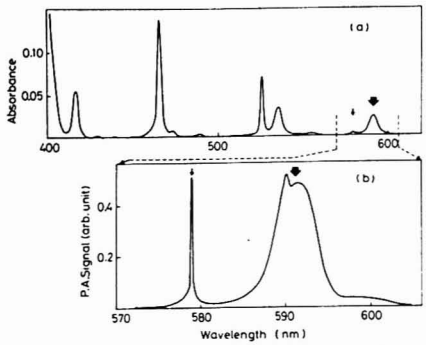

Figure 4. Absorption (a) and photoacoustic spectra (b) of Eu^{3+} ion in aqueous solution. Concentration: 0.2 M

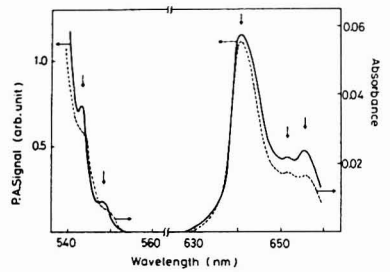

Figure 5. Absorption (---) and photoacoustic spectra (—) of Ho^{3+} ion in aqueous solution. Concentration: 2 mM

probably shows that the molecules of the solvent are under compression close to the Eu^{3+} ion and held relatively stable configuration in the region surrounding the ion, whereas the line at 591 nm shows fine structure. It is tentatively assigned as a magnetic dipole transition from thermally excited level, though it has not been clarified yet (*10*).

Holmium Ion. Figure 5 shows the photoacoustic spectrum in comparison with the absorption spectrum. All the lines did not evidence definite fine structure. For the case of the transitions to the upper $^5F_4$ and $^5S_2$ level from the ground level ($^5I_8$) around 540 nm, the absorption spectrum could not clearly be measured because of weak transitions, and the photoacoustic spectrum could not be observed over the whole wavelength region because of the limiting wavelength of the lasing dyes used. However, there were some differences between the photoacoustic and the absorption spectra, though precise comparison was somewhat difficult. Slight differences might arise from different cascade processes in the two excited states, radiatively and partly nonradiatively, to the ground state.

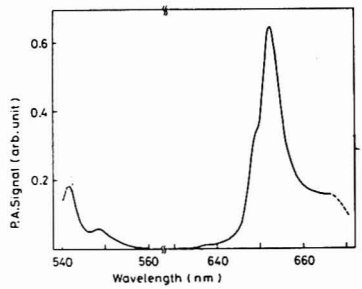

Figure 6. Photoacoustic spectrum of Er^{3+} ion in aqueous solution. Concentration: 2 mM

For the case of the $^5I_8$–$^5F_5$ transition at 641 nm, three peaks were observed. The intensity ratios of the peak at 641 nm to that at 656 nm, were 2.3:1 for the photoacoustic spectrum and 3.2:1 for the absorption spectrum. This result may be explained as follows. The peaks at 641 and 656 nm are considered to correspond to the transitions from the ground state ($^5I_8$) to two different excited states. The calculations of Crozier et al. (*11*) suggest that the terminal state of the transition at 641 nm was the $^5F_5$, and that at 656 nm might be one component of the level resulting from the spin-orbit coupling of the ^3G. The energy difference between the peaks at 641 and 651 nm was about 240 cm^{-1}, which is in good agreement with the magnitude of the ground state splitting (*7*). Therefore, the peak at 651 nm was interpreted as being due to the terminal population in the upper split ground state.

Erbium Ion. Figure 6 shows the photoacoustic spectrum of Er^{3+} ion. The spectrum at 542 nm is assigned to the $^4I_{15/2}$–^4S, and the spectrum at 652 nm, the $^4I_{15/2}$–$^4F_{9/2}$, respectively. Both spectra could not be measured over the whole wavelength region because of the limiting of lasing wavelength. Molar absorptivities of the above two electronic transitions are extremely small. The photoacoustic spectrum of Er^{3+} ion, which was clearly detected by the LIPAS, has revealed simple splitting features.

LITERATURE CITED

(1) Rosencwaig, A. *Anal. Chem.* **1975**, *47*, 592A–604A.
(2) Adams, M. J.; King, A. A.; Kirkbright, G. F. *Analyst (London)* **1976**, *101*, 73–85.
(3) Dixon, R. N.; Haner, D. A.; Webster, C. R. *Chem. Phys.* **1977**, *22*, 199–206.
(4) Lahmann, W.; Ludewig, H. J.; Welling, H. *Anal. Chem.* **1977**, *49*, 549–551.
(5) Oda, S.; Sawada, T.; Kamada, H. *Anal. Chem.* **1978**, *50*, 865–867.
(6) Sawada, T.; Oda, S.; Kamada, H. *Proc. Jpn. Acad. Ser. B*, **1978**, *54*, 189–193.
(7) Snitzer, E. *Phys. Rev. Lett.* **1961**, *7*, 444–446.
(8) Heller, A. *Appl. Phys. Lett.* **1966**, *9*, 106–108.
(9) Dawson, W. R.; Kropp, J. L. *J. Opt. Soc. Am.* **1965**, *55*, 822–828.
(10) Miller, D. G.; Sayer, E. V.; Freed, S. *J. Chem. Phys.* **1958**, *29*, 454–455.
(11) Crozier, M. H.; Dunciman, W. A. *J. Chem. Phys.* **1961**, *35*, 1392–1409.

RECEIVED for review December 22, 1978. Accepted February 5, 1979.

Constant Neutral Spectrum in Mass Spectrometry

Michael J. Lacey* and Colin G. Macdonald

CSIRO Division of Entomology, P.O. Box 1700, Canberra, A.C.T. 2601, Australia

A linked scan is proposed that generates a spectrum of metastable peaks for reactions related by a constant mass of the neutral fragment. An analysis of published data for *n*-decane demonstrates that a small number of such spectra would elicit genetic information for nearly all of the important fragmentations. Each constant neutral spectrum would provide a characteristic fingerprint for the molecule. Application to the direct analysis of the isotopic contents of labeled molecules is possible.

A three-dimensional surface can summarize the genetic relationships for all metastable ion transitions in a double focusing mass spectrometer and can be expected to show higher chemical specificity than any single (two-dimensional) spectrum (*1*). Some notable success has been achieved in plotting extensive regions of the surfaces for various molecules (*2–9*) but the acquisition and processing of the data can be laborious. Since many regions of an ion current surface provide limited or no information, the measurement of such regions would be redundant and a less thorough but more economical survey of a surface could be achieved by deliberately restricting the analysis to those regions in which the ion current is concentrated. In some cases, a three-dimensional examination of a limited region of a surface can illustrate particular aspects of ion chemistry (*1, 9, 10*). In other cases, a two-dimensional section through a selected metastable peak may provide sufficient information.

Coarse surveys of surfaces have been made by accumulating small numbers of constant daughter-ion spectra (*11*) or constant parent-ion spectra (*12*) (one spectrum for each normal daughter or parent ion of interest). The number of such spectra required to detect all important metastable peaks may be drastically reduced if the daughter or parent ion masses are chosen well, but this is difficult to achieve. The masses of the neutral fragments, however, are more distinctive of ion reactions than the mass-to-charge ratios of the parent and daughter ions, and the existence in a mass spectrum of pairs of peaks separated by familiar mass differences often facilitates the interpretation of the spectrum. If the ions responsible are indeed related as parent and daughter, the mass of the neutral fragment may be correlated with structural features (*13, 14*). An algorithm for evaluating the quality of reference mass spectra regards the existence of such pairs of peaks as relevant information (*15*).

Analyses of neutral fragments formed in an ionization chamber support the above structural inferences (*16, 17*). Also, it often happens that the same neutral fragment is common to two or more reactions of the one compound, and this phenomenon has been exploited in identifying molecular ions (*18*). It may be inferred that metastable ion transitions likewise will be determined by a limited choice of masses for the neutral fragments. We illustrate the validity of this prediction by reference to a schematic representation of the ion current surface for *n*-decane for an instrument of conventional geometry.

The Constant Neutral Spectrum. We consider the case of a metastable ion transition where the mass m_n of a neutral fragment is equal to the difference in masses of the parent and daughter ions. Thus,

$$m_n/z = \mu/\rho - \mu = (E_0/E)^2(V/V_0)m_B - (E_0/E)m_B$$

Since m_B is proportional to B^2, a constant neutral spectrum at constant V may be achieved, therefore, by a linked B, $(-E^{-1} + aE^{-2})^{-1/2}$ scan, where $a = E_0(V/V_0)$, or at constant B by a linked V, $(E + bE^2)$ scan, where $b = m_n/(zm_BE_0)$.

Model Surface for *n*-Decane. The $\ln(|\rho|)$, $\ln(|\mu|)$, ion current surface (*1*) for *n*-decane has been constructed from two published catalogues of metastable peaks (*2, 19*), and a normal mass spectrum (*20*). In the catalogue (*2*) based on constant daughter-ion spectra (first field-free region) for an instrument of conventional geometry, the major reaction (*19*) m/z 70 u → m/z 55 u was assigned incorrectly as m/z 71 u → m/z 55 u; and in the catalogue (*19*) based on constant parent-ion spectra (second field-free region) for an instrument of reversed geometry, the reaction (2) m/z 98 u → m/z 69 u was assigned incorrectly as m/z 98 u → m/z 70 u. Assignments of these and adjacent peaks have been corrected in the model, while minor peaks obscured by transitions in two field-free regions (*19*) have been ignored. The heights of metastable peaks for the same reactions in the first and second field-free regions are assumed to be equal. This and other arbitrary decisions are intended to give a surface that is useful for illustrating principles. The model surface is not designed to match quantitatively a surface measured in a specific experiment. Elemental compositions have been deduced from the nominal masses, and abundances of some minor isotopic peaks have been inferred from the ^{12}C data.

The height of the base peak in the normal mass spectrum is taken as 500 times the height of the highest metastable peak. It is assumed that the surface has been determined at a constant accelerating voltage of 3900 V and that the sensitivity of the detector is not dependent on the kinetic energy of the ions recorded. The peak heights in the model range from 0.05 unit to 50 000 units. All peaks are assumed to have Gaussian profiles both in the ρ-direction and in the μ-direction. Peak widths in the μ-direction are 0.0033 ($\delta m/m$, full width at 5% maximum height). The width ($\delta\rho/\rho$) of each metastable peak in the ρ-direction is taken to be the larger of the two following alternatives: the full width of the peak at 5% of maximum height is that required for release of 0.1 eV of kinetic energy, or the full width of the peak at half maximum height is 0.0033. The widths in the ρ-direction of peaks due to main beam ions are 0.0033. Ion currents due to fragmentations within fields (*1*) have not been included in our model surface.

RESULTS AND DISCUSSION

The schematic contour map of the ln ($|\rho|$), ln ($|\mu|$), ion current surface generated by the model is shown in Figure 1. Projections of the intersections with various surfaces, to simulate the spectra obtained by various scans, are shown in Figures 2 and 3.

Figure 2a shows the intersection of the surface with the plane $\rho = 1$; that is, the mass spectrum of the main beam ions and of metastable peaks for fragmentations in the second field-free region.

Figure 2b shows the constant parent-ion spectrum for the ^{12}C molecular ion. Principal metastable peaks are found for

0003-2700/79/0351-0691$01.00/0 © 1979 American Chemical Society

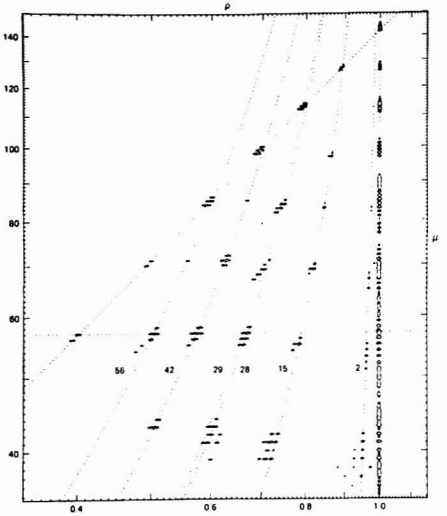

Figure 1. Schematic contour map of ln (|ρ|), ln (|μ|), ion current surface of *n*-decane for an instrument of conventional geometry. The contour level is 0.02 unit of ion current. The broken lines correspond to the surfaces $\rho = 1$, $\mu/\rho = 142.17$ u, $\mu = 57.07$ u, $\mu/\rho - \mu = 2.02$ u, $\mu/\rho - \mu = 15.02$ u, $\mu/\rho - \mu = 28.03$ u, $\mu/\rho - \mu = 29.04$ u, $\mu/\rho - \mu = 42.05$ u, and $\mu/\rho - \mu = 56.06$ u

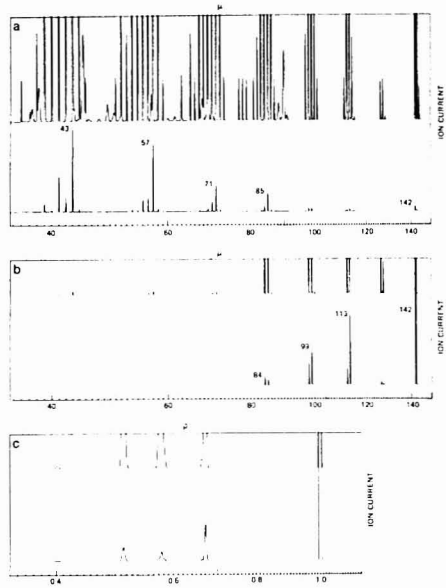

Figure 2. Intersections of surface in Figure 1 with the planes (a) $\rho = 1$, (b) $\mu/\rho = 142.17$ u, and (c) $\mu = 57.07$ u; corresponding to (a) mass spectrum of main beam ions, (b) constant parent-ion spectrum for ^{12}C molecular ion, and (c) constant daughter-ion spectrum for $C_4H_9^+$ ions

fragmentations in the first field-free region to $C_9H_{19}^+$, $C_9H_{18}^{+\cdot}$, $C_8H_{17}^+$, $C_8H_{16}^{+\cdot}$, $C_7H_{15}^+$, $C_7H_{14}^{+\cdot}$, $C_6H_{13}^+$ and $C_6H_{12}^{+\cdot}$ ions. The constant parent-ion spectrum for a molecular ion is usually the most important of the scans of metastable peaks for a compound and often its information content can be increased for molecular characterization by collision-induced dissociations (*21–23*).

Figure 2c shows the constant daughter-ion spectrum for $C_4H_9^+$ ions. Principal peaks are found at $\rho = 0.670$, $\rho = 0.577$, and $\rho = 0.505$, consistent with fragmentations of $C_6H_{13}^+$, $C_7H_{15}^+$, and $C_8H_{17}^+$ ions, respectively, to form $C_4H_9^+$ ions in the first field-free region. Although constant daughter-ion spectra are usually considered to be less easily applied to molecular characterization than constant parent-ion spectra, the peak profiles in the former case do reflect the kinetic energies released in the various fragmentations for an instrument of conventional geometry. For example, the minor metastable peak for formation of the $C_4H_9^+$ ion from the molecular ion is observed as a diffuse peak centered at $\rho = 0.402$ in the constant daughter-ion spectrum (Figure 2c) but as a narrow peak in the constant parent-ion spectrum (Figure 2b).

Figure 3a shows the constant neutral spectrum for H_2 loss. Principal peaks are observed for $C_6H_7^+$, $C_5H_5^+$, $C_4H_7^+$ to $C_4H_3^+$, $C_3H_6^{+\cdot}$ to $C_3H_3^+$, and C_3H^+ ions, formed in the first field-free region from parent ions containing an additional two hydrogen atoms in each case.

Figure 3b shows the constant neutral spectrum for $CH_3\cdot$ loss. The narrow profile of the peak for $C_9H_{19}^+$ ions formed from $C_{10}H_{22}^{+\cdot}$ ions (Figure 3b) is comparable with that for the same reaction in the constant parent-ion spectrum for the molecular ion (Figure 2b). Additional scanning modes for a double focusing mass spectrometer that involve energy discrimination have been distinguished previously (*1*, *24*).

Figure 3c shows the constant neutral spectrum for C_2H_4 loss. A peak appears to be present for the formation of $C_8H_{17}^+$ ions from $C_{10}H_{21}^+$ ions. The spectrum illustrates the caution that must be applied to the interpretation of peaks in those spectra that do not reflect the full profiles of kinetic energy released. As can be seen from the contour map (Figure 1), overlap of peaks in the ρ-direction for a given energy resolution and kinetic-energy release becomes more pronounced as the ρ- and μ-changes for a reaction increase. Thus with the present model, small peaks may appear in the constant neutral spectrum for C_2H_4 loss (Figure 3c) because of daughter ions formed by $C_2H_5\cdot$ loss and accelerated in the direction of the ion beam by the release of kinetic energy. Likewise, in the constant neutral spectrum for $C_2H_5\cdot$ loss (Figure 3d), small peaks may appear due to daughter ions formed by C_2H_4 loss and decelerated along the direction of the ion beam by the release of kinetic energy. A comparison of the peak heights in the constant neutral spectra (Figures 3c and 3d) may be used to minimize this problem, without the need for higher energy resolution or for three-dimensional analysis. For instance, the small peak at $\mu = 113$ u in Figure 3c may be due principally to daughter ions of the same reaction that gives rise to the large peak at $\mu = 113$ u in Figure 3d. Conversely, the small peaks at $\mu = 84$ u, $\mu = 57$ u, and $\mu = 43$ u in Figure 3d appear to be due principally to overlap of the large peaks at the same μ-values in Figure 3c. The peaks at $\mu = 113$ u and $\mu = 114$ u in Figure 3d are due to the loss of $C_2H_5\cdot$ from the ^{12}C molecular ion and ^{13}C molecular ion, respectively, and the peak heights are in the expected ratio.

Figure 3e shows the constant neutral spectrum for C_3H_6 loss. The peak at $\mu = 99$ u appears to be due to the formation of $C_7H_{15}^+$ ions from $C_{10}H_{21}^+$ ions, but it is mainly due to the same daughter ions formed from $C_{10}H_{22}^{+\cdot}$ ions and accelerated in the direction of the ion beam by the release of kinetic energy. This is evident from the contour map of the surface (Figure

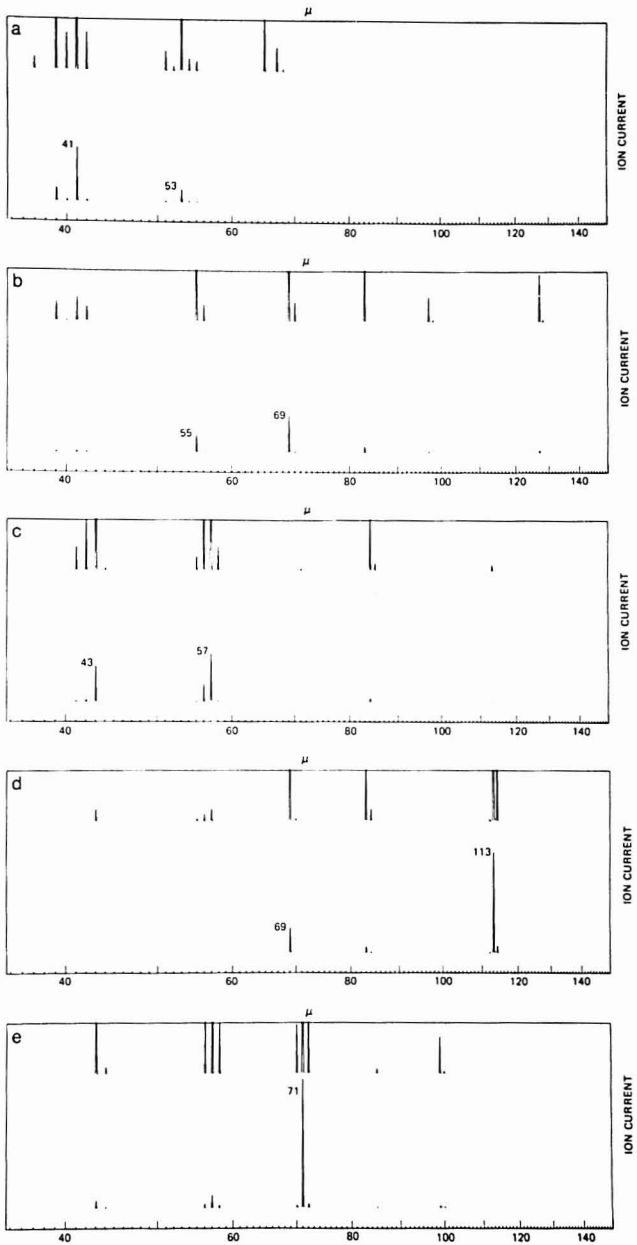

Figure 3. Intersections of surface in Figure 1 with the surfaces $\mu/\rho - \mu$ = (a) 2.02 u, (b) 15.02 u, (c) 28.03 u, (d) 29.04 u, and (e) 42.05 u; corresponding to constant neutral spectra for (a) H_2 loss, (b) $CH_3\cdot$ loss, (c) C_2H_4 loss, (d) $C_2H_5\cdot$ loss and (e) C_3H_6 loss

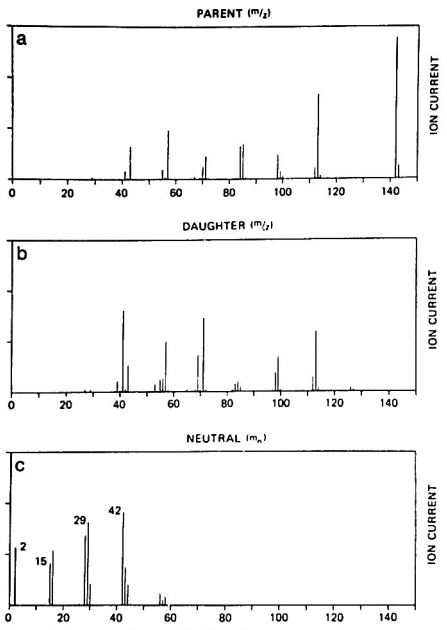

Figure 4. Normalized sums of heights of metastable peaks (first field-free region) for (a) constant parent-ion spectra, (b) constant daughter-ion spectra, and (c) constant neutral spectra

1) and from the constant neutral spectrum for C_3H_7· loss (derived but not shown).

The information content of the various spectra may be abbreviated as two-dimensional diagrams by expressing the integrated ion current for each spectrum as a fraction of the total ion current for the metastable peaks (first field-free region). Figures 4a–4c are approximations to such diagrams obtained by plotting the sums of the heights of metastable peaks for *n*-decane against masses of parent ion, daughter ion and neutral fragment. It is evident that the ion current is associated with fewer neutral fragments (Figure 4c) than parent ions (Figure 4a) or daughter ions (Figure 4b). This indicates that the genetic information contained in a surface may be surveyed more economically by the use of constant neutral spectra than by the use of constant parent-ion spectra or constant daughter-ion spectra.

Data for three-dimensional representation of the ion currents for various molecules may be obtained at low energy resolution with a focal plane mass spectrometer by synchronizing a *V*-scan (or preferably an E,B^2 scan) with a movement of the photoplate in its own plane and at right angles to the direction of the mass scale (*2*, *5–7*). The representations for a number of aromatic compounds (*5–7*) support our contention that metastable peaks are clustered along a limited number of lines determined by the masses of the neutral fragments. Spectra for integrated ion currents, analogous to those in Figures 4a–4c, have been deduced from the photoplate records in each case (*5–7*) and, as indicated above for *n*-decane, the total ion current for metastable peaks is associated with fewer neutral fragments than parent or daughter ions. The spectra of integrated ion current against mass of neutral fragment show sensitive correlations with structural features (*5–7*, *25*), as do the analogous spectra obtained by direct analysis of source reactions (*16*).

The concept of the constant neutral spectrum was used several years ago by Beynon, Baitinger, and Amy (*26*) to analyze the various reactions for loss of the elements of H·, H_2, and H_3· from ions of toluene. The spectra were gained by scanning *B* with iterative adjustments of *E*. The constant neutral spectrum for H· loss was used subsequently as a novel means of analyzing the deuterium content of labeled toluenes (*27*). It was necessary, however, to calibrate these spectra because of the possible isotope effects on the metastable peaks (*27*). A more direct measurement may be feasible by the use of a constant neutral spectrum where the loss of the neutral fragment is not subject to an isotope effect. Conversely, any isotope effects involved in the loss of a neutral fragment may be monitored directly by a comparison of the isotope distribution in the constant neutral spectrum with the known label distribution in the parent molecule.

Although ion currents due to reactions within fields have been omitted from our model for simplicity, they should not be ignored. For instance, in the above work (*26*) the approximation to the constant neutral spectrum for H· loss from toluene ions yielded an unusually broad metastable peak. This might be attributed to the reaction m/z 89 u → m/z 88 u in the first field-free region but, because of its broad character, we consider it more likely that the peak is due mainly to the formation of ions of m/z 89 u from ions of m/z 91 u within the electric sector. We have discussed more fully in a recent paper (*28*) the ambiguities that may arise because of ion reactions within fields.

It is probable that the great majority of unimolecular dissociations in the flight tube involve losses of single fragments. The constant neutral spectra obtained at low pressures, therefore, may reflect in general the masses of the neutral fragments lost in a single step. The feasibility of the *direct* analyses of the neutral products of metastable ions has been noted previously (*29*). A greater information content of several constant neutral spectra, particularly those for radical losses such as H·, may be obtained by the use of a collision cell to enhance the ion currents for fragmentations of singly or multiply charged ions. Such spectra can provide further fingerprints for molecular characterization. The spectra obtained at higher pressures do not necessarily reflect the masses of the neutral fragments since multistep dissociations may occur after collision.

A source of ambiguity may arise with an instrument of reversed geometry, since constant neutral spectra are possible both for fragmentations in the first field-free region and in the second field-free region with such an instrument. The scanning modes, however, do not necessarily transmit daughter ions uniquely from the selected field-free region. This is evident from the observations that daughter ions of transitions in the first field-free region of an instrument of reversed geometry can be transmitted during *E*-scans (*19*, *30*), while daughter ions from transitions in the second field-free region have been detected during *V*-scans (*31*, *32*) and *B,E* scans (*33*). Interference may be particularly noticeable in the constant neutral spectrum for H· loss using instruments of reversed geometry.

While linked scans for generating constant neutral spectra may be difficult to achieve by analogue techniques, computer control of the double focusing mass spectrometer should make the method feasible. We conclude that constant neutral spectra provide an efficient means of determining the affiliation of ions formed in a double focusing mass spectrometer. Correlations of constant neutral spectra with structure and applications to the analysis of labeled molecules should be possible.

SYMBOLS AND NOMENCLATURE

V = accelerating voltage.
E = electric sector voltage.
B = magnetic field.
V_0, E_0 = reference values of V and E for transmission of main beam ions by electric sector.
m_B = mass of singly charged ions transmitted by magnetic sector when $V = V_0$ and $E = E_0$.
$\rho = (V_0/V)(E/E_0)$.
$\mu = (E_0/E)m_B$.
Conventional geometry = geometry of double focusing mass spectrometer for which the electric sector precedes the magnetic sector.
Reversed geometry = geometry of double focusing mass spectrometer for which the magnetic sector precedes the electric sector.
First field-free region = field-free region preceding the first sector in the flight tube.
Second field-free region = field-free region preceding the second sector in the flight tube.
Constant parent-ion spectrum = spectrum of peaks due to the generation of different daughter ions from the same parent ion.
Constant daughter-ion spectrum = spectrum of peaks due to the generation of the same daughter ion from different parent ions.
Constant neutral spectrum = spectrum of peaks for reactions related by a constant mass of the neutral fragment.
P-scan = scanning mode in which all of the parameters V, E and B, except one (P), are kept constant.
Linked scan = scanning mode in which at least two of the parameters V, E, and B, are varied simultaneously while a specified relationship is maintained between them.
P,Q scan = linked scan in which P and Q, both functions of the parameters V, E, and B, are varied so that the ratio of P to Q remains constant. An example is an E,B^2 scan, in which E and B are varied at constant V so that E is proportional to B^2. Unlike the method of designating a linked scan by specifying a ratio that is kept constant (for example, an E/B^2 scan), the P,Q nomenclature for linked scans is consistent with the P nomenclature for simple scans.

LITERATURE CITED

(1) M. J. Lacey and C. G. Macdonald, *Org. Mass Spectrom.*, **12**, 587 (1977).
(2) T. W. Shannon, T. E. Mead, C. G. Warner, and F. W. McLafferty, *Anal. Chem.*, **39**, 1748 (1967).
(3) R. W. Kiser, R. E. Sullivan, and M. S. Lupin, *Anal. Chem.*, **41**, 1958 (1969).
(4) J. Coutant and F. W. McLafferty, *Int. J. Mass Spectrom. Ion Phys.*, **8**, 323 (1972).
(5) W. Schönfeld, *Int. J. Mass Spectrom. Ion Phys.*, **16**, 281 (1975).
(6) W. Schönfeld, *Org. Mass Spectrom.*, **10**, 321, (1975).
(7) W. Schönfeld, *Org. Mass Spectrom.*, **10**, 401 (1975).
(8) C. Hwang and R. W. Kiser, *Int. J. Mass Spectrom. Ion Phys.*, **27**, 209 (1978).
(9) M. J. Lacey and C. G. Macdonald, *Org. Mass Spectrom.*, **13**, 284 (1978).
(10) M. J. Lacey and C. G. Macdonald, *Org. Mass Spectrom.*, **13**, 243 (1978).
(11) M. A. Barber, W. A. Wolstenholme, and K. R. Jennings, *Nature (London)*, **214**, 664 (1967).
(12) U. P. Schlunegger, *Angew. Chem., Int. Ed. Engl.*, **14**, 679 (1975).
(13) D. H. Williams and I. Howe, "Principles of Organic Mass Spectrometry", McGraw-Hill, London, 1972, p 103.
(14) F. W. McLafferty, "Interpretation of Mass Spectra", 2nd ed., W. A. Benjamin, Reading, Mass., 1973, Table A-5.
(15) D. D. Speck, R. Venkataraghavan, and F. W. McLafferty, *Org. Mass Spectrom.*, **13**, 209 (1978).
(16) J. R. Reeher, G. D. Flesch, and H. J. Svec, *Org. Mass Spectrom.*, **11**, 154 (1976).
(17) F. B. Burns and T. H. Morton, *J. Am. Chem. Soc.*, **98**, 7308 (1976).
(18) R. G. Dromey, B. G. Buchanan, D. H. Smith, J. Lederberg, and C. Djerassi, *J. Org. Chem.*, **40**, 770 (1975).
(19) T. Wachs, P. F. Bente III, and F. W. McLafferty, *Int. J. Mass Spectrom. Ion Phys.*, **9**, 333 (1972).
(20) E. Stenhagen, S. Abrahamsson, and F. W. McLafferty, "Atlas of Mass Spectral Data", Wiley, New York, 1969, Spectrum API-0109.
(21) K. Levsen and H. Schwartz, *Angew. Chem., Int. Ed. Engl.*, **15**, 509 (1976).
(22) R. Robbiani, J. Kuster, and H. Seibl, *Angew. Chem., Int. Ed. Engl.*, **16**, 120 (1977).
(23) R. W. Kondrats and R. G. Cooks, *Anal. Chem.*, **50**, 81A (1978).
(24) R. K. Boyd and J. H. Beynon, *Org. Mass Spectrom.*, **12**, 163 (1977).
(25) P. Krenmayr, F. Kšica, and K. Varmuza, *Monatsh. Chem.*, **109**, 823 (1978).
(26) J. H. Beynon, W. E. Baitinger, and J. W. Amy, *Int. J. Mass Spectrom. Ion Phys.*, **3**, 55 (1969).
(27) J. H. Beynon, J. E. Corn, W. E. Baitinger, J. W. Amy, and R. A. Benkeser, *Org. Mass Spectrom.*, **3**, 191 (1970).
(28) M. J. Lacey and C. G. Macdonald, *Aust. J. Chem.*, **31**, 2161 (1978).
(29) J. H. Beynon and R. G. Cooks, *Int. J. Mass Spectrom. Ion Phys.*, **19**, 107 (1976).
(30) F. W. McLafferty and F. M. Bockhoff, *Anal. Chem.*, **50**, 69 (1978).
(31) W. V. Ligon and J. L. Webb, *Int. J. Mass Spectrom. Ion Phys.*, **22**, 359 (1976).
(32) A. Maquestiau, Y. Van Haverbeke, R. Flammang, and C. De Meyer, *Bull. Soc. Chim. Belg.*, **86**, 281 (1977).
(33) R. P. Morgan, C. J. Porter, and J. H. Beynon, *Org. Mass Spectrom.*, **12**, 735 (1977).

RECEIVED for review November 27, 1978. Accepted January 23, 1979.

Determination of Carbon in Steel by Secondary Negative Ion Mass Spectrometry

Naoharu Yamaguchi, Ken-ichi Suzuki, and Kimitaka Sato*

Fundamental Research Laboratories, Nippon Steel Corporation, 1618, Ida, Nakahara-ku, Kawasaki 211, Japan

Hifumi Tamura

Central Research Laboratory, Hitachi Ltd., 1-280, Higashi-Koigakubo, Kokubunji 185, Japan

The determination of carbon in steel by secondary negative ion mass spectrometry is described. Ions originating from adsorbates and gas phase were removed from solid-phase ions by the difference of their energies. The ions were collected by a new method for monitoring total ion intensity. The technique of removing only negative ions from secondary electrons in a magnetic field before mass analyzing was used. As a result, excellent linearity was obtained between carbon contents (0.001 to 0.61%) and ion intensities.

Ion mass analysis (IMA) employing negative ions offers advantages over Auger electron spectroscopy (AES) as already reported by Benninghoven (*1*). In particular, the use of negative ion improves detection sensitivity by 10 to 100 times over that using positive ions, especially for the determination of light elements such as carbon, oxygen, and sulfur. However, determination of light elements by secondary negative ions requires special consideration of the following factors: (1) influence of secondary ions originating from the specimen surface adsorbates and gas phase; (2) secondary negative ion yields of many matrix elements, for example, $^{56}Fe^-$, are very low, so that a standard element is necessary, to establish a relative ion intensity ratio; (3) influence of secondary electrons

0003-2700/79/0351-0695$01.00/0 © 1979 American Chemical Society

Table I. Chemical Composition of Specimens Used in the Present Investigation (%)

specimen	C	Si	Mn	P	S	Ti	V	Cr	Zr	Nb	Mo
pure iron	0.001										
steel A	0.09	0.23	1.05	0.001	0.004						
B	0.17	0.20	0.02	0.013	0.003			0.01			
C	0.35	0.23	0.69	0.025	0.026			0.07			
D	0.42	0.28	1.40								
E	0.51	0.27	0.80	0.017	0.027			0.01			
F	0.61	0.31	0.40	0.015	0.006			0.05			
NBS 461	0.15	0.047	0.36	0.053	0.025	0.01	0.024	0.13	0.005	0.011	0.30
462	0.40	0.28	0.94	0.045	0.034	0.037	0.058	0.74	0.063	0.096	0.080
463	0.19	0.41	1.15	0.031	0.024	0.010	0.10	0.26	0.20	0.19	0.12
464	0.54	0.48	1.32	0.017		0.004	0.29	0.078	0.010	0.037	0.029
465	0.037	0.029	0.03	0.008	0.008	0.20	0.002	0.004	0.002	0.001	0.005
466	0.065	0.025	0.11	0.012	0.007	0.057	0.007	0.011	0.005	0.005	0.011
467	0.11	0.26	0.27	0.033	0.010	0.26	0.041	0.036	0.094	0.29	0.021
468	0.26	0.075	0.47	0.023	0.028	0.011	0.17	0.54	0.005	0.006	0.20

having the same charge as negative ions and emitted from the specimens.

Here, the energy difference between the gas-phase and solid-phase ions is utilized to effect separation (2). In addition, a new method for monitoring total ion intensity (3) is used to make corrections. Furthermore, a novel approach was developed to ensure that only secondary ions are introduced into the mass analyzing system.

EXPERIMENTAL

The specimens used in this study were prepared so that the individual components would be present as a homogeneous solid solution. The chemical compositions of the specimens are shown in Table I.

IMA analysis was performed using a modified Hitachi IMA-2 Ion Microprobe Analyzer (4-7). Argon positive ions were used as primary ions and accelerated to 15 keV. The ion beam was 0.5 mm in diameter, and the specimen current was 1 μA. The acceleration voltage for secondary ions was ±3 keV.

RESULTS AND DISCUSSION

Solid- and Gas-Phase Ion Separation. The influence of gas-phase ions, originating from the specimen surface adsorption layer or the atmosphere, must be reduced to a minimum, in order to quantitatively analyze solid-phase ions accurately with IMA. For this purpose, two methods have been proposed.

First, the specimen surface is irradiated by an electron beam. The gas phase and adsorbates are examined by analyzing the electron impact desorbed ions generated on the specimen surface. Then, the secondary ions emitted during irradiation with an ion beam are analyzed and the spectra compared to distinguish between the gas-phase and solid-phase ions (8). In the second method, the energy difference between the gas-phase and solid-phase ions is utilized (2). In the present study, the second method was employed since the quantitative analysis is difficult and involves specialized instrumentation for the former one.

The concept of initial kinetic energy distribution for secondary ions has been discussed by Stanton (9) and Bradley (10). They suggested that there is an energy difference between solid-phase and gas-phase secondary ions and that energy analysis could be used to discriminate between these two types of ions.

The principle of the energy selection method is depicted in Figure 1. On the left, secondary ions with E_0 (eV) energy at a secondary ion acceleration voltage of V_0(V) pass through the β slit. However, on the right, secondary ions with $E_0 - \Delta E_0$ (eV) energy at a secondary ion acceleration voltage of $V_0 + \Delta V_0$ (V) pass through the β slit.

The results of energy distribution measurement for secondary ions from the steel specimens are shown in Figure 2.

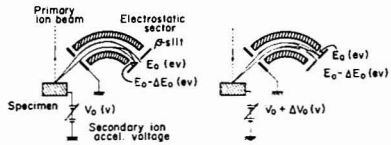

Figure 1. Principle of selection of secondary ion energy

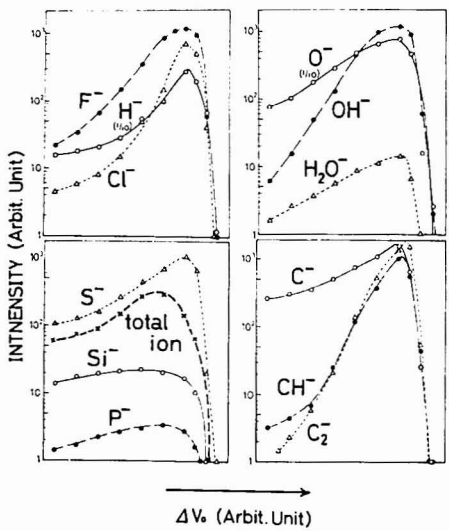

Figure 2. Energy distribution of secondary negative ions. Specimen, carbon steel. Primary ion, $^{40}Ar^+$ (15 keV, 1 μA). Beam diameter of primary ion; 0.5-mmi.d. Vacuum; 1×10^{-7} Torr

In all cases, gas-phase ions are distributed to a greater extent on the low energy side. Furthermore, the influence of gas-phase ions is held to a minimum and solid-phase ions are measured accurately. This is possible only if the specimen potential is set to permit detection of secondary ions with high initial kinetic energies.

As in the Figure, there is a difference in the energies of solid-phase and gas-phase ions, and the former are said to be 100 eV greater. This probably results from the fact that the energy of an ion depends on its potential at the point of

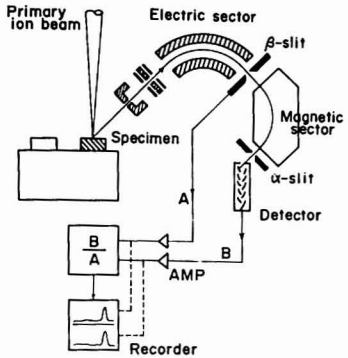

Figure 3. Principle of total ion monitoring method

ionization. The gas-phase species are ionized in a region where the field value is lower than for ions sputtered from the specimen surface.

Standard Relative Ion Intensity Ratio. In IMA analyses, the ionization efficiency or yield of secondary ions varies with specimen surface conditions. It is therefore necessary, especially in the case of quantitative analysis, to correct individual secondary ion intensities. At present, the following two methods are employed for this purpose:

(1) The secondary ion intensity of a matrix element is taken as the basis for determining the relative ion intensity ratio. In the case of steel, ^{56}Fe or ^{54}Fe is frequently used for this purpose.

(2) The current of total secondary ions introduced into the mass analyzing system is measured and used as the basis for determining the relative ion intensity ratio. This method is commonly known as the "total ion monitoring method" (*3*). Since secondary electrons have the same charge as negative ions, they must be eliminated to obtain accurate total negative secondary ion measurements. The solution to this problem is explained in the next section.

When performing negative ion spectroscopy, the ability to detect heavy elements sensitively deteriorates markedly. Therefore, when steel is analyzed, it is necessary to depend completely on the total ion intensity monitoring method. It is impractical to use iron (Fe) as a standard element.

The total secondary ion intensity monitoring method, as its name implies, has an important role of correcting individual secondary ion intensities for variations in extraction efficiency. Using this method, it is also possible to correct, to some extent, the influence of specimen surface variations or apparent surface work functions on secondary ion emission capacity. Namely, its purpose is to detect a part of the total ion current emitted from the specimen, which is, of course, proportional to the total ion current. In addition, this monitoring method determines the ratio of the total to the mass resolved ion current, reduces the effect of the above influences as much as possible, and then provides as correct a value as possible.

The principle of the total ion monitoring method is shown in Figure 3. Here, the ion current striking the β slit (resolving slit), located between the electric and magnetic sector fields, is used to represent the current. The reason for placing the β slit in this position is to avoid the influence of reflection ions.

Concrete application of this method for negative ions calls for the separation of secondary negative ions and secondary electrons. This is explained in the next section.

Separation of Secondary Electrons from Negative Ions. Secondary electrons having the same charge as total

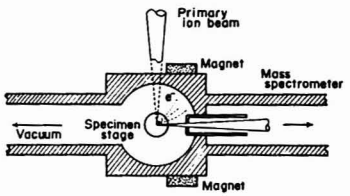

Figure 4. Method newly proposed for separating secondary electron from secondary ions

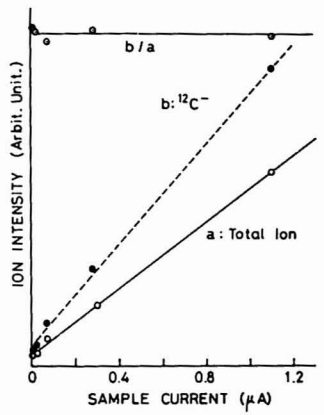

Figure 5. Effect of correction of ion intensity by total ion monitoring method

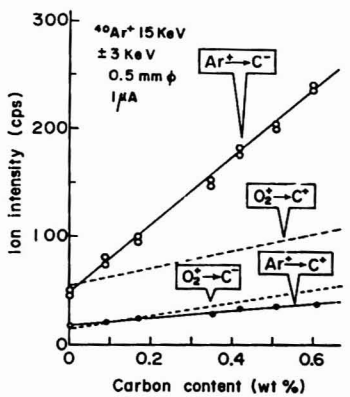

Figure 6. An example of calibration curve for carbon in steel and effect of primary ion species on sensitivity of carbon ion

secondary negative ions are also detected by the β slit. Therefore, accurate measurement of secondary negative ions becomes difficult. In the present study, secondary electrons were prevented from entering the mass analyzing system by the adoption of a magnetic field. The magnetic field is formed at right angles to the secondary ion path near the extraction electrode. The implementation of this separation method is shown in Figure 4. An example of total secondary negative

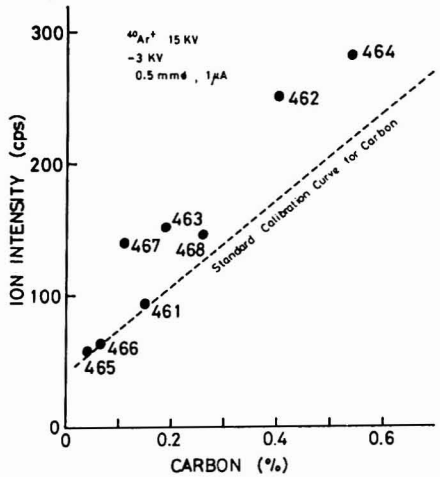

Figure 7. Relationship between carbon content in NBS standard steel and ion intensity of $^{12}C^-$

ion monitoring carried out after removal of secondary electrons is shown in Figure 5.

Quantitative Analysis of Carbon in Steel. After solving the problems discussed in the above sections, the feasibility of determining the carbon content in steel was studied. Here, the effect of primary ion species on the sensitivity to carbon ions was examined using steel specimens. It was found that $^{40}Ar^+$ was the most effective ion species as shown in Figure 6. Negative ions ($^{12}C^-$) show very good linearity in the carbon content range of 0 to 0.6%. Moreover, the two sets of measurement, taken on different days, reveal no differences as shown in Figure 6. A similar study using positive ions, showed that sensitivity was lower than with negative ions. This consistency in day-to-day measurements tends to substantiate the use of total ion monitoring.

Next, a similar experiment was carried out on commercially available standard steel specimens, NBS 461 to 468. The analysis conditions were the same as above and the results are shown in Figure 7. The NBS 461, 465, and 466 specimens are on the standard calibration line shown in Figure 6, but all other specimens show higher values.

It can be seen from Table I that all high value specimens contain significant amounts of so-called carbide formers such as vanadium and niobium. A similar phenomenon was also observed for positive ions by Tsunoyama et al. (*11*). They attributed the phenomenon to the presence of precipitation phases in the specimens and resultant variations in the ionization efficiency of alloy elements. Furthermore, they measured the ion intensity ratio of target elements to iron (Fe) where the concentration of target elements remained constant and the carbon content varied in order to study the influence of precipitation phases on ion intensity ratio in detail. In addition, they investigated these relationships with regard to the precipitation of carbides. As a result, Fe-V alloys, when annealed at 710 °C, released V_4C_3 and $(Fe\text{-}V)_3C$ precipitates. On the other hand, more complex precipitation phases were observed with Fe-Nb alloys. This fact suggests that such changes in the ion intensity ratio are due to the concentration of alloy elements present in the ferrite matrix and precipitation phases, to the actual state of combination with iron and carbon, and to the crystal structure. As a result, the present approach using negative ions appears to parallel the phenomena observed with positive ion analysis.

Light Elements Other than Carbon. Sulfur is another element that plays an important role and is contained in appreciable amounts in steel. The role of sulfur was investigated employing the linearity of the calibration curve. Approximate linearity was obtained, but more detailed studies will be necessary along with study of nitrogen, oxygen, and other light elements before meaningful conclusions can be proposed.

ACKNOWLEDGMENT

The authors express appreciation to S. Nagashima, Yokohama National University, for his encouragement and valuable suggestions. They are also indebted to H. Okada, the Director of the Nippon Steel Fundamental Research Laboratories, and H. Watanabe, the Director of the Hitachi Central Research Laboratory for their continued interest.

LITERATURE CITED

(1) A. Benninghoven, *Appl. Phys.*, 1, 3 (1973).
(2) K. Nakamura, H. Tamura, annd T. Kondo, *Jpn. J. Appl. Phys.*, **13**, 917 (1974).
(3) H. Tamura, T. Kondo, I. Kanomata, K. Nakamura, and Y. Nakajima, *Jpn. J. Appl. Phys., Suppl. 2*, Pt. 1, 379 (1974).
(4) K. Sato and H. Tamura, *J. Vacuum Soc. Jpn.*, **17**, 385 (1974).
(5) R. Matsumoto, K. Sato, and K. Suzuki, *Tetsu To Hagane*, **60**, 1980 (1974).
(6) R. Matsumoto, K. Sato, and K. Suzuki, *Jpn. J. Appl. Phys., Suppl. 2*, Pt. 1, 387 (1974).
(7) K. Sato, K. Suzuki, R. Matsumoto, and S. Nagashima, *Trans. Jpn. Inst. Met.*, **18**, 61 (1977).
(8) M. Stark, *Optik*, **36**, 139 (1972), and papers cited therein.
(9) H. E. Stanton, *J. Appl. Phys.*, **31**, 678 (1960).
(10) R. C. Bradley, *J. Appl. Phys.*, **30**, 1 (1959).
(11) K. Tsunoyama, Y. Ohashi, and T. Suzuki, *Anal. Chem.*, **48**, 832 (1976).

RECEIVED for review March 13, 1978. Accepted January 22, 1979.

Mechanism of Low-Pressure Chemical Ionization Mass Spectrometry

Richard L. Hunter and Robert T. McIver, Jr.*

Department of Chemistry, University of California, Irvine, California 92717

Chemical ionization mass spectrometry at sample pressures as low as 10^{-9} Torr can be accomplished with a Fourier transform mass spectrometer based upon the ion cyclotron resonance (ICR) principle. Generally ICR has been considered to be a low-performance mass spectrometer, but enormous progress has been made recently in improving the mass resolution, mass range, and scan rate. By combining a one-region ICR cell with a Fourier transform ion detection method, a truly high-resolution, rapid-scanning mass spectrometer has been developed. A mechanism for generation and storage of ions in the ICR cell is proposed and validated by a number of experimental tests. The chemical and physical processes in the ICR cell are well behaved, and projections are made of how even greater detection sensitivity can be achieved. By relying on computer technology rather than precision machining, ICR may become *the* high-performance mass spectrometric technique of the future.

In chemical ionization mass spectrometry, ionization of a sample is accomplished by interaction with gaseous reagent ions. Typically, a reagent gas such as methane, isobutane, or ammonia at a pressure of 1 Torr is ionized by high-energy electron impact, and the reagent ions thus formed undergo gas-phase reactions with the sample molecules to produce new ions characteristic of the sample (*1*). For example, the reagent ion CH_5^+ produced in methane reacts with sample molecules S in a bimolecular reaction to produce SH^+, an M + 1 ion of the sample:

$$CH_5^+ + S \xrightarrow{k} SH^+ + CH_4 \qquad (1)$$

The yield for conversion of CH_5^+ to SH^+ depends on three factors: (1) the magnitude of the ion–molecule reaction rate constant k, (2) the residence time of the reagent ions in the source region of the mass spectrometer, and (3) the pressure of sample molecules S. For reactions of this type, the rate constant k is usually about the same as the diffusion-controlled limiting rate and is determined by the long-range ion-induced dipole interaction potential (*2*, *3*). The magnitude of k generally depends on the nature of the particular reagent ion and sample, but typical values are in the range 10^{-9} to 10^{-11} cm^3/molecule-s. The second factor, residence time for reagent ions in the source region of the mass spectrometer, is limited to about 10 μs by diffusion of the ions to the walls of the source and by ion extraction fields of about 10 V/cm. This experimental limitation on the residence time of the reagent ions requires that the pressure of sample should be at least 10^{-3} to 10^{-4} Torr in order to produce significant ionization of the sample. Thus it is apparent that the residence time of the reagent ions in the apparatus sets a limit on the sensitivity of the method for detection of low-volatility compounds. Chemical ionization of the sample will not be detectable if the partial pressure of the sample is lower than about 10^{-5} Torr.

During the past 3 years we have developed a *low-pressure* chemical ionization mass spectrometer with the goal of extending the range of the chemical ionization technique to pressures as low as 10^{-10} Torr. In order to accomplish this, a static magnetic ion trap is utilized to store reagent ions for times typically of 10 to 20 s, about a million times longer than in a conventional source. Our interest in this area has been stimulated by a number of factors. First, lower sample pressures in the mass spectrometer imply greater ultimate detection sensitivity and the possibility of performing mass spectrometric analysis for ultralow-vapor-pressure compounds which cannot be detected in a conventional source. Another benefit is that far lower source temperatures could be used to minimize thermally induced rearrangement and decomposition of the sample.

In this paper, experimental techniques for Fourier transform mass spectrometry and low-pressure chemical ionization are described in detail. Also, a kinetic scheme is derived which accurately describes the storage of reagent ions and the yield of product ions.

EXPERIMENTAL

In order to accomplish chemical ionization of samples having very low partial pressures, it is essential that the reagent ions be trapped efficiently. For example, at a sample pressure of 1×10^{-6} Torr, the mean free time for collision between a gaseous ion and a sample molecule is about 3 s, and the mean free path of the ion is about 800 m (*4*). In our laboratory, we have met this requirement by using a one-region ion cyclotron resonance cell for generation, storage, and mass analysis of gaseous ions. The basic principles of this device have been explained previously (*5*). Essentially, static electric and magnetic fields are used to form a three-dimensional ion trap, and the cyclotron resonance principle is utilized to mass analyze the ions stored in the trap. In this section, the evolution of the trapped ion cyclotron resonance technique is described, and the performance of our latest instrument is demonstrated.

The first experiments involving analytical applications of the ion cyclotron resonance (ICR) technique showed that the technique suffered from many severe limitations (*6–8*). Mass resolution was rather low, limited to about 1 amu at m/e 200. Mass range was restricted to less than about m/e 280. The scan rate was very slow, taking typically 5 min for a single scan from m/e 10 to m/e 110. Furthermore, rather large samples, greater than 1 mg, were required. Truly then, during the late 1960s the ICR spectrometer was a low-performance mass spectrometer having very little potential as an analytical technique. The only saving grace was that it was an exceptionally powerful technique for studying gas-phase ion–molecule reactions. Two features, the ion cyclotron double resonance technique and the long pathlength of ions in the ICR analyzer cell, soon established it as the method of choice for elucidating the sequence of reactions in complex mixtures of ions and neutral molecules (*9*, *10*).

Enormous progress has been made during the past 5 years in improving the performance of the ICR technique. In fact, it appears now that ICR may be *the* mass spectrometer of the future for high-resolution, rapid scanning. Our evidence for this is presented in the Discussion section, but first we would like to analyze systematically how the performance of the ICR technique has been so greatly improved.

(1) Mass Resolution. During the 1960s the most widely used ICR analyzer cell was a three-section drift cell (*11–13*). A strong homogeneous magnetic field B restricts the motion of the ions in the plane perpendicular to the magnetic field, and the ions undergo cyclotron motion at a frequency ω, where

$$\omega = qB/m \qquad (2)$$

0003-2700/79/0351-0699$01.00/0 © 1979 American Chemical Society

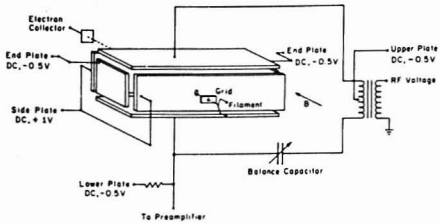

Figure 1. Schematic drawing of a one-region ICR cell for storage of gaseous positive ions. The combined effect of the strong homogeneous magnetic field B and an electrostatic field created by small dc voltages on the six metal plates traps ions inside the cell

In addition, voltages applied to the upper and lower plates of the cell cause the ions to drift slowly from the source region into the analyzer region where an alternating electric field at frequency ω_1 is provided by a marginal oscillator (*14*, *15*).

The mass resolution of this analyzer cell has been shown to be limited primarily by two factors: (1) pressure broadening of the peaks due to the ion–molecule collisions and (2) the limited time for drift of the ions through the analyzer region and into the total ion current region (*16*). In the low-pressure limit, mass resolution $M/\Delta M_{1/2}$ is given by

$$\frac{M}{\Delta M_{1/2}} = \frac{\omega\tau}{5.566} \tag{3}$$

where τ is the time for drift through the analyzer region (*17*, *18*). At pressures greater than 1×10^{-5} Torr, the peaks become even wider owing to ion–molecule collisions which interrupt the absorption of power from the rf electric field and damp the coherent motion of the resonant ions.

Equation 3 shows the close relationship between mass resolution and residence time τ in the analyzer region of the cell. All drift-type ICR cells suffer from low resolution because the residence time is limited to a few milliseconds by ion space charge, surface charges on the cell plates, and electric fields inside the analyzer cell. A very effective solution to this problem was found in 1970 when the one-region trapped ion analyzer cell, shown in Figure 1, was introduced (*19*). A pair of end plates causes the ions to drift slowly from one end of the cell to the other. All of the normal functions of ion formation by electron impact, reaction with added neutral molecules, and detection of product ions are performed in the one-region cell by utilizing a pulsed mode of operation and dispersing events in "time" rather than in "space". Ions formed by a pulse of the electron beam are stored with 50% efficiency for about 1.1 s at 9.7×10^{-6} Torr, and at lower pressures the trapping time increases proportionately. With a marginal oscillator detector, the mass resolution of the one-region cell is at least ten times better than the three-section cell because of the far longer residence time for the ions in the cell (*16*). Later it will be shown that even higher mass resolution is obtained if the marginal oscillator detector is replaced with the more advanced capacitance bridge detectors used in Fourier transform and rapid scan ICR experiments.

In summary, the key to high mass resolution in ICR experiments is a one-region cell which stores the ions and allows them to interact with the cyclotron resonance detector circuitry for times on the order of 0.1 s. In addition, pressures in the analyzer cell must be maintained lower than 1×10^{-6} Torr to avoid loss of resolution caused by pressure broadening of the peaks.

(2) Mass Range. The early ICR spectrometers were limited in mass range to about m/e 280 because of low mass resolution and practical difficulties in making a marginal oscillator detector operate at frequencies less than about 75 kHz. The detector design used now in our laboratory is a balanced capacitance bridge circuit which is driven by a frequency synthesizer (*20*, *21*). The capacitance bridge has many desirable features. First, ICR mass spectra can be recorded at constant magnetic field strength while the excitation signal from the frequency synthesizer is scanned over a wide range. Unlike a marginal detector, it is an untuned, broad-band detector which has no difficulty working at the low frequencies (around 20 kHz) required to observe ions up to m/e 1000. A second feature is that it responds much faster then the electrometer detector (*22*, *23*). More will be said about this in the next section on the factors which limit scan rate. A third feature is that higher mass resolution is obtained than with a marginal oscillator (*21*).

The only undesirable feature of the capacitance bridge detector is that it is more expensive (the Rockland Systems Corp. Model 5100 Programmable Frequency Synthesizer costs about $3300) and far more complex electronically than a marginal oscillator detector. However, we feel the greatly improved performance it provides more than offsets this disadvantage.

(3) Scan Rate. The scan rate of early ICR spectrometers was very slow, typically 5 min/decade. Mass spectra were obtained by setting the marginal oscillator frequency constant and slowly scanning the magnetic field strength to bring ions of different m/e into resonance. The electrometer detector method (*22*, *23*) operates at constant magnetic field strength while the frequency of the excitation signal is scanned, but it too is a slow-scan method because of the sluggish response to the electrometer.

Enormous progress has been made in the past 4 years in increasing the scan rate of ICR spectrometers. In 1974 Comisarow and Marshall introduced a *Fourier Transform Ion Cyclotron Resonance* (FT-ICR) technique which is capable of acquiring an entire mass spectrum in about 0.1 s (*24–28*). In an FT-ICR experiment, ions are generated in a one-region ICR cell by an electron beam pulse, and then, after a given delay period, the ions are subjected to an rf electric field pulse having a frequency which is varied linearly during the irradiating period of a few milliseconds. After the irradiating rf pulse is turned off, a high input impedance, broad-band amplifier detects the response of all the coherently accelerated ions. The resulting transient ICR signal is digitized, stored in a computer, and later subjected to Fourier transformation to recover the mass spectrum of ions stored in the ICR cell. A complete mass spectrum can be acquired in about 0.1 s, and ultrahigh mass resolution has been demonstrated (*29*).

In our laboratory another type of Fourier transform mass spectrometry called *rapid-scan ICR* has been developed for obtaining rapid, high-resolution mass spectra (*20*, *21*). A block diagram of the instrument is shown in Figure 2. Conceptually, the rapid-scan ICR technique is similar to correlation NMR spectroscopy (*30*, *31*) in that the excitation frequency from the frequency synthesizer is scanned rapidly across the spectrum under computer control. The transient response of resonant ions in the ICR cell is detected with a capacitance bridge detector, amplified, phase detected, filtered, digitized, and stored in a computer. The detected signal is greatly distorted by ringing due to the rapid scan rate, but a true mass spectrum can be recovered using Fourier transform computation methods.

Rapid-scan ICR has many desirable features in common with FT-ICR. Both are frequency sweep, constant magnetic field detection methods which allow the possibility of using permanent magnets and superconducting solenoids in ICR mass spectrometers. Both allow a full mass spectrum to be acquired orders of magnitude faster than was previously possible. Both utilize a one-region ICR cell for significantly improved mass resolution and mass range up to m/e 1000. Both require a computer data system to digitize the transient signals and compute the Fourier transforms.

Our interest in rapid-scan ICR developed because the computer equipment required for the experiment is less costly and more readily available than that required for FT-ICR. Comparisons are shown in Table I. In FT-ICR the transient signal from the detector is digitized at 2 MHz in a scan from m/e 20 (984 kHz) to m/e 1000 (19.7 kHz) at 1.2 T. Such high A/D conversion rates require essentially a transient recorder-type of buffer memory to store the digitized signal. In contrast, the phase-sensitive detector used in rapid-scan ICR experiments is very important because it allows digitization at 100 kHz of an audio beat signal rather than direct digitization at 2 MHz of the broad-band rf transient signal. This lower digitization rate allows medium-speed memory devices, such as core and magnetic disk, which are far less expensive and of greater storage capacity. One final comparison is that rapid-scan ICR requires irradiating rf voltage levels of only a few millivolts rather than about 100 V which is needed for FT-ICR, and the rf power distribution across the spectrum

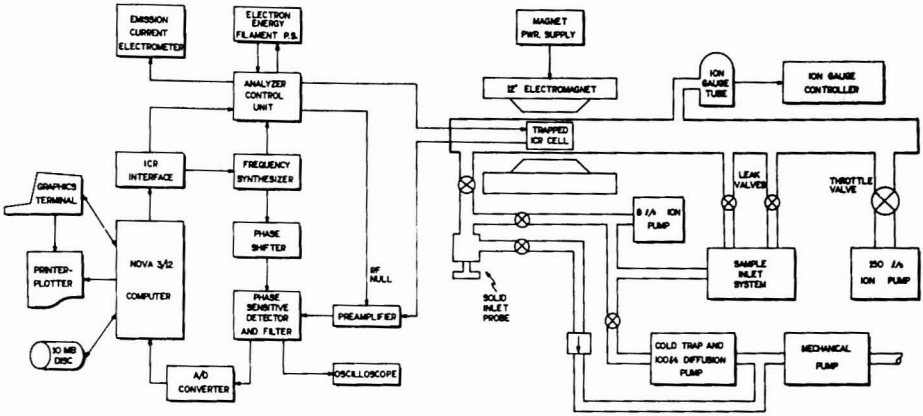

Figure 2. Block diagram of a Fourier transform mass spectrometer showing the computer and interface circuitry for rapid-scan ICR detection

Table I. Comparison of Instrumentation for Rapid-Scan ICR and Fourier Transform ICR

parameter	FT-ICR	rapid-scan ICR
1. analog/digital converter	2 MHz	100 kHz
2. computer memory	high-speed semiconductor	core or disk
3. size of FFT	limited by size of buffer memory	limited by size of disk memory
4. irradiating rf level	100 V	0.01 V

is far more uniform in rapid-scan ICR because the synthesizer scans the spectrum in several seconds rather than in just a few milliseconds. Uniform power distribution across the spectrum is important for ensuring that the ICR signals are linearly proportional to the number of ions in the ICR cell.

Both the FT-ICR and the rapid-scan ICR technique are still at a very early stage of development. However, it is clear that both methods provide such an enormous improvement in the scan rate, mass resolution, and mass range that the ICR spectrometer can now be classed as a truly high performance mass spectrometer.

(4) Sample Size. The first-generation ICR instruments relied on batch inlets and variable-leak values for introducing samples. Obviously, such a system would not be useful for small samples (less than a milligram) or low-volatility compounds. In addition, the scan speed of the earlier instruments was so slow that submicrogram-sized samples would be pumped away before a single mass scan could be completed.

This is an area where much work remains to be done, but the fast scan rates now available and exceedingly low partial pressures of sample required (as is discussed in the Results section) promise to make ICR a very sensitive analytical mass spectrometer. Figure 2 shows that our spectrometer at the University of California—Irvine has a direct insertion probe for admitting solid samples. Also, the probe, the vacuum system, and the ICR cell can be heated up to 250 °C. With this arrangement, a 1-μg sample can be detected with about the same sensitivity as commercial sector mass spectrometers which use a direct insertion probe. Quantitative studies of sensitivity are currently in progress, and we are confident that further improvements in the techniques for adding samples will further decrease the detection limit.

All reagent gases utilized for this work were obtained commercially and purified by several freeze–pump–thaw cycles on the ICR inlet system having a background pressure of less than 1×10^{-7} Torr. Pressures of samples and reagent gases in the ICR cell were measured with a Bayard-Alpert ionization gauge which was calibrated for the gases of interest with a Baratron capacitance manometer. The one-region ICR cell used for these experiments had dimensions of $1.9 \times 1.9 \times 7.6$ cm. For storing positive ions, the magnetic field strength was held constant at 1.28 T, the voltage applied to the upper plate, lower plate, and end plates was −1.0 V, and the voltage on the side plates was +1.0 V. An electron-impact energy of 20 eV was used, and emission currents of a few nanoamperes were measured with a Keithley Model 616 digital electrometer.

Table II. Comparison between Conventional Chemical Ionization Mass Spectrometry and Low-Pressure Chemical Ionization

	conventional CI	low-pressure CI
1. reagent gas pressure	1 Torr	10^{-6} Torr
2. sample pressure	10^{-3} Torr	10^{-9} Torr
3. ion residence time	10^{-6} s	10 s
4. ionic species	bipolar plasma: positive ions, electrons, and negative ions	free ions: only positive or negative species
5. variety of reagents	extensive clustering with polar reagents	no clustering

RESULTS

The Fourier transform mass spectrometer described in the Experimental section has proved to be a powerful method for chemical ionization mass spectrometry at low pressures. A comparison between conventional CI and low-pressure CI is shown in Table II. Reagent gas pressures and sample pressures roughly 10^6 times lower than in conventional CI mass spectrometers can be utilized because of the high trapping efficiency for the reagent ions. All ions of a given charge type, either positive or negative, are stored in the one-region ICR cell by a strong homogeneous magnetic field and a weak electrostatic field. To switch from storage of positive ions to storage of negative ions, the polarity of the electrostatic field is simply reversed. Since the ICR cell operates with ions of a single charge type, ion–electron and ion–ion recombination processes are not of importance in determining the lifetime of reagent ions in the cell. A final comparison shown in Table II concerns the variety of reagent ions which can be utilized. At pressures as high as 1 Torr, polar reagents such as H_2O, HCO_2H, and NH_3 cluster extensively around the sample ion

1. GENERATION OF REAGENT IONS:

$$NH_3 + e^- \xrightarrow{k_{ion}} NH_3^+ + 2e^-$$

$$NH_3^+ + NH_3 \xrightarrow{k_{rxn}} NH_4^+ + NH_2$$

2. ION LOSSES FROM THE ICR CELL:

$$NH_4^+ + NH_3 \xrightarrow{k_L} \text{LOSS}$$

Figure 3. Proposed mechanism for generation, storage, and loss of gaseous reagent ions

peaks and the reagent ions. This leads to uncertainty in the chemical processes occurring in the source because many reagent ions such as H_3O^+, $H^+(H_2O)_2$, $H^+(H_2O)_3$, etc., are all present at the same time. Since cluster ions usually form by a termolecular process such as

$$H_3O^+ + 2H_2O \rightarrow H^+(H_2O)_2 + H_2O \qquad (4)$$

the rate of formation of cluster ions depends on the *square* of the reagent gas pressure and is greatly suppressed at the 10^{-6} Torr pressures utilized in the ICR experiments.

Recently we have developed a model which accurately describes the physical and chemical processes occurring in the ICR cell under low-pressure CI conditions. Our mechanism for low-pressure chemical ionization will be presented here in two parts. First, the mechanism for generation and storage of reagent ions in the absence of sample will be treated. In the second part, steps for chemical ionization of a sample are added to the model, and the kinetic equations are solved to predict the yield for conversion of reagent ions to sample ions.

Mechanism for Generation and Storage of Reagent Ions. A simple mechanism which predicts the abundance of reagent ions in the ICR cell is shown in Figure 3. The first step in the mechanism is continuous ionization of the reagent gas by electron bombardment. Ions such as $NH_3^+\cdot$ formed in this way react very rapidly with the reagent gas at rate k_{rxn} to produce NH_4^+, the most stable reagent ion in ammonia. Clusters of ammonia with NH_4^+ do not form because the reagent gas pressure is very low, typically 10^{-6} Torr. The third and last step is bimolecular loss of the reagent ions from the ICR cell due to a random-walk-type process in which the centers of gyration are displaced perpendicular to the magnetic field.

With this mechanism the differential rate equation for formation of $NH_3^+\cdot$ can be written as

$$d[NH_3^+\cdot]/dt = k_{ion}[NH_3][e^-] - k_{rxn}[NH_3][NH_3^+\cdot] \qquad (5)$$

where brackets refer to the average concentrations (particles/cm^3) of each species in the ICR cell and t is time. This equation can be solved by assuming that the cell has no ions initially and that at $t = 0$ the electron emission current is set to a continuous and constant value. We will also assume throughout this treatment that pseudo-first-order kinetics apply, i.e., that the concentration of neutral molecules in the cell is constant and much greater than the concentration of ions. The solution of Equation 5 for the concentration of $NH_3^+\cdot$ in the ICR cell is

$$[NH_3^+\cdot] = (k_{ion}[e^-]/k_{rxn})(1 - e^{-k_{rxn}[NH_3]t}) \qquad (6)$$

From this it is apparent that the concentration of $NH_3^+\cdot$ begins at zero and eventually reaches a steady-state value equal to

$$t \rightarrow \infty, \quad [NH_3^+\cdot]_{ss} = k_{ion}[e^-]/k_{rxn} \qquad (7)$$

The steady-state is approached in an exponential manner with a half-life given by

$$\tau_{1/2} = (\ln 2)/k_{rxn}[NH_3] \qquad (8)$$

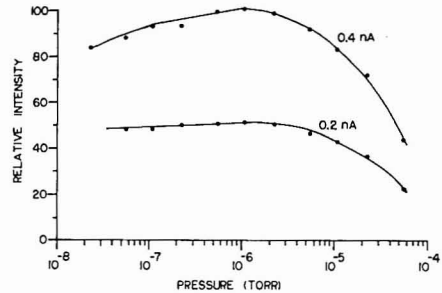

Figure 4. Experimental data for variation in size of the reagent ion signal with reagent gas pressure. The two sets of data shown correspond to electron emission currents regulated at 0.2 and 0.4 nA, and the magnetic field was fixed at 1.28 T

Typically, $\tau_{1/2}$ is about 0.02 s at a reagent gas pressure of 1×10^{-6} Torr.

The differential rate equation for formation of the terminal reagent ion NH_4^+ can also be written by referring to the mechanism in Figure 3.

$$d[NH_4^+]/dt = k_{rxn}[NH_3][NH_3^+\cdot] - k_L[NH_3][NH_4^+] \qquad (9)$$

Solution of this equation is simplified greatly by substituting the steady-state concentration of $NH_3^+\cdot$ (Equation 7), for $[NH_3^+\cdot]$ in the first term. The validity of this approximation will be demonstrated later. Proceeding with the solution gives

$$[NH_4^+] = (k_{ion}[e^-]/k_L)(1 - e^{-k_L[NH_3]t}) \qquad (10)$$

It is apparent from this solution that $[NH_4^+]$ is zero initially and increases to a final steady-state value given by

$$t \rightarrow \infty, \quad [NH_4^+]_{ss} = k_{ion}[e^-]/k_L \qquad (11)$$

The rate of approach for steady state is determined by the half-life

$$\tau_{1/2} = (\ln 2)/k_L[NH_3] \qquad (12)$$

Since k_L, the bimolecular rate constant for loss of ions due to diffusion to the plates of the ICR cell, is typically 10^{-12} cm^3/molecule-s, the half-life for attainment of steady state by NH_4^+ is typically 21 s at a reagent gas pressure of 1×10^{-6} Torr. Physically, one can imagine that $NH_3^+\cdot$ is slowly and continuously formed by electron impact and reacts rapidly after about 0.02 s to produce NH_4^+. The NH_4^+ ions thus formed are stored efficiently in the ICR cell, and their concentration continues to increase until after about 21 s some are slowly lost because of diffusion and neutralization at the plates of the ICR cell. The earlier substitution $[NH_3^+\cdot] \cong [NH_3^+\cdot]_{ss}$ used in solving Equation 9 is clearly justified because steady state for $NH_3^+\cdot$ occurs roughly 10^3 times faster than establishment of steady state for NH_4^+.

An experimental test of this mechanism is shown in Figure 4 for $(CH_3)_3NH^+$ (m/e 60) reagent ions in trimethylamine. Equation 11 predicts that the steady-state concentration of the protonated reagent ions is independent of the reagent gas pressure and linearly proportional to $[e^-]$, or the ionizing electron emission current. Figure 4 shows that the ICR power absorption signal for $(CH_3)_3NH^+$ is, in fact, substantially independent of trimethylamine reagent gas pressure from 5×10^{-8} to 5×10^{-6} Torr. At higher pressures the signal decreases owing most likely to pressure damping of the ion power absorption. In another test of Equation 11, a linear relationship is shown in Figure 5 between the observed ICR signal for $CH_3NH_3^+$ (m/e 32) reagent ions and electron emission current, for a constant methylamine reagent gas pressure of

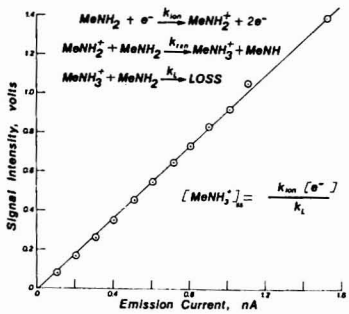

Figure 5. Experimental data showing the linearity between size of the reagent ion signal and electron emission current. Pressure of the reagent gas methylamine was maintained at 5×10^{-7} Torr

5×10^{-7} Torr. Both of these tests are in very good accord with the predictions of Equation 11 and demonstrate that the conditions in the ICR cell are well characterized by the mechanism shown in Figure 3.

One note of caution should be made, however, with regard to the effect of high electron emission currents. In the experiments above, emission currents of only a few nanoamperes were used to avoid an over-accumulation of ions in the ICR cell. Charge densities greater than about 10^6 ions/cm^3 cause the cyclotron frequencies to change, the ion trapping efficiency to decrease, and the power absorption signals to become distorted. For this reason, we monitor the electron emission current with an electrometer and avoid the tendency to "blast away" and make more ions.

Mechanism for Low-Pressure Chemical Ionization. A model for low-pressure chemical ionization can be obtained by extending the previous mechanism to include ionization of a sample S by the reagent ions. Such a mechanism for proton transfer to a sample S of higher proton affinity is shown in Figure 6. Reagent ions are formed in the same manner as before and may be removed from the ICR cell either by diffusion to the walls, k_L, or by proton transfer at rate k_{CI} to sample S. It is assumed that the partial pressure of the sample is much lower than the partial pressure of the reagent gas in order to produce a true chemical ionization spectrum. To complete the mechanism, provision is made for diffusional loss at rate k_L' of the protonated sample ions. Under these conditions, the differential rate equation for the concentration of the NH_4^+ reagent ions is

$$d[NH_4^+]/dt = k_{rxn}[NH_3][NH_3^{+\cdot}] - (k_{CI}[S] + k_L[NH_3])[NH_4^+] \quad (13)$$

This is similar to form to Equation 9 and can be solved in the same manner by substituting Equation 7 for $[NH_3^{+\cdot}]$. This substitution assumes that all the $NH_3^{+\cdot}$ ions formed by electron impact ionization react exclusively with ammonia to establish rapidly a steady-state concentration of $NH_3^{+\cdot}$ in the cell. The solution of Equation 13 is

$$[NH_4^+] = \frac{k_{ion}[NH_3][e^-]}{k_{CI}[S] + k_L[NH_3]}(1 - e^{-(k_{CI}[S]+k_L[NH_3])t}) \quad (14)$$

From this it is apparent that the NH_4^+ concentration is zero initially and eventually reaches a steady-state value equal to

$$t \to \infty, \qquad [NH_4^+]_{ss} = \frac{k_{ion}[NH_3][e^-]}{k_{CI}[S] + k_L[NH_3]} \quad (15)$$

The half-life for reaching steady state is similar to what was found earlier in Equation 12, but in the presence of sample is a bit shorter and is given by

$$\tau_{1/2} = (\ln 2)/(k_{CI}[S] + k_L[NH_3]) \quad (16)$$

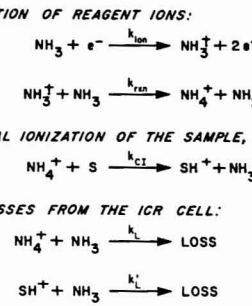

Figure 6. Proposed mechanism for low-pressure chemical ionization of sample S by reagent ions NH_4^+

According to the mechanism in Figure 6, the rate of appearance of protonated sample ions is

$$d[SH^+]/dt = k_{CI}[S][NH_4^+] - k_L'[NH_3][SH^+] \quad (17)$$

Integration of this is straightforward once Equation 14 is substituted for $[NH_4^+]$. However, the result is quite cumbersome and will not be reproduced in its entirety here. Of greater interest is the steady-state solution to Equation 17 given by

$$t \to \infty, \qquad [SH^+]_{ss} = \frac{k_{CI}k_{ion}[e^-][S]}{k_L'(k_{CI}[S] + k_L[NH_3])} \quad (18)$$

and the half-life for establishment of steady state for SH^+ given by

$$\tau_{1/2} \cong (\ln 2)/k_L[NH_3] \quad (19)$$

It is important to note that Equation 19 predicts that the rate for steady state of SH^+ is essentially independent of the pressure of the sample. This means that the $[SH^+]$ reaches the steady-state level on a time scale comparable to that of the reagent ions NH_4^+, even when the sample is introduced at a pressure three to four orders of magnitude lower than that of the reagent gas.

Of particular interest is the yield for conversion of reagent ions to sample ions. Comparison of Equation 18 for SH^+ and Equation 15 for NH_4^+ shows that the ratio of the two signals under steady-state conditions is predicted to be

$$[SH^+]/[NH_4^+] = k_{CI}[S]/k_L'[NH_3] \quad (20)$$

This is a strikingly simple expression which predicts a linear relationship between pressure of the sample, [S], and the ratio of the sample ion signal to the reagent ion signal. The results of an experimental test of this mechanism are shown in Figure 7. Methylamine was used as the reagent gas at a constant pressure of 2×10^{-6} Torr, and the pressure of a trimethylamine sample was varied from 5×10^{-9} to 1×10^{-7} Torr. Proton transfer occurs from the reagent ions $CH_3NH_3^+$ to the trimethylamine sample to form $(CH_3)_3NH^+$ (m/e 60).

$$CH_3NH_3^+ + (CH_3)_3N \xrightarrow{k_{CI}} (CH_3)_3NH^+ + CH_3NH_2 \quad (21)$$

At each pressure of sample, the ICR signals for the two ions were measured, and their ratio was calculated. The linear correlation shown in Figure 7 is exactly what is expected from Equation 20 and provides good evidence that the processes in the ICR cell are well characterized by this simple model.

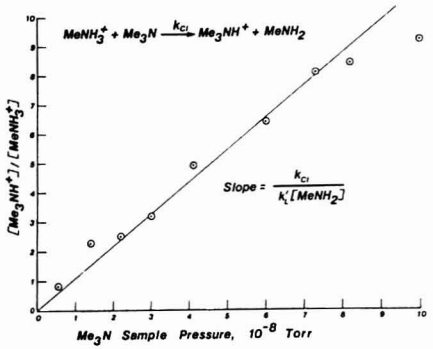

Figure 7. Experimental data for testing the validity of Equation 20. Methylamine at a pressure of 2×10^{-6} Torr was used as the reagent gas, and trimethylamine was the sample

In all of these experiments, ions are formed continuously and stored for as long as possible in the ICR cell until they finally diffuse to the walls. This *continuous mode* of operation is quite different from the pulsed ICR experiments described previously (*5*). For measurement of rate constants and equilibrium constants, a pulse sequence consisting of a grid pulse, detect pulse, and quench pulse is used to produce a packet of ions, allow them to react for a certain reaction period, detect the products, and finally neutralize all ions to stop the sequence and prepare for the beginning of a new pulse sequence. We have found, however, that greater detection sensitivity is achieved with the continuous mode, especially at pressures below 10^{-6} Torr. Another feature of the continuous mode of operation is that all the ionization tends to concentrate in the most stable species present. There are so many collisions in the ICR cell that unstable fragment ions usually react away quickly and do not appear in the mass spectrum. Problems arise if the sample of interest has a low proton affinity. If there are high proton affinity impurities present in the sample or the vacuum system, the sample ions will transfer a proton to the impurities and not appear in the mass spectrum. Often in cases such as this, it is desirable to switch to negative reagent ions or even to more specific reagent ions which react selectively with only the sample component of interest.

DISCUSSION

The previous results demonstrate that low-pressure chemical ionization is a well-behaved and well-characterized process. The proposed mechanisms explain the experimental results over several orders of magnitude in sample pressure. It is particularly interesting to notice that Figure 7 shows that at a sample pressure of 5×10^{-9} Torr the ratio of sample ion signal height to reagent ion signal height is 0.8. Therefore, about 44% of the reagent ions originally present in the ICR cell are converted through reaction to sample ions. This is a surprisingly high extent of conversion; the ionic composition in the cell is 44% sample ions and 56% reagent ions even at a sample pressure of 5×10^{-9} Torr. At higher pressures, for example, 4×10^{-8} Torr, the reagent ion signal is five times *smaller* than the sample ion signal.

The future outlook for this technique is very bright. The ICR cell itself is a simple device mechanically since none of the dimensions are critical. High performance as a mass spectrometer depends instead on maintaining reagent gas pressures below 1×10^{-6} Torr and having a large computer to acquire and process the transient ICR signals. In effect, the requirement for exceptionally high mechanical tolerances in double-focusing sector mass spectrometers is exchanged for a high-performance computer system and a clean vacuum system. Since the cost for precision machining can be expected to continue increasing and the cost of computer hardware can be expected to continue decreasing, Fourier transform mass spectrometry based on the ion cyclotron resonance principle may become the next generation high performance mass spectrometer.

In our research at the University of California—Irvine, attention will be focused on extending the low-pressure CI technique to even lower pressures to analyze for subnanogram quantities of low-volatility molecules. In terms of Equation 20, this can be accomplished by increasing the yield for conversion of reagent ions to sample ions by making k_L' smaller or, equivalently, by increasing the ion-trapping efficiency of the ICR cell. Several new cell designs are being tested for better trapping efficiency and for greater overall yield of ions from a given amount of sample. Also, it seems essential to improve the vacuum system so as to maintain as low a background pressure as possible. Our current system with a 150 L/s ion pump can be evacuated to only about 1×10^{-9} Torr. There should be no difficulty, however, in reaching lower pressures with larger commercially available pumps.

LITERATURE CITED

(1) For a recent review of chemical ionization mass spectrometry, see B. Munson, *Anal. Chem.*, **49**, 722A (1977).
(2) G. Giournousis and D. P. Stevenson, *J. Chem. Phys.*, **29**, 294 (1958).
(3) E. W. McDaniel, "Collision Phenomena in Ionized Gases", Wiley, New York, 1964, p 67.
(4) W. P. Allis in "Handbook der Physik", Vol. 21, S. Flügge, Ed., Springer, Berlin, 1956, p 383.
(5) See R. T. McIver, Jr., *Rev. Sci. Instrum.*, **49**, 111 (1978), and references therein.
(6) J. M. S. Henis, *J. Am. Chem. Soc.*, **90**, 844 (1968).
(7) J. M. S. Henis, *Anal. Chem.*, **41**(10), 22A (1969).
(8) M. L. Gross and C. L. Wilkins, *Anal. Chem.*, **43**(14), 65A (1971).
(9) H. Hartmann and K.-P. Wanczek, Ed., "Ion Cyclotron Resonance Spectrometry", Springer-Verlag, Berlin, 1978.
(10) T. A. Lehman and M. M. Bursey, "Ion Cyclotron Resonance Spectrometry", Wiley-Interscience, New York, 1976.
(11) J. L. Beauchamp, L. R. Anders, and J. D. Baldeschwieler, *J. Am. Chem. Soc.*, **89**, 4569 (1967).
(12) J. D. Baldeschwieler, *Science*, **159**, 263 (1968).
(13) J. L. Beauchamp, *Annu. Rev. Phys. Chem.*, **22**, 527 (1971).
(14) R. T. McIver, Jr., *Rev. Sci. Instrum.*, **44**, 1071 (1973).
(15) A. Warnick, L. R. Anders, and T. E. Sharp, *Rev. Sci. Instrum.*, **45**, 929 (1974).
(16) R. T. McIver, Jr., and A. D. Baranyi, *Int. J. Mass Spectrom. Ion Phys.*, **14**, 449 (1974).
(17) S. E. Buttrill, Jr., *J. Chem. Phys.*, **50**, 4125 (1969).
(18) M. B. Comisarow, *J. Chem. Phys.*, **55**, 205 (1971).
(19) R. T. McIver, Jr., *Rev. Sci. Instrum.*, **41**, 555 (1970).
(20) R. L. Hunter and R. T. McIver, Jr., *Chem. Phys. Lett.*, **49**, 577 (1977).
(21) R. L. Hunter and R. T. McIver, Jr., *Am. Lab.*, **9**, 13 (Nov 1977).
(22) R. T. McIver, Jr., E. B. Ledford, Jr., and J. S. Miller, *Anal. Chem.*, **47**, 692 (1975).
(23) E. B. Ledford, Jr., and R. T. McIver, Jr., *Int. J. Mass Spectrom. Ion Phys.*, **22**, 399 (1976).
(24) M. B. Comisarow and A. G. Marshall, *Chem. Phys. Lett.*, **25**, 282 (1974).
(25) M. B. Comisarow and A. G. Marshall, *Chem. Phys. Lett.*, **26**, 489 (1974).
(26) M. B. Comisarow and A. G. Marshall, *Can. J. Chem.*, **52**, 1997 (1974).
(27) M. B. Comisarow and A. G. Marshall, *J. Chem. Phys.*, **64**, 110 (1976).
(28) C. L. Wilkins, *Anal. Chem.*, **50**, 493A (1978).
(29) M. Comisarow, *Adv. Mass Spectrom.*, **7B**, p 1042 (1978).
(30) J. Dadok and R. F. Sprecher, *J. Magn. Reson.*, **13**, 243 (1974).
(31) R. K. Gupta, J. A. Ferretti, and E. D. Becher, *J. Magn. Reson.*, **13**, 275 (1974).

RECEIVED for review November 13, 1978. Accepted February 2, 1979. (R.T.M. acknowledges grant support from the National Institutes of Health (GM-23416-02) and the National Science Foundation (CHE 77-10024).

Comparison of the Negative Reactant Ions Formed in the Plasma Chromatograph by Nitrogen, Air, and Sulfur Hexafluoride as the Drift Gas with Air as the Carrier Gas

Timothy W. Carr

International Business Machines Corp., Dept. 350, Bldg. 310, Hopewell Junction, New York 12533

The negative reactant ions formed in the plasma chromatograph with zero grade air are examined with nitrogen, air, and SF_6 as the drift gas. The O_2^-, and O_4^- ions are observed in the mobility spectra of air carrier with both air and SF_6 as the drift gas but not when N_2 is used as the drift. The negative ion mass spectra as well as the total ion and individual mass-identified mobility spectra are shown for air with each of the three drift gases.

Plasma chromatography (*1–8*) and the coupled technique of plasma chromatography/mass spectroscopy (*9, 10*) have been investigated in recent years as methods to detect picogram quantities of both organic and inorganic compounds. The basis of the technique is the formation of both positive and negative ions through a series of ion-neutral molecule reactions occurring at atmospheric pressure. The phenomenon observed in the ionization process is similar to that observed in chemical ionization mass spectrometry (*11, 12*). The ions produced from the carrier gas are referred to as reactant ions, since they are used to react with the trace amount of sample molecules.

The identity of the reactant ions formed in the PC techniques is of particular importance in understanding the formation of product ions. Carroll, Horning, et al. (*13*) have identified the positive reactant ions formed using nitrogen for both the carrier and drift gases as being NH_4^+, NO^+, and $H(H_2O)_2^+$. Recently Kim, Karasek, et al. have also studied the positive reactant ions (*30*). The identity of the negative reactant ions formed with zero grade air as the carrier and nitrogen as the drift gas was the subject of a recent report by Carr (*14*). Most applications of the plasma chromatographic technique have involved the use of nitrogen as the drift gas. The purpose of this investigation is to compare the reactant ions produced with zero grade air as the carrier gas and nitrogen, zero grade air, and sulfur hexafluoride as the drift gas.

EXPERIMENTAL

The Alpha-II plasma chromatograph/mass spectrometer manufactured by Franklin GNO Corporation which was used in this investigation has been described previously (*14, 15*). This instrument consists of a Beta-VII plasma chromatograph coupled to a specifically modified Extranuclear Laboratories Spectr-El quadrupole mass spectrometer. The operating parameters of the plasma chromatograph used in this study are summarized in Table I.

A schematic of the combined PC-MS system is shown in Figure 1. This instrument has the capability of operating in several modes so that ion mobility spectra, mass spectra, total ion mobility spectra, and mass identified mobility spectra can be obtained. The ionic mobility may be measured in either a one-grid or two-grid pulsing procedure with the Beta-VII plasma chromatograph mode of operation. Both grids of the drift tube can be held open, allowing all the ions produced in the ionization source to continually drift down the tube and into the quadrupole mass spectrometer, which results in atmospheric pressure ionization mass spectra. Total ion mobility spectra can be obtained by operating the plasma chromatograph in the normal one-grid pulsing mode and the quadrupole mass spectrometer in the total ion mode, which enables the channeltron electron multiplier detector to measure the ionic distribution as a function of time. By adjusting the mass analyzer to respond only to a single m/e value and operating the plasma chromatograph in the normal one-grid pulsing mode, the distribution of an individual ion as a function of time can be obtained. The arrival time of the individual ions can then be compared with the arrival time of the ions measured in the total ion mode to produce the mass-identified mobility spectra.

Table I. Operating Parameters of the Alpha II Plasma Chromatograph–Mass Spectrometer

drift gas flow rate	500 cm³/min
carrier gas flow rate	100 cm³/min
applied voltage	+ 2800 V
gate width	0.2 ms
repetition rate	27.0 ms
temperature	210 °C

A Nicolet Model SD-721A integrating ADC mounted in a Nicolet Model 1074, 4096-channel signal averager was used to digitize the accumulated plasmagrams. Usually 512 scans of 27-ms duration were collected and stored on magnetic tape with a Nicolet Model NIC-28A magnetic tape coupler and Kennedy Model 9700 tape deck. As the data were being accumulated in memory, the information was displayed on a Tektronix Model D10 oscilloscope. The data stored on the magnetic tape were entered into an IBM System/370 computer and were subsequently analyzed using VSAPL under the operating system VM/370. The position and intensity of the peaks in the mobility spectra along with a plot of the mobility spectra were then displayed on a graphics terminal from which hard copies could be obtained.

The ultrahigh purity nitrogen and the zero grade air were obtained from MG Scientific Gases of Somerville, N.J.; the sulfur hexafluoride was obtained from Matheson Gas Products, Inc.

RESULTS AND DISCUSSION

The interpretation of plasma chromatographic data is dependent upon an understanding of ion-mobility theory and the nature of ion–neutral molecule interaction at atmospheric pressure in weak electric fields. Extensive studies have been made in the field of ionic mobility (*16, 17*); most studies of ion–neutral molecule reactions have been conducted at considerably lower pressures.

The drift time, t_D, of an ion in the plasma chromatograph can be expressed as

$$t_D = \frac{1}{K_0} \frac{P}{760} \frac{273}{T} \frac{L}{E} \qquad (1)$$

where K_0 is the reduced mobility of the ion, P is the pressure measured in Torr, T is the absolute temperature, E is the electric field, and L is the length of the drift tube. This equation shows that an increase in pressure or a decrease in temperature will result in an increase in the drift time of an ion. This is due to the increase of ion–neutral molecule collisions as a consequence of the increase in the molecular density in the drift tube.

0003-2700/79/0351-0705$01.00/0 © 1979 American Chemical Society

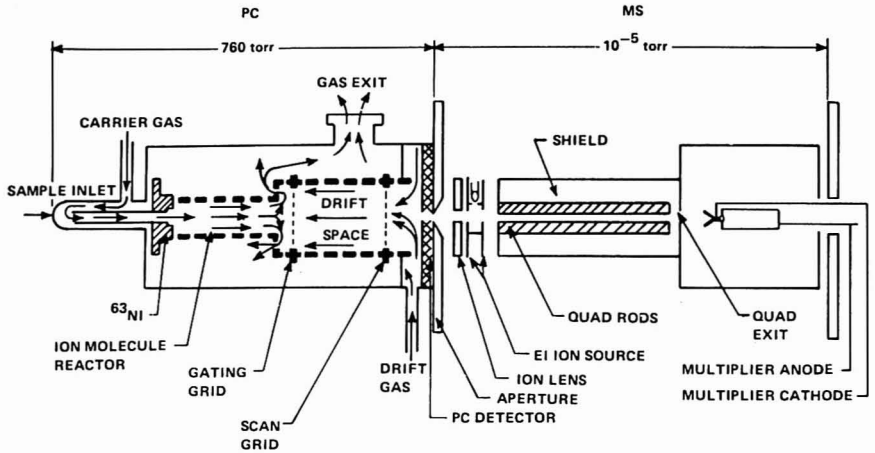

Figure 1. Schematic of the Alpha-II Plasma Chromatograph–Mass Spectrometer

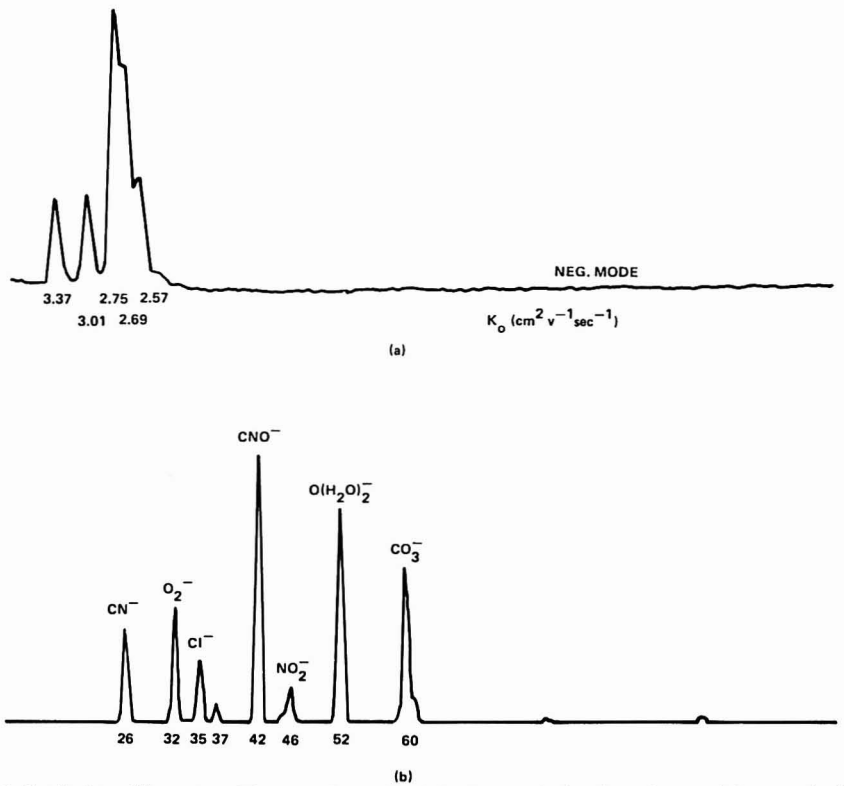

Figure 2. Negative ion mobility spectrum of the reactant ions produced with (a) zero grade air as the carrier gas and nitrogen as the drift gas and (b) the associated negative ion mass spectrum

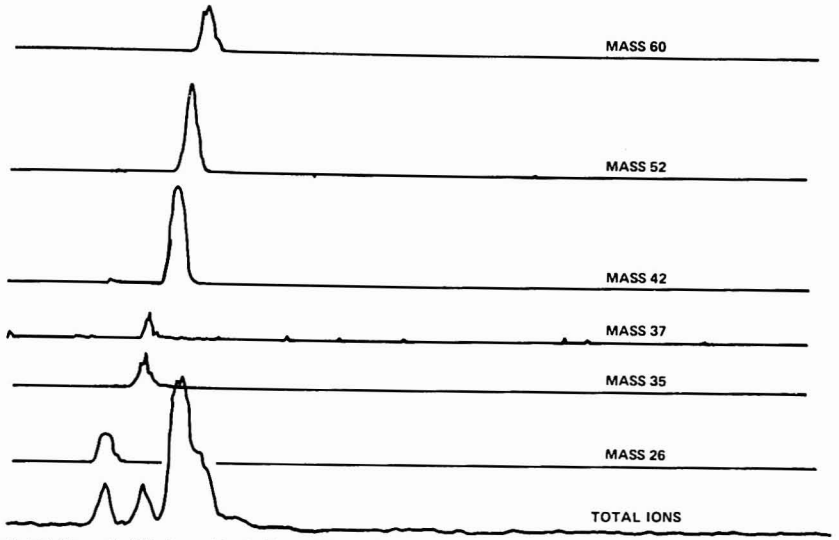

Figure 3. Total ion and individual mass-identified ion mobility spectra of the negative reactant ions produced with air as the carrier gas and nitrogen as drift

The general theory of ion mobility in weak electric fields, based upon the kinetic theory of gases, can be expressed as

$$K = \frac{3e}{16N}\left[\frac{1}{m} + \frac{1}{M}\right]^{1/2}\left(\frac{2\pi}{kT}\right)^{1/2}\frac{1}{\Omega_0} \qquad (2)$$

where K is the ionic mobility, N is the density of uncharged drift gas in molecules per cm^3, e is the charge on the ion, m is the mass of the ion, M is the mass of the neutral drift gas molecule, k is the Boltzmann constant, T is the absolute temperature, and Ω_0 is the average collisional cross section.

From Equation 2 it can be seen that as the mass of the ion becomes much larger than the mass of the drift gas molecules, the mass dependent term of the mobility equation becomes insignificant. Therefore, the mobility of a large ion is controlled by the average collisional cross section of the ion with the neutral drift molecules. The evaluation of the average collisional cross section is dependent upon several factors, the most important of which are ionic size and the nature of the interaction forces between the ions and neutral drift gas molecules (*18*, *19*). Therefore, it is desirable from the point of view of increasing the resolution of heavy ions in the mobility spectra to use a heavy drift gas. Xenon and sulfur hexafluoride are possible candidates, but xenon is economically unfavorable. Initially it was thought that sulfur hexafluoride would be unsuitable as a drift gas because of its high electron capture cross section. However, the results of this investigation showed that these fears were unwarranted.

The identity and formation of the negative reactant ions produced with air as the carrier and nitrogen as the drift gas have been discussed previously (*14*). For comparison purposes, the negative ion mobility spectrum and the total ion mobility, as well as the individual mass-identified mobility spectra, are shown in Figures 2 and 3, respectively. The most unexpected feature of these spectra is the absence of a mobility peak associated with O_2^- molecular ion under the experimental conditions used in this investigation.

At 483 K the coefficient of thermal detachment of an electron from the O_2^- ion is greater than the coefficient of thermal attachment (*20–22*). However, when the negative ion mobility spectra of the reactant ions produced from zero grade air carrier gas are compared with nitrogen, air, and sulfur hexafluoride as the drift gas, a definite mobility peak is observed for O_2^- with air and SF_6 as the drift gas as shown in Figures 4 and 5. The reason for this is the third-body efficiency of O_2 and SF_6 upon the stabilizing effect in the three-body electron attachment to O_2 (*20*).

$$e^- + O_2 + M \rightleftharpoons O_2^- + M \qquad (3)$$

The role of the third body in this reaction is to absorb the excess energy from the O_2^- ion after the electron attachment and to aid in the conservation of the total angular momentum of the system. In addition to the conservation of the orbital angular momentum, the spin angular momentum must also be conserved in the attachment process. Therefore, because O_2 and SF_6 have a greater stabilizing effect for thermal attachment than does N_2, the forward reaction rate of reaction 3 is greater than the reverse reaction rate in SF_6 and air. For N_2 as the drift gas the reverse reaction rate is greater. Nitrogen is roughly 100 times less effective than oxygen as a third body (*23*).

The negative ion mobility spectrum produced with air as both carrier and drift gas is shown in Figure 4a, the associated negative ion mass spectrum in Figure 4b. The same ionic species are observed in the negative ion mass spectra obtained from zero air carrier with both nitrogen and air as the drift. However, the intensities of the ions are significantly different between the two drift gases. With air as the drift gas, the O_2^- molecular ion with an m/e value of 32 is observed to be the most intense ion. In addition to the ions observed with nitrogen as the drift, an ion with an m/e value of 64 identified as O_4^- is found using air as the drift.

The negative ion mobility spectra of air carrier with air drift is strikingly different from the spectra of air carrier with nitrogen drift, which is readily seen from a comparison of Figures 2 and 4. The negative ion mobility spectrum with nitrogen drift contains five peaks which have been identified

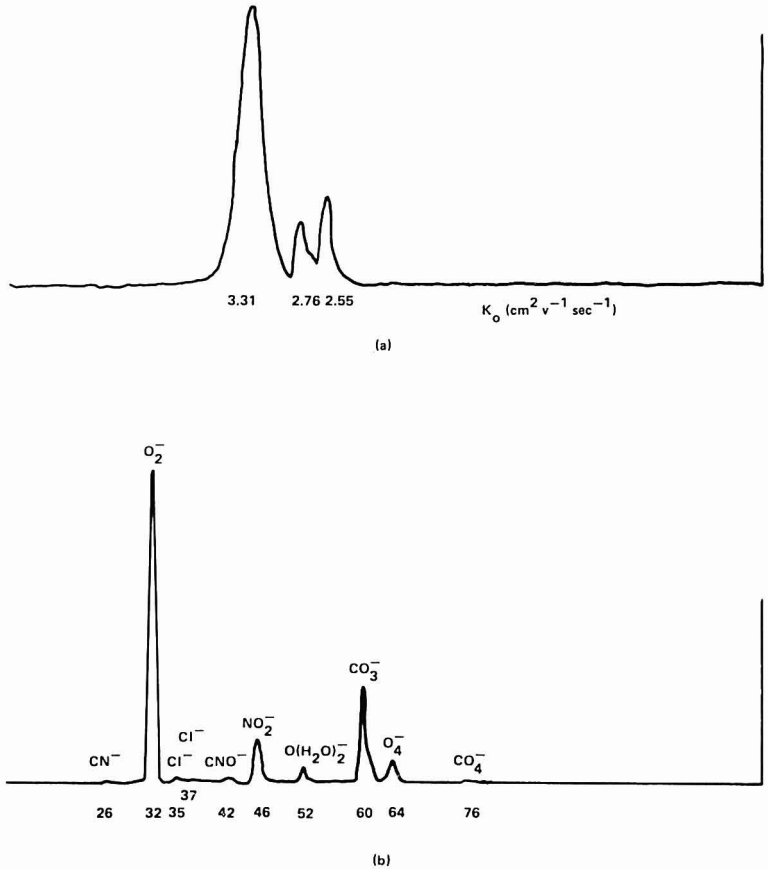

Figure 4. Negative ion mobility spectrum of the reactant ions produced with (a) air as both carrier and drift gases and (b) the associated negative ion mass spectra

as CN^-, Cl^-, CNO^-, $O(H_2O)_2^-$, and CO_3^- (*14*). The negative ion mobility spectrum obtained with air, on the other hand, contains three main peaks. The total ion mobility spectra and the individual mass-identified mobility spectra of the negative ions formed with air as the drift gas are shown in Figure 6. The distinct mobility peaks observed for the CN^- and Cl^- ions using nitrogen as drift are not observed when air is used as the drift gas. These peaks are obscured by the large mobility peaks comprised mainly of O_2^- and O_4^-. The O_2^- and O_4^- ions are observed under the same mobility peak due to the reversible reaction.

$$O_2^- + O_2 + M \leftrightarrows O_4^- + M \quad (4)$$

The mobility peak observed is equal to the mobility of the O_2^- ion times the fraction of the current carried by the O_2^- ion plus the mobility of the O_4^- ion times the fraction of the current carried by the O_4^- ion, which can be expressed as:

$$K_T = X_{O_2^-}K_{O_2^-} + X_{O_4^-}K_{O_4^-} \quad (5)$$

where K_T is the mobility of the peak observed in the spectrum, $X_{O_2^-}$ and $X_{O_4^-}$ are the fractions of the current carried by the respective ions and $K_{O_2^-}$ and $K_{O_4^-}$ are the mobilities of the specific ions. The mobilities of the NO_2^-, CNO^-, $O(H_2O)_2^-$, and CO_3^- ions are observed to be similar, whether air or nitrogen is the drift gas. These results are in agreement with the results obtained by Cohen and Wernlund (*24*).

The negative ion mobility spectrum associated with air carrier and SF_6 as the drift gas is shown in Figure 5a; the negative ion mass spectrum is shown in Figure 5b. As with air as the drift gas, the O_2^- molecular ion is the most intense ion in the negative mode mass spectra. Several ions in the mass spectra were also found with either nitrogen or air as drift, such as CN^- (m/e 26), Cl^- (m/e 35, 37), CNO^- (m/e 42), NO_2^- (m/e 46), $O(H_2O)_2^-$ (m/e 52), CO_3^- (m/e 60). As with the air drift gas, the O_4^- with an m/e value of 64 was also observed. A negative of m/e 50 is observed when the drift gas is SF_6, but not when the drift gas is air or nitrogen; this ion is most likely $O_2(H_2O)^-$. The thermodynamics of the hydration of O_2^- in the gas phase to yield $O_2^-(H_2O)_n$ with n values up to 3 have been studied by Arshadi and Kebarle (*25*); they determined that reaction 5 is 18.4 kcal/mole exothermic.

$$O_2^- + H_2O \leftrightarrows O_2(H_2O)^- \quad (6)$$

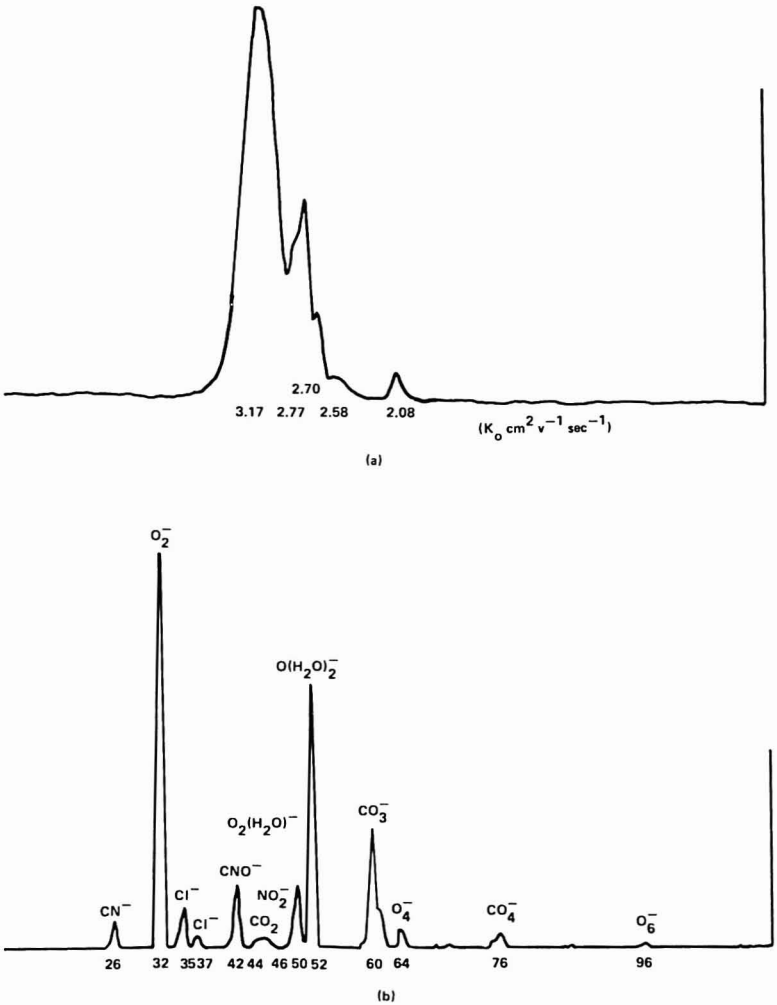

Figure 5. Negative ion mobility spectrum of the reactant ions produced with (a) air as the carrier and SF_6 as the drift and (b) associated negative ion mass spectrum between 10 and 110 amu

The bimolecular rate constant for the neutral interchange reaction of O_4^- and water at 300 K was measured by Adams, Bohme, Ferguson, et al. (26) to be 1.0×10^{-10} cm^3 $molecule^{-1}$ s^{-1} for reaction 7.

$$O_4^- + H_2O \rightleftharpoons O_2(H_2O)^- + O_2 \qquad (7)$$

Reaction 6 is probably the predominant mechanism for the formation of the $O_2(H_2O)^-$ ion because of the greater concentration of O_2^- ions compared with O_4^- ions. However, the rate constant measured for reaction 7 indicates that almost every encounter between water and O_4^- leads to the interchange reaction; therefore, this reaction cannot be neglected in a discussion of the formation mechanism. The reason the $O_2(H_2O)^-$ is observed with the SF_6 and not with the air drift gas is that the zero grade air is considerably drier than the SF_6.

The negative ion mobility spectrum with SF_6 drift is similar to that with air as the drift. Once again the CN^- and Cl^- mobility peaks are obscured by the O_2^-, O_4^-, and $O_2(H_2O)^-$ ion contribution. The total ion mobility spectra and the individual mass identified mobility spectra are shown in Figure 7. The ion of mass 42 (CNO^-), 60 (CO_3^-), and 52 ($O(H_2O)_2^-$) have been discussed previously. From Figure 7 it can readily be seen that the ions with m/e 32, O_2^-, and the ions with m/e 50, $O_2(H_2O)^-$, are under the same mobility peak. This suggests that reaction 6 is occurring. It should be noted that this peak, with SF_6 carrier, is of lower mobility than the corresponding peak with air as the drift gas. There are two possible ex-

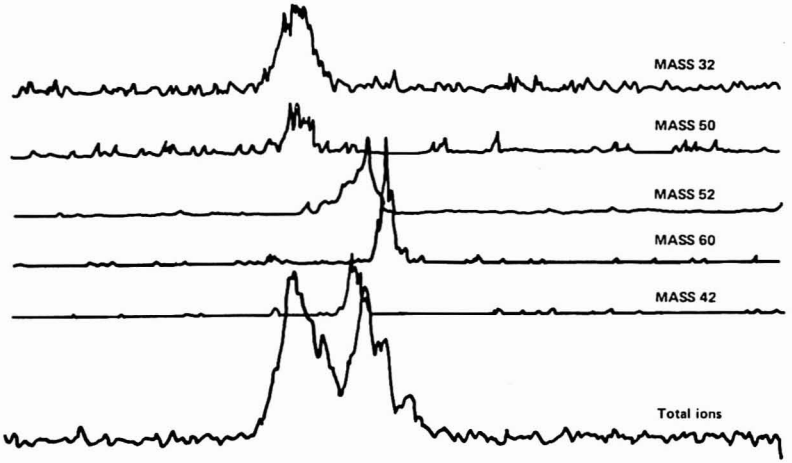

Figure 6. Total ion and selected individual mass-identified ion mobility spectra of the negative reactant ions produced with air as both the carrier and drift gas

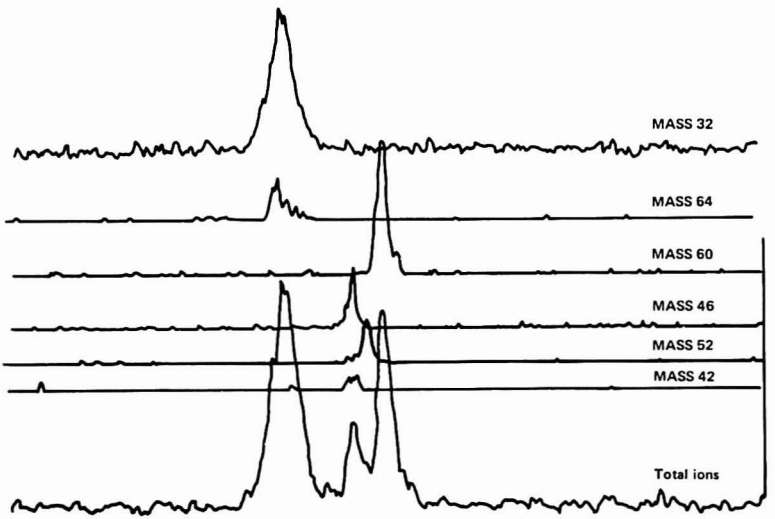

Figure 7. Total ion and selected individual mass-identified ion mobility spectra of the negative reactant ions produced with air as the carrier gas and SF_6 as the drift gas

planations for this. The $O_2(H_2O)^-$ ion may have a lower mobility than either the O_2^- or O_4^- ion, so that its contribution lowers the overall mobility of the peak. Also, SF_6 may increase the average collisional cross section, which would lower the mobility. Both of these mechanisms probably contribute to the observed result.

An additional peak of reduced mobility 2.08 $cm^2\ V^{-1}\ s^{-1}$ is observed in the mobility spectrum of Figure 5, and can be assigned to the SF_6^- ion based upon mass spectral data. This mobility is considerably higher than the value of 0.57 $cm^2\ V^{-1}\ s^{-1}$ obtained by McDaniel (27) and later by Morrison, Edelson, and McAfee (28). When the drift gas was changed from SF_6 back to nitrogen, the mobility of the SF_6^- was found to change drastically. The residual SF_6 left in the plasma chromatograph formed the SF_6^- and SF_6^- ions, and the peak in the mobility spectrum drifted toward a higher mobility after starting from a mobility approximating the value found by McDaniel. This phenomenon is presently under investigation in an attempt to elucidate the mechanism involved. The change in mobility when changing from SF_6 to N_2 as the drift is not surprising. This can be accounted for by the decreasing concentration of SF_6 in the mixed drift gas during the change-over, with the associated change in mobility from lower to higher value. However, the high mobility of SF_6^- in the SF_6 drift gas is not entirely clear. One explanation may be that charge transfer is taking place in the drift region of the PC tube which gives

Table II. Negative Reactant Ion Mobilities from N_2, Air, and SF_6 Drift Gas

ion	ionic weight, amu	mobility $cm^2 V^{-1} s^{-1}$		
		N_2	Air	SF_6
CN^-	26	3.37	3.37	3.37
Cl^-	35, 37	3.01	3.01	3.01
O_2^-	32	-	3.31	3.17
CNO^-	42	2.75	2.76	2.77
NO_2^-	46	2.76	2.76	2.77
$O_2(H_2O)^-$	50	-	-	3.17
$O(H_2O)_2^-$	52	2.69	-	2.70
CO_3^-	60	2.57	2.55	2.58
O_4^-	64	-	3.31	3.17
SF_6^-	146	-	-	2.08

rise to the apparent increase in mobility. Also the intensity of the SF_6^- ions is lower with the SF_6 drift gas. This may be due to the binary ionic recombination in the gas phase (29). The mobility of the negative reactant ions observed for air carrier gas with nitrogen, air, and sulfur hexafluoride as the drift gas are listed in Table II.

From this investigation, it is apparent that the negative ion mobility spectrum is dependent upon the nature of the drift as well as the carrier gas. For example, the examination of chlorinated compounds with plasma chromatography using air as the drift gas would have been complicated by the large mobility peak associated with the O_2^- ion. From this standpoint, the use of nitrogen as the drift gas was rather fortuitous. Also the negative ion mobility spectra associated with sulfur hexafluoride was a pleasant surprise. Because of its greater molecular weight and molecular size and because of its insulating characteristics, sulfur hexafluoride may prove to be of great value as a drift gas. Several other gases are now under investigation for use as carrier and drift gases in an effort to enhance the selectivity and sensitivity of the PC/MS technique.

ACKNOWLEDGMENT

The author expresses his appreciation to Gerald W. Peterson for programming the data acquisition and data analysis routines used in this study. The author is also indebted to Carl G. Majtenyi for the maintenance of the plasma chromatography–mass spectrometer instrument.

LITERATURE CITED

(1) H. E. Rivercomb and E. A. Mason, *Anal. Chem.*, **47**, 970 (1975).
(2) F. W. Karasek, *Anal. Chem.*, **46**, 710A (1974).
(3) R. A. Keller and M. M. Metro, *Sep. Purif. Methods*, **3**, 207 (1974).
(4) S. A. Benezra, *J. Chromatogr. Sci.*, **14**, 122 (1976).
(5) T. W. Carr, *J. Chromatogr. Sci.*, **14**, 85 (1977).
(6) R. A. Keller and M. M. Metro, *J. Chromatogr. Sci.*, **12**, 673 (1973).
(7) F. W. Karasek and D. A. Kane, *Anal. Chem.*, **46**, 780 (1974).
(8) F. W. Karasek and S. H. Kim, *Anal. Chem.*, **47**, 1166 (1975).
(9) F. W. Karasek, M. J. Cohen, and D. I. Carroll, *Anal. Chem.*, **43**, 390 (1971).
(10) G. W. Griffin, I. Dzidic, D. I. Carroll, R. N. Stillwell, and E. C. Horning, *Anal. Chem.*, **45**, 1204 (1973).
(11) F. W. Karasek, D. W. Denney, and E. H. DeDecker, *Anal. Chem.*, **46**, 970 (1974).
(12) R. A. Keller, *Am. Lab.*, **1975** (7) 35.
(13) D. I. Carroll, I. Dzidic, R. N. Stillwell, and E. C. Horning, *Anal. Chem.*, **47**, 1956 (1975).
(14) T. W. Carr, *Anal. Chem.*, **49**, 828 (1977).
(15) F. W. Karasek, S. H. Kim, and H. H. Hill, *Anal. Chem.*, **48**, 1133 (1976).
(16) E. W. McDaniel and E. A. Mason, "The Mobility and Diffusion of Ions in Gases", John Wiley and Sons, New York, 1973.
(17) E. A. Mason and H. W. Scharp, *Ann. Phys.*, **4**, 233 (1958).
(18) P. L. Patterson, *J. Chem. Phys.*, **56**, 3943 (1972).
(19) S. N. Lin, G. W. Griffin, E. C. Horning, and E. W. Wentworth, *J. Chem. Phys.*, **60**, 4994 (1974).
(20) A. V. Phelps and J. L. Pack, *Phys. Rev. Lett.*, **6**, 111 (1961).
(21) J. A. Ratcliffe and K. Weckes, "The Ionosphere in Physics of the Upper Atmosphere", Academic Press, New York, 1960.
(22) E. W. McDaniel, "Collision Phenomena in Ionized Gases", John Wiley and Sons, New York, 1964.
(23) L. M. Chanin, A. V. Phelps, and M. A. Biondi, *Phys. Rev. Lett.*, **2**, 344 (1959).
(24) M. J. Cohen and R. F. Wernlund, "Multiple Chemical Analysis with the Ion Molecule Reactor Mobility Spectrometer", presented at the 28th Pittsburgh Conference on Analytical Chemistry and Applied Spectroscopy, Cleveland, Ohio, Feb. 28–Mar. 4, 1977.
(25) M. Arshadi and P. Kebarle, *J. Phys. Chem.*, **74**, 1483 (1970).
(26) N. G. Adams, D. K. Bohme, D. B. Dunkin, F. C. Fehsenfeld, and E. C. Ferguson, *J. Chem. Phys.*, **52**, 3133 (1970).
(27) E. W. McDaniel and M. R. C. McDowell, *Phys. Rev.*, **114**, 1028 (1959).
(28) J. A. Morrison, D. Edelson, and K. B. McAfee, Fourteenth Annual Gaseous Electronics Conference, Schenectady, N.Y., October 31, 1961.
(29) M. J. Church and D. Smith, *Int. J. Mass Spectrom. Ion Phys.*, **23**, 137 (1977).
(30) S. H. Kim, K. R. Betty, and F. W. Karasek, *Anal. Chem.*, **50**, 2006 (1978).

RECEIVED for review December 6, 1978. Accepted February 9, 1979.

Light Intensity Measurements I: Large Area Bolometers with Microwatt Sensitivities and Absolute Calibration of the Rhodamine B Quantum Counter

D. G. Taylor[1] and J. N. Demas*

Department of Chemistry, University of Virginia, Charlottesville, Virginia 22901

A large area (1 inch × 1 inch) bolometer with microwatt sensitivity has been developed. Construction, calibration, and evaluation details are included. One of these bolometers was then used to calibrate the spectral responsivity of a Rhodamine B quantum counter (5 g/L in methanol). This counter is shown to be flat to ±2% over the 360–590 nm range.

Relative and absolute light intensity measurements are crucial for many spectroscopists, photochemists, and analytical chemists. For all but the most rudimentary relative intensity measurements, quantitative detectors are divided into two classes (1) thermal detectors and (2) quantum counters (*1, 2*). Thermal detectors which include bolometers, thermopiles, and pyroelectric radiometers, are thermally activated and respond by converting incident photons into heat by absorption in the sensor surface or volume. The incident flux is related to the sensor response to this heating. Bolometer, thermopile, or pyroelectric detectors sense temperature changes by variations in resistance, in developed EMF, or in capacitance, respectively. The key advantage of thermal detectors is that by making the absorber uniformly black at all wavelengths, the detector is energy flat in response (i.e., equal response for equal powers at different wavelengths) (*1–6*).

Spectroscopy, however, is more often concerned with the photon flux rather than the beam power. Only if the spectral distribution is known precisely, can the quantum flux be calculated from the incident power. Further, thermal detectors rarely have the large area, fast response time, sensitivity, or dynamic range required in spectroscopy. Although small in area (1 × 1 cm^2), the recently developed pyroelectric null radiometer avoids many of these problems (*3–6*).

Quantum flat quantum counter detectors (described below) have proved very useful in the spectral calibration of optical detectors and monochromator–source excitation systems, and the determination of absolute photoluminescence yields (*7, 8* and references therein). The first two calibrations are important in luminescence work to correct excitation and emission spectra. Absolute luminescent quantum yield determinations are hampered by the wavelength-dependent responses of photocells and phototubes while thermal detectors are not quantum flat and lack adequate sensitivity. Quantum counters avoid these problems.

An ideal quantum-flat detector is characterized by a response solely proportional to the incident photon flux regardless of its spectral distribution. Based on an idea of Vavilov (*9, 10*), Bowen (*11*) introduced a detector which very closely approximated this description. He gave the name "quantum counter" to the combination of an optically dense fluorescent screen placed before a phototube. The screen had a luminescence spectrum and quantum yield which was independent of excitation wavelength within its useful range. The phototube current was then directly proportional to the photon flux incident on the screen. Since this response was independent of wavelength within the useful range, the signal was proportional to the integral of the photon distribution incident on the counter which has led to the term "integrating screen". By combining a highly fluorescent dye counter and a photomultiplier, a very sensitive quantum-flat detector results.

The standard luminescent counter material for ~20 years has been the xanthene dye Rhodamine B (RhB) (*8, 12*) with a useful range from the UV out to ~600 nm. Luminescence research on red-IR emitting dyes and transition metal complexes has increased the need for quantum-counting materials with deeper red and IR sensitivity. In addition, the response of existing and new counters should be calibrated as accurately as possible.

This paper and the subsequent one (*13*) are devoted to the accurate calibration of several existing and some new quantum counter systems. This present paper describes the development, construction, and evaluation of large area (one square inch) bolometers. These bolometers are relatively simple and inexpensive to construct, may be built to accommodate almost any beam cross section, are sensitive (~10 μW), highly linear over more than a decade of intensity (5 ppt), and precise (3 ppt). One of these bolometers was used to recalibrate the RhB quantum counter with what we believe is the highest accuracy to date.

In the following paper (*13*), we describe the development and operation of a new design of quantum counter comparator. This system permits the rapid calibration of one optically dense quantum counter against another with a precision and accuracy of better than 0.5%. Using this comparator and the bolometer calibrated RhB counter, a critical evaluation of other RhB counters and of several new quantum counter systems is presented.

EXPERIMENTAL

Materials. The chemicals and solvent preparations are given in the subsequent paper (*13*).

Excitation System. The excitation source was a 1000-W Xe arc lamp run from an Oriel constant current power supply. The excitation beam was passed through 5 cm of aqueous $CuSO_4 \cdot 5H_2O$ (100 g/L) into an 0.25-m Bausch and Lomb grating monochromator (66 Å/mm resolution) equipped with an achromatic output lens. To further ensure low infrared stray light, an additional $CuSO_4$ solution filter (1 cm) was placed over the exit lens.

General Description of Bolometer. The bolometer sensor was a 1 inch × 1 inch square metal foil target with a positive temperature coefficient thermistor attached to it. The target was blackened to absorb and convert light energy into heat. The bolometer response was measured as the change in thermistor resistance upon irradiation. The bolometer was maintained at a constant temperature to minimize spurious signals and drift due to external temperature changes. Absolute calibration was achieved by electrical substitution whereby a known electrical power was dissipated on the target with a resistive heater. We

[1]Current address, School of Chemical Engineering, Purdue University, West Lafayette, Ind. 47907.

0003-2700/79/0351-0712$01.00/0 © 1979 American Chemical Society

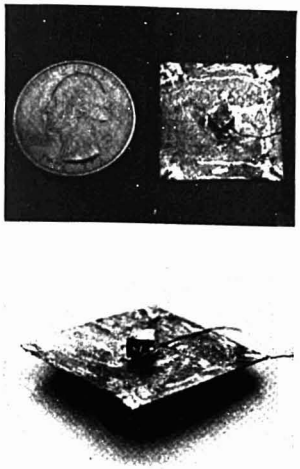

Figure 1. "U" bracket 1 inch × 1 inch silver foil bolometer sensor. (A) Back view. Thermistor is soldered inside "U" bracket at the top. The fine copper wires soldered at each corner are for mounting. (B) Details of thermistor and "U" bracket

now describe the bolometer target, the isothermal bolometer housing and temperature controller, and the performance of the system.

Bolometer Sensor. In our initial attempts at making large area sensors, we mounted thermistors directly onto the backs of 1 inch × 1 inch targets (thin aluminum sheet or 0.001-inch silver foil). Variations in surface sensitivity of the blackened sensor were probed with an ~1-mm diameter, 1-mW CW He-Ne laser. The sensitivity, which was ~10–20% less at the edges than directly over the centrally located thermistor, was inadequate for our work.

An improved version (~5% deviation) was obtained by mounting the thermistor on a small "U"-shaped silver bracket (Figures 1 and 2A) soldered onto the silver plate. The positive temperature coefficient (~20%/°C) thermistors in this and the subsequently described unit were from Pennsylvania Electronics Technology Inc. (Pittsburgh, Pa.) and gave 4–5 times the response of normal negative coefficient thermistors. These units were specially processed by the manufacturer for high resistances at their specified 30 °C operating point. One electrical contact of the thermistor bead was a flat copper surface which was sweat soldered onto the target, while a fine nickel wire made the other connection. A #40 enameled manganin wire calibration heater was threaded through the sensor plate (Figure 2A). The benzene-soot coated sensor was suspended by four #40 copper wires, one of which was used for a thermistor connection. The support wires were fastened onto an insulating support ring which was mounted on a $^1/_4$-inch copper plate by electrical standoffs (Figure 3). Entire sensor assemblies could then be interchanged in the bolometer head.

To further improve uniformity of surface sensitivity, the sensor of Figure 2B was constructed from 0.0025-inch copper foil. The rationale behind this design was to lengthen and increase the number of heat-flow paths to the thermistor. This detector surface was blackened with several thin coats of Krylon 1602 flat black spray paint which is much easier to apply and more durable than benzene soot. The maximum deviation in response across this device's surface was ~2.5%. For the relatively uniform ~$^3/_8$-inch diameter excitation beam used in the current work, response uniformity was probably an order of magnitude better and was deemed acceptable. This detector, shown in Figures 2B and 3, was used to calibrate the standard Rhodamine B quantum counter. Because of the fragile nature of the calibration heater mount, no attempt was made to convert this unit into an absolute bolometer.

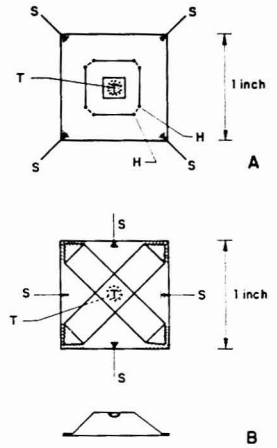

Figure 2. Diagram of bolometer sensing plates. (A) Absolute silver-foil (0.001-inch) sensing plate with manganin wire calibration heater. T-thermistor ("U" bracket as in Figure 1) and lead, H-manganin wire heater and leads, S-copper support wires and thermistor return lead, ////-solder connections. (B) Copper foil (0.0025-inch) sensor used in the RhB calibration. T-thermistor and lead, S-copper wires and thermistor return lead, ////-solder connections

Figure 3. Assembled copper foil sensor (Figure 2B) shown mounted on interchangeable copper plate with insulating plastic mounting

The thermistor resistances were measured with a Wheatstone bridge made from decade resistance boxes. Bridge power was from a 1.35-V RM42R Hg cell or from a 6-V lead acid battery with a series dropping resistor. The null detector was a Keithley Model 155 microvoltmeter.

The Bolometer Head. The bolometer head (Figure 4) was a solid aluminum cylinder $3^1/_4$ inches in diameter by 3 inches long. The ends were turned out to form two cavities $2^1/_4$ inches in diameter by $1^1/_8$ inches deep. The rear cavity housed a small signal preamplifier (See Figure 5) which was placed in the strictly temperature-controlled bolometer head to improve its already low (0.3 μV/°C) temperature drift. Head temperature was sensed by a Maier bridge (*14*) constructed from #40 copper wire (sensors R3 and R4) and #40 manganin (references R5 and R6) enameled wire wound around the forward section of the housing. The temperature control resistive heater (R15) was wound around the rear section of the head. A similar auxiliary heater was wound around the front section and was used to reduce the initial warm-up period. The thermal mass of the aluminum housing helped to smooth out heating and temperature variations at the detector.

The aluminum head was carefully isolated by an abundance of thermal insulation. The head was fit into two heavy woolen boot socks (large, Sears, Roebuck & Co.) to form six insulating layers except over the entrance window. This assembly was enclosed in a doubled up woolen stocking cap (R. W. Taylor,

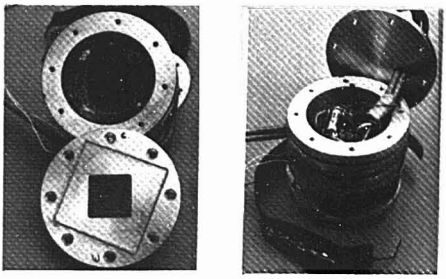

A B

Figure 4. Bolometer head. (A) Top view of bolometer head showing the sensor on interchangeable mount (Figure 3) installed, and the inner quartz window. (B) Rear view of the bolometer head showing the Maier bridge, preamplifier, and feedback network. The lower narrow winding is the auxiliary heater, the central broad band is the Maier bridge, and the upper narrow band is the control heater. The tape covered copper foil is an electrical shield which fits over the Maier bridge

Model 1974) and mounted snugly in a 1-foot cubic box made of $^1/_4$-inch plywood. The box was insulated inside by a minimum of 1-inch thickness of sheet Styrofoam. A $^1/_8$-inch thick quartz window on the head proper was complemented by a matching window at the light entrance to the box. This arrangement provided a very high thermal resistance which aided enormously in maintaining low background fluctuations. Heating power dissipated in R15 at 10 °C above room temperature was 2–3 W.

Temperature Controller. The proportional temperature controller was a modification of the design of West et al. (*15, 16*) (Figure 5). The Maier bridge sensor was wound on the outside of the sensor cavity of the aluminum head. The bridge imbalance corresponding to the temperature error was amplified by A1 (effective gain of $\sim 10^5$). Power for the bridge and preamplifier, heater current, and the boosted Maier bridge signal was passed through an umbilical cable to the main controller.

Ideally, the proportional temperature controller operated about the set point temperature of the copper–manganin bridge (i.e., the temperature at which the bridge imbalance is zero). The preamplified bridge imbalance was inverted (A2) with a gain of 5.6. A fraction of this amplified bridge imbalance voltage, adjustable by R2, was summed at unity gain by A3 with an adjustable bias set by R1. A3 controlled a current booster (T1 and T2) which varied the heating current supplied to R15 from a 15-V series pass voltage regulator (D, T3). One of the series resistors (R13) could be shunted to provide faster warmup while the other provided a measure of short circuit protection.

For optimum temperature control, R1 and R2 were adjusted after the head had equilibrated near the controller set point. R1 was adjusted to null M1 to within a few hundredths of a volt. R2 was then adjusted to increase the fraction of imbalance signal summed by A3 until any further increase caused the controller to oscillate. R1 and R2 interacted and several adjustments were initially required. The long response time of the system required $\sim$0.5–2 h for transient effects to subside after major adjustments, but, once adjusted, the system was stable for weeks. If power was interrupted for more than a few seconds, R2 was backed off and readjusted as the system again settled into the non-oscillatory operating range; therefore, the controller was run continuously in this work.

Measurement of the Reflectance of the Bolometer Absorber. The reflectance of Krylon 1602 flat black enamel was measured at 10-nm intervals using the Xe arc excitation system. An aluminum plate was blackened on one side with the paint and freshly smoked on the other with MgO. Excitation was normal to the surface, and reflected intensities were monitored at 45° (6 inches from the surface) using a United Detector Technology PIN 10DP photodiode operating as a current source. Currents were measured either directly on a Keithley Model 160 digital voltmeter, or after current-to-voltage conversion (Analog Devices 40 J operational amplifier with a 20-MΩ feedback resistor). At each wavelength, signals were measured for the MgO coated and the blackened sides of the plate with both in the same orientation. The reflectance of the enamel, $(r_{fb})_\lambda$ was the ratio of the

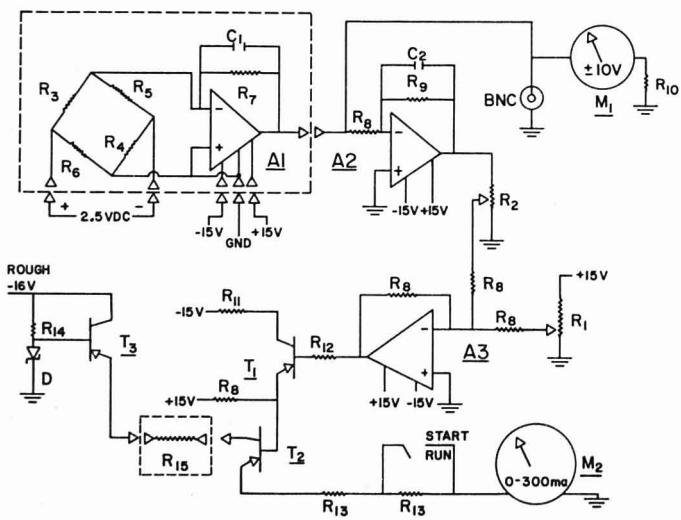

Figure 5. Schematic of the proportional temperature controller. Components within the dashed lines are located in or on the bolometer head. R1, 10-kΩ 20-turn trimpot; R2, 20-kΩ 20-turn trimpot; R3, 117-Ω #40 enameled Cu wire; R4, 117-Ω #40 enameled Cu wire; R5, 127-Ω #40 enameled manganin wire; R6, 116-Ω #40 enameled manganin wire; R7, 10 MΩ; R8, 100 kΩ; R9, 560 kΩ; R10, 10 k-Ω; R11, 1 kΩ; R12, 2.7 kΩ; R13, 10 Ω, 3-W; R14, 330 Ω; R15, 28Ω #40 enameled Cu wire; all resistors $^1/_4$ W unless specified. CI, 0.1 μF; C2, 0.047 μF; D, 1N4744 15-V Zener; TI, GE 22318; T2, T3, Sylvania ECG 121; A1, Analog Devices 233J; A2, A3, Analog Devices 741K. The 2.5 V is derived from a 7805 three-terminal regulator and a series dropping resistor

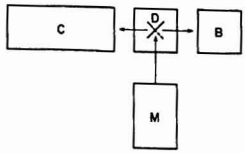

Figure 6. Schematic diagram of the Rhodamine B calibration apparatus. (B) Bolometer; (D) front surfaced deflection mirror; (M) excitation light source and monochromator; (C) comparator consisting of RhB counter cell and photomultiplier. (See Ref. 13 for details)

black-to-MgO photodiode signals at each wavelength; the paint and MgO are both near Lambertian reflectors, and MgO is a near perfect reflector over the wavelength range of interest (*17*, *18*).

Measurement of Window Transmittance. The transmittances of the bolometer windows and quantum counter cells were measured on a Cary 11 recording spectrophotometer using the 0–0.1 absorbance slidewire. In each case, the air vs. air spectrum was run at the same instrument settings and subtracted from the sample spectrum. The quantum counter cell contained methanol and the effective absorbance of a single cell window was taken as half the measured absorbance of the cell.

Absolute Calibration of Rhodamine B. The standard reference cell and solution of RhB (5 g/L methanol) was calibrated by measuring the responsivity of the quantum counter vs. the bolometer using the apparatus shown in Figure 6. This sealed cell and solution was also used throughout the quantum counter comparator measurements of the next paper. The excitation beam was alternately directed onto the quantum counter cell or the bolometer by means of a front surfaced mirror with adjustable positioning stops. Measurements were made at 10-nm intervals over the range 320–600 nm using a 19-nm (FWHM) optical slit width. This bandwidth was larger than that used with the quantum counter comparator (*13*) to provide measurable bolometer response at the spectral extremes.

The bolometer thermal time constant was ~30–50 s and, after a change in illumination, the resistance was stable to within ±2 Ω after ~3 min. Bolometer equilibrium was therefore assumed to attain within 4 min. Compensation for slow drifts in excitation intensity and bolometer temperature was effected by a semi-symmetrical dark–light–dark measurement cycle at each calibrated wavelength. Data collection efficiency was optimized through the multiple use of bolometer dark resistance values for base-line correction of adjacent illuminated bolometer readings. The complete measurement cycle required 8 min per calibrated wavelength and was subdivided into three periods of 2, 4, and 2 min, respectively. Figure 7 illustrates the measurement cycle for calibration at λ_i.

Upon entering Period #1 (from Period #3) the bolometer had only half completed equilibration to darkness so the average illuminated quantum counter signal $V_{1L}(i)$ was recorded in the interim. The bolometer dark resistance $R_{1D}(i)$ was then recorded and the excitation beam deflected to illuminate the bolometer, thus initiating Period #2. Quantum counter dark signal $V_{2D}(i)$ was recorded at Period #2 midpoint, and the bolometer illuminated resistance $R_{2L}(i)$ was recorded as Period #2 was terminated by illumination of the quantum counter. During Period #3 the average illuminated quantum counter signal at λ_i was again recorded as $V_{3L}(i)$. Period #3 ends by advancing the excitation wavelength to λ_{i+1}, thus restarting the measurement cycle at Period #1 for the new λ_{i+1}. As the cycle began again, the quantum counter was illuminated at λ_{i+1} and the bolometer was half equilibrated to darkness.

The bolometer response $(\Delta R/R_0)_{\lambda_i}$ and the quantum counter response $V(\lambda_i)$ were calculated using the following equations:

$$(\Delta R/R_0)_{\lambda_i} = \left\{\frac{R_{2L}(i)}{0.5[R_{1D}(i) + R_{1D}(i+1)]}\right\}^{-1} \quad (1)$$

$$\bar{V}(\lambda_i) = 0.5\,[\bar{V}_{1L}(i) + \bar{V}_{3L}(i)] - \bar{V}_{2D}(i) \quad (2)$$

Rhodamine B Calibration Data Treatment. $(\Delta R/R_0)_\lambda$ is directly proportional (see below) to the incident power. The quantum counter signal $V(\lambda)$ is proportional to the incident *number of photons* per unit time under the same conditions. Each $(\Delta R/R_0)_\lambda$ was converted to relative quanta per unit time by multiplying by λ. The apparent variation in relative luminescence quantum yield (quanta emitted per quanta absorbed) for Rhodamine B ($I'(\lambda)$) was calculated from

$$I'(\lambda) = V(\lambda)/[(\Delta R/R_0)_\lambda \cdot \lambda] \quad (3)$$

$I'(\lambda)$ was not the true relative luminescence quantum yield; the transmittances of the bolometer and quantum counter windows, and reflectance from the bolometer's black paint varied slightly with wavelength.

The true relative response of the quantum-counter quartz windowed dye-cell combination, $I_Q(\lambda)$, was obtained from

$$I_Q(\lambda) = I'(\lambda)\{(t_{bw})_\lambda^2[1 - (r_{fb})_\lambda]\}/N \quad (4)$$

where $(t_{bw})_\lambda$ was the transmittance of a single bolometer window at λ, $(r_{fb})_\lambda$ was the reflectance of the flat black paint at λ, and N was a normalization factor making $I_Q(\lambda)$ average unity over the wavelength range reported.

$I_Q(\lambda)$ represented the real responsivity of a quartz windowed RhB counter. The true relative luminescence quantum yield of Rhodamine B, $\phi(\lambda)$, differed slightly from $I(\lambda)$, because of variation in the transmittance of the quantum counter cell window, $(t_{CW})_\lambda$. $\phi(\lambda)$ is given by

$$\phi(\lambda) = [I(\lambda)/(t_{CW})_\lambda]/N' \quad (5)$$

where N' is a new normalization factor for $\phi(\lambda)$. Since t_{CW} increased by only ~0.3% from 360 to 590 nm, $I(\lambda)$ and $\phi(\lambda)$ differ only slightly.

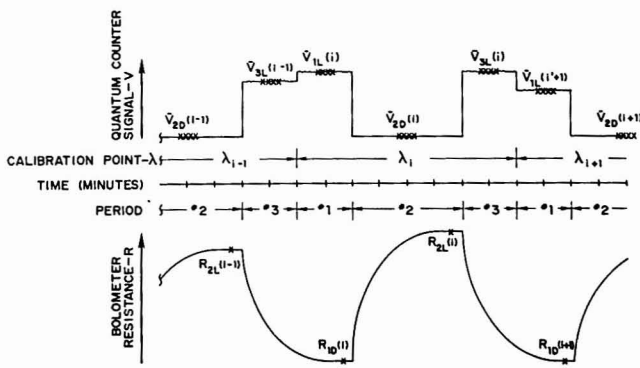

Figure 7. Measurement cycle for calibration of the standard RhB counter against the large area bolometer. X's indicate recorded measurements

RESULTS AND DISCUSSION

Bolometer-Controller Performance. The temperature controller's performance was judged by the drift in the bolometer's dark resistance vs. time. When fully equilibrated, detector drift over the ~12 min required for a dark, light, dark measurement cycle was at the very worst 300 μ°C and nominally 75–150 μ°C (~4-Ω maximum change in the 70-kΩ thermistor). The bridge noise corresponded to ~±2 Ω, so the temperature drift and measurement "noise" were comparable.

Using the detector with calibration heater, short term drift and noise corresponded to ~±5–10 μW of incident power. Also, this absolute version had constant sensitivity within 0.5% over the power range 300–4000 μW ($\Delta R/R_0$ ~ 0.2–4%) as determined using the internal calibration heater. The relative bolometer had very nearly the same sensitivity as the absolute one, and since the two thermistors came from the same supplier and batch, we assumed the relative bolometer to be equally linear over the same range of ($\Delta R/R_0$).

Over the region 340–590 nm in the RhB calibration, ΔR ranged over 400 to 2500 Ω. We estimated an upper bound on the measurement precision to be ±$^1/_2$% based on the null noise level of ±2 Ω. The mean relative deviation of the pairs of resistance changes

$$([R_{2L}(i) - R_{1D}(i)] \text{ and } [R_{2L}(i) - R_{1D}(i+1)])$$

in the RhB calibration (370–590 nm) was 0.17% for 23 measurements with 410 Ω ≤ ΔR ≤ 2530 Ω (mean resistance 1665 Ω). This mean relative deviation agreed quite well with an estimated mean uncertainty of 2/1665 = 0.12% using the 2-Ω observed noise level. Thus, the upper bound figure of $^1/_2$% is certainly conservative at the higher power levels.

We turn now to the bolometer accuracy, which we estimate at ~1–2%. The response of a thermistor is given by Equation 6 (*19*).

$$(R_T - R_0)/R_0 = (\Delta R/R_0) = \exp[B(T_0^{-1} - T^{-1})] - 1 \quad (6)$$

where R_0 and R_T are resistances at T_0 and T, respectively, and B is the thermistor sensitivity factor. When used over a narrow temperature range, the exponential can be expanded in a power series and truncated after the squared term to yield

$$(\Delta R/R_0) = B(T - T_0)/T_0^2 + (\tfrac{1}{2})[B(T - T_0)/T_0^2]^2 \quad (7)$$

For very small temperature changes, the second term may be ignored and ($\Delta R/R_0$) is proportional to $T - T_0$ and thus the incident power. For somewhat higher values of ($\Delta R/R_0$), the second term represents an error in the linearity of the bolometer response. The largest ($\Delta R/R$) encountered in the RhB calibration was ~3.6% ($T - T_0$ ~ 0.2 K), and our assumption of a linear power dependence in ($\Delta R/R_0$) is in error by no more than 2%. While Equation 6 is accurate over a wide temperature range for negative coefficient thermistors, it is not an exact representation of the actual sigmoidal R vs. T response of positive temperature coefficient thermistors. Thus, the real error was less than the maximum 2% figure derived above. The measurements made with the absolute bolometer suggest that the errors were, in fact, under 1%. Thus, we conservatively estimated our measurement accuracy in the RhB calibration at better than 2%.

Rhodamine B Calibration. The results of our bolometer calibration of the standard RhB (5 g/L in methanol) quantum counter are shown in Figure 8 and Table I. This counter was the one used as the reference counter in the following paper. $I_Q(\lambda)$ represents the responsivity of a quartz windowed counter; $\phi(\lambda)$ is the true relative luminescence yield corrected for cell reflections.

Quantum counters are most commonly used to calibrate the wavelength dependence of the intensities of spectral sources. The use of $I_Q(\lambda)$ and $\phi(\lambda)$ occurs in these calibrations

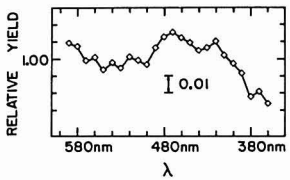

Figure 8. Relative variation in luminescence quantum yield $\phi(\lambda)$ of the rear viewed standard Rhodamine B counter (5 g/L) in methanol 1-cm optical path

Table I. Relative Response of a Standard Rhodamine B Quantum Counter[a]

λ, nm	$I_Q(\lambda)$	$\phi(\lambda)$
590	1.009	1.009
580	1.007	1.007
570	0.999	0.998
560	1.001	1.000
550	0.993	0.993
540	0.998	0.997
530	0.994	0.994
520	1.001	1.001
510	0.999	0.999
500	0.997	0.996
490	1.006	1.006
480	1.013	1.013
470	1.016	1.016
460	1.012	1.013
450	1.009	1.010
440	1.005	1.005
430	1.007	1.007
420	1.010	1.011
410	1.002	1.003
400	0.997	0.998
390	0.992	0.993
380	0.978	0.980
370	0.981	0.983
360	0.974	0.976

[a] Methanol solution of RhB (5 g/L).

in two different cases. The basic equations for the use of quantum counters are

$$V(\lambda) = KF_{ext}(\lambda)t_{CW}(\lambda)\phi(\lambda) \quad (8A)$$

$$= KF_{ext}(\lambda)I_Q(\lambda) \quad (8B)$$

$$= KF_{int}(\lambda)\phi(\lambda) \quad (8C)$$

where $V(\lambda)$ is the quantum counter's photomultiplier signal, K is a proportionality constant, $F_{ext}(\lambda)$ is the relative free air quantum flux of the source, $t_{CW}(\lambda)$ is the transmittance of the front window of the quantum counter cell, $F_{int}(\lambda)$ is the flux delivered to the sample within the quantum counter cell, and $\phi(\lambda)$ and $I_Q(\lambda)$ are as defined previously. Equation 8A is used to calculate the relative free air spectral distribution of the source given knowledge of the cell window transmittance and $\phi(\lambda)$. Equation 8B is used to directly calculate $F_{ext}(\lambda)$ when the quantum counter solution is contained in a high quality quartz cell as was used by us to obtain $I_Q(\lambda)$. Equation 8C yields the light flux delivered in a cell when the quantum counter and unknown solutions are contained in equivalent cells.

The $\phi(\lambda)$ vs. λ data yield a standard deviation (360–590 nm) of 1.04% about the mean with a maximum spread of 4.2%. As discussed above, we conservatively estimate our experimental precision to be ±0.5% except toward the long and short wavelength limits where our diminished arc intensity might increase errors slightly. The accuracy rests on the linearity of thermistor response, which we conservatively estimate to be 1–2%.

We believe that our present calibration is at least a factor of 2 more accurate and precise than previous thermopile calibrations. Errors in earlier calibrations accrued from the failure to correct for the reflection and transmission properties of the optical paths, the use of thermopiles, the variable collection efficiency of the detector, and purity problems with RhB (see ref. 13). Distortions in beam splitter systems can arise from variations in reflection coefficients caused by beam polarization. Thermopiles are small area detectors with very nonuniform sensitivities. Thus, even if the excitation beam underfills the thermopile sensor, changes in beam size with wavelength caused by chromatic optics (e.g., lens) produce differing sensitivity factors for the detector. For large area beams which overfill the sensor, chromatic aberrations in the optics produce large variations in the collection efficiency.

Thus, conditions such that a sampled beam accurately represents the whole beam are very difficult to obtain and verify. In the current measurements, however, the excitation optical train was relatively achromatic, optical losses were corrected, and the entire excitation beam was intercepted by both the quantum counter cell and a uniformly sensitive bolometer. Thus, this calibration makes a sound reference for the examination of other counter materials.

ACKNOWLEDGMENT

We gratefully acknowledge R. B. Martin for use of his Cary 11, E. D. West for the gift of the manganin wire, and A. Norvelle for his skill and assistance in machining the bolometer head.

LITERATURE CITED

(1) Parker, C. A. "Photoluminescence of Solutions"; Elsevier: New York, 1968.
(2) Calvert, J. G.; Pitts, J. N., Jr. "Photochemistry"; J. Wiley & Sons: New York, 1966.
(3) Geist, J.; Blevin, W. R. *Appl. Opt.* **1973**, *12*, 2532.
(4) Doyle, W. M.; McIntosh, B. C.; Geist, J. *Opt. Eng.* **1976**, *15*(6), 541.
(5) Geist, J.; Lind, M. A.; Schaefer, A. R.; Zalewski, E. F. "Spectral Radiometry: A New Approach Based on Electro-Optics"; *Natl. Bur. Stand. (U.S.) Tech. Note* **954**, 1977.
(6) Geist, J. *Natl. Bur. Stand. (U.S.) Tech. Note* **954-1**, June 1971.
(7) Demas, J. N.; Crosby, G. A. *J. Phys. Chem.* **1971**, *75*, 991.
(8) Melhuish, W. H. *J. Res. Natl. Bur. Stand., Sect. A* **1972**, *76*, 547.
(9) Vavilov, S. J. *Z. Phys.* **1927**, *42*, 311.
(10) Vavilov, S. J. *Z. Phys.* **1924**, *22*, 266.
(11) Bowen, E. J. *Proc. R. Soc. London, Ser. A* **1938**, *154*, 349.
(12) Melhuish, W. H. *N. Z. J. Sci. Technol., Sect. B* **1955**, *37*, 142.
(13) Taylor, D. G.; Demas, J. N. *Anal. Chem.*, following paper in this issue.
(14) Maier, C. G. *J. Phys. Chem.* **1930**, *34*, 2860.
(15) West, E. D.; Case, W. E.; Rasmussen, A. L.; Schmidt, L. B. *J. Res. Natl. Bur. Stand.* **1972**, *76A*, 13.
(16) West, E. D., National Bureau of Standards, Boulder, Colo., private communication, 1975.
(17) Killick, D. E.; Bateman, D. A.; Brown, D. R.; Moss, T. S.; de la Perrelle, T. E. *Infrared Phys.* **1966**, *6*, 85, Figure 10.
(18) Middleton, W. E. K.; Sander, C. L. *J. Opt. Soc. Am.* **1951**, *41*, 419.
(19) Gunn, S. R., *J. Chem. Educ.* **1973**, *50*, 515.

RECEIVED for review September 14, 1978. Accepted January 23, 1979. Support by the National Science Foundation (MPS 74-17916 and CHE 77-20379), the Air Force Office of Scientific Research (78-3590), the Research Corporation, and the donors of the Petroleum Research Fund, administered by the American Chemical Society, is gratefully acknowledged. This work was taken in part from the M.S. Thesis of D. G. Taylor at the University of Virginia, 1976.

Light Intensity Measurements II: Luminescent Quantum Counter Comparator and Evaluation of Some Luminescent Quantum Counters

D. G. Taylor[1] and J. N. Demas*

Department of Chemistry, University of Virginia, Charlottesville, Virginia 22901

The design, construction, and evaluation of a very precise and accurate instrument for comparing optically dense luminescence quantum counters is described. The system is capable of making intercomparisons with an accuracy and precision of better than 0.5%. A series of Rhodamine B, Rhodamine 6G, and blue dye quantum counters are calibrated over the 360–590 nm region. The Rhodamine B counters offer the best spectral flatness of response, but are sensitive to photolysis. The blue dyes, especially Nile Blue A, promise to extend quantum counting to ~700 nm.

The term "quantum counter" was originally used by Bowen in 1936 (*1*) to describe a spectrally flat quantum responsive detector composed of a fluorescent screen placed before a photodetector. Using a thermopile for the calibrations, his original measurements gave suitable results for a 1-mm thickness of crystalline uranyl ammonium sulfate in paraffin (252–436 nm) and aesculin (1-cm cell, 1 g/L in water; 252–367 nm), but not so for fluorescein owing to an absorption minimum around 367 nm. The independence of luminescence efficiency with wavelength, however, was a concept demonstrated qualitatively by Vavilov (*2*, *3*) a decade earlier. With great insight, Vavilov described the very application of this property which was developed by Bowen and Sawtell (*4*) and finds most extensive use today.

In 1955, Melhuish (*5*) introduced Rhodamine B (RhB) as a new quantum counter material which provided a useful range to ~600 nm. Using a standard lamp, he found that the luminescence yield of a front viewed 4 g/L solution in glycerol was wavelength independent with the exception of an ~5% reduction in yield around 450 nm. Weber and Teale (*6*) followed with a thermopile calibration of RhB (9.6 g/L in ethylene glycol) in a side viewed counter; they found a similar 10% reduction in yield at 440 nm (*6*). Melhuish (*7*), attributing this dip to the dye's absorption minimum, introduced a mixed-dye counter of acriflavin (1 g/L) and RhB (4 g/L). This system was based on the strong absorption of acriflavin at ~450 nm and its demonstrated efficient energy transfer

[1]Current address, School of Chemical Engineering, Purdue Univerity, West Lafayette, Ind. 47907.

0003-2700/79/0351-0717$01.00/0 © 1979 American Chemical Society

to RhB. This combination was not calibrated and has not found acceptance.

In his 1962 report describing a method for calibrating monochromator-photodetector systems, Melhuish (*8, 9*) again calibrated a RhB counter (3 g/L in ethylene glycol). The counter appeared flat (against a thermopile) to within ca. ±2–3% from 340–600 nm; however, this result is probably no more accurate than previous reports. Melhuish did not correct for the spectral variation in optical reflection, transmission, and polarization since these corrections were much less significant than his measurement uncertainty. Also, the source and purity of the RhB is reported only in the work of Weber and Teale. Taken together, the measurements by these workers do, however, set an upper bound on counter spectral uniformity at ~5–10%.

More recently Yguerabide (*10*) and later Demas (*11, 12*) calibrated a rear-viewed RhB counter (8 g/L in ethylene glycol) with thermopiles. Yguerabide found it flat to within ±4% from 250–600 nm with an estimated precision of ±2%. Demas checked the same counter system from 400–600 nm with an apparent precision and flatness of ±1.5%. Taking a different approach, Melhuish (*13*) and Velapoldi (*14*) examined optically dilute ($\sim 10^{-7}$ M, $A \leq 0.05$) dye solutions for their potential as luminescence emission standards. Their absorption and excitation spectra from 250–600 nm agreed to ca. ±5%. Aggregation effects at high solute concentrations (up to 0.01 M) preclude extending these results on monomeric solutions to optically dense counters. Their results do support, however, the fundamental premise of quantum counters: the luminescence quantum yield of suitable materials can be wavelength invariant.

More recent measurements by Melhuish strongly suggest a substantial dip (~6%) in the efficiency of RhB below 350 nm (*15*). Also, Cehelnik and Mielenz (*16*) have shown severe polarization and emission spectral changes with excitation wavelength for RhB in ethylene glycol. The latter workers have developed a long path "mushroom" shaped quantum counter cell to overcome these difficulties.

We present here the details of the development, construction, and evaluation of a new, very accurate quantum counter comparator. Using this comparator and our previous absolute calibration of RhB (5 g/L in methanol) (*17*), we then describe a critical evaluation of a number of RhB systems and the performance of some new dye counters which may prove suitable for the 600–700 nm region.

QUANTUM COUNTER COMPARATOR DESIGN CRITERIA

An ideal quantum counter comparator should have the following attributes: (1) simplicity of construction and low cost; (2) ease of operation; (3) extremely high reproducibility and insensitivity to the matching of components and optical alignment; (4) extremely high accuracy and elimination of all systematic errors; (5) versatility. We outline the considerations which led to our final design.

First, quantum counters can be viewed from either the front or rear surfaces. The optical density is usually large (≥99% absorption in the first millimeter); however, the counters absorption spectrum modulates the depth of excitation penetration with wavelength. Thus, for either viewing geometry, the emission path will vary with penetration depth. The penetration depth will usually vary by no more than a millimeter. For front viewing, however, this corresponds to large changes in the optical path length traversed by the emission to reach the detector (e.g., 0.01 vs. 1 mm). Since emission and absorption spectra typically overlap strongly for quantum counters, the fraction of the emission escaping the front face will then vary strongly with wavelength. Thus uncontrollable and unacceptable distortions of the response vs. wavelength can result. In marked contrast, a rear viewing detector sees only a very small fractional change in emission path length since the bulk of the cell thickness is always traversed (e.g., 9 vs. ~10 mm). See Ref. 16 for this concept pushed to the limit. Emission intensities observed at the rear face more accurately reflect variations in the luminescence efficiency. Rear viewing also protects against reflected or scattered source illumination; the counter is an excellent blocking filter to all wavelengths in its usable range. Thus, we considered the rear viewed detector essential to our design.

The method of optical comparison is crucial. A simple frequently used method is to measure the complete spectrum for one sample, change samples, then repeat the measurements on the second sample. Relative yields are then compared point-by-point. Large uncertainties can be introduced, however, from two difficultly controlled sources: (1) variations in excitation source flux between the two measurements and (2) irreproducibility of excitation wavelength selection. Most high-pressure arcs exhibit output fluctuations of 5% or more over an hour. Reproducible excitation wavelength selection is especially difficult in regions where the source spectrum contains sharp structure or the lamp intensity is changing rapidly with λ (e.g., toward the UV). We therefore rejected this approach for one in which the monochromator was set and measurements were made in quick succession on both samples at that wavelength.

Alignment and other systematic errors can be minimized by: (1) keeping the optical paths as direct as possible and (2) making the optical paths for the two samples identical if possible. Therefore, we avoided separate lenses, mirrors, and apertures in the samples' optical paths. This reduced optical component matching problems (there is no matching other than the cells) and corrections for their chromatic characteristics (*18*).

We envisaged two designs which incorporate these features. (1) Multiple detectors indirectly view sample emissions from the rear. Identical sample cell detector pairs are then placed alternately in the excitation beam. (2) A single detector sequentially views emissions from several samples. The samples are fixed symmetrically about the detector (i.e., the detector at the apex and samples around the base of a cone) and are moved selectively into the excitation beam.

We discarded the multidetector system. The added expense of multiple units and the problems of matching photodetector linearities made the single detector system much more appealing. Our design would thus be a rear viewed single detector comparator.

A very subtle error must be avoided in the cell compartment design. The cells must be completely masked around their rear margin. This masking prevents light pipe transmission of both excitation and emission light through the cell wall.

Although silicon photodiodes have been used with quantum counters (*19*), a photomultiplier tube (PMT) was the only suitable choice. Only PMTs have the necessary sensitivity for use with low intensity sources and low stray light optical systems. PMTs also have a large dynamic range and excellent linearity. For use with common red emitting quantum counters, the PMT should also have an extended red response. A large photocathode was considered essential to increase collection efficiency. We rejected the use of a lens to collect and focus the emission onto the detector because of optical alignment problems and variations in lens collection efficiency with wavelength (*18*).

The comparator design is rounded out by the selection of a method for measuring the PMT signal. PMT dark currents (typically nanoamperes at the maximum voltage rating) are generally orders of magnitude below the luminescence signals observed with a PMT matched to the emission region; this

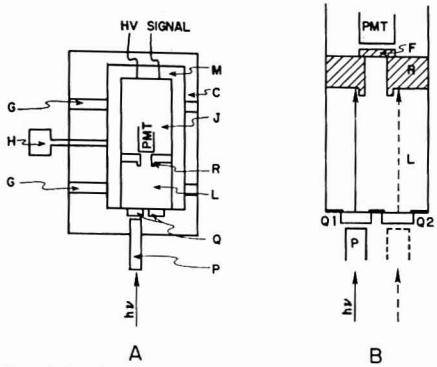

Figure 1. Top view of quantum counter comparator (A) with expanded view of cell holder in (B). PMT photomultiplier. (M) Kinematic mounting plate for holding photomultiplier and quantum counter assembly. (G) Guides for sliding M along. (H) External handle for positioning counter cells. (J) PMT housing (4 × 5 × 10 in. Budbox). (L) Quantum counter cell holder and optical baffling (4 × 5 × 6 in. Budbox). (Q) Quantum counter cells. (R) 2-in. spacer and internal light baffle for reducing transmitted excitation source to PMT. (P) Entrance pipe for light baffling. (F) Red pass blocking filter to further attenuate exciting light. Directly transmitted excitation did not strike the PMT

is the case in our comparator. Where the small dark currents are significant, emission data are easily corrected by subtraction. We therefore chose to make dc signal measurements, thus avoiding the use of ac techniques which in this case would add unnecessary complexity (e.g., chopper) and expense. Further, ac methods may introduce errors from chopper waveform shapes and poor linearity.

For accuracy and ease of measurement, we decided to use a digital voltmeter (DVM), thus reducing operator reading error and substantially improving accuracy over mechanical readouts. For our experiments, a potentiometer would have added negligible accuracy, and operator fatigue and the longer elapsed time of each measurement would probably have reduced precision and accuracy.

EXPERIMENTAL

Materials. Rhodamine B (Aldrich) was purified by repeated recrystallization from 1-propanol and from 2-propanol (cooled in dry ice); yield was ~70% after four recrystallizations. TLC (silica gel or neutral alumina plates, E. Merck; 1/8:v/v methanol–chloroform eluant) showed the eight to ten visible fluorescing impurities found in the commercial material to be effectively removed.

Eastman Rhodamine 6G (Rh6G) was purified by column chromatography (5 cm × 40 cm column of Sephadex LH-20 with methanol eluant). Two passes were required (~40–50% yield). TLC (alumina with methanol eluant) showed the purified dye to have only traces of colored or luminescent impurities.

Eastman Nile Blue A (NBA) was purified by two recrystallizations from chloroform (yield ~60%). The dye was chromatographically pure on TLC (silica gel, chloroform eluant).

Aldrich Methylene Blue (MB) and Eastman Azures A, B, and C (AzA, AzB, AzC) were examined by TLC (neutral alumina; 1/1:v/v methanol–chloroform). MB was relatively pure, but all attempts to further purify it by recrystallization and column chromatography failed. It was used as supplied. The Azures were very impure with at least five major components common to all including a major component of MB. All attempts at purification failed, and AzB was used as supplied.

Analytical Reagent grade anhydrous methanol, ethylene glycol, and distilled water were used without further purification.

Excitation System. The excitation system is described in the preceding paper (*17*).

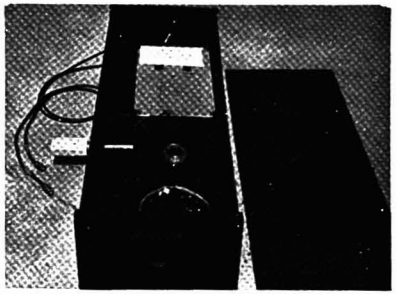

Figure 2. The quantum counter comparator apparatus, showing the PMT and cell holder mounted on a sliding, externally actuated tray. Excitation enters through the black tube at the bottom of the photograph

Comparator Construction. The comparator was constructed as shown in Figures 1 and 2. The PMT enclosure and cell holder (Budd Boxes) were mounted on a pine board equipped with guides which engaged a track perpendicular to the excitation beam. Travel was limited at both extremes so as to reproducibly center each cell in the excitation beam. The track was firmly attached to the base of the light-tight (tongue-and-groove construction) plywood box which completely surrounded the PMT enclosure and cells. All internal surfaces were generously painted with flat-black enamel. Cells could be exchanged swiftly (~1 s) and surely by means of a dowel connected to the sliding tray mount and passing to the outer side of the box.

The excitation beam was focused onto the cell face. A blackened entrance pipe, which extended to within ~1 cm of the cell face, blocked stray room illumination and minimized off-axis stray light from the monochromator and arc. The conduit arrangement ensured that only the cell in position was excited by the source. Direct PMT viewing of the excitation beam was prevented by symmetrical viewing from a PMT position off the excitation beam axis.

An RCA C7164R 5-cm diameter extended-red response (400–900 nm) photomultiplier gave good sensitivity to the dye emissions ($\lambda > 570$ nm). Emissions were viewed through a Corning 2-62 red pass filter (shortwave cutoff at ~610 nm). High voltage was supplied to the PMT by a very well regulated Pacific Photometric Instruments Model 200 variable supply.

Current was measured as the voltage developed across a 50-kΩ load resistor using a Heath UDI-905 DVM (resolution of 1 in 100 000). A matched pair of 1-cm optical path, 5-cm diameter "Quarasil" cells (Precision Cells, Hicksville, N.Y.) were masked around their diameter and window margins with black tape to prevent light piping and were used for all samples.

Comparator Measurement Procedure. The xenon arc and all electronics were allowed to warm up for at least 3 h. At earlier times, arc output variations (~5%) prohibited extremely precise measurements. After warmup, typical experimental uncertainty was 2–5 ppt. Unless otherwise specified, all comparisons were made against the same sealed RhB (5 g/L in absolute methanol) standard reference sample which was calibrated against the large area bolometer (see preceding paper (*17*)).

We selected methanol as the solvent because it is available in very high purity. Further, its viscosity is low which minimizes or avoids polarization errors; these include anisotropic emission and detection sensitivity variations with polarization. The work of Cehelnik and Mielenz (*16*) on RhB in the widely used ethylene glycol clearly justified our concern about the use of more viscous solvents.

All comparisons were made in a darkened room. At the maximum PMT voltage (1700 V), however, dark current (~0.2 nA) was unaffected by room lights or by probing the apparatus with a flashlight. This dark current was at least 100 times smaller than the weakest luminescence signal.

The monochromator was set to the source maximum at 466 nm (6.6-nm bandpass FWHM). The PMT voltage was adjusted to give a maximum of 20 μA.

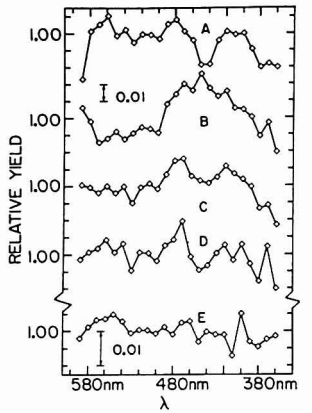

Figure 3. Wavelength dependence of the relative luminescence quantum yield of Rhodamine B quantum counters ($\phi(\lambda)$). (A) 8 g/L methanol; mean of two experiments. (B) 2 g/L methanol; single experiment. (C) 5 g/L ethylene glycol; mean of two experiments. (D) 8 g/L ethylene glycol; single experiment. (E) Identical RhB (5 g/L methanol) solution in both cells, single experiment; note expanded scale in E

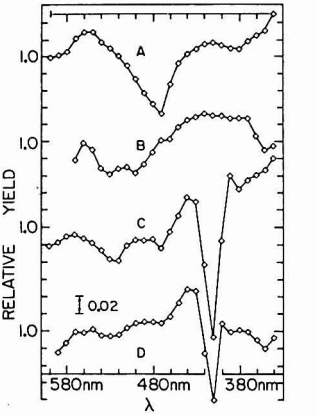

Figure 4. Uncorrected variation in relative quantum yield ($R(\lambda)$) of some organic dyes relative to Rhodamine B (5 g/L methanol). (A) Nile Blue A (2 g/L methanol); mean of two experiments. (B) Rhodamine 6G (5 g/L methanol); mean of three experiments. (C) Commercial Azure B (1 g/L methanol); mean of two experiments. (D) Commercial Methylene Blue (1 g/L methanol); mean of two experiments

Luminescence intensities were then measured for both cells at 10-nm intervals between 340–600 nm. With the wavelength set, 3 or more successive values taken about 3 s apart were read into an audio tape recorder for the first cell; the second cell was quickly positioned in the excitation beam (~1 s), and the process was repeated. A comparison required 45–50 s per wavelength. The next wavelength was selected, and the sequence repeated until a complete spectrum was recorded. Three to five readings were observed before data recording was begun. If instability was noted, the data for that wavelength were voided, and the full comparison was repeated. It was usual to experience about one arc flicker lasting ~2 min per hour of operation.

After recording one complete spectrum, the two cells were exchanged and the measurement sequence was repeated to obtain a second complete spectrum. A full comparison, consisting of two complementary spectra, required ~45 min. The raw data were later transcribed from the tape under more illuminated conditions.

Comparator Data Treatment. For the first cell arrangement, the sample-to-reference intensity $R(1,\lambda)$ was computed at each wavelength:

$$R(1,\lambda) = [(X_1 + X_2 + X_3)/(S_1 + S_2 + S_3)]_\lambda \quad (1)$$

where X and S refer to the dark current corrected detector signals of the unknown and standard, respectively. The data were normalized to yield $\bar{R}(1,\lambda)$ by

$$\bar{R}(1,\lambda) = R(1,\lambda)/M(1) \quad (2)$$

where $M(1)$ is the mean of $R(1,\lambda)$ for the region of best data (generally 340–580 nm).

These calculations were repeated for the second data set taken with the cells interchanged to yield $\bar{R}(2,\lambda)$. The final relative sensitivity $R(\lambda)$ of the unknown relative to the RhB standard was then calculated from

$$R(\lambda) = 0.5[\bar{R}(1,\lambda) + \bar{R}(2,\lambda)] \quad (3)$$

This calculation procedure minimized any possible contribution from nonsymmetric optical paths at the two cell positions. The above results are qualitatively interesting, but the true spectral luminescence responsivity of Rhodamine B must be known in order to interpret comparator results on an absolute basis. We accomplished this by measuring the response of the RhB standard reference counter against our bolometer (*17*). With this calibration, our RhB standard functioned as a transfer standard to rapidly relate the response of other luminescent materials to the bolometer, and thus measure their absolute spectral sensitivity or relative yield.

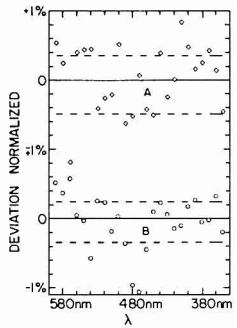

Figure 5. Reproducibility of Quantum Counter Comparator. (A) Agreement between cell positions $\{[\bar{R}(1,\lambda) - \bar{R}(2,\lambda)] \times 100\%\}$ obtained for Nile Blue A (2 g/L methanol) (Figure 4A). Dashed lines indicate mean positive (+3.53 ppt) and negative (−4.84 ppt) deviations; RMS deviation is 4.06 ppt. (B) Agreement between two separate experiments for Nile Blue A (2 g/L methanol) from two apparatus operators. Dashed lines as above: +2.35 ppt, −3.52 ppt; RMS is 2.91 ppt

RESULTS AND DISCUSSION

Figure 3 shows the relative quantum yield ($\phi_x(\lambda)$ vs. λ) of different RhB counters. All data were measured relative to the standard RhB counter calibrated in the preceding paper, and $\phi_x(\lambda)$ were calculated from

$$\phi_x(\lambda) = KR(\lambda)\phi_s(\lambda) \quad (4)$$

where $\phi_s(\lambda)$ is the relative quantum yield of the standard quantum counter sample (Table I, Ref. 17) and K is a normalization factor. Figure 4 shows $R(\lambda)$'s of several blue dyes and Rh6G. Figure 5A shows the equivalence of the two cell positions. Figure 5B shows the reproducibility for two different operators evaluating the same sample. Figure 6 shows the effect of photolyzing an RhB counter.

Because of the symmetrical arrangement of the two quantum counter cells, and the use of a single detector it is also easy to evaluate the relative sensitivities of different

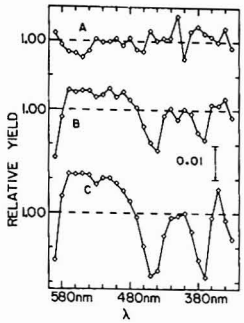

Figure 6. Relative luminescence yield ($R(\lambda)$) of Rhodamine B (5 g/L methanol) upon photolysis (4–5 mW at 467 nm). Data for each photolysis time are normalized to unity; luminescence yields between runs cannot be compared. Photolysis times: (A) 0 h. (B) 66 h. (C) 140 h

Table I. Relative Sensitivity of Organic Dye Quantum Counters[a,b]

Rhodamine B (2 g/L methanol)	1.71
Rhodamine B (5 g/L methanol)	1.00
Rhodamine B (8 g/L methanol)	0.49
Rhodamine B (5 g/L ethylene glycol)	0.92
Rhodamine B (8 g/L ethylene glycol)	0.61
Rhodamine 6G (5 g/L methanol)	1.67
Methylene Blue (1 g/L methanol)	0.064
Azure B (1 g/L methanol)	0.092
Nile Blue A (2 g/L methanol)	0.15

[a] Mean sensitivity over the 360–590 nm range compared to standard Rhodamine B (5 g/L MeOH) counter. [b] All counters 1-cm optical path and viewed from the rear. Emissions were viewed through a Corning C.S. 2-62 red-pass filter with a RCA C7164R photomultiplier tube.

quantum counters used in our configuration. Table I shows the sensitivity of the different dye systems relative to our standard RhB (5 g/L in methanol).

Estimation of Comparator Error. First, we consider the precision with which counters may be compared. An important test of comparator precision is the deviation of $R(\lambda)$ from unity for the comparison of identical samples. Figure 3E shows this comparison ($R(\lambda)$) for identical RhB counters (5 g/L in methanol), which yields an RMS deviation of 0.32%.

Next we examined the equivalence of the two cell positions $\{[\bar{R},\lambda) - \bar{R}(2,\lambda)] \times 100\%\}$. Figure 5A, derived from the raw data of Figure 4A, is representative. The distribution by sign (15 +'s, 10 −'s) and the signed average magnitudes (+3.5 ppt, −4.8 ppt) of $\{[\bar{R}(1,\lambda) - \bar{R}(2,\lambda)] \times 100\%\}$ reveal no strong distinction between the cell positions; this was reaffirmed by an average deviation of +0.18 ppt. The average RMS deviation between the two positions was 0.41% agreeing well with 0.32% obtained for identical counters (Figure 3E). While we could detect no significant bias toward either cell position, all results have been reported as the average of $\bar{R}(1,\lambda)$ and $\bar{R}(2,\lambda)$ as a precaution.

A similar analysis may be applied to independent comparisons performed by different operators to provide a different test of experimental reproducibility. Figure 5B shows the difference in $R(\lambda)$'s obtained by one of the authors (D.G.T.) and B. H. Blumenthal from comparisons made on the same day; the average of these comparisons is shown in Figure 4A. Again we detect no bias toward either experiment, and found quite acceptable reproducibility (0.3% RMS deviation) between experiments.

These results show the comparator to be remarkably insensitive to operator and experimental parameters. The precision of comparison is 2–5 ppt and represents substantial improvement in spectrofluorometric measurements of this type.

Rhodamine B Quantum Counters. Figure 3, A–D shows $\phi(\lambda)$ for several RhB solutions. Subtle changes in response occur with changes in solvent and concentration. Of particular interest are the changes in the 400–480 nm region. Melhuish (5) as well as Weber and Teale (6) noticed a decrease in the luminescence response in this region (5% and 10%, respectively, at 450 nm). The source and purity of Melhuish's RhB was not given; Weber and Teale used recrystallized "stock" RhB. As we shall show, sample impurity may well be the cause of these variations.

Our standard RhB counter was prepared from 4-week-old recrystallized RhB. This standard counter and the remaining RhB were used for the four months of this work. The commercial RhB contained 8–10 highly colored luminescent impurities. Freshly purified RhB showed only traces of these impurities. Pure solid RhB, however, upon standing in closed, clear glass containers under fluorescent room lights for eight weeks degraded to a purity only slightly better than the original unpurified dye. A high purity laser grade RhB (Exciton Chemical Co.) on hand for several months showed smaller amounts of similar impurities. Obviously, RhB is air, moisture, light, or thermally sensitive.

A counter solution identical in composition and from the same RhB sample as the standard counter was made up four weeks after the preparation of the standard. This freshly prepared counter has a sensitivity decrease of 1.5% at 450 nm relative to the standard counter. Thus, it appears that the crystalline material degrades faster than the 5 g/L methanolic solution.

In another experiment both counter cells were filled from the same freshly prepared solution of 5 g/L RhB in methanol using three-month-old purified crystalline RhB. The two counters were compared immediately, and again after one had been irradiated (~4–5 mW at 467 nm) for 66 h and still again after a total of 140 h of irradiation (Figure 6).

After 140 h of irradiation, TLC of the solutions showed the photolyzed solution to be enriched in the impurities. This result strongly indicates the origin of the previously observed sensitivity decrease at 450 nm and again demonstrates the quite remarkable sensitivity of the comparator for the detection of small changes in luminescent efficiency.

The major impurities in RhB observed by TLC luminesced in the blue-green region, which suggested that they absorbed strongly in the 300–450 nm region. RhB has absorption minima centered at 450 nm and 370 nm with $\epsilon \sim 5000\ M^{-1}\ cm^{-1}$. Thus, these impurities may absorb at the RhB absorption minima since these wavelengths both correspond to dips in the observed luminescence yield. If the impurities have ϵ's at 450 nm similar to RhB at its maximum ($\epsilon \sim 120\,000$ at 560 nm), then an impurity need only be present at 0.1% for it to absorb ~3% of the excitation in this region and decrease the luminescence yield a like amount. A photolysis quantum yield of 4×10^{-5} was calculated based on total impurities of 0.1% after the 140-h photolysis. This agrees qualitatively with the value of 10^{-5}–10^{-6} reported by Diennes (20). Agreement would be closer if the impurity absorbed less strongly than assumed. While overly simple, this model does qualitatively explain our results. The apparently more rapid degradation of the crystalline RhB material should also be kept in mind.

Thus, we believe that at least some of the luminescence efficiency variations of RhB counters are attributable to the differing purities of the counter solutions. At 450 nm, this effect is especially clear (see Figures 3A, C, D). RhB counters

may be even flatter than our data indicate because of the variable impurity levels and the fact that our standard had been photolyzed to some extent during the course of the measurements. A complete recalibration using freshly purified RhB would be highly desirable. Nevertheless, the observed flatness of $\phi(\lambda)$ is quite remarkable considering the probable variations in the solution compositions.

RhB can aggregate even at $\sim 10^{-4}$ M; several workers (*21–23*) have shown that in aqueous and ethanolic solutions the monomer–dimer equilibrium predominates. Since we see no appreciable differences in $\phi(\lambda)$ vs. λ with concentration and solvent, the RhB probably exists predominantly as a dimer at our concentrations. Because of polarization errors at high viscosity, however, we recommend using methanol or other low viscosity solvents. In part, many of the strange observations of Cehelnik and Mielenz (*16*) for RhB in ethylene glycol can probably be traced to polarization errors and the slow establishment of excited state conformational or chemical equilibrium; such problems would be minimized or eliminated in methanol.

Other Dye Counter Materials. Figure 4 shows the $R(\lambda)$'s of three blue dyes and Rhodamine 6G. Nile Blue A, an oxazine dye with an emission maximum at ~700 nm, gave a peak-to-peak variation in yield of ~10% (Figure 4A). This counter probably has a flatter response in the 600–700 nm region where the main absorption bands are located. It is also possible that a combination of dyes exhibiting energy transfer could be used to fill in the regions of low yield.

Rhodamine 6G, a xanthene dye related to RhB, luminesces at a slightly shorter wavelength than RhB. Rh6G seemed an ideal counter candidate. It is a better laser dye than RhB and exhibits higher luminescence yields. Its yield is virtually temperature independent as opposed to RhB (50% decrease from 19 to 50 °C (*24*). Unfortunately, as Figure 4B shows, Rh6G is more variable in response than RhB (7% vs. 4%) and yields only a minor increase in sensitivity (1.5 times) at the same concentration and with our filter detector combination.

Azure B (AzB) and Methylene Blue (MB) are very similar thiazine dyes which we have examined as suggested by Seely's (*25*) unchecked use of MB as a counter in the 550–700 nm region (Figures 4C, D). The absorption spectra of these dyes suggest their potential use as quantum counters with sensitivity well to the red of RhB. The gross decrease in emission intensity at 410 nm, however, greatly limits their usefulness as broad-band counters. They may, however be useful at longer wavelengths ($\lambda \leq 700$ nm), and indeed our results suggest their response may be flat to 500 nm rather than the 550 nm suggested by Seely (*25*). Use of binary dye mixtures may also extend the useful spectral region.

As expected, the lower luminescence yields of the blue dyes coupled with their emissions in the near-IR where our PMT is less sensitive makes them substantially less sensitive than the RhB and R6G counters. The blue dyes do promise use to $\lambda \leq \sim 700$ nm, however, which would represent a 100-nm improvement over the 600-nm limit of RhB. Further work is in progress.

CONCLUSIONS

A very precise method for the comparison of rear viewed optically dense quantum counter solutions was designed and implemented. An absolutely calibrated RhB standard (5 g/L in methanol) was then employed in the comparator to calibrate other dyes.

RhB counters were examined and found to have quite flat responses (±2%) for several combinations of solvent and concentration. The probable cause of past problems with RhB counters appears to arise from readily formed degradation products. We recommend that RhB counters be prepared from chromatographically pure, freshly purified crystalline material. Counter solution and solids should be stored in darkness.

Several organic dyes were examined for use as quantum counting materials. Nile Blue A and Methylene Blue show potential for use in the 500–700 nm region.

LITERATURE CITED

(1) Bowen, E. J. *Proc. R. Soc. London, Ser. A* **1936**, *154*, 349.
(2) Vavilov, S. J. *Z. Phys.* **1927**, *42*, 311.
(3) Vavilov, S. J. *Z. Phys.* **1924**, *22*, 266.
(4) Bowen, E. J.; Sawtell, J. W. *Trans. Faraday Soc.* **1937**, *33*, 1425.
(5) Melhuish, W. H., *N. Z. J. Sci. Technol., Sect. B* **1955**, *37*, 142.
(6) Weber, G.; Teale, F. W. J. *Trans. Faraday Soc.* **1957**, *53*, 646.
(7) Melhuish, W. H. *J. Phys. Chem.* **1961**, *65*, 229.
(8) Melhuish, W. H. *J. Opt. Soc. Am.* **1962**, *52*, 1256.
(9) Melhuish, W. H. *Rev. Sci. Instrum.* **1962**, *33*, 1213.
(10) Yguerabide, J. *Rev. Sci. Instrum.* **1968**, *39*, 1048.
(11) Demas, J. N., Ph.D. Dissertation, University of New Mexico, Albuquerque, N.M., 1970.
(12) Demas, J. N. "Creation and Detection of the Excited State", Vol. IV; Ware, W. R., Ed.; Marcel Dekker: New York, 1976.
(13) Melhuish, W. H. *J. Res. Natl. Bur. Stand., Sect. A* **1972**, *76*, 547.
(14) Velapoldi, R. A. *J. Res. Natl. Bur. Stand., Sect. A* **1972**, *76*, 641.
(15) Melhuish, W. H. *Appl. Opt.* **1975**, *14*, 26.
(16) Cehelnik, E. D.; Mielenz, K. D. *Appl. Opt.* **1976**, *15*, 2259.
(17) Taylor, D. G.; Demas, J. N. *Anal. Chem.*, preceding paper in this issue.
(18) Borresen, H. C.; Parker, C. A. *Anal. Chem.* **1966**, *38*, 1073.
(19) Amrein, W.; Gloor, J.; Schaffner, K. *Chimia* **1974**, *28*, 185.
(20) Melhuish, W. H. *Rev. Sci. Instrum.* **1968**, *39*, 1048, in Figure 4.
(21) Selwyn, J. E.; Steinfeld, J. I. *J. Phys. Chem.* **1972**, *76*, 762.
(22) Rohatgi, K. K.; Singal; G. S. *J. Phys. Chem.* **1963**, *67*, 2844.
(23) Rohatgi, K. K.; Singal, G. S. *J. Phys. Chem.* **1966**, *70*, 1695.
(24) Schwerzel, R. E. Abstract A2, The 12th Informal Conference on Photochemistry, Extended Abstracts, National Bureau of Standards, Gaithersburg, Md., 1976.
(25) Seely, G. R. *J. Phys. Chem.* **1969**, *73*, 125.

RECEIVED for review September 14, 1978. Accepted January 23, 1979. We gratefully acknowledge support by the National Science Foundation (MPS 74-17916 and CHE 77-20379), Air Force Office of Scientific Research (78-3590), the Research Corporation, and the donors of the Petroleum Research Fund, administered by the American Chemical Society. This work is taken in part from the M.S. Thesis of D.G.T. at the University of Virginia, 1976.

Calibration Curves with Nonuniform Variance

Lowell M. Schwartz

Department of Chemistry, University of Massachusetts, Boston, Massachusetts 02125

Methods are shown for calculating statistical uncertainties in the form of confidence limits for an assay obtained through a calibration curve of arbitrary form when the precision or variance of the data is nonuniform along the curve. Illustrative examples are based on photometric and chromatographic analyses. The ramifications of ignoring variance nonuniformity are discussed.

In a recent communication (*1*), it was shown how to find confidence limits for the quantitative analysis of an unknown sample determined by projecting its response measurement through a nonlinear calibration curve of arbitrary form. Several calculational methods were discussed but all were based on an assumption that the precision of the data points was uniform along the calibration curve, the so-called "homoscedastic" or uniform variance condition. Although this assumption is a valid one for many analytical procedures, there are several for which it is not. These include all methods based on counting measurements (*2*), either photon or radioactive, and also photometric and chromatographic analyses under certain conditions. It is the purpose of this paper to offer means of extending the previously discussed methods to cases such as these, i.e., those for which the data points along the calibration curve are inherently nonuniformly precise, the "heteroscedastic" or nonuniform variance condition. An extensive literature exists on statistical treatments of this same problem in radioligand assay (*3*, *4*), i.e., radioimmunoassay (RIA) and immunoradiometric assay (IRMA).

SUMMARY OF UNIFORM VARIANCE TREATMENT

An understanding of the complications caused by nonuniformity of variance requires a brief reiteration of the principles involved in calculating confidence limits in the homoscedastic case. The notation used here is the same as that used previously (*1*). A calibration curve $y_{cal}(x)$ is constructed by measuring the responses y_i of n standard samples having concentrations x_i. Each such standard may be measured repeatedly n_i times. Then samples having unknown concentrations X_i are each measured N_i times generating response data Y_i. An unknown X_i is found in the usual way by projecting the mean $\bar{Y}_i$ of the N_i replicates through the calibration curve and onto the x-axis. If both y_i and Y_i are normally (gaussian) distributed random variables, then confidence limits for X_i at a prescribed level of significance α are calculated by finding two values of X which satisfy the equation

$$[\bar{Y}_i - y_{cal}(X)]^2 = t_\alpha^2 \, \mathrm{var}[\bar{Y}_i - y_{cal}(X)] \qquad (1)$$

The statistic t_α is selected from a Student's t-table using the level α and the number of degrees of freedom inherent in the variance. The development of Equation 1 requires no assumption as to the uniformity of variance along the calibration curve.

It is now assumed that all standard samples y_i and unknown responses Y_i have the same precision so that each such measurement is a random variable drawn from a population having variance σ^2. In many cases σ^2 is not known to the analyst and so must be estimated as the sample variance s^2 from the experimental data at hand. Equation 2 of Reference 1 is used to calculate s^2 by pooling the replicate measurements made on all the samples. An important ramification of the homoscedastic condition is that s^2 then enters into the variance on the right-hand side of Equation 1 as shown explicitly in Equations 5, 9, and 12 of Reference 1. Yet if the y_i and Y_i have nonuniform variance, there exists no such common population variance σ^2, Equation 2 of Reference 1 is irrelevant, and we must find another means of calculating the variance in Equation 1.

A second problem arises if the calibration curve is to be constructed as a polynomial function (*1*) for which the degree is selected using statistical fitting criteria. If a value of s^2 is available from Equation 2 or Reference 1, then the appropriate polynomial is selected as the one with smallest degree for which the variance of residuals of the y_i data points about $y_{cal}(x)$ is near s^2. Alternatively, if s^2 is not available because of insufficient replication, polynomials of increasing degree are fitted and F-tests on the successive residual variances can select the minimum degree for which lack-of-fit has been eliminated. The F statistic, however, is the ratio of two sample variances drawn from a common population and this procedure, as well as the former alternative, rests upon the existence of a uniform variance. Without this condition, some other method must be developed to select the appropriate polynomial degree.

THE VARIANCE FUNCTION

The heteroscedastic condition implies that the variances of points change in a regular way along the calibration curve and so the population variance at a particular point σ_i^2 can in principle be expressed as a function of y_i or x_i. The analyst must have prior knowledge that the data have nonuniform variance, for experience has shown that this condition cannot be determined from a limited number of measurements (*3*). The paper by Rodbard et al. (*4*) serves as a typical illustration of the extensive statistical experimentation required to establish the nature of the variance function. The prior knowledge may be theoretical as may be the case in a counting method for which the variance of a count, if determined by the Poissonian distribution, is exactly equal to the expected count. On the other hand, the variance function may be the result of extensive replication experiments. In either case, this function serves as the basis of the right-hand side of Equation 1 and so the associated number of degrees of freedom is infinite if the function is theoretical or very large otherwise. We will also allow the possibility that the variance function involves an unknown multiplying factor.

Finally, we will regard the variance of measurements y_i as being inherently a function of the measurement (y) rather than of the concentration (x). It is important to make this choice even though either could be regarded as the independent variable for this function since y and x are interdependent through the calibration curve. Had we regarded σ^2 as an inherent function of x, $\sigma_i^2(x_i)$ would be determinate (not random) because x_i values are not random variables. The choice that σ^2 be a function of y makes the calculations more difficult but is more realistic. The variance of a measurement logically depends on the measurement itself, not on some other

0003-2700/79/0351-0723$01.00/0 © 1979 American Chemical Society

experimental factor that influences the level of the measurement. The difficulty arises because to evaluate $\sigma_i^2(y)$ for a given standard sample using $y = \bar{y}_i$, the mean of a few replications, leads to spuriously erratic $\sigma^2(y)$ behavior. Instead $\sigma^2(y)$ should be smoothed by using the expected value of y, i.e., the mean of a great many replications. Because of practical limitations, however, this information is not available and so the next best recourse is to base $\sigma_i^2(y)$ on the predicted value of y for a given x_i, which is $y_{cal}(x_i)$. But at the start of a calculation, the function $y_{cal}(x)$ involves at least unknown parameter values and perhaps also a yet undetermined number of terms. Thus an iterative procedure is required since $y_{cal}(x)$ depends on evaluations of $\sigma_i^2(y)$ and σ_i^2 depends on $y_{cal}(x_i)$. Nevertheless, we have a variance function $\sigma^2(y)$ which is either completely specified or of the form

$$\sigma^2(y) = V\phi(y) \tag{2}$$

where $\phi(y)$ is a completely specified function and V is a constant multiplier whose value in any particular calibration experiment is unknown.

DETERMINING THE CALIBRATION CURVE

The calibration curve is constructed from the n calibrating points $\bar{y}_i$ vs. x_i by the method of least-squares. Weighting factors w_i must reflect the number of replications n_i and also the variance at the locality of the point so that

$$w_i = n_i/\sigma_i^2 \tag{3}$$

The sum to be minimized is

$$S = \sum_{i=1}^{n} \frac{n_i}{\sigma_i^2}[y_{cal}(x_i) - \bar{y}_i]^2 \tag{4}$$

and minimization is understood to be with respect to adjustable parameters in the $y_{cal}(x)$ function. Brownlee (5) shows how to calculate the parameters a and b and the parameter variances for the particular case of a linear calibration line $y_{cal} = a + b(x - \bar{x})$ and with variances σ_i^2 completely known (5, Section 11.12) or with variances involving an unknown multiplying factor (5, Section 11.13). Brownlee obtains the parameter variances using analysis-of-variance which we will follow. Previously (1) we offered three strategies for dealing with general nonlinear calibration curves: a linear segmented approximation, a three-parameter nonlinear function of specified form, and a polynomial function of adjustable degree but, in the following development, we abandon the linear segmented method because of its crudity.

TWO- OR THREE-PARAMETER FUNCTION OF SPECIFIED FORM

As previously (1) we assume a three-parameter equation $y_{cal} = \bar{y} + c_1(x - \bar{x}) + c_2[f(x) - \bar{f}]$ where $f(x)$ is a nonlinear function specified by the analyst as representing the curvature of his particular line and c_1 and c_2 are adjustable parameters to be determined by multiple regression techniques. It will also be convenient sometimes to omit the linear term and use the two-parameter model $y_{cal} = \bar{y} + c_2[f(x) - \bar{f}]$. If this is done, several formulas given in Reference 1 are changed and these are that in addition to $c_1 = \text{cov}(c_1, c_2) = 0$,

$$c_2 = S_{fy}/S_{ff} \tag{5}$$

and

$$\text{var}(c_2) = \sigma^2/S_{ff} \tag{6}$$

When the variance is nonuniform, these equations and those for the three-parameter model require some modifications. The weighting factors w_i (simply equal to n_i for uniform variance) are given by Equation 3 with σ_i^2 evaluated as $\sigma^2[y_{cal}(x_i)]$ or by $\phi[y_{cal}(x_i)]$ if the multiplier V is unknown. The formulas for c_1 and c_2 are unchanged, but the constants σ^2 which appear in the formulas for var (c_1), var (c_2) and cov (c_1, c_2) are replaced by unity if the variance function is completely specified (5, Section 11.12). If V is not known a priori, it must be estimated from the sum of weighted residuals about the calibration curve and the values of V so determined then replace the constant σ^2 in the parameter variance formulas. Following Brownlee (5, Section 11.13), if p is the number of terms in the model equation (2 or 3), the sum S of Equation 4 is distributed as the product of V and the chi square statistic with $(n - p)$ degrees of freedom, $V\chi^2(n - p)$. The expected value of S is $V(n - p)$ and, therefore, $V = S/(n - p)$ is the estimate of σ^2 required. The sum S is evaluated with the calibration curve as found by regression. But, as mentioned above, an iteration is necessary since the parameters c_1 and c_2 cannot be found without w_i and w_i cannot be calculated without $\sigma^2[y_{cal}(x_i)]$ which involves c_1 and c_2. It is, nevertheless, a simple matter to program a computer to begin with provisional $w_i = n_i$, find c_1 and c_2 on this basis, recalculate $w_i = n_i/\sigma_i^2$, and reiterate until c_1 and c_2 cease to change.

POLYNOMIAL FUNCTION OF UNSPECIFIED DEGREE

A calibration curve is sought in the form of a polynomial of degree m expressed either as a power series or as a linear combination of orthogonal polynomials. The degree is selected to fit the curvature of the calibrating data to statistical criteria which, for data of uniform variance, are based on that variance. If the variances are nonuniform and completely specified, the sum S of Equation 4 follows a chi square distribution with $(n - m - 1)$ degrees of freedom provided that the scatter of data points about the calibrating polynomial is random, i.e., has no systematic error component due to lack-of-fit. Therefore, we may adopt a strategy, analogous to F-testing in the homoscedastic case, of calculating a series of calibrating polynomials with degrees from 1 to $(n - 2)$ and calculating S for each. To test a given polynomial, we make the null hypothesis that the corresponding sum S is distributed as χ^2, adopt, say, a 95% confidence level for the test, and compare S with $\chi^2(n - m - 1)$ from a table of probability points at $\alpha = 0.05$. If the tabulated χ^2 exceeds S, we reject the null hypothesis and assume lack-of-fit as the cause. The polynomial of least degree for which $\chi^2 \leq S$ is selected. The power series or orthogonal polynomial coefficients and their variances are then available from the polynomial fitting routines.

Again each polynomial in the test series requires an iteration involving w_i as described but this is not difficult. A less tractable problem arises though if the multiplier V is not known and is, therefore, omitted from w_i. The resulting sum S is distributed as $V\chi^2(n - m - 1)$ which quantity is useless for χ^2 testing. This author knows no method of circumventing this problem and hopes that some reader with greater knowledge of statistical techniques will offer a solution. Meanwhile, we cannot proceed to select the degree of a calibrating polynomial from data at hand when the response variances are nonuniform yet dependent on an unknown multiplying factor.

CALCULATING CONFIDENCE LIMITS

Two confidence limits for an assay X_i are found as two appropriate values of X which satisfy Equation 1. A most important feature of this equation is that the right-hand side includes var ($\bar{Y}_i$), the variance of the mean of N_i response measurements made on the unknown. Whereas for a homoscedastic case, this quantity depends only on N_i and the constant σ^2, for a heteroscedastic case it depends on the location of $\bar{Y}_i$ along the calibration curve. This dependence is expressed as

$$\text{var}(\bar{Y}_i) = \frac{\sigma_i^2}{N_i} = \frac{\sigma^2[y_{cal}(X)]}{N_i} \tag{7}$$

which shows its explicit dependence on X, a confidence limit yet to be found.

The other variance term on the right-hand side of Equation 1 depends on the nature of the calibration curve and on whether or not an unknown multiplier V is involved in the variance function. If $\sigma^2(y)$ is completely specified without an unknown V, a three-parameter calibration curve leads to

$$\text{var}\,[y_{cal}(X)] = \frac{1}{\nu} + (X - \bar{x})^2\frac{S_{ff}}{\Delta} + [f(x) - \bar{f}]^2\frac{S_{xx}}{\Delta} - 2(X - \bar{x})\,[f(X) - \bar{f}]\frac{S_{fx}}{\Delta} \quad (8a)$$

a two-parameter model leads to

$$\text{var}\,[y_{cal}(X)] = \frac{1}{\nu} + [f(X) - \bar{f}]^2\frac{S_{fy}}{S_{ff}} \quad (8b)$$

and a polynomial of degree m to

$$\text{var}\,[y_{cal}(X)] = \sum_{j=0}^{m} [P_j(X)]^2\,\text{var}\,(a_j) \quad (8c)$$

In these expressions, weighting factors are

$$w_i = n_i/\sigma^2[y_{cal}(x_i)] \quad (9a)$$

If, however, $\sigma^2(y) = V\phi(y)$ and V is found from the residuals of calibrating points about the line, then weighting factors are

$$w_i = n_i/\phi[y_{cal}(x_i)] \quad (9b)$$

and Equations 8a and 8b are modified by multiplying the right-hand sides by V. These options are summarized by writing Equation 1 in the alternative forms A calculation

$$[Y_i - y_{cal}(X)]^2 =$$

$$\begin{cases} t_\alpha^2\left(\dfrac{\sigma^2[y_{cal}(X)]}{N_i} + \text{var}\,[y_{cal}(X)]\right) & (10a) \\ t_\alpha^2 V\left(\dfrac{\phi[y_{cal}(X)]}{N_i} + \text{var}\,[y_{cal}(X)]\right) & (10b) \end{cases}$$

is done using Equations 10a, 9a, and any one of 8a, 8b, or 8c or it is done with Equation 10b, 9b, and 8a or 8b. Either form of Equation 10 can be solved numerically or graphically as the intersection of the horizontal line $y = \bar{Y}_i$ with two confidence bands as shown previously (*1*).

ILLUSTRATIVE EXAMPLE 1

Although photometric analysis is normally done under conditions which yield a linear calibration line due to Beer's law and uniform variances, we have deliberately chosen an experiment which is more complicated so that it may serve as an example of the methods described here. The system is aqueous copper(II) chloride, which in the near ultraviolet has an absorption band severely deviating from Beer's law so that a calibration curve of absorbance A vs. formal concentration at a fixed wavelength in this band is distinctly nonlinear as is shown in Figure 1.

The variance of an absorbance measurement is due to many sources of variability but we can classify these into those associated with sample preparation and those arising within the spectrophotometer itself. If standard samples are prepared by diluting a known stock solution into volumetric flasks using transfer pipets of differing volumes, the variance due to this operation is more-or-less uniform if the pipet volume range is not excessive. However, nonuniform variance is introduced if the photometer noise level is roughly independent of transmittance because the absorbance is a logarithmic transformation of transmittance and, hence, its variance cannot be uniform. In order to ensure that the overall variance

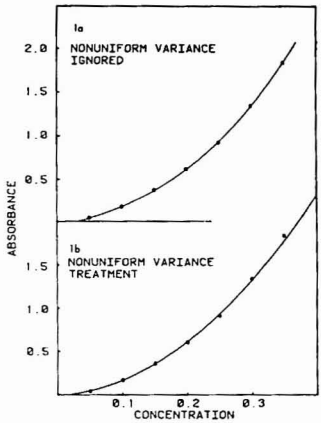

Figure 1. Illustrative Example 1: Potentiometric calibration curves fit to the data given in Table I. Figure 1a is a cubic polynomial obtained by F-testing (*1*) but ignoring variance nonuniformity. Figure 1b is the quadratic polynomial Equation 12 fit to the same data by χ^2-testing and taking into account the variance function Equation 11

of absorbance vs. concentration be nonuniform, one simply reduces the spectrophotometer slit width to increase the dynode voltage which increases the noise level. When the variance due to this noise is large enough compared to the sample preparation variance, the overall variance is nonuniform and the calibration data are thus heteroscedastic.

The proper statistical procedure for determining the variance function is to prepare many (perhaps 20 or more) replicate standard samples at each of several (perhaps 6 or more) concentration levels and record a single instantaneous absorbance reading A for each such sample. These measurements (perhaps 120 or more) are then studied to deduce the manner in which var (A) actually varies with the A level and this would constitute the desired variance function. Since the purpose here is not to find a truly accurate representation of the variance function but to demonstrate a calculational method, this procedure was shortcut in the following manner. A series of 20 replicate solutions was prepared at the same concentration level and the absorbance of each of these was recorded using a Beckman ACTA C III spectrophotometer set at 330 nm and with the slits sufficiently wide (0.40 mm) that the noise level was minimal and easily time-averaged. The variance s_c^2 of these 20 was 43. × 10^{-6}, and this was presumed to be due only to sample preparation variability. Then a second series of seven solutions ranging in absorbance from 0.05 to 2. was measured at 330 nm with the slit width reduced to 0.025 mm. In this series, however, 20 instantaneous absorbance readings were recorded from the fluctuating digital display for each solution. The variances $s_n^2(A)$ so recorded were due to spectrophotometric noise and appeared to increase exponentially with absorbance level. A plot of log $s_n^2(A)$ vs. A yielded a good straight line represented by $s_n^2(A) = 17.7 \times 10^{-6} \exp(3.05\,A)$. We then hypothesized that a calibration curve constructed by making a single instantaneous absorbance reading under narrow slit conditions for each of several standard solutions prepared as in the first series above would have a variance function given by

$$\sigma^2(A) = s_c^2 + s_n^2(A) = 43. \times 10^{-6} + 17.7 \times 10^{-6} \exp(3.05\,A) \quad (11)$$

The calibrating data recorded in this way are given in Table

Table I. Illustrative Example 1: A Photometric Calibration Experiment[a]

calibrating data: concentration, x_i	calibrating data: absorbance, y_i	absorbance, Y_i	concentration, X_i	95% confidence limits		(interval)	true X_i
		"Unknowns" Treated Using Variance Function Equation 11					
0.050	0.042	0.172	0.1017	0.0954	0.1079	(0.0125)	0.100
0.100	0.170	0.619	0.2014	0.1965	0.2064	(0.0099)	0.200
0.150	0.361	1.318	0.2995	0.2915	0.3092	(0.0177)	0.300
0.200	0.606						
0.250	0.913	"Unknowns" Treated by Methods of Reference 1 Ignoring Variance Nonuniformity					
0.300	1.339	0.172	0.0993	0.0889	0.1092	(0.0203)	0.100
0.350	1.840	0.619	0.2029	0.1976	0.2082	(0.0106)	0.200
		1.318	0.2985	0.2950	0.3019	(0.0069)	0.300

[a] Single instantaneous absorbance measurements of aqueous $CuCl_2$ are taken at 330 nm using a Beckman ACTA C III spectrophotometer with slits set at 0.025 mm.

Table II. Illustrative Example 2: Gas Chromatographic Quantitative Analysis[a]

calibrating data: injected charge, x_i	calibrating data: peak height, y_i	calibrating data: replications n_i	peak height, Y_i	charge, X_i	95% confidence limits		(interval)	true X_i
			"Unknowns" Treated Using Variance Function Equation 13					
0.564	1.433	1	1.433	0.551	0.486	0.625	(0.139)	0.564
1.107	3.00	1	9.24	3.358	3.052	3.734	(0.682)	3.44
1.715	4.90	3	16.47	5.956	5.407	6.630	(1.223)	5.73
2.27	6.10	4						
2.28	7.85	4	"Unknowns" Treated by Methods of Reference 1 Ignoring Variance Nonuniformity					
3.44	9.51	8						
4.61	12.78	4						
5.16	13.89	4	1.433	0.532	0.213	0.843	(0.630)	0.564
5.73	15.97	4	9.24	3.362	3.065	3.658	(0.593)	3.44
			16.47	5.980	5.675	6.292	(0.617)	5.73

[a] Data are taken from Reference 7, Figure 4.

I together with response measurements also taken singly on three "unknowns" with narrow slit width setting. The determinations of unknown concentrations and 95% confidence limits were calculated from these data using a polynomial calibrating curve and the variance function in Equation 11. This polynomial is

$$y_{cal} = -0.01072 + 0.4407x + 13.34x^2 \quad (12)$$

and is plotted in Figure 1b. A polynomial of degree 2 was chosen because with four degrees of freedom (seven data points less three parameters), the 5% tail of the chi square distribution is greater than $\chi^2 = 9.5$ whereas this polynomial yielded a weighted sum of squares $S = 3.1$. The conclusion is that lack-of-fit cannot be justified, whereas when a polynomial of degree 1 was tried, S greatly exceeded χ^2. Equation 12 was used to find the unknown concentrations for the three unknown responses and Equation 10a was used to find the 95% confidence limits on these concentrations. The results are shown in Table I. In Equation 10a, $t_{0.05} = 1.960$ was selected corresponding to infinite degrees of freedom because of $\sigma^2(A)$ of Equation 11 represents the combined results of 160 measurements. Finney (6) discusses the problem of combining heteroscedastic variances and advises that using infinite degrees of freedom cannot be seriously in error when this many measurements are taken.

ILLUSTRATIVE EXAMPLE 2

Bocek and Novak (7) report that gas chromatographic quantitative analysis may under certain conditions involve nonuniform variance. The second illustrative example is based on such a case where the calibration curve is constructed by measuring the peak heights corresponding to different injected molar charges of benzene. The charge is varied by injecting equal volumes v of different solutions of benzene in toluene having known concentrations M_i. If the charges $q_i = M_i v$ have variances s_q^2 due only to a uniform variance s_v^2 in the injected volume, then $s_q^2 = M_i^2 s_v^2 = (s_v^2/v^2)q_i^2$ showing the proportionality between s_q^2 and q_i^2. If the peak height measuring procedure itself introduces negligible variance, and if peak heights h_i are proportional to q_i, it follows that the variance in h_i is proportional to h_i^2. This case is Variant 1b discussed in Reference 7 and illustrated there as Figure 4 (mislabelled as Variant 2b). We have enlarged Figure 4 and have read off 33 visible calibrating values. These are grouped together into nine sets having virtually the same q level, each set is regarded as a replication series, and these will constitute nine calibrating points. The members of each series are averaged and these values are shown in Table II and plotted in Figure 2. For our purposes the charge q corresponds to x and height h to y, which has nonuniform variance given by the a priori variance function

$$\sigma_y^2 = Vy^2 \quad (13)$$

where the multiplier V will be regarded as unknown although its value can be estimated as about 1.3×10^{-3} from information given in Reference 7. To fit a calibration curve to these data, we recognize the obviously linear relationship between x and y and so fit a two-parameter model equation with $f(x) = x$. The calibrating line so obtained was

$$y_{cal} = -0.0993 + 2.782x \quad (14)$$

and the variance of weighted residuals was $V = 1.80 \times 10^{-3}$.

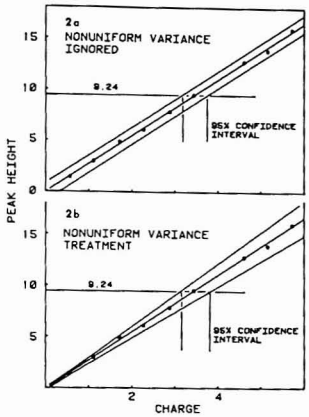

Figure 2. Illustrative Example 2: Chromatographic calibration data from Figure 4 of Reference 7 as summarized in Table II. Figure 2a shows treatment according to procedures in Reference 1 ignoring variance nonuniformity; Figure 2b uses heteroscedastic methodology. The middle line in both Figures 2a and 2b is the calibration line and the bounding lines are plots of Equation 14 which together with the $y = 9.24$ line comprise the graphical solutions for 95% confidence limits

We selected three of the original 33 data points to serve as "unknowns" and calculated 95% confidence limits for these using Equations 8b and 10b with $t_{0.05} = 2.365$ corresponding to the seven degrees of freedom inherent in V. These confidence limits are given in Table II.

DISCUSSION

If a calibrating procedure is known to be heteroscedastic but the analyst does not know the variance function, the effort required to establish this function is generally greater than that required to find the calibration curve. Therefore, it is of interest to discuss the effects of nonuniform variance on calibration results in order to understand the conditions under which these effects are important.

Firstly, there is one point of agreement among statistics texts and that is the minimal effect of weighting factors on fitted regression curves. Unless the variance nonuniformity is quite severe, the curve fitted to calibration data is likely to be nearly the same, whether or not the variance nonuniformity is included in the weighting factors. To show this effect in the two illustrative examples, we have repeated all the calculations using methods of Reference 1. In the photometric experiment, the calibrating polynomial obtained by F-testing turns out to be a cubic and this is plotted along with the calibrating data in Figure 1a for comparison with the heteroscedastic curve shown in Figure 1b. The similarity between these two curves is also evident by examining the assays X_i given in Table I obtained by projecting the "unknown" absorbances through the respective curves. In all three cases, the difference between the X_i values obtained by the two methods is a small fraction of the statistical uncertainties as represented by the 95% confidence intervals. Similarly, in the chromatographic example, F-testing yields the linear calibration curve drawn as the middle line in Figure 2a. The similarity between this line and the heteroscedastic calibration line below in Figure 2b is visually evident and again an examination of the corresponding X_i values given in Table I shows how little these are affected.

Variance nonuniformity may be more important in the confidence limit calculations and this is more obvious in the chromatographic example. The two outer lines drawn in both Figures 2a and 2b are plots of

$$y = y_{cal}(x) \pm t_a[\text{var}\,[Y_i - y_{cal}(x)]] \qquad (14)$$

for the unknown sample with $Y_i = 9.24$. The intersections of these bands with the horizontal $y = 9.24$ represent graphical solutions to Equations 1 or 10b. The difference between homoscedastic and heteroscedastic treatments is pronounced. In Figure 2a, the spacing between these bands increases slightly at both extremities as the variance in Equation 14 is at a minimum near the center of the calibrating points. However, in Figure 2b the bands diverge as y increases and this is due to the y^2 dependence of the variance. The trend of the 95% confidence intervals in Table II shows the same effect. These intervals increase markedly with increasing Y_i value, but if variance nonuniformity is ignored, they vary much less. A similar discussion of the photometric example is complicated by the variation in local slope of the calibration curve but the following conclusions can be drawn from both. An analyst wishing to avoid the labor of a heteroscedastic treatment will sacrifice statistical reliability by ignoring variance nonuniformity but will generally obtain roughly the same assays X_i and roughly the same confidence intervals for samples falling in the region of the calibration curve where the variance is an average over the nonuniform range. This region typically falls somewhere in the mid-range of the curve and so confidence limits obtained near the extremities of the curve are likely to be severely in error.

Interested readers will be sent FORTRAN program listings on request to the author.

LITERATURE CITED

(1) L. M. Schwartz, *Anal. Chem.*, **49**, 2062 (1977).
(2) L. M. Schwartz, *Anal. Chem.*, **50**, 980 (1978).
(3) D. J. Finney, *Biometrics*, **32**, 721 (1976) and other references cited therein.
(4) D. Rodbard, R. H. Lenox, H. L. Wray, and D. Ramseth, *Clin. Chem. (Winston-Salem, N.C.)*, **22**, 350 (1976) and other references cited therein.
(5) K. A. Brownlee, "Statistical Theory and Methodology in Science and Engineering", 1st ed., John Wiley and Sons, New York, 1960.
(6) D. J. Finney, "Statistical Method in Biological Assay" 2nd ed., Hafner Publishing Co., New York, 1964, Chapter 14.
(7) P. Bocek and J. Novak, *J. Chromatogr.*, **51**, 375 (1970).

RECEIVED for review November 6, 1978. Accepted February 5, 1979.

Laser Induced Thermal Lens Effect for Calorimetric Trace Analysis

N. J. Dovichi and J. M. Harris*

Department of Chemistry, University of Utah, Salt Lake City, Utah 84112

The thermal lens effect, generated in condensed phase by absorption of a laser beam, produces a loss of radiation in the center of the beam which is enhanced relative to normal Beer's law behavior by increasing laser power. The time dependence of the effect provides a reference or blank measurement without requiring a double-beam arrangement. An application of the technique to the determination of trace level Cu(II) with EDTA is presented. Using a 4-mW He:Ne laser, a minimum detectable absorbance of 1.0×10^{-5}, corresponding to 3.3 ng copper, is found.

To reduce detection limits for a solution absorbance measurement of a very weakly fluorescent sample (*1*), one can determine a temperature rise associated with the nonradiative relaxation of the excited molecules. Since the magnitude of heat delivered to the solvent depends linearly on source power, the sensitivity of this approach can benefit from the high power of a laser source. Several methods for measuring small absorbances in condensed phase by a laser-induced temperature increase have recently been compared in the review literature (*2–4*). These methods, listed in order of decreasing detection limits, include thermocouple calorimetry, photoacoustic calorimetry, interferometry, thermal lens calorimetry, and several laser intracavity effects such as spot size variation, beat frequency shift, and resonator gain variations (*5*). The intracavity effects generally produce the lowest limit of detection because of the large average power in the resonator and the sensitivity of the oscillator to small refractive index gradients produced by absorption by the sample. Thermal lens calorimetry, although somewhat less sensitive, provides a much simpler method for decreasing the detection limits in absorption measurements.

The thermal lens effect, first reported by Gordon et al. (*6*), is produced in an experimental arrangement similar to normal single-beam absorption spectrometry. The major difference is that laser radiation passing through a sample is detected only at the center of the beam by restricting the field of view of the detector with a pinhole. The sample causes a loss of radiation from the beam center by thermal defocusing; that is, light absorbed by the sample is converted to heat by nonradiative relaxation and increases the temperature of the solvent by an amount which is greatest at the center of the beam. This temperature increase results in a lowering of the refractive index, producing a negative lens which defocuses the beam.

If the path from the laser to the sample is initially blocked and then opened with a shutter, the thermal lens takes a finite time to build up. A steady-state condition is obtained when the rate of laser heating equals the rate of heat loss due to the thermal conductivity of the solvent and the finite temperature rise. The buildup of the lens can take place on time scales from tens of microseconds to hundreds of milliseconds depending on the thermal conductivity of the solvent and the radius of the laser beam through the sample (*6, 7*).

The intensity measured at the beam center, $I(t)$, will initially ($t = 0$) reflect only the Beer's law response of the sample:

$$I(0)/I_0 = 10^{-A} \tag{1}$$

or for small A,

$$(I_0 - I(0))/I_0 = 2.303A \tag{2}$$

where A is the sample absorbance and I_0 is the incident light intensity. After sufficient time, when a steady state temperature difference is reached, the intensity at the detector, $I(\infty)$, depends on the optical arrangement of the system. An optimum configuration which minimizes $I(\infty)$ is obtained when the sample is placed one confocal length beyond the beam waist formed by a long focal length lens. In this configuration, using a TEM_{00} laser beam to probe a sample whose length, l, is sufficiently small ($l << 2\pi\omega_0^2 n/\lambda$, where ω_0 is the beam waist, n is the refractive index, and λ is the laser wavelength), the following expression governs the initial and final intensities (*2*):

$$\frac{I(0) - I(\infty)}{I(\infty)} = -\frac{2.303P(dn/dT)}{\lambda k}A = 2.303EA \tag{3}$$

where P is the laser in watts, dn/dT is the change in solvent refractive index with temperature (usually negative), λ is the laser wavelength, k is the thermal conductivity in W cm^{-1} K^{-1}, and E is the enhancement of this effect relative to Beer's law behavior. This expression assumes that all of the absorbed light is converted into heat. If the quantum yield of fluorescence is finite, then a correction term which includes the quantum yield and Stokes shift may be applied (*8*).

Several analytically significant characteristics are apparent in Equation 3. First, the relative change in intensity due to the thermal lens, for a given sample absorbance and solvent, depends linearly on the laser power. Thus, increasing the laser power increases the enhancement and therefore the sensitivity of the technique, even in the presence of proportional noise on $I(0)$ and $I(\infty)$. A second advantage, gained by repetitive chopping of the laser beam, is that a nearly simultaneous measurement of a "blank" signal, $I(0)$, can be made in the *presence* of the sample. Although $I(0)$ is not a true blank since it is reduced from I_0 by 10^{-A}, this factor cancels in determining $(I(0) - I(\infty))/I(\infty)$ since $I(\infty)$ is reduced by the same proportional amount. Since a blank and sample measurement can be made each time the beam is chopped, the $1/f$ contribution to the proportional noise will be reduced relative to typical single beam absorption measurements.

The thermal lens effect offers several attractive attributes for trace level determinations of solutes in the liquid phase. Historically the technique has been used to measure very weak absorbances of neat solvents (*3, 9, 10*); the only reports of solution measurements have been for characterization of thermal lens physics (*2, 11*) and, most recently, for determination of nonradiative quantum yields (*8*). Our interest in this work is to study the application of the thermal lens technique to trace solute determinations; in particular we would like to focus attention on the potential use of low power, discrete wavelength, CW lasers (for example He:Ne, He:Cd, or Ar^+) since lasers of this type are inexpensive enough to be

0003-2700/79/0351-0728$01.00/0 © 1979 American Chemical Society

Table I. Thermooptical Properties of Solvents for Thermal Lens Measurements[a]

solvent	k, mW/cm K	$10^4 \times dn/dT$, K^{-1}	E/P, mW^{-1}[b]
CCl_4	1.02	5.8	8.93
benzene	1.44	6.4	7.02
acetone	1.60	5.0	4.97
methanol	2.01	3.9	3.06
water	6.11	0.8	0.21

[a] Data taken from Solimini (*10*). [b] Enhancement per unit laser power in milliwatts, λ = 632.8 nm.

accessible to a wide range of analytical chemists.

The thermal lens technique and this particular choice of laser impose several constraints on the design of an analytical method. The lack of tunability of the source precludes the measurement of spectra; therefore the selectivity of a method must be provided by chemical means, e.g., chromogenic reaction or separation technique, while the thermal lens apparatus acts as a sensitive, quantitative, although nonselective detector. The choice of solvent for a determination governs the enhancement, E, that one realizes for a particular laser power. Equation 3 shows that a solvent of choice will have a small thermal conductivity and a large dn/dT. Table I lists several solvents, their pertinent thermooptical properties, and the enhancement of the effect relative to Beer's law per unit laser power in milliwatts, taking as the wavelength λ = 632.8 nm from the He:Ne laser transition. The inverse of this factor, P/E, would represent the breakeven power in milliwatts, where the magnitude of the thermal lens effect would equal the Beer's law response. A general trend shown from these data is that the enhancement in more polar solvents suffers from larger thermal conductivity and a smaller dn/dT. The order of magnitude of E/P predicts that milliwatt power lasers will produce only modest enhancements in nonpolar solvents and a loss of sensitivity in water, relative to Beer's law.

For this work we have chosen to study the determination of Cu(II) (*12*), which forms an EDTA complex having a sufficiently large stability constant to allow trace level determinations, a larger molar absorbtivity at 632.8 nm than the reactant species, and a negligible quantum yield of fluorescence. The small molar absorbtivity of the Cu(II)–EDTA complex, $\epsilon = 47\ M^{-1}\ cm^{-1}$, will result in a larger detection limit than for more strongly absorbing solutes. However, to quantitate the minimum detectable absorbance of the thermal lens technique, the small molar absorbtivity reduces the chance of error due to sample handling.

EXPERIMENTAL

Instrument. A block diagram for the thermal lens experiment is shown in Figure 1. The optical system is constructed on a 4 ft × 5 ft × $2^1/_2$ in., vibrationally isolated optical breadboard NRC model XS-45. The He:Ne laser, CW Radiation model LS4P, produces a 4-mW, linearly polarized beam at 632.8 nm. The laser beam is chopped at 0.4 Hz, and a small portion of the beam is directed to a reference vacuum photodiode, RCA 929, powered with a 67-V battery. The main beam is directed toward a mirror, M1, which is mounted on an adjustable rotation–translation stage to provide alignment relative to the table surface and the sample. The beam is focused with a 13.6-cm focal length biconvex achromatic lens into the 1-cm square cell which holds the sample. The power of the laser beam at the sample is 2.35 mW due to reflective losses. The cell holder is mounted on a magnetic block, which can be slid along the table surface against a steel rail, to allow reproducible positioning of the cell relative to the beam waist. Three additional mirrors were used to fold a 9-m optical path between the cell and detector. The final mirror, represented schematically by M2, is placed in an adjustable mount to allow positioning of the center of the beam over a 0.1-mm pinhole in front of a detector, identical to that of the reference channel.

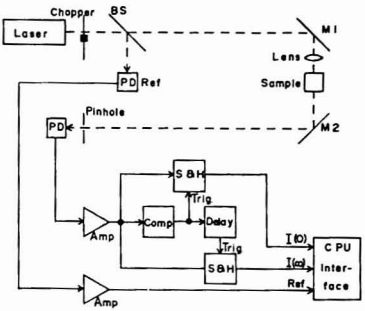

Figure 1. Thermal lens experimental arrangment. BS is a beam splitter; M1 and M2 are mirrors; PDs are vacuum photodiodes; Comp is a comparator; S & Hs are sample-and-hold circuits

The current from both the signal and reference detectors is converted to a voltage with a TI TL084 quad operational amplifier wired in an i-to-v mode with a 10-MΩ feedback resistor. The signal voltage is sent in parallel to two sample-and-hold circuits, RCA CD4098 and CD4016, and a comparator, NS LM311. The comparator determines when the chopper unblocks the beam and strobes the first sample-and-hold to measure $I(0)$. After a 1.2-s delay, provided by a NS LM555, the second sample-and-hold is strobed to measure $I(\infty)$. All the signals transfered to the computer are first buffered with NS LM310 voltage followers. The computer is a DEC LSI-11 microprocessor with a Data Translation 12-bit interface. The computer is programmed to calculate the expression $(I(0) - I(\infty))/I(\infty)$ and to divide this expression by the reference signal to correct for laser power fluctuations. Typically 150 results of this kind are gathered, deviant results are eliminated, and the average and standard deviation are computed.

Reagents. All chemicals are analytical reagent grade or better. A 0.05 M copper solution is prepared by dissolving 1.59 g of copper turnings (>99.9%) in 5 mL of concentrated sulfuric acid and diluting to 500 mL with water. Aqueous EDTA reagent is prepared by transfer of 200 μL of a 0.1 M solution to a 2-mL volumetric flask and dilution to volume with 0.4 M, pH 7 aqueous phosphate buffer. The 1:1 acetone:water reagent is similarly prepared with dilution to volume by a solution composed of one part acetone and one part aqueous phosphate buffer. The 3:1 acetone:water reagent is prepared in 1 mL 1:1 acetone:aqueous buffer solution and diluted to volume with acetone.

Procedure. Since the magnitude thermal lens effect is a function of the distance between the cell and the beam waist (*2*), one must vary this distance to optimize the measurement. A cell containing a sample of methylene blue in 2:1 methanol:water is placed in the cell holder and the position of the beam on the pinhole is varied with M2 until a maximum current is observed from the detector. The cell distance from the beam waist is then varied by sliding the magnetic block along the rail parallel to the beam until a maximum thermal lens effect is found. The alignment cell is replaced with a cell containing the EDTA reactant solution, and the beam position on the pinhold is realigned for maximum detector current, again using M2. When the cell faces are exactly perpendicular to the beam, a series of interference fringes are observed, which are probably caused by the cell windows acting as a Fabry-Perot interferometer. The magnitude of the interference is sensitive to mechanical vibrations giving rise to large fluctuations in the signal. This condition was avoided by deliberately tilting the cell faces slightly with respect to the beam perpendicular.

The determination of copper proceeds as follows. A 1-mL aliquot of EDTA reagent is pipetted into the 1-cm cell. After a blank measurement is made, a series of 1- to 4-μL aliquots of 0.05 M copper solution are added to the cell; the solution is mixed and allowed to stand for 60 s, and the thermal lens measurement is made. This general method of multiple addition of sample to the reagent solution provides convenient standardization for analytical

Table II. Analytical Results of the Thermal Lens Determination of EDTA

solvent	observed enhancement	limits of detection[a] A	Cu(II), μg/mL	ng, in-beam vol.[b]
water	0.22 ± 0.01[c]	5.1×10^{-3}	5.5	17
1:1 acetone:water	0.59 ± 0.02	3.5×10^{-3}	3.7	12
3:1 acetone:water	2.0 ± 0.1	1.0×10^{-3}	1.0	3.3

[a] Extrapolated 2σ limits or 95% confidence. [b] Absolute detection limit for Cu(II) in a cylindrical volume defined by the 1-cm cell length times an area enclosing 90% of the beam intensity, $4\pi\omega^2$, where the beam radius, ω, equals 1.6×10^{-3} cm. [c] Uncertainty defined as $\pm 2\sigma$ or 95% confidence.

work, since aliquots of unknown and standard may be alternately determined without cleaning the cell or disturbing the alignment.

RESULTS AND DISCUSSION

The thermal lens technique differs from normal absorption spectrometry in that the position of the cell along the light path influences the magnitude of the measured effect. The influence of position has been derived by Hu and Whinnery (2) in terms of the beam waist, ω_0 produced by the focusing lens, and the beam radius, ω, at the sample.

$$\frac{I(0) - I(\infty)}{I(\infty)} = -\frac{4.606P(dn/dT)}{\lambda k}\left[\frac{\omega_0(\omega^2 - \omega_0^2)^{1/2}}{\omega^2}\right]A \quad (4)$$

The expression inside the brackets has a maximum equal to $^1/_2$ when $\omega = \omega_0(2)^{1/2}$ which reduces Equation 4 to Equation 3. To obtain the dependence of the thermal lens effect on a more easily measured parameter, the distance between the beam waist and the sample, z, the expression (13):

$$\omega^2 = \omega_0^2 + \frac{z^2\lambda^2}{\pi^2\omega_0^2} \quad (5)$$

is substituted for ω^2 in Equation 4 to give:

$$\frac{I(0) - I(\infty)}{I(\infty)} = -\frac{4.606P(dn/dT)}{\lambda k}\left[\frac{zz_c}{z_c^2 + z^2}\right]A \quad (6)$$

where z_c is the confocal length, $z_c = \pi\omega_0^2/\lambda$. The expression inside the brackets maximizes when the distance from the beam waist to the cell, z, is one confocal length, z_c.

The experimental results for the dependence of the thermal lens effect as a function of cell position, using a methylene blue sample in 2:1 methanol: water having an absorbance of $A = 0.18$ at 632.8 nm, are shown in Figure 2. A beam waist for this experiment, $\omega_0 = 1.2 \times 10^{-2}$ cm, was calculated from the manufacturer's specification for the divergence of this laser, $\theta = 0.9$ mrad, and focal length of the focusing lens, $f =$ 13.6 cm using the formula (13)

$$\omega_0 = f\theta \quad (7)$$

This beam waist was applied to Equation 6 which predicts a maximum effect at $z = 7.1$ cm. The least squares fit of the data to Equation 6 shows that the actual divergence is closer to 0.8 mrad, with a maximum effect at 6.2 cm. The fit of the data over the 20-cm range is generally good. One can see from these results that the position of the sample strongly influences the measurement. The variation near the optimum, however, is small, and errors of the order of ±1 cm in cell placement are tolerable for the particular focal length of focusing lens chosen in this experiment.

The analytical results for the determination of copper with EDTA are presented in Table II. The individual calibration curves for each solvent are linear. The chi squared statistic, relating the variance of the least squares fit to the variance of the individual points, is typically $\chi^2 = 3.2$ for $N = 11$ data points; the error in the individual points therefore accounts for all of the uncertainty in the fit at 95% confidence. A clear improvement is shown in the enhancement of the effect by decreasing polarity of solvent. To assure that the trend was not due to a change in the molar absorbtivity of the complex, the absorbances of the highest concentration solutions for each solvent were checked spectrophotometrically, and no difference in molar absorbtivity with solvent was noted. An enhancement measurement that can be checked against theory is that for water, for which the thermooptical constants are known. Equation 3 predicts an enhancement of 0.49 compared to the experimental value of 0.22. Loss of enhancement could be attributed to imperfect alignment of the beam on the pinhole or a change in the thermooptical constants compared with pure water due to the presence of the buffer.

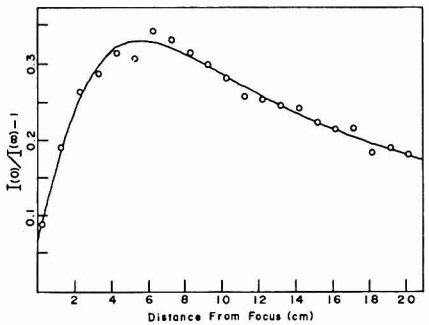

Figure 2. Variation of thermal lens effect with cell position. The distance is measured relative to the beam waist. Open circles are experimental data; solid line is a least-squares fit to Equation 6

The enhancements observed with the low laser power are near unity in the best case. The small detection limits for absorbance that were measured can therefore only be attributed to the reduction in $1/f$ noise discussed in the introduction. Since the standard deviation of the thermal lens measurement has no apparent systematic variation, the detection limits depend inversely on enhancement. This observation, together with the experimental verification by Akhmanov that the enhancement is linear with laser power (11), allows extrapolation of these results to ultimate detection limits. Using a 1-W laser in the same experimental apparatus, the limit of detection for a species having a molar absorptivity of 10^4 in the 3:1 acetone:water solvent is predicted to be 10^{-10} M or about 10^{-16} mol in the probe volume. We expect that the thermal lens technique, in light of its potential capability compared to its simplicity in concept and execution, will make a significant contribution to the field of spectrophotometric analysis.

ACKNOWLEDGMENT

The authors acknowledge the assistance of S. Painter and

S. M. Warnick with the design of the signal processing electronics.

LITERATURE CITED

(1) T. Hirschfeld, *Appl. Spectrosc.*, **31**, 238 (1977).
(2) C. Hu and J. R. Whinnery, *Appl. Opt.*, **12**, 72 (1973).
(3) J. R. Whinnery, *Acc. Chem. Res.*, **7**, 225 (1974).
(4) A. Hordvik, *Appl. Opt.*, **16**, 2827 (1977).
(5) T. D. Harris, Ph.D. Thesis, Purdue University, Lafayette, Ind., 1978.
(6) J. P. Gordon, R. C. C. Leite, R. S. Moore, S. P. S. Porto, and J. R. Whinnery, *J. Appl. Phys.*, **36**, 3 (1965).
(7) F. W. Dabby, R. W. Boyko, C. V. Shank, and J. R. Whinnery, *IEEE J. Quantum Electron.*, **qe-5**, 516 (1969).
(8) J. H. Brannon and D. Magde, *J. Phys. Chem.*, **82**, 705 (1978).
(9) M. E. Long, R. L. Swafford, and A. C. Albrecht, *Science*, **191**, 183 (1976).
(10) D. Solimini, *J. Appl. Phys.*, **37**, 3314 (1966).
(11) S. A. Akhmanov, D. P. Krindach, A. V. Migulin, A. P. Sukhorukov, and R. V. Khokhlov, *IEEE J. Quantum Electron.* **qe-4**, 568 (1968).
(12) P. B. Sweetser and C. E. Bricker, *Anal. Chem.*, **25**, 253 (1953).
(13) J. R. Arnaud, "Beam and Fiber Optics", Academic Press, New York, 1976.

RECEIVED for review November 9, 1978. Accepted January 12, 1979. This research was supported in part by the donors of the Petroleum Research Fund administered by the American Chemical Society, and by the University of Utah Research Fund.

Comparison of Digestion Methods for Determination of Organoarsenicals in Wastewater

Charles E. Stringer

Dallas Water Utilities, 1020 Sargent Road, Dallas, Texas 75216

Moses Attrep, Jr.*

Department of Chemistry, East Texas State University, Commerce, Texas 75428

Two digestive methods were investigated and compared as to their effectiveness in releasing arsenic from three organoarsenicals introduced into wastewater samples. The digestive methods utilized included a wet method employing hydrogen peroxide–sulfuric acid and ultraviolet photodecomposition. The organoarsenicals investigated were disodium methanearsonate, dimethylarsinic acid, and triphenylarsine oxide. All the digestive methods gave quantitative arsenic recoveries for the three organoarsenic compounds when added to wastewater samples. The ultraviolet photodecomposition proved to be an effective digestive technique, requiring a 4-h irradiation to decompose a primary settled raw wastewater sample containing spiked quantities of the three organoarsenicals.

The knowledge and concern about the environmental impact and the ultimate fate of organoarsenicals applied to soils and other ecosystems is steadily growing. The extensive number of analytical procedures which have been reported in the literature would seem to indicate inherent difficulties in the analysis of arsenic. Most procedures intended to measure total arsenic incorporate some mode of wet or dry digestion to destroy any organically bound arsenic, in addition to any other organic constituents present in the sample.

Probably the most frequently used method of digestion incorporates the use of nitric and sulfuric acids. Kopp (*1*) used this digestion method and experienced 91 to 114% recovery of arsenic trioxide added to deionized water and 86 to 100% recovery of the compound added to river water. Evans and Bandemer (*2*) recovered 87% of the arsenic trioxide added to eggs. By modifying the above digestive method by the addition of perchloric acid, Caldwell et al. (*3*) observed 80 to 90% arsenic recovery with *o*-nitrobenzene arsonic acid, 85 to 94% arsenic recovery with *o*-arsanilic acid, and 76.7% arsenic recovery with disodium methylarsenate.

Two uncertainties seem to arise when reviewing the previous digestive methods using nitric and sulfuric acid. First, the addition of inorganic arsenic to an organic matrix and subsequent recovery of all the inorganic arsenic added is not definitive proof of total recovery of any organoarsenicals present. Secondly, the choice of *o*-nitrobenzene arsonic acid and *o*-arsanilic acid seems unfortunate since both compounds represent arsenic attached to an aromatic ring which is atypical of cacodylic acid and disodium methyl arsonate, two widely used organoarsenicals.

Aside from nitric and sulfuric acid, a relatively simple digestive method employing 30% hydrogen peroxide in the presence of sulfuric acid was reported by Kolthoff and Belcher (*4*) and subsequently used by Dean and Rues (*5*) to determine arsenic in triphenylarsine. The application of this digestive method to environmental samples including wastewater is the subject, in part, of this investigation.

Armstrong et al. (*6*) observed that organic matter in seawater could be oxidized to carbon dioxide on exposure to sufficient ultraviolet radiation from a medium pressure mercury arc vapor lamp. Tam (*7*) also used this approach to decompose organoarsenicals and observed 111% for *o*-arsanilic acid, 97% for sodium cacodylate, and 108% for arsenazo. The feasibility of this digestive method to organoarsenicals added to wastewater samples warrants further investigation.

This research was undertaken to determine to what extent hydrogen peroxide–sulfuric acid and ultraviolet irradiated liberated inorganic arsenate from organoarsenicals added to treated wastewater samples. Arsenic determinations were performed by either the colorimetric procedure described by Kopp (*1*) or the arsine–atomic absorption method described by Manning (*8*).

EXPERIMENTAL

Apparatus. All colorimetric determinations were made using a Bausch and Lomb Spectronic 20 colorimeter equipped with a

0003-2700/79/0351-0731$01.00/0 © 1979 American Chemical Society

1-cm absorption cell at a wavelength of 520 nm. Arsine was collected in a arsine generation apparatus, Fischer No. 1405.

High sensitivity arsenic determinations were obtained on a Perkin-Elmer 403 Atomic Absorption Spectrophotometer equipped with deuterium background correction and a 10 mu Hitachi model 165 recorder.

Samples were irradiated by a medium pressure 450-W mercury arc photochemical lamp (Hanovia lamp no. 67A0100) mounted vertically in the middle of an aluminum cylinder large enough in diameter to accommodate ten 1-inch diameter silica tubes which had been fashioned by sealing the ends of discarded germicidal ultraviolet lamps. A blower fan was attached to the bottom of the lamp housing and served as an extractor fan to provide cooling of the lamp and samples. Excessive cooling of the lamp and resulting dimming of the lamp discharge was alleviated by enclosing the lamp in a 2-inch diameter quartz liner which had been tapered at one end to retard air flow. The silica tubes which contained the samples were approximately 20 cm long and set 2 cm parallel to the lamp.

Reagents. The following arsenic compounds were used in this study without further purification: arsenic trioxide (99.98% As_2O_3), Baker Reagent; triphenylarsine oxide (no purity listing), Research Organic/Inorganic Chemical Corporation; disodium methane arsonate (95%), Alpha Inorganics; and dimethylarsinic acid (no listing of purity), Research Organic/Inorganic Chemical Corporation. All other reagents were reagent grade or the highest purity obtainable.

Analysis of Organoarsenicals. Quadruplicate samples of each of the three organoarsenicals were subjected to vigorous digestion with hydrogen peroxide and sulfuric acid as described by Kolthoff and Belcher (*4*). Arsenate, resulting from the decomposition of the organoarsenicals, was reduced to arsenite with hydrazine sulfate and titrated with potassium bromate. The yellow color of free bromine liberated by oxidation of bromide ion in the presence of excess bromate titrant served to distinguish the end point of the titration. Stock solutions of 1000 mg/L as As were prepared for each organoarsenical in addition to As_2O_3.

Analytical Procedures. (*a*) *Hydrogen Peroxide–Sulfuric Acid Digestion—AgDDC Analysis.* Aliquots of each of the three organoarsenicals containing 5 μg of arsenic were added to 125-mL Erlenmeyer flasks which also served as arsine generators. To each organic compound and a complete set of arsenic trioxide standards, ranging from reagent blank to 6 μg of arsenic, 5 mL of concentrated sulfuric acid and 5 mL of 30% hydrogen peroxide were added. Samples and standards were boiled off and fumed for an additional 2 min. The samples were cooled and to each flask the following were added in succession: 25 mL of water, 7 mL of HCl (concentrated), 5 mL of 15% KI, and after 10 min, five drops of 40% $SnCl_2$. The samples were refrigerated for 20 min to allow for reduction to occur. Arsine was generated into an absorption tube containing 4 mL of the AgDDC reagent for 1 h.

The applicability of this digestive procedure to real samples was investigated by adding known quantities of the three organoarsenic compounds to wastewater samples and observing the arsenic recovery after digestion with sulfuric acid–hydrogen peroxide. The samples chosen for spiking with organoarsenicals were a primary settled raw sewage sample being fed into an activated sludge plant (Aeration Feed) and the effluent (SBE) from the discharge of this process. These samples were taken from the Dallas Water Utilities Pilot Plant facility.

This portion of the study was accomplished by dividing each sewage sample into four separate subsamples of 100 mL volume and spiking separately three of the four subsamples with each of the three organoarsenicals equivalent to 5 μg arsenic. The samples and accompanying standards were then subjected to hydrogen peroxide–sulfuric acid digestion with analysis to AgDDC.

(*b*) *Hydrogen Peroxide-Sulfuric Acid—Analysis by AA.* Aliquots of each of the three organoarsenicals containing 0.50 μg of arsenic were added to 125-mL Erlenmeyer flasks which were also to serve as arsine generators. The samples were digested in an analogous manner as described in the previous digestion. To the samples and standards, ranging from reagent blank to 1.0 μg of arsenic, 25 mL of water, 10 mL of concentrated hydrochloric acid, and 5 mL of 15% KI were added. After 10 min, five drops of 40% stannous chloride were added and the samples were allowed to react at room temperature for 20 min prior to analysis. Each flask, after addition of a stirring bar, was connected to the dosing column by means of a Teflon seal and purged of air with argon. The two-way purge valve was then closed and 2 g of arsenic-free zinc was delivered through the dosing stopcock to the flask. A magnetic stirrer was used to stir the contents of the flask during the 240 s the arsine and hydrogen were being generated and collected in a ballon reservoir for analysis by atomic absorption.

(*c*) *Ultraviolet Decomposition—AgDDC Analysis.* Samples were irradiated by a medium pressure 450-W mercury arc photochemical lamp (Hanovia lamp no. 679A0100) mounted vertically in the middle of an aluminum cylinder large enough in diameter to accommodate ten 1-inch diameter silica tubes which had been fashioned by sealing the ends of discarded germicidal ultraviolet lamps. A 12-V blower fan was attached to the bottom of the lamp housing and served as an extractor fan to provide cooling of the lamp and samples. Excessive cooling of the lamp and resulting dimming of the lamp discharge was alleviated by enclosing the lamp discharge in a 2-inch diameter quartz liner which was tapered at one end to retard air flow. The silica tubes which contained the samples were approximately 20 cm long and set 2 cm parallel to the lamp.

An assessment of the length of irradiation time necessary to decompose photochemically the three organoarsenicals was investigated. This was accomplished by placing into each of ten silica tubes 50 mL of cacodylic acid equivalent to 50 μg of arsenic and removing each tube from the unit after irradiation for a predetermined exposure up to 3.5 h. Triphenylarsine oxide and DSMA were experimentally treated in a analogous manner.

Prior to irradiation, each sample was acidified with three drops of nitric acid and also three drops of 30% hydrogen peroxide. Following irradiation, each sample was transferred to a 100-mL volumetric flask and made to volume. Then, 10 mL of the 100 mL was volumetrically transferred to a 125-mL Erlenmeyer flask, which also served as the arsine generator. The inorganic arsenic content was determined colorimetrically with AgDDC and the extent of photodecomposition based on the experimentally observed quantity over the 5-μg arsenic total in the 100-mL volume taken for analysis.

The applicability of ultraviolet decomposition to wastewater samples was investigated by spiking the same samples which had previously been evaluated using the hydrogen peroxide–sulfuric acid digestion with the organoarsenicals. The aerator feed and settling basin effluent samples were handled separately.

The aerator feed sample contained a substantial amount of particulate matter and was blended for approximately 5 min beforehand. After blending, 50 mL of the aerator feed sample was volumetrically pipetted into each of four silica tubes. To three of the four tubes, 1-μg quantities of the three organoarsenicals were added. Sufficient nitric acid was added to bring the pH to 2 and three drops of 30% hydrogen peroxide were added. The samples and a 50-mL arsenic trioxide standard containing 10 μg of arsenic were irradiated for 4 h. After irradiation, the aerator feed samples were transferred to 100-mL volumetric flasks and made to volume. Arsenic analysis was carried out on 25-mL aliquots using atomic absorption.

The analysis of the effluent sample (SBE) was performed in a similar manner, except that 25-mL sample volumes spiked with 0.5 μg of the three organoarsenicals were utilized in the study. In an effort to shorten the time of irradiation, the smaller sample volumes were used in conjunction with 2-h irradiations.

RESULTS

Since reagent grade purities of the three organoarsenicals utilized in this study were not available, it was necessary to get a comparison of the arsenic content of each compound by several different methods. The arsenic content of the three organoarsenicals was determined by three independent methods of analysis including bromate titration of arsenious acid, neutron activation, and X-ray fluorescence. The arsenic content for triphenylarsine oxide revealed arsenic percentages of 22.0, 22.3, and 27.2% arsenic (as As) by each of the above methods, respectively. Dimethylarsinic acid was observed to contain 34.6, 34.4, and 34.9%, respectively. Disodium methanearsonate was found to contain 25.6% arsenic by

Table I. Recovery of Arsenic from Triphenylarsine Oxide, Disodium Methanearsonate, and Dimethylarsinic Acid Employing Wet Digestion with 5 mL of 30% Hydrogen Peroxide and 5 mL of Sulfuric Acid with Analyses by AgDDC and Atomic Absorption

compound	recovery, %[a] AgDDC	atomic absorption
triphenylarsine oxide	101.0 ± 5.2 (4)	100.8 (2)
disodium methanearsonate	103.5 ± 1.2 (4)	100.8 (2)
dimethylarsinic acid	99.9 ± 2.3 (3)	99.2 (2)

[a] Each sample contained 5 μg As. Number in parentheses indicates the number of samples run.

Table II. Recovery of Arsenic from Triphenylarsine Oxide, Disodium Methanearsonate, and Dimethylarsinic Acid Spiked into AF and SBE Sample with Wet Digestion Employing 15 mL of 30% Hydrogen Peroxide and 5 mL of Sulfuric Acid with Analysis by AgDDC[a]

sample	recovery, %[b] sample 1	sample 2
100 mL AF	(9.7 μg As/L)	(6.9 μg As/L)
100 mL AF + triphenylarsine oxide	92.4	94.1
100 mL AF + disodium methanearsonate	90.4	89.1
100 mL AF + dimethylarsinic acid	96.0	90.2
100 mL SBE	(22.6 μg As/L)	(18.5 μg As/L)
100 mL SBE + triphenylarsine oxide	101.1	100.6
100 mL SBE + disodium methanearsonate	98.1	104.4
100 mL SBE + dimethylarsinic acid	89.4	96.6

[a] All 5-μg weights are as arsenic. [b] Corrected for amount of arsenic initially present.

bromate titration and 24.5% As by neutron activation.

The values of arsenic obtained by the volumetric determinations were used in the preparation of the 1000 mg/L stock solutions of the three organoarsenicals. As an additional check on each stock solution, 50 mL of each of the three solutions was placed into separate flasks, digested with sulfuric acid and hydrogen peroxide, and titrated with 1.0 N potassium bromate. Each sample required 13.3 mL of 0.1 N potassium bromate which is equivalent to 49.8 mg of the 50 mg of arsenic known to be present in the sample. A final check was made on the stock solutions by atomic absorption. A 10-, 50-, and 100-mg per liter solution was made from each organoarsenic stock solution and compared to arsenic trioxide solutions of the same concentrations. Each sample was aspirated into a hydrogen–argon flame and observed to give identical signals—any one compound could be used as a standard for the others. The Perkin-Elmer 403 Atomic Absorption Spectrophotometer was operated with deuterium background correction.

The percent recoveries obtained by the digestion procedure using 5 mL of 30% hydrogen peroxide and 5 mL of sulfuric acid with AgDDC analysis and atomic absorption analysis are given in Table I. The recovery results obtained by this digestion method applied to the aeration feed and settling basin effluent samples spiked with each of the three organoarsenicals equivalent to 5 μg of arsenic are presented in Table II.

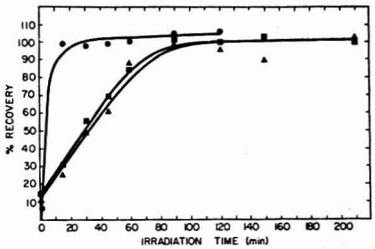

Figure 1. Recovery of arsenic after ultraviolet exposure as a function of time. ●, triphenylarsine oxide; ■, disodium methanearsonate; ▲, dimethylarsinic acid

Table III. Recovery of Arsenic from Triphenylarsine Oxide, Disodium Methanearsonate, and Dimethylarsinic Acid Spiked into Aerator Feed (AF) and Settling Basin Effluent (SBE) with Digestion by UV and Analysis by High Sensitivity Atomic Absorption

compound	recovery, %[a] aerator feed sample 1	aerator feed sample 2	settling basin effluent
triphenylarsine oxide	110.0	100.0	102.8
disodium methanearsonate	100.0	102.4	102.8
dimethylarsinic acid	100.0	109.8	88.6

[a] Corrections were made for arsenic present in the samples.

Table IV. Chemical Analysis of the Aerator Feed Sample and the Settling Basin Effluent Sample Taken at Dallas

parameter[a]	samples aerator feed	settling basin
pH @ 25 °C	7.3	7.6
total alkalinity as $CaCO_3$	216.0	160.0
ammonia nitrogen	12.7	1.93
organic nitrogen	12.8	3.70
nitrite–nitrate nitrogen	0.2	1.7
nitrite nitrogen	0.01	0.08
total phosphorus as P	5.5	6.5
chemical oxygen demand	222.2	42.65
total organic carbon as C	57.0	12.0
total inorganic carbon as C	50.9	33.0
total carbon as C	107.0	45.0
suspended solids	132	21

[a] All values reported in mg/L units.

The effects of ultraviolet irradiation as a function of time for triphenylarsine oxide, disodium methanearsonate, and dimethylarsinic acid are illustrated in Figure 1. The extent of arsenic recovery using photo-oxidation in conjunction with high sensitivity arsenic analysis when applied to the aerator feed and settling basin effluent samples is shown in Table III.

A chemical analysis of the aerator feeding and settling basin effluent samples is provided in Table IV in order to illustrate the overall water quality of the samples used in this study.

DISCUSSION

The digestive method employing hydrogen peroxide and sulfuric acid with analysis by AgDDC gave extremely good

results with arsenic recoveries ranging from a low of 98.5 to a high of 104.9%. This same digestive method when applied to a primary settled raw sewage sample gave arsenic recoveries ranging from 89.1 to 96.0%. Arsenic recoveries of 89.4 to 104.4% were experienced from an activated sludge effluent sample. The same digestive method employing the high sensitivity arsenic analysis by atomic absorption resulted in arsenic recoveries of 99.2 to 100.8%.

The hydrogen peroxide–sulfuric acid digestion seemed to provide the most consistent and complete recoveries of any of the wet digestive procedures previously examined. Previous studies using nitric–sulfuric acid, with and without ammonium oxalate, revealed arsenic recoveries ranging from 80.2 to 105.9% and from 100.5 to 110.5%, respectively. This digestion procedure coupled with the AgDDC colorimetric analysis resulted in quantitative arsenic recoveries from wastewater samples. The hydrogen peroxide–sulfuric acid digestion combined with the high sensitivity arsenic analysis gave acceptable recoveries of arsenic and should be considered a viable technique.

The most encouraging digestive technique examined during the course of this investigation was the photodecomposition approach using ultraviolet light. The time-dependent study of the digestive effects of ultraviolet irradiation of the three organoarsenicals resulted in some interesting observations. A 15-min exposure of triphenylarsine oxide resulted in greater than 99% photodecomposition of the compound. The monoalkylated arsenic compound reacted much slower than triphenylarsine oxide, requiring 2 h for complete decomposition.

The application of ultraviolet photodecomposition with high sensitivity atomic absorption analysis was demonstrated on the same set of wastewater samples used in the hydrogen peroxide–sulfuric acid digestion. Four-hour irradiation of the aerator feed samples spiked with the three organoarsenicals resulted in arsenic recoveries of 100 to 110%. During the 4 h of irradiation, the total organic carbon (TOC) content of the sample was diminished from an initial value of 57 mg/L carbon to 1 mg/L carbon. The total carbon content was reduced from 107 mg/L carbon to 5 mg/L carbon—a drastic reduction in both organic and total carbon content.

The settling basin effluent sample showed 102.8% recoveries for both disodium methanearsonate and triphenylarsine oxide. An 88.6% recovery of dimethylarsinic acid added to SBE indicated that 2-h irradiation was insufficient for all of this compound to photodecompose in the presence of other organic matter. The total organic carbon content was reduced from an initial value of 12 mg/L carbon to 6 mg/L carbon—a 50% reduction.

There were several observations made concerning the arsenic analysis by both the AgDDC technique and the high sensitivity atomic absorption procedure during the course of this investigation. Turbidity problems were initially encountered in the AgDDC colorimeteric procedure.

Following the generation and collection of arsine into the chloroform solution containing *l*-epedrine and AgDDC, a precipitate would form which would seriously interfere with the absorbance measurements. The apparent cause of this problem was traced to the AgDDC. Of three different lots of AgDDC on hand, all three lots were distinctively different in color. The colors ranged from brown to pale green with the brown compound apparently responsible for the difficulty.

In conclusion, it is felt that the data support the premise that the recovery of arsenic from the organoarsenic compounds studied—triphenylarsine oxide, disodium methanearsonate, and dimethylarsenic acid—is complete by wet digestion using hydrogen peroxide–sulfuric acid and by photodecomposition using ultraviolet light.

LITERATURE CITED

(1) J. F. Kopp, *Anal. Chem.*, **45**, 1789 (1973).
(2) R. J. Evans and S. L. Bandemer, *Anal. Chem.*, **26**, 595 (1954).
(3) J. S. Caldwell, R. L. Lishka, and E. F. McFarren, *J. Am. Water Works Assoc.*, **65**, 731 (1973).
(4) I. M. Kolthoff and R. Belcher, "Volumetric Analysis", Vol. 3, Interscience Publishers, New York, 1957, pp 511–13.
(5) J. A. Dean and R. E. Rues, *Anal. Lett.*, **2**, 105 (1969).
(6) F. A. J. Armstrong, P. M. Williams, and J. D. H. Strickland, *Nature (London)*, **211**, 418 (1966).
(8) D. C. Manning, *At. Absorpt. Newsl.*, **10**, 6 (1971).

RECEIVED for review June 5, 1978. Accepted January 26, 1979.

Analytical Techniques for 2,3,7,8-Tetrachlorodibenzo-*p*-dioxin Detection in Environmental Samples after the Industrial Accident at Seveso

A. di Domenico* and F. Merli

Istituto Superiore di Sanità, Sezione presso la Regione Lombardia, c/o Laboratorio Provinciale di Igiene e Profilassi, Via F. Juvara 22, 20129 Milan, Italy

L. Bonifortl, I. Camoni, A. Di Muccio, F. Taggi, and L. Vergori

Istituto Superiore di Sanità, Viale Regina Elena 299, 00161 Rome, Italy

G. Colli, G. Elli, A. Gorni, P. Grassi, G. Invernizzi, A. Jemma, and L. Luciani

Laboratorio Provinciale di Igiene e Profilassi, Reparto Chimico, Via F. Juvara 22, 20129 Milan, Italy

F. Cattabeni, L. De Angelis, and G. Galli

Istituto di Farmacologia e Farmacognosia, Università di Milano, Via A. del Sarto 21, 20129 Milan, Italy

C. Chiabrando and R. Fanelli

Istituto di Ricerche Farmacologiche "Mario Negri", Via Eritrea 62, 20157 Milan, Italy

Analytical techniques for the determination of 2,3,7,8-tetrachlorodibenzo-*p*-dioxin (TCDD) contents in environmental samples taken from the Seveso, Italy, area are described. Low-resolution gas–liquid chromatography in combination with mass fragmentography has proved to be a highly sensitive and specific means to detect trace amounts (parts per trillion) of TCDD when appropriate clean-up procedures are applied. Detection thresholds were found to be in the range of 10 to 0.2 ppt for agricultural soil, 50 to 2 ppt for vegetation, and 20 to 1 ng/m² for cotton swab "wipe tests". No false positive results were yielded over a 14-month period (~7000 samples). Doubtful results, classified as "undetermined", occurred with an average frequency of <5%.

On July 10, 1976, a mixture of chemicals, containing a still unknown quantity of TCDD, was inadvertently released into the northern Italian sky following the rupture of a pressure valve equipping a trichlorophenol-producing reaction vessel at the ICMESA plant owned by Givaudan, a Hoffmann-La Roche subsidiary, about 20 km north of Milan, Italy. The wind-driven fall of the dangerous medley resulted in a major chemical catastrophe because an extremely toxic component, 2,3,7,8-tetrachlorodibenzo-*p*-dioxin (*1–3*), spread over inhabited areas to yield a highly contaminated and very hazardous environment (*4–7*). Shortly after the event, alarming biological effects were noticed on the local animal and vegetable life. Quite clearly, one thing was essential: to obtain a picture of the unsafe area in order to take the appropriate sanitary measures (*8–10*). For this reason, most of the initial analytical work concerned soil and vegetation sampling which was used to define contamination maps. Much of the later work stemmed from the former experimental experiences as a natural carry-over.

The analytical techniques described herein were developed from a platform of basic procedures (*11–16*) in order to deal with the great variety of individual cases encountered while examining thousands of samples. Efforts were made to obtain a fast and reliable method which would ensure good detection thresholds in spite of initial substrata chemical complexity. Without being a remedy to all problems, such a method proved to be of unquestionable utility when applied to the analyses of earth, vegetation, "wipe tests", mud, and similar materials. Attention also deserves to be drawn to the inter-group liaison and to the quality test criteria used for checking the reliability of results.

EXPERIMENTAL

Solvents. Iso-octane, hexane, pentane, petroleum ether, acetone, acetonitrile, and dichloromethane were all pesticide or, when not available, spectral-grade quality, and obtained from Carlo Erba, Milan, Italy. Periodic quality checks were run by applying selected parts of the analytical procedure to the residue obtained by concentrating a 0.5- to 1-L volume of the solvent being checked: absence of unexpected signals on the chosen fragmentographic tracks was taken as proof that the solvent was suitable for use. If signals interfering with those due to TCDD did appear, the solvent was either discarded or distilled in a glass apparatus for further cleanup.

Reagents. Anhydrous Na_2SO_4, $NaHCO_3$, and concentrated H_2SO_4 were analytical-reagent grade and supplied by Carlo Erba; 70–230 mesh silica gel and activated alumina were purchased from E. Merck, Darmstadt, Germany: the latter, neutral aluminum oxide 90, was sifted with a 170-mesh sieve. The coarser part was collected and activated for 12 h at 130 °C (Brockmann activity 1). Celite 545 was obtained from BDH, Poole, England.

Standard Solutions. Concentrated standard solutions of pure TCDD (100 μg/mL, EC-GLC assay ≥98%) in benzene were supplied by Carlo Erba. They were diluted with iso-octane to concentrations (0.01 to 0.1 μg/mL) suitable for external standard use during GLC or GLC-MS runs. TCDD was also provided by Givaudan, Geneva, Switzerland, by D. Lee, of the Plant Pathology Laboratory, Ministry of Agriculture, Fisheries, and Food, U.K., and by the University of Rochester, Rochester, N.Y.: all dioxin standards exhibited similar EC-GLC patterns (assay >95%) and were employed indiscriminantly. EC-GLC checks were confirmed by combined gas chromatography–mass spectrometry.

Sample Preparation for Recovery Tests. Known amounts of TCDD standard solution were added to dioxin-free agricultural soil, vegetation, or cotton swab hosts to simulate certain levels of contamination. Dioxin-free soil and vegetation were selected on the basis of their similarities to field samples collected in the contaminated area; soil samples were normally obtained from agricultural land and stripped of random pebbles prior to analysis; large vegetation pieces were chopped up before any kind of

0003-2700/79/0351-0735$01.00/0 © 1979 American Chemical Society

Table I. Gas Chromatography-Mass Spectrometry Systems Available for TCDD Determination and Gas Chromatographic Operating Conditions (Carrier Gas: He)

instrument	column: i.d., 2.5 mm; length, 4-7 ft	approximate flow rate, mL/min	temperature, °C injector	oven	separator
LKB 9000	3% OV-17 on 100-120 Gaschrom Q	50	270	255	270
Finnigan 3000	3% OV-17 on 100-120 Gaschrom Q	15 psi	270	240	210
LKB 9000 S	3% OV-61 on 80-100 Chromosorb W-HP	25	270	250	250
Finnigan 3200	2% OV-101 on 80-100 Chromosorb W-HP	24 psi	270	220	210
LKB 9000	3% OV-1 on 100-120 Gaschrom Q	30	260	250	280
HP 5984 A	3% OV-17 on 100-120 Chromosorb W-HP	30	300	240	240

Table II. Fragmentographic Setups in Three GC-MS Systems Used for Routine TCDD Determination and Average Instrumental Sensitivities at *m/e* 322 (S/N > 2)

GC-MS system	monitored ion fragments, *m/e*	multiple ion detection technique	detection threshold, pg
LKB 9000 S	320, 322, 324	Hardware: MID control unit with multichannel light beam oscillograph as graphic terminal. Simultaneous mass scanning and recording on photographic paper	40
Finnigan 3200	320, 322, 324	Hardware: MID control unit with multichannel strip chart recorder as graphic terminal. Simultaneous mass scanning and recording	20
HP 5984 A	320, 322, 324	Software: MID program handled through computerized equipment. Simultaneous mass scanning and recording with real-time mass chromatogram visual display. Information stored on disk and recalled through computer display terminal for visual graphics, data reduction, and display permanent copy	20

chemical treatment. TCDD was allowed to settle in for at least 24 h prior to analysis. The TCDD solution was added by means of GC microsyringes, small volumes being released at several internal and external sites of the soil or cotton swab samples. Where vegetation was concerned, the TCDD solution was sprinkled over the sample exposed surface.

Apparatus. A number of GLC-MS systems located in five different laboratories(*8,9*) were used for a considerable number of determinations. Table I summarizes the setup of instruments and indicates gas chromatographic conditions. Column glass tubing, $^1/_4$ inch o.d. × ~2.5 mm i.d., was machined to the required shape and length, from 4 to 7 ft. Under the afore-cited conditions, TCDD appeared within 6 min of injection, although instrumental parameters were usually set for a routine retention time of less than 4 min.

All mass spectrometers were equipped for multiple ion detection either by means of specific hardware accessories (LKB and Finnigan), or by means of a computer-driven software program (Hewlett-Packard). Table II reports some information on operative fragmentographic setups. It may be added that parameters were set to maximize signal intensities while maintaining fine stability and nominal resolution: at *m/e* 322, for $\Delta M = 1$, valley overlap was less than 20% for all instruments. Ionization potential was chosen within the range of 40 to 70 eV, while dwell times were between 100 and 500 ms.

Precautions. Most of the precautinary measures enforced when working with TCDD-containing samples were suggested by the literature (*17*). Mass spectrometer fore pump exhausts were connected to 20–30 mesh activated charcoal traps (~8 cm i.d. × 40 cm length). Wastes from analytical and instrumental processes (glassware, towels, laboratory coats, residues from extraction, oil from MS pumps, etc.) were gathered in sealed containers and disposed of by transfer to a restricted area near Seveso; TCDD-contaminated materials resulting from all kinds of analytical and decontamination processes are, normally, collocated in that area.

Sampling Procedures. *Soil Samples.* Sampling sites were established superimposing a North–South grid over a topographical map of the area. Grid blocks were 50 × 50 m within the evacuated area (*8–10*), and 150 × 150 m elsewhere. Sites were preferentially chosen in open meadows or on farmed land, away from physical obstacles cutting through the ICMESA-to-site line, and set at, or close to, each of the grid block intersections. To evaluate top soil contamination, 50-cm long steel probes (~7 cm i.d.) were vertically sunk to a 7-cm depth: cores were retrieved and stored in separate sealed plastic bags after removal of eventual vegetation. No particular techniques were developed to collect silt and mud. Atmospheric dust was, normally, collected by means of dust-jars.

To determine the vertical distribution of TCDD in soil, samples were taken from the vertical faces of specifically dug trenches (maximum depth, 2 m). Trench walls were first cleaned by careful scraping; then the required number of 10 × 20 × 4 cm steel boxes, or of the aforementioned core cylinders, were inserted horizontally into the trench face, from bottom to top. Collection devices were extracted, emptied, and individual samples were stored as before.

Vegetation Samples. Grass was collected within an area bordered by a 20 × 20 cm steel frame laid on the ground by cutting it off as close as possible to the soil. Sites were established as described. Considerable quantities of diverse vegetation were also obtained from random sampling and from fruit and vegetables markets.

"*Wipe Tests*". Cotton swabs were used to pick up any TCDD on smooth, solid, nonabsorbing surfaces, such as polished marble, waxed stoneware, ceramic tiles, glass panes, Formica surfaces, and synthetic varnish used for metal or wood. "Wipe tests" were extensively used to determine contamination levels of walls, floors, and windows of private and public places; these tests were also employed to detect any TCDD presence on varnished metal such as the exposed parts of large industrial machines.

A square sampling area of 0.25 m^2 (different areas were occasionally used) was wiped back and forth, vertically and horizontally, with a 5- to 10-g degreased cotton swab dowsed with approximately 20 to 30 mL of 20% acetone in hexane. Before changing wiping direction, the swab was turned over to present a fresh side for the pick-up action. The cotton swab was held in a clean metal clamp from start to finish; it was then stored in a glass-stoppered glass jar where extraction was later performed.

Thirty experiments were carried out to determine the pick-up efficiency of the wiping action. Quantities of TCDD, 0.01 or 0.1

μg, were distributed in the form of small droplets of standard solution over test surfaces and allowed to dry naturally and rest for at least 1 h before collecting. All test places were chosen at random and used without any prior cleaning; it was sought to simulate a typical host background. Tested materials were as mentioned above. The average percent recovery was found to be 87 ± 12, two evaluations being discarded from the average as outliers.

Analytical Techniques. *Extraction.* Some anhydrous Na_2SO_4 and approximately 400 mL of 20% acetone in hexane (*14*) were added to a suitable-volume Erlenmeyer flask containing a weighed quantity of sample. The flask was then stoppered. After shaking vigorously for 5 min, the solid residue was allowed to settle. The liquid phase was removed by filtering through a thin layer of anhydrous Na_2SO_4 laid over a qualitative paper filter. Extraction was repeated twice again with additional 300-mL volumes of the same mixture. The three extracts were collected together in a round-bottomed evaporating flask, and evaporated until almost dry in a Büchi Rotavapor under mild vacuum at room temperature. The hexane–acetone mixture was, at times, replaced by dichloromethane.

Weight was in the range of 0.5 to 1.5 kg for soil samples after their water contents had been reduced by allowing for natural under-hood evaporation until weight variations were <5% at 12-h intervals. Samples, 50 to 200 g, were normally used for vegetation owing to its lower specific weight; large vegetation pieces were chopped up before extraction.

Clean-up Steps. Clean-up steps *A* through *D* were selected as deemed most appropriate as a result of extensive use in the early stages (*9*). Any individual step could be readily opted for to clean up the dried extraction product; clean-up step combinations, for certain substratum types, were selected on the basis of progressively acquired experience with samples of similar origins.

Steps *B* and *D* were used in most cases (>50%). Combinations *A-B-D* or *B-C-D* were employed for soil, silt, and mud samples obtained from industrial or urban areas, that is whenever additional cleanup was reckoned to be necessary. Sequence *B-C-D* was, often, applied to extracts of vegetation other than grass as combined steps *B* and *D* generally failed to eliminate some sources of interference. Some soil samples (~2%) containing relatively large quantities of TCDD (>200 μg/m²) were subjected to clean-up step *B* only. Generally, samples were seldom cleaned up any further if instrumental determination appeared to be inadequate because of interference. In such cases, the policy was to analyze a replacement sample purified with a more complete clean-up combination.

A. Large quantities of interfering substances were reduced by adding 5 mL of concentrated H_2SO_4 (*11, 15*) in small draughts to the extract previously diluted to approximately 20 mL with 40–60 °C petroleum ether, and by swirling the mixture vigorously after each addition to permit the organic material to decompose gradually without clotting, thereby avoiding major TCDD losses. Some 20 mL of the same solvent were added, followed by enough anhydrous Na_2SO_4 to produce a semi-fluid system which was, in turn, treated with 15 10-mL portions of 40–60 °C petroleum ether to remove the organic matter from the mineralized part by combined stirring and decanting. Each liquid fraction was drained separately through the multilayer column described hereafter before being pooled with the others in appropriate glassware to be carefully Rotavapor-reduced nearly to dryness.

B. Some anhydrous Na_2SO_4 was added to the extraction residue and the slush treated with ten 5-mL portions of 40–60 °C petroleum ether. Each liquid fraction was purified by a multilayer chromatographic column made from a 20 cm long × 20 mm i.d. glass tubing filled, from bottom to top, with: a glass wool plug, 0.5 cm anhydrous Na_2SO_4, 1.5 cm 70–230 mesh silica gel, 1.5 cm 9:1 (w/w) Na_2SO_4–$NaHCO_3$ mixed layer, 8 cm 1:1 (w/w) 96% H_2SO_4–celite 545 mixture obtained by careful mixing in mortar, and 1.5 cm anhydrous Na_2SO_4. Prior to use, the column was thoroughly washed with petroleum ether. Approximately a 50-mL eluate was collected in a 100-mL Erlenmeyer flask to be concentrated as reported.

C. The residue from *B* was drawn up three times with 5-mL portions of 40–60 °C petroleum ether. The final solution (<20 mL) was extracted with three 30-mL portions of petroleum ether–saturated acetonitrile (*14*) by shaking vigorously for 1 min in a separatory funnel. Each time layers were allowed to separate out completely before removing the acetonitrile layer. The polar phase pool (~90 mL) was washed with 10 mL petroleum ether in a separatory funnel, then transferred to an appropriate glass container to be gently and thoroughly dried by Rotavapor.

This clean-up step proved to be an alternative to *A*. However, it also proved not to be as reproducible as other steps and was excessively time-consuming; consequently, the process was omitted whenever possible.

D. The residue from either *B* or *C* was treated three times with 2-mL portions of hexane. Each fraction was transferred to a 0.5-cm i.d. glass column packed with 1.2 g freshly activated dry alumina(*11, 12, 15*) resting on a glass wool plug. The 3-portion pool was first eluted with 8 mL 99:1 (v/v) hexane–dichloromethane, and then with 7 ml 20% dichloromethane in hexane. The latter fraction was collected in a 25-mL Erlenmeyer flask and Rotavapor-evaporated just to dryness, as described above.

When hexane was replaced by pentane in the eluent mixture, the final forced evaporation was dispensed with; the 7-mL eluate was collected in a 10-mL cone-shaped bottom vial with approximately 3 cm² cross section, and allowed to desiccate under air at room temperature.

Because of the great variety of sample matrices, it was left to the operator's skill and experience to adjust glassware size and chemical quantities to the specific requirements of the analysis. Clean-up steps were selected likewise. This policy proved practical and, in the end, sufficiently straightforward to give reliable results in a fast and steady fashion, rapid output rate being one of the main objectives of the entire technical setup.

Dried samples were kept in collection containers which were sealed either with glass stoppers or Teflon-lined screw caps to enable safe handling. Once delivered to instrumental laboratories, samples were dissolved in known volumes of iso-octane (usually, 0.1 mL or larger) of which an aliquot was injected for mass fragmentographic determination.

Mass Fragmentography. Although TCDD was occasionally recognized and determined by EC gas–liquid chromatography, most work was carried out by combined gas chromatography–mass spectrometry which gave similar sensitivity limits and a more trustworthy identification technique; the latter owing to the combination of gas chromatographic retention time with a typical feature of TCDD mass spectrum, that is the intense lines associated with the first three masses of the molecular ion pentuplet (*18*). The occurrence of the expected intensity ratio 77:100:49, relative to peaks at nominal *m/e* 320, 322, and 324, was taken as evidence that TCDD was present. Differences from standard TCDD pattern of ±10% and ±0.1 min on isotopic ratios and retention time, respectively, were admitted.

When interfering compounds appeared at the correct retention time and the actual quantity of TCDD could not be measured, the analysis output was defined as "undetermined", generally giving a numerical upper limit. Subsequently, a substitute sample was analyzed for more accurate results. If one or both identification criteria proved to be starkly absent, TCDD presence was ruled out and the analytical outcome was defined as "undetected", namely below sensitivity limit. It must be pointed out that near detection threshold (S/N > 2 at *m/e* 322), only the intensity ratio of peaks at *m/e* 320 and 322 could be used; data yielded were never contradicted by later checks. A summary of the analytical work up until October 1977 is reported in Table III.

Weekly or daily tests were performed to ascertain the linear response range of each GLC-MS system and the minimum TCDD amount capable of producing a S/N > 2 at *m/e* 322. Although response was normally linear over a wide range of injected dioxin amounts (Table IV), all operators agreed to compare sample-originated signals with standard TCDD peaks of similar intensity. Standard-to-sample injections were in the ratio of 1 to 2 in most analysis runs.

It should be noticed that most packings yielded slightly asymmetrical peaks, and that would suggest using areas instead of heights for quantity calculation. Both methods, however, were used with comparable results even at faint signal intensities, this being possible owing to the modest degree of accuracy called for. Tailing was negligible when 1.5% OV-17/1.95% QF-1 on 80–100 Chromosorb W-HP packing was used. However, this mixed

Table III. "Undetected"-,[a] "Undetermined"-,[b] and "Determined"-Category Samples Analyzed up until October 1977, and Their Group Subdivision by Analytical Result

samples (month, N_o)		"undetected" N_1	"undetected" $N_1/N_o \times 100$	"undetermined" N_2	"undetermined" $N_2/N_o \times 100$	"determined" N_3	"determined" $N_3/N_o \times 100$
Sep	1019	559	54.9	47	4.6	413	40.5
Oct	593	167	28.2	10	1.7	416	70.1
Nov	475	161	33.9	32	6.7	282	59.4
Dec	311	57	18.3	7	2.3	247	79.4
Jan	197	137	69.5	7	3.6	53	26.9
Feb	472	360	76.2	39	8.3	73	15.5
Mar	455	305	67.0	20	4.4	130	28.6
Apr	617	262	42.5	98	15.9	257	41.6
May	755	351	46.5	53	7.0	351	46.5
Jun	424	279	65.8	19	4.5	126	29.7
Jul	482	287	59.5	22	4.6	173	35.9
Aug	438	242	55.3	1	0.2	195	44.5
Sep	711	536	75.4	13	1.8	162	22.8
Oct	374	312	83.4	8	2.1	54	14.5
total	7323	4015	54.8	376	5.1	2932	40.1

[a] Below detection threshold. [b] Doubtful results due to presence of interfering compounds.

Table IV. Check on Fragmentographic Response Reproducibility: Normalized Signal Intensity[a] as Function of TCDD Injected Quantities. Apparatus: Hewlett-Packard 5984 A

TCDD, pg	injected volume, μL	operator 1, m/e 322	operator 2, m/e 322	operator 2, m/e 324[b]
40	4	0.40 ± 0.01[c]	0.40 ± 0.01	0.19 ± 0.02[d]
100	1	1.05 ± 0.06		
200	2	1.95 ± 0.13	2.07 ± 0.14	1.01 ± 0.10
400	4	4.06 ± 0.18		
500	5		5.30 ± 0.22	2.47 ± 0.07

[a] Each value averaged from 5 determinations. [b] Normalized against m/e 322, Operator 2. [c] Standard deviation. [d] Average detection threshold.

stationary phase proved to be rather unsuitable when mass fragmentography was performed because of some unwanted background from column bleeding and rather rapid deterioration with respect to other packings.

RESULTS AND DISCUSSION

Recovery Data. Individual steps, and their selected combinations, were tested to ascertain recovery yields for all, or parts, of the analytical process.

To check the reliability of TCDD recovery rates for the separate clean-up steps, a 1-mL volume of the standard solution, containing either 0.01 or 0.1 μg of TCDD, was subjected to the clean-up step in question. Table V summarizes our results. We should like to emphasize that between-step residue transfers may be responsible for some TCDD loss. Our data show that at least three 2-mL solvent volumes are required to transfer an average 96% of the dioxin present in the residue from one container to the next. Repeated transfers may quite possibly contribute to the total TCDD loss in the *B-C-D* clean-up step combination, which is considerably higher than what might be expected on the basis of the recovery values for individual steps.

Table V. Results of Recovery Tests Performed on the Analytical Procedure, or Its Single Parts.[a] TCDD Quantity Used: 0.1 and 0.01 μg/Test in 1 mL Solvent

operation and number of tests	TCDD % recovery minimum	maximum	average
clean-up step *B*, 12	80	124	101 ± 12[b]
clean-up step *C*, 15	73	114	91 ± 13
clean-up step *D*, 14	95	120	102 ± 7
clean-up steps *B-D*, 18	80	115	96 ± 12
clean-up steps *B-C-D*, 8	58	93	76 ± 11
extraction (soil)[c]			90
extraction (grass)[c]			89
extraction (cotton swabs)[c]			90

[a] Clean-up step *A* did not introduce any appreciable TCDD loss provided the operation was performed with the utmost care. This conclusion was reached after a number of recovery tests had been carried out by applying a sequence of clean-up steps including *A*. [b] Standard deviation. [c] Obtained from values shown in Table VI by taking into account TCDD losses due to clean-up steps.

Table VI. TCDD Recovered from Laboratory-Contaminated Agricultural Soil, Grass, and Cotton Swabs. Sample Weights: 500, 100, and 10 g, Respectively. Main Analytical Operations Employed: Extraction and Clean-up Steps *B-D*. Total Added Quantities in the Range of 0.005 to 0.55 μg/Sample

type of sample and number of tests	TCDD % recovery minimum	maximum	average	confidence interval[a]
soil, 28[b]	74	101	86 ± 7[c]	83-90
grass, 12	72	98	85 ± 7	79-92
cotton swabs, 46[b]	68	112	86 ± 10	82-90

[a] Probability level, 99.0%. [b] Groups originally containing 30 and 49 samples. Two, and three, outcomes, respectively, were considered as outliers and disregarded. [c] Standard deviation.

Table VI shows TCDD recovery yields obtained when agricultural soil, grass, and cotton swab substrata were analyzed. Samples, prepared as previously described, were extracted and subjected to a clean-up procedure involving steps *B* and *D*, with the following exceptions: 10 soil samples were subjected to step *B* only, and 19 cotton swab samples were taken through the *B-C-D* combination. In the latter case, the individual recovery yields were corrected because of the loss caused by combining step *C* with *B* and *D*, as can be seen in Table V. The group formed by these corrected values did not exhibit any significant statistical difference when compared to the group of remaining 27 samples processed through steps *B* and *D* only. It was, therefore, assumed that the whole ensemble could be dealt with as a homogeneous group. Recovery yields appear to be very similar for the substrata investigated.

It should be noticed that the vegetation analyzed up to the end of 1976 was thought to carry TCDD as a result of the initial fallout and, therefore, distributed over the exposed surface of samples. Recovery tests were conducted accordingly. However, as time went by, it seemed reasonable to assume that soil-to-vegetation transfer would occur and take over the previous contamination mechanism; data obtained from parallel external–internal laboratory-contamination preliminary experiments give a somewhat unclear picture, but sufficient to show that recovery yields, for both contamination mechanisms, may strongly depend on the type of vegetation.

On the whole, it may be concluded that, for grass and grass-like vegetation exhibiting external contamination states, consistent recovery yields >70% were found, though they were also seen to drop to less than 40% when other types of vegetation were considered (for instance, fruit and vegetables). Recovery of TCDD from internal sites is under investigation and no definitive conclusions may be drawn.

Silt, mud, and city soil were treated similarly to agricultural soil. Mean recovery yields for groups of 10 to 15 samples were found to coincide with those reported in Table VI within statistical meaningfulness. However, occurrence of "undetermined" results was generally above average.

Recovery statistical dispersions appear to be influenced somewhat by the number of operators working on the analytical process, larger variation coefficients (>10%) being related to the intervention of several people (>2). With only one operator, <5% variation coefficients were attainable.

Finally, Tables V and VI concern only the data obtained from one specific investigation; data are, however, borne out by the results of a great number of various recovery tests performed on every 10- to 20-sample set, and aimed at ascertaining if the procedure selected for the analysis, as a whole or in its separate stages, would match the optimized yields previously discussed. When mismatches were found, the procedure was reviewed, chemicals checked, and, if necessary, substituted until analysis could be carried out with the correct recovery values. From Table VI, the following three coefficients were worked out to correct numerical outputs due to manipulation losses: soil, 1.16; grass and grass-like vegetation, 1.18; "wipe tests", 1.33, obtained by assuming that "wipe test" pick-up efficiency (see last paragraph of "Wipe Tests" under "Sampling Procedures") and analytical treatment account for average losses of 13% and 14%, respectively, and, therefore, the final overall recovery may have a 75% yield.

The average detection threshold for soil, vegetation, and "wipe tests" can be calculated by using the information previously reported. If the available instrumental sensitivity is taken as approximately 20 pg, and the injected aliquot is 10% of the extract final volume, then 0.2 ng/extract can be detected. We may extrapolate the expected sensitivity for soil, grass, and "wipe tests" to be 0.2 ppt, 2 ppt, and 1 ng/m^2, respectively. However, these values are not supported by experimental evidence as no recovery tests were carried out at such concentrations. On the other hand, data shown in Table VI assess 10 ppt, 50 ppt, and 20 ng/m^2 as being clearly detectable, thereby suggesting detection thresholds to be in the 10 to 0.2 ppt, 50 to 2 ppt, and 20 to 1 ng/m^2 ranges. Many analytical results seem to indicate that apparent thresholds are definitely better than the upper limits, and can consistently approach the lower ones when operations are performed appropriately.

Inter-Group Liaison. As there were several instrumental laboratories working independently on TCDD detection in samples prepared elsewhere (*8*, *9*), GLC-MS operators thought it advisable to avoid yielding data unless compliant with common standard procedures (*8*). The ensuing check criterion was to have unidentifiable test samples circulate among others in the ratio of approximately 1 to 20 and, for them, to be blind-analyzed by all operators. In the end, the outcome of each single determination for a particular sample was compared with the value obtained by averaging all results relative to that one sample; separate determinations were considered to be acceptable if their deviations from the average were within a preset check value.

In most instances, test samples were handled by two laboratories only; if the numerical difference in the results was greater than the preset value, a third laboratory would carry out a blind determination to identify the erroneous result, the genesis of which would be fully investigated.

Table VII. Pertinent Statistical Parameters in a Group of Recycled Test Samples

found TCDD quantity, μg/sample			mean variation coefficient, %	mean maximum deviation, %	number of samples
range	minimum	maximum			
$Q \leq 0.1$	0.0020	0.10	32	53	44
$0.1 < Q \leq 1$	0.11	0.79	13	21	33
$1 < Q$	1.5	146	11	18	6

To obtain check values, found TCDD quantities were grouped into classes, the number and nominal limits of which were identified through statistical evaluation mainly by minimizing the mean variation coefficient relative to each quantity range in order to keep each result dispersion homogeneous in its own range. The results of 83 test samples cropped off from a 4-month period are shown in Table VII. Checks were quickly carried out by utilizing mean variation coefficients: for instance, most measures (95%) in the 0.1- to 1-μg/sample range were expected to fall within ±26% of the average. Whatever result lay outside was viewed as suspicious and, therefore, investigated.

Finally, it should be pointed out that the remarkable increase of the high-sensitivity range mean variation coefficient complies with what one would expect when utilizing a highly sensitive analytical procedure.

High-Resolution GLC. A number of samples were analyzed first by our instrumental technique and later by combined high-resolution GLC-mass fragmentography (*19–21*), analyses being performed at the Swiss Federal Research Station, Wädenswil, Switzerland. High-resolution GLC was introduced as a check test for routine GLC-MS outputs any time an "undetermined" result was thought to be critical and whenever analytical results did not fit into statistical expectancy. All checks were carried out to either ascertain or rule out TCDD presence, no particular attention being given to quantitative aspects. However, later evaluations, obtained by comparing sample fragmentograms to those of external standards, yielded the results reported in Table VIII. All "undetermined" samples were found to contain TCDD. For samples 1, 6, and 8, the new estimates were below, though comparable with, the previously given upper limits. In all other cases but one, attributed to an operator's mistake (sample 7), TCDD presence was clearly confirmed and calculated amounts compared well with the previous findings.

It is noteworthy that samples reported in Table VIII underwent a further instrumental analysis because of some suspicion cast upon our original results. However, all results but one were found to agree with those obtained later when a more sophisticated technique was applied.

Statistical Evaluation. The relationship between "undetermined" outcomes, so classified as to avoid biasing findings on TCDD presence, and the frequency of these outcomes during the 14-month period merits analysis in greater depth. Data shown in Table III agree with a statistical evaluation of the "undetermined" result frequency expressed in terms of median, mean value, and 99% confidence interval.

When 14 months are considered, one obtains: 0.045, 0.048, and 0.017 . . . 0.080, respectively. If the April results are disregarded as being outliers, one has: 0.044, 0.040, and 0.020 . . . 0.060, respectively. If the lower limit of the confidence interval is considered as an optimistic estimate, then approximately 2% of the analytical results may be expected to

Table VIII. TCDD Evaluation in Soil (1-10) and Vegetation (11-20) Samples: This Laboratory's Results and Those Obtained in Check Tests by High-Resolution GLC-Mass Fragmentography

sample	this laboratory's result, μg[a]	check test outcome, μg[b]	
1	⩽1.2	positive	1.8
2	0.69	positive	1.0
3	0.69	positive	1.0
4	0.0020	positive	<0.01
5	0.46	positive	0.50
6	⩽0.19	positive	0.10
7	0.53	negative[c]	
8	⩽1.3	positive	0.70
9	0.060	positive	0.090
10	⩽0.090	positive	<0.03
11	0.10	positive	0.080
12	0.13	positive	0.064
13	0.51	positive	0.41
14	0.43	positive	0.22
15	0.30	positive	0.14
16	0.47	positive	0.56
17	0.21	positive	0.24
18	1.1	positive[d]	
19	0.028	positive	
20	0.0097	positive	

[a] The sign ⩽ stands for "undetermined". [b] Approximate values calculated in our laboratory from previously recorded mass fragmentograms (see text). [c] Erroneous retention time. [d] Check tests on samples 18 through 20 were performed in our laboratory.

classify as "undetermined", a trend which may be expected when the analytical procedure is applied to a restricted class of materials, and carried out with the utmost care.

On the other hand, doubtful results occur with an average frequency <5%, as may be derived from medians and mean values. No realistic upper limits can be established for cases of pessimistic expectancy as the analytical techniques described herein were applied only to samples of somewhat preselected substrata. It must be pointed out that no false positive results were found in the high sensitivity range. More critical information is lacking.

CONCLUSIONS

The information presented in this work holds enough critical evidence to strongly support, contrary to some criticism (22), the combined use of low-resolution gas chromatography and low-resolution mass spectrometry (mass fragmentography) for TCDD detection in environmental samples at a ppt level, provided certain conditions are observed. Our experience also allows us to recommend the technique, once adequate clean-up steps have been taken, as a definite alternative to more sophisticated techniques whenever the latter are unavailable or unsuitable for the actual task.

Because the samples supplied of various types and gathered over an extended period presented a broad spectrum of analytical problems, some changes have since been introduced to accelerate the clean-up procedure, reduce the chance of TCDD losses, and extend the applicability of this method to substrata other than those reported upon. These modifications appear to offer promising possibilities and will be described elsewhere after thorough operative testing has been performed.

ACKNOWLEDGMENT

We thank H. R. Buser for the high-resolution GLC-MS analyses and C. Rossi and L. Manara for providing helpful suggestions and discussions. We also thank P. Adamoli, G. Bandi, A. Bonetta, G. Camarda, D. Caruso, M. G. Castelli, M. Fittipaldi, G. P. Martelli, D. Pontecorvo, F. Rizzello, G. Rossi, G. P. Schmidt, P. Tancioni, and E. Zaino for their technical assistance in the laboratory.

LITERATURE CITED

(1) A. Poland and A. Kende, *Fed. Proc.*, **35**, 2404 (1976).
(2) IARC, *IARC Monogr., Evaluation of Carcinogenic Risk of Chemicals to Man*, **15** (1977), Lyon, France.
(3) N. Frontali, G. L. Gatti, and C. Rossi, "Toxicological Data and Operational Decisions Concerning TCDD Contamination: A Discussion of Guidelines Particularly in Relation to the Limits of Analytical Methods", report of the Istituto Superiore di Sanità, ISTISAN 1977/1 (1977), Rome, Italy.
(4) R. L. Rawls and D. A. O'Sullivan, *Chem. Eng. News*, **54**, 27 (1976).
(5) A. Hay, *Nature (London)*, **263**, 338 (1976).
(6) B. Commoner and R. E. Scott, "U.S. Air Force Studies on the Stability and Ecological Effects of TCDD (Dioxin): An Evaluation Relative to the Accidental Dissemination of TCDD at Seveso, Italy", report of the Center for Biology of Natural Systems, Washington University, St. Louis, Mo., 1976.
(7) L. Canonica, *Chim. Ind. (Milan)*, **59**, 87 (1977).
(8) A. di Domenico, "Valutazione della TCDD nel Terreno: Sviluppo della Metodologia Analitica e Definizione del Sistema di Approntamento di una Mappa di Contaminazione", report of the Istituto Superiore di Sanità (Rome) and Laboratorio Provinciale di Iglene e Profilassi (Milan) for the EEC, ISTISAN 1977/4 (1977), Rome, Italy.
(9) P. Adamoli et al., "Analysis of 2,3,7,8-Tetrachlorodibenzo-*p*-dioxin in the Seveso Area", in "Chlorinated Phenoxy Acids and Their Dioxins: Mode of Action, Health Risks, and Environmental Effects", *Ecol. Bull.*, **27**, 31 (1978), C. Ramel, Ed., Stockholm, Sweden.
(10) A. di Domenico, F. Pocchiari, V. Silano, and G. Zapponi, *CODATA Bull.*, **29**, 53 (1978).
(11) D. Firestone, J. Ress, N. L. Brown, R. P. Barron, and J. N. Damico, *J. Assoc. Off. Anal. Chem.*, **55**, 85 (1972).
(12) H. R. Buser and H. P. Bosshardt, *J. Chromatogr.*, **90**, 71 (1974).
(13) H. R. Buser, *J. Chromatogr.*, **107**, 295 (1975).
(14) P. Slade, *J. Assoc. Off. Anal. Chem.*, **58**, 1244 (1975).
(15) E. C. Villanueva, R. W. Jennings, V. W. Burse, and R. D. Kimbrough, *J. Agric. Food Chem.*, **23**, 1089 (1975).
(16) W. W. Blaser, R. A. Bredeweg, L. A. Shadoff, and R. H. Stehl, *Anal. Chem.*, **48**, 984 (1976).
(17) O. Anilline, *Adv. Chem. Ser.*, **120**, 126 (1973).
(18) R. Baughman and M. Meselson, *Adv. Chem. Ser.*, **120**, 92 (1973).
(19) H. R. Buser, *J. Chromatogr.*, **114**, 95 (1975).
(20) H. R. Buser, *Anal. Chem.*, **48**, 1553 (1976).
(21) H. R. Buser, *Anal. Chem.*, **49**, 918 (1977).
(22) R. A. Hummel, *J. Agric. Food Chem.*, **25**, 1049 (1977).

RECEIVED for review March 15, 1978. Accepted January 18, 1979.

Electrochemical Removal of Phenolic Films from a Platinum Anode

Ross C. Kolle and Dennis C. Johnson*

Department of Chemistry, Iowa State University, Ames, Iowa 50011

The polymeric film which can form on a Pt electrode during anodic detection of phenol produces a loss of electrode activity. The electrochemical removal of the film from the electrode surface and simultaneous reactivation of the electrode are quickly achieved by anodic polarization in an acidic solution of ferric chloride. A mechanism is suggested for the cleaning process.

The chemical literature contains numerous reports of the loss of electrode activity which accompanies the buildup of polymeric films on the surfaces of solid electrodes during oxidation of phenol and various other aromatic hydrocarbons (*1-12*). The accumulation of reaction products which produces the loss of electrode activity is commonly referred to as "blocking", "poisoning", or "fouling". Fichter and co-workers (*1-4*), as early as the second decade of this century, reported that surface films are formed during anodic oxidations of some aromatic compounds and that a consequential instability and lack of precision were observed in subsequent electroanalytical measurements. The authors did not offer a practical solution to the problems created by the films. Reporting on their efforts to develop a voltammetric method for the determination of phenolic compounds at a Pt electrode, Hedenberg and Freiser (*5*) commented: "A black deposit was formed on the electrode . . . . This deposit was insoluble in acetone, dioxane, chromic acid, nitric acid, and strong alkali. The formation of the deposit gradually insulated the electrode from the cell causing the observed current to drop . . . . The only way found to clean the electrode was to burn off the deposit in the flame of a Bunsen burner for 30 seconds prior to each run". Other workers have reported similar difficulties when attempting to remove organic films from fouled electrode surfaces (*6, 7*).

Several suggestions have been given to diminish the problems caused by these surface films (*6, 7, 11*) but they are of questionable practicality for routine electroanalysis. A patent covering the electrochemical synthesis of hydroquinone, starting with the electrochemical oxidation of phenol, describes the use of a cellophane membrane to cover the electrode surface for the purpose of retarding the loss of electrode activity (*11*). The application of membrane-covered electrodes for amperometric analysis results in a sacrifice of sensitivity because transport of analyte through a membrane is slow relative to convective-diffusional transport in the solution phase.

The primary reaction in the oxidation of phenol at Pt electrodes is concluded by Gileadi et al. (*9, 10, 12*) and others (*13, 14*) to be a one-electron oxidation to produce the phenoxy radical which is adsorbed at the electrode surface.

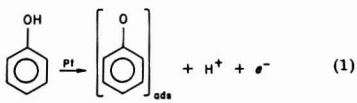

(1)

Strong lateral attractions exist between adsorbed radicals, according to Gileadi et al. (*12*). Mechanisms by which adjacent phenoxy radicals can couple to form dimers, oligomers, and eventually polymers are discussed by Taylor and Battersby (*13*). The adsorbed phenoxy radical can undergo a subsequent oxidation to produce the phenoxonium cation. This cation, acting as a strong electrophile, can react with water to produce quinone or with a phenol molecule to produce a dimer.

Reliance on certain rituals of electrochemical pretreatment for maintaining a high level of electrode activity is an integral part of most voltammetric methods of analysis with noble-metal electrodes (*15*). The pretreatment usually consists of alternate anodic and cathodic polarization of the electrode. This method of pretreatment is ineffective for removal of the adsorbed products from oxidation of phenol at a Pt electrode. We report here the first electrochemical method for the in situ cleaning and reactivation of a Pt electrode which has been severely fouled by a polymeric phenoxy film. The method consists of anodic polarization in an acidic solution of ferric chloride. Also described is the detection of phenol in water at a Pt electrode by flow-injection analysis to 1 ppb ($\mu g\ L^{-1}$) without preconcentration. At this concentration, no electrode fouling was observed.

EXPERIMENTAL

Instrumental. Current–potential (*I–E*) curves were obtained with a rotating Pt disk electrode, area equal to 0.459 cm^2, from Pine Instrument Co., Grove City, Pa. The rotator was model PIR, also from Pine Instrument Co. A Pt disk electrode, area equal to 0.32 cm^2, was constructed in the Chemistry Shop at Iowa State University for use in the PIR rotator. This electrode was of special construction to permit easy detachment of the Pt tip from the mounting shaft for entry of the Pt electrode into a scanning electron microscope. The Pt disk surfaces were polished by the usual metallurgical process to a mirror finish. The flow-through electrode, shown in Figure 1, was constructed by the Chemistry Shop from 16-gauge (0.130-cm) Pt wire and silica-loaded Teflon. The channel containing the wire electrode had the dimensions 0.152 cm (i.d.) × 2.1 cm. The area of the wire electrode exposed to the flowing stream was 0.858 cm^2.

Potentiostatic control for all electrochemical experiments was provided by a three-electrode potentiostat assembled in our laboratory from operational amplifiers according to the conventional design (*16*). A booster was included in the potentiostat to give the control amplifier a value of current saturation equal to approximately ±600 mA. The large current capacity was necessary only for the cleaning procedure applied to fouled electrodes. In those cases, the current-to-voltage converter was removed from the potentiostatic circuit and the working electrode was attached directly to ground. Measurement of the electrode current during cleaning was accomplished by observing the potential drop (IR) produced across a small, standard resistor inserted between the output of the control amplifier and the counter electrode. The reference electrode was a miniature SCE from Beckman Instruments, with a saturated solution of NaCl as the filling solution. All potentials are reported vs. the SCE reference.

A diagram of the flow-injection analyzer is shown in Figure 2. Compression seals were made from $^1/_8$-inch Fetfe, a pliable fluoroelastomer obtained from Ace Glass, Inc., Vineland, N.J. Fetfe is inert to strong acids and corrosive solutions. All tubing, tube-end fittings and valves were of the Cheminert variety from Laboratory Data Control of Riviera Beach, Fla. Tubing (0.787-mm

0003-2700/79/0351-0741$01.00/0 © 1979 American Chemical Society

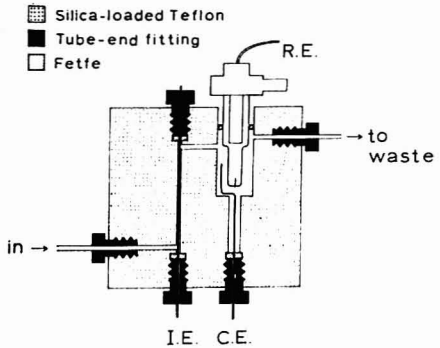

Figure 1. Platinum detector electrode. I.E., Pt indicating electrode; C.E., Pt counter electrode; R.E., calomel reference electrode

i.d.) was made of Teflon; tube-end fittings were polypropylene; and valves were made from Kel-F. The sample loop on the sample-injection valve had a capacity of 0.0709 mL. Flow of the carrier and reagent streams was maintained by compressed He applied to the reagent bottles. Flow rate was adjusted by a needle valve, constructed in the Chemistry Shop from Kel-F, and monitored by a calibrated flowmeter from Gilmont Instruments Inc., Great Neck, N.Y.

The scanning electron microscope was model JSM-U3 from JEOL, Inc., and micrographs were recorded on Polaroid film. Three-dimensional microscopic observation of the electrode surface was possible by obtaining micrographs at two angles differing by about 8°. Each resulting pair of micrographs was then observed with aid of a stereoscopic viewer.

Chemicals. Phenol was the analytical reagent from Mallinckrodt Chemical Works and was used without further purification. All other chemicals were reagent grade from J. T. Baker Chemical Co. Water was triply distilled with demineralization after the first distillation; the second distillation was from an alkaline solution of permanganate.

Procedure for Cleaning Electrodes. Platinum electrodes which had become fouled during oxidation of phenol were successfully cleaned of the adherent, polymeric film by anodic polarization in a solution of 0.1 M $HClO_4$ containing $Fe(ClO_4)_3$ and NaCl. The concentrations of Fe(III) and Cl^- were 1 mM for the rotating disk electrodes, and 0.1 M for the flow-through detector. A signal voltage of 3 V was applied at the input of the potentiostat for polarization periods of 30 s to 2 min, depending on the extent of fouling. The current density at the electrodes during anodic polarization was approximately 0.4 A cm^{-2}. No attempt was made to calculate the true electrode potential during cleaning because of the unknown and variable value of the uncompensated cell resistance.

RESULTS AND DISCUSSION

Detection of Phenol by Flow-Injection Analysis. Typical anodic current peaks for detection of phenol at a concentration of 10 μM in a solution of 0.10 M $HClO_4$ are shown in Figure 3A for a flow rate of 2.0 mL min^{-1}. Each injection corresponds to 67 ng phenol. The average value of peak height for the 20 peaks in Figure 3A is 1.12 μA, with a relative standard deviation of 9.7 ppt. At the concentration of phenol used for Figure 3A, loss of electrode activity was negligible with successive injections. A linear calibration curve based on peak area was obtained for detection of phenol in the concentration range 0.01–10 μM with a slope of 1.436 C M^{-1} and a correlation factor of greater than 0.999. The detection limit was approximately 0.01 μM which corresponds to 0.1 ng phenol per injection.

Fouling of Pt Electrodes. Electroanalysis of solutions of phenol at concentrations much greater than 10 μM resulted in rapid loss of electrode activity for oxidation of phenol, as observed in Figure 3B for 1.0 mM phenol (6.7 μg per injection). The electrode activity is lost not only for subsequent anodic detection of phenol but also for anodic detection of Br^-. Detection peaks are shown in Figure 3C for injections of 1.0 mM Br^- (5.7 μg per injection) in 0.1 M $HClO_4$ made alternately with the injections of 1.0 mM phenol in Figure 3B. The peak in Figure 3C labeled with a zero corresponds to the injection of Br^- for a fully active electrode prior to detection of any phenol. The area of peak 0 in Figure 3C is 4.62×10^{-4} C. This corresponds to a detector efficiency of 6.8%.

Figure 4 is a plot of the peak area observed in a separate study for injections of Br^- as a function of the cumulative electrical charge passed for oxidation of phenol prior to the injection of Br^- sample. Response of our detector for Br^- was eliminated when a total of 5.0 mC of charge had passed for oxidation of phenol at a concentration of 1.0 mM. Assuming a perfectly smooth electrode surface, i.e. true area/geometric area = 1, and a 1:1 correspondence of Pt atoms at the surface with the product of a one-electron oxidation of phenol, 5.0 mC corresponds to the equivalent of 24 monolayers of phenoxy product on the electrode surface. Gileadi reported that several

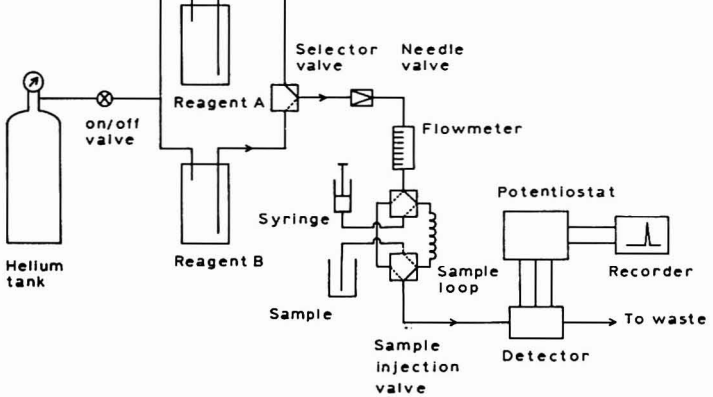

Figure 2. Flow injection analyzer. Reagent A: 0.1 M $HClO_4$; reagent B: 0.1 M $HClO_4$, 0.1 M $Fe(ClO_4)_3$, and 0.1 M NaCl

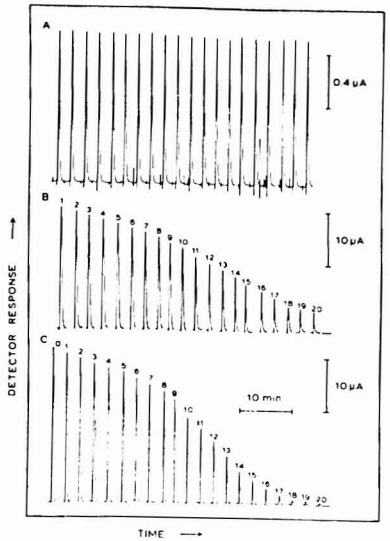

Figure 3. Detection peaks for phenol and bromide. $E = 1.2$ V, $v_f = 2.0$ mL min^{-1}. A: 67 ng phenol per injection; B: 6.7 μg phenol per injection; C: 5.7 μg Br^- per injection

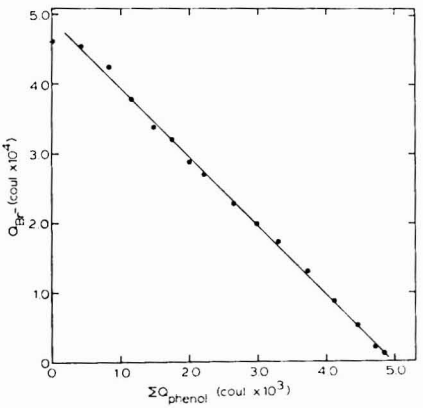

Figure 4. Peak area for bromide detection as a function of accumulated area for prior phenol detections

hundred monolayers of the phenoxy radical must be adsorbed to produce complete fouling of the Pt electrode (*9*). Little quantitative emphasis should be placed on these data because the assumption of a perfectly smooth electrode surface can never be valid. Furthermore, the retention of the phenoxy radicals on the electrode is probably not quantitative. The total charge for phenol oxidation required to totally foul the electrode is larger at low concentrations of phenol than at high concentrations. For example, we observed negligible loss of electrode activity following 20 injections of samples containing 1 nmol phenol per injection, whereas loss of activity was appreciable for a single injection of 5 nmol of phenol. Obviously the fouling process is more efficient at higher fluxes

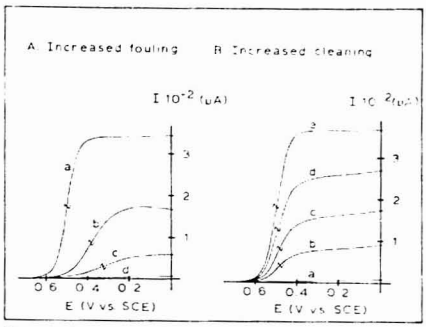

Figure 5. Current–potential curves for reduction of iron(III). Rotating disk electrode, 1600 rev min^{-1}, 0.1 M $HClO_4$, 1.0 mM $Fe(ClO_4)_3$; A: curves obtained for successive degrees of electrode fouling, curve a corresponds to "clean" electrode at start of experiment; B: curves obtained for successive stages during electrochemical cleaning of a fouled electrode, curve e corresponds to "clean" electrode

of phenol which is consistent with a mechanism for film formation which involves coupling of radicals at the electrode surface (*17*).

There was no readily observed change in the appearance of a Pt electrode which had been fouled just to the extent that Br was electroinactive. Continuation of the fouling process for many hours was accompanied by an increasing intensity in the color of the electrode surface: light yellow, gold, tan, and finally a deep brown after periods of 24–48 h. The films were not soluble in CH_2Cl_2, CCl_4, $(CH_3)_2CO$, or dimethylformamide. Severe anodization and cathodization in dilute solutions of $HClO_4$ or H_2SO_4 was similarly unsuccessful in reactivating the fouled electrode surface. Likewise, anodic polarization in acidic solutions containing either Fe(III) or Cl^-, but not in combination, did not result in cleaning of the electrode surface.

Comparison of Fouling and Cleaning Reactions. The accumulation of adsorbed products from the oxidation of organic materials onto a "clean" Pt electrode surface has two effects on current–potential curves (I–E) obtained for an electroactive analyte. The heterogeneous exchange current decreases, as noted by the shift of the half-wave potential ($E_{1/2}$). Also, the apparent value of the limiting current decreases as the thickness of the surface film increases to an extent where the analyte cannot gain access to the electrode surface. These two effects are clearly evident in I–E curves obtained for reduction of Fe(III) at a rotating Pt disk electrode and shown in Figure 5A. The electode was fouled by oxidation of phenol at 1.20 V in 0.1 M $HClO_4$ containing 1.0 mM phenol. The fouling process was interrupted periodically and the electrode transferred to a solution of 0.1 M $HClO_4$, containing 1.0 mM $Fe(ClO_4)_3$, for the purpose of recording I–E curves in the potential range 0.7–0.0 V.

When the electrode had been completely fouled, as determined by the virtual loss of a cathodic signal for Fe(III), the electrode was subjected to the cleaning procedure described in a previous section. The cleaning process was interrupted periodically and the I–E curves for Fe(III) were immediately recorded. The resultant curves are shown in Figure 5B. The values of $E_{1/2}$ for the cathodic waves obtained for Fe(III) during the process of cleaning are approximately equal to the reversible value. This is in sharp contrast to the curves in Figure 5A obtained in the process of fouling. Clearly, the cleaning process does not occur by a mechanism which is simply the reverse of that for fouling. The data in Figure 5B are consistent with a mechanism for cleaning in which

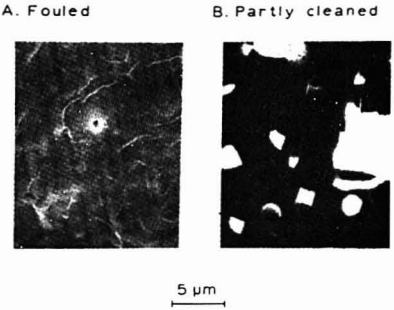

Figure 6. Scanning electron micrographs of fouled electrode (A) and partially cleaned electrode (B)

perforations of the surface film occur which result in exposure of finite portions of clean Pt surface.

No definite conclusions can be made at this time regarding the role of Fe(III) and Cl^- in the cleaning process. Certainly Cl_2 is produced by oxidation of any Cl^- which permeates the film and the chlorination of aromatic compounds is catalyzed by Fe(III) (*18*). Perhaps the chlorination of the phenolic film occurs with concurrent degradation of the polymeric matrix. We observed that the potentials for onset of O_2 and H_2 evolution are not shifted significantly by formation of a surface film, even of sufficient thickness to be observed with the eye. Hence, the film is concluded to be permeable to H_2O, H^+, H_2, and O_2. However, the partial pressure of O_2 at the interface of the Pt and the film during anodic polarization is probably not trivial for a large anodic current density. When the polymeric film has been weakened sufficiently by the chlorination process, the O_2 pressure between the electrode surface and the film is probably sufficient to produce a series of mild explosions. These events quite literally tear pieces of the weakened film from the electrode surface.

Scanning Electron Microscopy. Photographs taken with the scanning electron microscope and shown in Figure 6 are consistent with the previous conclusions. A micrograph of the disk electrode obtained after fouling had occurred to an extent so that the electrode surface appeared dark brown is shown in Figure 6A. The grooves left in the electrode surface by the polishing process are clearly evident even though the surface is completely covered by the polymeric film. Figure 6B is a micrograph of a fouled electrode after partial cleaning of the surface. Numerous small sections of film, 1–6 μm in cross section, have been removed from the electrode surface revealing the Pt substrate. The reduction of Fe(III) on these exposed regions of Pt would be expected to occur by a reversible reaction, which is consistent with the data in Figure 5B. The total area of Pt exposed in Figure 6B was less than the geometric area of the electrode, and the limiting current for Fe(III) at the partially cleaned electrode was less than for the fully cleaned electrode surface. Stereoscopic examination of partially cleaned surfaces frequently revealed fragments of the film, attached to the electrode surface along an edge, which projected away from the surface. The visual appearance was similar to that of a sheet of paper which has been pierced by a blunt object.

Healing of Surface Films. The *I–E* curves for reduction of Fe(III) obtained immediately after partial cleaning of a fouled Pt disk electrode are shown in Figure 5B and were discussed above. If the electrode potential was allowed to scan in a cyclic manner in the range 0.7–0.0 V for several minutes, the value of $E_{1/2}$ for the cathodic Fe(III) wave was observed to shift slowly in a negative direction from the reversible value. Also, the limiting current was observed to decrease simultaneously with the shift of $E_{1/2}$. Subsequent micrographs of the electrode revealed that the edges of the film surrounding the exposed regions of Pt had become very diffuse. Apparently small organic molecules dissolved in the polymeric film, e.g., oligomers, flow from the film onto the freshly cleaned Pt regions resulting in a loss of electrochemical activity on those sections of the Pt surface. Thus, the polymeric films damaged by partial cleaning can undergo a healing process. When the electrodes had been completely cleaned, as noted by a return of the limiting current to the mass transport-limited value, no loss of electrode activity was detected for extended voltammetric application in acidic solutions of Fe(III).

CONCLUSIONS

Platinum electrodes have been demonstrated to be applicable for amperometric detection of phenolic compounds. No loss of electrode activity is observed for detection at low concentrations of phenol (*17*). Occasionally, unintentional fouling of the detector electrode can result if analysis is performed on a solution of phenol at high concentration. In the event of electrode fouling, the adherent surface film is quickly and conveniently removed by brief anodic polarization of the electrode in an acidic solution of ferric chloride. Routine application of Pt electrodes for flow-through detectors in the determination of phenolic compounds by flow-injection analysis or liquid chromatography is now feasible without fear of lengthy down-time for removal of polymeric films from the electrode surface.

ACKNOWLEDGMENT

The authors are grateful to Jerry Amenson of the Engineering Research Institute for performing the microscopy.

LITERATURE CITED

(1) Fichter, F. *Z. Electrochem.* **1913**, *19*, 781.
(2) Fichter, F.; Stocker, R. *Ber.* **1914**, *47*, 2003.
(3) Fichter, F.; Brumner, E. *Bull. Soc. Chem.* **1916**, *19*, 281.
(4) Fichter, F.; Ackerman, F. *Helv. Chim. Acta* **1919**, *2*, 583.
(5) Hedenburg, J. F.; Freiser, H. *Anal. Chem.* **1953**, *25*, 1355.
(6) Lord, S. S.; Rogers, L. B. *Anal. Chem.* **1954**, *26*, 284.
(7) Ginzburg, W. I. *Zhur. Fiz. Khim.* **1959**, *33*, 1504; Eng. transl. in Russ. *J. Phys. Chem.* **1959**, 33(7), 26.
(8) Kondrikor, N. B. *Uch. Zap. Dal'nevost. Univ.* **1966**, *8*, 61; cf. *Ref. Zh. Khim.* **1967**, Pt. 1, 21B1119.
(9) Bejerano, T.; Forgacs, C.; Gileadi, E. *J. Electroanal. Chem.* **1970**, *27*, 69.
(10) Zeigerson, E.; Gileadi, E. *J. Electroanal. Chem.* **1970**, *28*, 421.
(11) Covtiz, F. H. French Patent No. 1 544 350, 1969; *Chem. Abstr.* **1969**, *71*, 91080f.
(12) Gileadi, E. *Isreali J. Chem.* **1971**, *9*, 405.
(13) Taylor, W. I.; Battersby, A. R. "Oxidative Coupling of Phenols", Marcel Dekker, Inc.: New York, 1967, pp 54–55.
(14) Shimizu, T.; Kunugi, A.; Nagaura, S. *Denki Kogaku Oyobi Kogyo Butsuri Kagaku* **1975**, *43*, 269; *Chem. Abstr.* **1975**, *83*, 170102.
(15) Adams, R. "Electrochemistry at Solid Electrodes", Marcel Dekker, Inc.: New York, 1969, pp. 206–208.
(16) Underkofler, W. L.; Shain, I. *Anal. Chem.* **1963**, *35*, 1778.
(17) Kissinger, P. Purdue University, Lafayette, Ind., personal communication, 1978.
(18) Morrison, R. T.; Boyd, R. N. "Organic Chemistry", 2nd ed.; Allyn and Bacon, Inc.: Boston, 1966, pp 351–352.

RECEIVED for review December 4, 1978. Accepted February 5, 1979. Grateful acknowledgment for support of this research is given to the U.S. National Science Foundation, for grants CHE76-17826 A01 and CHE78-01566; and to Iowa State University for a summer research fellowship for R.C.K. in 1976.

Immobilization, Electrochemistry, and Surface Interactions of Tetrathiafulvalene on Chemically Modified Ruthenium and Platinum Oxide Electrodes

Kuo-nan Kuo, P. R. Moses,[1] J. R. Lenhard, D. C. Green,[2] and Royce W. Murray*

Kenan Laboratories of Chemistry, University of North Carolina, Chapel Hill, North Carolina 27514

A monocarboxylic acid derivative of tetrathiafulvalene is immobilized on RuO_2 and PtO electrodes using alkylaminesilane chemistry. The cyclic voltammogram for oxidation of this molecular surface state to the radical cation involves larger surface activity non-ideality parameters than does that for further oxidation to the dication. Oxidation to the radical cation is facilitated by addition of chloride to the acetonitrile solvent medium.

Alkylaminesilane reagents such as 3-(2-aminoethylamine)propyltrimethoxysilane (*en* silane) bind stably from anhydrous reaction media to metal oxide electrodes such as SnO_2 (*1*), RuO_2 (*2*), TiO_2 (*3*), and Pt/PtO (*4*). The thus immobilized amine function can be employed to further immobilize electrochemically interesting molecular charge transfer states (*2*, *4–12*). Of special interest has been the degree to which thus immobilized chemicals usefully mimic chemical (*3*, *6*, *11*) and electrochemical (*10*) characteristics of their molecular analogues dissolved in the solution phase.

Existing immobilized molecular charge transfer states emphasize molecules probing the electrode–solution interface and molecules where the dissolved solution analogue has interesting properties. To the extent that molecular immobilization on a "two-dimensional" solid electrode surface can be considered a special case of the solid state, examples of compounds having special solid state properties are also of interest in modified electrode experiments. Tetrathiafulvalene (TTF) is such a case in view of its unusual solid state conductivity and crystal structure properties as salts with tetracyanoquinodimethane and halides. A carboxylic acid derivative of TTF well suited for an immobilization study has recently been prepared (*13*).

This paper describes experiments in which the carboxylic acid of tetrathiafulvalene (TTFCOOH) has been amide coupled to *en* silanized RuO_2 and Pt/PtO electrode surfaces, producing, ostensibly, the surface structure

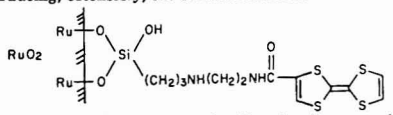

(1)

Various aspects of representing the silicon bonding center have recently been discussed (*3*). The tetrathiafulvalene moiety on this surface undergoes electron transfer communication with the underlying RuO_2 and Pt/PtO electrode surfaces to form the radical cation and dication

$$RuO_2/en/COTTF \rightleftarrows RuO_2/en/COTTF^+ \rightleftarrows RuO_2/en/COTTF^{2+} \quad (2)$$

In keeping with its reputation as an interesting solid state chemical, the immobilized form of tetrathiafulvalene exhibits some unusual electrochemical features which are described.

EXPERIMENTAL

The RuO_2 electrodes were prepared using a spray aspiration method and the Pt/PtO electrode by electro-oxidation. Details are given elsewhere (*14*). After washing with methanol and acetonitrile, and vacuum oven drying (50 °C), the electrode was silanized with a 5% solution of *en* silane in dry benzene and washed copiously with dry benzene, acetonitrile, and $CHCl_3$ in sequence. Amide coupling between this surface and the TTFCOOH derivative was *N,N'*-dicyclohexylcarbodiimide (DCC) assisted; after 36 h reaction in $CHCl_3$ the modified electrodes, designated $RuO_2/en/COTTF$ and $PtO/en/COTTF$, were thoroughly washed with $CHCl_3$ and then acetonitrile.

Electrochemical experiments were carried out in acetonitrile dried over molecular sieves. Benzene was dried over Na^0; 0.1 M $Et_4N^+ClO_4^-$ was supporting electrolyte except as otherwise specified. X-ray photoelectron (XPES) spectra were obtained using a DuPont Model 650B Electron Spectrometer (*1*).

RESULTS AND DISCUSSION

Reaction of *en* silane with the RuO_2 electrodes was verified by observation of the expected (*1*, *3*) N 1s, Si 2p, and O 1s XPES bands on the RuO_2/en surface at 399.8, 102.2, and 532.2 eV, respectively. After the coupling reaction with TTFCOOH, a S 2p band additionally appears at 164.0 eV in good agreement with that obtained for a sample of pure TTF powder (163.6 eV). Contact of an unsilanized RuO_2 surface with a solution of TTFCOOH plus DCC yields, after thorough washing, no S 2p band indicating no adsorption interference.

Cyclic voltammetry of $RuO_2/en/COTTF$ and $PtO/en/COTTF$ electrodes prepared by the amidization procedure produced in most experiments two well-defined oxidation waves (Figure 1) with the peak current–potential scan rate proportionality (for both anodic and cathodic branches) characteristic (*15*) of an immobilized charge transfer state. The formal potentials of the observed surface waves are essentially the same on RuO_2 and PtO modified electrodes, and are furthermore close to those measured by cyclic voltammetry of a solution of an authentic sample of the *n*-propylamide of TTFCOOH as shown by data given in Table I. Treatment of unsilanized PtO electrodes with TTFCOOH solutions yields no evidence of the surface waves. On RuO_2 surfaces, such treatment erratically produces small waves at +0.39 and +0.76 V vs. SSCE which persist for only ca. 10 potential cycles and correspond by their charge to a coverage of zero to 0.6×10^{-10} mol/cm^2. This result indicates either a minor adsorption interference or more likely material trapped in pores of the RuO_2 surface.

The results overall are consistent with covalent coupling of TTFCOOH to the *en* silanized metal oxide electrodes as represented by the amide structure in Equation 1. The immobilized tetrathiafulvalene acts predictably (*10*) as a molecular charge transfer state by undergoing electron transfer communication with the electrode surface at approximately the same formal potential as the solution analogue. It is reasonable to represent the chemical process occurring in the

[1] Present address, P. R. Mallory Company, Burlington, Mass. 01803.
[2] IBM Watson Research Center, Yorktown Heights, N.Y. 10598.

0003-2700/79/0351-0745$01.00/0 © 1979 American Chemical Society

Table I. Cyclic Voltammetry of Immobilized and Solution Tetrathiafulvalene Amidocarboxylic Acid in Acetonitrile

modified electrodes	$E^{o\prime}_{surf}$, volt vs. SSCE[a]	$E^{o\prime}_{soln}$, volt vs. SSCE[a]	ΔE_p, mV[b]	$\Gamma \times 10^{10}$, mol/cm^2 [c]
RuO_2/*en*/COTTF	0.42, 0.77		60, 39	2.9
	0.42, 0.77		81, 51	4.2
	0.40, 0.74		74, 42	5.0
	0.42, 0.78		59, 51	9.5
	0.40, 0.78		80, 70	12
Average[d]	0.41 ± 0.01, 0.77 ± 0.02		70, 54	7.5
PtO/*en*/COTTF	0.45, 0.78		98, 55	3.2 (1.9)
	0.43, 0.78		55, 42	2.5 (1.5)
solution of TTFCONHPr[e]				
at Pt		0.38, 0.75	61, 78	
at RuO_2		0.38, 0.74	60, 63	
at RuO_2/*en*		0.38, 0.75	62, 72	

[a] Average of anodic and cathodic E_{peak}, vs NaCl saturated calomel electrode. [b] At 0.1 V/s. [c] Coverage usually measured on cathodic branch of +0.41 V wave, and based on geometrical area except Pt electrodes where coverage corrected for 1.7 microscopic roughness is shown in parentheses. [d] Average for nine modified electrodes. [e] 0.2 mM solution in 0.1 M $Et_4N^+ClO_4^-/CH_3CN$.

surface waves of Figure 1 as Reaction 2.

Geometrical coverages of immobilized tetrathiafulvalene as measured by charge under the cyclic voltammetric wave are given in Table I. Coverages on RuO_2/*en*/COTTF electrodes are higher than expected for the ca. 2×10^{-10} mol/cm^2 model-estimated monolayer coverage but the coverages on RuO_2 involve a microscopic roughness factors of unknown value. On PtO/*en*/COTTF, a roughness correction can be obtained from the Pt hydrogen adsorption waves (*11*) and application of the measured 1.7 there leads to coverages ($1.5–1.9 \times 10^{-10}$ mol/cm^2) plausibly consistent with monomolecular coverage levels.

Tetrathiafulvalene immobilized using *en* silane is, on both RuO_2 and PtO surfaces, notably stabler than similarly immobilized nitroaromatics (*2*, *4*) but considerably less stable than selected ferrocenes (*11*). Continuous potential cycling through both steps of Reaction 2 causes a gradual diminution of the charge under the surface wave, with no change in waveshape. Attenuation of the charge under the surface wave by 95% requires 100–300 potential scan cycles. Restriction of the potential scan range to the first (cation radical) reaction step only provides greatly enhanced lifetime of the surface charge transfer state; half-lives ($\Gamma = 0.5\,\Gamma_{init}$) exceed 500 cycles as illustrated in Figure 1, curves C. The neutral (unoxidized) electrode state is very stable to exposure to solvent; prepared electrodes are stored under acetonitrile for days with no ill effects. The oxidized forms of the tetrathiafulvalene are then the least stable charge states for the immobilized molecule, particularly the dication. XPES of extensively cycled RuO_2/*en*/COTTF electrodes shows considerable attenuation of the S 2p band but little change in N 1s or Si 2p. Details of the chemical reaction decay pathway are not available, but it appears that, like nitroaromatics and ferrocenes on PtO surfaces (*4*, *11*), decay of the surface charge transfer state is not determined by rupture of the electrode–silane linkage.

Consistent with fast charge transfer of immobilized species, peak potential separations in both steps of Reaction 2 are small. ΔE_p between the anodic and cathodic waves on modified electrodes are shown in Table I. The magnitude of ΔE_p varies somewhat but on both RuO_2/*en*/COTTF and PtO/*en*/COTTF surfaces, ΔE_p for the more anodic ($TTF^+ \rightleftarrows TTF^{2+}$) reaction is smaller than that for the first ($TTF \rightleftarrows TTF^+$) step. This difference in ΔE_p is opposite to that observed for the solution molecule where ΔE_p tends to be, if anything, slightly larger for the $TTF^+ \rightleftarrows TTF^{2+}$ reaction.

Cyclic Voltammetric Waveshapes. It is obvious in Figure 1 that the surface charge transfer for the second ($TTF^+ \rightleftarrows TTF^{2+}$) immobilized tetrathiafulvalene reaction leads to a sharper cyclic voltammetric peak than that for the first ($TTF \rightleftarrows TTF^+$) step. This is a curious effect not paralleled in the electrochemistry of the solution analogue which is normally shaped (Figure 1).

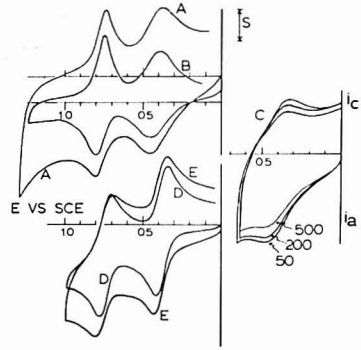

Figure 1. Cyclic voltammograms of immobilized and dissolved tetrathiafulvalene in 0.1 M Et_4N^+ ClO_4^-/CH_3CN, 0.1 V/s. Curve A. RuO_2/*en*/COTTF electrode. 3rd cycle. $S = 16\ \mu A/cm^2$. Curve B. PtO/*en*/COTTF electrode. 10th cycle. $S = 26\ \mu A/cm^2$. Curve C. RuO_2/*en*/COTTF electrode, scan first wave only for indicated number cycles. $S = 12\ \mu A/cm^2$. Curve D. ca. 0.2 mM *n*-PrNHCOTTF at RuO_2 electrode. $S = 16\ \mu A/cm^2$. Curve E. ca. 0.2mM *n*-PrNHCOTTF at RuO_2/*en* electrode. $S = 32\ \mu A/cm^2$

All cyclic voltammetric results reported thus far for immobilized redox molecules display a broadening of the cyclic voltammetric wave as compared to that expected in the ideal reversible situation (*15*). Brown and Anson have proposed that such broadening may reflect surface activities differing from surface concentrations (*16*), and present theory exponentially relating activity to surface coverage and interaction or non-ideality parameters r_O and r_R. Application of the resulting theoretical relations has produced reasonable shape fits to surface waves for both adsorbed (*16*) and covalently immobilized molecules (*11*, *17*).

A comparison of immobilized tetrathiafulvalene to the surface activity theory is illustrated in Figure 2 and Table II. The shape of the background curve underneath the waves on RuO_2/*en*/COTTF electrodes, using a cubic expression, was adjusted for the best overall fit of current above background to the theory (*17*). The appearance of the thus assumed background curve is reasonable, and considering the size of

Table II. Non-ideality Parameters[a] for RuO_2/*en*/COTTF Electrodes

	reaction							
	$TTF \rightarrow TTF^+$		$TTF^+ \rightarrow TTF^{2+}$		$TTF^{2+} \rightarrow TTF^+$		$TTF^+ \rightarrow TTF$	
procedure[b]	$r_{a_1} \times 10^{-9}$	$\Gamma \times 10^{10}$	$r_{a_2} \times 10^{-9}$	$\Gamma \times 10^{10}$	$r_{c_2} \times 10^{-9}$	$\Gamma \times 10^{10}$	$r_{c_1} \times 10^{-9}$	$\Gamma \times 10^{10}$
scan-hold-scan[c]	−1.4	12.5	−0.55	9.6	−0.55	11.2	−1.5	10.3
free scan[d]	−2.0	10.8	...[e]	...[e]	−0.41	9.4	−1.7	11.4
free scan[d]	−2.5	8.6	...[e]	...[e]	−0.69	7.7	−2.3	7.4

[a] Assuming $r_O = r_R$. [b] Results are for three different electrodes. [c] Scan through anodic waves, hold potential at +0.9 V for 10 s, then scan through cathodic waves. [d] Free running cyclic voltammogram, data from 20th cycle. [e] Results not accurate because of excessive base-line current.

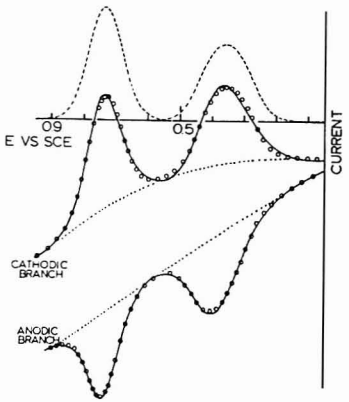

Figure 2. Comparison of cyclic voltammogram of RuO_2/*en*/COTTF electrode (—) with surface activity theory (O). Cubic equation base line (...) for best overall fit. Zero of base line is offset to aid comparison of anodic and cathodic waves. Theoretical curve (---) for cathodic branch without base line. Experimental example corresponds to first entry of Table II

the background correction, the agreement of experiment and theory is fairly good for both waves. There is some shape (skewing) mismatch for the $TTF \rightleftarrows TTF^+$ wave. An additional useful criterion for a satisfactory comparison is obtaining the same calculated surface coverage (using the assumed background) from the areas under all four waves. Except for problems evident with background in several cases for the $TTF^+ \rightarrow TTF^{2+}$ anodic step, coverages evaluated for the four waves through the entire potential cycle are in satisfactory mutual agreement.

Non-ideality parameters obtained from the comparison of the surface activity theory and experiment confirm the visual impressions of the cyclic voltammograms; the wave broadening does differ for the two reaction steps. The non-ideality parameters for the second ($TTF^+ \rightleftarrows TTF^{2+}$) reaction step are numerically 3–5 times smaller than those for the first ($TTF \rightleftarrows TTF^+$) reaction step. Parameters for both waves are negative meaning according to the theory that reactants are destabilized.

Lennox and Murray (*18*) have pointed out that heterogeneity of structural characteristics (e.g., oxide site properties, details of bonding, etc.) of a modified electrode surface could yield a spread in $E^{0\prime}$ in an ensemble of immobilized species, which would have a broadened cyclic voltammetric wave as a consequence. While a contribution from structural diversity remains possible, the mere fact that wave broadening differs for two reaction steps of the same immobilized chemical strongly implies that gross structural heterogeneity is not the dominant factor here.

Correspondence of the experimental results to the surface activity theory of course provides no direct *physical* picture of the electrode–solution interfacial phenomenon which provokes the difference between the two tetrathiafulvalene reactions. Certainly contributions from interactive effects between the immobilized tetrathiafulvalenes are indicated (and in this sense a parallel between the surface and solid state properties exists). Intuitively, heightening of destabilizing electrostatic effects might have been expected for the $TTF^+ \rightleftarrows TTF^{2+}$ reaction as compared to the $TTF \rightleftarrows TTF^+$ step and, activity-wise, on this ground the $TTF + TTF^{2+}$ reaction should be further removed from ideality. The reverse situation, however, is that which is experimentally observed, and thus simple electrostatic considerations do not suffice. It is possible a connection exists between the pattern of ΔE_p and interaction parameters. However, without a better appreciation of the general physical significance of surface activity non-ideality parameters, it is premature to speculate further as to the nature of this unusual characteristic of the immobilized tetrathiafulvalene electrochemistry.

Since reactant and product mass transport (migration) is not a consideration when a charge transfer species is immobilized on an electrode, it is conveniently possible to explore consequences of supporting electrolyte concentrations over a wide range. RuO_2/*en*/COTTF electrodes were examined in 0.005 to 0.2 M $Et_4N^+ClO_4^-$ electrolyte. While ΔE_p increases (for both waves) at low electrolyte concentration, owing to the ohmic effect, and the apparent $E^{0\prime}$ shifts due to liquid junction changes, there is no substantial alteration of the difference in cyclic voltammetric peak sharpness for the first and second tetrathiafulvalene waves with electrolyte concentration.

Effect of Chloride. The interaction of halide ions with tetrathiafulvalene cation radical to form nonstoichiometric conducting halide salts has been reported (*19–21*) as have been the advantages and consequence of electrochemically oxidizing tetrathiafulvalene in the presence of halide in acetonitrile solvent. Stacking of radical cation occurs in the conducting solid. The alterations of TTF electrochemistry in the presence of halide are at least in part associated with the low solubility of the TTF^+X^- salts in acetonitrile.

Figure 3 illustrates the effect of added small concentrations of chloride ion, as $Et_4N^+Cl^-$ to the 0.1 M $Et_4N^+ClO_4^-$ solution contacting a RuO_2/*en*/COTTF electrode. A discernible negative shift in $E^{0\prime}$ occurs for the $TTF \rightleftarrows TTF^+$ reaction, and for a series of chloride additions an approximate 60-mV shift per decade of chloride concentration is identified (Figure 3). The electrochemical wave also becomes less distinct. The second tetrathiafulvalene wave becomes immeasurably buried in the enhanced background attendant to the presence of the halide.

The $E^{0\prime}$ shift shown in Figure 3 corresponds to a stabilization of immobilized tetrathiafulvalene cation radical relative to the reduced form of TTF, as could occur by some specific 1:1 interaction between chloride ion and the radical cation. Of some interest is whether this interaction occurs as "monomer" TTF^+Cl^- units, or by *cooperative* effects between

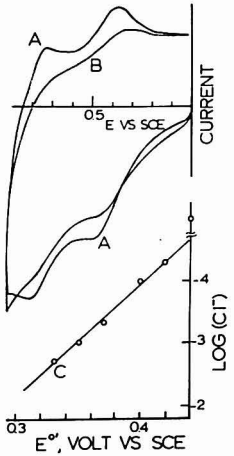

Figure 3. Effect of added $Et_4N^+Cl^-$ on cyclic voltammograms of RuO_2/*en*/COTTF in 0.1 M $Et_4N^+ClO_4^-/CH_3CN$. Curve A; no added $Et_4N^+Cl^-$. Curve B; 10^{-4} M $Et_4N^+Cl^-$. Curve C; shift of $E^{0\prime}$ of TTF $\rightleftarrows$ TTF^+ with $[Et_4N^+Cl^-]$

neighboring immobilized molecules (e.g., $(TTF^+Cl^-)_x$). This question is undergoing further study. Of present note, however, is that the "concentration" of immobilized tetrathiafulvalene amide, if we imagine a monolayer $\Gamma = 2 \times 10^{-10}$ mol/cm^2 confined to a 20-Å surface volume increment, is ca. 1.0 M. The minimum chloride concentration estimated from Figure 3 to yield a shift in $E^{0\prime}$ is 2×10^{-5} M. The product of these two concentrations, 2×10^{-5}, is within a factor of 80 of the solubility measured (*20*) for TTF^+Cl^- in acetonitrile. Also, alterations in the electrochemistry of 10^{-3} M dissolved tetrathiafulvalene occur for addition of 10^{-3} M chloride. This exercise in numbers does not of course provide an interpretation or demonstrate ordering or cooperativity between adjacent tetrathiafulvalene radical cation sites, merely that the interfacial TTF "concentration" is sufficiently high that solubility considerations are not completely implausible.

Whether the chloride effect on immobilized tetrathiafulvalene and the differences in wave sharpness and ordering of ΔE_p values have any common roots will require further study to ascertain. Clear at this point, however, is that tetrathiafulvalene immobilized on a solid electrode surface has unusual properties, possibly due to neighbor sites just as does tetrathiafulvalene in crystalline salt form. From this we speculate that inspection of properties of other immobilized charge transfer chemical selected on the basis of solid state characteristics may be worthwhile.

ACKNOWLEDGMENT

The authors gratefully acknowledge the assistance of M. Umana with XPES measurements and D. N. Smith with surface activity calculations.

LITERATURE CITED

(1) P. R. Moses, L. Wier, and R. W. Murray, *Anal. Chem.*, **47**, 1882 (1975).
(2) P. R. Moses and R. W. Murray, *J. Electroanal. Chem.*, **77**, 393 (1975).
(3) P. R. Moses, L. M. Wier, J. C. Lennox, H. O. Finklea, and R. W. Murray, *Anal. Chem.*, **50**, 576 (1978).
(4) J. R. Lenhard and R. W. Murray, *J. Electroanal. Chem.*, **78**, 195 (1977).
(5) R. J. Burt, G. J. Leigh, and C. J. Pickett, *J. Chem. Soc., Chem. Commun.* 940 (1976).
(6) A. Diaz, *J. Am. Chem. Soc.*, **99**, 5838 (1977).
(7) M. Fujihira, T. Osa, D. Hursh, and T. Kuwana, *J. Electroanal. Chem.*, **88**, 285 (1978).
(8) A. F. Diaz and K. K. Kanazawa, *J. Electroanal. Chem.*, **86**, 441 (1978).
(9) B. E. Firth and L. L. Miller, *J. Am. Chem. Soc.*, **98**, 8272 (1976).
(10) J. R. Lenhard, R. Rocklin, H. Abruna, K. Willman, K. Kuo, R. Nowak, and R. W. Murray, *J. Am. Chem. Soc.*, **100**, 5213 (1978).
(11) J. R. Lenhard and R. W. Murray, *J. Am. Chem. Soc.*, **100**, 7870 (1978).
(12) K. Itaya and A. J. Bard, *Anal. Chem.*, **50**, 1487 (1978).
(13) D. C. Green, *J. Chem. Soc., Chem. Commun.*, 161 (1977).
(14) D. R. Rolison, K. Kuo, M. Umana, D. Brundage, and R. W. Murray, *J. Electrochem. Soc.*, **126**, 407 (1979).
(15) R. F. Lane and A. T. Hubbard, *J. Phys. Chem.*, **77**, 1401 (1973).
(16) A. P. Brown and F. C. Anson, *Anal. Chem.*, **49**, 1589 (1977).
(17) D. N. Smith, K. Willman, K. Kuo, and R. W. Murray, *J. Electroanal. Chem.*, **95**, 217 (1979).
(18) J. C. Lennox and R. W. Murray, *J. Am. Chem. Soc.*, **100**, 3710 (1978).
(19) F. B. Kaufman, E. M. Engler, D. C. Green, and J. Q. Chambers, *J. Am. Chem. Soc.*, **98**, 1596 (1976).
(20) J. Q. Chambers, D. C. Green, F. B. Kaufman, E. M. Engler, B. A. Scott, and R. R. Schumaker, *Anal. Chem.*, **49**, 802 (1977).
(21) F. Wudl, *J. Am. Chem. Soc.*, **97**, 1962 (1975).

RECEIVED for review August 2, 1978. Accepted February 5, 1979. This research was supported in part by the National Science Foundation under Grant CHE76-24564. This is Part XVI of a series on Chemically Modified Electrodes.

Optical Monitoring of Electrogenerated Species via Specular Reflection at Glancing Incidence

Richard L. McCreery,* Richard Pruiksma, and Robert Fagan

Department of Chemistry, The Ohio State University, Columbus, Ohio 43210

Light reflected from a planar electrode at small angles relative to the electrode surface was used to carry out conventional absorbance measurements on electrogenerated species. Compared to measurements involving optically transparent electrodes, the effective optical path length of the new technique is longer by factors of 100–200, leading to greatly increased absorbance values. The absorbance is linear with the square root of time for times greater than 20 ms after the beginning of electrolysis, and its magnitude can be predicted from the geometry of the optical apparatus. The advantages of the new technique include the ability to monitor weak or short-lived chromophores, the absence of a need for time averaging, and the lack of the requirement of an optically transparent electrode.

Numerous methods have evolved in recent years which make use of an optical probe to obtain UV–VIS spectral characteristics of solution components generated by an electrochemical reaction (*1–3*). These methods have been used to identify and characterize electrogenerated materials and to monitor the kinetics of decay of reactive species. The most common methods for examining electrogenerated materials in solution involve an optically transparent electrode (OTE), either a thin-film metal or metal oxide electrode on a transparent substrate or a "minigrid" electrode made from commercially available metal grids. While these spectroelectrochemical methods have proved extremely useful, they suffer from several drawbacks which hinder their use for examining weakly absorbing species or electrogenerated materials with short lifetimes.

The main problem is a very short path length for both an optically transparent thin-film electrode or a minigrid, resulting in very small absorbance values for either short-lived or weakly absorbing species. The absorbance for an optically transparent electrode, where the optical beam is perpendicular to the electrode surface, is given by Equation I,

$$A(t) = \epsilon_R C_{ox}{}^b \left[\frac{2}{\pi^{1/2}} D_{ox}{}^{1/2} t^{1/2} \right] \qquad (1)$$

where $C_{ox}{}^b$ is the bulk concentration of a species undergoing a diffusion controlled reaction: $Ox + ne^- \rightarrow Red$, D_{ox} is its diffusion coefficient, ϵ_R is the molar absorptivity of the reduced form (assumed to be the only absorbing species at the wavelength used), and t is the time after the initiation of generation of Red (*4, 5*). By analogy to the Beer–Lambert law, the term in brackets is the effective path length of the optical beam. This path length is very short for typical species ($D_{ox} \cong 10^{-6}$ cm^2/s), with values of 3.6×10^{-5} cm at 1 ms to 10^{-3} cm at 1 s. Clearly, a strong chromophore is necessary to obtain measurable absorbance with the concentrations used in electrochemistry (ca. 1 mM). With short-lived species, it is necessary to time average thousands of runs even for strong chromophores (*6*).

A minigrid electrode does not improve these path-length problems and has the added problem of the lag time required for the absorbing species to "fill" the holes between the grid wires (*7*). Internal reflection spectroscopy has also been used to monitor transient species, but the path length is limited to a few multiples of the length of the evanescent wave (ca. 2000 Å) (*8*). A problem with both thin-film and minigrid electrodes is internal resistance which limits the magnitude of the current and creates uncompensated IR drops. This problem is severe with thin-film electrodes and results in poor transient response and uneven distribution of applied potential.

Changes in specular reflectance accompanying electrochemical events have long been used to characterize electrode surface changes and in a few cases to examine electrogenerated species in solution (*9–11*). Specular reflectance in a thin-layer cell was used to monitor stable solution species, with the beam reflected off the electrode at a 40° angle (*12*). While this approach avoids the problem of electrode transparency and resistance, the effective path length is only a factor of about two greater than that for an OTE. In addition, the magnitude of the incident beam angle is constrained by refraction from the walls of the thin-layer cell. Thus the sensitivity is only slightly improved, and the technique is still limited to strong chromophores of relatively stable species. A method based on multiple reflections within a reflective tube has been presented (*13*) and an attempt made to detect electrogenerated solvated electrons. Long effective path lengths were reported, but quantitation was difficult because of large variations in path length with beam geometry and position.

In the technique reported here, light reflected from a planar electrode at glancing incidence is used to make conventional absorption measurements. As the angle of incidence, measured relative to the electrode plane, is decreased, the optical path length through the diffusion layer increases greatly compared to an OTE experiment. A large enhancement in absorbance, and therefore sensitivity, results, making spectroelectrochemical observation of weak chromophores and short-lived species possible.

THEORY

For a light beam reflecting off a planar electrode at an angle α relative to the surface (Figure 1), the absorbance due to an electrogenerated species will be given by Equation 2.

$$A(t) = 2\epsilon_R \int_0^\infty C_R(x,t)\,dl \qquad (2)$$

$C_R(x,t)$ is the concentration profile of the electrogenerated species as a function of distance from the electrode and dl is a path length increment. Since dx/dl equals $\sin \alpha$,

$$A(t) = \frac{2\epsilon_R}{\sin \alpha} \int_0^\infty C_R(x,t)\,dx$$

$$A(t) = \frac{2\epsilon_R}{\sin \alpha} C_{ox}{}^b \frac{2}{\pi^{1/2}} D_{ox}{}^{1/2} t^{1/2} \qquad (3)$$

As before, this equation is based on the assumption that only

0003-2700/79/0351-0749$01.00/0 © 1979 American Chemical Society

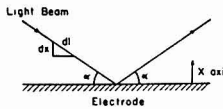

Figure 1. Specular reflection of a light beam from a planar electrode. See text for details

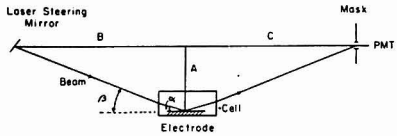

Figure 2. Optical arrangement for absorbance measurements using reflected light. B = C = 67.0 cm; A = 0.3–3.0 cm. Beam and electrode aligned as described in text

the reduced form absorbs at the chosen wavelength and that the charge transfer reaction is diffusion controlled. The factor $(2/\sin \alpha)$ represents the path length enhancement of the reflection measurement over that calculated for an OTE experiment with the beam perpendicular to the electrode. Except for this enhancement, the absorbance has the same behavior as that observed with an OTE, with a $t^{1/2}$ dependence of absorbance for a stable electrogenerated species.

EXPERIMENTAL

A schematic diagram of the optical apparatus is shown in Figure 2. Distances B and C are equal, and have magnitudes of about 70 cm. The light source was a 0.5 mW, He/Ne laser (632.8 nm) whose beam was directed by two mirrors (beam steering device, Newport Research). The mirrors, cell, and photomultiplier were mounted on an optical rail (Newport Research). The working electrode was made by vapor deposition of 5000 Å of gold film onto glass. The electrode was mounted on a three-dimensional micromanipulator and placed in a $2 \times 1 \times 1^1/_2$ inch quartz cell made from $^1/_{16}$-inch-thick quartz plate. The dimension of the working electrode along the optical axis was 37 mm. A platinum wire auxiliary electrode and an SCE were placed in the cell without special positioning. A 1P28 photomultiplier (PMT) with standard electronics served as a detector.

The alignment of the working electrode with respect to the laser beam is of obvious importance and was accomplished as follows. The cell was lowered away from the working electrode, and the beam positioned to pass through a 3 mm^2 hole on the face of the PMT housing, without reflecting off the electrode. The distance from the beam to the electrode (A in Figure 2) was measured, with values ranging from 0.3 to 3 cm. Then the beam was directed onto the electrode using the steering device, and the electrode was rotated until the reflected spot impinged on the hole in the PMT housing. This adjustment ensures that the electrode plane is parallel to a line between the source and the PMT. Finally, the cell was repositioned without moving the working electrode and rotated to place the beam back on the PMT, to ensure the beam position is not altered by refraction within the cell.

Provided the distances B and C of Figure 2 are equal, the apparent incidence angle β is $\sin^{-1}$ (A/C). To determine the true incidence angle α (again relative to the electrode surface), refraction by the solution must be taken into account. From Snell's law, $\sin \alpha = \sin \beta/1.331$, where 1.331 is the refractive index of water at 632.8 mm. The α values reported herein have been so corrected. The index of refraction of the buffer used here was assumed to equal that of water to the required accuracy. Changes in index of refraction by dissolved salts are generally in the third or fourth decimal place (*14*).

The reduction of methyl viologen to a blue cation radical was used as a test system in this work, since the radical absorbs well at the He/Ne laser wavelength and the system is well behaved electrochemically. An accurate concentration of methyl viologen is difficult to prepare from commercially available methyl viologen chloride, since the water content varies. To avoid this compli-

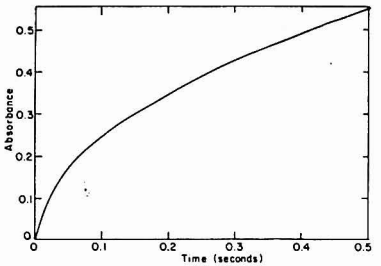

Figure 3. Absorbance vs. time response for a potential step from –0.3 to –0.8 V vs. SCE; 0.59 mM methyl viologen in 0.3 M phosphate buffer, pH 7.0. Average of three runs

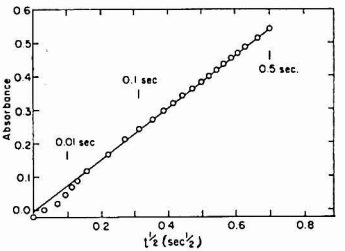

Figure 4. Absorbance vs. square root of time for data of Figure 3

cation, the glancing incidence technique was evaluated by comparing the absorbance of light incident at small values of α to the absorbance of light which is incident normal to the surface. The normally incident light will experience a path length twice that of an OTE experiment, and will have twice the absorbance given by Equation 1. The ratio of absorbance at any angle α to one half the absorbance at normal incidence is the absorbance enhancement of the present technique over an OTE experiment, and should have a value of $2/\sin \alpha$. Using this approach, it is unnecessary to know D_{ox} or ϵ at 632.8 nm to compare the two methods, but literature values (*15*, *16*) under similar conditions are: $D_{ox} = 0.86 \times 10^{-5}$ cm^2 s^{-1} and $\epsilon_{632.8} \cong 9700$ M^{-1} cm^{-1}.

Methyl viologen dichloride (K and K Laboratories) was dissolved in 0.3 M phosphate buffer with pH 7.0. The potential was controlled by a PARC model 173 potentiostat and was stepped from –0.3 to –0.8 V vs. SCE. The PMT output was monitored before and during the potential step with a minicomputer, and the absorbance vs. time curves were calculated by the computer. Three runs were averaged in all cases. Despite the negative potential of the step, hydrogen generation was too slow under these conditions to cause any apparent problems.

RESULTS

The absorbance vs. time curve for reduction of a 0.6-mM viologen solution with an α angle of 1.48° is shown in Figure 3. The small noise level of the curve, which is typical, results from the large absorbance values compared to an OTE experiment. A plot of A vs. $t^{1/2}$ for the same experiment is shown in Figure 4, and demonstrates a $t^{1/2}$ dependence of absorbance at times longer than 20 ms. Good A vs. $t^{1/2}$ linearity was observed for angles greater than 0.4°; deviations at smaller angles are discussed below.

Table I lists data from experiments at different incident angles at times from 25 to 500 ms after the beginning of the potential pulse. The theoretical enhancement is the value $2/\sin \alpha$, determined from the experimental geometry and Equation 3. The observed enhancement is the observed average $A/t^{1/2}$ divided by one half the $A/t^{1/2}$ value for a normal incidence ($\alpha = 87°$) experiment. This enhancement

Table I. Predicted and Observed Absorbance Enhancements as a Function of α

α (°)	mean $A/t^{1/2}$	predicted enhancement	observed enhancement
87.	0.0200	2.00	---
1.99	0.546	57.5	54.6
1.48	0.759	77.5	75.9
1.22	0.966	93.9	96.6
0.96	1.126	118	113
0.71	1.336	162	134
0.45	1.890	254	189
0.19	2.187	594	219

Table II. Observed Absorbance Enhancement as a Function of Time after Initiation of Electrolysis

	seconds					predicted
α (°)	0.05	0.025	0.013	0.005	0.001	enhancement
1.99	56.7	54.6	50	30	11	57.5
1.48	75.1	74.7	61	28	3.4	77.5
1.22	80.5	66.7	44	9.5	~0.1	96.6
0.96	98.0	82.4	45	9.8	~0.1	118
0.71	120	81.9	47	15	0.3	189
0.45	123	67.4	34	11	-1.2	254
0.19	81.5	39.3	18	1.0	-11	594

is the increase in absorbance for the glancing incidence experiment over an experiment using an OTE with the beam perpendicular to the electrode surface.

Table II lists the observed enhancement as a function of time for points at 50 ms and less after the beginning of the potential pulse. At times longer than 50 ms, the enhancement is constant to within 5%, and equal to the observed values from Table I. However, at times shorter than 50 ms, the enhancement decreases both with decreasing time and with decreasing angle. As mentioned earlier, the absorbance is not linear in $t^{1/2}$ in this time region. For a light beam at normal incidence to the electrode surface, an A vs. $t^{1/2}$ plot was linear after 21 ms. At times below 21 ms, the A vs. $t^{1/2}$ curve for a normal incidence experiment had a shape similar to that in Figure 4.

Finally, no significant change in reflectance of the gold electrode was observed when a background experiment was conducted with buffer containing no viologen.

DISCUSSION

The agreement between the predicted and observed absorbance enhancement for incident angles of 0.96° and above (Table I) confirms Equation 3. The agreement with theory allows the calculation of an effective path length for a given experimental configuration and pulse time, and absorbance may be related to concentration in the same fashion as an experiment based on an OTE. The theory for kinetic systems developed for OTE experiments (*1*) also applies to the glancing incidence approach, with the latter technique having much greater sensitivity. When it is necessary to know the absorbance enhancement accurately, enhancements of at least a factor of 100 over conventional OTE experiments may be achieved, when all other parameters are equal.

For angles at 0.71° and 0.45°, the absorbance was linear with $t^{1/2}$, but the enhancement was 18–25% lower than expected. While an effective path length cannot be calculated accurately at these small angles, the A vs. $t^{1/2}$ linearity allows the experiments to be used for many purposes, such as spectral characterization and kinetics. The enhancements of up to a factor of 200 over OTE experiments will make such experiments valuable even when absolute quantitation is difficult. For the smallest angle used here (0.19°) the absorbance was not linear with $t^{1/2}$ until late in a 500-ms run. Data acquired at this angle may be useful for detecting short-lived species, but the absorbance vs. time behavior is too unpredictable for quantitation.

The decrease in the enhancement at times below 50 ms cannot arise from the optical geometry, so it must be caused either by electrode surface roughness or by slow response of the potentiostat/cell combination. At times below 10 ms, the diffusion layer thickness approaches the magnitude of surface irregularities of the electrode. A beam reflected at glancing incidence may not interact with the electrogenerated species within the microscopic depressions of the electrode surface and, therefore, will not have the predicted path length. An additional surface effect which may be important in some cases is the change in reflectance of the electrode caused by changes in potential or the electrolysis of solution components. Changes in reflectance of the gold electrode were negligible in background runs with viologen absent, ruling out significant error in absorbance from an interaction between the buffer and the electrode. The linearity of observed absorbance with $t^{1/2}$ for viologen solutions is unlikely if the reflectance of the gold surface were changed by electrolysis; thus electrode reflectance changes can be assumed negligible for the gold/viologen system.

No attempts were made to optimize the transient response of the potentiostat/cell combination, and at least some of the slow response of the absorbance was caused by this deficiency. The fact that the deviations from linearity for A vs. $t^{1/2}$ plots at short times are similar for both glancing and normal incidence implies that cell response is a significant source of deviation below 25 ms. Clearly, the cell response could be improved when experiments require measurements in this short time frame.

The lack of agreement between theory and experiment at angles of 0.7° and below is caused at least in part by scattered light from the incident beam which is not reflected directly off the electrode. At small incident angles, deflection of the incident beam by diffraction, dust in the solution or air, or imperfections in the glass optics and cell will create stray light which will decrease the observed absorbance.

A laser source for this work is a convenience, but not a necessity. The only quality of the source which is important is collimation, and sufficiently parallel light can be achieved easily without a laser. An experiment using a continuum source and a monochromator would be conducted in the same fashion as one using a laser source, provided the light is collimated before entering the electrochemical cell. Work at small angles would require a narrow beam which could be easily generated by a suitable mask.

The vapor-deposited gold electrode used to examine the glancing incidence technique was not difficult to fabricate and is useful for a variety of systems. However, any electrode having sufficient reflectance and planarity can be used with success. Platinum foil (0.005 inch thick) and a mercury film on platinum were tested, and yielded results comparable to the gold film electrode. When sufficiently polished, glassy carbon would also be a suitable electrode. As pointed out by others (*12*), reflectivity changes with wavelength can be significant with metals in the UV. The thick gold film or any bulk metal electrode will have much lower resistance than thin films used for OTE experiments, so uncompensated IR effects will usually be negligible.

The effective path length increases of factors of 100–200 allowed by this reflection technique have four important implications. First, electrogenerated species with lifetimes in the region of 10 ms and greater create much larger absorbances than those from the corresponding OTE experiment, resulting in improved sensitivity and signal-to-noise ratio.

While the present experiments did not yield satisfactory results below 10 ms, the problems in this time region are technical and amenable to improvement. Second, the relatively long path lengths of the reflection mode permit weak chromophores to be monitored, in contrast to most OTE experiments. Third, extensive time averaging is not usually necessary, again in contrast to OTE methods. Many reactions of electrogenerated species are irreversible, and a long period of time must elapse between runs to re-establish initial conditions. In many cases this is impractical, so time averaging is commonly applied to mechanisms involving reversible coupled reactions, such as redox reactions between an electrogenerated component and a solution species. The present technique will be useful where time averaging is not permissible or is very time-consuming. Fourth, a wider range of concentrations may be used with the present method compared to OTE experiments. Lower concentrations are usable because of the longer optical path length, and higher concentrations are possible because of the lower resistance of the working electrode relative to thin-film electrodes.

The concept of using reflected light for absorbance measurements on electrogenerated species is not a new one. However, when the reflection angle is very small with respect to the electrode surface, significant enhancements in path length are observed and important experimental advantages result.

LITERATURE CITED

(1) Winograd, N.; Kuwana, T. "Spectroelectrochemistry at Optically Transparent Electrodes", in "Electroanalytical Chemistry", Vol. 7, Bard, A. J., Ed.; Marcel Dekker: New York, 1974.
(2) Kuwana, T. *Ber. Bunsen, Phys. Chem.* **1973**, *77*, 858.
(3) Heineman, W. R. *Anal. Chem.* **1978**, *50*, 390A.
(4) Strojek, J.; Kuwana, T. *J. Electroanal. Chem.* **1968**, *16*, 471.
(5) Winograd, N.; Blount, H. N.; Kuwana, T. *J. Phys. Chem.* **1969**, *73*, 3456.
(6) Winograd, N.; Kuwana, T. *J. Am. Chem. Soc.* **1971**, *93*, 4343.
(7) Petek, M.; Neal, T. E.; Murray, R. W. *Anal. Chem.* **1971**, *43*, 1069.
(8) Winograd, N.; Kuwana, T. *J. Electroanal. Chem.* **1969**, *23*, 333.
(9) McIntyre, J. D. E. "Specular Reflection Spectroscopy of the Electrode Solution Interphase", in "Advances in Electrochemistry and Electrochemical Engineering", Vol. 9, Muller, R., Ed.; Wiley-Interscience: New York, 1973.
(10) Bewick, A.; Tuxford, A. M. *Symp. Faraday Soc.* **1970**, *4*, 116.
(11) Aylmer-Kelly, A. W. B.; Bewick, A.; Cantrill, P.; Tuxford, A. M. *Faraday Diss. Chem. Soc.* **1973**, *56*, 96.
(12) Kissinger, P. T.; Reilley, C. N. *Anal. Chem.* **1970**, *42*, 12.
(13) Walker, D. C. *Anal. Chem.* **1967**, *39*, 896.
(14) O'Brien, R. *J. Chem. Eng. Data* **1973**, *18*, 142.
(15) Steckhan, E.; Kuwana, T. *Ber. Bunsen. Phys. Chem.* **1974**, *78*, 253.
(16) Landrum, H. L.; Salmon, R. T.; Hawkridge, F. *J. Am. Chem. Soc.* **1977**, *99*, 3154.

RECEIVED for review December 6, 1978. Accepted January 25, 1979. This work was supported in part by grant 28412 from the National Institute of Mental Health.

Electrochemical Study of the Degradation of Vitamin K_3 and Vitamin K_3 Bisulfite

J. C. Vire, G. J. Patriarche,* and G. D. Christian[1]

Institut de Pharmacie, Université Libre de Bruxelles 205/1, Boulevard du Triomphe, 1050 Bruxelles, Belgium

Polarography is used to follow the degradation and the products of vitamin K_3 bisulfite (I) and vitamin K_3 (II). The degradation scheme is outlined in Figure 2. The predominant degradation of I in alkaline solution is to II. In neutral solution, gradual isomerization to the naphthoquinone sulfonate (VIII) becomes significant. II is degraded primarily via rearrangment to the epoxynaphthohydroquinone (VI) in the absence of oxygen, except in very alkaline medium (pH 12) where formation of the naphthohydroquinone (VII) becomes significant. Small amounts of the epoxnaphthoquinone (III) occur by reaction of II with O_2 or H_2O_2 formed with VII. VI and IV degrade to the phthiocol (IV) and the dinaphthalenetetrone dimer (V), the former becoming more dominant at higher pH. I is more stable than II at pH $\geq$ 7. The relative rates of degradation are reported.

K vitamins are present in vegetables where they seem to play an active role in photosynthetic mechanisms (*1*). They also play a role in cellular respiration as electron transporters (*2*) and in oxidative phosphorylation (*3*). These properties result from the reversible character of this quinone/hydroquinone redox system.

In the human body, they are synthesized by microorganisms in the intestine to provide required physiological quantities and are implicated in synthesis of four blood coagulation factors in the liver (*4*, *5*). Deficiencies of vitamin K in the body are infrequent, but may occur if obstruction of the bile or intestine occurs and in cases of liver disease such as cirrhosis (*4*, *5*). Deficiencies are generally accompanied by a decrease in the prothrombin level with an increase in blood coagulation time. At advanced stages, the capillaries may become fragile and hemorrhage. Symptoms are reversed by incorporation of K vitamins in the diet, except in cases of some liver diseases.

In recent spectrophotometric studies of naphthoquinones of the important K group vitamins, we have observed several properties related to complex formation with titanium(IV) (*6*). We have also studied the electrochemistry of vitamin K_3 (menadione) and its bisulfite derivative (*7–10*). We were interested in the stability of the active forms of these compounds in aqueous solution. The present work was undertaken to determine both the rates of degradation and the degradation products of vitamin K_3 and vitamin K_3 bisulfite in neutral and alkaline media.

EXPERIMENTAL

Direct current (dc), alternating current (ac), and differential pulse (dp) polarographies were used to identify and monitor the compounds resulting from the degradation of these two vitamins. Polarograms were obtained with solutions of pH 6–12 at regular intervals during periods ranging up to between 20 and 50 days. These periods correspond to stabilization of the developed chemical degradation processes. The solutions were stored in the dark. They were deaerated with nitrogen and stored in Teflon-stoppered volumetric flasks to exclude oxygen. Control experiments with electrolyte solutions demonstrated no po-

[1] Permanent Address: Department of Chemistry, University of Washington, Seattle, Wash. 98195.

0003-2700/79/0351-0752$01.00/0 © 1979 American Chemical Society

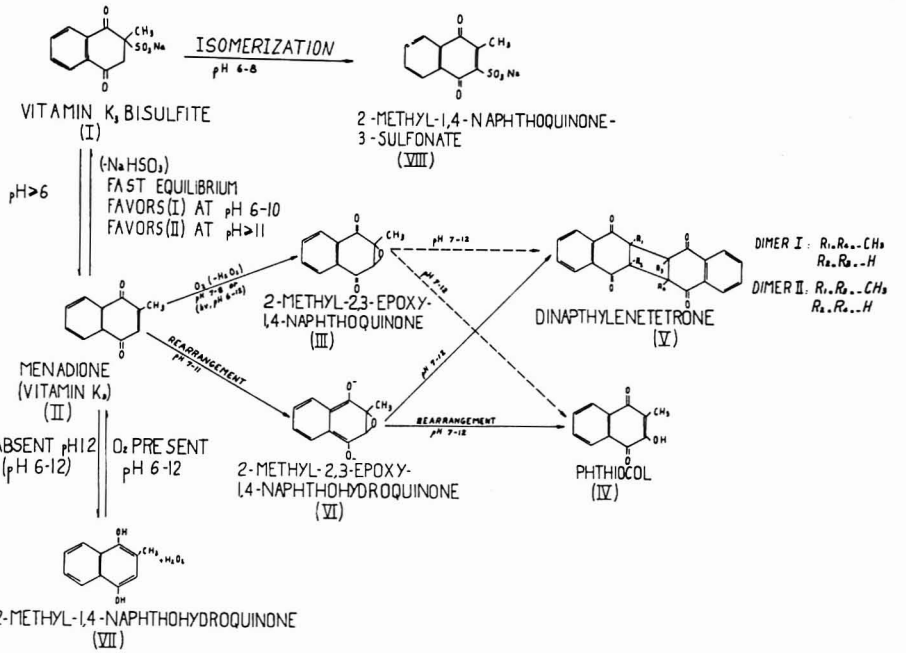

Figure 1. Degradation scheme for vitamin K_3 and vitamin K_3 bisulfite

larographically measurable oxygen entered the solutions stored in the flasks.

Apparatus and Reagents. Polarograms, dc, ac, and dp, were obtained on a Tacussel polarograph type PRG 34, using a saturated calomel reference electrode. The following parameters were used unless otherwise stated.

Alternating current polarography: 10 mV superimposed, frequency 90 Hz., drop time 1.1 s; dp polarography: sweep rate 2 mV/s, drop time 2 s, current sampled 40 ms, starting 1.9 s after initiating the drop, pulse amplitude 40 mV.

Direct current polarography: drop time 1.1 s. A nitrogen atmosphere was maintained above solutions during recording of polarograms. Nitrogen was initially bubbled in the solution for a few minutes to remove any traces of oxygen that may have been introduced during transfer of solutions.

The photochemical degradation of menadione was studied in a quartz polarographic cell with the aid of a 100-W high pressure mercury vapor lamp. A Hanovia high voltage dc power supply was used for the lamp. The lamp was placed 60 cm from the solution.

Menadione (Merck 5793) and Vitamin K_3 bisulfite (PCB c 813930) were used without further purification. Solutions were prepared immediately before initiation of the measurements, and final solutions contained 10% methanol (Merck 6008). Buffers used were phosphate/HCl and phosphate/NaOH at 0.05 M.

RESULTS AND DISCUSSION

General Reaction Scheme. As many as eight different polarographic waves or peaks were observed in these studies, corresponding to the reduction of eight different compounds, some with multiple waves. Some of the waves overlapped. In order to facilitate discussions, a summary of the degradation reaction scheme as evolved from the electrochemical studies is presented in Figure 1, and a dp polarogram identifying most of the peaks is shown in Figure 2. We shall refer to the various peak numbers as waves throughout the discussion.

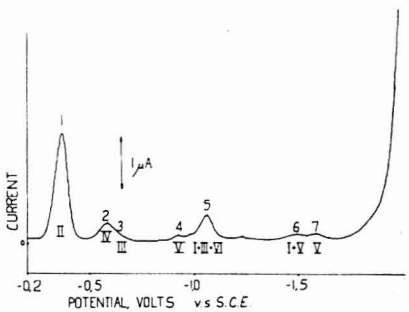

Figure 2. Differential pulse polarogram of a 5×10^{-4} M solution of menadione at pH 9 after 600 h. The waves (peaks) are due to reduction of compounds identified by roman numerals as follows. Wave 1, reduction of carbonyl groups of menadione (II). Wave 2, reduction of carbonyl groups of phthiocol (IV). Wave 3, reduction of carbonyl groups of 2-methyl-2,3-epoxy-1,4-naphthoquinone (III). Wave 4, reduction of first carbonyl groups of dinaphthylenetetrone (V). Wave 5, reduction of first carbonyl group of vitamin K_3 bisulfite (I), and of epoxy groups of 2-methyl-2,3-epoxy-1,4-naphthoquinone (III) and hydroquinone (VI). Wave 6, reduction of second carbonyl group of vitamin K_3 bisulfite (I) and of second carbonyl groups of dinaphthylenetetrone (V). Wave 7, reduction of cyclobutane groups of dinaphthylenetetrone (V)

Vitamin K_3 Bisulfite Degradation. At pH 6, vitamin K_3 bisulfite (I) is degraded, and the rate of degradation progressively increases with increased pH (Figure 3). One observes a simultaneous decrease of the two waves of this compound and the appearance of another wave at more positive potentials as the compound degrades. The half-wave

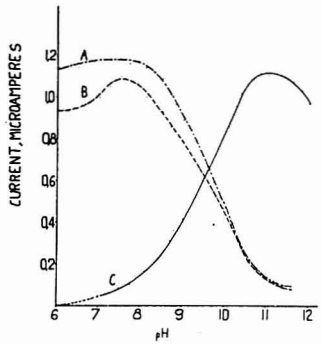

Figure 3. Equilibrium concentrations of vitamin K_3 bisulfite and menadione as function of pH measured 30 min after preparation of vitamin K_3 bisulfite solution. (A) First wave of vitamin K_3 bisulfite (5). (B) Second wave of vitamin K_3 bisulfite (6). (C) Menadione wave (1)

potential and the pH dependence of this wave, and its adsorption characteristics identify it as being due to menadione (wave 1) (*8, 9*). This compound is formed by a β cleavage mechanism which eliminates the bisulfite ion. This reaction confirms the results of Carmack et al. (*11*). Although degradation begins at pH 6, the new wave cannot be detected until pH 7. It diminishes starting at pH 11 because this molecule is rapidly decomposed in very alkaline media.

Except at very alkaline pH, the vitamin K_3 bisulfite decomposes slowly. For example, at pH 9, a freshly prepared solution preserved in a nitrogen atmosphere for 8 h and measured at regular times showed no significant degradation. The same experiment at pH 11 showed about 40% degradation, but greater for the menadione product (about 60%) than for the parent dioxotetraline form. So it appears that the dioxotetraline form is a more stable form in alkaline medium than the naphthoquinone structure. A polarographic study of the reaction between menadione and sodium bisulfite in neutral (pH 7) and alkaline (pH 9) media at different ratios of reactants indicated that at equal concentrations of bisulfite and menadione, the reaction was incomplete and that it was favored at the lower pH (Figure 4). Extrapolation of the curves in Figure 4 indicates that complete reaction should be obtained at ratios of about 0.26 and 0.85 menadione/bisulfite, respectively, for pH 9 and 7. These results suggest that there is an equilibrium reaction as follows

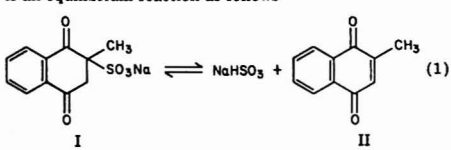

I II (1)

which is governed by the concentrations of menadione and bisulfite, and the pH. This reaction is reversible in neutral and alkaline media. In acidic media, no reaction is observed between bisulfite and either menadione or vitamine K_3 bisulfite.

The vitamin K_3 bisulfite derivative quickly degrades by β cleavage to give equilibrium concentrations of menadione and bisulfite via reaction (*1*), producing the menadione wave and a diminished vitamin K_3 bisulfite wave. The equilibrium lies toward compound I at pH 6–10 and toward compound II at pH 11 or above.

The produced menadione degrades to produce new waves, causing a further shift in the equilibrium and a decrease in both the vitamin K_3 bisulfite wave and the menadione wave. The kinetics of these decompositions are considered below.

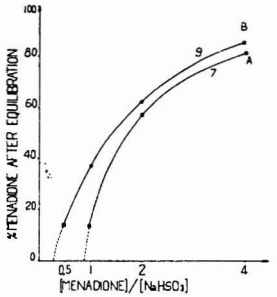

Figure 4. Percentage of menadione remaining at equilibrium after reaction with $NaHSO_3$, as a function of the ratio of the initial concentrations of menadione/$NaHSO_4$ measured after 30 min. (A) pH 7, (B) pH 9

For the bisulfite, another peak appears between pH 6 and 8 at a potential more positive than the menadione (wave 1) peak. Its intensity goes through a maximum with time, being reached sooner at the higher pH. The peak is attributed to the formation of an isomer of the vitamin K_3 bisulfite: 2-methyl-1,4-naphthoquinone-3-sulfonate (VIII). The formation of this isomer is small compared to the formation of menadione in alkaline solution, but it can become significant at neutral pH over long periods of time when the equilibrium between menadione and the bisulfite lies towards the bisulfite. This isomer has been demonstrated by Ksenzhek et al. (*12*) using voltammetry with a carbon paste electrode. The relatively positive potential of its peak is due to the inductive effect of the sulfonate group on the quinone structure of the isomer. The dc polarographic wave of this isomer shifts in a cathodic direction with increased pH from 6 to 7 (near −0.15 V vs. SCE).

Menadione Degradation. Several authors (*13–16*) have studied the photochemical decomposition of menadione in various media. Results obtained can be described as follows. In the absence of oxygen, light promotes reduction of vitamin K_3 (II) to 2-methyl-1,4-naphthohydroquinone (VII) with simultaneous formation of hydrogen peroxide. In the presence of oxygen, the naphthohydroquinone is reoxidized to menadione. This oxidation is reported to be accompanied by formation of 2-methyl-2,3-epoxy-1,4-naphthoquinone (III), which is said to then be transformed into phthiocol (IV) or a dimer (V) which has the structure of dinaphthylenetetrone.

Asahi (*14, 17*) proposed the use of polarography for the study of the photochemical decomposition of vitamine K_3. We have employed polarography to study the chemical degradation.

Figure 5 shows a dc polarogram (curve A) of menadione at pH 9 after 600 h. Curve B shows a dc polarogram obtained at the same pH, but for a fresh solution irradiated for 1 h with UV radiation. (A fresh solution exhibits primarily only the menadione wave.) The similarity of the two polarograms is evident, the only difference being at the menadione wave. In the first instance only the cathodic wave of the quinone form is seen, but, after irradiation, about two thirds of the menadione present is in the reduced hydroquinone form (VII), as seen from the anodic wave. This anodic wave is also seen at pH 12 upon standing in the presence of nitrogen. The conclusion is that chemical and photochemical decomposition result in the same degradation products. Note also the similarity of the dc polarograms with the dp polarogram in Figure 2. The dp polarographic technique is more useful in

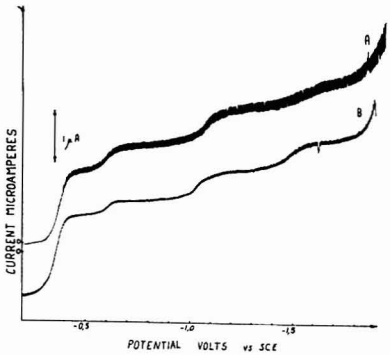

Figure 5. Direct current polarograms of 5×10^{-4} M menadione at pH 9. (A) after 600 h. (B) After UV irradiation for 1 h

resolving new waves at low concentrations.

Both menadione and its degradation product phthiocol are reduced at the DME to the corresponding naphthohydroquinones.

In addition, the chemical degradation intermediate 2-methyl-2,3-epoxy-1,4-naphthoquinone (III) is reduced in two 2-electron steps at the DME. The reduction of the epoxy form may be represented by

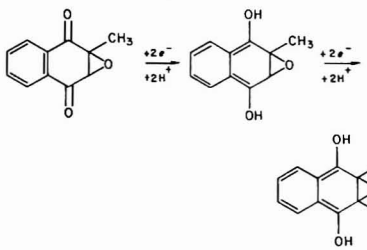

(2)

The first wave (3) occurs at −0.6 V vs. SCE and corresponds to the reduction of the two carbonyl groups. This reduction potential is due to the fact that the epoxy form is intermediate in structure between the quinone form, which is conjugated (and which is reduced at −0.3 V), and the *o*-benzenedicarbonyl form

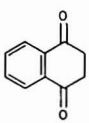

which is not conjugated (and is reduced at −1.0 V). The second wave (5) is due to reduction of the epoxy function to an alcohol, and appears between −1.00 and −1.13 V for pH 7 to 11. The hydroquinone epoxy intermediate (VI) also exhibits this wave (see below).

The dimer produced from the epoxy intermediate (probably the hydroquinone (VI) is reduced in two 2-electron steps in a manner similar to the reduction of the epoxy form, with half-wave potentials of −0.80 to −1.05 V for the first wave (4) and −1.45 to −1.55 V. for the second wave (6) at pH 7 to 11. The waves for the two different dimers occur at identical potentials and can not be resolved (*14*, *17*). But dimer I also exhibits a third ill-defined wave (7) at −1.6 V which corresponds to the electrochemical opening of the cyclobutane ring,

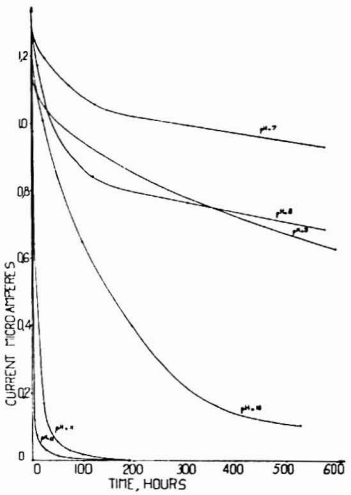

Figure 6. Intensity of menadione (5×10^{-4} M) dc polarographic wave (1) as a function of time at different pH values

Table I. Time Required for 50% of the Menadione Initially Present to Disappear

	pH					
	7	8	9	10	11	12
$T_{1/2}$, h	1500[a]	700	550	110	2	*b*

[a] Obtained by extrapolation. [b] Not measurable after 2 h, less than 10% remains.

with addition of two protons (*14*, *17*). This wave can only be resolved from the second wave (6) using dp polargraphy.

From the above electrochemical properties, it is possible to interpret the degradation of vitamin K_3 in alkaline solution. Figure 6 represents the change in the menadione concentration as a function of time at different pH values, obtained from dc polarograms. The decomposition of this compound is initially rapid and then slows down after 150 h at pH 7 and 8. Above pH 8, the behavior of the curves changes somewhat, indicating more gradual degradation throughout. This behavior could be due to the fact that the buffering capacity of phosphate is small at pH 9. Above pH 10, the degradation is very rapid. Table I lists the times required for decomposition of one half the menadione at the different pH values. Note the short half-life above pH 10.

Similar rate curves are obtained using dp polarography with improved sensitivity. But ac polarography gives irregular curves because the intensity of the peaks is modified by adsorption which accompanies the reduction of menadione. This adsorption phenomenon also results in an anodic shift in the dc half-wave potential of the menadione wave as a function of time (due to decreased concentration of menadione with time).

When the degradation is very fast, it is not possible to observe significant quantities of 2-methyl-1,4-naphthohydroquinone (VII), except at pH 12 with the solution maintained under a nitrogen atmosphere. It is not observed if the solution is contacted with oxygen between measurments, and increased amounts of III are observed at pH 7–8.

The first dp polarographic peak (5) appears at pH 7 after 24 h, corresponding to the reduction of the epoxy function

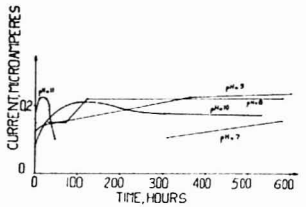

Figure 7. Intensity of second epoxy derivative wave (5) as a function of time at different pH values. Starting solution 5×10^{-4} menadione

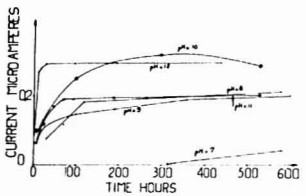

Figure 8. Intensity of phthiocol wave (2) as a function of time at different pH values. Starting solution 5×10^{-4} M menadione

of either compound III or VI. A DC polarographic wave is observed only after 300 h. But a dc wave appears rapidly at pH 8 and above due to compound VI (Figure 7). At pH 7 and 8, the wave remains stable after 120 h, and at pH 9 after 360 h. However, at pH 10 and 11, the epoxy form goes through a maximum, indicating rapid degradation.

A second dp polarographic peak of the epoxy form can be observed at more positive potentials after 28 h at pH 7, and is due to the reduction of the two carbonyl functions (wave 3). It increases with time, but its height is never more than one fifth of the other wave. It also appears at pH 8, but is smaller, and is not seen at higher pH.

These results indicate the intermediate character of the epoxy derivative in the degradation of vitamin K_3, especially at pH 10 and 11.

The predominance of the more negative potential peak over the other and the fact that the more positive one is not present above pH 8 indicates that the carbonyl form of the epoxy compound exists at pH 7 and 8 only, while the hydroxy form can exist up to pH 11.

These results suggest that menadione undergoes chemical oxidation, by two different pathways depending on the pH. At pH ≥7, an internal oxidation occurs by rearrangement of the molecule as follows:

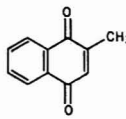

+ $2OH^-$ ⟶

II

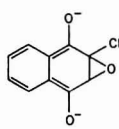

+ H_2O (3)

VI

The corresponding hydroxy form of the epoxy product is electrochemically reduced (wave 5). This compound can only exist in the ionic form at these pH values because its pK_a is about 5 (*17*). In neutral and weakly alkaline solution, a second oxidation can occur by reaction with oxygen:

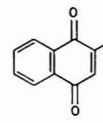

+ O_2 + H_2O $\xrightarrow{OH^-}$

II

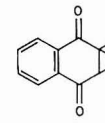

+ H_2O_2 (4)

III

The hydrogen peroxide in turn can oxidize menadione:

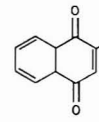

+ H_2O_2 $\xrightarrow{OH^-}$

II

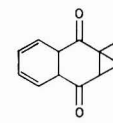

+ H_2O (5)

III

However, this reaction would be a minor one. The quinone epoxy compound results in the more positive wave (3) observed, only at pH 7 and 8. The hydroxy epoxy compound produced in reaction 3 can also react with oxygen to give the carbonyl compound at pH 7 and 8, but this is only a minor side reaction.

The 2-methyl-2,3-epoxy-1,4-naphthoquinone (III) isomerizes at pH 7 to produce a small amount of phthiocol (IV). This isomerization increases at pH 8 and above (Figure 8). The abnormally high current (wave 2) at pH 10 is resolved into two peaks using dp polarography indicating the presence of another compound at this pH. As seen in the figure, the phthiocol is stable in alkaline medium and does not undergo further degradation.

The dimerization reaction of the epoxy form starts at pH 7 (very small) and increases with increasing pH. The first dimer wave (4) is generally only detected by dp polarography. It can be seen by dc polarography only at pH 11 because it coincides with the epoxy wave and is not resolved; at this pH, the epoxy wave is diminished (Figure 7).

The dimerization reaction can be monitored more easily with the second appearing wave of the dimer (wave 6). It appears immediately at pH 8 with dp polarography, and after 300 h at pH 9 with dc polarography. It increases regularly up to pH 11 (Figure 9), as the rate of degradation of menadione increases. At pH 12, it diminishes, suggesting further degradation of the dimer in very alkaline solution.

A third dimer peak appears between pH 9 and 10 (the last peak (7) in Figure 2), and is probably due to electrochemical breaking of the cyclobutane ring of the dimer. The intensity remains small.

Rate of Degradation of Vitamin K_3 Bisulfite. As we have indicated, the principal decomposition product of vitamin K_3 bisulfite following the β cleavage reaction is menadione, which is then further degraded by the reactions given above.

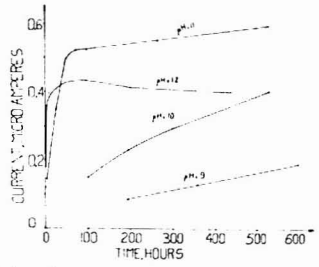

Figure 9. Intensity of second dimer wave (6) as a function of time at different pH values. Starting solution 5×10^{-4} M menadione

The degradation of vitamin K_3 bisulfite as a function of time was investigated using dp polarography. The degradation products exhibited many polarographic waves which could be neither resolved nor detected by dc polarography.

The first vitamin K_3 bisulfite wave is overlapped with the second wave of the epoxy derivative (wave 5) at pH 9 to 10, while its second wave is fused with the second wave of the dimer (wave 6) at pH 7–10.

The concentration of vitamin K_3 bisulfite decreased regularly starting at pH 6. The degradation rate increased progressively with increased pH, but decreased with time. The two peaks of the compounds disappeared after 100 h at pH 11, and did not appear at pH 12 because of immediate decomposition.

The menadione peak increases as the concentration of vitamin K_3 bisulfite decreases, passing through a maximum between pH 7 and 9, at which time the vitamin K_3 bisulfite and its menadione product are decaying at equal rates. At pH 6, there is no degradation of menadione for up to 50 days.

The reduction peak of the epoxy function (wave 5) develops starting at pH 7, and its intensity remains significant at pH 11 after 30 days. In contrast, when starting with menadione, this peak disappears after 2 days at pH 11, indicating the slower rate of decay of the bisulfite compound. The phthiocol peak can be detected only at pH 9 or above in traces when starting with vitamin K_3 bisulfite, but with menadione it is seen starting at pH 7. So the rate of formation of menadione from the bisulfite is sufficient to produce only traces of phthiocol from the menadione degradation. This is in contrast to the results of Kallmayer (*18*) and Fieser (*19*) who reported that phthiocol could come directly from the bisulfite degradation.

The two reduction peaks of the dimer form appear starting at pH 7 for both the bisulfite and menadione, and their evolution with time is similar at the different pHs.

This different behavior from the phthiocol compound may be due to differences in the rates of formation of each at different pHs, with the dimer formation rate being independent of pH and the phthiocol formation rate accelerated with increased pH.

CONCLUSION

The predominant degradation of vitamin K_3 bisulfite (I) in alkaline solution is to menadione (II), but in neutral solution, significant degradation to the naphthoquinone sulfonate (VIII) gradually occurs since the equilibrium between I and II lies towards I. The degradation of menadione is primarily via rearrangement to the epoxynaphthohydroquinone (VI) in the absence of oxygen, except in very alkaline medium (pH 12) where formation of the naphthohydroquinone (VII) becomes significant. Formation of the epoxynaphthoquinone (III) can be accounted for from either the presence of traces of oxygen in solution or from reaction of II with hydrogen peroxide or oxygen produced from the hydrogen peroxide formed with VII.

The end products of degradation are significant quantities of either the phthiocol (IV) or dinaphthylenetetrone dimer (V), primarily from VI, the formation of the phthiocol becoming more dominant with increasing pH. Vitamin K_3 bisulfite is more stable than menadione at pH $\geq$ 7.

LITERATURE CITED

(1) J. F. Pennock, in "Vitamin A, E, und K", H. Frhr. Von Kress and K. U. Blum, F. K. Schattauer Verlag, Stuttgart, 1969, p 181.
(2) A. F. Brodie and T. Watanabe, *Vitam. Horm. (Leipzig)*, **24**, 447 (1966).
(3) E. Lederer and M. Vilkas, *Vitam. Horm. (Leipzig)*, **24**, 409 (1966).
(4) H. A. Harper, "Précis de Biochimie", 3rd ed, A. Colin, Paris 1973.
(5) L. S. Goodman and A. Gilman, "The Pharmacological Basis of Therapeutics", 4th ed., Macmillan, New York 1970.
(6) J.-C. Vire, G. J. Patriarche, R. J. Nowak, and H. B. Mark, Jr., *Anal. Chem.*, **49**, 1943 (1977).
(7) J.-C. Vire and G. J. Patriarche, *Analusis*, in press.
(8) J.-C. Vire, G. J. Patriarche, *Analusis*, in press.
(9) J.-C. Vire, G. J. Patriarche, *Analusis*, in press.
(10) J.-C. Vire, G. J. Patriarche, *Analusis*, **6**(4), 155 (1978).
(11) M. Carmack, M. B. Moore, and M. E. Ballis, *J. Am. Chem. Soc.*, **72**, 844 (1950).
(12) O. S. Ksenzhek, S. A. Petrova, M. V. Kolodyazhny, and S. V. Oleinik, *Bioelectrochem. Bioenerg.*, **4**, 335 (1977).
(13) F. Poupe, *Collect. Czech. Chem. Commun.*, **12**, 225 (1947).
(14) Y. Asahi, *J. Pharm. Soc. Jpn.*, **76**, 373 (1956).
(15) K. Thoma and G. Pfaff, *Pharmazie*, **31**, H7, 447 (1976).
(16) S. Patai, "The Chemistry of the Quinonoid Compounds", Vol. I, John Wiley and Sons, London, 1974, Chap. 9.
(17) Y. Asahi, *J. Pharm. Soc. Jpn.*, **76**, 365 (1956).
(18) H. J. Kallmayer, *Sci. Pharm.*, **41**(4), 314 (1973).
(19) L. F. Fieser, *J. Biol. Chem.*, **133**, 391 (1940).

RECEIVED for review November 13, 1978. Accepted January 19, 1979. Thanks are expressed to the Fonds National de la Recherche Scientifique (F.N.R.S. Belgium) (G.J.P.) and the Commission for Educational Exchange between the United States of America, Belgium, and Luxembourg (G.D.C.) for support of this research.

Estimation of Particle Size Distributions from Turbidimetric Measurements

K. C. Yang[1] and Richard Hogg*

Mineral Processing Section, Department of Mineral Engineering, The Pennsylvania State University, University Park, Pennsylvania 16802

A method is described in which simple measurements of the turbidity of a suspension of fine particles can be used to obtain realistic estimates of the mean and range of particle sizes present. By assuming that the actual distribution can be fitted to a simple, two-parameter function such as the log normal, the values of the parameters can be estimated from turbidity data obtained at two wavelengths. Experimentally, it has been found that for dispersions of several different minerals, the estimation procedure yields results which agree remarkably well with direct measurements using centrifugal sedimentation. Simulation studies, of the effect of significant deviations from the proposed log normal form, indicate that the estimation procedure yields results which are reasonably representative of the central part of the distribution. There is no evidence of strong bias toward the tails of the distributions.

Light scattering offers an attractive means of studying dispersions of fine particles, particularly when the particle size is too small for other methods such as sedimentation to be used effectively. The principal attractions of light scattering as a method of particle size analysis are:

(i) There is no practical lower limit to the particle sizes to which the technique can be applied.

(ii) Measurements are rapid and simple.

(iii) Sampling problems are minimized since the method can be employed in situ.

(iv) Measurement causes no disturbance of the system which is simply illuminated with a beam of light.

Unfortunately, however, there are also several disadvantages to the use of light scattering for particle size measurement. The relationship between the size of a particle and its ability to scatter light is complex and is known only for particles of simple shape. Furthermore, this relationship is not generally unique insofar as similar scattering can result from particles of several different sizes. Nevertheless, light scattering measurements can be used relatively easily to obtain equivalent spherical diameters for essentially monodisperse suspensions of particles.

Scattering techniques can be used to determine average sizes of polydisperse suspensions provided that essentially all of the particles are either much smaller or much larger than the wavelength of the incident light. In addition, an instrument has recently been developed (*1*) which uses a complex optical filtering system to evaluate the scattering behavior and can be used to obtain several moments of the distribution. However, it has not yet proved possible to develop general methods for the direct determination of particle size distributions from light scattering measurements alone. Techniques have been described from which size distributions can be evaluated from the combination of light scattering with other methods such as sedimentation (*2*) or from scattering by individual particles passing through a beam of light, one at a time (*3–5*). These approaches, however, lose several of the important advantages of light scattering techniques. Specifically, they can no longer take advantage of the speed, simplicity, and range of applicability of a simple measurement of the light scattering behavior of a suspension of particles.

Information on the average and approximate range of sizes in a polydisperse suspension can be obtained by comparing light scattering data with theoretical results based on an assumed form for the distribution. In particular, Meehan and Beattie (*6*) have described a technique which permits an estimate of the size distribution to be obtained from simple measurements of turbidity at two wavelengths. The purpose of the work described in this paper has been to extend the method of Meehan and Beattie to materials with broad size distribution, to evaluate the limitations of the method, and to present experimental data comparing the estimated size distributions for several materials with the results of direct measurement by centrifugal sedimentation.

THEORY

The turbidity τ of a suspension of particles is a measure of the reduction in intensity of the transmitted beam due to scattering and is defined by

$$\tau = \frac{1}{l} \ln \frac{I_0}{I} \tag{1}$$

where l is the length of the light path in the suspension and I_0 and I are the intensities of the incident and transmitted beams, respectively.

For a dilute suspension of identical, spherical particles, the turbidity is given by

$$\tau = \nu \pi r^2 K_t \tag{2}$$

where ν is the number concentration of particles in the suspension, r is the radius of the particles, K_t is the total scattering coefficient, defined as the ratio of scattering cross section to geometric cross section. In general, K_t values can be evaluated from the exact Mie (*7–9*) theory of light scattering by spherical particles.

Measurement of turbidity as defined by Equation 2 is not generally feasible. In any practical instrument, the measured intensity is made up of contributions from the transmitted light plus the light scattered in the forward direction in a cone of solid angle ω determined by the geometry of the optical system. Equation 2 accounts only for light scattered exactly in the forward direction, i.e., for $\omega \to 0$. This problem has been considered in detail by Gumprecht and Sliepevich (*10*) who introduced a correction factor, R, defined as

$$R = K_\omega / K_t \tag{3}$$

where K_ω is an effective scattering coefficient defined so as to account for the light scattered in the near-forward direction. Thus, the measured turbidity of a monodisperse suspension of spherical particles of radius r is given by

$$\tau = R K_t \pi r^2 \nu \tag{4}$$

In the more practical case of a suspension of particles which are not all identical, i.e., when there is a distribution of particle sizes, Equation 4 can be expressed as

[1] Present address, Handy and Harman, 1770 Kings Highway, Fairfield, Conn. 06430.

0003-2700/79/0351-0758$01.00/0 © 1979 American Chemical Society

$$\tau = \pi \int_0^\infty RK_t r^2 d\nu(r) \quad (5)$$

where $d\nu(r)$ is defined as the number of particles, per unit volume of suspension, whose radius lies between r and $r + dr$. If the particle size distribution can be described in terms of a density function $n(r)dr$, the mass fraction of particles whose radius lies between r and $r + dr$, Equation 5 can be rewritten:

$$\frac{\tau}{c} = \frac{3}{4\rho} \int_0^\infty R(r)K_t(r)r^{-1}n(r)dr \quad (6)$$

where c is the concentration (mass per unit volume) of particles in the suspension and ρ is the density of the particles. The quantity τ/c is known as the specific turbidity of the suspension.

It is convenient to express the particle size in terms of the dimensionless parameter α which leads to

$$\frac{\tau\lambda}{c} = \frac{3\pi}{2\rho} n_0 \int_0^\infty R(\alpha)K_t(\alpha)\alpha^{-1}n(\alpha)d\alpha \quad (7)$$

In the special cases when all particles are either very much smaller or very much larger than the wavelength of the incident light, the integral in Equation 7 can be related to simple moments of the distribution. Thus, for very small particles, the specific turbidity is proportional to the mean particle volume while at the other extreme, turbidity is a measure of specific surface area. For such cases, turbidity measurements yield no further information on the particle size distribution.

In order to apply Equation 7 to the evaluation of real systems, it is convenient to assume a specific form for the size distribution. A suitable form is the two-parameter log-normal distribution defined by

$$n(r)dr = \frac{1}{\sqrt{2\pi}\ln\sigma} \exp\left[-1/2\left(\frac{\ln r - \ln r_{50}}{\ln\sigma}\right)^2\right]\frac{dr}{r} \quad (8)$$

where r_{50} is the geometric mean radius and σ is the geometric standard deviation. If Equation 8 is expressed in terms of the dimensionless variable α and substituted into Equation 7, the integral can be evaluated numerically yielding a theoretical relationship between the specific turbidity and the parameters of the distribution.

Meehan and Beattie (*6*) described a simple graphical technique which can be used to estimate the parameters from measurements of specific turbidity at two wavelengths. Briefly, the method involves simultaneous solution of the theoretical expressions obtained by integration of Equation 7. At any given wavelength, the measured turbidity corresponds to pairs of values for the parameters r_{50} and σ. By plotting theoretical r_{50} vs. σ curves using values corresponding to the experimental turbidity, an estimate of the parameters of the actual distribution can be obtained from the intersection of the curves for different wavelengths. This technique will be described in more detail in a subsequent section of this paper.

It should be emphasized that these measurements yield only an estimate of the size distribution since they provide no means of determining the actual form of the distribution. However, for many applications, an estimate of the mean and standard deviation is probably sufficient. Furthermore, in view of the gross approximations (spherical particles, isotropic, homogeneous materials, etc.) implicit in the use of these methods, it is probably unrealistic to expect them to provide more than an estimate of the actual distribution.

CALCULATIONS

Computation of Total Scattering Coefficients. According to the Mie theory, the scattering coefficients, K_t can be evaluated from an expression of the form (*10*)

$$K_t(m,\alpha) = \frac{2}{\alpha^2}\sum_{n=1}^{\infty}\frac{[R(A_n)]^2 + [I(A_n)]^2 + [R(P_n)]^2 + [R(P_n)]^2}{(2n+1)/[n(n+1)]^2} \quad (9)$$

The quantities A_n and P_n are functions of m and α only and are defined in terms of J-type Bessel functions.

The calculations were carried out on an IBM 370/168 computer at the Pennsylvania State University. The computations, which were performed in double precision arithmetic, were arranged to terminate when the absolute values of each of the four quantities $R(A_n)$, $I(A_n)$, $R(p_n)$, and $I(P_n)$ became smaller than 10^{-7}. Bessel functions whose orders had absolute values of less than 35 were evaluated using a standard, built-in function. For larger orders, the recurrence formula (*11*, *12*)

$$J_{p+1}(\beta) = \frac{2p}{\beta}J_p(\beta) - J_{p-1}(\beta) \quad (10)$$

where p need not be an integer, was used. Derivatives were determined by means of the relation (*11*, *12*)

$$\frac{dJ_p(\beta)}{d\beta} = 1/2[J_{p-1}(\beta) - J_{p+1}(\beta)] \quad (11)$$

The computer program was carefully checked by comparing selected K_t values with those published by Gumprecht and Sliepcevich (*13*) and Pangonis et al. (*14*).

Calculation of Theoretical Turbidities. Theoretical values of the quantity $\tau\lambda/c$ for dispersions of the minerals used in this study were calculated for different values of the size distribution parameters α_{50} and σ. The values were obtained by numerical integration of Equation 7, with $n(\alpha)$ as given by the log normal distribution. Typical plots of theoretical $\tau\lambda/c$ values vs. the dimensionless mean size α_{50} are shown in Figures 1 and 2 for several values of the standard deviation σ.

EXPERIMENTAL

Two polystyrene latices (obtained from the Dow Chemical Company) and the minerals: quartz (SiO_2), anatase (TiO_2), gibbsite ($Al(OH)_3$), and corundum (α-Al_2O_3) were selected for this study. Quartz suspensions were obtained by the dry grinding of silica sand for 7 h in a mechanized agate mortar, dispersing in a 0.1% sodium pyrophosphate solution and removing the remaining coarse particles (>10 μm) in a sedimentation column.

The anatase was prepared from type T-315 titanium oxide which was supplied by Fisher Scientific Company and was dispersed in double distilled water containing a few drops of 1.5% aerosol OT surfactant solution.

The corundum dispersion was prepared from type A-591 alumina also supplied by Fisher Scientific. Three hundred grams of the material were ground in a $^1/_7$-gal. alumina ball mill jar using $^1/_2$-in. to 1-in. alumina balls as grinding media. The grinding was carried out wet in a solution of 10 mL glacial acetic acid and 5 g of aluminum hydroxide gel in 400 mL distilled water. After grinding, the coarser particles (>10 μm) were removed by sedimentation. The finer portion of the suspension was siphoned out and stored in a 1-gal. glass bottle.

The gibbsite $Al(OH)_3$ suspension was prepared in exactly the same manner as the alumina. The starting material was supplied by Atlas-Mason Company.

The suspensions were sampled (for turbidity measurement etc.) by carefully pipetting a known volume from the stock suspension. The suspension was thoroughly agitated prior to sampling to ensure uniformity. Suspension concentrations were checked repeatedly by drying and weighing samples.

The exact crystalline form of each material was examined by X-ray diffraction techniques. Refractive index values were obtained from tabulations given by Deer, Howie, and Zussman (*15*) using the averaging procedure described by Jaffe (*16*).

The relevent physical properties of the materials are summarized in Table I.

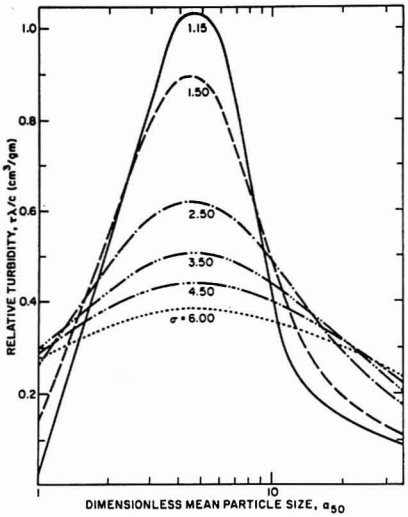

Figure 1. Theoretical light scattering curves for polydisperse suspensions of corundum (α-Al_2O_3) which conform to the log-normal distribution

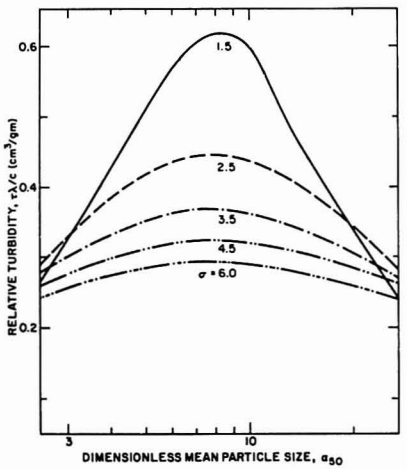

Figure 2. Theoretical light scattering curves for polydisperse suspensions of quartz (SiO_2) which conform to the log-normal distribution

Turbidity measurements were carried out in a Coleman-Hitachi Model 124, double-beam, recording spectrophotometer for various concentrations of the minerals at wavelengths of 436, 546, 650, and 800 nm. In each case, it was determined that there was no appreciable change in turbidity with time, indicating that effects due to coagulation or sedimentation were not significant.

Since the theoretical expressions are valid only for extremely dilute suspensions, when each particle acts as an independent source of scattered light and secondary scattering is negligible, the standard procedure of determining turbidity as a function of concentration and extrapolating to infinite dilution was followed in all cases. Experimental plots of specific turbidity vs. concentration are given in Figures 3 and 4 for the polystyrene latex and the corundum dispersions, respectively.

Table I. Physical Properties of Materials Investigated

material	average refractive index	specific gravity, g/cm³
polystyrene latex, LS-1132-E	1.592	1.05
polystyrene latex, LS-1047-E	1.592	1.05
corundum (Al_2O_3)	1.767	3.97
quartz (SiO_2)	1.547	2.65
gibbsite ($Al(OH)_3$)	1.577	2.42
anatase (TiO_2)	2.537	3.84

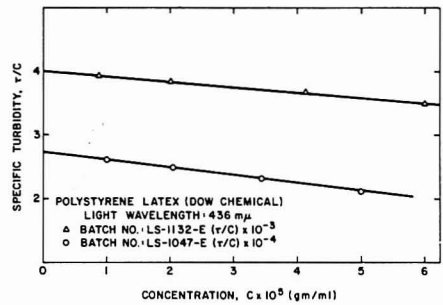

Figure 3. Experimental turbidities of polystyrene latex suspensions

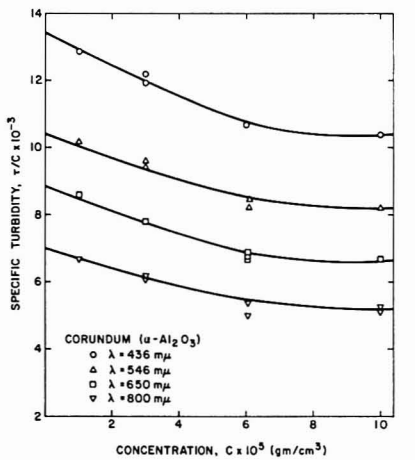

Figure 4. Experimental turbidities of corundum (α-Al_2O_3) suspensions

For comparison purposes, particle size distributions were obtained for each of the mineral suspensions by centrifugal sedimentation using an MSA-Whitby Particle Sizer Analyzer (*17*). At least four replicate tests were performed on each suspension and good reproducibility was obtained in all cases.

RESULTS AND DISCUSSION

Evaluation of Experimental Procedure. The experimental methods used in this study were evaluated using results obtained for the polystyrene latex suspensions. Average particle sizes for these, essentially monodisperse, systems can be obtained directly from Equation 2 which can be rewritten.

$$\frac{\tau\lambda}{c} = \frac{3\pi n_0}{2\rho}\left(\frac{K_t}{\alpha}\right) \qquad (12)$$

Table II. Experimental Results for Polystyrene Latex Beads

latex	average particle diameter, μm: manufacturers figure	average particle diameter, μm: estimated from turbidity	specific turbidity $(\tau/c)_{c=0}$: measured	specific turbidity $(\tau/c)_{c=0}$: theoretical	correction factor
LS-1132-E	0.091	0.095	3.45×10^{-3}	3.45×10^{-3}	1.000
LS-1047-E	0.234	0.231	21.38×10^{-3}	21.50×10^{-3}	0.995

Table III. Experimental Results for Mineral Suspensions

mineral	mean particle diameter, μm: estimated from turbidity	mean particle diameter, μm: centrifugal sedimentation	standard deviation, σ: estimated from turbidity	standard deviation, σ: centrifugal sedimentation
corundum (α-Al_2O_3)	0.60	0.55	2.84	2.76
quartz (SiO_2)	1.25	1.18	2.89	2.97
gibbsite ($Al(OH)_3$)	0.34	0.32	2.56	2.30
anatase (TiO_2)	0.30	0.60	1.54	1.86

Theoretical values of the quantity K_t/α as a function of the dimensionless size α are shown in Figure 5. Experimental average sizes for the two materials, evaluated using Equation 12 and Figure 5 are given in Table II.

These results can be used to obtain experimental estimates of the correction factor R defined by Equation 3. Thus, R can be calculated from

$$R = \tau_{exp}/\tau_{theor}$$

where τ_{exp} is the experimental turbidity of the suspension and τ_{theor} is the theoretical value calculated from the known size of the particles. The values of R, so determined, are also given in Table II. It should be noted that, in general, R depends on the relative particle size α. Thus, the values shown in Table II are not necessarily valid under all conditions. However, in view of the small corrections involved, it seems reasonable to assume that the correction factor is insignificant for the optical system used in this study.

Size Distribution of Polydisperse Mineral Suspensions. For each of the measured turbidities, the theoretical scattering curves (Figures 1 and 2, for example) can be used to obtain a pair of values of the dimensionless median size α_{50} corresponding to each value of the standard deviation σ. Thus, for the corundum system, a relative turbidity $(\tau\lambda/c)$ of 0.5 would be obtained if $\sigma = 1.15$ and $\alpha_{50} = 2.0$ or 9.5. Similarly, if $\sigma = 2.50$, the same relative turbidity (0.5) would be obtained if $\alpha = 2.1$ or 9.7. By plotting these theoretical σ values vs. the corresponding mean particle radii, a curve is obtained for each measured turbidity. Examples of these curves are shown in Figure 6 for measurements on the corundum system at four different wavelengths. An estimate of the "true" values of the parameters can be obtained from the intersection of the curves. It should be noted that, in fact, it is necessary to obtain data only at two wavelengths. In the present study, however, we have used four wavelengths as a check on the consistency of the results. Ideally, all four curves should intersect in a single point; the observed discrepancies are surprisingly small in view of the approximate nature of the model.

The size distributions estimated from the light scattering data are compared to those obtained by centrifugal sedimentation in Figures 7 and 8 for the corundum and quartz suspensions respectively; the log normal distribution parameters are compared for all of the minerals in Table III. Clearly, the agreement between the turbidimetric and sedimentation results is remarkable. An exception is found, however, in the case of anatase where the light scattering technique appears to underestimate the mean size by a factor

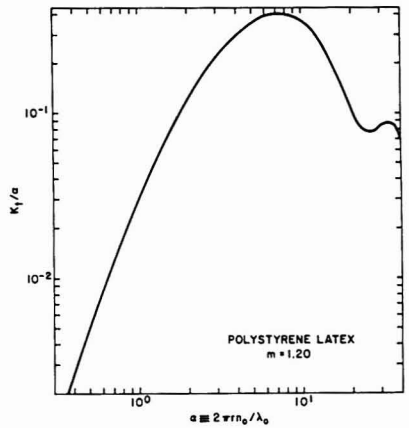

Figure 5. Theoretical relationship for the light scattering behavior of monodisperse polystyrene latex suspension

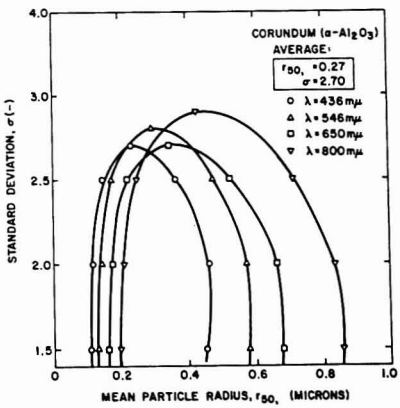

Figure 6. Experimental plot for graphical evaluation of the size distribution parameters for corundum (α-Al_2O_3)

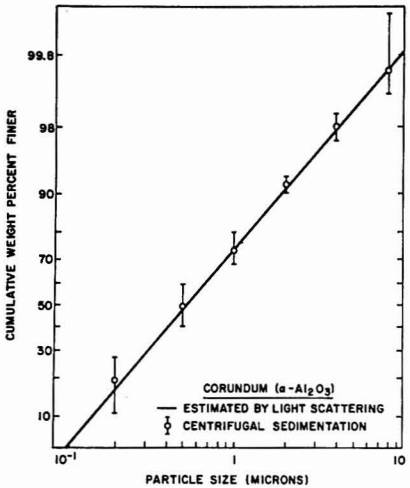

Figure 7. Comparison of the particle size distribution of a corundum (α-Al_2O_3) suspension as estimated from turbidimetry with direct measurement by centrifugal sedimentation

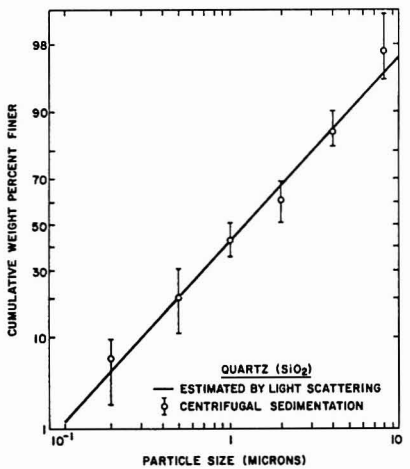

Figure 8. Comparison of the estimated particle size distribution of a quartz (SiO_2) suspension with direct measurement by centrifugal sedimentation

of two. The reasons for this discrepancy are not fully clear, though it may very possibly be the result of using improper values for the refractive indices. Titanium oxides have high refractive indices which are known (*18*) to be strongly dependent on wavelength.

Effect of Deviations from the Log Normal Distribution. In the previous sections of this paper, it has been shown that, for materials which conform quite closely to the log normal size distribution, reasonable estimates of the parameters of the distribution can be obtained from simple turbidity measurements. Clearly, however, there is no a priori reason to expect any given material to conform to this particular distribution. It is of considerable interest, therefore,

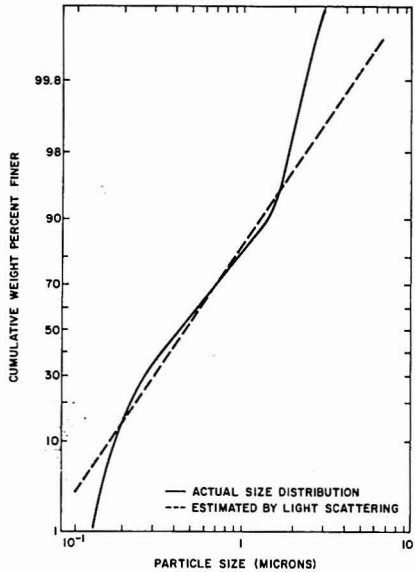

Figure 9. Simulation of the result of applying the estimation procedure to particle size distributions which do not conform to the log normal law

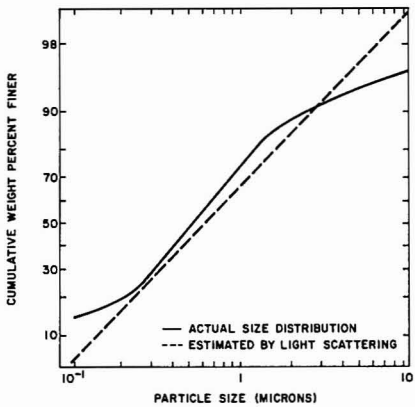

Figure 10. Simulation of the result of applying the estimation procedure to particle size distributions which do not conform to the log normal law

to examine the results which would be obtained by applying this technique to particulate systems which do not conform to the log normal distribution.

Theoretical turbidities have been calculated, using Equation 7, for a series of hypothetical distributions which deviate significantly from the log normal form. Examples of two such distributions are shown, as the solid lines, in Figures 9 and 10. These theoretical turbidities have, in turn, been used as "experimental" values in our estimation procedure. The dashed lines in Figures 9 and 10 represent the apparent distributions which would be obtained if we were to apply our estimation procedure to particulate systems whose true size

distributions were given by the solid curves. In each case, it is found that the estimated distribution conforms quite closely to the central portion of the true distribution and is not strongly biased toward either of the tails. Thus, it appears that the estimation procedure described in this paper can reasonably be applied to real systems which may not necessarily conform to the log normal size distribution. The resulting, estimated distribution will be a kind of "best-fit" log normal approximation to the true particle size distribution.

SUMMARY OF ESTIMATION PROCEDURE

The procedure to be followed in using this approach to estimate particle size distributions can be summarized as follows.

(1) Obtain the appropriate values of the light scattering coefficients K_t either from tables (see, for example, ref. 13 and 14) or by numerical solution of Equation 9.

(2) Determine the theoretical turbidity curves for the material by numerical integration of Equation 7.

(3) Measure the specific turbidity of the suspension as a function of solids concentration and extrapolate to infinite dilution. Obtain such measurements for at least two wavelengths.

(4) From the measured turbidities and the theoretical curves obtained in (2) above, determine the possible values of the mean size parameter α_{50} corresponding to each value of the standard deviation σ.

(5) Plot σ vs. mean particle radius for each measured turbidity.

(6) Read off the estimated mean and standard deviation for the actual distribution from the intersection of the curves.

LITERATURE CITED

(1) E. L. Weiss and H. N. Frock, *Powder Technol.*, 14, 287 (1976).
(2) T. Allen, "Particle Size Measurement", 2nd ed., Halstead Press, Wiley, New York, 1975.
(3) F. T. Gucker, C. T. O'Konski, H. G. Pickard, and J. H. Pitts, *J. Am. Chem. Soc.*, 69, 2422 (1949).
(4) C. T. O'Konski and G. J. Doyle, *Anal. Chem.*, 27, 694 (1955).
(5) A. E. Martens and J. D. Keller, *Am. Ind. Hyg. Assoc. J.*, 29, 257 (1968).
(6) E. J. Meehan and W. H. Beattie, *J. Phys. Chem.*, 64, 1006 (1960).
(7) G. Mie, *Ann. Physik*, 25, 377 (1908).
(8) H. C. van der Hulst, "Light Scattering by Small Particles", Wiley, New York, 1957.
(9) M. Kerker, "The Scattering of Light and Other Electromagnetic Radiation", Academic Press, New York, 1969.
(10) R. O. Gumprecht and C. M. Sliepcevich, *J. Phys. Chem.*, 57, 90 (1953).
(11) S. A. Stekunoff "Applied Math for Engineers and Scientists", van Nostrand, New York, 1965, p 406.
(12) R. Weast, Ed., "Handbook of Tables for Mathematics", 6th ed., Chemical Rubber Company, Cleveland, Ohio, 1970.
(13) R. O. Gumprecht and C. M. Sliepcevich, "Tables of Light Scattering Functions for Spherical Particles", University of Michigan, Engineering Research Institute Special Publication: Tables, Ann Arbor, Mich., 1951.
(14) W. J. Pangonis, W. Heller, and A. Jacobson, "Tables of Light Scattering Functions for Spherical Particles", Wayne State University Press, Detroit, Mich., 1957.
(15) W. A. Deer, R. A. Howie, and J. Zussman, "An Introduction to the Rock Forming Minerals", Wiley, New York, 1966.
(16) H. W. Jaffe, *Am. Mineral.*, 41, 757 (1956).
(17) K. T. Whitby, *Am. Soc. Heat. Refrig. Air-Cond. Eng., J. Sect., Heat., Piping, Air Cond.*, June 1965.
(18) T. Radhakrishnan, *Proc. Indian Acad. Sci., Sec A*, 35, 117 (1952).

RECEIVED for review May 18, 1978. Accepted January 29, 1979. This work described in this paper was supported in part by the National Science Foundation under an Institutional Grant to The Pennsylvania State University. The paper was presented at the Eastern Analytical Symposium, New York, November 1973.

Chemically Bonded Aryl Ether Phase for the High Performance Liquid Chromatographic Separation of Aromatic Nitro Compounds

Thomas H. Mourey and Sidney Siggia*

Chemistry Department, GRC Tower I, University of Massachusetts, Amherst, Massachusetts 01003

A chemically bonded aryl ether stationary phase which shows novel selectivity in the reverse-phase liquid chromatographic separation of aromatic nitro compounds has been prepared. Differentiation between nitroaromatic isomers is a result of partitioning and charge transfer interactions. Comparisons with octadecyl and phenyl silica show both the differences and the advantages of the aryl ether phase. A modified Hammett equation is used to relate retention to electrophilic aromatic substitution rates for meta- and para-substituted compounds. Absorption spectra of the charge transfer complexes involved are presented, and the significance of the complexation is discussed in terms of its effect on chromatographic behavior.

Selectivity in high performance liquid chromatographic separations is often influenced by the electron donor–acceptor properties of the solute molecules and the bonded phase. While investigating the reverse-phase separation of a number of aromatic nitro compounds, we hoped to take advantage of the strong electron accepting properties of these compounds by using a stationary phase which contained strong electron donating groups. The resultant charge transfer complexes are well documented in the literature (*1–3*), and it is basically accepted that there is a partial or complete transfer of electrons from donor to acceptor. Complex stability is a function of the electronic character and number of substituents on the acceptor molecule, their steric effects, and the solvent system employed. The interaction is highly suited for chromatographic application. Complexation kinetics are rapid (*4*), reversible, and discriminative enough to add functional group selectivity that is not possible in adsorption and partition chromatography.

The electron donor of choice for a nitroaromatic selective stationary phase is an aromatic ether. The ether linkage increases the electron density of the aromatic ring. The result is that the phenoxy group is one of the most powerful electron donors for nitroaromatics (*1*) as evidenced by formation of

0003-2700/79/0351-0763$01.00/0 © 1979 American Chemical Society

solid picrates. An organohalosilane incorporating the phenoxy group can be synthesized by the platinum catalyzed addition of a silicon hydride to an olefin (*5, 6*). The result is a terminally substituted silanizing reagent which may be chemically bonded to a silaceous chromatographic support material.

EXPERIMENTAL

Chlorodimethyl-(3-phenoxy)propylsilane Synthesis. The platinum catalyzed addition of chlorodimethylsilane to allyl phenyl ether,

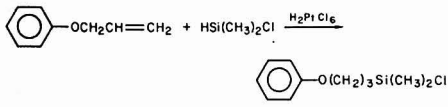

was run as follows: 7 g of allyl phenyl ether (0.0522 mol, 96% from Aldrich Chemical Corp., Inc.) and approximately 1.0×10^{-5} mol of chloroplatinic acid (Fisher Chemical) were heated to 85 °C with stirring in a 100-mL round bottom flask equipped with an efficient reflux condenser and dropping funnel. Five grams (0.05742 mol) of chlorodimethylsilane (Ventron Corp.) were added dropwise with stirring so that the heat of the reaction maintained the temperature between 90–100 °C. Total addition time was approximately 45 min. The solution was heated for an additional 8 h, the product vacuum distilled, and the fraction boiling between 90–92 °C at 0.25 mm Hg collected. The yield was 82% chlorodimethyl-(3-phenoxy)propylsilane. The 60-MHz proton magnetic resonance spectrum showed a 6-proton singlet at 0.40 ppm, a distorted 2-proton triplet at 0.90 ppm, 2-proton multiplet from 1.62 to 2.11 ppm, 2-proton triplet at 3.86 ppm, 3-proton multiplet at 6.89 ppm, and a 2-proton multiplet at 7.20 ppm. Aromatic resonances showed no significant differences from the starting material. A 70-eV mass spectrum gave results consistent with the position of addition and also with the absence of dimer resulting from hydrolysis.

Bonded Phase Preparation. Five grams of LiChrosorb SI60 5 μm silica (E. M. Merck) were refluxed in 100 mL of 6 N hydrochloric acid for 2 h, filtered, washed thoroughly with neutral, distilled, deionized water, and dried under vacuum at 150 °C for 15 h. The above prepared silica and 50 mL of dry toluene were placed in a 250-mL round bottom flask equipped with an efficient reflux condenser. Three milliliters of chlorodimethyl-(3-phenoxy)propylsilane in 25 mL of dry toluene were added, and the whole was refluxed for 2 h. The bonded phase was filtered, washed thoroughly with dry toluene and methanol, and dried at 60 °C under vacuum for 15 h. Elemental carbon and hydrogen analysis showed percent loading to be 12.51% by weight, corresponding to 0.76 mmol of aryl ether per gram of support. This dry phase was suspended in 50 mL of dry toluene and treated with 4 mL of trimethylchlorosilane, refluxed for 1 h, filtered, washed with dry toluene and methanol, and dried under vacuum at 60 °C before use.

Column Packing Procedure. Stainless steel columns, 4 mm by 200 mm, were equipped with zero dead volume fittings. The packing (1.65 g) was slurried in 12 mL of isopropanol, sonicated for 30 s, and introduced into the column and packing reservoir. Filtered, distilled, deionized water, (200 mL) were pumped through at 6000 psi, and the column was conditioned with the appropriate mobile phase under normal operating conditions before use. Octadecyl and phenyl phases used in comparison studies were packed similarly.

Chromatography. The chemically bonded phenyl column used in comparison studies was prepared by treating 5-μm LiChrosorb SI60 with dichloromethylphenylsilane. The 5-μm octadecyl phase (ODS) was obtained from Johns-Manville. Column efficiencies were matched to range between 3000–3500 plates per 100 mm for comparison of the three columns. All flow rates were 1.00 mL/min. Mobile phases used for comparison studies were 50/50, 35/65, 6/94 methanol–water (v/v) for the aryl ether, ODS, and phenyl columns, respectively.

Molecular Complex Formation Studies. Solutions of allyl phenyl ether, nitroaromatic, and the two together in a 1 to 1 molar ratio, were prepared in 50/50 (v/v) methanol–water, and their ultraviolet absorption spectra run vs. 50/50 methanol–water. All references were prepared identically to samples, excluding the nitro compound under investigation, when examining absorption shifts and intensity changes near the visible region.

Reagents and Instrumentation. The structure of chlorodimethyl-(3-phenoxy)propylsilane was confirmed with a Varian A-60 nuclear magnetic resonance spectrometer and a Perkin-Elmer–Hitachi RMU 6L mass spectrometer. A Perkin-Elmer 202 UV-vis spectrophotometer and a Beckman IR10 infrared spectrophotometer were used in complex formation studies. Liquid chromatograms were run on a Laboratory Data Control Constametric IIG liquid chromatograph equipped with a Model 1202 Spectromonitor II variable wavelength UV detector. Samples were introduced through a 10-μL high pressure Valco injection valve. Methanol was Fisher Spectranalyzed grade. Water was distilled, run through cation- and anion-exchange columns as well as activated charcoal. All solvents were filtered through 0.45-μm membrane filters. Most nitro compounds were commercially obtained. Others were synthesized using standard procedures and their identities were confirmed spectroscopically. All sample compounds were either fractionally distilled or recrystallized from the appropriate solvents, and their purities were checked by melting and boiling points.

RESULTS AND DISCUSSION

Synthesis of the monochlorosilane is more desirable than the di- or trichloro derivative for several reasons. Hydride addition of chlorodimethylsilane proceeds much more slowly than the di- and trichloro reactions, making the addition easier to control. The resulting product is considerably more volatile than the di and tri derivatives which makes it easier to purify by fractional distillation. In addition, the effects of monofunctional vs. di- and trifunctional reagents on chromatographic performance have been reviewed in the literature (*7, 8*), showing that the monochloro reagent is more desirable because of its homogeneous, single layer coverage of the support material. Synthesis via silicon hydride addition is favored in this instance over other synthetic methods because of its high yield and selectivity for the terminally substituted isomer.

Column efficiencies for the aryl ether averaged 3500 plates in 100 mm using the loop injector. Up to 5000 plates per 100 mm were obtained by direct injection onto the same column. Peak shouldering and rapid column deterioration reduced the usefulness of this technique, however. Results of chromatography on the aryl ether, octadecyl, and phenyl columns are given in Table I in terms of k' values. Several general trends are evident. The elution order for the aryl ether is nonnitro, mononitro, dinitro, trinitro, showing that increased retention corresponds to decreasing electron density. A similar trend is not evident with either ODS or phenyl columns. These columns tend to retain polynitro compounds less strongly than mono and nonnitro because of the high polarity of the nitro group. The result, as shown in Table I, is that polynitro compounds of one class (i.e., dinitrobenzenes) have k' values similar to mononitro compounds of a different class (i.e., nitroacetanilides and nitrobenzaldehydes for ODS and phenyl respectively). The chromatograms in Figures 1a and 1b show the aryl ether elution order more clearly for a random mixture of nitro compounds varying widely in nature of substituents and solubility in the mobile phase. Of this mixture of 23 test compounds, ODS gave 16 distinct peaks while the phenyl column showed only 13. The latter two columns gave poor separation of the mixture in both cases due to co-elution of polynitros with mononitros.

Comparison separations of the three phases are shown in Figures 2 and 3. Separations of nitrobenzenes in Figure 2 show that the elution order for ODS is the inverse of the aryl ether. The phenyl phase (Figure 2c) gives a separation similar to ODS except for the early elution of benzene. Elution orders tend to indicate that ODS and, suprisingly, phenyl show little or no selectivity for electron density of the solutes. Hy-

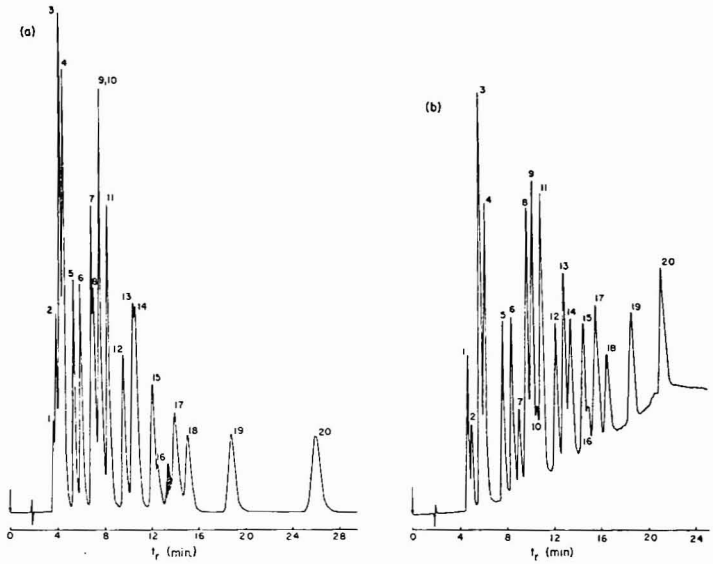

Figure 1. (a) Mixture of aromatic nitro compounds separated isocratically on 4 mm i.d. × 200 mm long chemically bonded aryl ether phase. Mobile phase, 45% MeOH/55% H_2O. Flow rate, 1.00 mL/min. UV detection at 254 nm, 0.08 AUFS. (1) *o*-Nitrobenzenesulfonamide, 236 ng; (2) *p*-nitrobenzenesulfonamide, 194 ng; (3) *p*-nitrobenzamide, 240 ng; aniline, 660 ng; (4) acetanilide, 210 ng; (5) *p*-nitroaniline, 376 ng; (6) *o*-nitroacetanilide, 234 ng; (7) *o*-nitroaniline, 376 ng; (8) benzene, 3580 ng; *o*-nitrobenzonitrile, 236 ng; (9) *p*-nitrobenzonitrile, 236 ng; (10) *p*-nitroacetanilide, 362 ng; (11) nitrobenzene, 378 ng; (12) *p*-dinitrobenzene, 178 ng; (13) *m*-dinitrobenzene, 158 ng; (14) 2,4-dinitroaniline, 222 ng; (15) *m*-nitroanisole, 184 ng; 2,4-dinitroacetanilide, 258 ng; (16) *p*-nitroanisole, 172 ng; (17) 1,3,5-trinitrobenzene, 120 ng; (18) 2,4-dinitroanisole, 176 ng; (19) 2,4,6-trinitroaniline, 176 ng; (20) 3,5-dinitromethylbenzoate, 210 ng. (b) Same mixture as in (a) run with a linear gradient from 35% MeOH to 65% MeOH. Gradient time equals 20 min

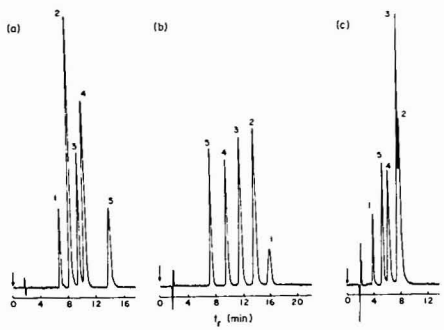

Figure 2. Comparison separations of nitrobenzenes on (a) aryl ether, (b) ODS, (c) phenyl. UV detection at 254 nm, 0.08 AUFS. (1) Benzene, 1790 ng; (2) nitrobenzene, 189 ng; (3) *p*-dinitrobenzene, 89 ng; (4) *m*-dinitrobenzene, 79 ng; (5) 1,3,5-trinitrobenzene, 60 ng

drophobic interaction appears to primarily govern distribution between the mobile and stationary phases in these latter two cases. Figure 3a distinctly shows separation according to the number of nitro substituents for compounds of similar polarity and solubility, yet different substituent classes. ODS and phenyl phases (Figures 3b and 3c) lack this selectivity, resulting in ineffective separation. This particular separation is of some significance to organic synthesis. Direct nitration of acetanilide is a common route to the *o*-, *p*-, and 2,4-dinitroanilines since these isomers cannot be obtained from the

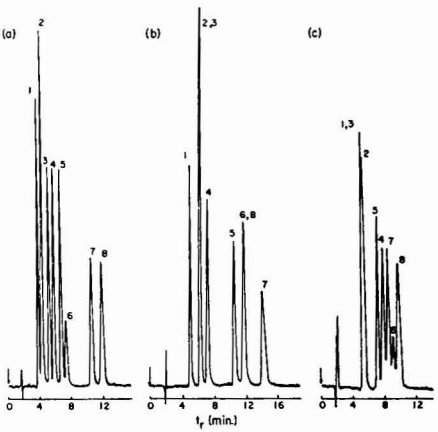

Figure 3. Comparison separations of nitroanilines and nitroacetanilides on (a) aryl ether, (b) ODS, (c) phenyl. UV detection at 254 nm, 0.08 AUFS. (1) Aniline, 165 ng; (2) acetanilide, 52 ng; (3) *p*-nitroaniline, 94 ng; (4) *o*-nitroacetanilide, 84 ng; (5) *o*-nitroaniline, 74 ng; (6) *p*-nitroacetanilide, 90 ng; (7) 2,4-dinitroaniline, 56 ng; (8) 2,4-dinitroacetanilide, 64 ng

direct nitration of aniline. Mixtures of all isomers are possible in the process, and all are readily separated by the aryl ether bonded phase.

Table I. k' Values for Standard Compounds

compound	aryl ether	ODS	phenyl
nonnitro			
aniline	1.17	1.71	2.09
phenol	1.19	2.26	2.40
acetanilide	1.49	2.57	0.06
benzaldehyde	2.38	3.71	2.69
benzonitrile	2.76	3.76	2.62
benzene	2.98	8.18	1.28
anisole	3.91	8.14	5.27
mononitro			
o-nitrobenzenesulfonamide	1.00	0.93	1.40
p-nitrobenzenesulfonamide	1.24	1.23	0.90
p-nitrobenzamide	1.31	1.76	1.42
p-nitroaniline	1.98	2.50	2.11
m-nitroaniline	2.06	2.57	2.14
p-nitrophenol[a]	2.19	3.86	1.24
m-nitrophenol[a]	2.19	4.29	1.51
o-nitroacetanilide	2.33	4.78	1.25
p-nitrobenzaldehyde	2.67	3.39	2.60
o-nitrophenol[a]	2.79	5.90	2.43
m-nitrobenzaldehyde	2.86	3.53	3.26
o-nitroaniline	2.87	5.20	3.12
m-nitroacetanilide	2.91	4.78	4.23
o-nitrobenzonitrile	2.98	3.43	4.55
p-nitrobenzonitrile	3.22	3.36	2.47
p-nitroacetanilide	3.24	5.81	4.24
nitrobenzene	3.76	6.95	3.48
o-nitroanisole	4.86	6.40	2.39
m-nitroanisole	5.76	11.79	5.20
p-nitroanisole	6.19	8.82	5.11
p-nitro methyl benzoate	7.47	14.14	6.13
1-chloro-4-nitrobenzene	8.18	16.14	5.06
dinitro			
3,5-dinitrobenzamide	2.90	4.42	1.90
2,6-dinitrophenol[a]	3.28	4.13	2.25
2,5-dinitrophenol[a]	3.85	5.17	1.94
2,4-dinitrophenol[a]	4.22	4.78	1.94
p-dinitrobenzene	4.40	5.54	3.29
m-dinitrobenzene	4.88	4.58	2.43
2,4-dinitroaniline	5.11	7.30	3.89
2,4-dinitroacetanilide	5.84	5.84	4.60
2,4-dinitroanisole	8.02	14.14	6.31
3,5-dinitro methyl benzoate	13.81	11.79	6.54
trinitro			
1,3,5-trinitrobenzene	6.94	3.13	1.77
2,4,6-trinitroaniline	9.60	5.64	3.27

[a] Mobile phase modified with 1% by volume acetic acid.

Results of complex formation studies show absorption spectra characteristic of weakly bound molecular complexes. Figure 4 shows that the complex absorption spectrum of allyl phenyl ether and 1,3,5-trinitrobenzene is roughly the sum of the reactants, with slight anomaly in the 250- to 300-nm region. A significant increase in intensity, measured as the total area under the absorption curve, is present in 4.5×10^{-6} M solutions (Figure 4a). Such increases are characteristic of complex formation (*9*). An absorption shift toward the visible region, also indicative of charge transfer interactions, is not immediately apparent. It has been shown, however, that molecular complexes of this type often show spectra which are no more than the sum of the reactants when observed in dilute solutions (*10*). Increasing the molar concentration (Figure 4b) results in a significant increase in the absorption intensity between 300 and 350 nm. At higher concentrations, the intensity increase can be observed visually as a change from pale to deep yellow. Examination of the molecular complex formed between allyl phenyl ether and 2,5-dinitrophenol

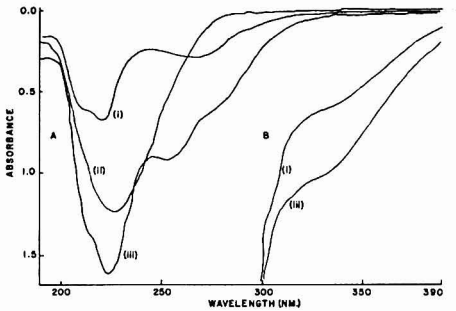

Figure 4. Ultraviolet absorption spectra of 1,3,5-trinitrobenzene–allyl phenyl ether molecular complex. (Ai) 4.5×10^{-6} M allyl phenyl ether; (Aii) 1:1 molecular complex, 4.5×10^{-6} M; (Aiii) 4.5×10^{-6} M 1,-3,5-trinitrobenzene. (Bi) 1.9×10^{-2} M 1,3,5-trinitrobenzene; (Bii) 1:1 complex with allyl phenyl ether at same molar concentration

showed a 10-nm shift toward the visible region as well as increased spectrum intensity. At higher concentrations, this effect was also observed visually.

No significant changes were found in the infrared spectra of products compared to reactants. It has been shown (*11*) that changes in infrared bands do not necessarily appear, especially in weakly bound, noncrystalline complexes.

These data indicate that the complexes are weakly formed, and that partitioning into the stationary phase should be as much a factor in retention as is charge transfer interaction. This is particularly true with mononitro compounds which are only moderately electron deficient.

There is evidence of a relationship between molecular complex formation and the rate of electrophilic aromatic substitution in donors and acceptors (*1*, *12*). Therefore, it should be possible to plot a modified Hammett equation (*13*) which relates the nature of substituents in substituted nitrobenzenes to chromatographic retention on the aryl ether. Since complex formation studies show that partitioning effects are important to retention, they must be taken into account by an approximation which gives a k' factor as a measure of electron density or charge transfer alone. A first approximation is to ratio the k' values of the aryl ether with those for a phase such as ODS which separates by partitioning. Incorporating this adjustment into the original Hammett equation gives

$$\log [A(k'_{ae}/k'_{ods})] = \rho\Sigma\sigma$$

where σ is the Hammett substituent constant, ρ the reaction constant, and A equal to the ratio of k'_{ods} to k'_{ae} for nitrobenzene. The equation gives a measure of the effects of substituents in nitrobenzenes compared to nitrobenzene through normalization by constant A. The calculations give a linear free-energy relationship which holds for para- and meta-substituted compounds only. The additivity principle (*14*) extends the application to poly-substituted compounds.

A plot of Hammett substituent constants (*15*) vs. the ODS normalized capacity factors is shown in Figure 5. σ^+ values were used for the nitrobenzaldehydes and *p*-nitromethylbenzoate because of the unavailability in the literature of Hammett constants. The approximation roughly gives a linear relationship as predicted by theory. The nitroanilines, *p*-nitrophenol, and *p*-nitroanisole deviate markedly in a positive direction, corresponding to retention greater than predicted. An explanation may lie in additional retention mechanisms, typically hydrogen bonding between the nitroanilines and *p*-nitrophenol and the bonded phase either linkage. In ad-

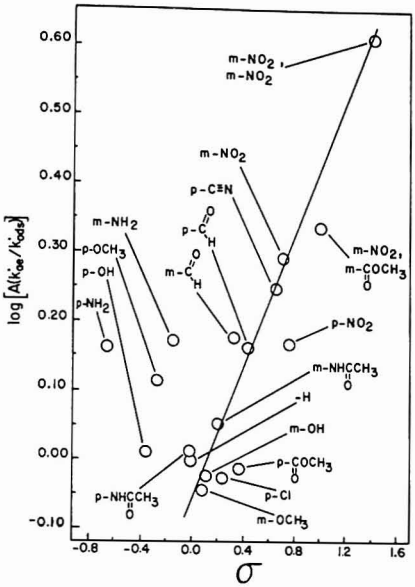

Figure 5. Hammett function data for para- and meta-substituted nitrobenzenes

dition, Hammett constants may not be accurate choices for these compounds since resonance effects of the substituents are not taken into account. Modified Hammett constants (*15*) improve the linearity and include some of the deviating points in the line.

A linear relationship between log k' values and percent methanol in the mobile phase was observed for methanol contents between 35 and 65%. Ten nitrobenzenes, nitroanilines, and nitroacetanilides were investigated. This behavior is typical of other reverse-phase systems (*16*). Higher methanol contents showed positive deviation, or retention greater than expected.

In conclusion, we have found that the microparticulate aryl ether phase provides selectivity for aromatic nitro compound isomers that is not present in other nonpolar reverse-phase systems. It provides rapid and efficient separation of a large cross section of compounds typically found in nitration reaction mixtures and high explosive preparations, many of which are presently difficult to isolate by other means because of similarities in polarity and partitioning behavior.

LITERATURE CITED

(1) Rose, J. "Molecular Complexes" Pergamon Press: New York, 1967.
(2) Foster, R. "Organic Charge Transfer Complexes"; Academic Press: New York, 1969.
(3) Mulliken R. S.; Person, W. B. *Ann. Rev. Phys. Chem.* **1962**, *13*, 107.
(4) Hammick, D. L.; Sixsmith, G. *J. Chem. Soc.* **1935**, 580.
(5) Sommer, L. H.; MacKay, F. P.; Steward, O. W.; Campbell, P. C. *J. Am. Chem. Soc.* **1957**, *79*, 2764.
(6) Speier, J. L.; Webster, J. A.; Barnes, G. H. *J. Am. Chem. Soc.* **1957**, *79*, 974.
(7) Kitka, E. J.; Grushka, E. *Anal. Chem* **1976**, *48*, 1098.
(8) Kirkland, J. J. *Chromatographia* **1975**, *8*, 661.
(9) White, W. N. *J. Am. Chem. Soc.* **1959**, *81*, 2912.
(10) Hunter, R. F.; et al. *J. Chem. Soc.* **1938**, 1576.
(11) Burton, W. R.; Richards, R. E. *J. Chem. Soc.* **1950**, 1316.
(12) Stone, E. W.; Maki, A. H. *J. Chem. Phys.* **1963**, *39*, 1635.
(13) Hammett, L. P. "Physical Organic Chemistry"; McGraw Hill: New York, 1940; Chapter 6.
(14) Jaffe, H. H. *Chem. Rev.* **1953**, *53*, 191.
(15) Stock, L. M.; Brown, H. C. "Advances in Physical Organic Chemistry"; Gold, Ed.; V., Academic Press: New York, 1963; Chapter 2.
(16) Karch, K.; Sebastian, I.; Halasz, I.; Engelhardt, H. *J. Chromatogr.* **1976**, *122*, 171.

RECEIVED for review August 16, 1978. Accepted January 31, 1979. This research was supported in part by an American Chemical Society Division of Analytical Chemistry Summer Fellowship, sponsored by the Division of Analytical Chemistry Chairman.

Retention Indices for Programmed-Temperature Capillary-Column Gas Chromatography of Polycyclic Aromatic Hydrocarbons

Milton L. Lee* and Daniel L. Vassilaros

Department of Chemistry, Brigham Young University, Provo, Utah 84602

Curt M. White

Pittsburgh Energy Technology Center, U.S. Department of Energy, Pittsburgh, Pennsylvania 15213

Milos Novotny

Department of Chemistry, Indiana University, Bloomington, Indiana 47401

In this study the retention index which employs a homologous series of *n*-alkanes as internal standards was evaluated for use with SE-52 capillary columns, and was found to lack good statistical reliability for the PAH. Therefore, a new retention index was defined based on the series of PAH internal standards: naphthalene, phenanthrene, chrysene, and picene. The retention indices of over 200 PAH were determined using this system. The average 95% confidence limits for four measurements on each PAH are ±0.25 index unit.

The main purpose of any chromatographic system is to resolve mixtures of elements or compounds into less complex mixtures or ultimately into pure components. In many instances, chromatography serves as the sample preparation or clean-up step prior to analysis by methods such as infrared spectrometry, UV absorption, fluorescence, and mass spectrometry. In addition to this function, the chromatographic system can provide retention data which can serve as complementary information for the positive identification of resolved components. For example, knowledge concerning structure vs. retention among isomers can greatly help in the correct structural assignment of an unknown compound when there is a choice between several possible isomers. In addition, it is a generally accepted practice that excellent retention data correlation between an unknown and a selected reference compound on two columns of different polarity is sufficient for positive identification of the unknown, although additional spectrometric evidence lends weight to the argument. These considerations have led to much effort by many users to develop simple and reproducible retention parameters which could be used by themselves and other laboratories. A number of systems have been proposed to tabulate and present retention data, and descriptions of these systems are reviewed in the literature (*1*, *2*). The relative retention, which presents retention data relative to a single arbitrary standard, and the retention index introduced by Kovats (*3*), in which the retention is determined relative to a series of homologous *n*-hydrocarbons, are the most widely accepted methods for reporting data. With well-defined chromatographic columns, isothermal conditions, and operational procedures, these systems can be used to provide sufficiently reproducible data. Unfortunately, the degree of reproducibility is dependent on a number of factors, some of which cannot be easily controlled by the laboratory worker. For instance, it is not unusual to find differences in chemical composition from batch-to-batch of a particular stationary phase (*4*). Furthermore, chemical reactions such as polymerization or catalytic decomposition (*5*) of the stationary phase which change the chemical nature and, hence, the retention characteristics of the phase can occur during use. The effects of column materials on solute retention with identical stationary phases have been described (*6*). The degree of deactivation of the stationary phase support material has a profound effect upon retention, especially when thin films of stationary phase are used. The active surface can "look through" the film layer and interact with polar compounds leading to an increase in their retention (*7*). Thermal degradation of silylated support surfaces and bleeding of the stationary phase during repeated use add to these effects. The relationship between retention behavior and operating temperature has been the subject of a number of investigations (*2*). Retention and, hence, retention data oftentimes differ greatly when determined at different operating temperatures. Furthermore, it has been shown that temperature has an effect on the polarity of stationary phases (*2*).

Table I. Retention Indices from Capillary Columns with Different Stationary Phase Film Thicknesses

	normal retention index		PAH index	
compound	column A	column B	column A	column B
naphthalene	1168.74	1166.21	200.00	200.00
ace-naphthylene	1425.03	1413.00	244.65	244.67
fluorene	1555.87	1549.28	268.14	268.22
phenanthrene	1744.70	1734.95	300.00	300.00
anthracene	1754.20	1744.40	301.73	301.76
4*H*-cyclo-penta[*def*]-phenanthrene	1876.18	1864.28	321.95	322.09
pyrene	2063.99	2048.56	351.13	351.25
benzo[*a*]-fluorene	2167.27	2153.04	366.64	366.75
benzo[*e*]-pyrene	2770.65	2751.03	450.66	450.80
perylene	2812.49	2815.42	456.12	456.23

The reproducibility of retention data increases with the similarity of the sample to chosen standard reference compounds. The use of homologous series other than the normal paraffins as calibration standards for the retention index system has been proposed by a number of workers. Among these are the methyl esters of the linear saturated acids (*8*, *9*), selected steranes (*10*), primary straight-chain alcohols (*11*), *n*-propyl ethers (*11*), and 2-alkanones (*12*, *13*). The use of a chemically similar homologous series is even more critical

0003-2700/79/0351-0768$01.00/0 © 1979 American Chemical Society

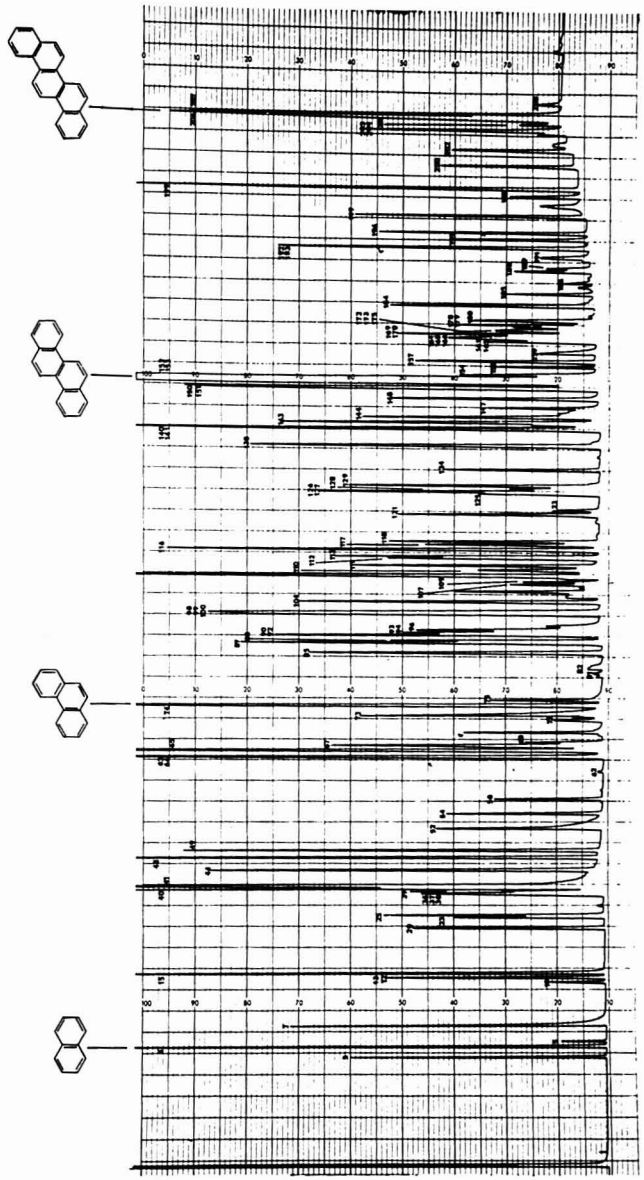

Figure 1. Capillary column gas chromatogram of standard PAH on a 12 m × 0.29 mm, i.d., glass capillary coated with a 0.34-μm film of SE-52. Numbered peaks refer to compounds listed in Tables II and III

Table II. PAH Retention Indices

compound no.	compound name	average index	standard deviation
1	1,2-dihydronaphthalene	197.01	0.07[c]
2	1,4-dihydronaphthalene	197.01	0.07[c]
3	tetralin	197.04	0.05[d]
4	naphthalene	200.00	
5	benzo[*b*]thiophene	201.47	0.05[f]
6	indoline	204.74	0.04[c]
7	indole	205.26	0.08[d]
8	quinoline	209.70	—[b]
9	isoquinoline	215.61	1.01[d]
10	2-methylnaphthalene	218.14	0.28[h]
11	2-methylbenzo[*b*]-thiophene	218.74	0.04[c]
12	azulene	219.95	0.24[c]
13	quinoxaline	220.37	0.05[d]
14	3-methylbenzo[*b*]-thiophene	221.02	0.03[c]
15	1-methylnaphthalene	221.04	0.25[e]
16	8-methylquinoline	223.02	0.06[e]
17	1,2,3,4-tetrahydroquinoline	225.97	0.10[c]
18	6-methylquinoline	229.82	0.03[c]
19	1,2,2a,3,4,5-hexahydro-acenaphthylene	232.70	—[b]
20	biphenyl	233.96	0.24[d]
21	2-ethylnaphthalene	236.08	0.16[c]
22	1-ethylnaphthalene	236.56	0.14[e]
23	3-methylindole	236.66	—[b]
24	2-methylindole	237.42	0.21[f]
25	2,6-dimethylnaphthalene	237.58	0.17[f]
26	2,7-dimethylnaphthalene	237.71	0.07[d]
27	5-ethylbenzo[*b*]-thiophene	238.46	0.37[d]
28	2-methylbiphenyl	238.77	0.04[c]
29	1,3-dimethylnaphthalene	240.25	0.16[e]
30	1,4-naphthoquinone	240.82	0.04[c]
31	1,7-dimethylnaphthalene	240.66	0.25[c]
32	1,6-dimethylnaphthalene	240.72	0.09[d]
33	2,2′-dimethylbiphenyl	241.94	—[b]
34	2,6-dimethylquinoline	242.43	0.29[e]
35	2,3-dimethylnaphthalene	243.55	0.19[c]
36	1,4-dimethylnaphthalene	243.57	0.16[f]
37	1,5-dimethylnaphthalene	244.98	0.16[c]
38	diphenylmethane	243.35	0.11[f]
39	acenaphthylene	244.63	0.19[g]
40	2,2′-bipyridyl	245.48	0.27[c]
41	1,2-dimethylnaphthalene	246.49	0.30[e]
42	1,8-dimethylnaphthalene	249.52	—[b]
43	2-ethylbiphenyl	250.85	—[b]
44	acenaphthene	251.29	0.14[g]
45	4-methylbiphenyl	254.71	0.17[d]
46	3-methylbiphenyl	254.81	0.15[f]
47	2,3-dimethylindole	255.48	—[b]
48	dibenzofuran	257.17	0.05[c]
49	2-methyl-1,4-naphthoquinone	259.23	0.11[c]
50	2,3,6-trimethylnaphthalene	263.31	0.12[c]
51	1-methylacenaphthylene	265.24	0.02[d]
52	2,3,5-trimethylnaphthalene	265.90	0.14[e]
53	dibenzo-*p*-dioxin	267.27	0.20[h]
54	fluorene	268.17	0.15[g]
55	*trans*-1,2,3,4,4a,9a-hexahydrodibenzothiophene	269.67	0.37[f]
56	*cis*-1,2,3,4,4a,9a-hexahydrodibenzothiophene	271.39	0.27[f]
57	3,3′-dimethylbiphenyl	271.87	—[b]
58	9-methylfluorene	272.38	0.17[c]
59	2,3,5-trimethylindole	272.57	—[b]
60	4,4′-dimethylbiphenyl	274.59	—[b]
61	5*H*-indeno[1,2-*b*]pyridine	279.31	0.19[c]
62	xanthene	280.48	0.22[c]
63	9,10-dihydroanthracene	284.89	0.19[e]
64	9-ethylfluorene	284.99	0.20[c]
65	9,10-dihydrophenanthrene	287.09	0.16[c]
66	1,2,3,4,5,6,7,8-octahydroanthracene	287.69	0.20[c]
67	2-methylfluorene	288.21	0.15[d]
68	1-methylfluorene	289.03	0.04[d]
69	1,2,3,4,5,6,7,8-octahydrophenanthrene	292.03	0.06[c]
70	1,2,3,4-tetrahydrodibenzothiophene	294.30	0.12[c]
71	9-fluorenone	294.79	0.26[d]
72	dibenzothiophene	295.81	0.03[g]
73	1,2,3,4-tetrahydrophenanthrene	297.21	—[b]
74	phenanthrene	300.00	
75	anthracene	301.69	0.08[g]
76	benzo[*h*]quinoline	302.22	0.11[d]
77	9,10-dihydroacridine	304.33	—[b]
78	acridine	304.50	0.05[c]
79	1,2,3,4-tetrahydrocarbazole	306.76	0.19[d]
80	phenanthridine	308.79	0.28[a]
81	benzo[*f*]quinoline	309.25	0.19[d]
82	carbazole	312.13	—[b]
83	9-ethylcarbazole	313.97	0.13[d]
84	1-phenylnaphthalene	315.19	0.05[c]
85	1,2,3,10b-tetrahydrofluoranthene	316.37	0.14[d]
86	9-*n*-propylfluorene	318.01	0.20[c]
87	3-methylphenanthrene	319.46	0.12[e]
88	2-methylphenanthrene	320.17	0.12[d]
89	3-methylbenzo[*f*]-quinoline	320.77	0.24[d]
90	2-methylanthracene	321.57	0.12[c]
91	*o*-terphenyl	321.99	0.16[d]
92	4*H*-cyclopenta[*def*]-phenanthrene	322.08	0.15[d]
93	9-methylphenanthrene	323.06	0.24[d]
94	4-methylphenanthrene	323.17	—[b]
95	1-methylanthracene	323.33	—[b]
96	1-methylphenanthrene	323.90	0.08[c]
97	2-methylacridine	324.46	0.05[c]
98	9-*n*-butylfluorene	328.99	0.37[d]
99	9-methylanthracene	329.13	0.19[d]
100	4,5,9,10-tetrahydropyrene	329.69	0.24[c]
101	4,5-dihydropyrene	330.01	0.02[d]
102	thianthrene	330.13	0.26[e]
103	anthrone	330.53	0.67[c]
104	2-phenylnaphthalene	332.59	0.14[e]
105	9-ethylphenanthrene	337.05	0.08[d]
106	2-ethylphenanthrene	337.50	—[b]
107	3,6-dimethylphenanthrene	337.83	0.14[d]
108	2,7-dimethylphenanthrene	339.23	0.16[d]
109	1,2,3,6,7,8-hexahydropyrene	339.38	0.17[c]
110	6-phenylquinoline	342.45	0.40[c]
111	fluoranthene	344.01	0.16[g]
112	9-isopropylphenanthrene	345.78	0.28[c]
113	1,8-dimethylphenanthrene	346.26	0.27[c]
114	2-phenylindole	347.47	0.07[c]
115	indeno[1,2,3-*ij*]-isoquinoline	347.57	0.19[c]
116	9-*n*-hexylfluorene	348.54	0.10[c]
117	9-*n*-propylphenanthrene	350.30	0.17[c]
118	pyrene	351.22	0.08[d]
119	9,10-dimethylanthracene	355.49	0.03[c]
120	benzo[*lmn*]phenanthridine	358.53	0.28[c]
121	9-methyl-10-ethylphenanthrene	359.91	0.19[c]
122	*m*-terphenyl	360.73	0.03[c]
123	benzo[*kl*]xanthene	361.38	0.15[c]
124	4*H*-benzo[*def*]carbazole	364.22	0.12[d]
125	*p*-terphenyl	366.10	0.16[g]
126	benzo[*a*]fluorene	366.74	0.13[g]
127	11-methylbenzo[*a*]-fluorene	367.04	0.14[d]
128	9,10-diethylphenanthrene	367.97	0.15[d]

Table II. (*Continued*)

compound no.	compound name	average index	standard deviation
129	1-methyl-7-isopropyl-phenanthrene	368.67	0.19[c]
130	benzo[*b*]fluorene	369.39	0.15[c]
131	4-methylpyrene	369.54	0.13[c]
132	2-methylpyrene	370.15	0.44[d]
133	4,5,6-trihydrobenz[*de*]-anthracene	370.86	—[b]
134	1-methylpyrene	373.55	0.11[c]
135	3,5-diphenylpyridine	373.79	0.18[e]
136	5,12-dihydronaphthacene	381.56	—[b]
137	9,10-dimethyl-3-ethyl-phenanthrene	381.85	0.18[e]
138	9-phenylcarbazole	382.09	—[b]
139	1-ethylpyrene	385.35	—[b]
140	2,7-dimethylpyrene	386.34	0.06[d]
141	1,2,3,4,5,6,7,8,9,10,11,12-dodecahydrotriphenylene	386.36	0.29[e]
142	11-benzo[*a*]fluorenone	386.41	0.06[d]
143	1,1′-binaphthyl	388.38	0.23[d]
144	benzo[*b*]naphtho[2,1-*d*]-thiophene	389.26	0.16[e]
145	benzo[*ghi*]fluoranthene	389.60	0.06[d]
146	benzo[*c*]phenanthrene	391.39	0.40[c]
147	benz[*c*]acridine	392.50	0.13[e]
148	9-phenylanthracene	396.38	—[b]
149	cyclopenta[*cd*]pyrene	396.54	0.08[d]
150	benz[*a*]anthracene	398.50	0.08[c]
151	benz[*a*]acridine	398.74	—[b]
152	chrysene	400.00	
153	triphenylene	400.00	0.01[c]
154	benzo[*a*]carbazole	401.81	—[b]
155	1,2′-binaphthyl	405.35	0.50[c]
156	7-benz[*de*]anthrene	406.54	0.34[d]
157	9-phenylphenanthrene	406.90	0.14[c]
158	naphthacene	408.30	0.22[d]
159	benzo[*b*]carbazole	410.12	—[b]
160	11-methylbenz[*a*]-anthracene	412.72	—[b]
161	2-methylbenz[*a*]-anthracene	413.78	0.44[c]
162	1-methylbenz[*a*]-anthracene	414.37	0.17[c]
163	1-*n*-butylpyrene	414.87	0.12[d]
164	1-methyltriphenylene	416.32	—[b]
165	9-methylbenz[*a*]-anthracene	416.50	0.20[d]
166	3-methylbenz[*a*]-anthracene	416.63	—[b]
167	9-methyl-10-phenyl-phenanthrene	417.16	—[b]
168	8-methylbenz[*a*]-anthracene	417.56	0.04[c]
169	6-methylbenz[*a*]-anthracene	417.57	0.30[c]
170	3-methylchrysene	418.10	0.17[d]
171	5-methylbenz[*a*]-anthracene	418.72	—[b]
172	2-methylchrysene	418.80	—[b]
173	12-methylbenz[*a*]-anthracene	419.39	0.45[d]
174	4-methylbenz[*a*]-anthracene	419.67	—[b]
175	5-methylchrysene	419.68	—[b]
176	6-methylchrysene	420.61	0.04[c]
177	4-methylchrysene	420.83	0.16[c]
178	2,2′-biquinoline	421.12	—[b]
179	1-phenylphenanthrene	421.66	0.31[c]
180	1-methylchrysene	422.87	0.06[c]
181	7-methylbenz[*a*]-anthracene	423.14	—[b]
182	*o*-quaterphenyl	423.63	—[a]
183	2,2′-binaphthyl	423.91	—[b]
184	2,(2′-naphthyl)-benzo[*b*]-thiophene	428.11	0.37[d]
185	1,3-dimethyltriphenylene	432.32	—[b]
186	1,12-dimethylbenz[*a*]-anthracene	436.82	—[b]
187	benzo[*j*]fluoranthene	440.92	—[b]
188	benzo[*b*]fluoranthene	441.74	0.48[c]
189	benzo[*k*]fluoranthene	442.56	—[b]
190	7,12-dimethylbenz[*a*]-anthracene	443.38	0.12[c]
191	1,6,11-trimethyltri-phenylene	446.24	—[b]
192	dinaphtho[1,2-*b*; 1′,2′-*d*]-furan	450.20	—[b]
193	benzo[*e*]pyrene	450.73	0.17[c]
194	dibenzo[*c,kl*]xanthene	451.57	—[b]
195	benzo[*a*]pyrene	453.44	—[b]
196	perylene	456.22	0.29[c]
197	1,3,6,11-tetramethyl-triphenylene	461.72	—[b]
198	3-methylcholanthrene	468.44	—[b]
199	*m*-quaterphenyl	472.81	0.23[c]
200	indeno[1,2,3-*cd*]pyrene	481.87	0.09[c]
201	pentacene	486.81	—[b]
202	*p*-quaterphenyl	488.18	0.38[d]
203	dibenz[*a,c*]anthracene	495.01	0.08[b]
204	dibenz[*a,h*]anthracene	495.45	—[a]
205	benzo[*b*]chrysene	497.66	—[a]
206	picene	500.00	
207	benzo[*ghi*]perylene	501.32	0.18[e]
208	dibenzo[*def,mno*]chrysene	503.89	—[b]
209	2,3-dihydrodibenzo-[*def,mno*]chrysene	503.91	—[b]

[a] 1 determination. [b] 2 determinations. [c] 3 determinations. [d] 4 determinations. [e] 5 determinations. [f] 6 determinations. [g] 7 determinations. [h] 8 determinations.

under temperature programming conditions in which the retention data are not only dependent on temperature but also on the rate of temperature programming (*14*, *15*). In temperature-programmed gas chromatography, the simple expression of elution behavior as retention relative to an arbitrary standard is not applicable, and the logarithmic relationship which exists under isothermal operation between *n*-alkane carbon number and retention in the Kovats Index is replaced by the approximately linear relationship:

$$I = 100\frac{T_{R(substance)} - T_{R(C_z)}}{T_{R(C_{z+1})} - T_{R(C_z)}} + 100\,z \qquad (1)$$

where $T_{R(substance)}$ is the retention time of the substance for which the retention index is to be determined, $T_{R(C_z)}$ and $T_{R(C_{z+1})}$ are the retention times for the *n*-alkane standards which bracket the substance of interest, and z is the number of carbon atoms in the *n*-alkane standard that elutes just prior to the substance of interest (*14*). The retention indices of a number of standard PAH have been calculated using this approach (*16*, *17*).

In studies involving the analysis of complex mixtures of polycyclic aromatic hydrocarbons, reports have demonstrated the resolution of over 150 compounds by capillary-column gas chromatography (*18–20*). The extremely large number of possible isomers coupled with the unavailability of standard reference compounds in many laboratories makes standardization of retention data almost essential. Because of the problems encountered with the retention index using the

Table III. Structure, Numbering System, and Ring Orientation for Standard PAH

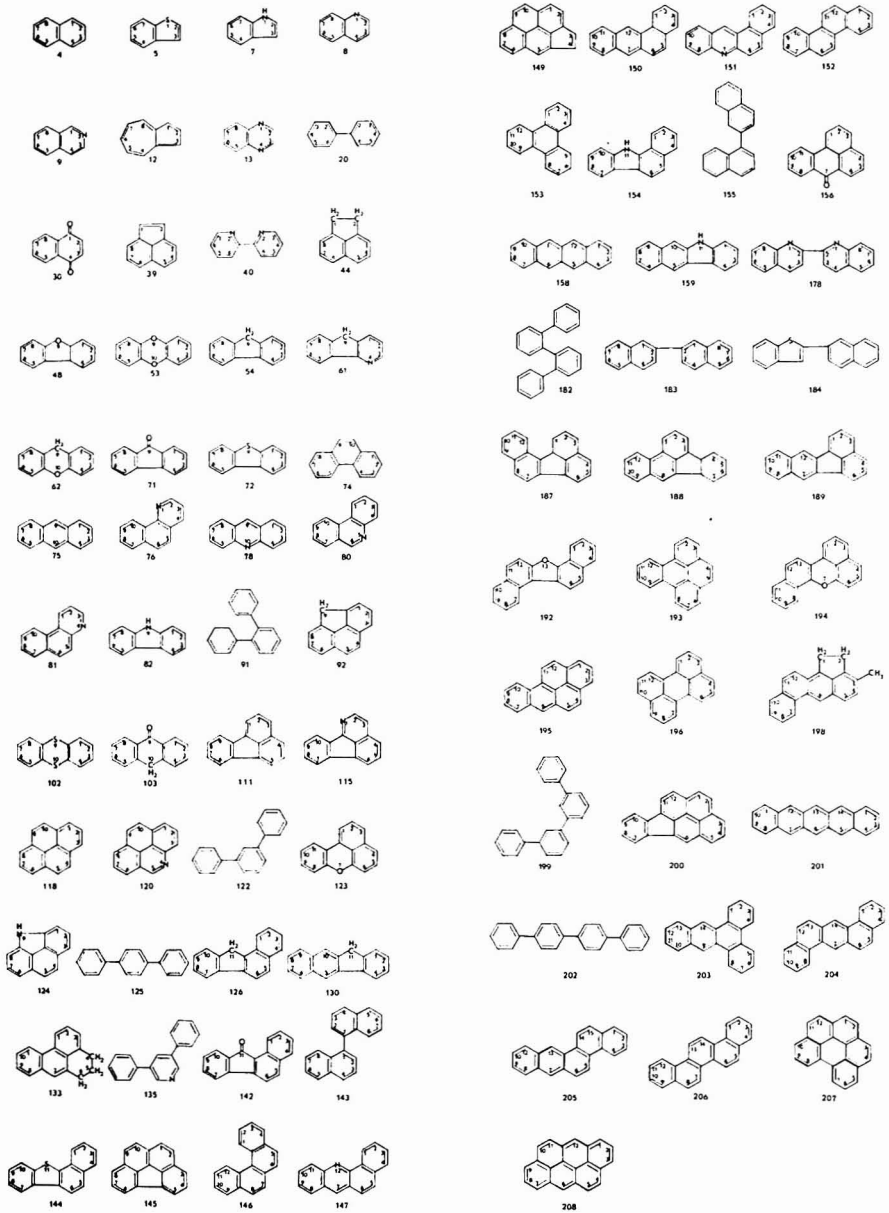

n-alkanes as standard references, a new set of standards was chosen: naphthalene, phenanthrene, chrysene, and picene. In this study, retention indices based on this system were determined for over 200 standard compounds.

EXPERIMENTAL

Retention indices were calculated from data obtained by co-chromatographing a number of polycyclic aromatic hydrocarbon standard compounds and the series of *n*-alkanes on glass capillary

columns coated with an SE-52 methylphenylsilicone stationary phase. Five columns were used to generate the retention data in this study. (Column A was 12 m × 0.30 mm, i.d., with 0.34-μm film thickness, column B was 12 m × 0.28 mm, i.d., with a film thickness of 0.17 μm, and three additional columns were 12 m × 0.29 mm, i.d., with 0.34-μm film thickness). All columns were drawn from Kimble R6 soda lime glass capillary tubing, and were treated by variations of the following general procedure: HCl gas phase etch, HCOOH wash, HMDS/TMCS gas phase silylation, and static coating. A Varian Model 3700 gas chromatograph with precisely controlled oven temperature was programmed from 50 to 250 °C at 2 °C/minute during each chromatographic run. Carrier gas flow rate was varied from 1–3 mL/min of He. Data acquisition was accomplished with a Varian CDS 101 integrator. The retention index for each standard compound was calculated according to Equation 1.

The new PAH retention indices were generated in the same manner except naphthalene, phenanthrene, chrysene, and picene were used as internal standards instead of the normal hydrocarbons. These retention indices were calculated from Equation 1 where $T_{R(C_z)}$ and $T_{R(C_{z+1})}$ were defined as the retention times for the PAH internal standards which bracket the substance of interest, and z is the number of rings in the PAH standard that elutes prior to the substance of interest.

The retention indices for compounds that eluted before naphthalene were calculated from an extension of the naphthalene–phenanthrene interval. In the same manner, indices for compounds that have longer retention than picene were calculated from an extension of the chrysene–picene interval.

It should be stressed that all four standards must be eluted during the temperature programming period; and programming should start 30 to 40 °C less than the elution temperature of naphthalene.

RESULTS AND DISCUSSION

In selecting a chromatographic column, it is important to consider both the efficiency and selectivity of the column to achieve the desired resolution of solutes of interest. Lysyuk and Korol (*21*) measured the relative retention, heats, and entropies of solution for 16 PAH in seven different stationary phases and found that the selectivities of different stationary phases for PAH are similar. The new liquid crystal phases have shown quite pronounced selectivities (*22*), but the efficiencies and thermal stabilities of columns prepared with these phases leave much to be desired, especially in the field of capillary-column gas chromatography. For this reason, the main effort in the resolution of PAH has been made in the direction of developing high resolution columns rather than in searching for new, more selective stationary phases. A methylphenylsilicone stationary phase, SE-52 (5% phenyl), was used in this study because of the well-documented high efficiencies for PAH demonstrated by columns coated with this stationary phase (*18–20*).

Grob and Grob (*7*) have recently studied the effects of film thickness on PAH retention for capillary columns coated with SE-52. Dependence of retention, separation efficiency, inertness, capacity, and thermal stability on film thickness was shown. It was found that doubling the film thickness of the liquid phase causes elution of a PAH compound under programmed temperature conditions at about 16 °C higher temperature. It was also found that surface effects were reduced, and capacities and thermal stabilities were increased with thicker films. One is forced to compromise between boiling point range of interest and these other effects. In this study, we chose two different intermediate film thicknesses such that a 12 m × 0.30 mm, i.d., capillary column with the thicker film would elute the dibenzanthracene isomers at a column temperature of approximately 250 °C.

The effect of film thickness on the retention index using both the normal alkanes and the proposed PAH standards can be seen in Table I. While one sees a maximum variation of almost 20 index units (benzo[*e*]pyrene) in the ordinary retention system, 0.14 is the largest difference in the new PAH system. Similar variations can be seen with the *n*-hydrocarbon system after using the same column for several weeks. On the other hand, the PAH retention index system maintained excellent reproducibility over several months of heavy column usage.

The PAH retention indices determined for over 200 compounds are listed in Table II. Table III gives the structures of these compounds. As can be seen from the statistical data given in Table II, the precision is, in most cases, quite good. A capillary column gas chromatogram of over 100 standard PAH is shown in Figure 1. The efficiency of these capillaries is approximately 3000 plates per meter, and the peak width at half-height averages, over the range of PAH, 0.80 index unit. This means that two PAH whose retention indices differ by 1 index unit should have better than 50% area resolution.

To test the reliability of the retention indices under different temperature programming rates, 10 chromatographic runs were made; 3 runs were at 4 °C/min and 7 runs were at 2 °C/min. The average 95% confidence limits for the series of PAH retention indices calculated from these runs are ±0.16 index unit.

The selection of the standard compounds as references in the new index system was based on a number of considerations. A plot of elution temperature, as a function of retention index for the four standards, approaches linearity. Furthermore, these compounds are quite soluble in the usual organic solvents and are generally commercially available. Our first attempt was to use a series of PAH with linear arrangement of aromatic rings (naphthalene, anthracene, naphthacene, and pentacene) but the low solubility of naphthacene and pentacene in methylene chloride and other organic solvents encouraged a selection of another series. (A similar series of compounds has been used in high-performance liquid chromatography (*23, 24*)).

In summary, a new PAH retention index is now available which maintains a high degree of reproducibility under varying conditions, and retention indices have been calculated for over 200 standard compounds. We believe that this system offers significant advantages in attempts to identify isomeric PAH in complex mixtures. The new PAH retention index system facilitates reliable interlaboratory comparisons as well as improved analyses in any one laboratory.

LITERATURE CITED

(1) L. S. Ettre, *Chromatographia*, **6**, 489 (1973).
(2) J. K. Haken, *Adv. Chromatogr.*, **14**, 367 (1976).
(3) E. Kovats, *Helv. Chim. Acta*, **41**, 1915 (1958).
(4) W. O. McReynolds, *J. Chromatogr. Sci.*, **8**, 685 (1970).
(5) K. Grob, G. Grob, and K. Grob, Jr., *Chromatographia*, **10**, 181 (1977).
(6) K. Tesarik and M. Novotny, *Chromatographia*, **2**, 383 (1969).
(7) K. Grob, Jr., and K. Grob, *Chromatographia*, **10**, 250 (1977).
(8) F. P. Woodford and C. M. van Gent, *J. Lipid Res.*, **1**, 188 (1960).
(9) T. K. Miwa, K. L. Mikolajczak, F. R. Earle, and I. A. Wolff, *Anal. Chem.*, **32**, 1739 (1960).
(10) W. J. A. VandenHeuvel and E. C. Horning, *Biochim. Biophys. Acta*, **64**, 41 (1962).
(11) S. J. Hawkes, *J. Chromatogr. Sci.*, **10**, 535 (1972).
(12) H. F. Dymond and K. D. Kilburn, in "Gas Chromatography 1966", A. B. Littlewood, Ed., Institute of Petroleum, London, 1967, p 353.
(13) R. G. Ackman, *J. Chromatogr. Sci.*, **10**, 536 (1972).
(14) H. van Den Dool and P. Dec. Kratz, *J. Chromatogr.*, **11**, 463 (1963).
(15) P. Majlat, Z. Erdos, and J. Takacs, *J. Chromatogr.*, **91**, 89 (1974).
(16) G. Alberini, V. Cantuti, and G. P. Cartoni, *Gas Chromatogr., Int. Symp. Anal. Instrum. Div. Instrum. Soc. Am.*, **6**, 258 (1966).
(17) N. Carugno and S. Rossi, *J. Gas Chromatogr.*, **5**, 103 (1967).
(18) M. L. Lee, M. Novotny, and K. D. Bartle, *Anal. Chem.*, **48**, 405 (1976).
(19) M. L. Lee, M. Novotny, and K. D. Bartle, *Anal. Chem.*, **48**, 1566 (1976).
(20) M. L. Lee, G. P. Prado, J. B. Howard, and R. A. Hites, *Biomed. Mass Spectrom.*, **4**, 182 (1977).
(21) L. S. Lysyuk and A. N. Korol, *Chromatographia*, **10**, 712 (1977).
(22) G. M. Janini, G. M. Muschik, J. A. Schroer, and W. L. Zielinski, Jr., *Anal. Chem.*, **48**, 1879 (1976).
(23) M. Popl, V. Dolansky, and J. Mostecky, *J. Chromatogr.*, **91**, 649 (1974).
(24) S. A. Wise, S. N. Chesler, H. S. Hertz, L. R. Hilpert, and W. E. May, *Anal. Chem.*, **49**, 2306 (1977).

RECEIVED for review November 6, 1978. Accepted January 29, 1979. This work was accomplished at the Pittsburgh Energy Technology Center during the summer of 1978 at which time M.L.L. and D.L.V. were Fossil Energy Summer Research Participants under the administration of the Oak Ridge Associated Universities, University Programs. This work was partially aided by support from the National Science Foundation Grant No. MPS 75-04932 to one of us (M.N.).

CORRESPONDENCE

Reverse Phase Liquid Chromatography at Increased Temperature

Sir: The recent article by Saner and associates (*1*), concerning resolution of reverse phase columns at increased temperature, sparked considerable interest in our laboratory, where we have been using this technique for drug analysis for some time. The authors' statement that "elevated temperatures are infrequently utilized as a means of improving resolution since the net improvement is small relative to the improvement gained by particle size reduction" must be investigated further, even though it is basically true. Particle size has for now reached a practical limit at 5 μm because of the tremendous pressure that would be required by smaller particles. Therefore, increasing column temperature is the next logical step toward increased resolution, since the pressure decrease that results will allow increased flow rate. Here we reach the point of interest because increased flow rate at lower mobile phase strength can give greatly enhanced resolution at the same or lower pressure than would be encountered in a room temperature system.

However, in the application of temperature it is neither sufficient nor beneficial to heat only the analytical column. An obvious point that is usually neglected is that for maximum efficiency, the mobile phase must be heated to the system temperature before it enters the column.

EXPERIMENTAL

Reagents. 3-Bromocinnamamide (I); its *N*-methyl (II), *N*-ethyl (III), and *N*-isopropyl (IV) homologues (Burroughs Wellcome Company, Research Triangle Park, N.C.); and clonazepam (V) (Applied Science Laboratories, Inc., State College, Pa.) were used as received.

Apparatus. The liquid chromotograph consisted of a reciprocating piston pump with a pressurized tube pulse dampener, a fixed wavelength UV absorption detector (Laboratory Data Control, Riviera Beach, Fla.) operated at 254 nm, and a six-port sample injection valve with a 50-μL loop (Valco Instruments Company, Houston, Tex.). The columns were 250 mm × 4.6 mm i.d. tubes packed with a 10-μm microparticulate reverse phase (Partisil 10-ODS, Reeve-Angel, Liquid Chromatography Division, Clifton, N.J.) and a 5-μm totally porous spherical reverse phase (Spherisorb ODS, Laboratory Data Control). A 50 mm × 1.09 mm i.d. precolumn was connected directly to the main column inlet fitting and dry-packed in place with a pellicular C-18 phase (Vydac Reverse Phase, Applied Science Laboratories, Inc.) by vibration for 10 min. A $^1/_{16}$-inch Swagelok union was attached, and the constricted portion was also packed. A small pad of glass wool was placed on top of the packing, and the entire system was connected to the sampling valve. The main columns were heated with a water jacket (Altex Scientific Inc., Berkeley, Calif.). A water jacket was made for the precolumns from a length of 9.5 mm i.d. × 6.4 mm wall Tygon tubing. Water ports were made by boring holes through the wall and inserting short lengths of glass tubing. The ends were sealed at the $^1/_{16}$-inch nuts with O-rings.

RESULTS AND DISCUSSION

The column–precolumn system described was designed for maximum chromatographic efficiency. Precolumns that are commercially available at the present time generally have the same internal diameter as the common analytical columns, 4.6 or 3.2 mm. These require a short length of tubing for connection to the main column. The $^1/_{16}$-inch (1.09-mm i.d.) precolumn used here can be attached directly to the analytical column and dry-packed in place so that the inlet frit of the main column is the outlet frit of the precolumn. Heating the precolumn is a simple and efficient means of preheating mobile phase.

Figure 1 shows chromatograms of a standard mixture containing approximately 0.1 μg/50 μL of compounds I and II, and 0.2 μg/50 μL of compounds III, IV, and V. Equivalent samples were injected in each case into the 10-μm Partisil ODS column, and chromatograms A, B, and C were obtained with the mobile phase, acetonitrile:water (22:78), flowing at 120 mL/h. Sample A was run with the column and precolumn at 60 °C, sample B with the column at 60 °C and precolumn at 25 °C, and sample C with the column and precolumn at 25 °C. Sample D was run with acetonitrile:water (16:84) flowing at 160 mL/h and the column and precolumn at 60 °C. Pressures for systems A, B, C, and D were 10.8 MPa (1550 psi), 12.4 MPa (1800 psi), 18.6 MPa (2700 psi), and 14.1 MPa (2050 psi), respectively. Resolution of peaks II and V in systems A, C, and D are 0.57, 0.64, and 1.3, respectively, with *R* calculated simply as separation distance divided by peak width (assumed equal for peaks II and V). A similar experiment performed on the 5-μm Spherisorb ODS column with acetonitrile:water (32:68) flowing at 160 mL/h gave resolution of peaks II and V of 1.15 and 1.07 in the room temperature (C) (29.1 MPa, 4230 psi) and the heated (A) (16.1 MPa, 2330 psi) systems, respectively. A run with the precolumn at 25 °C and the main column at 60 °C also resulted in almost complete loss of resolution of peaks II and V. Retention volumes for the final peaks in chromatograms C and D (10-μm Partisil ODS) are 31.6 and 30.4 mL, respectively.

The advantages of the application of temperature in reverse phase liquid chromatography are clearly seen. However, chromatogram B, obtained without preheating the mobile phase, is seriously lacking in resolution and peak symmetry. Actually, the peaks are not simply broadened or skewed, but each component elutes as two unresolved bands. This is seen more clearly in Figure 2, which shows the difference in peak shape and retention of a single component (III) injected into the 5-μm Spherisorb ODS column with acetonitrile:water (32:68) flowing at 120 mL/h. Peak A was obtained with a heated precolumn and peak B with an unheated precolumn. Symmetry appears to be maintained in this case; however, the splitting of the single component would lead one to think that each compound travels through the analytical column under at least two different sets of conditions. In a very gross sense, at a particular flow rate, an equilibrium exists in which there

This article not subject to U.S. Copyright. Published 1979 by the American Chemical Society

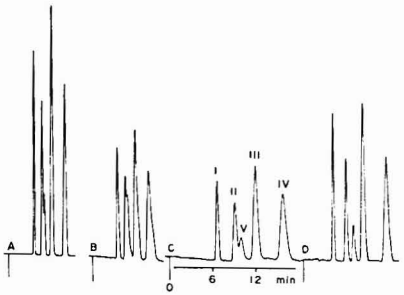

Figure 1. Chromatograms of a standard mixture obtained with acetonitrile:water (22:78) flowing at 120 mL/h, and column (10-μm Partisil ODS) and precolumn at 60 °C (A), column at 60 °C and precolumn at 25 °C (B), and column and precolumn at 25 °C (C). Chromatogram obtained with acetonitrile:water (16:84) flowing at 160 mL/h, and column and precolumn at 60 °C (D). Compounds are 3-bromocinnamamide (I) and 3-bromo-*N*-methyl cinnamamide (II) at 0.1 μg/50 μL, and 3-bromo-*N*-ethyl cinnamamide (III), 3-bromo-*N*-isopropyl cinnamamide (IV), and clonazepam (V) at 0.2 μg/50 μL

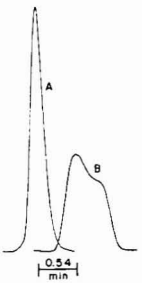

Figure 2. Chromatograms of identical samples of 3-bromo-*N*-ethyl cinnamamide (III) indicating changes in peak shape and retention with heated (A) and unheated (B) precolumn. Analytical column was 5-μm Spherisorb ODS with flow rate of 120 mL/h (acetonitrile:water (32:68). Retention time for peak A is 9.42 min

is a cone of room temperature mobile phase surrounded by cones of higher temperature mobile phase that extend into the column to the point where the mobile phase temperature all the way across the column equals the set temperature. The reduced rates of mobile phase and stationary phase mass transfer in this low temperature area account for the variation in peak shape and retention.

The depth of this temperature differential increases with flow rate and column temperature so that at low flow or low temperature or both, the effect may be difficult to detect. Figures 3 and 4 illustrate this flow dependence for the 5-μm Spherisorb ODS column. As shown in Figure 3, identical samples containing components II and V were injected at 40, 80, and 120 mL/h with unheated (a) and heated (b) precolumns. Resolution decreases dramatically for the former samples while it is maintained for the latter. Figure 4 shows the variation in peak shape and size with flow rate. Curves A, B, and C were obtained after injections of identical samples of III onto the 5-μm Spherisorb column with an unheated precolumn at flow rates of 58, 115, and 230 mL/h, respectively. Although retention volume (to center of band) remains approximately the same in the three cases, elution volume increases from 0.76 mL (A) to 1.65 mL (B) to 3.34 mL (C), accounting for the decreased response. In the usual case, as in the b chromatograms of Figure 3, both retention volume

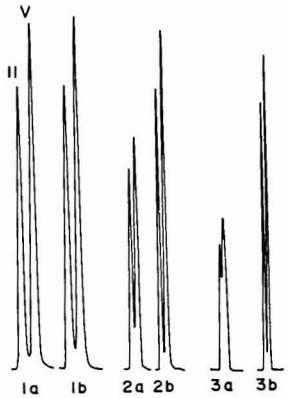

Figure 3. Chromatograms of identical samples, containing 3-bromo-*N*-methyl cinnamamide (II) and clonazepam (V), run at 40 mL/h (1), 80 mL/h (2), and 120 mL/h (3) with unheated (a) and heated (b) precolumns on 5-μm Spherisorb ODS column

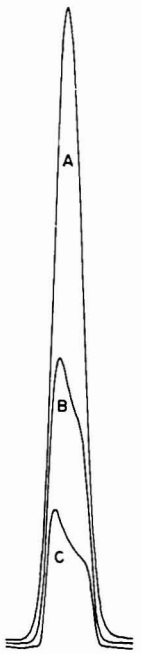

Figure 4. Chromatograms of identical samples of 3-bromo-*N*-ethyl cinnamamide (III) run at 58 mL/h (A), 115 mL/h (B), and 230 mL/h (C) on 5-μm Spherisorb ODS with unheated precolumn

and elution volume are constant with increasing flow rate, so that peak area decreases while peak height remains relatively constant.

These data show that, in reverse phase chromatography, the effects of using high temperature with unequilibrated and equilibrated mobile phase are similar for both 5- and 10-μm

particle columns. From Figure 1 for the 10-μm Partisil ODS column and from the similar data presented for the 5-μm Spherisorb ODS column, we see that in going from a room temperature system to an equilibrated (heated precolumn) high temperature system, there is a slight loss in resolution but a significant reduction in system pressure and retention volume. This allows modification of mobile phase strength and flow rate to give complete resolution (Figure 1D). In the unequilibrated systems (unheated precolumn, Figure 1B), there is almost complete loss of resolution at high flow rates.

The exact flow rate at which these effects become evident would be determined by the mobile phase composition, column temperature, and column configuration (length and diameter) of each system. In the unequilibrated systems used here, the variation in peak shape and resolution appears between 40 and 80 mL/h. In Figure 3, parts 1a and b, obtained at 40 mL/h, resolution are actually greater in the unequilibrated system, indicating that flow is low enough that the mobile phase comes to temperature almost immediately in the main column and that the additional time the solutes spend in the room temperature precolumn and the main column contributes to the separation. However, at 80 mL/h (Figure 2a), the peaks are distorted enough to decrease resolution. Since most reverse phase work is done at flow rates at or above 60 mL/h, it is important that a totally equilibrated system be used.

Reverse phase chromatography is a powerful tool; however, in room temperature systems, in which the operational constraints of pressure and time are maximized, much of the power of the medium is wasted and instrumentation can unnecessarily be pushed to its limits. In most cases, selectivity is achieved with a reverse phase column by decreasing mobile phase strength. The exception occurs infrequently when there is some specific solute–solvent interaction that contributes to the separation. Barring this occurrence, operation of these columns above room temperature with equilibrated, low-strength mobile phase at high flow rate will allow separations that are impossible at room temperature because of instrumental or temporal restraints. Any separation that is already possible at room temperature can be done at higher temperature in a shorter time, with less consumption of mobile phase, at a lower pressure, and with greater sensitivity.

ACKNOWLEDGMENT

The authors thank D. M. Mitchell for technical assistance.

LITERATURE CITED

(1) Saner, W. A.; Jadamic, J. R.; Sager, R. W. *Anal. Chem.* **1978**, *50*, 749.

Robert J. Perchalski*
Research Chemist, Research Service (151)
Veterans Administration Medical Center
Gainesville, Florida 32602

B. J. Wilder
Neurology Service
Veterans Administration Medical Center
Department of Neurology, College of Medicine
University of Florida
Gainesville, Florida 32602

RECEIVED for review November 6, 1978. Accepted February 5, 1979. This work was supported in part by the Medical Research Service of the Veterans Administration, the Epilepsy Research Foundation of Florida, Inc., and Burroughs-Wellcome Co.

Gas Chromatographic Determination of Glycols at the Parts-per-Million Level in Water by Graphitized Carbon Black

Sir: The analysis of very polar compounds, such as glycols and glycerol in particular, is still a problem due to the limited availability of thermally stable, highly polar stationary phases and inert solid supports.

Poly(ethylene glycol) (PEG) 400 (*1*), poly(ethylene glycol) pentaerythritol adipate (LAC-2R-446) (*2*), and poly(vinyl-formal-propionitrile) (*3*) have been used for the analysis of free glycols. However, in the first two cases no results were reported concerning very dilute solutions of glycols and, in the third case, tailed peaks for glycols were reported.

Porous polymers (*4*, *5*) have been used in the analysis of diols but, also in this case, the reported procedures were not concerned with the determination of part-per-million quantities.

An original approach for the analysis of glycols was suggested by Phifer and Plummer (*6*) who used water as the stationary phase and water vapor as the carrier gas.

More recently, tetrahydroxyethylenediamine (THEED)-coated Chromosorb W (*7*) has been used generally for separating light molecular weight diols and specifically for determining traces of 2,3-butanediol in 1,2-propanediol. Severe drawbacks of this method are that a long analysis time is necessary and the column deteriorates rapidly at the temperature of operation.

The object of this paper is to show that the use of THEED as a tailing reducer and selectivity modifier on an inert adsorbing medium such as Carbopack C yields untailed peaks even for a few nanograms of diols and glycerol. The separation of seven diols from 1,2-ethanediol to 1,4-butanediol, including diethylene glycol, in aqueous solution at the level of 10 ppm has been achieved in 12 min at 115 °C by Carbopack C modified with 0.8% THEED. At the column operating temperature, the packing had a good stability. By raising the column temperature to 125 °C, it was possible to chromatograph a water solution containing 50 ppm of glycerol and triethylene glycol with an analysis time of about 30 min.

Table I. Capacity Ratio Data at 115 °C

	THEED percentages				
compound	0.45	0.60	0.70	0.80	1.0
1,4-butanediol	250	148	160	185	235
glycerol	850	810	900	1050	1700

At this column temperature, however, a slow deterioration of the packing occurs. The separating ability of the THEED + Carbopack C system has been investigated by varying the relative amount of THEED.

EXPERIMENTAL

Carbopack C, which is an example of Graphitized Carbon Black, was supplied in the 80–100 mesh range by Supelco, Bellefonte, Pa. It was ground and sieved to obtain the 100–120 mesh range.

The procedure of coating Carbopack C was similar to that reported previously (*8*).

Glass columns (55 cm × 0.2 cm i.d.) were filled with the packing material by following a procedure described elsewhere (*8*). After this, the columns were conditioned under flow at 115 °C for 24

0003-2700/79/0351-0776$01.00/0 © 1979 American Chemical Society

Table II. Relative Retention Times at 115 °C

compound	THEED percentages				
	0.45	0.60	0.70	0.80	1.0
1,2-ethanediol	395	725	740	775	945
1,2-propanediol	560	830	835	890	945
2,3-butanediol	1000	1000	1000	1000	1000
1,3-propanediol	1150	1460	1630	1835	2070
1,3-butanediol	1780	2050	2120	2220	2315
1,4-butanediol	3510	3970	4240	4525	4840

h. This long conditioning time is necessary to eliminate some impurities from THEED which cause undesirable variations in the separation factors of glycols. Hydrogen was used as carrier gas. The advantage of using hydrogen has been reported elsewhere (8).

A Carlo Erba gas chromatograph (Model GI, Milan, Italy) equipped with a flame ionization detector was used.

DISCUSSION AND RESULTS

In Table I, capacity ratio (k) data for glycerol and 1,4-butanediol are reported as a function of the percentage of THEED added to the Carbopack C.

At low THEED percentages, a decrease is observed in the retention of the two glycols as the amount of liquid phase is increased. This decrease is sharper for the less polar compound. Conversely, at THEED percentages higher than 0.6%, there is an increase in the capacity ratio values, which is sharper for glycerol.

As already reported (9), this effect can be accounted for by assuming that deposition of THEED molecules occurs as "adsorption on a uniform surface" and that 0.6% THEED is the relative amount needed to form one monolayer on the Carbopack C surface. Therefore, at THEED percentages lower than 0.6%, this modifying agent deactivates the adsorbing solid for glycols and also reduces the solid surface available for adsorption of eluates. At THEED percentages higher than 0.6%, adsorption of eluates occurs on preadsorbed THEED molecules. Consequently, retention of glycols increases on increasing the surface concentration of THEED and the extent of this effect is dependent upon the degree of polarity of glycols.

The gradual increase of the polarity degree of the Carbopack + THEED system on increasing the relative amount of the liquid phase is evident by observing the variations in the relative retention times at 115 °C of some diols (see Table II). At low THEED percentages, glycols are retained mainly on the basis of their molecular weight. It is interesting to note that on THEED-modified Carbopack C, the elution order of 1,2-ethanediol, 1,3-propanediol, and 2,3-butanediol is reversed as compared with a THEED gas–liquid chromatographic column (7). As the surface concentration of THEED is made larger, the column packing tends to fractionate glycols on the basis of their polarity. Indeed, 1% THEED-modified Carbopack C yields poor separations for 1,2-ethanediol, 1,3-propanediol, and 2,3-butanediol.

The minimum relative amount of THEED needed to obtain peaks for diols was found to be 0.5%. From the examination of the data reported above, it appears that Carbopack C modified with 0.6% THEED is the best column packing for analytical purposes. With this THEED percentage, however, the peak for glycerol is still somewhat tailed. Therefore, with a view to obtaining a general purpose chromatographic column for the analysis of glycols, we made use of Carbopack C + 0.8% THEED.

Using this column packing, quantitative measurements were carried out for 1,4-butanediol and glycerol at various concentrations and using two appropriate internal standards, that is octanol and dodecanol, respectively (Table III). The data reported in Table III make it evident that THEED is effective

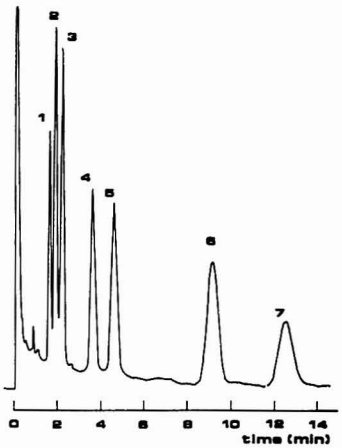

Figure 1. Chromatogram showing the separation of some diols. Column packing, Carbopack C + 0.8% THEED; column, 51 cm × 2 mm i.d.; temperature, 115 °C; dead time, 3 s; carrier gas, hydrogen; sample, 0.4 μL water containing about 10 ppm of each glycol: (1) ethanediol; (2) 1,2-propanediol; (3) 2,3-butanediol; (4) 1,3-propanediol; (5) 1,3-butanediol; (6) 1,4-butanediol; (7) diethyleneglycol

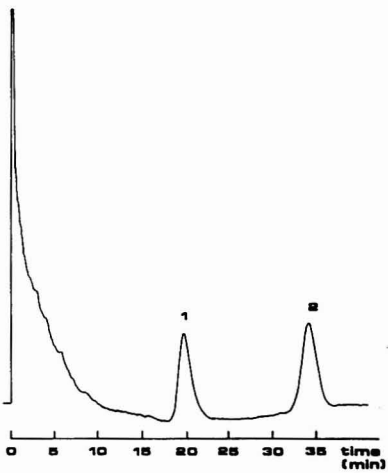

Figure 2. Chromatogram showing the elution of 50 ppm of glycerol (1) and triethyleneglycol (2) in water. Temperature, 125 °C; sample, 0.6 μL of a water solution; other conditions as in Figure 1

in eliminating anomalous effects of adsorption for glycols on the Carbopack C surface. Also, it appears that few ppm of diols can be determined with an error not higher than 4%. The appearance of some peak tailing when glycerol is injected in tiny amounts does not allow accurate determination of this compound to be made at concentrations lower that 50 ppm.

Figure 1 is the reproduction of a chromatogram of an aqueous solution of some diols, including diethylene glycol, obtained at 115 °C by using the column packing cited above. The good tolerance to water of THEED deposited on the carbon surface coupled with the absence of peak tailing allowed us to chromatograph glycols at the ppm level. It is

Table III. Quantitation Data for 1,4-Butanediol and Glycerol

concn, ppm	response factor for 1,4-butanediol vs. *n*-octanol	concn, ppm	response factor for glycerol vs. *n*-dodecanol
80	0.521 ± 0.008	200	0.446 ± 0.008
40	0.258 ± 0.004	100	0.221 ± 0.004
16	0.104 ± 0.002	50	0.109 ± 0.004
8	0.051 ± 0.001	30	0.056 ± 0.005
4	0.026 ± 0.001		

noteworthy that using hydrogen as carrier gas lowers the analysis time to a matter of minutes.

Figure 2 is the reproduction of a chromatogram of glycerol and triethylene glycol contained in water at the level of about 50 ppm. The column packing used is the same as that cited above, but the column temperature was raised to 125 °C in order to contain the analysis time within about 30 min.

As far as column stability is concerned, we noted that an uninterrupted use of 0.8% THEED-coated Carbopack C at 115 °C for ten days caused a final decrease of the retention time of 1,4-butanediol not larger than 10%. A more evident column deterioration was observed keeping the temperature at 125 °C.

ACKNOWLEDGMENT

We thank E. Sebastiani for his experimental assistance.

LITERATURE CITED

(1) G. Manius, F. P. Mahn, V. S. Venturella, and B. Z. Senkowski, *J. Chromatogr. Sci.*, **9**, 367 (1971).
(2) I. L. Weatherall, *J. Chromatogr.*, **26**, 251 (1967).
(3) K. Assmann, O. Serfas, and G. Geppert, *J. Chromatogr.*, **26**, 495 (1967).
(4) Applied Science Labs., State College, Pa., Technical Bulletin, no. 24.
(5) S. B. Dave, *J. Chromatogr. Sci.*, **7**, 390 (1969).
(6) L. H. Phifer and H. K. Plummer, *Anal. Chem.*, **38**, 1652 (1966).
(7) B. A. Swinehart, *Anal. Chem.*, **40**, 427 (1968).
(8) A. Di Corcia, A. Liberti, and R. Samperi, *J. Chromatogr.*, **122**, 459 (1976).
(9) A. Di Corcia and A. Liberti, *Adv. Chromatogr.*, **14**, 305 (1976).

Antonio Di Corcia*
Roberto Samperi

Istituto di Chimica Analitica
Università di Roma 00185
Rome, Italy

RECEIVED for review July 19, 1978. Accepted December 5, 1978.

Time-Resolved Matrix-Isolation Fluorescence Spectrometry of Mixtures of Polycyclic Aromatic Hydrocarbons

Sir: The environmental presence of complex mixtures of polycyclic aromatic hydrocarbons (PAH) containing species which are mutagenic or carcinogenic has long been recognized as a potential health hazard. Identification and quantitative determination of specific constituents in such mixtures remains a difficult task because of the large number of species usually occurring in a given sample and the similarities of their chemical and spectroscopic properties (*1*). Steady-state fluorometric analysis of PAH mixtures using matrix isolation (MI) as a sampling technique has been developed in this laboratory as a procedure for qualitative and quantitative analyses of PAH in mixtures; the method has been demonstrated useful in very challenging cases, including the resolution of PAH isomers (*2–4*). We now report the application and potential utility of laser-excited time-resolved fluorescence procedures for characterization of matrix-isolated PAH mixtures.

EXPERIMENTAL

A block diagram of the time-resolution spectrofluorometer is shown in Figure 1. When operated in the mode locked/cavity dumped regime, the argon ion laser produced light pulses of 800 ps FWHM at repetition rates ranging from single shot to 1 MHz. The 5145-Å line was frequency doubled with an Interactive Radiation 5-1 temperature phase-matched SHG system (ADP crystal). The doubled beam, which was separated from the fundamental by a prism, was directed onto an MI sample deposited on a sapphire window in a closed-cycle cryostat (*2, 5*). Fluorescence from the sample was analyzed with a Spex 1702 0.75-m grating spectrometer equipped with a 600 groove/mm grating and was detected by an Amperex XP2020 photomultiplier. Temporal resolution was achieved by use of a sampling oscilloscope, which limited the sampling rate (and hence the repetition rate of the laser) to a maximum of 32 kHz. Control of the sampling sweep by an external ramp generator was used to plot fluorescence decay curves with an X-Y recorder. Use of a "waveform hold" control of the ramp generator permitted plotting of time-resolved fluorescence spectra in which the "time window width" was defined by the rise time of the sampling oscilloscope (e.g., 75 ps for the Tektronix S-2 head), and the delay (with respect to the laser pulse) was defined by the voltage at which the ramp was "held". Performance of a time-resolved spectrometer of similar design for temporal separation of fluorescence and Raman scattering has been characterized by Harris et al. (*6*).

RESULTS AND DISCUSSION

In Figure 2 are shown steady-state MI fluorescence spectra for a six-component PAH mixture in N_2 at 16 K. Excitation at a minimum of two wavelengths (248 and 280 nm) is required to fully illustrate the presence of all six components. While the major spectral peaks are sufficiently well resolved to be identified easily, quantitation is complicated by the presence of partially-overlapping band systems and the resulting difficulty in base-line definition. Note, for example, the partial overlap of the anthracene and pyrene bands at ca. 3700 Å, that of pyrene and benzo[*e*]pyrene at 3900 Å, and the severe overlap of the benzo[*a*]pyrene and benzo[*k*]fluoranthene features at ca. 4000 Å in Figure 2. In this mixture (which was deliberately chosen to highlight partial overlap of spectral features), quantitation of anthracene, benzo[*e*]pyrene, benzo[*a*]pyrene, and benzo[*k*]fluoranthene would be extremely difficult.

Time-resolved MI fluorescence spectra of this same mixture, at three different delay times, are shown in Figure 3; use of a somewhat larger emission monochromator bandpass than that employed in steady-state MI fluorometry was required to observe an adequate signal. Despite the loss in spectral resolution thereby introduced, comparison of Figures 2 and 3 shows that time resolution succeeds in alleviating the difficulties of band overlap and base-line definition evident in Figure 2. For example, though anthracene absorbs only weakly at 2573 Å, its temporal resolution from pyrene is apparent. In addition, while benzo[*a*]pyrene (BaP) and benzo[*k*]fluoranthene (BkF) cannot readily be distinguished from each other by steady-state MI fluorometry, their fluorescence decay times in N_2 matrices are sufficiently different (78 ns for BaP and 13 ns for BkF) to produce excellent temporal "separation" of the emission spectra for these

0003-2700/79/0351-0778$01.00/0 © 1979 American Chemical Society

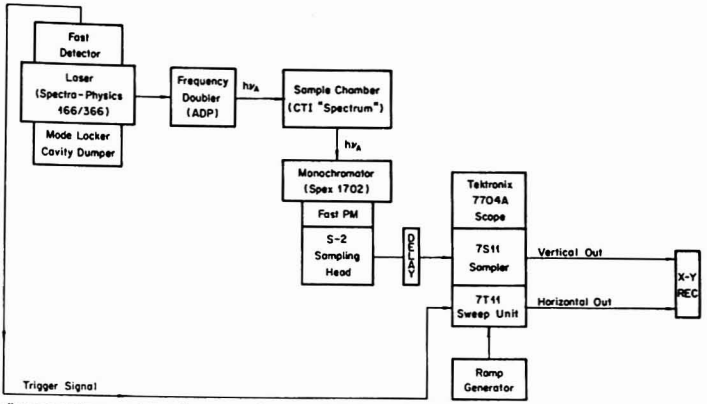

Figure 1. Block diagram of time-resolution fluorometer for matrix-isolation studies

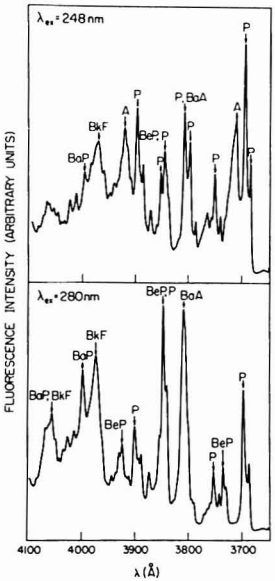

Figure 2. Steady-state matrix-isolation fluorescence spectrum of six-component PAH mixture. Sample contained pyrene (P; 3 μg), anthracene (A; 1.5 μg), benz[*a*]anthracene (BaA; 400 ng), benzo[*e*]pyrene (BeP; 3.5 μg), benzo[*a*]pyrene (BaP; 27 ng), and benzo[*k*]fluoranthene (BkF; 258 ng). Matrix: N_2; temperature: 16 K

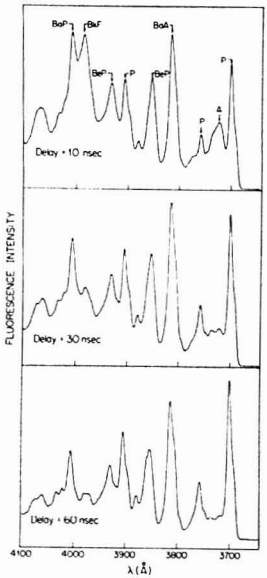

Figure 3. Time-resolved MI fluorescence spectra, obtained at three different delay times, for the same mixture used to obtain the steady-state spectra in Figure 2. Fluorescence decay times in N_2 matrix (not corrected for finite laser pulse width): BaP, 78 ns; BkF, 13 ns; A, 8 ns; BeP, 100 ns; BaA, 115 ns; P, 430 ns

compounds. The presence of BaP fluorescence in the virtual absence of interference from BkF is especially noticeable at long delay times (e.g., 60 ns in Figure 3), though it is obvious that use of very long delay times in time-resolved fluorometry involves a trade-off of sensitivity for resolution.

Time resolution can be especially useful for identification of minor sample constituents. For example, Figure 4 compares steady-state and time-resolved MI fluorescence spectra of BaP in the presence of a large excess of BkF. While the steady-state spectrum provides only a vague indication of the presence of BaP, the time-resolution data provide strong confirmatory evidence for the presence of (carcinogenic) BaP in this mixture. In cases of this type, the fluorescence decay time serves as an additional parameter useful for identification of minor sample constituents in complex samples and thus serves to enhance the utility of MI fluorescence as a "fingerprinting" technique.

Quantitation of BaP in the presence of 1 μg BkF is compared for steady-state and time-resolved MI fluorometry in Figure 5. In both cases, measurements were made at 4006 Å, using benzo[*b*]fluorene (BbF) as internal standard (2). Fluorescence spectra for all samples and a "blank" (containing

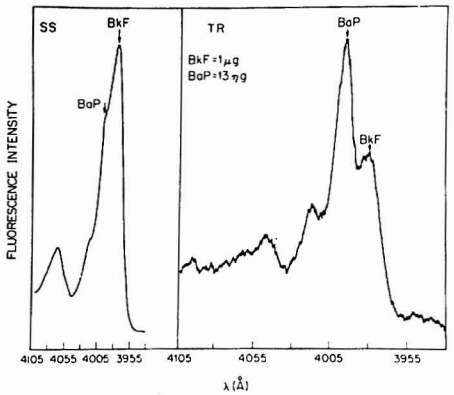

Figure 4. Steady-state (left) and time-resolved (right; delay = 90 ns) MI fluorescence spectra of two-component mixture (benzo[*k*]-fluoranthene, 1 μg; benzo[*a*]pyrene, 13 ng)

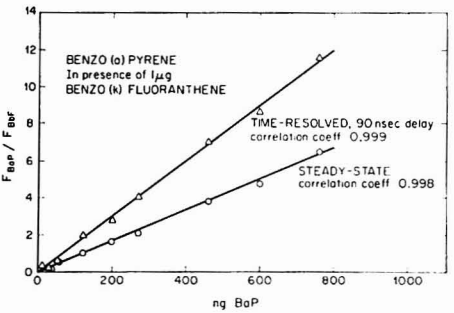

Figure 5. Analytical calibration curves (λ = 4006 Å) for benzo[*a*]pyrene in the presence of 1 μg benzo[*k*]fluoranthene, by time-resolved (Δ) and steady-state (O) MI fluorometry. In all cases, benzo[*b*]fluorene (BbF) was used as internal standard

1 μg BkF and no BaP) were normalized to yield the same intensity for the internal standard, BbF, at 3377 Å. The normalized blank intensity at 4006 Å was then subtracted from each of the normalized "sample" intensities at 4006 Å; the resulting BaP fluorescence signals were expressed as the ratio of BaP (4006 Å) to BkF (3377 Å) fluorescence intensities. The greater slope in the analytical calibration curve observed for time resolution arises largely from the fact that the analyte, BaP, exhibits a greater fluorescence decay time (78 ns) than the internal standard, BbF (τ_F = 37 ns); the data plotted in Figure 5 were obtained at a long delay time (90 ns). The limit of detection for BaP (defined as the quantity of BaP required to produce a difference in fluorescence intensity between a sample and a "blank", containing 1 μg BkF and no BaP, equal to 3 times the standard deviation of the "blank" fluorescence intensity at 4006 Å) in the presence of 1 μg BkF was 40 ng by steady-state MI fluorometry but was reduced to 2 ng by use of time resolution. Additional improvement in detection limits in cases of this type should be possible by using the argon ion laser to synchronously pump a dye laser (7). A major shortcoming of the fluorometer shown in Figure 1 is its restriction to a single excitation wavelength (2573 Å); this is an especially important limitation in MI fluorometry because excitation as well as emission spectra are sharpened by use of cryogenic matrices.

While time resolution is unlikely to achieve the status of a routine technique in low-temperature fluorescence spectrometry, it should prove very useful in special cases (as, for example, when a carcinogenic PAH such as benzo[*a*]pyrene is a minor constituent of a complex sample). Future developments in time-resolved MI fluorometry in this laboratory will include use of a synchronously-pumped dye laser (7) as a tunable source, and the complementary use of time-resolved and steady-state MI fluorescence spectra to obtain detailed profiles of PAH content of complex real samples, such as coal liquids and shale oils.

LITERATURE CITED

(1) Jones, P. W.; Freudenthal, R. K. "Polynuclear Aromatic Hydrocarbons: Second International Symposium on Analysis, Chemistry, and Biology"; Raven Press: New York, 1978.
(2) Stroupe, R. C.; Tokousbalides, P.; Dickinson, R. B., Jr.; Wehry, E. L.; Mamantov, G. *Anal. Chem.* **1977**, *49*, 701.
(3) Tokousbalides, P.; Hinton, E. R., Jr.; Dickinson, R. B., Jr.; Bilotta, P. V.; Wehry, E. L.; Mamantov, G. *Anal. Chem.* **1978**, *50*, 1189.
(4) Mamantov, G.; Wehry, E. L.; Kemmerer, R. R.; Stroupe, R. C.; Hinton, E. R.; Goldstein, G. *Adv. Chem. Ser.* **1978**, *170*, 99.
(5) Mamantov, G.; Wehry, E. L.; Kemmerer, R. R.; Hinton, E. R. *Anal. Chem.* **1977**, *49*, 86.
(6) Harris, J. M.; Chrisman, R. W.; Lytle, F. E.; Tobias, R. S. *Anal. Chem.* **1976**, *48*, 1937.
(7) Harris, J. M.; Gray, L. M.; Pelletier, M. J.; Lytle, F. E. *Mol. Photochem.* **1977**, *8*, 161.

Richard B. Dickinson, Jr.
E. L. Wehry*

Department of Chemistry
University of Tennessee
Knoxville, Tennessee 37916

RECEIVED for review December 1, 1978. Accepted February 2, 1979. This research was supported by the National Science Foundation (Grants MPS75-05364 and CHE77-12542).

Electron Mobility in a Plasma Chromatograph

Sir: A plasma chromatograph is one of the analytical instruments for investigating both positive and negative ions resulting from a series of ion–molecule reactions, taking place at atmospheric pressure, between molecules of interest and the reactant ionic species (*1*). The generation of positive reactant ions has recently been studied in detail (*2*) and that of negative reactant ions has also been discussed in many reports (*3*). However, when nitrogen gas is used as both drift and carrier gases, only thermal electrons are expected to be generated as the negative species, which were found to be much less reactive than the positive or negative reactant ions (*4*). This mode of the plasma chromatograph operation has been utilized by Karasek, Tatone, and Kane (*5*) in studying the electron capture mechanism, which is of interest to many gas chromatographers. However, with use of a Franklin GNO Beta/VI model plasma chromatograph, the authors reported that these thermal electrons appeared as a continuum across the plasma chromatographic scan because the gate grids did

0003-2700/79/0351-0780$01.00/0 © 1979 American Chemical Society

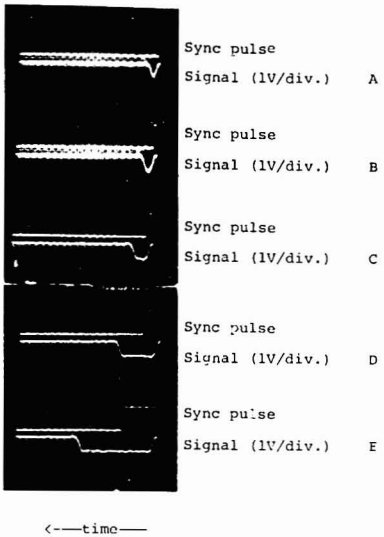

Figure 1. Thermal electron peak shapes at a field strength of 214 V/cm and at gate pulse widths of (A) 50 μs, (B) 100 μs, (C) 200 μs, (D) 500 μs, (E) 1 ms. The sync pulse widths are one-half of the gate pulse widths

not close perfectly to exclude such high speed particles. If the grid could exclude these electrons, they predicted that the ion drift spectrum would show a single peak with a drift time of 10 μs, which would be too fast for the response of the recording system. However, Spangler and Collins (6) did detect a very sharp peak near the start of the spectrum and observed a base-line current in some of the ion drift spectra obtained on a Franklin GNO Beta/VII plasma chromatograph when nitrogen was used as drift gas and a considerable lower flow of air as carrier gas. Because their interest was in the generation of negative reactant ions, no discussion was made about their observation.

Because of the above described ambiguity, the electron mobility, i.e., the electron velocity per unit field strength, was re-investigated with use of a plasma chromatography and the results obtained are discussed in this paper.

EXPERIMENTAL

A model Beta/VII-S plasma chromatograph, manufactured by the Franklin GNO Company, now PCP, Inc., of Palm Beach, Fla., was employed in this study. The detailed description of the instrumentation and the experimental conditions have been reported elsewhere (7). The plasma chromatographic oven was kept at 200 °C and prepurified nitrogen, after passing through a Linde Molecular Sieve 13X trap, was used as both drift and carrier gases with flow rates of 500 cm^3/min. and 150 cm^3/min, respectively. The data obtained were recorded by the following ways: a Polaroid camera attached to a dual beam Tektronix oscilloscope for measuring electron drift times, a Varian CAT, a digital signal averager, for obtaining the ion drift spectra, and a PAR Boxcar integrator, an analog signal averager, for monitoring the reaction between electrons and CCl_4.

RESULTS AND DISCUSSION

When nitrogen was used as both drift and carrier gases, a very sharp peak was observed on the oscilloscope near the origin of the negative ion mobility spectrum. The oscilloscope was triggered by the positive slope of the plasma chromatographic sync pulse, which is one half of the gate pulse. As

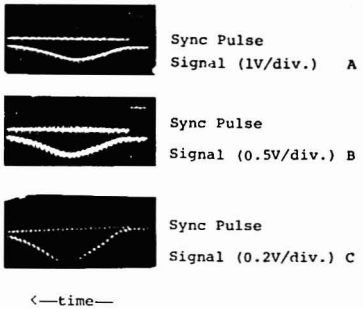

Figure 2. Electron drift velocities at a gate width of 50 μs and at field strengths of (A) 214 V/cm, (B) 143 V/cm, and (C) 107 V/cm. The sync pulse width is 25 μs, which is one-half of the gate pulse width

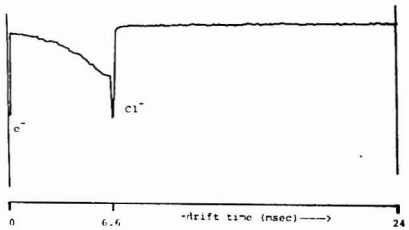

Figure 3. Ion mobility spectrum after the introduction of 2 μL of CCl_4 vapor into the drift gas stream

the pulse width increased, the peak width of the observed peak also increased. This flatness of the peak indicates the time required for the negative species to arrive at the collector is shorter than the gate pulse width. This is shown in Figure 1, where the gate pulse width varied from 50 μs to 1 ms and the plasma chromatographic drift field strength was 214 V/cm, or in other words, 3 kV was applied to the entire 14-cm plasma chromatographic tube. The tube consists of two regions — the ion-molecule reaction region, 6 cm in length, and the ion drift region, 8 cm in length. With the shortest gate pulse available which is 50 μs, the drift times of these negative peaks were measured as referenced to the time of the one-half of the gate pulse, as shown in Figure 2, to be 100, 110, and 120 μs at the drift field strengths of 214, 143, and 107 V/cm, respectively. Assuming that these negative particles are thermal electrons, the drift times are much longer than 10 μs, predicted by Karasek et al. (5). The drift velocities at the above drift field strengths were calculated to be 0.80, 0.73 and 0.67×10^5 cm/s. The reduced mobilities,

$$k_0 = \frac{d}{tE}\left(\frac{P}{760}\right)\left(\frac{273}{T}\right)$$

where d is the drift distance, t the drift time, E the drift field strength, P the pressure in mm Hg and T the temperature in K at the experimental conditions, were calculated to be 0.22, 0.30, and 0.36×10^3 cm^2/V-s at the above respective field strengths. Under the present ambient pressure experimental conditions, the E/N values, where N is the number density of the gaseous molecules, were calculated to be 0.85, 0.57, and 0.43 Td at 293 K (1 $Td = 10^{-17}$ V cm^2 $molecule^{-1}$). The electron drift velocities at the corresponding E/N value at 293 K were found to be 4.2, 3.7, and 3.3×10^5 cm/s (8). The reduced mobilities are therefore calculated to be 1.8, 2.4, and 2.9×10^3 cm^2/V-s which are much higher than our experi-

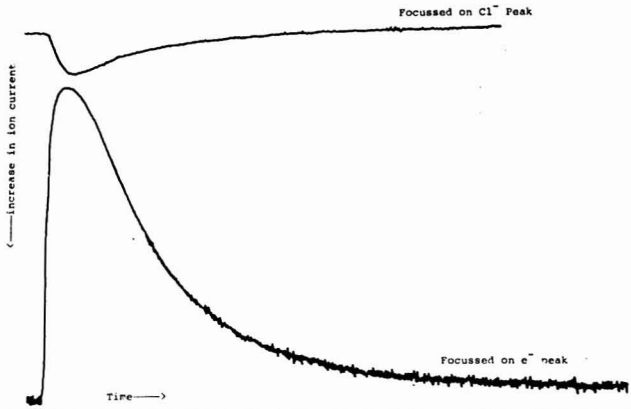

Figure 4. Reaction of $CCl_4 + e^- \rightarrow Cl^- + CCl_3$ after the introduction of 2 μL of CCl_4 vapor into the drift gas stream

mental values, even though the effect of the gate width time (t_g) is taken into consideration (*9*).

In order to understand more about these observed peaks, 2 μL of CCl_4 vapor was injected into the drift gas stream by adding a T connection with a septum inlet in the drift gas line. The ion mobility spectrum was obtained and is shown in Figure 3. The first peak (peak A) is the aforementioned negative peak and the second peak (peak B) is at the same drift time as Cl^-, which is the expected dissociative electron capture product from CCl_4. The distorted portion between these two peaks is interpreted to result from the reaction between the negative reactant of peak A and CCl_4 in the plasma chromatographic drift region. This experiment indicates that not only did the detected negative reactant of peak A transfer charge to CCl_4 but also that the drift gas got into the ion–molecule reaction region. Spangler and Collins (*6*) also observed similar distorted reactant ion peaks toward the shorter drift time when the air carrier gas flow was increased. This was explained to be due to the presence of oxygen and water in the drift region, which trap detected electrons to recycle them through ion–molecule cluster reactions before arrival at the collector. Both experiments point out that the drift gas can get into the carrier gas region and vice versa, which then would affect the plasma chromatographic performance as well as the relative densities of thermal electrons and negative reactant ions in the ion source.

When the plasma chromatograph was tuned to the peaks shown in Figure 3, the intensities of the two peaks were recorded as function of time after 2 μL CCl_4 vapor was introduced into the drift gas stream. This is shown in Figure 4. That an increase of the Cl^- peak intensity correlated with a decrease of the negative reactant peak intensity is direct evidence for the reaction between CCl_4 and the negative reactant of peak A.

Because of their extremely high mobility, peak A cannot be due to negative species with significant mass. The smallest negative reactant species other than electrons would be H^-. The generation of H^- under the present experimental conditions is chemically unlikely. Furthermore, the collision cross section was estimated to be 43 $Å^2$ when the radii of H^- and the N_2 molecule were assumed to be 2.08 Å (*10*) and 1.6 Å (*11*), respectively. The reduced mobility of H^- was then estimated, according to the Langevin equation (*11*, *12*), to be 12 $cm^2/V\text{-}s$. This value is much smaller than the reduced mobilities obtained herein for peak A. Therefore, the evidence presented above indicates that peak A is due to thermal electrons. With use of a plasma chromatograph of the same model as that of this study, M. Cohen and R. Wernlund (*13*) confirmed the magnitude of our measured value of the electron mobility. The discrepancy between the electron mobilities reported in literature and measured by a plasma chromatograph is attributed to the undesired capacitance coupling in the plasma chromatographic detection system. This will result in a longer integration time of a signal from the fast arriving electrons than the actual drift time of the electrons. Therefore, the present plasma chromatograph is not suitable for an accurate measurement of the electron drift mobility.

ACKNOWLEDGMENT

The authors express their gratitude to M. Cohen and R. Wernlund of PCP, Inc., for their efforts in confirming our measurement and to D. Ruhl for his assistance in characterizing the electrometer.

LITERATURE CITED

(1) Karasek, F. W. *Anal. Chem.* **1974**, *46*, 710A–20A.
(2) Carrol, D. I.; Dzidic, I.; Stillwell, R. N.; Horning, E. C. *Anal. Chem.* **1975**, *47*, 1956–9.
(3) Carr, T. W. *Anal. Chem.* **1977**, *49*, 828–31.
(4) Karasek, F. W.; Kane, D. M. *J. Chromatogr.* **1974**, *93*, 129–39.
(5) Karasek, F. W.; Tatone, O. S.; Kane, E. M. *Anal. Chem.* **1973**, *45*, 1210–14.
(6) Spangler, G. E.; Collins, C. I. *Anal. Chem.* **1975**, *47*, 393–402.
(7) Tou, J. C.; Boggs, G. U. *Anal. Chem.* **1976**, *48*, 1351–6.
(8) Huxley, L. G.; Crompton, R. W. "The Diffusion and Drift of Electrons in Gases", Wiley: New York, 1974; Chap. 14.
(9) Spangler, G. E.; Collins, C. I. *Anal. Chem.* **1975**, *47*, 403–7.
(10) Coulson, C. A. "Valence", Oxford University Press: London, 1961; p 316.
(11) Griffin, G. W.; Horning, E. C.; Wentworth, W. E. *J. Chem. Phys.* **1974**, *60*, 4994–9.
(12) Hasse, H. R. *Phil. Mag.* **1926**, *1*, 139–60.
(13) Cohen, M. J.; Wernlund, R. F., PCP Inc. Palm Beach, Fla., private communication, 1978.

J. C. Tou*
T. Ramstad
T. J. Nestrick

Analytical Laboratories
The Dow Chemical Co.
Midland, Mich. 48640

RECEIVED for review May 5, 1978. Accepted January 15, 1979.

Application of Anion-Exchange Resin-Loaded Filters to the X-Ray Fluorescence Determination of Sulfate

Sir: The use of anion-exchange resin-loaded filters (SB-2) for the enrichment of small amounts of various anions followed by X-ray fluorescence (XRF) measurement was first described by Campbell in 1966 (*1*). He reported a detection limit of 0.6 μg for sulfur. Since 1966 this approach to anion analysis has received little attention, the main interest centering on trace metal enrichment with cation-exchange resins (*2–6*). Recently, Warren (*7*) reported on the use of SB-2 ion-exchange filters for preconcentration and found a limit of detection of 0.1 μg for the iodide ion.

The purpose of this work was to establish the conditions necessary to permit quantitative analysis of sulfate by enrichment on SB-2 filters. A procedure for cleaning and preconditioning the filters to obtain sufficiently low and reproducible blanks is described. In order to analyze sulfur in samples where particle size effects are appreciable, dissolution of the sample is often necessary. Since wet-digestion methods utilizing perchloric and nitric acids are commonly used for sample dissolution, perchlorate and nitrate ions were tested as possible interferences. As an alternative to measuring the sulfur K X-ray lines which are strongly absorbed in the filter, conversion of the sulfate to barium sulfate directly in the SB-2 paper was investigated. The sulfur was then determined indirectly by measuring the higher energy Ba $L\beta_2$ line. This procedure was applied to the analysis of sulfur in NBS-SRM 1621 Fuel Oil (certified value = 1.05% sulfur).

EXPERIMENTAL

Apparatus. The Philips vacuum spectrograph and associated instrumentation have been described in a previous publication (*8*). LiF (100) and graphite crystals were used for measuring the Ba $L\beta_2$ and S Kα lines, respectively, with a Cr target tube operated at 40 kV and 30 mA. The sample holders were adapted to maintain the filters in a reproducible position during measurement. The filters were rotated, and X-ray measurements of either the S Kα or Ba $L\beta_2$ lines were made in vacuum (70 Pa, or 0.5 mm Hg). An average of the X-ray intensity of the top and bottom sides of each filter was taken. Reeve-Angel SB-2 filters in the chloride form (Whatman, Inc.), 47-mm diameter, lot number 6865 were used and held in commercial filter holders (Bio-Rad Lab.). All chemicals were analytical reagent grade and the water was triple-distilled (*9*).

Filter Preparation. The anion affinity of the SB-2 resin according to Samuelson (*10*) decreases in the following order: citrate, sulfate, oxalate, iodide, perchlorate, nitrate, chromate, bromide, thiocyanate, chloride, formate, hydroxide, and acetate.

To obtain maximum retention of sulfate, the filters were converted first to the hydroxide and then to the acetate form. XRF measurements of the SB-2 filters showed unacceptably high blank levels of about 300 ppm of sulfur. They were cleaned by first treating the filters with distilled water for several hours to allow the resin to swell. They were then immersed in a 4 wt.% NaOH solution and allowed to stand for 12–15 h. This treatment was found to remove about 90% of the sulfur present in the blank. The remaining 10% of the sulfur in the filters could not be removed by washing and is believed to be bound within the cellulose matrix of the paper. The sulfur blank after washing was found to be reproducible within ±3%. After a second treatment with a fresh NaOH solution, the filters were rinsed with water and immersed in a 5 wt.% acetic acid solution for 12–15 h. The filters were removed, washed, and then stored in a 0.01 M sodium acetate solution (pH 5.0) before use.

Procedure. *Preparation of Calibration Curves.* (a) To prepare filters containing from 10 to 1000 μg of sulfur, aliquots of a standard ammonium sulfate solution were added to 2.0 mL of 0.1 M acetate buffer and made up to 50-mL volume with water.

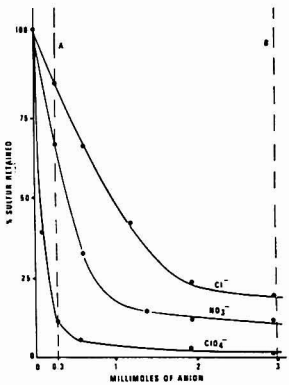

Figure 1. Percent sulfur retained as a function of anion added. Dotted line A represents the total anion capacity of the filter (0.3 mmol). Dotted line B represents ten times the anion capacity. Initial sulfate loading is 0.1 mmol

The pH was adjusted between 3 and 6 with either dilute acetic acid or ammonium hydroxide and then passed through a cleaned filter four times. The filter was rinsed with 10 mL of water and allowed to dry.

(b) To convert the sulfate to barium sulfate in the filters, the filters were loaded with sulfate as described in a. They were immersed in 10 mL of a 0.4 wt.% solution of barium chloride (pH 2) for 1 h. They were then washed with water and dried.

Analysis of NBS-SRM 1621 Fuel Oil. One gram of NBS-SRM 1621 Fuel Oil was ignited in an oxygen-bomb calorimeter according to the ASTM Standard Test Method D2382-65-[70]. The sample cup was then washed with water, and the washings were collected quantitatively. About 80 mL of solution was obtained containing 132 μg/mL of sulfur. Aliquots of this solution were taken and treated as described in a and b above.

RESULTS AND DISCUSSION

To test the influence of perchlorate, nitrate, and chloride as possible interferences, varying amounts of these ions were added to solutions each containing 0.01 mmol of sulfate ion. These solutions were then passed through filters. The loading of each of the above anions ranged from zero to ten times the anion capacity of the filter which was calculated to be 0.3 mmol, and the results are plotted in Figure 1. It can be seen that these anions have a strong effect. For example, 0.3 mmol of perchlorate displaces 92%, nitrate 35%, and chloride 10% of the sulfate initially present. Therefore, quantitation of sulfur is possible only in analyte solutions where chloride or more weakly held anions are present.

When the S Kα line was measured directly, strong X-ray absorption from filter to filter was observed because of the changing distribution of sulfate with depth within the filter. The half-thickness of paper for sulfur X rays was calculated to be 0.01 mm. Because the filter is 0.2 mm thick, it is not transparent to sulfur X rays. Also, each side of the filter has different topography caused by the manufacturing process, and microscopic examination showed that the amount of ion-exchange resin varies from side to side. Figure 2A shows a calibration curve which is linear up to 400 μg prepared with ammonium sulfate solutions.

0003-2700/79/0351-0783$01.00/0 © 1979 American Chemical Society

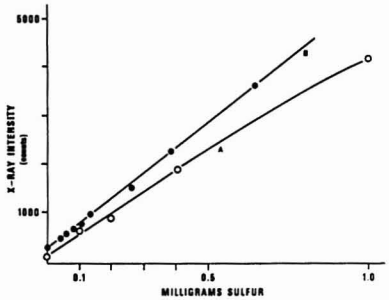

Figure 2. X-ray intensity vs. milligrams of sulfur. Legend: (-A-) Sulfur Kα line measured. (-B-) Ba Lβ_2 line measured

Another procedure was investigated in an effort to overcome the strong X-ray absorption effects in the filter. This consisted of converting the sulfate loaded on the filter to barium sulfate followed by measurement of the Ba Lβ_2 line. Because of the higher energy of the barium line (e.g., filter attenuates 50% of Ba Lβ_2), it was expected that differences in the distribution of sulfate in the filter would have a much smaller effect in the analysis. Figure 2B shows a calibration curve where the sulfate loaded on the filter was converted to barium sulfate with subsequent measurement of the Ba Lβ_2 line. It is evident from Figure 2B that the linear range is greater compared to figure 2A where the sulfur Kα line was measured directly. Nine measurements of sulfur in the NBS-SRM 1621 Fuel Oil gave an average value of 1.10% with a standard deviation of a single measurement of 0.13%.

XRF analysis of sulfur with anion-exchange resin-loaded filters is primarily influenced by interfering anions, filter thickness, and uneven distribution of the resin in the filter. This technique requires that anions which form insoluble salts with barium such as phosphate also be absent. It is not recommended that filters which have been previously loaded with sulfate and exposed to direct X-ray radiation be cleaned and reused. We have observed partial radiation damage to the resin in such filters and this can lead to less than 100% retention of the sulfate in the filter. To improve the precision of the X-ray measurements in general it would be advantageous to use filters in which the ion-exchange resin is of a very fine particle size and uniformly distributed throughout the filter matrix.

LITERATURE CITED

(1) Campbell, W. J.; Spano, E. F.; Green, T. E. *Anal. Chem.* **1966**, *38*, 987.
(2) Hooton, K. A. H.; Parsons, M. L. *Anal. Chem.* **1973**, *45*, 436.
(3) James, H. *Analyst (London)* **1973**, *98*, 274.
(4) Blaedel, W. J.; Niemann, R. A. *Anal. Chem.* **1975**, *47*, 1455.
(5) Kerfoot, W. B.; Crawford, R. L., submitted for publication in *Anal. Chem.*
(6) Toussaint, C. J.; Alna, G.; Bo, F. *Anal. Chim. Acta* **1977**, *88*, 193.
(7) Warren P. L. *Proc. Anal. Div. Chem. Soc.*, **1977**, January.
(8) Rasberry, S. D.; Heinrich, K. F. J. *Anal. Chem.* **1974**, *46*, 81.
(9) Kuehner, E. C.; Alvarez, R.; Paulsen, P. J.; Murphy, T. J. *Anal. Chem.* **1972**, *44*, 2050.
(10) Samuelson, O. "Ion Exchangers in Analytical Chemistry", Wiley; New York, 1953.

B. Schreiber

Sandoz Ltd.
CH-4002
Basle, Switzerland

P. A. Pella*

National Bureau of Standards
Washington, D.C. 20234

RECEIVED for review November 3, 1978. Accepted January 15, 1979.

Author Index

Adams, D. F. 609
Apffel, J. 594
Attrep, M., Jr. 731

Bamesberger, W. L. 609
Barnett, S. A. 641
Bentz, B. L. 673
Boniforti, L. 735
Bruhn, C. G. 673
Busch, K. W. 670

Camoni, I. 735
Cantwell, F. F. 623
Carr, T. W. 705
Cattabeni, F. 735
Chiabrando, C. 735
Christian, G. D. 752
Clark, H. A. 616
Coleman, H. J. 602
Colli, G. 735

De Angelis, L. 735
Demas, J. N. 712, 717
Dickinson, R. B., Jr. 778
Di Corcia, A. 776
DiCosimo, R. 679
di Domenico, A. 735
Di Muccio, A. 735
Dovichi, N. J. 728

Eatough, D. J. 633
Elli, G. 735

Fagan, R. 749
Fanelli, R. 735
Farwell, S. O. 609
Feldman, C. 664
Ford, C. D. 659
Frick, L. W. 641
Fukumoto, K. 651

Galli, G. 735
Gloor, R. 645
Gluck, S. J. 609
Gorni, A. 735
Grassi, P. 735
Green, D. C. 745
Grizzle, P. L. 602

Hansen, L. D. 633
Harris, J. M. 728
Harrison, W. W. 673
Hirao, Y. 651
Hogg, R. 758
Holcombe, J. A. 648
Hunter, R. L. 699
Hurtubise, R. J. 659

Invernizzi, G. 735
Issaq, H. J. 657

Jablonski, B. B. 681
Janca, J. 637
Jemma, A. 735
Johnson, D. C. 741
Jurs, P. C. 616

Kamada, H. 686, 688
Kim, S. 679
Kimura, K. 651
Koile, R. C. 741
Kuo, K-n. 745

Lacey, M. J. 691
Lamb, J. D. 633
Lee, M. L. 768
Leidner, H. 645
Lenhard, J. R. 745
Leyden, D. E. 681
Luciani, L. 735

McCreery, R. L. 749
Macdonald, C. G. 691
McIver, R. T., Jr. 699
Malloy, B. 670
Merli, F. 735
Moses, P. R. 745
Mourey, T. H. 763
Murray, R. W. 745

Nakashima, S. 654
Nestrick, T. J. 780
Nomura, M. 686
Novotny, M. 768

Oda, S. 686, 688

Paasivirta, J. 598
Patriarche, G. J. 752
Pearson, R. M. 683
Pecsok, R. L. 594
Pella, P. A. 783
Perchalski, R. J. 774
Pruiksma, R. 749
Puon, S. 623

Ramstad, T. 780
Richter, B. E. 633
Rollins, D. K. 633
Salmon, S. G. 648
Samperi, R. 776
San Filippo, J., Jr. 679
Sato, K. 695
Sattar, M. A. 598
Sawada, T. 686, 688
Schreiber, B. 783
Schutte, T. M. 609
Schwartz, L. M. 723
Shimizu, H. 688
Siggia, S. 763
Stringer, C. E. 731
Sugisaki, H. 651
Suzuki, K-i. 695

Taggi, F. 735
Talmi, Y. 670
Tamura, H. 695
Taylor, D. G. 712, 717
Tou, J. C. 780

Vassilaros, D. L. 768
Vergori, L. 735
Vire, J. C. 752

Wehry, E. L. 778
White, C. M. 768
Wilder, B. J. 774

Yamaguchi, N. 695
Yang, K. C. 758

Future Articles

Derivation Methods of Stoichiometric Empirical Formulas from Elemental Analysis Results
B. W. Tattershall

Chemical Analysis and Structural Characterization of Transition Metal Disulfide Intercalates
S. L. Suib, L. R. Faulkner, G. D. Stucky, and R. J. Blattner

Colorimetric Determination of Hexuronic Acids in Plant Materials
R. W. Scott

Adsorption of Mercury Vapor by Gold and Silver
T. T. Mercer

Separation of Mass Spectra of Mixtures by Factor Analysis
F. J. Knorr and J. H. Futrell

Direct Pyrolysis of Cellulose and Cellulose Derivatives in a Mass Spectrometer with a Data System
W. E. Franklin

Time-Resolved Phosphorescent Spectrometry with Silicon Intensified Target Vidicon and Regression Analysis Methods
D. E. Goeringer and H. L. Pardue

Radiative Auger Effect in X-ray Fluorescence Analysis
P. Van Espen, H. Nullens, and F. Adams

Flow Electrolysis on a Reticulated Vitreous Carbon Electrode
W. J. Blaedel and J. Wang

Characterization of Asphaltenes Isolated from a Coal-Derived Liquid
B. C. Bockrath, K. T. Schroeder, and F. W. Steffgen

Determination of Asphaltenes in Fuels from Coal Hydrogenation
F. W. Steffgen, K. T. Schroeder, and B. C. Bockrath

Thermometric Titrations of Polyprotic Acids
J-L. Burgot and M. A. Bernard

Microcomputer-Controlled Potentiometric Analysis System
C. R. Martin and H. Freiser

Determination of Pentachlorophenol in Water by Mass Spectrometric Isotope Dilution
L. L. Ingram, Jr., G. D. McGinnis, and S. V. Parikh

Now you can weigh with analytical precision (0.1mg) on a fully automatic electronic top-loader or on a fully automatic electronic suspended-pan balance, as the weighing situation or your personal preference dictates.

The new top-loader that weighs with analytical precision is our Model 1201MP. Compact and very affordable, this addition to our popular 1200 Series has a capacity of 30g and weighs to 0.1mg at the touch of a button. Its many advanced features include a built-in microprocessor, instant electronic taring, memory and weight recall, BCD output for printer connection, and a large, bright digital display with reading stability indicator. Pan access is provided from the top and both sides of the glass enclosed weighing chamber.

For 0.1mg precision in an electronic analytical balance, we offer our new Model 2003MP. Fully automatic push-button operation and other features are similar to our electronic top-loaders. In addition, a door-activated switch blocks display of the last digit except when both chamber doors are closed, thereby preventing air current-induced instability of the readout. With a capacity of 166g, larger pan and larger weighing chamber, the 2003MP is more versatile and somewhat more costly.

For literature write: Sartorius Balances, Division of Brinkmann Instruments, Inc., Cantiague Road, Westbury, N.Y. 11590.

Sartorius introduces an electronic top-loader with the same precision (0.1mg) as our new electronic analytical balance.

FULLY AUTOMATIC ELECTRONIC ANALYTICAL BALANCE WITH 0.1mg PRECISION, MODEL 2003MP

FULLY AUTOMATIC ELECTRONIC TOP-LOADING BALANCE WITH 0.1mg PRECISION, MODEL 1201MP

sartorius

CIRCLE 21 ON READER SERVICE CARD